

Structure and function of chloroplasts, volume III

Edited by

Hongbo Gao, Yan Lu, Rebecca L. Roston and Alistair McCormick

Published in

Frontiers in Plant Science



FRONTIERS EBOOK COPYRIGHT STATEMENT

The copyright in the text of individual articles in this ebook is the property of their respective authors or their respective institutions or funders. The copyright in graphics and images within each article may be subject to copyright of other parties. In both cases this is subject to a license granted to Frontiers.

The compilation of articles constituting this ebook is the property of Frontiers.

Each article within this ebook, and the ebook itself, are published under the most recent version of the Creative Commons CC-BY licence. The version current at the date of publication of this ebook is CC-BY 4.0. If the CC-BY licence is updated, the licence granted by Frontiers is automatically updated to the new version.

When exercising any right under the CC-BY licence, Frontiers must be attributed as the original publisher of the article or ebook, as applicable.

Authors have the responsibility of ensuring that any graphics or other materials which are the property of others may be included in the CC-BY licence, but this should be checked before relying on the CC-BY licence to reproduce those materials. Any copyright notices relating to those materials must be complied with.

Copyright and source acknowledgement notices may not be removed and must be displayed in any copy, derivative work or partial copy which includes the elements in question.

All copyright, and all rights therein, are protected by national and international copyright laws. The above represents a summary only. For further information please read Frontiers' Conditions for Website Use and Copyright Statement, and the applicable CC-BY licence.

ISSN 1664-8714
ISBN 978-2-83251-989-9
DOI 10.3389/978-2-83251-989-9

About Frontiers

Frontiers is more than just an open access publisher of scholarly articles: it is a pioneering approach to the world of academia, radically improving the way scholarly research is managed. The grand vision of Frontiers is a world where all people have an equal opportunity to seek, share and generate knowledge. Frontiers provides immediate and permanent online open access to all its publications, but this alone is not enough to realize our grand goals.

Frontiers journal series

The Frontiers journal series is a multi-tier and interdisciplinary set of open-access, online journals, promising a paradigm shift from the current review, selection and dissemination processes in academic publishing. All Frontiers journals are driven by researchers for researchers; therefore, they constitute a service to the scholarly community. At the same time, the *Frontiers journal series* operates on a revolutionary invention, the tiered publishing system, initially addressing specific communities of scholars, and gradually climbing up to broader public understanding, thus serving the interests of the lay society, too.

Dedication to quality

Each Frontiers article is a landmark of the highest quality, thanks to genuinely collaborative interactions between authors and review editors, who include some of the world's best academicians. Research must be certified by peers before entering a stream of knowledge that may eventually reach the public - and shape society; therefore, Frontiers only applies the most rigorous and unbiased reviews. Frontiers revolutionizes research publishing by freely delivering the most outstanding research, evaluated with no bias from both the academic and social point of view. By applying the most advanced information technologies, Frontiers is catapulting scholarly publishing into a new generation.

What are Frontiers Research Topics?

Frontiers Research Topics are very popular trademarks of the *Frontiers journals series*: they are collections of at least ten articles, all centered on a particular subject. With their unique mix of varied contributions from Original Research to Review Articles, Frontiers Research Topics unify the most influential researchers, the latest key findings and historical advances in a hot research area.

Find out more on how to host your own Frontiers Research Topic or contribute to one as an author by contacting the Frontiers editorial office: frontiersin.org/about/contact

Structure and function of chloroplasts, volume III

Topic editors

Hongbo Gao — Beijing Forestry University, China

Yan Lu — Western Michigan University, United States

Rebecca L. Roston — University of Nebraska-Lincoln, United States

Alistair McCormick — University of Edinburgh, United Kingdom

Citation

Gao, H., Lu, Y., Roston, R. L., McCormick, A., eds. (2023). *Structure and function of chloroplasts, volume III*. Lausanne: Frontiers Media SA.

doi: 10.3389/978-2-83251-989-9

Table of contents

- 05 **Editorial: Structure and function of chloroplasts, Volume III**
Hongbo Gao, Alistair J. McCormick, Rebecca L. Roston and Yan Lu
- 09 **Visualizing the Integrity of Chloroplast Envelope by Rhodamine and Nile Red Staining**
Jinjie An, Xin Miao, Lulu Wang, Xu Li, Xiaomin Liu and Hongbo Gao
- 18 **Gene Replacement in Arabidopsis Reveals Manganese Transport as an Ancient Feature of Human, Plant and Cyanobacterial UPF0016 Proteins**
Natalie Hoecker, Yvonne Hennecke, Simon Schrott, Giada Marino, Sidsel Birkelund Schmidt, Dario Leister and Anja Schneider
- 33 **Functional Relationship of Arabidopsis AOXs and PTOX Revealed via Transgenic Analysis**
Danfeng Wang, Chunyu Wang, Cai Li, Haifeng Song, Jing Qin, Han Chang, Weihai Fu, Yuhua Wang, Fei Wang, Beibei Li, Yaqi Hao, Min Xu and Aigen Fu
- 51 **The Physiological Functionality of PGR5/PGRL1-Dependent Cyclic Electron Transport in Sustaining Photosynthesis**
Mingzhu Ma, Yifei Liu, Chunming Bai, Yunhong Yang, Zhiyu Sun, Xinyue Liu, Siwei Zhang, Xiaori Han and Jean Wan Hong Yong
- 60 **How to Measure Grana – Ultrastructural Features of Thylakoid Membranes of Plant Chloroplasts**
Radostaw Mazur, Agnieszka Mostowska and Lucja Kowalewska
- 69 **A Novel Chloroplast Protein RNA Processing 8 Is Required for the Expression of Chloroplast Genes and Chloroplast Development in *Arabidopsis thaliana***
Mengmeng Kong, Yaozong Wu, Ziyuan Wang, Wantong Qu, Yixin Lan, Xin Chen, Yanyun Liu, Perveen Shahnaz, Zhongnan Yang, Qingbo Yu and Hualing Mi
- 82 **Molecular Characterization of Mg-Chelatase CHL1 Subunit in Pea (*Pisum sativum* L.)**
Cai-jun Wu, Jie Wang, Jun Zhu, Jing Ren, You-xin Yang, Tao Luo, Lu-xi Xu, Qing-hong Zhou, Xu-feng Xiao, Yu-xin Zhou and Sha Luo
- 95 **Stromal Protein Chloroplast Development and Biogenesis1 Is Essential for Chloroplast Development and Biogenesis in *Arabidopsis thaliana***
Weijie Chen, Jingang Huang, Shiwei Chen, Lin Zhang, Jean-David Rochaix, Lianwei Peng and Qiang Xin
- 109 **Rubredoxin 1 Is Required for Formation of the Functional Photosystem II Core Complex in *Arabidopsis thaliana***
Liping Che, Han Meng, Junxiang Ruan, Lianwei Peng and Lin Zhang
- 121 **AtRsmD Is Required for Chloroplast Development and Chloroplast Function in *Arabidopsis thaliana***
Zi-Yuan Wang, Wan-Tong Qu, Tong Mei, Nan Zhang, Nai-Ying Yang, Xiao-Feng Xu, Hai-Bo Xiong, Zhong-Nan Yang and Qing-Bo Yu

- 137 **A Tissue-Chopping Based Immunofluorescence Staining Method for Chloroplast Proteins**
Lulu Wang, Mingdong Tang, Wenwen Huang, Jinjie An, Xiaomin Liu and Hongbo Gao
- 143 **Reduction in chloroplastic ribulose-5-phosphate-3-epimerase decreases photosynthetic capacity in Arabidopsis**
Yonghong Li, Lianwei Peng, Xiaoqin Wang and Lin Zhang



OPEN ACCESS

EDITED AND REVIEWED BY

Anna N Stepanova,
North Carolina State University,
United States

*CORRESPONDENCE

Hongbo Gao
✉ gaohongbo@bjfu.edu.cn

SPECIALTY SECTION

This article was submitted to
Plant Physiology,
a section of the journal
Frontiers in Plant Science

RECEIVED 16 January 2023

ACCEPTED 06 February 2023

PUBLISHED 01 March 2023

CITATION

Gao H, McCormick AJ, Roston RL and Lu Y
(2023) Editorial: Structure and function of
chloroplasts, Volume III.
Front. Plant Sci. 14:1145680.
doi: 10.3389/fpls.2023.1145680

COPYRIGHT

© 2023 Gao, McCormick, Roston and Lu.
This is an open-access article distributed
under the terms of the [Creative Commons
Attribution License \(CC BY\)](#). The use,
distribution or reproduction in other
forums is permitted, provided the original
author(s) and the copyright owner(s) are
credited and that the original publication in
this journal is cited, in accordance with
accepted academic practice. No use,
distribution or reproduction is permitted
which does not comply with these terms.

Editorial: Structure and function of chloroplasts, Volume III

Hongbo Gao^{1*}, Alistair J. McCormick², Rebecca L. Roston³
and Yan Lu⁴

¹College of Biological Sciences and Technology, Beijing Forestry University, Beijing, China, ²Institute of Molecular Plant Sciences, School of Biological Sciences, University of Edinburgh, Edinburgh, United Kingdom, ³Department of Biochemistry, University of Nebraska-Lincoln, Lincoln, NE, United States, ⁴Department of Biological Sciences, Western Michigan University, Kalamazoo, MI, United States

KEYWORDS

chloroplast, photosynthesis, envelope, thylakoid, ribosome

Editorial on the Research Topic

Structure and function of chloroplasts, Volume III

Chloroplasts are endosymbiotic organelles derived from cyanobacteria. They have a double envelope membrane, including the outer envelope and the inner envelope. A complex membrane system, thylakoids, exists inside the chloroplast. It is the site of the light-dependent reactions of photosynthesis. The stroma is the main site of the carbon fixation reactions. Although photosynthesis is a very complicated process with many proteins involved, there are many other important processes that occur in chloroplasts, including the regulation of photosynthesis, the biogenesis and maintenance of the structures, carbohydrate, lipid, tetrapyrrole, amino acid, and isoprenoid metabolism, production of some phytohormones, production of specialized metabolites, regulation of redox, and interactions with other parts of the cell (Sabater, 2018). During evolution, most of the cyanobacterial genes were lost and many of them were transferred into the nuclear genome. A majority of chloroplast proteins are nuclear-encoded and possess an N-terminal transit peptide which helps the protein to be targeted into chloroplasts. Chloroplasts have their own highly reduced genome which works coordinately with the nuclear genome for the biogenesis and function of chloroplasts (Liebers et al., 2022). This Research Topic presents studies covering different aspects of chloroplast function, including photosynthesis, biogenesis, structure, and maintenance. These works push the frontiers of chloroplast research further in the field of plant biology.

Photosynthesis and its regulation

The chloroplast thylakoid protein RUBREDOXIN1 (RBD1) has previously been proposed to play a role in photosystem II (PSII) assembly in *Chlamydomonas* and *Synechocystis* (Calderon et al., 2013; Garcia-Cerdan et al., 2019; Kiss et al., 2019), but this had not been investigated in land plants. Che et al. examined an *Arabidopsis* mutant lacking *RBD1*, *rbd1*, and observed a severe reduction in intact PSII complexes, an increased abundance of assembly intermediates, and a reduction in translation of the central D1 subunit. Although newly synthesized mature D1 and precursor D1/D2 could assemble into

the PSII reaction center, larger complexes were nearly completely absent. Thus, RBD1 appears to be critical for PSII assembly and may also be involved in the translation of *D1*.

Alternative oxidase (AOX) is responsible for the alternative electron transfer pathway in mitochondria (Juszczuk and Rychter, 2003), while plant plastid terminal oxidase (PTOX) mediates the chloroplast oxygen-consuming respiratory electron transfer pathway (Nawrocki et al., 2015). Wang et al. found that when AOXs are directed to chloroplasts *via* a chloroplast-specific targeting sequence in Arabidopsis, all five AOXs (AOX1a, 1b, 1c, 1d, and AOX2) are able to either partially or fully suppress the variegation phenotype of a PTOX-deficient mutant *immutans* indicating that all AOXs could act as a PQH2 oxidase and active PTOX in chloroplasts. The authors also found that native versions of AOX1a, AOX1b and AOX2 were partially dual-localized to chloroplasts, whereas AOX1c and AOX1d are found only in mitochondria. This research revealed the interaction between mitochondria and chloroplasts and shed light on the complex mechanisms of redox control in plant cells.

Li et al. studied the role of the plastidial enzyme ribulose-5-phosphate-3-epimerase (RPE) which plays an important role in the Calvin-Benson-Bassham (CBB) cycle and oxidative pentose phosphate pathways in plants. Using *rpe* knockdown mutants in *Arabidopsis thaliana*, these researchers showed that reduced levels of RPE resulted in decreased leaf CO₂ assimilation and photosynthetic electron transport rates under high light levels. Together their findings indicate that RPE may be an additional putative target for increasing flux through the CBB cycle to enhance photosynthesis.

Mn²⁺ is critical for PSII function. It is supplied to the thylakoid lumen by PAM71, a Mn²⁺ transporter and a member of the Uncharacterized Protein Family 0016 (UPF0016, Eisenhut et al., 2018). Although Mn²⁺ transport appears to be a common feature of UPF0016 proteins, little is known about their history. Hoecker et al. used a phylogenetic approach to classify eukaryotic UPF0016 genes into two subgroups. Furthermore, the authors investigated if UPF0016 transporters from different origins could substitute for PAM71, including a cyanobacterial protein MNX, human TMEM165 and an Arabidopsis chloroplast envelope protein CMT1, when directed to the thylakoid membrane in an Arabidopsis *pam71* mutant. In all three cases, the transporters could substitute for PAM71 in a non-native environment, indicating that Mn²⁺ transport is an ancient feature of the family.

Chlorophyll biosynthesis is catalyzed by the rate-limiting heterotrimeric enzyme, Mg-chelatase. Recent genome sequencing of pea (*Pisum sativum* L.) showed there were two genes of one Mg-chelatase subunit, *PsCHLI1* and *PsCHLI2* (Kreplak et al., 2019). Wu et al. studied the two genes and showed that *PsCHLI1* was more highly expressed than *PsCHLI2* in leaves, that silencing *PsCHLI1* resulted in yellow leaves and reduced chlorophyll content, and that silencing *PsCHLI2* produced no obvious phenotype. The researchers concluded that *PsCHLI1* was the essential CHLI subunit for maintaining Mg-chelatase activity, and a potential target for improving photosynthetic efficiency by manipulating Mg-chelatase.

The majority of the light energy is transferred through the linear electron transport (LET) pathway, which includes PSII, cytochrome b6f complex (Cytb6f), photosystem I (PSI) and ferredoxin-NADP reductase (FNR), to ultimately reduce NADP⁺ to NADPH. However, additional pathways, such as a Proton Gradient Regulation5 (PGR5)/PGR5-Like Photosynthetic Phenotype1 (PGRL1)-dependent cyclic electron transport (CET) pathway around PSI, also exist (Joliot and Johnson, 2011). In the minireview of Ma et al., the authors provide an overview on this CET pathway and how it coordinates with other related photosynthesis processes, such as state transition, non-photochemical quenching (NPQ), and the balance of ATP/NADPH, to protect photosystems and chloroplasts during various stress conditions. A deeper understanding of PGR5/PGRL1-CET will be beneficial for the agricultural production.

Biogenesis and development of chloroplasts

In higher plants, chloroplast development requires coordinated expression of plastid-encoded and nuclear-encoded genes (Lieber et al., 2022). Kong et al. discovered that a novel chloroplast protein, RNA PROCESSING8 (RP8), is required for chloroplast gene expression and chloroplast development in *Arabidopsis thaliana*. Loss-of-function mutation in the *RP8* gene results in reduced accumulation of the mature *rpoA* transcript, which encodes the alpha subunit of the plastid-encoded RNA polymerase (PEP) complex. Consequently, the pale-green *rp8* mutant displays impaired transcription of PEP-dependent genes, such as *psaA*, *psbA*, *psbB*, *petB*, and *rbcL*. Thylakoids are either absent or barely visible in the cotyledons and true leaves of the *rp8* mutant. Therefore, Kong et al. proposed that RP8 is involved in the processing of *rpoA* transcripts.

Ribosome biogenesis is a multistep process that includes the synthesis, processing, and folding of rRNAs, the synthesis, processing, and folding of ribosomal proteins, and finally integration of the ribosomal proteins with the mature rRNAs (Weis et al., 2015). Chen et al. characterized a chloroplast protein CDB1 which is indispensable for chloroplast development through its involvement in chloroplast ribosome assembly. CDB1L, the paralog of CDB1, is localized in both chloroplasts and mitochondria; it may play a similar role during ribosome assembly in both organelles. These findings provide a better understanding of the regulation mechanisms controlling chloroplast development and ribosome assembly in plant organelles.

Arabidopsis thaliana Ribosomal small subunit methyltransferaseD (*AtRsmD*) encodes a 16S rRNA methyltransferase in chloroplasts (Ngoc et al., 2021). In the study of Wang et al., the *atrsmd-2* mutant exhibited impaired chloroplast development and reduced photosynthetic efficiency in emerging leaves under normal growth conditions. Amounts of chloroplast-encoded photosynthetic proteins, such as D1, D2, CP43, and CP47, were reduced in the emerging leaves of the *atrsmd-2* mutant, resulting in the decreased accumulation of the photosynthetic super complex. Knockout of the *AtRsmD* gene affected the accumulation of chloroplast rRNAs and chloroplast ribosomal proteins, as well as altered the RNA loading of

chloroplast ribosomes in *Arabidopsis*, with cold stress exacerbating the effect of the mutation on chloroplast development and chloroplast ribosome biogenesis. This work extends our understanding of the significance of chloroplast rRNAs methylation in chloroplast development and photosynthesis.

Methods for chloroplast research

Chloroplast isolation is a method frequently used in the study of chloroplasts (Fitzpatrick and Keegstra, 2001; Seigneurin-Berny et al., 2008). In many experiments, the intactness of isolated chloroplasts is essential for the validity of conclusions made. However, the intactness of chloroplast envelope was not checked in the many publications, even though this is an essential quality control. An et al. developed a quick and easy method to visualize the intactness of chloroplast envelopes by staining isolated chloroplasts with fluorescent dyes, Rhodamine or Nile red, and then observing the chloroplasts with a fluorescence microscope. Broken chloroplasts and intact chloroplasts can be directly observed. Moreover, the authors have also reported that the middle-layer chloroplasts in Percoll density gradient centrifugation methods may contain mostly broken plastids, a finding that has important practical consequences.

In wild-type plants, chloroplast division proteins are known to form a ring at the division site, with the patterns of these proteins being disordered in several chloroplast division mutants (Wang et al., 2017; Chen et al., 2018; Chen et al., 2019; Liu et al., 2022; Sun et al., 2023). This is often observed *via* immunofluorescence staining (IFS). However, the traditional IFS method uses wax-embedding and sectioning, which is time-consuming and tedious. Wang et al. developed a method that is very simple and fast. They cut leaves into irregular small pieces and performed the IFS directly. The leaf tissue was lysed so that the samples could separate into single cells, which provided a clear view of individual cells. The authors demonstrated the utility of this method by studying the localization of chloroplast division protein FtsZ1 in the wild-type and mutant *Arabidopsis* and various other plants.

In chloroplasts, stacked thylakoid membranes, grana, are connected by unstacked thylakoid membranes, lamella, forming a complicated membrane network (Kirchhoff, 2019). Thylakoid structure, usually observed *via* electron microscopy, affects the photosynthesis efficiency and is regulated by various developmental and physiological factors. The minireview by Mazur et al. overviews the recent approaches for measuring the ultrastructural features of grana. The authors outline and define structural parameters, such as granum height and diameter, thylakoid thickness, end-membrane length, stacking repeat distance, and granum lateral irregularity, highlighting the basic measurements and related workflows. The paper also discusses how to correctly interpret such data by taking into account the 3D nature of grana stacks projected onto 2D images.

Together, the studies collected here in this special issue represent advances across the topics related to the structure and function of chloroplasts, from biogenesis to regulation, from energy fixation to dissipation, from physical to analysis methods. They will empower future research to delve a little further into the critical questions surrounding chloroplast structure and function.

Author contributions

All authors listed have made a substantial and intellectual contribution to the work and approved it for publication.

Funding

HG was supported by the Fundamental Research Funds for the Central Universities (2022BLRD14) and National Nature Science Foundation of China (Grant No. 32070696, 31570182). AM acknowledges funding from UK Biotechnology and Biological Sciences Research Council (BBSRC) grants (BB/S020128/1, BB/S015531/1 and BB/W003538/1). RR was supported by the United States Department of Energy (DE-SC0021101), the National Science Foundation (IOS-1845175), and the Nebraska Agricultural Experiment Station with funding from the Hatch Multistate Research capacity funding program (NEB-30-131, 1017736). YL was supported by the National Science Foundation of the United States (Grant No. DBI-2146882).

Acknowledgments

We thank all the authors and reviewers that have contributed to this Research Topic.

Conflict of interest

The authors declare that the research was conducted in the absence of any commercial or financial relationships that could be construed as a potential conflict of interest.

Publisher's note

All claims expressed in this article are solely those of the authors and do not necessarily represent those of their affiliated organizations, or those of the publisher, the editors and the reviewers. Any product that may be evaluated in this article, or claim that may be made by its manufacturer, is not guaranteed or endorsed by the publisher.

References

- Calderon, R. H., Garcia-Cerdan, J. G., Malnoe, A., Cook, R., Russell, J. J., Gaw, C., et al. (2013). A conserved rubredoxin is necessary for photosystem II accumulation in diverse oxygenic photoautotrophs. *J. Biol. Chem. Sep* 13; 288, 26688–26696. doi: 10.1074/jbc.M113.487629
- Chen, C., Cao, L., Yang, Y., Porter, K. J., and Osteryoung, K. W. (2019). ARC3 activation by PARC6 promotes FtsZ-ring remodeling at the chloroplast division site. *Plant Cell* 31, 862–885. doi: 10.1105/tpc.18.00948
- Chen, C., Maccready, J. S., Ducat, D. C., and Osteryoung, K. W. (2018). The molecular machinery of chloroplast division. *Plant Physiol.* 176, 138–151. doi: 10.1104/pp.17.01272
- Eisenhut, M., Hoecker, N., Schmidt, S. B., Basgaran, R. M., Flachbart, S., Jahns, P., et al. (2018). The plastid envelope CHLOROPLAST MANGANESE TRANSPORTER1 is essential for manganese homeostasis in arabidopsis. *Mol. Plant Jul* 2; 11, 955–969. doi: 10.1016/j.molp.2018.04.008
- Fitzpatrick, L. M., and Keegstra, K. (2001). A method for isolating a high yield of arabidopsis chloroplasts capable of efficient import of precursor proteins. *Plant J.* 27, 59–65. doi: 10.1046/j.0960-7412.2001.01061.x
- Garcia-Cerdan, J. G., Furst, A. L., McDonald, K. L., Schunemann, D., Francis, M. B., and Niyogi, K. K. (2019). A thylakoid membrane-bound and redox-active rubredoxin (RBD1) functions in de novo assembly and repair of photosystem II. *P Natl. Acad. Sci. U.S.A.* 116, 16631–16640. doi: 10.1073/pnas.1903314116
- Joliot, P., and Johnson, G. N. (2011). Regulation of cyclic and linear electron flow in higher plants. *Proc. Natl. Acad. Sci.* 108, 13317–13322. doi: 10.1073/pnas.1110189108
- Juszczuk, I. M., and Rychter, A. M. (2003). Alternative oxidase in higher plants. *Acta Biochim. Pol.* 50, 1257–1271. doi: 10.18388/abp.2003_3649
- Kirchhoff, H. (2019). Chloroplast ultrastructure in plants. *New Phytol.* 223, 565–574. doi: 10.1111/nph.15730
- Kiss, E., Knoppova, J., Aznar, G. P., Pilny, J., Yu, J. F., Halada, P., et al. (2019). A photosynthesis-specific rubredoxin-like protein is required for efficient association of the D1 and D2 proteins during the initial steps of photosystem II assembly. *Plant Cell. Sep*; 31, 2241–2258. doi: 10.1105/tpc.19.00155
- Kreplak, J., Madoui, M.-A., Cápál, P., Novák, P., Labadie, K., Aubert, G., et al. (2019). A reference genome for pea provides insight into legume genome evolution. *Nat. Genet.* 51, 1411–1422. doi: 10.1038/s41588-019-0480-1
- Liebers, M., Cozzi, C., Uecker, F., Chambon, L., Blanvillain, R., and Pfannschmidt, T. (2022). Biogenic signals from plastids and their role in chloroplast development. *J. Exp. Bot.* 73, 7105–7125. doi: 10.1093/jxb/erac344
- Liu, X., An, J., Wang, L., Sun, Q., An, C., Wu, B., et al. (2022). A novel amphiphilic motif at the c-terminus of FtsZ1 facilitates chloroplast division. *Plant Cell* 34, 419–432. doi: 10.1093/plcell/koab272
- Nawrocki, W. J., Tourasse, N. J., Taly, A., Rappaport, F., and Wollman, F. A. (2015). The plastid terminal oxidase: its elusive function points to multiple contributions to plastid physiology. *Annu. Rev. Plant Biol.* 66, 49–74. doi: 10.1146/annurev-arplant-043014-114744
- Ngoc, L. N. T., Park, S. J., Cai, J., Huong, T. T., Lee, K., and Kang, H. (2021). RsmD, a chloroplast rRNA m2G methyltransferase, plays a role in cold stress tolerance by possibly affecting chloroplast translation in arabidopsis. *Plant Cell Physiol.* 62, 948–958. doi: 10.1093/pcp/pcab060
- Sabater, B. (2018). Evolution and function of the chloroplast: current investigations and perspectives. *Int. J. Mol. Sci.* 19 (10), 3095. doi: 10.3390/ijms19103095
- Seigneurin-Berny, D., Salvi, D., Joyard, J., and Rolland, N. (2008). Purification of intact chloroplasts from arabidopsis and spinach leaves by isopycnic centrifugation. *Curr. Protoc. Cell Biol.* 3, 30. doi: 10.1002/0471143030.cb0330s40
- Sun, Q., Cao, X., Liu, Z., An, C., Hu, J., Wang, Y., et al. (2023). Structural and functional insights into the chloroplast division site regulators PARC6 and PDV1 in the intermembrane space. *Proc. Natl. Acad. Sci. United States America* 120, e2215575120. doi: 10.1073/pnas.2215575120
- Wang, W. H., Li, J. Y., Sun, Q. Q., Yu, X. Y., Zhang, W. W., Jia, N., et al. (2017). Structural insights into the coordination of plastid division by the ARC6-PDV2 complex. *Nat. Plants* 3, 17011. doi: 10.1038/nplants.2017.11
- Weis, B. L., Kovacevic, J., Missbach, S., and Schleiff, E. (2015). Plant-specific features of ribosome biogenesis. *Trends Plant Sci.* 20, 729–740. doi: 10.1016/j.tplants.2015.07.003



Visualizing the Integrity of Chloroplast Envelope by Rhodamine and Nile Red Staining

Jinjie An^{1,2}, Xin Miao^{1,2}, Lulu Wang^{1,2}, Xu Li^{1,2}, Xiaomin Liu^{1,2} and Hongbo Gao^{1,2*}

¹ Beijing Advanced Innovation Center for Tree Breeding by Molecular Design, Beijing Forestry University, Beijing, China,

² College of Biological Sciences and Technology, Beijing Forestry University, Beijing, China

OPEN ACCESS

Edited by:

Jirong Huang,
Shanghai Institute for Biological
Sciences, Chinese Academy of
Sciences (CAS), China

Reviewed by:

Aigen Fu,
Northwest University, China
Hualing Mi,
Shanghai Institute for Biological
Sciences, Chinese Academy of
Sciences (CAS), China

*Correspondence:

Hongbo Gao
gaohongbo@bjfu.edu.cn

Specialty section:

This article was submitted to
Plant Physiology,
a section of the journal
Frontiers in Plant Science

Received: 16 February 2021

Accepted: 30 March 2021

Published: 26 April 2021

Citation:

An J, Miao X, Wang L, Li X, Liu X and
Gao H (2021) Visualizing the Integrity
of Chloroplast Envelope by
Rhodamine and Nile Red Staining.
Front. Plant Sci. 12:668414.
doi: 10.3389/fpls.2021.668414

Chloroplasts are essential organelles in plant cells with many important functions. Chloroplasts isolated by Percoll density gradient centrifugation are widely used in the study of chloroplasts. The intactness of isolated chloroplasts is necessary for many of the experiments. In the past, those isolated chloroplasts were either simply believed to be intact or had to be analyzed by indirect biochemical methods. Here we show a new method to check the intactness of isolated chloroplasts by staining their envelope with fluorescent dyes, Rhodamine or Nile red, and then observing them with a fluorescence microscope. With this method, broken chloroplasts and intact chloroplasts can be distinguished easily and their integrity can be checked in a few minutes. Results of this method agreed well with those of biochemical methods. Moreover, we have also found that sometimes the middle layer chloroplasts from the Percoll gradient centrifugation could be mostly broken, which could cause mistakes in the experiment. With our method, this problem can be easily found. This chloroplast envelope staining method can be used in the preparation of isolated chloroplasts to ensure the intactness.

Keywords: chloroplast isolation, chloroplast integrity, envelope, staining, Rhodamine, Nile red

INTRODUCTION

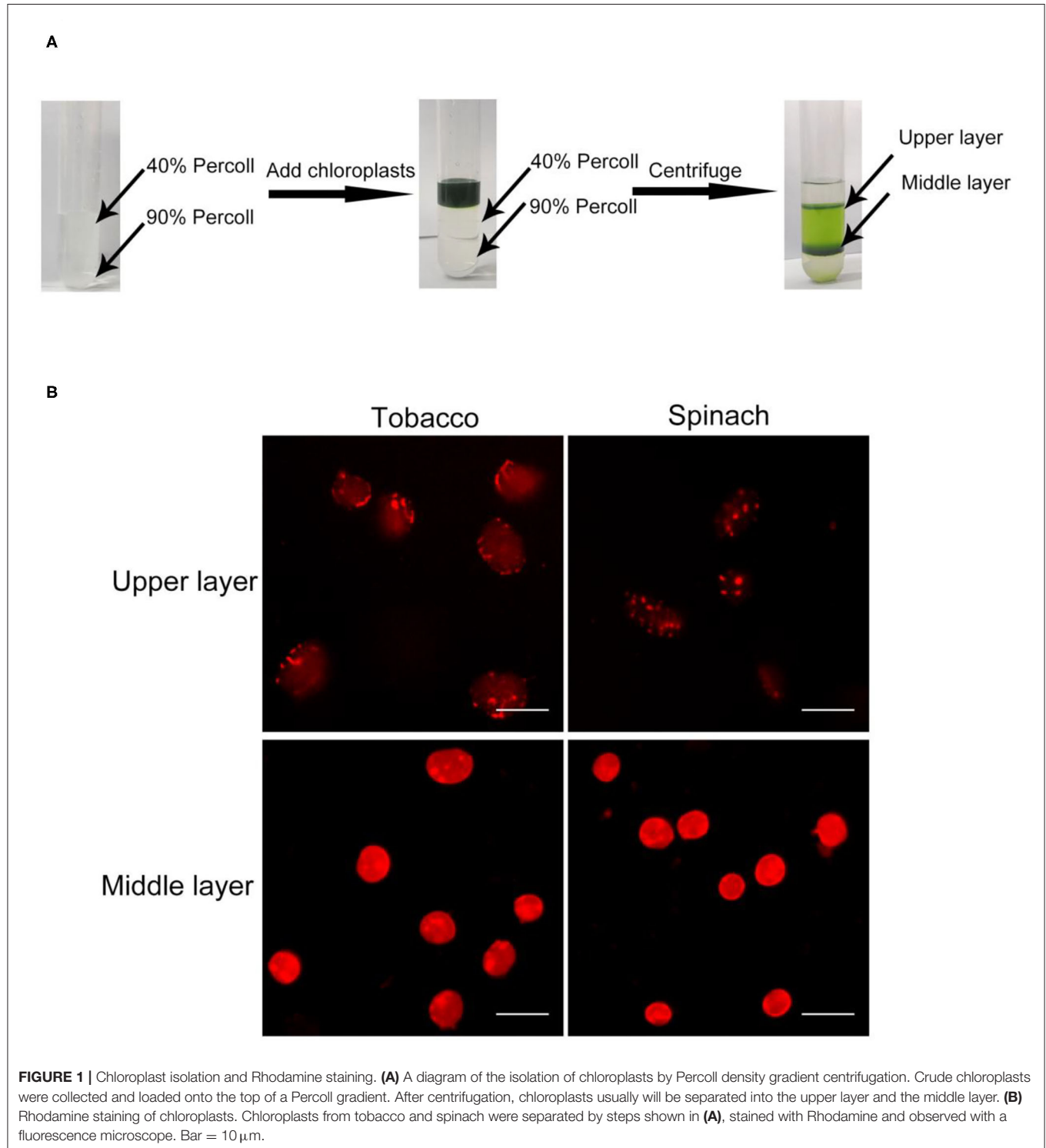
Chloroplasts are plant-specific organelles encapsulated by double membranes, inside which contain thylakoids, stroma, and other structures. Chloroplasts are the major site of photosynthesis. They are also involved in many other important biochemical processes in plants, such as the biosynthesis of fatty acids, amino acids, and plant hormones (Azevedo et al., 2006; Lopez-Juez, 2007; Schaller and Stintzi, 2009; Sendon et al., 2011; Mano and Nemoto, 2012; Wang and Benning, 2012). Chlorophyll in the thylakoids of chloroplasts can emit autofluorescence upon excitation (Ruhle et al., 2018), which is often used for the observation chloroplasts with fluorescence microscope (Gao et al., 2013).

Biochemical, physiological, and proteomic analyses are common methods to study the functions and development of chloroplasts (Gao et al., 2003, 2006; Baginsky and Gruissem, 2004; Block et al., 2007; Lopez-Juez, 2007; Su and Lai, 2017; Fuertauer et al., 2019). During the process of these analyses, chloroplasts are often isolated and the intactness of chloroplasts are required to maintain their metabolic activity and the functional surrounding envelope membrane at the maximum (Seigneurin-Berny et al., 2008b; Su and Lai, 2017). The density of chloroplasts will be decreased once they are broken. Due to the difference of the densities between broken chloroplasts and intact

chloroplasts, Percoll density gradient centrifugation method is widely used to separate broken chloroplasts and obtain pure and intact chloroplasts (Fitzpatrick and Keegstra, 2001; Seigneurin-Berny et al., 2008a). After centrifugation, broken chloroplasts

usually stay in the upper layer, and intact chloroplasts usually stay in the middle layer between the Percoll of two different densities.

In the past, it was generally believed that chloroplasts obtained by Percoll density gradient centrifugation are intact



(Seigneurin-Berny et al., 2008b; Lang et al., 2011; Vieira Ldo et al., 2014), but this may not always be true. During the day, starch granules are accumulated in chloroplasts, which not only make chloroplasts fragile during the isolation process but also increase the density of chloroplasts. Therefore, broken chloroplasts with high starch content may stay in the middle layer of Percoll gradient and misled the experiment. The integrity of chloroplasts can be analyzed by SDS-PAGE analysis (Seigneurin-Berny et al., 2008a,b). However, it will take hours to 1 day get the final results. Hill reaction is a quick method widely used to check the intactness of chloroplasts (Mills and Joy, 1980). It estimates the intactness of chloroplasts based on biochemical reactions indirectly. Direct observation with bright field, phase contrast, and autofluorescence are difficult to discern broken chloroplasts with good shapes. In this study, we developed a new method using fluorescent dyes, such as Rhodamine or Nile red, to stain the envelop membrane of isolated chloroplasts and then directly check their integrity by microscopy observation. This method is very simple. With this method, we found that isolated chloroplasts from the middle layer of Percoll gradient are not totally intact and this can be quickly observed with a fluorescence microscope.

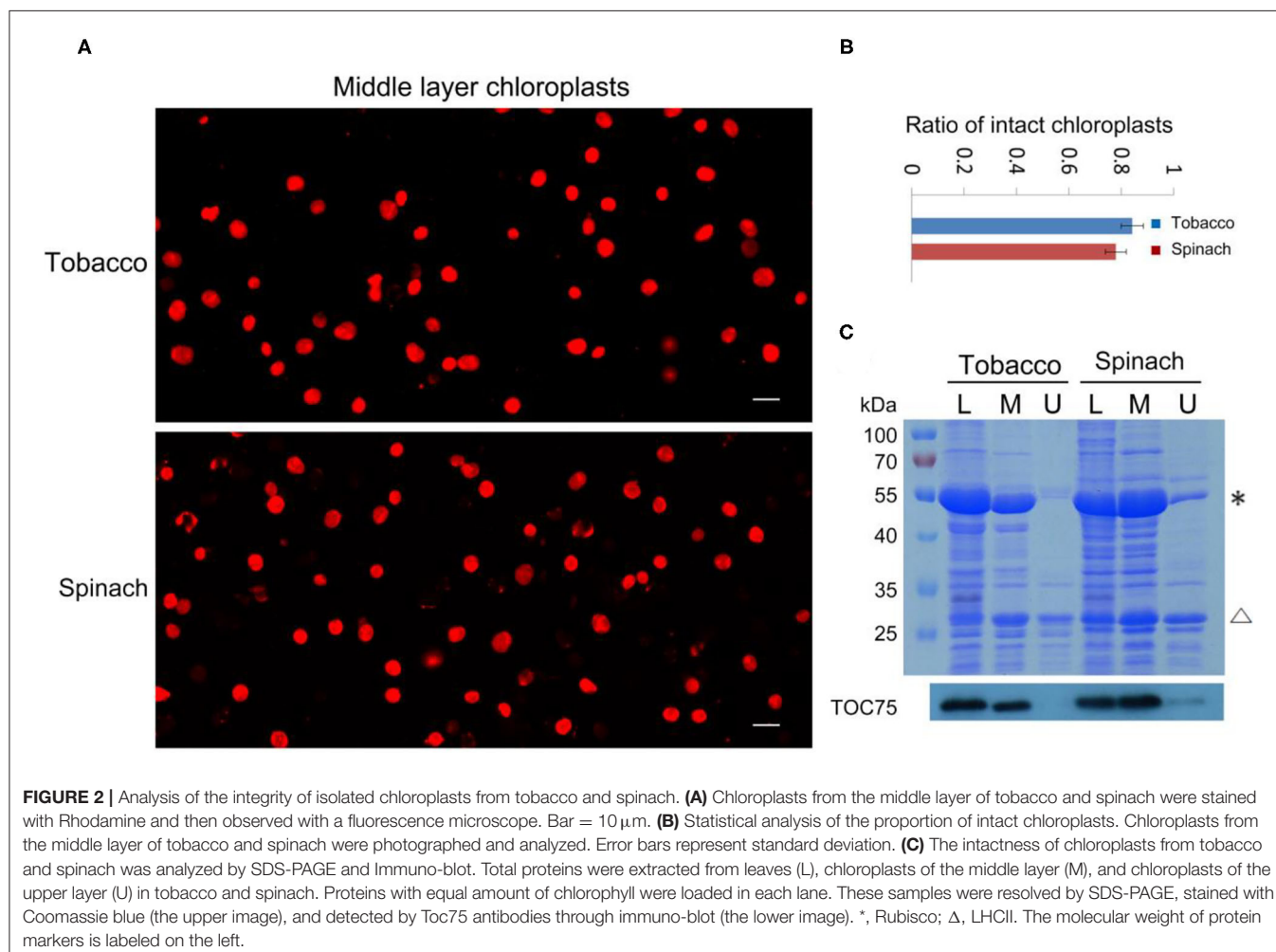
MATERIALS AND METHODS

Plant Materials and Growth Conditions

Arabidopsis thaliana plants used are Columbia-0 (Col) wild type. Plants were grown in soil in a growth chamber at 22°C with 40–60% relative humidity and 16-h-light/8-h-dark cycles. Tobacco (*Nicotiana benthamiana*) and poplar (*Populus alba* × *Populus tremula* var. *glandulosa*) plants were grown under the same growth condition. Tobacco plants were 5-week-old and poplar plants were 6-month-old. Spinach, pea and lettuce were bought from a vegetable shop. *Peperomia tetraphylla* and orchid were grown on a sunny windowsill at room temperature and 6-month-old.

Chloroplast Isolation

All the steps were carried out at 4°C. For each sample, 7 g leaves were harvested, put into a blender, and added with 100 mL GB solution [50 mM HEPES/KOH (pH 7.9), 0.33 M sorbitol, 1 mM MgCl₂, 1 mM MnCl₂, 2 mM EDTA (pH8.0), 5 mM Na-ascorbate, 0.1% BSA]. These leaf tissues was ground five times, 3 s each time. The ground samples were filtered into 50 mL tubes, centrifuged at 2000 g for 2 min. After removing the



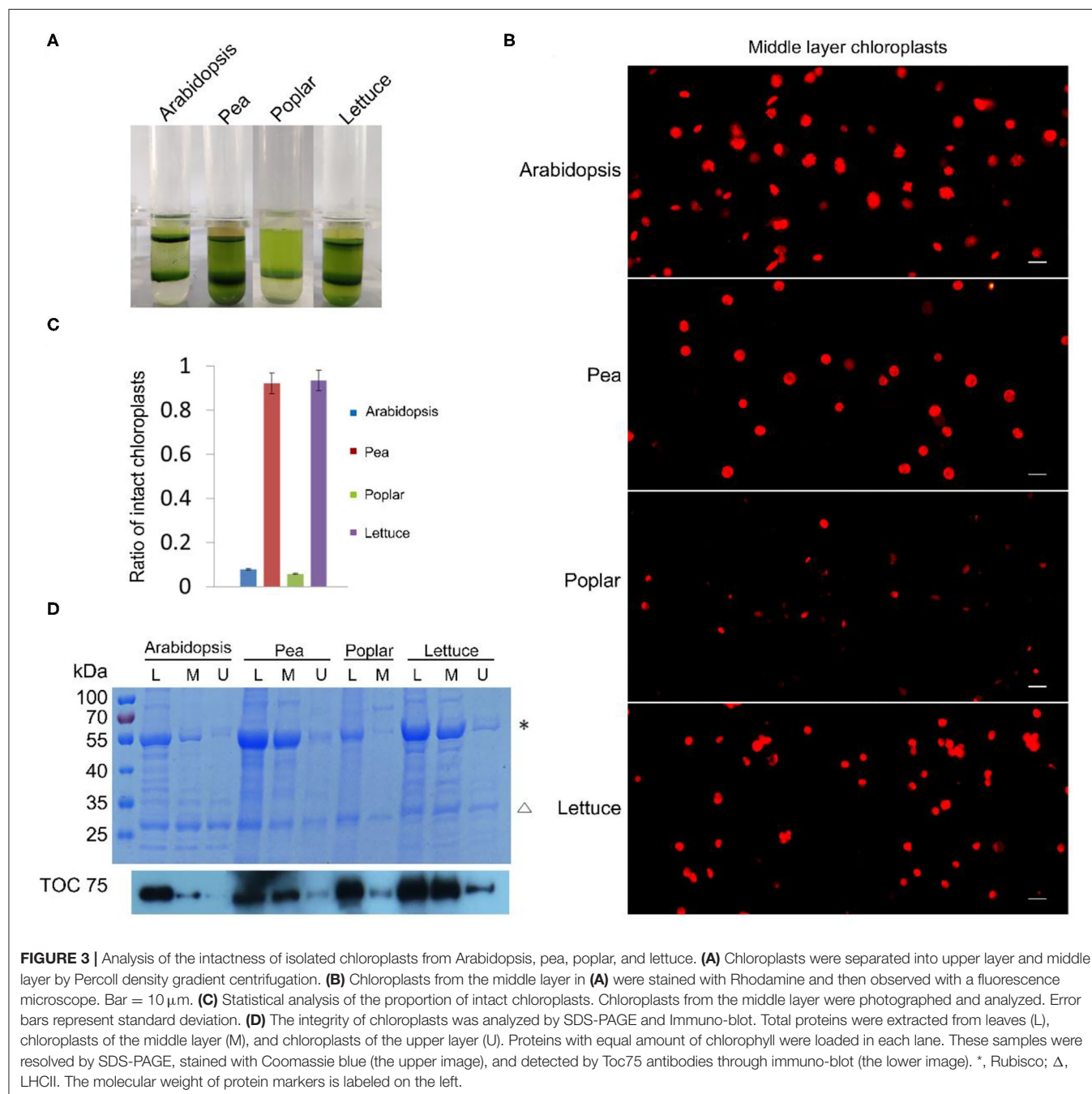
supernatant, 500 μ L RB solution [50 mM HEPES-KOH (pH 7.9), 0.33 M sorbitol, 0.8 mM CaCl_2 , 5 mM Na-ascorbate] was added to the chloroplast pellet. The chloroplasts were resuspended and carefully added to the surface of a Percoll density gradient solution in RB with 40% (v/v) Percoll on the top, and 90% (v/v) Percoll at the bottom. After a centrifugation at 2000 g for 10 min, chloroplasts were separated by Percoll gradient into upper layer and middle layer. For washing, chloroplasts from each layer were carefully transferred into a new tube and resuspended with 3 mL RB, centrifuged at 400 g for 3 min, and resuspended in RB again.

Chloroplast Staining

1 μ L Rhodamine B (0.1 mg/mL) or Nile red (1 mg/mL) were added into 100 μ L chloroplast suspension. Then the chloroplasts were stained on ice for 2–10 min. After being collected by centrifugation at 3000 g for 7 s and washed with RB twice, chloroplasts were observed with a fluorescence microscope.

Microscopy and Image Analysis

Isolated chloroplasts were observed with a NEXCOPE NE910 microscope equipped with 40 \times and 20 \times objectives, and images were captured with an E3ISPM camera. Autofluorescence of



chlorophyll, and red fluorescence of Rhodamine and Nile red were observed with an excitation filter set of 510–580 nm and an emission filter set of 600–700 nm. Image analysis was carried out using ImageJ (<http://rsbweb.nih.gov/ij/>; version 1.52v) and Photoshop (Adobe Photoshop CC 2015).

Statistical Analysis of Chloroplast Integrity

For each stained chloroplast sample of the middle layer, 20 fields observed with 40× objective were taken to count the intact and broken chloroplasts. The ratio of intact or broken chloroplasts to the total chloroplasts ($n > 400$) was calculated. Data was analyzed by Excel.

Coomassie Blue Staining and Immunoblotting

Proteins were extracted from the leaves, chloroplasts of the upper layer and the middle layer, respectively. Protein samples with equal amount of chlorophyll were loaded in each lane, resolved by SDS-PAGE, stained in Coomassie brilliant blue solution (1 g Coomassie brilliant blue R250, 200 mL ethanol, 100 mL acetic acid, add deionized water to 1 L) for 4 h. Subsequently, the gel was destained in destaining solution (200 mL ethanol, 100 mL acetic acid, add deionized water to 1 L) for several hours. Protein samples resolved by SDS-PAGE gels were also transferred to Immun-Blot PVDF membrane (Bio-Rad). Blots were probed with anti-TOC75 primary antibodies (Chen et al., 2016) (1:40,000

dilution) for 1 h and HRP conjugated anti-rabbit secondary antibodies (1:10,000 dilution) for 1 h. Films were developed using eECL Western Blot Kit (Beijing ComWin Biotech Company).

RESULTS

Conventional Microscopy Method Is Not Good at Discerning Broken and Intact Chloroplasts

Chloroplast isolation is a common experiment in many labs. Obtaining intact chloroplasts is important for the study of chloroplasts. Isolated chloroplasts can be observed with a bright field, phase contrast or fluorescence microscope to check their integrity. If a chloroplast is highly disintegrated, its shape will be abnormal and can be easily recognized. However, it is difficult to directly observe the integrity of isolated chloroplasts with broken envelope and relatively good shapes (**Supplementary Figure 1**). In some cases (see below), a majority of isolated chloroplasts could be broken with unawareness and this could cause a serious problem to the experiment.

Rhodamine Can Be Used to Discern Broken and Intact Chloroplasts by Staining Their Envelope

In order to discern intact chloroplasts and broken chloroplasts, we developed a method to evaluate the intactness of isolated

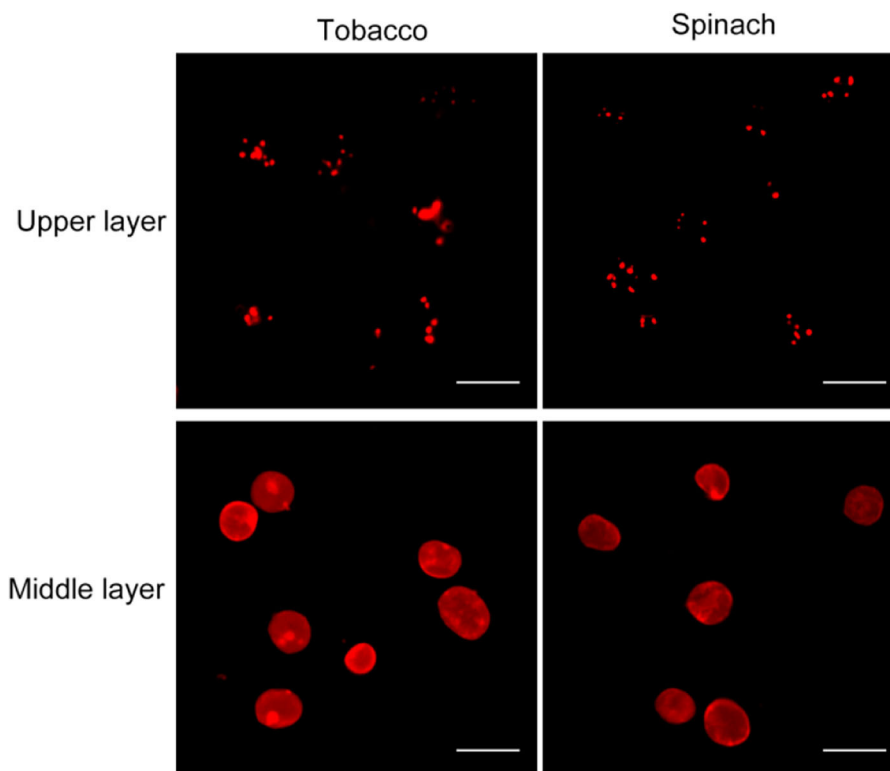


FIGURE 4 | Nile red staining of chloroplasts. Chloroplasts from tobacco and spinach were isolated by steps shown in **Figure 1A**, stained with Nile red and observed with a fluorescence microscope. Bar = 10 μ m.

chloroplasts. At first, crude chloroplasts isolated from plant leaves were applied to a Percoll density gradient centrifugation to get the upper layer chloroplasts and middle layer chloroplasts (**Figure 1A**). These chloroplasts were stained with Rhodamine for 2–10 min and washed twice. Rhodamine is a dye with red fluorescence under the excitation of a 550 nm laser (Chen and Wood, 2009), and it can bind to chloroplast envelope and show the integrity through microscopy observation (**Figure 1B**).

In the beginning, we isolated chloroplasts from tobacco and spinach leaves, and checked the integrity of isolated chloroplasts with the above method. After staining, the envelope of chloroplasts can be visualized clearly (**Figure 1B**). For most of the chloroplasts from the upper layer, the envelope was discontinuous and apparently broken. In contrast, for most of the chloroplasts from the middle layer, the envelope was continuous and obviously intact. This staining method allowed us to visually identify intact and broken chloroplasts.

Rhodamine Staining Is a Reliable Method to Check the Integrity of Chloroplasts

With our method, the ratio of intact and broken chloroplasts could be calculated in a relatively precise way (**Figures 2A,B**). It indicated that 84 and 78% of the middle layer chloroplasts from tobacco and spinach were intact, respectively. To further verify the effectiveness of this method, we carried out SDS-PAGE, Coomassie Blue staining and immuno-blot analysis. Proteins of the leaves, upper layer chloroplasts and middle

layer chloroplasts from tobacco and spinach were extracted for comparison (**Figure 2C**). Rubisco is a key enzyme for carbon fixation in photosynthesis, it is a soluble and highly abundant protein localized to the stroma of chloroplasts (Suzuki et al., 2010). LHCII is a key protein for light harvesting in photosynthesis, it is also highly abundant and localized to the grana of thylakoids (Gao et al., 2018; Liu et al., 2019). If the envelope of a chloroplast is broken, its Rubisco will be mostly lost, but its LHCII can be mostly kept. So, the integrity of isolated chloroplasts can be deduced by comparing the ratio of Rubisco and LHCII to that of the leaves. As we can see from **Figure 2C**, the Rubisco from the middle layer chloroplasts of tobacco and spinach were close to those of leaves, while the Rubisco from the upper layer chloroplasts were very low compared with those of leaves, suggesting that the chloroplasts from the middle layer were mostly intact and the chloroplasts from the upper layer were mostly broken. Toc75 is an outer envelope membrane protein of chloroplasts (Chen et al., 2016), it can also be used to reveal the integrity of isolated chloroplasts. Our immuno-blot assay results indicated that Toc75 level in the middle layer chloroplasts was close to that of the leaf, while its level in the chloroplasts of upper layer was very low (**Figure 2C**), suggesting that the envelope of the middle layer chloroplasts was mostly kept and intact, and the envelope of the upper layer chloroplasts was mostly broken and lost. These results are consistent with each other, suggesting that Rhodamine staining method is good for evaluating the intactness of isolated chloroplasts.

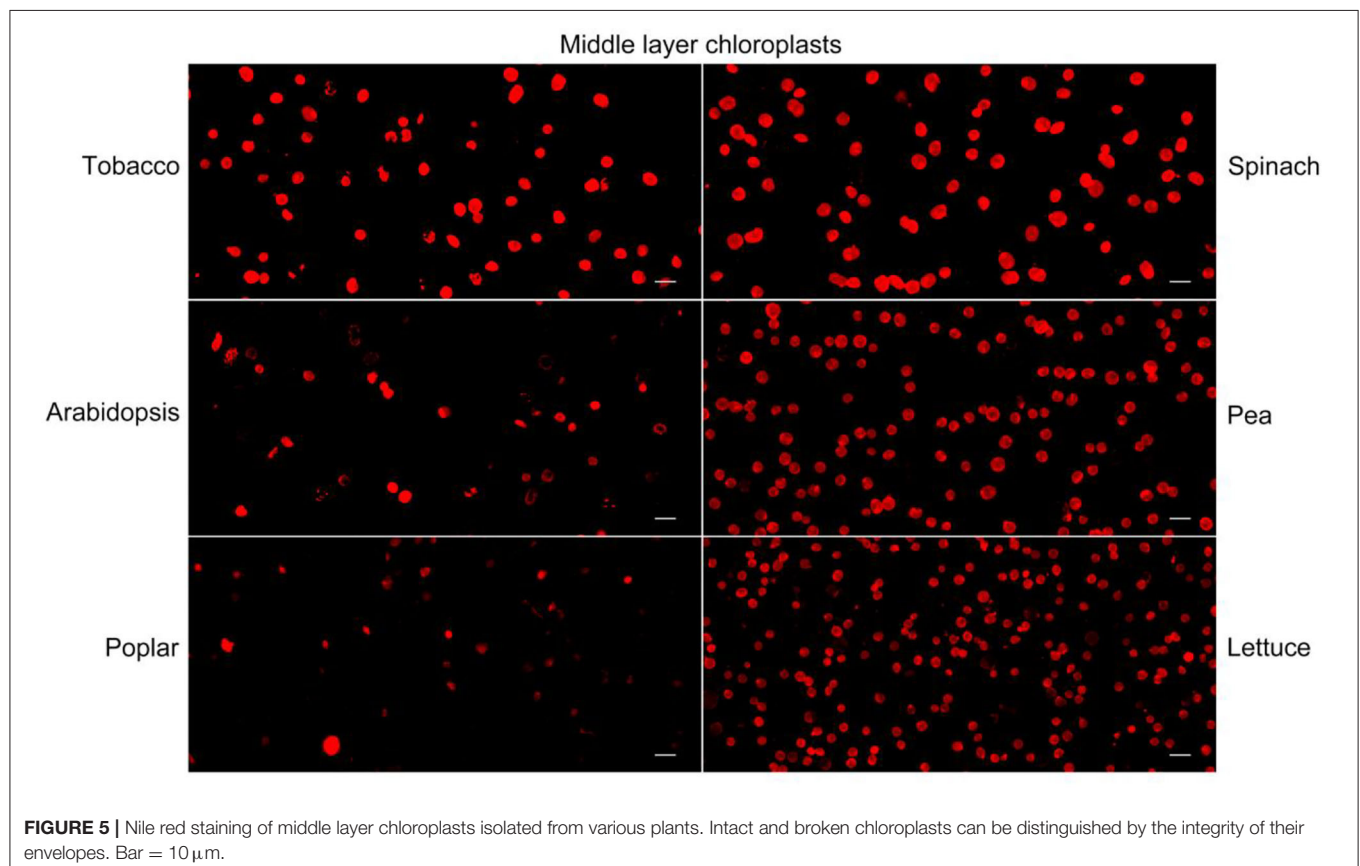


FIGURE 5 | Nile red staining of middle layer chloroplasts isolated from various plants. Intact and broken chloroplasts can be distinguished by the integrity of their envelopes. Bar = 10 μm.

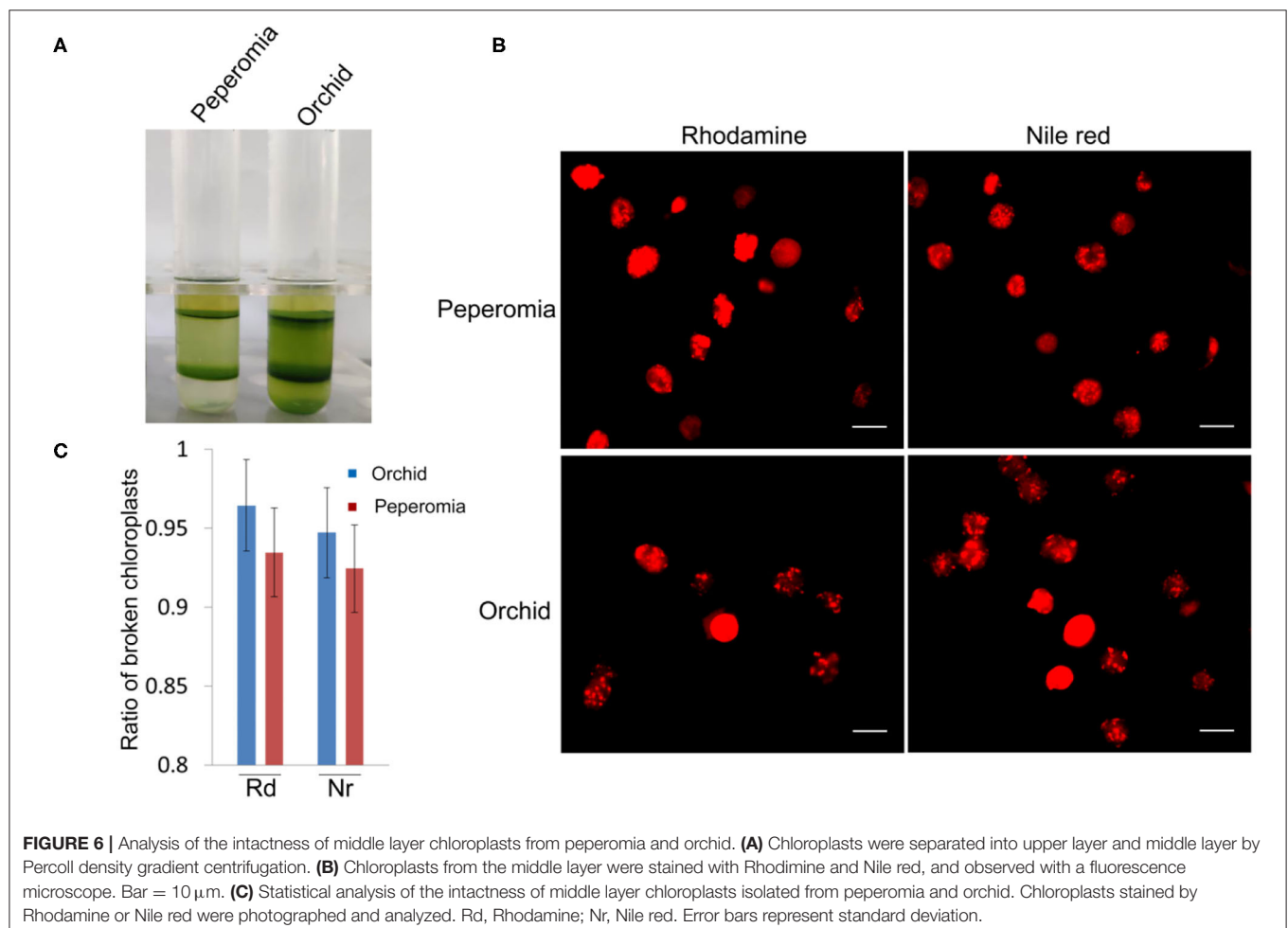
Rhodamine Can Be Used to Check the Integrity of Chloroplasts Isolated From Various Plants

Besides tobacco and spinach, we also tested our method with the chloroplasts isolated from other plants. We isolated chloroplasts from Arabidopsis, pea, poplar, and lettuce, stained the chloroplasts from the middle layer, and observed them with a fluorescence microscope (**Figure 3A**). A majority of the chloroplasts from pea and lettuce were intact. But surprisingly, chloroplasts from the middle layer of Arabidopsis and poplar looked to be mostly broken. We further calculated the proportion of intact chloroplasts to total chloroplasts of these plants (**Figure 3B**). The results indicated that ratios of intact chloroplasts from pea and lettuce were 92 and 93%, whereas those of Arabidopsis and poplar were only 8 and 6%, respectively (**Figure 3C**). Although a large part of the chloroplasts from Arabidopsis were well-stained, their envelopes were not smooth, suggesting they were fragile and mostly broken. Moreover, we used Coomassie blue staining and immuno-blot methods to analyze the intactness of chloroplasts from the middle layer (**Figure 3D**). The conclusions were similar to that of Rhodamine

staining, further suggesting that our method is reliable and it can be applied to other plants.

Chloroplast Envelope Integrity Can Also Be Visualized by Nile Red Staining

Nile red is a commonly used lipophilic dye that shows strong red fluorescence at the excitation wavelength of 550 nm (Fowler and Greenspan, 1985; Greenspan et al., 1985; Rumin et al., 2015). We test our method with Nile red as the dye on chloroplasts isolated from tobacco and spinach first as before (**Figures 1, 4**). Most of the chloroplasts from the middle layer have a relatively uniform fluorescence with clear and smooth boundaries, suggesting they were intact. In contrast, most of the chloroplasts from the upper layer were stained as small bright spots, suggesting they were broken. Then the chloroplasts isolated from other plants, including Arabidopsis, pea, poplar, and lettuce, were also stained with Nile red to see the effect of envelope membrane staining (**Figure 5**). The results were similar to that of Rhodamine staining (**Figures 2, 3**). As we can see, most of the chloroplasts from the middle layer of tobacco, spinach, pea and lettuce were intact, and a small part of the chloroplasts were



broken. For the chloroplasts from the middle layer of *Arabidopsis* and poplar, most of them were broken. Overall, the staining results of Nile red looks to be similar to those of Rhodamine. Thus, Nile red can also be used as a dye like Rhodamine to stain the envelope membrane of chloroplasts to check their intactness.

Chloroplasts From the Middle Layer May Be Mostly Broken

As shown above, isolated chloroplasts from the middle layer of *Arabidopsis* and poplar were mostly broken (Figures 3, 5). We also isolated chloroplasts from other plants, such as *peperomia* and orchid. The isolated chloroplasts were separated well into upper layer and middle layer (Figure 6A). However, after being stained with Rhodamine and Nile red, most of those chloroplasts were found to be broken (Figure 6B). This was also confirmed by the statistical analysis, which showed that more than 90% of those chloroplasts were broken (Figure 6C). These data further suggest that checking the integrity of chloroplast envelope is necessary and our method is good at this.

DISCUSSION

Chloroplasts are involved in a variety of important biological processes in plants. Isolated chloroplasts are widely used in the study of chloroplasts, such as biochemical, physiological and cellular experiments (Gao et al., 2003, 2006; Baginsky and Gruissem, 2004; Lopez-Juez, 2007). It is essential to obtain intact chloroplasts in these experiments. Direct microscopy observation with bright field, phase contrast and autofluorescence might be used to check their intactness. However, we found this often could be misleading and cause serious problem to the experiments. For the chloroplasts isolated from plants in extended darkness, thylakoids will shrink and the envelope may look clear, and their intactness probably can be judged this way. However, in most cases, chloroplasts were isolated from healthy plants or plants grown under normal growth condition, they were almost fully filled with thylakoids and looked to have good shapes under microscope even if their envelopes were broken (Figure 3B; Supplementary Figure 1).

Although the intactness of chloroplasts can be checked by biochemical methods such as Coomassie blue staining or immuno-blot analysis of chloroplast proteins (Figures 2, 3) (Seigneurin-Berny et al., 2008a), it is relatively time consuming to obtain the results. Hill reaction method is a fast and simple method to estimate the intactness of chloroplasts based on biochemical reaction (Mills and Joy, 1980). In this study, we developed a method that use two dyes, Rhodamine or Nile red, with strong red fluorescence to stain the chloroplast envelope

membrane and then show its integrity in several minutes. It can easily distinguish intact and broken chloroplasts by direct microscopy observation. It can also obtain a ratio of the intact or broken chloroplasts in a sample of isolated chloroplasts through statistical analysis (Figures 2, 3). The results of this method were validated by traditional biochemical methods (Figures 2, 3). In contrast to the traditional biochemical methods, it is simple, fast and accurate. Therefore, our method is very useful. In this study, we have tested our method only in several plants, but it could be used in many other plants.

It is usually believed that the chloroplasts in the middle layer of Percoll density gradient are intact (Seigneurin-Berny et al., 2008a,b), since chloroplasts in the upper layer are mostly broken. In many cases, this could be true. In our experiments, with our chloroplast staining method, we found that chloroplasts in the middle layer of Percoll density gradient could also be mostly broken (Figures 3, 6). Percoll density gradient centrifugation method mainly relies on the density of chloroplasts, so broken chloroplasts with higher density could stay in the middle layer. But their integrity can be easily revealed by our method to avoid mistakes in the experiment. Since chloroplasts from different plants could be in different physiological conditions, their isolation methods may not always be same. Hence, our method can also be used to quickly optimize the protocol for chloroplast isolation.

DATA AVAILABILITY STATEMENT

The original contributions presented in the study are included in the article/Supplementary Material, further inquiries can be directed to the corresponding author.

AUTHOR CONTRIBUTIONS

HG designed the experiments. JA, XM, LW, and XuL carried out the experiments. XiL, JA, and HG prepared the manuscript. All authors contributed to the article and approved the submitted version.

FUNDING

This work was supported by grants from the National Natural Science Foundation of China (No. 32070696, No. 31570182).

SUPPLEMENTARY MATERIAL

The Supplementary Material for this article can be found online at: <https://www.frontiersin.org/articles/10.3389/fpls.2021.668414/full#supplementary-material>

REFERENCES

- Azevedo, R. A., Lancien, M., and Lea, P. J. (2006). The aspartic acid metabolic pathway, an exciting and essential pathway in plants. *Amino Acids* 30, 143–162. doi: 10.1007/s00726-005-0245-2
- Baginsky, S., and Gruissem, W. (2004). Chloroplast proteomics: potentials and challenges. *J. Exp. Bot.* 55, 1213–1220. doi: 10.1093/jxb/erh104
- Block, M. A., Douce, R., Joyard, J., and Rolland, N. (2007). Chloroplast envelope membranes: a dynamic interface between plastids and the cytosol. *Photosyn. Res.* 92, 225–244. doi: 10.1007/s11120-007-9195-8

- Chen, Y. L., Chen, L. J., and Li, H. M. (2016). Polypeptide transport-associated domains of the Toc75 channel protein are located in the intermembrane space of chloroplasts. *Plant Physiol.* 172, 235–243. doi: 10.1104/pp.16.00919
- Chen, Y. Y., and Wood, A. W. (2009). Application of a temperature-dependent fluorescent dye (Rhodamine B) to the measurement of radiofrequency radiation-induced temperature changes in biological samples. *Bioelectromagnetics* 30, 583–590. doi: 10.1002/bem.20514
- Fitzpatrick, L. M., and Keegstra, K. (2001). A method for isolating a high yield of Arabidopsis chloroplasts capable of efficient import of precursor proteins. *Plant J.* 27, 59–65. doi: 10.1046/j.0960-7412.2001.01061.x
- Fowler, S. D., and Greenspan, P. (1985). Application of Nile red, a fluorescent hydrophobic probe, for the detection of neutral lipid deposits in tissue sections: comparison with oil red O. *J. Histochem. Cytochem.* 33, 833–836. doi: 10.1177/33.8.4020099
- Fuertauer, L., Kuestner, L., Weckwerth, W., Heyer, A. G., and Naegele, T. (2019). Resolving subcellular plant metabolism. *Plant J.* 100, 438–455. doi: 10.1111/tjp.14472
- Gao, H., Sage, T. L., and Steryoung, K. W. (2006). FZL, an FZO-like protein in plants, is a determinant of thylakoid and chloroplast morphology. *Proc. Natl. Acad. Sci. U.S.A.* 103, 6759–6764. doi: 10.1073/pnas.0507287103
- Gao, H. B., Kadirjan-Kalbach, D., Froehlich, J. E., and Steryoung, K. W. (2003). ARC5, a cytosolic dynamin-like protein from plants, is part of the chloroplast division machinery. *Proc. Natl. Acad. Sci. U.S.A.* 100, 4328–4333. doi: 10.1073/pnas.0530206100
- Gao, J. L., Wang, H., Yuan, Q. P., and Feng, Y. (2018). Structure and function of the photosystem supercomplexes. *Front. Plant Sci.* 9:357. doi: 10.3389/fpls.2018.00357
- Gao, Y. F., Liu, H., An, C. J., Shi, Y. H., Liu, X., Yuan, W. Q., et al. (2013). Arabidopsis FRS4/CPD25 and FHY3/CPD45 work cooperatively to promote the expression of the chloroplast division gene ARC5 and chloroplast division. *Plant J.* 75, 795–807. doi: 10.1111/tjp.12240
- Greenspan, P., Mayer, E. P., and Fowler, S. D. (1985). Nile red: a selective fluorescent stain for intracellular lipid droplets. *J. Cell Biol.* 100, 965–973. doi: 10.1083/jcb.100.3.965
- Lang, E. G., Mueller, S. J., Hoernstein, S. N., Porankiewicz-Asplund, J., Vervliet-Scheebaum, M., and Reski, R. (2011). Simultaneous isolation of pure and intact chloroplasts and mitochondria from moss as the basis for sub-cellular proteomics. *Plant Cell Rep.* 30, 205–215. doi: 10.1007/s00299-010-0935-4
- Liu, J., Lu, Y., Hua, W., and Last, R. L. (2019). A new light on photosystem II maintenance in oxygenic photosynthesis. *Front. Plant Sci.* 10:975. doi: 10.3389/fpls.2019.00975
- Lopez-Juez, E. (2007). Plastid biogenesis, between light and shadows. *J. Exp. Bot.* 58, 11–26. doi: 10.1093/jxb/erl196
- Mano, Y., and Nemoto, K. (2012). The pathway of auxin biosynthesis in plants. *J. Exp. Bot.* 63, 2853–2872. doi: 10.1093/jxb/ers091
- Mills, W. R., and Joy, K. W. (1980). A rapid method for isolation of purified, physiologically active chloroplasts, used to study the intracellular distribution of amino acids in pea leaves. *Planta* 148, 75–83. doi: 10.1007/BF00385445
- Ruhle, T., Reiter, B., and Leister, D. (2018). Chlorophyll fluorescence video imaging: a versatile tool for identifying factors related to photosynthesis. *Front. Plant Sci.* 9:55. doi: 10.3389/fpls.2018.00055
- Rumin, J., Bonnefond, H., Saint-Jean, B., Rouxel, C., Sciandra, A., Bernard, O., et al. (2015). The use of fluorescent Nile red and BODIPY for lipid measurement in microalgae. *Biotechnol. Biofuels* 8:42. doi: 10.1186/s13068-015-0220-4
- Schaller, A., and Stintzi, A. (2009). Enzymes in jasmonate biosynthesis—Structure, function, regulation. *Phytochemistry* 70, 1532–1538. doi: 10.1016/j.phytochem.2009.07.032
- Seigneurin-Berny, D., Salvi, D., Dorne, A. J., Joyard, J., and Rolland, N. (2008a). Percoll-purified and photosynthetically active chloroplasts from *Arabidopsis thaliana* leaves. *Plant Physiol. Biochem.* 46, 951–955. doi: 10.1016/j.plaphy.2008.06.009
- Seigneurin-Berny, D., Salvi, D., Joyard, J., and Rolland, N. (2008b). Purification of intact chloroplasts from Arabidopsis and spinach leaves by isopycnic centrifugation. *Curr. Protoc. Cell Biol.* 3:30. doi: 10.1002/0471143030.cb0330s40
- Sendon, P. M., Seo, H. S., and Song, J. T. (2011). Salicylic acid signaling: biosynthesis, metabolism, and crosstalk with jasmonic acid. *J. Korean Soc. Appl. Biol. Chem.* 54, 501–506. doi: 10.3839/jksabc.2011.077
- Su, P. H., and Lai, Y. H. (2017). A reliable and non-destructive method for monitoring the stromal pH in isolated chloroplasts using a fluorescent pH probe. *Front. Plant Sci.* 8:2079. doi: 10.3389/fpls.2017.02079
- Suzuki, Y., Kihara-Doi, T., Kawazu, T., Miyake, C., and Makino, A. (2010). Differences in Rubisco content and its synthesis in leaves at different positions in Eucalyptus globulus seedlings. *Plant Cell Environ.* 33, 1314–1323. doi: 10.1111/j.1365-3040.2010.02149.x
- Vieira Ldo, N., Faoro, H., Fraga, H. P., Rogalski, M., De Souza, E. M., De Oliveira Pedrosa, F., et al. (2014). An improved protocol for intact chloroplasts and cpDNA isolation in conifers. *PLoS ONE* 9:e84792. doi: 10.1371/journal.pone.0084792
- Wang, Z., and Benning, C. (2012). Chloroplast lipid synthesis and lipid trafficking through ER-plastid membrane contact sites. *Biochem. Soc. Trans.* 40, 457–463. doi: 10.1042/BST20110752

Conflict of Interest: The authors declare that the research was conducted in the absence of any commercial or financial relationships that could be construed as a potential conflict of interest.

Copyright © 2021 An, Miao, Wang, Li, Liu and Gao. This is an open-access article distributed under the terms of the Creative Commons Attribution License (CC BY). The use, distribution or reproduction in other forums is permitted, provided the original author(s) and the copyright owner(s) are credited and that the original publication in this journal is cited, in accordance with accepted academic practice. No use, distribution or reproduction is permitted which does not comply with these terms.



Gene Replacement in *Arabidopsis* Reveals Manganese Transport as an Ancient Feature of Human, Plant and Cyanobacterial UPF0016 Proteins

Natalie Hoecker¹, Yvonne Hennecke¹, Simon Schrott¹, Giada Marino^{1,2}, Sidsel Birkelund Schmidt³, Dario Leister¹ and Anja Schneider^{1*}

¹ Molekularbiologie der Pflanzen (Botanik), Fakultät für Biologie, Ludwig-Maximilians-Universität München, Martinsried, Germany, ² Massenspektrometrie von Biomolekülen an der LMU (MSBioLMU), Fakultät für Biologie, Ludwig-Maximilians-Universität München, Martinsried, Germany, ³ Department of Plant and Environmental Sciences, Faculty of Science, University of Copenhagen, Frederiksberg, Denmark

OPEN ACCESS

Edited by:

Alistair McCormick,
University of Edinburgh,
United Kingdom

Reviewed by:

Pierre Morsomme,
UCLouvain, Belgium
Greg B. Moorhead,
University of Calgary, Canada

*Correspondence:

Anja Schneider
anja.schneider@lrz.uni-muenchen.de

Specialty section:

This article was submitted to
Plant Physiology,
a section of the journal
Frontiers in Plant Science

Received: 20 April 2021

Accepted: 20 May 2021

Published: 14 June 2021

Citation:

Hoecker N, Hennecke Y,
Schrott S, Marino G, Schmidt SB,
Leister D and Schneider A (2021)
Gene Replacement in *Arabidopsis*
Reveals Manganese Transport as an
Ancient Feature of Human, Plant
and Cyanobacterial UPF0016
Proteins. *Front. Plant Sci.* 12:697848.
doi: 10.3389/fpls.2021.697848

The protein family 0016 (UPF0016) is conserved through evolution, and the few members characterized share a function in Mn^{2+} transport. So far, little is known about the history of these proteins in Eukaryotes. In *Arabidopsis thaliana* five such proteins, comprising four different subcellular localizations including chloroplasts, have been described, whereas non-photosynthetic Eukaryotes have only one. We used a phylogenetic approach to classify the eukaryotic proteins into two subgroups and performed gene-replacement studies to investigate UPF0016 genes of various origins. Replaceability can be scored readily in the *Arabidopsis* UPF0016 transporter mutant *pam71*, which exhibits a functional deficiency in photosystem II. The N-terminal region of the *Arabidopsis* PAM71 was used to direct selected proteins to chloroplast membranes. Transgenic *pam71* lines overexpressing the closest plant homolog (*CMT1*), human *TMEM165* or cyanobacterial *MINX* successfully restored photosystem II efficiency, manganese binding to photosystem II complexes and consequently plant growth rate and biomass production. Thus AtCMT1, HsTMEM165, and SynMINX can operate in the thylakoid membrane and substitute for PAM71 in a non-native environment, indicating that the manganese transport function of UPF0016 proteins is an ancient feature of the family. We propose that the two chloroplast-localized UPF0016 proteins, CMT1 and PAM71, in plants originated from the cyanobacterial endosymbiont that gave rise to the organelle.

Keywords: PAM71, manganese transporter, *Arabidopsis*, UPF0016 evolution, endosymbiosis, gene replacement, *Synechocystis*

INTRODUCTION

Cross-species replacement of genes in model organisms is a powerful tool with which to investigate whether the corresponding proteins retain their ancestral functions over a billion years of evolution. There are several examples in which human genes have been shown to supply the functions of their orthologous counterparts in plants (Jha et al., 2018; Huber et al., 2020), and plant genes can

frequently be replaced by the cyanobacterial ortholog or vice versa (Savidge et al., 2002; Sattler et al., 2003; Lv et al., 2009; Armbruster et al., 2013; Proctor et al., 2018; Yoon et al., 2019). These examples of pairwise replacements can be expanded further with multiple replacement assays to gain insight into the history and evolution of gene families. Gene duplication and subsequent divergence is a major driver of evolution, and each gene/protein family has its own evolutionary history.

The uncharacterized protein family 0016 (UPF0016), also referred to as the Gcr1-dependent translation factor1 (GDT1) family (Thines et al., 2020), is a highly conserved membrane transporter family with members in many lineages of the tree of life (Demaegd et al., 2014). One prominent member, which is responsible for the alternative family name just mentioned, is the Golgi-localized Gdt1p, originally identified as a $\text{Ca}^{2+}/\text{H}^{+}$ antiporter in *Saccharomyces cerevisiae* (Demaegd et al., 2013; Colinet et al., 2016). A second, the human transmembrane protein 165 (TMEM165), attracted much interest when its involvement in the rare condition known as congenital disorders of glycosylation (CDG) was demonstrated in 2012 (Foulquier et al., 2012; Rosnoblet et al., 2013; Zeevaert et al., 2013; Bammens et al., 2015; Potelle et al., 2016; Schulte Althoff et al., 2016; Krzewinski-Recchi et al., 2017; Morelle et al., 2017). Several studies have hypothesized that TMEM165 is a Golgi-localized Mn^{2+} and/or Ca^{2+} transporter (Demaegd et al., 2013; Potelle et al., 2016; Stribny et al., 2020).

In the model plant *Arabidopsis thaliana*, the chloroplast manganese transporter1 (CMT1) and photosynthesis-affected mutant71 (PAM71) proteins were found to transport Mn^{2+} across the chloroplast envelope and the thylakoid membrane, respectively (Schneider et al., 2016; Eisenhut et al., 2018; Zhang et al., 2018). Two additional members of the family are located in the endoplasmic reticulum (ER) compartment (Hoecker et al., 2020) and a third, pam71-like3 (PML3), found in the Golgi membrane, facilitates Mn^{2+} import under conditions of Mn deficiency (Yang et al., 2021).

It has been shown that, in bacteria, members of UPF0016 are located in the plasma membrane, where their main function is the export of excess Mn^{2+} to prevent Mn toxicity. One prominent example is the manganese exporter A (MneA), a UPF0016 protein found in *Vibrio cholerae* (Fisher et al., 2016; Zeinert et al., 2018). Cyanobacteria, such as *Synechocystis*, possess additional internal membranes, at which photosynthesis takes place. Here, the manganese exporter (MNX) protein presumably needs to be targeted to both the thylakoid and the plasma membrane in order to perform its physiological function and prevent accumulation of toxic levels of Mn^{2+} in the cytosol (Brandenburg et al., 2017; Gandini et al., 2017; Eisenhut, 2019).

Eukaryotic proteins of the UPF0016 family share a conserved overall structure, comprising two regions consisting of three transmembrane (TM) domains each, which are connected by an acidic loop, and contain a highly conserved Glu-x-Gly-Asp-(Arg/Lys)-(Ser/Thr) motif in TM1 and TM4, respectively (Demaegd et al., 2014; Hoecker et al., 2017; Thines et al., 2020). This type—with six TM domains—is also found in many prokaryotes, while some others harbor one or two genes coding for a version that consists of only three TM domains,

which are assumed to form homo- or heterodimers (Demaegd et al., 2014). Besides the high degree of conservation, eukaryotic representatives of the UPF0016 family exhibit additional features, among them high sequence diversity within their N-terminal segments (Hoecker et al., 2017). While the ER-localized proteins lack an N-terminal extension, ScGdt1p, HsTMEM165 and AtPML3 all have an N-terminal signal peptide that directs them to the Golgi membrane (Foulquier et al., 2012; Demaegd et al., 2013; Hoecker et al., 2020; Yang et al., 2021). The chloroplast-targeting peptide (cTP) sequences of Arabidopsis PAM71 and CMT1 direct these proteins to the thylakoid and inner-envelope membranes, respectively (Schneider et al., 2016; Eisenhut et al., 2018; Zhang et al., 2018).

In this study, we set out to define the ancestor(s) of eukaryotic members of the UPF0016 family and determine whether individual members have retained the ancestral function. We performed a phylogenetic analysis to identify appropriate candidates. We selected MNX of *Synechocystis* (Brandenburg et al., 2017; Gandini et al., 2017), human TMEM165 and Arabidopsis CMT1 (Eisenhut et al., 2018; Zhang et al., 2018) and directed the proteins to the thylakoid membrane of the Arabidopsis *pam71* knock-out line. Appropriate control constructs were generated and transgenic *pam71* plants were analyzed for complementation of growth deficiencies as a measure of the degree to which these transporters have retained the ancestral mode of action.

MATERIALS AND METHODS

Phylogenetic Analysis

Protein sequences were retrieved by protein Blast searches at NCBI¹ using *Arabidopsis thaliana* PAM71 or *Vibrio cholerae* MneA as query sequences. Target organisms either represent ten eukaryotic model species or were manually selected from a list of 393 prokaryotes (Hanikenne and Baurain, 2013). Evolutionary analyses were conducted in MEGA X (Kumar et al., 2018) using the maximum-likelihood method and the Le_Gascuel_2008 model (Le and Gascuel, 2008). Initial tree(s) were obtained automatically by first applying Neighbor-Join and BioNJ algorithms to a matrix of pairwise distances estimated using a JTT model, and then selecting the topology with the superior log likelihood value. A discrete Gamma distribution was used to model evolutionary rate differences among sites (+G). Estimates of evolutionary divergence between sequences were obtained by using a pairwise distance calculation that assumes uniform rates among sites. All positions with less than 95% site coverage were eliminated; i.e., fewer than 5% alignment gaps, missing data, and ambiguous bases were allowed at any position (partial deletion option).

Generation of Arabidopsis Lines

The mutants *pam71* or *cmt1* were stably transformed by the floral-dip method (Clough and Bent, 1998) using Silwet L-77 (Lehle Seeds, Round Rock, TX, United States) as the detergent.

¹<https://blast.ncbi.nlm.nih.gov/Blast.cgi>

Both mutations are in the Colombia-0 background. The first step employed primer pairs 1/2 or 16/17 (see **Supplementary Table 1**), and first-strand cDNA of *Arabidopsis* for cloning of the cTP sequences into the pENTR vector (Thermo-Fisher Scientific/Invitrogen, Waltham, MA, United States), yielding pENTR-cTP_(PAM71) and pENTR-cTP_(CMT1). The Phusion High-Fidelity DNA polymerase (New England Biolabs, Frankfurt, Germany) was used for this and all subsequent steps, and all further primer sequences are listed in **Supplementary Table 1**. The plasmids pENTRcTP_(PAM71) and pENTR-PAM71 were used as templates for the amplification of two PCR products using primers 1/2 and primers 3/4, respectively. The two PCR products were then digested with *Xho*I (New England Biolabs), ligated with T4 DNA ligase (New England Biolabs), and a second PCR was performed using primers 1/4. The resulting PCR product was cloned into pENTR, yielding the plasmid pENTR-cTP_(PAM71):PAM71_{core}. The plasmid pENTR-cTP_(PAM71):CMT1_{core} was assembled in an analogous manner, using primers 1/2 with pENTRcTP_(PAM71) and primers 6/7 with pENTR-CMT1 as templates for the first PCR, and primers 1/7 for the second PCR. The plasmid pENTR-cTP_(PAM71):TMEM165 was assembled in the same way, using primers 1/2 with pENTRcTP_(PAM71) and primers 8/9 with pDNR-LIP-TMEM165 (transOMIC technologies, Huntsville, AL, United States) as templates for the first PCR and primers 1/9 for the second PCR. Plasmid pENTR-PAM71_{core} was created using primers 5/4 and pENTR-PAM71 as a template. Plasmids pENTR-cTP_(CMT1):CMT1_{core} and pENTR-cTP_(CMT1):PAM71 were constructed accordingly. All plasmids were sequenced and recombined into the destination vector pB2GW7 (Karimi et al., 2002) using the LR Clonase Gateway system (Thermo-Fisher Scientific/Invitrogen). Plasmid pB2GW7p35S:cTP_{extended(PAM71)}:MNX was assembled using three PCR products and the Gibson assembly cloning kit (New England Biolabs). The three PCR products were obtained with primer pairs 10/11, 12/13, and 14/15, and pENTR-PAM71, *Synechocystis* sp. PCC6803 genomic DNA (Gandini et al., 2017) and pB2GW7, respectively, as templates. The final construct was then sequenced. All plasmids harboring the pB2GW7 backbone were transformed into *Agrobacterium* and plated on media containing Rif/Gent/Spec. Individual colonies were selected, verified and used to transform *Arabidopsis*. Transgenic T₁ plants were selected by spraying seedlings twice with BASTA at a final concentration of 100 mg L⁻¹ glufosinate-ammonium. T₂ plants were assayed for segregation by genotyping, and appropriate homozygous T₃ seed stocks were generated.

Growth Conditions

Arabidopsis seeds were stratified for 3 days at 4°C to synchronize germination, and plants were grown for 4–5 weeks in growth chambers on a 12–12 h light-dark cycle at 18–22°C and 100 μmol photons m⁻² s⁻¹ during the light period. The *Arabidopsis* plants used for transformation and seed production, and *Nicotiana benthamiana* plants were grown in a temperature-controlled greenhouse with additional lighting for up to 16 h to reach a fluence of at least 140 μmol photons m⁻² s⁻¹.

Plant growth was analyzed on the basis of leaf area, which was determined from photographs taken at different times after germination and quantified using the ImageJ software (Schneider et al., 2012).

Transient Expression

The plasmids pENTR-cTP_(PAM71) and pENTR-cTP_(CMT1) were recombined into the destination vector pB7FWG2 (Karimi et al., 2002), resulting in pB7FWG2p35S:cTP_(PAM71):GFP and pB7FWG2p35S:cTP_(CMT1):GFP, respectively, which were then transformed into *Agrobacterium*. *Agrobacterium*-mediated infiltration of 4-week-old *N. benthamiana* leaves and protoplast isolation were performed as described (Schweiger and Schwenkert, 2014). In brief, 48 h after infiltration, protoplasts were released from leaf tissue by incubation in the dark for 4 h, with mild shaking at 40 rpm, in an enzyme solution (osmolarity: 550 mOsm) containing 1% (w/v) cellulase (Duchefa Biochemie, Haarlem, Netherlands) and 0.3% (w/v) macerozyme (Duchefa Biochemie). The protoplasts were then filtered through a 100 μm gauze filter and washed with W5 buffer [150 mM NaCl, 125 mM CaCl₂, 5 mM KCl, 2 mM MES (pH 5.7), 550–580 mOsm], then centrifuged at 100 g for 1 min and resuspended in W5 buffer. The fluorescence signals were recorded with a confocal laser-scanning microscope (Leica microsystems TCS SP5, Leica Microsystems, Wetzlar, Germany) with a 63x objective. The argon laser was set to 30%, GFP fluorescence was excited at 488 nm and the emission was recorded with a PMT detector at 515 nm. Chlorophyll autofluorescence was detected at 650–705 nm with a second PMT detector. The gain settings for both PMT detectors were chosen within the interval 760–900 to reduce background noise. Z-stacking images were generated with a maximum of 0.5 μm distance between each layer.

Chlorophyll *a* Fluorescence Measurements

The photosynthetic performance of PSII was quantified by measuring chlorophyll *a* fluorescence using a Dual PAM fluorometer (Walz, Effeltrich, Germany). Plants were dark-adapted for 30 min and single leaves were exposed to probe light (3–4 μmol photons m⁻² s⁻¹) for 30 s to measure minimal chlorophyll *a* fluorescence (F₀). A light pulse of 10,000 μmol photons m⁻² s⁻¹ was then applied for 800 ms to determine the maximum chlorophyll *a* fluorescence (F_m). Quantitative information was obtained by calculating the maximum quantum yield of PSII as F_v/F_m = (F_m - F₀)/F_m (Maxwell and Johnson, 2000). *In vivo* chlorophyll *a* fluorescence was captured as a photograph by the Imaging PAM fluorometer (Walz, Effeltrich, Germany). Plants were dark-adapted for 30 min and whole plants exposed to blue probe light (3–4 μmol photons m⁻² s⁻¹) for 30 s, followed by a light pulse of 2,800 μmol photons m⁻² s⁻¹ for 800 ms.

Real-Time PCR Analysis

Total RNA was isolated from *Arabidopsis* leaves using the Monarch Total RNA Miniprep Kit including the on-column DNase digest, and cDNA was synthesized according to the

instructions supplied with the iScript cDNA Synthesis Kit (Bio-Rad, Hercules, CA, United States). For quantitative real-time (qRT) PCR, SYBR Green Supermix (Bio-Rad) was used and PCR was performed with the CFX light cycler (Bio-Rad). Selected regions of the *cTP_(PAM71)* sequence (primers 30/31) or the *PAM71_(core)* sequence (primers 32/33) were used to record expression of the target gene and the reference gene *Actin* (primers 28/29). Relative transcript levels were quantified according to the comparative cycle threshold (C_T) method (Schmittgen and Livak, 2008): $\Delta C_T = C_T(\text{Gene}_{\text{TransgenicLine}}) - C_T(\text{Actin}_{\text{TransgenicLine}})$ or $\Delta C_T = C_T(\text{Gene}_{\text{Col-0}}) - C_T(\text{Actin}_{\text{Col-0}})$; $\Delta \Delta C_T(\text{TransgenicLine}) = \Delta C_T(\text{Gene}_{\text{TransgenicLine}}) - \Delta C_T(\text{Gene}_{\text{Col-0}})$ and $2^{-\Delta \Delta C_T}$ calculated. Expression in Col-0 is: $\Delta \Delta C_T(\text{Col-0}) = \Delta C_T(\text{Gene}_{\text{Col-0}}) - \Delta C_T(\text{Gene}_{\text{Col-0}}) = 0$ and $2^0 = 1$.

Blue-Native PAGE and SEC-ICP-MS Analysis

For the isolation of thylakoid membrane-protein complexes, leaf samples (5 g fresh weight) were homogenized in 0.4 M sucrose, 10 mM NaCl, 5 mM MgCl_2 , 20 mM Tricine (pH 7.9), 10 mM ascorbate and 10 mM NaF, then filtered through two layers of Miracloth (GE Healthcare, Chicago, IL, United States) and centrifuged at 5,000 g for 10 min at 4°C. The pellet was dissolved in 5 mM Tricine (pH 7.9) and 10 mM NaF, and centrifuged at 10,000 g for 10 min at 4°C. The resulting thylakoid membranes were dissolved in storage buffer [0.4 M sucrose, 10 mM NaCl, 5 mM MgCl_2 , 20 mM Tricine (pH 7.9), 20% (v/v) glycerol, 10 mM NaF] and the protein concentration was determined using the Pierce BCA Protein Assay (Thermo-Fisher Scientific/Invitrogen, Waltham, MA, United States). Samples were stored at −80°C. For Blue-Native PAGE analysis, samples equivalent to 18 µg protein were solubilized in the presence of 1% (w/v) β-dodecyl-maltoside (Sigma-Aldrich, St. Louis, MO, United States) for 10 min on ice in the dark. Native-PAGE sample buffer was then added and protein complexes were separated by non-denaturing Bis-Tris gel electrophoresis (3–12% acrylamide gradient, Thermo-Fisher Scientific/Invitrogen) for 3.5 h. For SEC-ICP-MS analysis, samples equivalent to 50 µg protein were solubilized in the presence of 1% (w/v) α-dodecyl-maltoside (Biomol, Hamburg, Germany) for 10 min on ice in the dark. Solubilized protein complexes were filtered through a 0.45-µm nylon membrane and applied to a size-exclusion column (BioBasic SEC1000, a silica-based high-pressure steel column; Thermo-Fisher Scientific/Invitrogen) using an inert HPLC system. Protein elution was performed with 25 mM Bis-Tris (pH 7.0) and 0.03% (w/v) α-dodecyl-maltoside as the mobile phase at a flow rate of 1 mL min^{−1}. The outlet of the column was coupled to a triple quadrupole ICP-MS (Agilent 8800 ICP-QQQ-MS, Agilent, Santa Clara, CA, United States) for online detection of Mn binding in the size-fractionated PSII complexes. The ICP-QQQ-MS was operated in MS/MS scan mode with oxygen as the reaction gas, which allowed for simultaneous detection of manganese as the parent ion (⁵⁵Mn⁺) and sulfur as the oxide product ion (⁴⁸SO⁺). The external calibration for quantification of the stoichiometric ratios of Mn to S in

photosynthetic complexes was carried out using flow-injection analysis (Schmidt et al., 2015).

Proteome Analysis

For the isolation of chloroplasts, leaf samples (12 g fresh weight) were homogenized in a mixture of 0.4 M sorbitol, 20 mM Tricine-NaOH (pH 8.4), 10 mM EDTA, 0.1% (w/v) BSA, 5 mM NaHCO_3 , 1 mM MgCl_2 and 1 mM MnCl_2 . The extract was filtered through two layers of Miracloth (GE Healthcare) and concentrated by centrifugation for 5 min at 1,500 g. The pellet was resuspended in 80 mM sorbitol, 4 mM Tricine-NaOH (pH 8.4), 0.5 mM EDTA, 1 mM MgCl_2 and then layered onto a discontinuous 40% (w/v)/80% (w/v) Percoll gradient (GE Healthcare). Intact chloroplasts were isolated from the interphase after centrifugation for 15 min at 7,000 g. To separate envelope and thylakoid membranes, the chloroplasts were lysed in 10 mM HEPES-KOH (pH 7.6) and 5 mM MgCl_2 by incubation on ice for 10 min, then layered onto a discontinuous sucrose gradient consisting of 1.2 M, 1.0 M, and 0.46 M sucrose, and centrifuged at 58,000 g for 2 h. The stroma in the top fraction was discarded, the envelopes were collected from the middle fraction, and the thylakoids were recovered as a pellet. The envelope fraction was further concentrated by centrifugation at 135,200 g for 1 h at 4°C. Both fractions were stored in TMK buffer [10 mM Tris-HCl pH 6.8, 10 mM MgCl_2 , 20 mM KCl including protease inhibitor cocktail (Roche, Basel, Switzerland)] at −80°C.

Thylakoid and envelope fractions were resuspended in 200-µl aliquots of guanidine-HCl, and incubated at 60°C for 30 min. Samples were then disrupted by applying two 10-s bursts of sonication using a Branson Sonifier B-12 (Branson Ultrasonics, Brookfield, CT, United States). After removing cell debris by centrifugation at 10,000 g for 15 min, samples were loaded onto a Microcon-30 kDa filter. On-column reduction, alkylation and tryptic digestion were performed as previously described (Janowski et al., 2018). After elution, the peptide mixtures were acidified to pH ≤ 3 using formic acid, desalted with home-made C18 stage tips (Rappsilber et al., 2003), vacuum dried to near dryness and stored at −80°C until further use.

LC-MS/MS was performed on an Ultimate 3000 RSLCnano HPLC system (Thermo-Fisher Scientific/Invitrogen), coupled online to an Impact II Ultra-High Resolution Qq-Time-Of-Flight (Bruker Daltonics, Billerica, MA, United States). The nano-LC system (Thermo-Fisher Scientific/Invitrogen) was operated in a two-column setup with an Acclaim Pepmap nano-trap column (C18, 100 Å, 100 µm × 2 cm) and an Acclaim Pepmap RSLC analytical column (C18, 100 Å, 75 µm × 50 cm). The columns were kept at 50°C throughout the run. The peptide mixtures were separated at a constant flow rate of 250 nl/min, using a linear gradient 3–30% solvent B (0.1% formic acid in acetonitrile) over 60 min, followed by a linear increase from 30 to 45% solvent B within 15 min. Full MS scans in the mass range 200–2,000 m/z were acquired at a rate of 3 Hz, and the 18 most intense peaks were selected for MS2 analysis using an intensity-dependent spectrum acquisition rate of between 4 and 16 Hz. To minimize repeated sequencing, the dynamic exclusion duration was set to 30 s.

The raw MS files were processed using the MaxQuant software (Cox and Mann, 2008). Peak lists were searched against the Arabidopsis reference proteome (Uniprot, version April 2019) using the built-in Andromeda search engine (Cox et al., 2011). The database was modified to include the sequences of the chimeric constructs. The search parameters were set as follows: Cysteine carbamidomethylation as fixed modification, methionine oxidation and acetylation of protein N-termini as variable modifications. The specific protease was set to trypsin (Thermo-Fisher Scientific/Invitrogen), allowing a maximum of two missed cleavage sites. The false-discovery rate at the protein and PSM level was set to 1%. The match-between-runs option was disabled, whereas the intensity-based-absolute-quantification (iBAQ) (Schwanhauser et al., 2011) option was enabled. Downstream data analysis was performed using Microsoft Excel. Potential contaminants, reverse hits and proteins identified only by site modification were removed. The protein group iBAQ values were then normalized to the sum of all iBAQ values within one sample, generating relative iBAQ (riBAQ) values. To compare the thylakoid and envelope fractions of single chloroplast preparations, the abundances of a given protein group were expressed as relative percentages of the total riBAQ values. Data were analyzed from three independent biological replicates.

Data and Code Availability

The mass spectrometry proteomics data have been deposited with the ProteomeXchange consortium <http://proteomecentral.proteomexchange.org> via the PRIDE partner repository (Vizcaino et al., 2016) under the accession number PXD022763.

RESULTS

Phylogenetic Analysis of UPF0016 Proteins

The family was first described in 2014 (Demaegd et al., 2014) and members have now been identified in more than 2,800 species across all three domains of life (Supplementary Figure 1). We were particularly interested in examining the ancestry of plant UPF0016 proteins, which are encoded by small gene families (Hoecker et al., 2017). In order to embed plant UPF0016 proteins in a broader context, proteins of prokaryotic and eukaryotic origins were retrieved and subjected to a phylogenetic analysis. A dataset of 33 proteins was selected from 33 prokaryotic organisms, which were chosen from a taxonomically representative set of phyla (Hanikenne and Baurain, 2013), taking into account phyla that appear to encompass many species that code for UPF0016 proteins (Supplementary Figure 1). This set was supplemented by 24 eukaryotic proteins obtained from 10 species, representing both photosynthetic and non-photosynthetic model organisms. Clear phylogenies could not be identified within prokaryotic phyla, except for those proteins of α -Proteobacteria that displayed a bootstrap value of 100%, indicating that these could be monophyletic (Figure 1). Intriguingly, cyanobacterial proteins were found to be closely

related to eukaryotic proteins (as indicated by a single branch supported by a bootstrap value of 100%) and were clearly separated from all other prokaryotic phyla. Closer inspection of the members of Viridiplantae confirmed the previous findings (Hoecker et al., 2017) that chloroplast-localized members and Golgi/ER-localized members form separate subgroups (Figure 1). The latter subgroup comprises members found in all Eukaryotes, including Metazoa and Fungi, and was named subgroup one. The chloroplast-localized proteins were named subgroup two. These proteins presumably arose separately, because they form a single defined monophyletic group. Next, we extracted the well characterized proteins of Arabidopsis, Synechocystis and human, and estimated the evolutionary divergence between these seven sequences by pairwise comparisons. In terms of their amino-acid sequences, PAM71 and AtPML4 are most dissimilar, while AtPML4 and AtPML5 display the highest similarity (Figure 2). HsTMEM165 shows less resemblance to SynMNX, AtPAM71, and AtCMT1 than to the three AtPML proteins, or in other words SynMNX, AtPAM71, and AtCMT1 form a cluster. Taken together, these observations allow us to conclude that the gene(s) encoding the chloroplast-localized proteins PAM71 and CMT1 are derived from the cyanobacterial endosymbiosis that gave rise to chloroplasts. Because the gene(s) encoding Golgi/ER-localized proteins have close counterparts in non-photosynthetic Eukaryotes, this clade must have arisen prior to the cyanobacterial endosymbiosis.

The Arabidopsis Mutant *pam71* as a Platform for UPF0016 Gene-Replacement Studies

To test the hypothesis that UPF0016 proteins share an ancient functionality, we chose the *pam71* Arabidopsis mutant for a gene-replacement study. We selected AtCMT1 and HsTMEM165 as representative members of each subgroup and SynMNX as the cyanobacterial representative. The nucleus-encoded PAM71 protein is equipped with a chloroplast-targeting signal peptide at the N-terminus, which is predicted to be cleaved at amino acid position 74 (Schneider et al., 2016; Hoecker et al., 2017) during uptake into the organelle from the cytoplasm. To verify that the cTP is sufficient to direct proteins of interest into this plant organelle, we cloned the first 255 bp of the PAM71 ORF upstream of the GFP sequence and transiently expressed the fusion protein in *Nicotiana benthamiana* leaves (Figure 3A). Indeed, the GFP fluorescence signal was found to coincide precisely with the red autofluorescence emitted by chlorophyll *a* molecules in isolated protoplasts. Next, a series of chimeric constructs was generated (Figure 3B), including a positive control containing the native PAM71 sequence and a negative control containing a truncated version of PAM71 lacking the first 255 bp at the 5' end. Furthermore, we linked the PAM71 cTP sequence to the full-length TMEM165 sequence and replaced the original cTP sequence of CMT1. An extended cTP sequence was used to generate the MNX construct, in order to increase the size of the protein (Supplementary Figure 2), as the naturally occurring MNX/SynPAM71 is smaller than any of the other three proteins (Thines et al., 2020). The

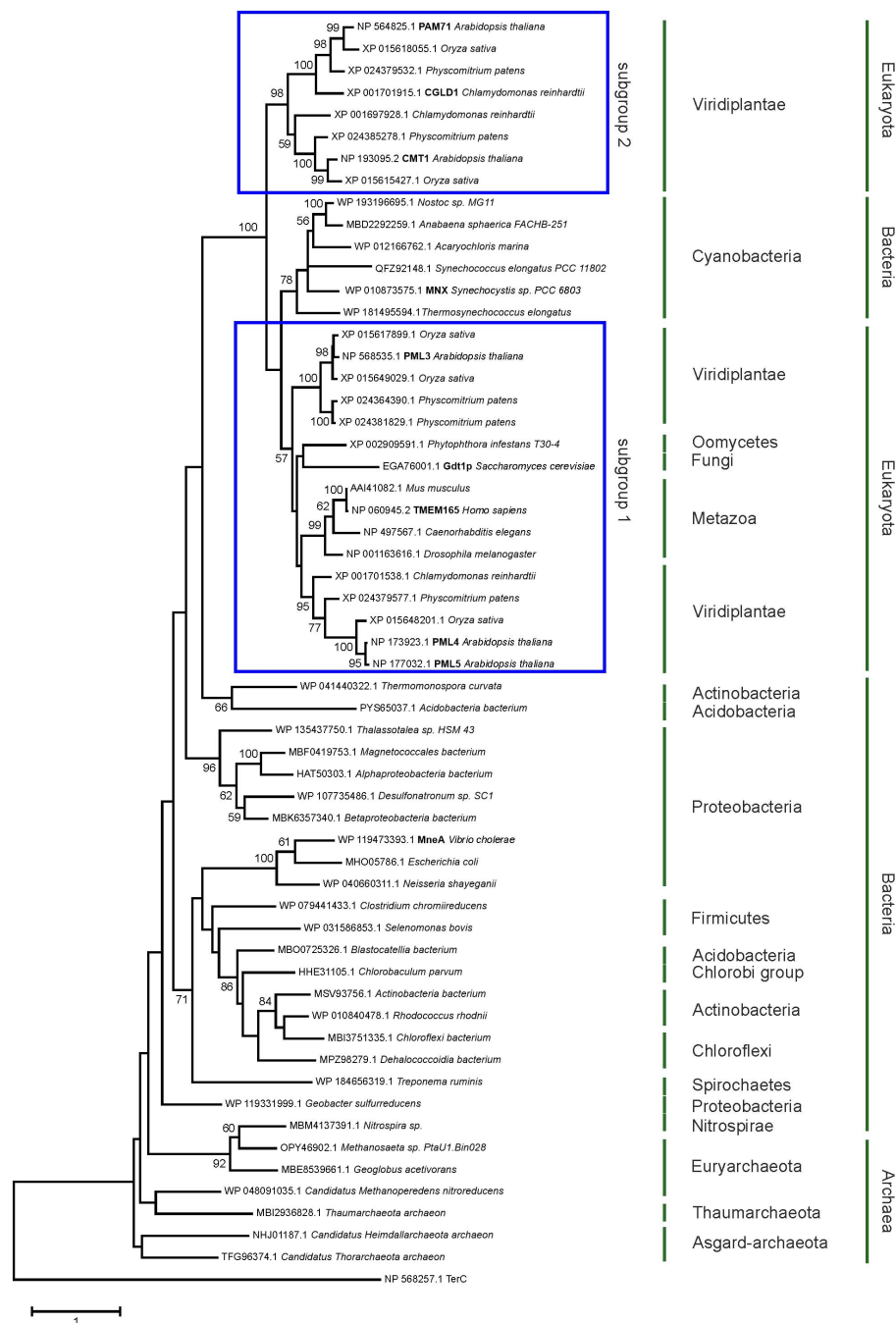


FIGURE 1 | Evolutionary analysis of UPF0016 members using the maximum-likelihood method. Protein sequences were retrieved by protein BLAST search using AtPAM71 as query sequence, except for those from *Alphaproteobacterium bacterium*, *Vibrio cholera*, *Escherichia coli*, *Neisseria shayegani*, and *Treponema ruminis*, which were identified using MneA of *Vibrio cholera* as query sequence. The tree with the highest log likelihood is shown. The percentage (>50%) of trees in which the taxa grouped together is also shown (bootstrap values based on 500 replicates). The tree is drawn to scale with branch lengths measured in numbers of substitutions per site. The tree is rooted on *Arabidopsis thaliana* TerC. The TerC and UPF0016 families form part of the LysE transporter superfamily (<http://pfam.xfam.org/clan/CL0292>). NCBI accession numbers are indicated and proteins mentioned throughout the text are highlighted.

five constructs were introduced into *Agrobacterium* cells and successfully transformed into the *pam71* background. The *pam71* mutant is characterized by a reduced growth rate and a lower maximum quantum yield of photosystem II (PSII) (Fv/Fm,

Figures 3C,D) (Schneider et al., 2016; Wang et al., 2016). Several independent transgenic lines per construct were selected based on their resistance to glufosinate, assayed for the presence of the transgene in the homozygous *pam71* background and

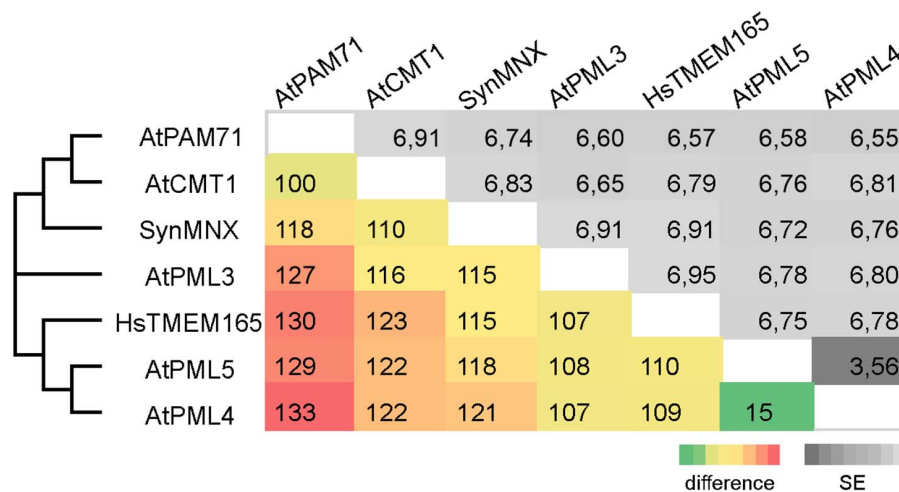


FIGURE 2 | Pairwise comparison of UPF0016 members of Arabidopsis, Synechocystis and human. The numbers of amino-acid differences between the indicated sequences are shown. Standard-error (SE) estimates are shown above the diagonal and were obtained by a bootstrap procedure (1,000 replicates). The consensus tree in which the associated proteins clustered together is indicated on the left.

characterized with respect to their Fv/Fm values. Transgenic lines were named as follows: *cP* refers to *cTP_{PAM71}* and *pos* and *neg* indicate presence or absence of *cTP_{PAM71}* respectively, followed by the protein name. Fv/Fm was significantly reduced in the twelve *cP_{neg}PAM71* lines relative to the twenty-five *cP_{pos}PAM71* control lines (Figure 3D), indicating that the presence of a cTP is required for functional complementation. Interestingly, the Fv/Fm values of the thirty-four selected *cP:CMT1* lines were comparable to those of the positive control lines (Figure 3D). However, it is worth noting that the endogenous proteins PAM71 and CMT1 have non-redundant functions in chloroplasts (Eisenhut et al., 2018; Zhang et al., 2018; Frank et al., 2019; Schmidt et al., 2020). Moreover, it was found that the thirty-four *cP:TMEM165* lines and the thirty-four selected *cP:MNX* lines have significantly increased Fv/Fm values in comparison to the negative control lines and *cP:TMEM165* lines are significantly improved in comparison to *pam71* (Figure 3D). Both groups (*cP:TMEM165* lines and *cP:MNX* lines) showed a wide range of Fv/Fm values, for instance from 0.4 to 0.8 in the *cP:MNX* lines, maybe due to very different levels of expression of the respective non-plant transgene across the populations. Taken together, these results suggested that the approach is feasible, and we proceeded to analyze individual lines in more detail.

In Transgenic Lines Both the Quantum Yield of Photosystem II and Growth Rate Are Enhanced

To select suitable lines for detailed investigations, two criteria were applied: T1 plants should exhibit an increased Fv/Fm value and harbor a single-locus transgene insertion, because this is less likely to cause (post)-transcriptional gene silencing in subsequent generations. We selected two lines that met these criteria from each group (Supplementary Figure 3). Single-locus insertion events were identified based on a segregation analysis

of T2 plants, assuming a 3:1 mode of dominant inheritance of the transgene (Supplementary Figure 3). Furthermore, we confirmed that the phenotypes of positive *cP_{pos}PAM71* and negative *cP_{neg}PAM71* control plants were close to wild-type and *pam71* plants, respectively (Supplementary Figure 4A). All selected transgenic lines were grown side by side, and on visual inspection just before the transition to the reproductive state, the rosette diameter was found to be larger in all cases than in either of the negative control lines (Figure 4A). Growth recovery to almost control levels was observed in the *cP:CMT1*, *cP:TMEM165*, and *cP:MNX* lines (Figure 4B). Furthermore, Fv/Fm values in both *cP_{pos}PAM71* lines reached almost 0.8, indicative of optimal PSII efficiency and photosynthesis, while both *cP_{neg}PAM71* lines had Fv/Fm values around 0.6 (Figure 4C). These results are similar to those of wild-type and *pam71* plants respectively (Supplementary Figure 4B). Optimal PSII efficiency was also observed in the two *cP:CMT1* lines, in one of the *cP:TMEM165* lines (#39) and in both *cP:MNX* lines (Figure 4C). The second *cP:TMEM165* line #13 did not quite reach the control value (Figure 4C), but this can probably be explained by variation in the levels of transgene expression. Based on wild-type *cTP* expression, in fact, an approximately twofold higher transgene expression was observed in *cP:TMEM165* #13 (Figure 4D), whereas transgene expression was increased by at least 10-fold in the two positive control lines, in *cP:CMT1* #16 and #27, in *cP:TMEM165* #39, and in *cP:MNX* #1 and #34 (Figure 4D). Notably, we also found transgene expression in the negative control lines to be well above the *pam71* level, which can be attributed to the use of the 35S promoter (Supplementary Figure 4C). Overall, we concluded that transgene overexpression in the *cP_{pos}PAM71*, *cP:CMT1*, *cP:MNX* and *cP:TMEM165* lines resulted in the restoration of optimal PSII efficiency, and consequently boosted plant growth and biomass production. It is worth pointing out here that no leaf abnormalities were detected in any of the lines (Figure 4A). In contrast, overexpression

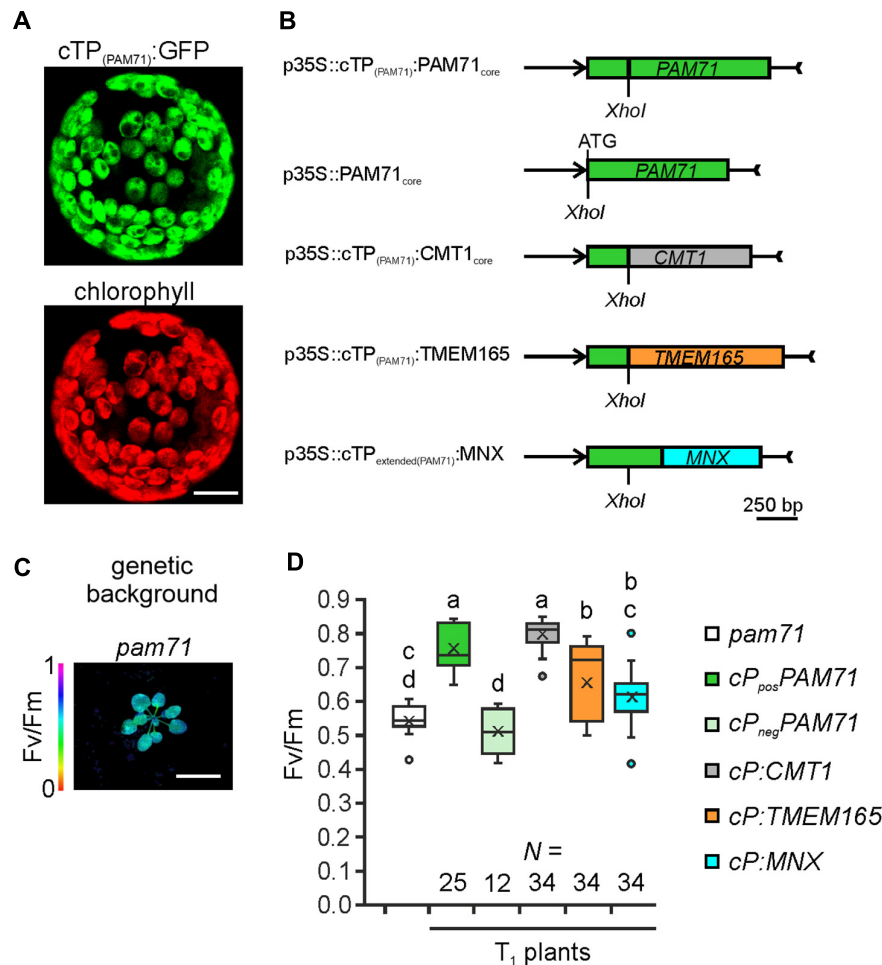


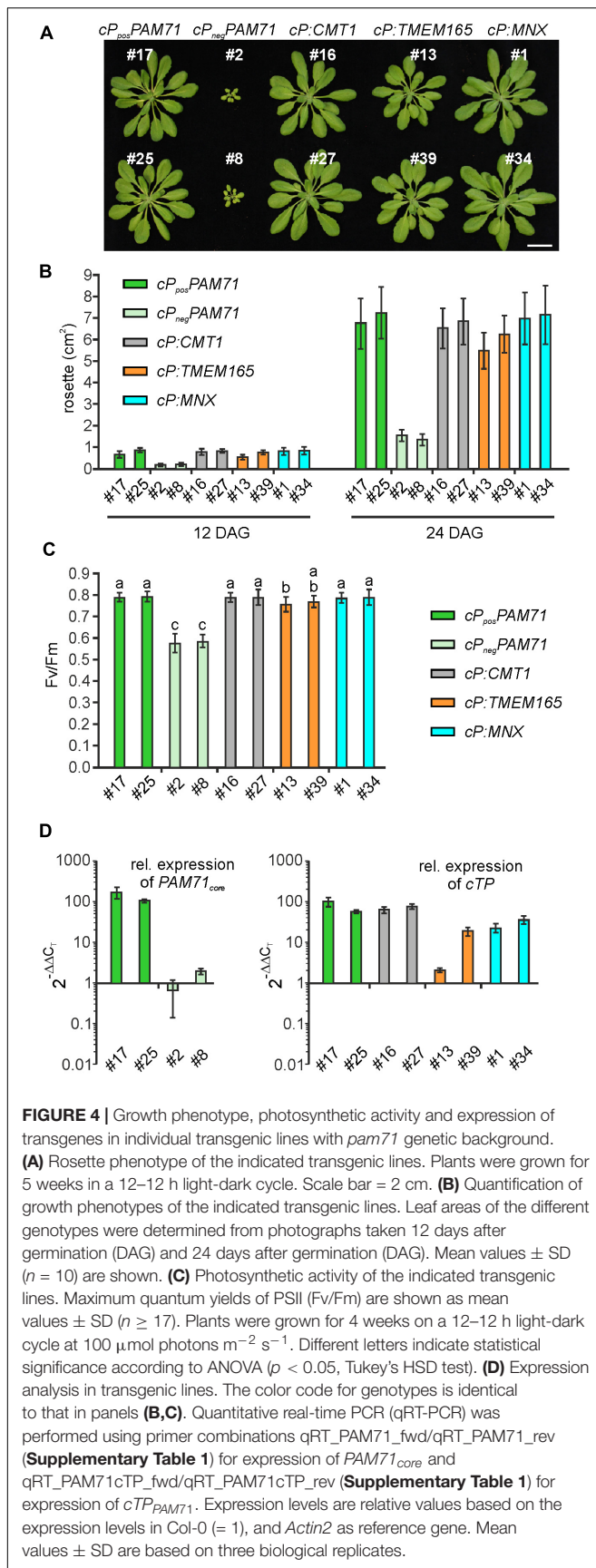
FIGURE 3 | Experimental setup for gene replacement assays. **(A)** Verification of the N-terminal PAM71 sequence as a chloroplast-targeting peptide. *Nicotiana benthamiana* leaves were infiltrated with the *Agrobacterium* strain containing p35S::cTP_(PAM71)::GFP; protoplasts were isolated after 48 h and analyzed by confocal microscopy. Scale bar = 12.5 μ m. **(B)** Scheme depicting the chimeric constructs used for transformation of *pam71*. **(C)** The *pam71* mutant as genetic background. The maximum quantum yield of PSII (Fv/Fm) of a 4-week-old plant is shown. Scale bar = 1 cm. **(D)** Photosynthetic activity of BASTA-resistant T₁ transgenic plants in comparison to *pam71*. The maximum quantum yields of PSII (Fv/Fm) of T₁ plants are depicted as box plots representing the range of values, the exclusive median and the mean, indicated as x. The number of independent individuals is given (N). Outliers are indicated as dots. Different letters indicate statistical significance based on ANOVA ($p < 0.01$, Tukey's honestly significant difference (HSD) test).

of the UPF0016 transporter *PML3* in the Golgi apparatus of *Arabidopsis* was accompanied by stunted plant growth and a curled leaf morphology (Hoecker et al., 2020).

Human TMEM165, Plant CMT1, and Cyanobacteria MNX All Facilitate Incorporation of Manganese Into the Photosynthetic Complexes in the Thylakoid Membrane

To unequivocally demonstrate the subcellular localization of cP:TMEM165, cP:CMT1 and cP:MNX in the *pam71* mutant background, proteomic analysis was employed. In this approach, envelope and thylakoid membrane fractions were isolated from purified chloroplasts, and several membrane proteins with known localizations were chosen as marker proteins

for quality control. All selected marker proteins could be assigned to the correct fraction in wild-type chloroplasts (Supplementary Table 2), including the endogenous CMT1 protein, whereas the endogenous PAM71 was not detectable. We also verified that PAM71, TMEM165 and MNX were all undetectable in the negative control line, and only the endogenous CMT1 protein was found to be enriched in the envelope fraction (Supplementary Table 2). Chloroplasts were isolated from *cP_{pos}PAM71* #25, *cP:CMT1* #27, *cP:TMEM165* #39, and *cP:MNX* #1, and the envelope and thylakoid fractions were analyzed for the presence of the respective test proteins and marker proteins (Figure 5A). PAM71 was found to be equally enriched in both fractions in *cP_{pos}PAM71* plants, as was the MNX protein in *cP:MNX* plants (Figure 5A and Supplementary Tables 3, 4). The majority of the TMEM165 protein was found in the envelope fraction in



cP:TMEM165 plants, but a small portion was also present in the thylakoid membrane (Figure 5A and Supplementary Table 5). Owing to the presence of the endogenous CMT1 protein, *cP:CMT1* is difficult to quantify accurately, but nearly 40% of all CMT1 could be assigned to the thylakoid fraction of *cP:CMT1* plants (Figure 5A and Supplementary Tables 6, 7). This result differs from the distribution of endogenous CMT1 in the other genotypes, which had about 19% in their thylakoid enriched fractions (Supplementary Table 7). Thus, we concluded that overexpression of *cP:TMEM165*, *cP:MNX* or *cP:CMT1* in the *pam71* mutant background enables the production of significant amounts of the corresponding proteins, which were eventually inserted into the thylakoid membrane.

One physiological consequence of the *PAM71* knock-out mutation is a marked decrease in the amounts of photosynthetic complexes, for instance PSII dimer, PSI monomer and PSII LHCII supercomplexes (Schneider et al., 2016; Wang et al., 2016). Thus, we tested the ability of *cP:CMT1*, *cP:TMEM165* and *cP:MNX* plants to enhance levels of photosynthetic membrane complexes. To this end, we employed Blue-Native PAGE analysis to determine the amounts of these complexes in the transgenic lines relative to wild-type and *pam71*. As expected, the steady-state levels of PSII_{di}/PSII_{mono} and PSII-LHCII_{super} were reduced in the negative control line (*cP_{neg}PAM71*) to quantities comparable to those in *pam71* (Figure 5B). On the other hand, steady-state levels of these protein complexes were restored to wild-type amounts in *cP_{pos}PAM71*, *cP:CMT1*, and *cP:MNX* and almost to wild-type levels in *cP:TMEM165* plants. In the *pam71* mutant, inadequate amounts of Mn are bound in PSII complexes (Schneider et al., 2016) and, as expected, the same effect was observed in the negative control line (Figures 5C,D and Supplementary Figure 4D). In contrast, the levels of Mn bound in PSII complexes in *cP:CMT1*, in *cP:TMEM165* and in *cP:MNX* plants matched those seen in the positive control (Figure 5C), as determined by SEC-ICP-MS analysis. Moreover, the Mn:S ratios (the relative amount of Mn incorporated into PSII per unit of S, used here as a proxy for protein) in these three lines were indistinguishable from that in *cP_{pos}PAM71* (Figure 5D), indicating sufficient transport of Mn²⁺ into the thylakoid lumen.

CMT1 of Arabidopsis Cannot Be Replaced by PAM71

Following the observation that overexpression of *CMT1* can complement the *pam71* phenotype, we also investigated the reverse configuration. First, we verified that the *cTP* of *CMT1* was able to direct GFP into the chloroplast (Figure 6A). Next, a fusion construct consisting of the *cTP* of *CMT1* (designated as *cC*) and the core sequence of *PAM71* (Figure 6B) was assembled. This construct and a positive control (*cTP* of *CMT1* fused to the *CMT1* core sequence) were introduced into the *cmt1* genetic background, and several independent transgenic lines per construct were selected (Figure 6C). Comparison of the Fv/Fm values for both groups of plants revealed that, in contrast to *cC_{pos}CMT1* lines, the Fv/Fm ratios in *cC:PAM71*

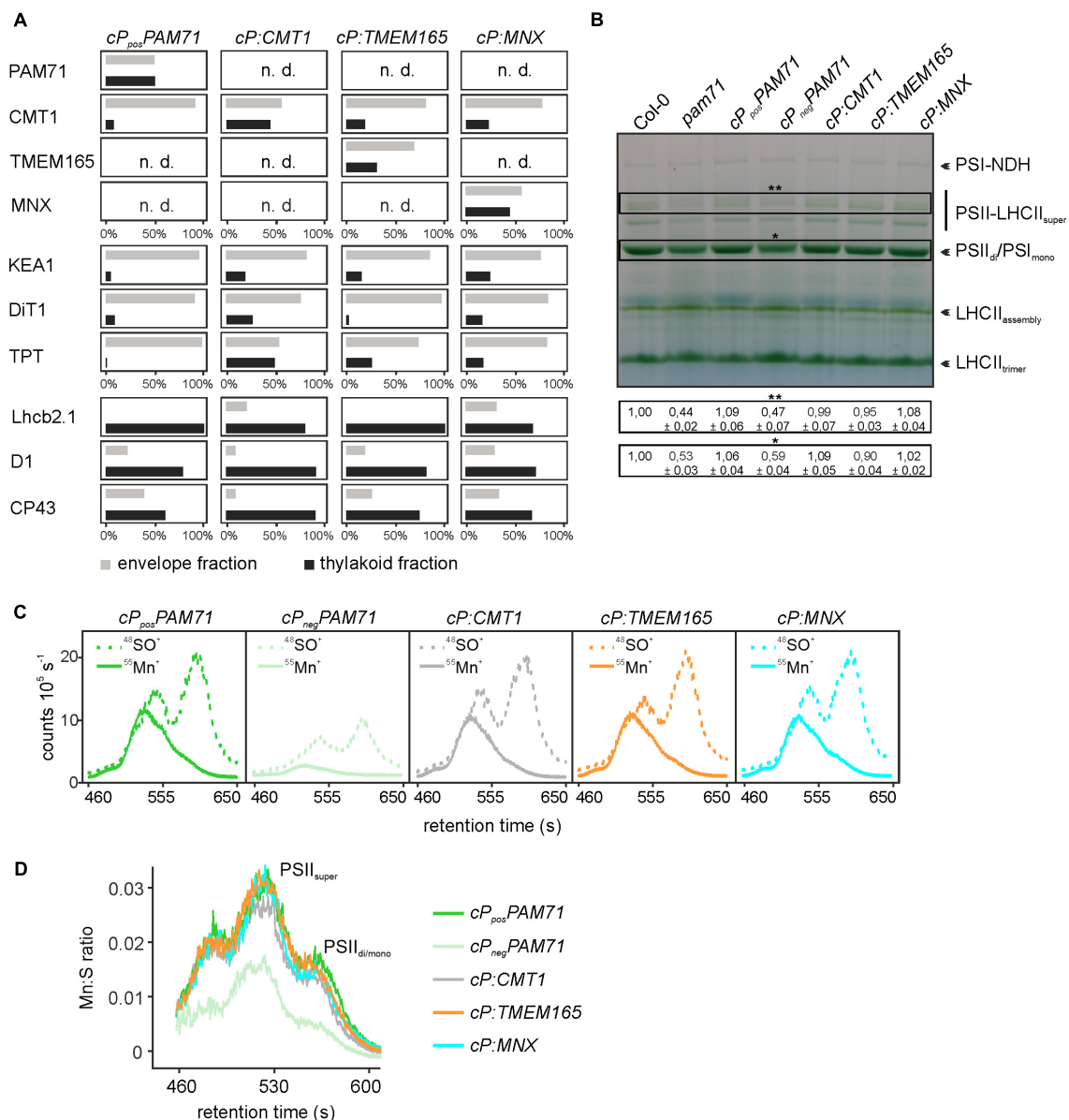


FIGURE 5 | Proteomic and ICP-MS analysis of individual transgenic lines with *pam71* genetic background. **(A)** PAM71, CMT1, TMEM165, MNX and marker proteins of envelope and thylakoid enriched fractions of the indicated plant lines. The K⁺ efflux antiporter 1 (KEA1), dicarboxylate transporter 1 (DiT1) and triosephosphate/phosphate translocator (TPT) were used as envelope marker proteins, and chlorophyll a-b binding protein 2.1 (Lhcb2.1), photosystem II protein D1 (D1) and photosystem II CP43 reaction center protein (CP43) served as thylakoid markers. The proteomic analysis is based on three independent experiments and data depicted are derived from Experiment 2 (**Supplementary Tables 3–6**). n.d., not detected. **(B)** Accumulation of thylakoid photosynthetic complexes in transgenic lines in comparison to levels in Col-0 and *pam71*. Thylakoid membrane samples (equivalent to 18 μ g of protein) were solubilized with 1% (w/v) β -dodecyl-maltoside, and protein complexes were fractionated by Blue-Native gel electrophoreses. NDH, NADH dehydrogenase-like; PSI, photosystem I; PSII, photosystem II; LHCII, light-harvesting complex of photosystem II. The different assembly states are indicated. Quantification of the indicated complexes (**PSII-LHCII supercomplexes and *PSII dimer/PSI monomer complexes) is based on intensity levels in Col-0 (=1,00). Mean values \pm SD ($n = 3$) are shown. **(C)** Size-exclusion chromatograms depicting the relative intensities of the non-oxide ion $^{55}\text{Mn}^{+}$ and the oxide ion $^{48}\text{SO}^{+}$ in the transgenic lines. Thylakoid membranes (equivalent to 50 μ g of protein) were solubilized with 1% (w/v) α -dodecyl-maltoside, and protein complexes were fractionated on a size-exclusion column. Analysis was performed with two independent experiments. **(D)** Quantification of the Mn:S ratios in the transgenic lines. Mn:S ratios are shown for the fractionated photosynthetic complexes from the samples analyzed in panel **(C)**. PSII, Photosystem II; different assembly states are indicated. The data are based on two independent experiments.

lines resembled that of *cmt1* mutant plants (**Figure 6D**). Because subtle effects might not be detectable in the T1 generation, we selected two lines per group for closer inspection. The

lines chosen exhibited the highest Fv/Fm values within their group in the respective T1 plant, carried a single-copy transgene insertion, and the magnitude of transgene expression was at

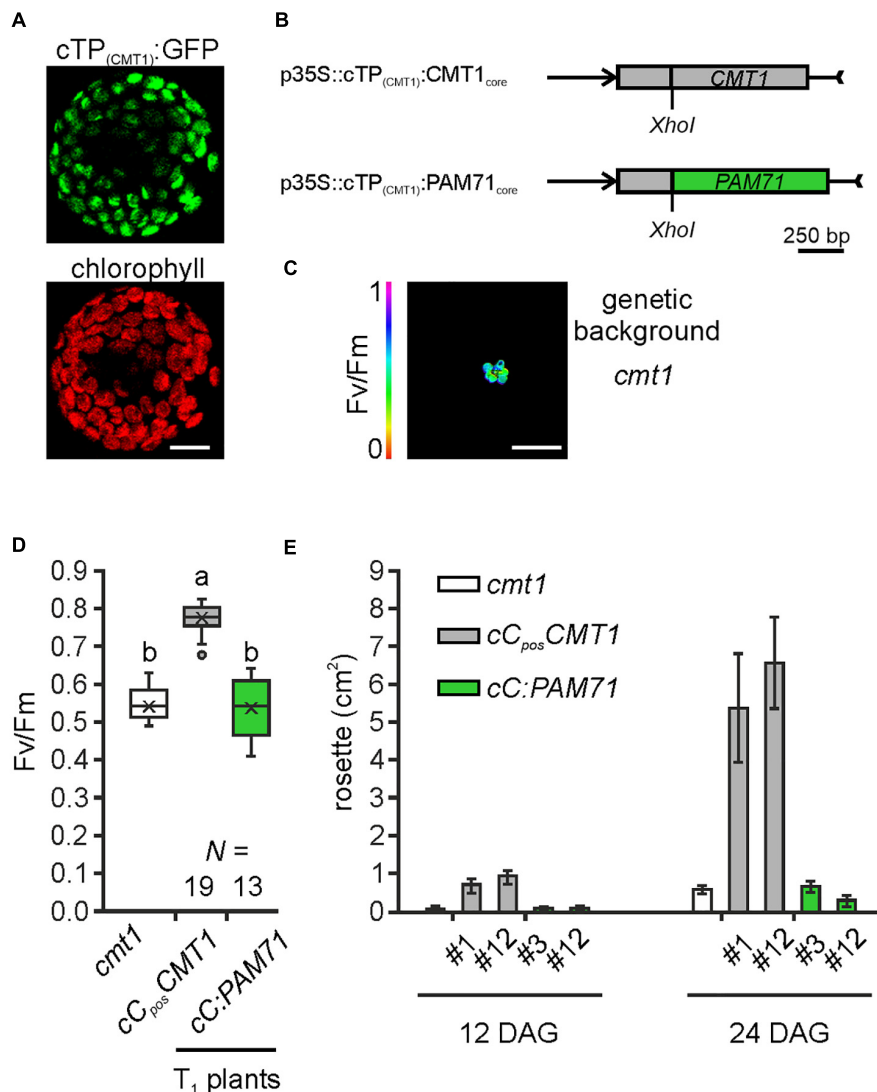


FIGURE 6 | Experimental setup for gene replacement assay and analysis of individual transgenic lines in the *cmt1* genetic background. **(A)** Verification of the N-terminal CMT1 sequence as a chloroplast-targeting peptide. *Nicotiana benthamiana* leaves were infiltrated with the Agrobacterium strain containing p35S::cTP_(CMT1):GFP; protoplasts were isolated after 48 h and analyzed by confocal microscopy. Scale bar = 12.5 μ m. **(B)** Schematic depiction of the chimeric constructs used for transformation of *cmt1*. **(C)** The *cmt1* mutant as genetic background. The maximum quantum yield of PSII (Fv/Fm) of a 4-week-old plant is shown. Scale bar = 1 cm. **(D)** Photosynthetic activity of BASTA resistant T₁ transgenic plants in comparison to *cmt1*. The maximum quantum yield of PSII (Fv/Fm) of T₁ plants is depicted as box plots representing the range of values, the exclusive median and the mean, indicated as x. The number of independent plant lines is given (N). Outliers are indicated as dots. Different letters indicate statistical significance according to ANOVA ($p < 0.01$, Tukey's HSD test). **(E)** Quantification of growth phenotypes of the indicated genotypes. Leaf areas of selected transgenic lines in comparison to *cmt1* were determined from photographs taken 12 days after germination (DAG) and 24 days after germination (DAG). Mean values \pm SD ($n = 10$) are shown.

least 10 times higher than the wild-type level (Supplementary Figures 5A,B). A re-examination of Fv/Fm values in subsequent generations revealed that, in both selected *cC:PAM71* lines, the Fv/Fm values were not significantly different from those of *cmt1* mutant plants, whereas Fv/Fm recovered to almost 0.8 in both positive control lines (Supplementary Figure 5C). In addition, growth of both *cC:PAM71* lines was markedly retarded, as in the case of *cmt1* mutant plants (Figure 6E). Taken together, these data showed that PAM71 cannot substitute CMT1 in the envelope membrane.

DISCUSSION

Our phylogenetic analysis indicates that eukaryotic and cyanobacterial members of the UPF0016 transporter family share a common ancestor, which is reflected in their functional conservation. A gene-replacement analysis was conducted in the *Arabidopsis* mutant *pam71* (Figure 3), which is characterized by diminished growth. This phenotype is readily discernible under standard cultivation conditions, and *pam71* is accessible to genetic manipulations resulting in inheritable traits. For our

purposes, these features make it more suitable than systems in which the knock-out mutation generates a conditional phenotype. For instance, a conditional phenotype has been found in the yeast UPF0016 mutant *gdt1*, which is sensitive to high concentrations of Ca^{2+} (Demaegd et al., 2013). However, its growth rate is otherwise unaffected, i.e., similar to that of wild-type strains. It has been shown that sensitivity to excess Ca^{2+} can be suppressed by transient expression of TMEM165 (Demaegd et al., 2013).

As targets for our analysis, we selected the *Synechocystis* gene *MNX*, the *Arabidopsis* gene *CMT1* and the human gene *TMEM165*. Their protein products share with PAM71 the predicted topology of two clusters of three transmembrane domains, including the consensus motifs (Supplementary Figure 2). Variations at the N-terminus are assumed to be required for correct membrane targeting (Hoecker et al., 2017), and indeed the N-terminal portion of PAM71 is sufficient for targeting to chloroplasts (Figure 3A). Notably, a derivative of PAM71 lacking the chloroplast targeting signal peptide is incapable of complementing the *pam71* phenotype (Figures 3D, 4, 5B–D), indicating that the cTP is specifically required for correct targeting. Thus, the proteins MNX, CMT1 and TMEM165 could be successfully targeted to the thylakoid membrane of *pam71* plants by equipping them with the cTP of PAM71 (Figure 5A) and overexpressed from the respective transgenes (Figure 4D). We demonstrate that the paralog CMT1, as well as both orthologs SynMNX and HsTMEM165, are functional in *Arabidopsis* thylakoid membranes when introduced into the *Arabidopsis pam71* mutant background. These findings show that all four proteins have retained the ancestral function. Like PAM71, CMT1, MNX and TMEM165 are capable of transporting Mn^{2+} into the thylakoid lumen for efficient reconstitution of inorganic Mn clusters in photosystem II (Figures 5C,D)—as demonstrated by the recovery of photosystem II efficiency (Figure 4C), which eventually increased plant growth (Figure 4B). A strong proton gradient across the thylakoid membrane (Hohner et al., 2016; Pottosin and Shabala, 2016) is established upon illumination, which presumably energizes Mn^{2+} uptake into the acidic thylakoid lumen, in accordance with the current model of a cation/proton antiport mechanism for the UPF0016 protein family (Thines et al., 2020). In this respect, it is interesting to note that CMT1 can functionally replace PAM71 at the thylakoid membrane, but not *vice versa* (Figure 6 and Supplementary Figure 5). It is tempting to speculate that CMT1 has acquired additional features that allow it to cope with the conditions prevailing at the envelope membrane, where the proton gradient is much weaker (Hohner et al., 2016).

Our findings indicate that UPF0016 members function independently of additional factors and/or of the lipid composition of the membrane. It is particularly remarkable that the human ortholog TMEM165 can replace PAM71 in the thylakoid membrane, which is rich in monogalactosyldiacylglycerol and digalactosyldiacylglycerol (Li-Beisson et al., 2013; Rocha et al., 2018), in contrast to the Golgi membrane. TMEM165 (Foulquier et al., 2012; Potelle et al., 2016; Dulary et al., 2017; Lebredonchel et al., 2019; Foulquier and Legrand, 2020), like its plant counterpart PML3

(Hoecker et al., 2020; Yang et al., 2021), naturally resides in the Golgi membrane, where the Mn^{2+} imported into the Golgi lumen acts as an essential cofactor in the synthesis of N-glycans. In the present study an LC_MS/MS-based approach was employed to gain insight into the partitioning of overexpressed TMEM165, MNX, PAM71, and CMT1 between the envelope and thylakoid membranes, because quantitative proteomics studies on purified chloroplast membranes and their subfractions have been shown in the past to be an efficient method for this purpose (Ferro et al., 2010). The expected enrichment of marker proteins in the two membrane fractions allowed us to conclude that the method is reliable (Figure 5A). As observed in the past (Ferro et al., 2010), it was not possible to identify the endogenous PAM71 in wild-type samples (Supplementary Table 2); only in the overexpressor line *cP_{pos}PAM71* could it be successfully identified (Figure 5A). Clearly, fractions of the overexpressed TMEM165, MNX, and PAM71 proteins were retained in the envelope membrane. However, at least in the case of PAM71, presumably non-functional (Figure 6).

UPF0016 proteins are of interest not only because of their conserved ability to facilitate Mn^{2+} transport, but also in terms of their evolutionary history—given that members have been identified across Archaea, Bacteria, and Eukaryota (Supplementary Figure 1). Small UPF0016 gene/protein families exist in plants, and in *Arabidopsis* the genes that code for both ER-localized proteins (PML4/PML5) are derived from a chromosomal duplication event in the progenitor of *Arabidopsis* (Hoecker et al., 2017)—indeed, these two share the highest similarity (Figure 2). This study suggests that the genes coding for the chloroplast-localized proteins CMT1 and PAM71 arose during the establishment of endosymbiosis, after the cyanobacterial precursor of chloroplasts contributed its gene copy to the eukaryotic host genome, which then gave rise to a gene duplication that is widely conserved in Viridiplantae (Figure 1). In green algae, the PAM71 homolog CGLD1 (conserved in the green lineage and diatoms 1) maintained the structure and function of PSII, and contributed to its protection under photo-oxidative stress conditions (Xing et al., 2017). It is well established that genes of the cyanobacterial ancestor have been transferred to the nucleus, that many of the proteins they encode are rerouted to the chloroplast (Leister, 2003, 2016; Lee and Hwang, 2018) and that numerous proteins can functionally replace each other (Savidge et al., 2002; Sattler et al., 2003; Lv et al., 2009; Armbruster et al., 2013; Proctor et al., 2018; Yoon et al., 2019). Yet, what makes the evolution of the UPF0016 family particularly interesting is that it suggests all members of Eukaryota and Cyanobacteria (Figure 1) might have a common ancestor, which would explain why human TMEM165 can functionally substitute for PAM71 in chloroplast membranes. We suggest that plants received UPF0016 gene copies *via* two independent events. Although speculative, lateral gene transfer, perhaps involving Cyanobacteria, could be at the origin of subgroup one proteins, which are present in all Eukaryota, as there is no indication of an archaeal and/or protobacterial origin of this subgroup (Figure 1). In a second event, through cyanobacterial endosymbiotic gene transfer, subgroup two proteins were then introduced into the green

lineage. We have not succeeded in tracing UPF0016 protein members to the last common ancestor of all cells, which is proposed to have lived about 3.8 billion years ago and to have had 355 protein clusters (Weiss et al., 2016, 2018). Thus, it is reasonable to assume that UPF0016 genes spread extensively by lateral gene transfer later in evolution.

It has also been suggested that PAM71 acquired an additional Ca^{2+} transport function (Wang et al., 2016; Frank et al., 2019). In this study, we have shown that the cyanobacterial MNX protein is functional in *pam71* plants and fully complements all aspects of the latter's mutant phenotype (Figure 5). This enables us to conclude that only the Mn^{2+} transport activity of PAM71 plays a significant physiological role in chloroplasts. At the thylakoid membrane it can be replaced by its paralog (CMT1) and by its orthologs from *Zea mays* (Wang et al., 2020), cyanobacteria and human, yet there is no indication that PAM71 can function at the envelope membrane. A future challenge is to determine the molecular basis for the adaptation of CMT1 to the conditions prevailing in the envelope membrane of chloroplasts, and this study opens the door to further investigations of how far proteins can diverge without losing their ancient function.

DATA AVAILABILITY STATEMENT

The mass spectrometry proteomics data have been deposited at <https://www.ebi.ac.uk/pride> under the accession number PXD022763.

REFERENCES

- Armbruster, U., Labs, M., Pribil, M., Viola, S., Xu, W., Scharfenberg, M., et al. (2013). *Arabidopsis* curvature thylakoid1 proteins modify thylakoid architecture by inducing membrane curvature. *Plant Cell* 25, 2661–2678. doi: 10.1105/tpc.113.113118
- Bammens, R., Mehta, N., Race, V., Foulquier, F., Jaeken, J., Tiemeyer, M., et al. (2015). Abnormal cartilage development and altered N-glycosylation in Tmem165-deficient zebrafish mirrors the phenotypes associated with TMEM165-CDG. *Glycobiology* 25, 669–682. doi: 10.1093/glycob/cwv009
- Brandenburg, F., Schoffman, H., Kurz, S., Kramer, U., Keren, N., Weber, A. P., et al. (2017). The *Synechocystis* manganese exporter Mnx is essential for manganese homeostasis in cyanobacteria. *Plant Physiol.* 173, 1798–1810. doi: 10.1104/pp.16.01895
- Clough, S. J., and Bent, A. F. (1998). Floral dip: a simplified method for *Agrobacterium*-mediated transformation of *Arabidopsis thaliana*. *Plant J.* 16, 735–743. doi: 10.1046/j.1365-3113x.1998.00343.x
- Colinet, A. S., Sengottaiyan, P., Deschamps, A., Colsoul, M. L., Thines, L., Demaegd, D., et al. (2016). Yeast Gdt1 is a Golgi-localized calcium transporter required for stress-induced calcium signaling and protein glycosylation. *Sci. Rep.* 6:24282.
- Cox, J., and Mann, M. (2008). MaxQuant enables high peptide identification rates, individualized p.p.b.-range mass accuracies and proteome-wide protein quantification. *Nat. Biotechnol.* 26, 1367–1372. doi: 10.1038/nbt.1511
- Cox, J., Neuhauser, N., Michalski, A., Scheltema, R. A., Olsen, J. V., and Mann, M. (2011). Andromeda: a peptide search engine integrated into the MaxQuant environment. *J. Proteome Res.* 10, 1794–1805. doi: 10.1021/pr101065j
- Demaegd, D., Colinet, A. S., Deschamps, A., and Morsomme, P. (2014). Molecular evolution of a novel family of putative calcium transporters. *PLoS One* 9:e100851. doi: 10.1371/journal.pone.0100851
- Demaegd, D., Foulquier, F., Colinet, A. S., Gremillon, L., Legrand, D., Mariot, P., et al. (2013). Newly characterized Golgi-localized family of proteins is involved in calcium and pH homeostasis in yeast and human cells. *Proc. Natl. Acad. Sci. U.S.A.* 110, 6859–6864. doi: 10.1073/pnas.1219871110
- Dulavy, E., Potelle, S., Legrand, D., and Foulquier, F. (2017). TMEM165 deficiencies in congenital disorders of glycosylation type II (CDG-II): clues and evidences for roles of the protein in Golgi functions and ion homeostasis. *Tissue Cell* 49, 150–156. doi: 10.1016/j.tice.2016.06.006
- Eisenhut, M. (2019). Manganese homeostasis in cyanobacteria. *Plants* 9:18. doi: 10.3390/plants9010018
- Eisenhut, M., Hoecker, N., Schmidt, S. B., Basgaran, R. M., Flachbart, S., Jahns, P., et al. (2018). The plastid envelope chloroplast manganese transporter1 is essential for manganese homeostasis in *Arabidopsis*. *Mol. Plant* 11, 955–969. doi: 10.1016/j.molp.2018.04.008
- Ferro, M., Brugiere, S., Salvi, D., Seigneurin-Berny, D., Court, M., Moyet, L., et al. (2010). AT_CHLORO, a comprehensive chloroplast proteome database with subplastidial localization and curated information on envelope proteins. *Mol. Cell. Proteomics* 9, 1063–1084. doi: 10.1074/mcp.m900325-mcp200
- Fisher, C. R., Wyckoff, E. E., Peng, E. D., and Payne, S. M. (2016). Identification and characterization of a putative manganese export protein in *Vibrio cholerae*. *J. Bacteriol.* 198, 2810–2817. doi: 10.1128/jb.00215-16
- Foulquier, F., Amyere, M., Jaeken, J., Zeevaert, R., Schollen, E., Race, V., et al. (2012). TMEM165 deficiency causes a congenital disorder of glycosylation. *Am. J. Hum. Genet.* 91, 15–26. doi: 10.1016/j.ajhg.2012.05.002
- Foulquier, F., and Legrand, D. (2020). Biometals and glycosylation in humans: congenital disorders of glycosylation shed lights into the crucial role of Golgi manganese homeostasis. *Biochim. Biophys. Acta Gen. Subj.* 1864:129674. doi: 10.1016/j.bbagen.2020.129674
- Frank, J., Happeck, R., Meier, B., Hoang, M. T. T., Stribny, J., Hause, G., et al. (2019). Chloroplast-localized BICAT proteins shape stromal calcium signals

AUTHOR CONTRIBUTIONS

AS: conceptualization. NH, YH, SS, GM, and SBS: investigation and analysis of data. DL and AS: resources. SBS and AS: funding acquisition and writing—review and editing. NH and AS: writing—original draft. All authors contributed to manuscript revision, read, and approved the submitted version.

FUNDING

This research was supported by the German Science Foundation (SCHN560/4-1 to AS) and by the Independent Research Fund Denmark—Technology and Production Sciences (Grant No. DFF-5054-00042 to SBS).

ACKNOWLEDGMENTS

We would like to thank Sabine Jarzombski for excellent technical assistance, Serena Schwenkert for *Nicotiana benthamiana* seeds and support with confocal microscopy, and Paul Hardy for critical reading of the manuscript.

SUPPLEMENTARY MATERIAL

The Supplementary Material for this article can be found online at: <https://www.frontiersin.org/articles/10.3389/fpls.2021.697848/full#supplementary-material>

- and are required for efficient photosynthesis. *New Phytol.* 221, 866–880. doi: 10.1111/nph.15407
- Gandini, C., Schmidt, S. B., Husted, S., Schneider, A., and Leister, D. (2017). The transporter SynPAM71 is located in the plasma membrane and thylakoids, and mediates manganese tolerance in *Synechocystis* PCC6803. *New Phytol.* 215, 256–268. doi: 10.1111/nph.14526
- Hanikenne, M., and Baurain, D. (2013). Origin and evolution of metal P-type ATPases in Plantae (Archaeplastida). *Front. Plant Sci.* 4:544. doi: 10.3389/fpls.2013.00544
- Hoecker, N., Honke, A., Frey, K., Leister, D., and Schneider, A. (2020). Homologous proteins of the manganese transporter PAM71 are localized in the Golgi apparatus and endoplasmic reticulum. *Plants* 9:239. doi: 10.3390/plants9020239
- Hoecker, N., Leister, D., and Schneider, A. (2017). Plants contain small families of UPF0016 proteins including the photosynthesis affected MUTANT71 transporter. *Plant Signal. Behav.* 12:e1278101. doi: 10.1080/15592324.2016.1278101
- Hohner, R., Aboukila, A., Kunz, H. H., and Venema, K. (2016). Proton gradients and proton-dependent transport processes in the chloroplast. *Front. Plant Sci.* 7:218. doi: 10.3389/fpls.2016.00218
- Huber, M., Bienvenut, W. V., Linster, E., Stephan, I., Armbruster, L., Sticht, C., et al. (2020). NatB-mediated N-terminal acetylation affects growth and biotic stress responses. *Plant Physiol.* 182, 792–806. doi: 10.1104/pp.19.00792
- Janowski, M., Zoschke, R., Scharff, L. B., Martinez Jaime, S., Ferrari, C., Proost, S., et al. (2018). AtRsgA from *Arabidopsis thaliana* is important for maturation of the small subunit of the chloroplast ribosome. *Plant J.* 96, 404–420. doi: 10.1111/tj.14040
- Jha, S. G., Larson, E. R., Humble, J., Domozych, D. S., Barrington, D. S., and Tierney, M. L. (2018). Vacuolar protein sorting 26C encodes an evolutionarily conserved large retromer subunit in eukaryotes that is important for root hair growth in *Arabidopsis thaliana*. *Plant J.* 94, 595–611. doi: 10.1111/tj.13880
- Karimi, M., Inze, D., and Depicker, A. (2002). GATEWAY vectors for *Agrobacterium*-mediated plant transformation. *Trends Plant Sci.* 7, 193–195. doi: 10.1016/s1360-1385(02)02251-3
- Krzewinski-Recchi, M. A., Potelle, S., Mir, A. M., Vicogne, D., Dulary, E., Duvet, S., et al. (2017). Evidence for splice transcript variants of TMEM165, a gene involved in CDG. *Biochim. Biophys. Acta Gen. Subj.* 1861, 737–748. doi: 10.1016/j.bbagen.2017.01.011
- Kumar, S., Stecher, G., Li, M., Knyaz, C., and Tamura, K. (2018). MEGA X: molecular evolutionary genetics analysis across computing platforms. *Mol. Biol. Evol.* 35, 1547–1549. doi: 10.1093/molbev/msy096
- Le, S. Q., and Gascuel, O. (2008). An improved general amino acid replacement matrix. *Mol. Biol. Evol.* 25, 1307–1320. doi: 10.1093/molbev/msn067
- Lebedonchel, E., Houdou, M., Potelle, S., De Bettignies, G., Schulz, C., Krzewinski Recchi, M. A., et al. (2019). Dissection of TMEM165 function in Golgi glycosylation and its Mn(2+) sensitivity. *Biochimie* 165, 123–130. doi: 10.1016/j.biochi.2019.07.016
- Lee, D. W., and Hwang, I. (2018). Evolution and design principles of the diverse chloroplast transit peptides. *Mol. Cells* 41, 161–167.
- Leister, D. (2003). Chloroplast research in the genomic age. *Trends Genet.* 19, 47–56. doi: 10.1016/s0168-9525(02)00003-3
- Leister, D. (2016). Towards understanding the evolution and functional diversification of DNA-containing plant organelles. *F1000Res.* 5:F1000FacultyRev-330.
- Li-Beisson, Y., Shorrosh, B., Beisson, F., Andersson, M. X., Arondel, V., Bates, P. D., et al. (2013). Acyl-lipid metabolism. *Arabidopsis Book* 11:e0161.
- Lv, H. X., Guo, G. Q., and Yang, Z. N. (2009). Translocons on the inner and outer envelopes of chloroplasts share similar evolutionary origin in *Arabidopsis thaliana*. *J. Evol. Biol.* 22, 1418–1428. doi: 10.1111/j.1420-9101.2009.01755.x
- Maxwell, K., and Johnson, G. N. (2000). Chlorophyll fluorescence—a practical guide. *J. Exp. Bot.* 51, 659–668. doi: 10.1093/jxb/51.345.659
- Morelle, W., Potelle, S., Witters, P., Wong, S., Climer, L., Lupashin, V., et al. (2017). Galactose supplementation in patients with TMEM165-CDG rescues the glycosylation defects. *J. Clin. Endocrinol. Metab.* 102, 1375–1386. doi: 10.1210/je.2016-3443
- Potelle, S., Morelle, W., Dulary, E., Duvet, S., Vicogne, D., Spriet, C., et al. (2016). Glycosylation abnormalities in Gdt1p/TMEM165 deficient cells result from a defect in Golgi manganese homeostasis. *Hum. Mol. Genet.* 25, 1489–1500. doi: 10.1093/hmg/ddw026
- Pottosin, I., and Shabala, S. (2016). Transport across chloroplast membranes: optimizing photosynthesis for adverse environmental conditions. *Mol. Plant* 9, 356–370. doi: 10.1016/j.molp.2015.10.006
- Proctor, M. S., Chidgey, J. W., Shukla, M. K., Jackson, P. J., Sobotka, R., Hunter, C. N., et al. (2018). Plant and algal chlorophyll synthases function in *Synechocystis* and interact with the YidC/Alb3 membrane insertase. *FEBS Lett.* 592, 3062–3073. doi: 10.1002/1873-3468.13222
- Rappsilber, J., Ishihama, Y., and Mann, M. (2003). Stop and go extraction tips for matrix-assisted laser desorption/ionization, nanoelectrospray, and LC/MS sample pretreatment in proteomics. *Anal. Chem.* 75, 663–670. doi: 10.1021/ac026117i
- Rocha, J., Nitenberg, M., Girard-Egrot, A., Jouhet, J., Marechal, E., Block, M. A., et al. (2018). Do galactolipid synthases play a key role in the biogenesis of chloroplast membranes of higher plants? *Front. Plant Sci.* 9:126. doi: 10.3389/fpls.2018.00126
- Rosnoblet, C., Legrand, D., Demaegd, D., Hacine-Gherbi, H., De Bettignies, G., Bammens, R., et al. (2013). Impact of disease-causing mutations on TMEM165 subcellular localization, a recently identified protein involved in CDG-II. *Hum. Mol. Genet.* 22, 2914–2928. doi: 10.1093/hmg/ddt146
- Sattler, S. E., Cahoon, E. B., Coughlan, S. J., and Dellapenna, D. (2003). Characterization of tocopherol cyclases from higher plants and cyanobacteria. Evolutionary implications for tocopherol synthesis and function. *Plant Physiol.* 132, 2184–2195. doi: 10.1104/pp.103.024257
- Savidge, B., Weiss, J. D., Wong, Y. H., Lassner, M. W., Mitsky, T. A., Shewmaker, C. K., et al. (2002). Isolation and characterization of homogentisate phytyltransferase genes from *Synechocystis* sp. PCC 6803 and *Arabidopsis*. *Plant Physiol.* 129, 321–332. doi: 10.1104/pp.010747
- Schmidt, S. B., Eisenhut, M., and Schneider, A. (2020). Chloroplast transition metal regulation for efficient photosynthesis. *Trends Plant Sci.* 25, 817–828. doi: 10.1016/j.tplants.2020.03.003
- Schmidt, S. B., Persson, D. P., Powikrowska, M., Frydenvang, J., Schjoerring, J. K., Jensen, P. E., et al. (2015). Metal binding in photosystem II super- and subcomplexes from barley thylakoids. *Plant Physiol.* 168, 1490–1502. doi: 10.1104/pp.15.00559
- Schmittgen, T. D., and Livak, K. J. (2008). Analyzing real-time PCR data by the comparative C-T method. *Nat. Protoc.* 3, 1101–1108. doi: 10.1038/nprot.2008.73
- Schneider, A., Steinberger, I., Herdean, A., Gandini, C., Eisenhut, M., Kurz, S., et al. (2016). The evolutionarily conserved protein photosynthesis affected MUTANT71 is required for efficient manganese uptake at the thylakoid membrane in *Arabidopsis*. *Plant Cell* 28, 892–910.
- Schneider, C. A., Rasband, W. S., and Eliceiri, K. W. (2012). NIH image to ImageJ: 25 years of image analysis. *Nat. Methods* 9, 671–675. doi: 10.1038/nmeth.2089
- Schulte Althoff, S., Gruneberg, M., Reunert, J., Park, J. H., Rust, S., Muhlhausen, C., et al. (2016). TMEM165 deficiency: postnatal changes in glycosylation. *JIMD Rep.* 26, 21–29. doi: 10.1007/8904_2015_455
- Schwanhauser, B., Busse, D., Li, N., Dittmar, G., Schuchhardt, J., Wolf, J., et al. (2011). Global quantification of mammalian gene expression control. *Nature* 473, 337–342. doi: 10.1038/nature10098
- Schweiger, R., and Schwenkert, S. (2014). Protein-protein interactions visualized by bimolecular fluorescence complementation in tobacco protoplasts and leaves. *J. Vis. Exp.* 9:51327. doi: 10.3791/51327
- Stribny, J., Thines, L., Deschamps, A., Goffin, P., and Morsomme, P. (2020). The human Golgi protein TMEM165 transports calcium and manganese in yeast and bacterial cells. *J. Biol. Chem.* 295, 3865–3874. doi: 10.1074/jbc.ra119.012249
- Thines, L., Stribny, J., and Morsomme, P. (2020). From the uncharacterized protein family 0016 to the GDT1 family: molecular insights into a newly-characterized family of cation secondary transporters. *Microb. Cell* 7, 202–214. doi: 10.15698/mic2020.08.725
- Vizcaino, J. A., Csordas, A., Del-Toro, N., Dienes, J. A., Griss, J., Lavidas, I., et al. (2016). 2016 update of the PRIDE database and its related tools. *Nucleic Acids Res.* 44, D447–D456.
- Wang, C., Ou, D., Wang, C., Lu, X., Du, J., Li, J., et al. (2020). Functional characterization of a chloroplast-localized Mn(2+)(Ca(2+))/H(+) antiporter, ZmmCCHA1 from *Zea mays* ssp. mexicana L. *Plant Physiol. Biochem.* 155, 396–405. doi: 10.1016/j.plaphy.2020.08.002

- Wang, C., Xu, W., Jin, H., Zhang, T., Lai, J., Zhou, X., et al. (2016). A putative chloroplast-localized Ca(2+)/H(+) antiporter CCHA1 is involved in calcium and pH homeostasis and required for PSII function in *Arabidopsis*. *Mol. Plant* 9, 1183–1196. doi: 10.1016/j.molp.2016.05.015
- Weiss, M. C., Preiner, M., Xavier, J. C., Zimorski, V., and Martin, W. F. (2018). The last universal common ancestor between ancient Earth chemistry and the onset of genetics. *PLoS Genet.* 14:e1007518. doi: 10.1371/journal.pgen.1007518
- Weiss, M. C., Sousa, F. L., Mrnjavac, N., Neukirchen, S., Roettger, M., Nelson-Sathi, S., et al. (2016). The physiology and habitat of the last universal common ancestor. *Nat. Microbiol.* 1:16116.
- Xing, J., Liu, P., Zhao, L., and Huang, F. (2017). Deletion of CGLD1 impairs PSII and increases singlet oxygen tolerance of green alga *Chlamydomonas reinhardtii*. *Front. Plant Sci.* 8:2154. doi: 10.3389/fpls.2017.02154
- Yang, C. H., Wang, C., Singh, S., Fan, N., Liu, S., Zhao, L., et al. (2021). Golgi-localised manganese transporter PML3 regulates *Arabidopsis* growth through modulating Golgi glycosylation and cell wall biosynthesis. *New Phytol.* doi: 10.1111/nph.17209 [Epub ahead of print].
- Yoon, J., Han, Y., Ahn, Y. O., Hong, M. K., and Sung, S. K. (2019). Characterization of HemY-type protoporphyrinogen IX oxidase genes from cyanobacteria and their functioning in transgenic *Arabidopsis*. *Plant Mol. Biol.* 101, 561–574. doi: 10.1007/s11103-019-00925-8
- Zeevaert, R., De Zegher, F., Sturiale, L., Garozzo, D., Smet, M., Moens, M., et al. (2013). Bone dysplasia as a key feature in three patients with a novel congenital disorder of glycosylation (CDG) type II due to a deep intronic splice mutation in TMEM165. *JIMD Rep.* 8, 145–152. doi: 10.1007/8904_2012_172
- Zeinert, R., Martinez, E., Schmitz, J., Senn, K., Usman, B., Anantharaman, V., et al. (2018). Structure-function analysis of manganese exporter proteins across bacteria. *J. Biol. Chem.* 293, 5715–5730. doi: 10.1074/jbc.m117.790717
- Zhang, B., Zhang, C., Liu, C., Jing, Y., Wang, Y., Jin, L., et al. (2018). Inner envelope chloroplast manganese transporter 1 supports manganese homeostasis and phototrophic growth in *Arabidopsis*. *Mol. Plant* 11, 943–954. doi: 10.1016/j.molp.2018.04.007

Conflict of Interest: The authors declare that the research was conducted in the absence of any commercial or financial relationships that could be construed as a potential conflict of interest.

Copyright © 2021 Hoecker, Hennecke, Schrott, Marino, Schmidt, Leister and Schneider. This is an open-access article distributed under the terms of the Creative Commons Attribution License (CC BY). The use, distribution or reproduction in other forums is permitted, provided the original author(s) and the copyright owner(s) are credited and that the original publication in this journal is cited, in accordance with accepted academic practice. No use, distribution or reproduction is permitted which does not comply with these terms.



Functional Relationship of Arabidopsis AOXs and PTOX Revealed via Transgenic Analysis

Danfeng Wang¹, Chunyu Wang^{1,2}, Cai Li¹, Haifeng Song¹, Jing Qin¹, Han Chang¹, Weiha Fu¹, Yuhua Wang¹, Fei Wang¹, Beibei Li¹, Yaqi Hao¹, Min Xu^{1*} and Aigen Fu^{1*}

¹ Chinese Education Ministry's Key Laboratory of Western Resources and Modern Biotechnology, Key Laboratory of Biotechnology Shaanxi Province, College of Life Sciences, Northwest University, Xi'an, China, ² College of Life Sciences, Northeast Agricultural University, Harbin, China

OPEN ACCESS

Edited by:

Hongbo Gao,
Beijing Forestry University, China

Reviewed by:

Deqiang Duanmu,
Huazhong Agricultural University,
China

Dawei Zhang,
Sichuan University, China

Fang Huang,
Institute of Botany, Chinese Academy
of Sciences, China

*Correspondence:

Aigen Fu
aigenfu@nwnu.edu.cn
Min Xu
xumin@nwnu.edu.cn

Specialty section:

This article was submitted to
Plant Physiology,
a section of the journal
Frontiers in Plant Science

Received: 09 April 2021

Accepted: 07 June 2021

Published: 02 July 2021

Citation:

Wang D, Wang C, Li C, Song H,
Qin J, Chang H, Fu W, Wang Y,
Wang F, Li B, Hao Y, Xu M and Fu A
(2021) Functional Relationship
of Arabidopsis AOXs and PTOX
Revealed via Transgenic Analysis.
Front. Plant Sci. 12:692847.
doi: 10.3389/fpls.2021.692847

Alternative oxidase (AOX) and plastid terminal oxidase (PTOX) are terminal oxidases of electron transfer in mitochondria and chloroplasts, respectively. Here, taking advantage of the variegation phenotype of the Arabidopsis PTOX deficient mutant (*im*), we examined the functional relationship between PTOX and its five distantly related homologs (AOX1a, 1b, 1c, 1d, and AOX2). When engineered into chloroplasts, AOX1b, 1c, 1d, and AOX2 rescued the *im* defect, while AOX1a partially suppressed the mutant phenotype, indicating that AOXs could function as PQH₂ oxidases. When the full length AOXs were overexpressed in *im*, only AOX1b and AOX2 rescued its variegation phenotype. *In vivo* fluorescence analysis of GFP-tagged AOXs and subcellular fractionation assays showed that AOX1b and AOX2 could partially enter chloroplasts while AOX1c and AOX1d were exclusively present in mitochondria. Surprisingly, the subcellular fractionation, but not the fluorescence analysis of GFP-tagged AOX1a, revealed that a small portion of AOX1a could sort into chloroplasts. We further fused and expressed the targeting peptides of AOXs with the mature form of PTOX in *im* individually; and found that targeting peptides of AOX1a, AOX1b, and AOX2, but not that of AOX1c or AOX1d, could direct PTOX into chloroplasts. It demonstrated that chloroplast-localized AOXs, but not mitochondria-localized AOXs, can functionally compensate for the PTOX deficiency in chloroplasts, providing a direct evidence for the functional relevance of AOX and PTOX, shedding light on the interaction between mitochondria and chloroplasts and the complex mechanisms of protein dual targeting in plant cells.

Keywords: alternative oxidase (AOX), plastid terminal oxidase (PTOX), mitochondria, chloroplasts, targeting peptide, protein dual targeting

INTRODUCTION

Plant cells harbor two energy-converting organelles, mitochondria and chloroplasts, which evolved from ancient prokaryotes through different endosymbiotic events (Cavalier-Smith, 2000; Leister, 2003). Most of the symbiont genes were lost or transferred to their host genomes during evolution. Expression of the remaining small genomes in organelles and of the nuclear genome of host

cells is highly coordinated (Martin and Hermann, 1998; Abdallah et al., 2000). Mitochondria and chloroplasts are tightly linked to each other, sharing some common conserved proteins (Mueller and Reski, 2014). Photosynthesis provides carbon substrates to sustain mitochondrial respiration, and mitochondria contribute essential metabolites to maintain chloroplast functions as well (Blanco et al., 2014; Zhao et al., 2018).

The respiratory electron transfer chain (RETc) in plant mitochondria consists of a main cytochrome pathway and an alternative pathway (Møller, 2001; Finnegan et al., 2004; Schertl and Braun, 2014). Electron transfer in the cyanide-sensitive cytochrome pathway is coupled to transmembrane proton translocation and responsible for ATP synthesis (Juszczuk and Rychter, 2003). The alternative pathway, mediated by a cyanide-resistant alternative oxidase (AOX), catalyzes electron transfer from UQH₂ (ubiquinol) to oxygen (Vanlerberghe and McIntosh, 1997; Juszczuk and Rychter, 2003). This energy-wasteful alternative pathway oxidizes reducing equivalents without coupling to proton translocation across the mitochondrial membrane and ATP synthesis (Rogov et al., 2014; Vishwakarma et al., 2015).

The photosynthetic electron transfer chain (PETc) in chloroplasts consists of photosystem II, PQ (plastoquinone), cytochrome b₆f complex, plastocyanin and photosystem I (Rochaix, 2011; Hasan et al., 2013). In prokaryotic cyanobacteria, PETc and RETc coexist in the thylakoid membrane and share some intermediate components (Myers, 1986; Cooley et al., 2000). As the evolutionary remnants of cyanobacteria, chloroplasts also contain an O₂-dependent electron transfer pathway, referred to as chlororespiration, which involves the NADH dehydrogenase complex, the PQ pool, and the plastid terminal oxidase (PTOX) (Bennoun, 2002). As a distant homolog of mitochondrial AOX (Carol et al., 1999; Wu et al., 1999), PTOX transfers electrons from PQH₂ to oxygen at the thylakoid membrane, mimicking the function of AOX at the mitochondrial inner membrane (Nawrocki et al., 2015).

PTOX and AOX are derived from an ancient di-iron oxidase, but they diverged early on different evolutionary routes before the endosymbiotic events giving rise to mitochondria and chloroplasts (McDonald and Vanlerberghe, 2006; Nobre et al., 2016). AOX is a UQH₂ oxidase in mitochondria, while PTOX is a PQH₂ oxidase in chloroplasts. *In vitro* enzyme assays showed that PTOX specifically uses PQH₂ as substrate and AOX exclusively uses UQH₂ (Josse et al., 2003; Fu et al., 2012; Yu et al., 2014).

The PTOX-mediated electron transfer pathway does not contribute significantly in chloroplasts when PETc develops and functions well (Fu et al., 2009; Nawrocki et al., 2015). However, it might be a major force to drive electron transfer in darkness, in non-photosynthetic plastids, or at the early stage of chloroplast development (Wang and Fu, 2016). PTOX is a key factor for maintaining the PQ pool redox balance and functions as a “safety valve” to protect photosynthesis (Wang and Fu, 2016). It is a stress-responsive protein and could protect plants from various harmful stresses (Laureau et al., 2013; Stepien and Johnson, 2018). PTOX is also critical for

carotenoid biosynthesis since inactivation of PTOX results in a deficiency of phytoene desaturation, a key step in carotenoid biosynthesis (Okegawa et al., 2010; McDonald et al., 2011). Consequently, the Arabidopsis PTOX null mutant, *immutans* (*im*), shows a striking light-dependent variegation phenotype due to the absence of protective carotenoids (Wu et al., 1999; Fu et al., 2005, 2009, 2012). In addition, PTOX participates in chloroplast development and plant photomorphogenesis (Foudree et al., 2012; Tamiru et al., 2013).

As a non-energy conserving terminal oxidase, AOX keeps a balance between mitochondrial carbon and energy metabolism. Similar to PTOX, AOX also plays a critical role in response to different types of stress conditions, including low/high temperature (Murakami and Toriyama, 2008; Wang et al., 2011), salinity (Wang et al., 2010), metal toxicity (Tan et al., 2010), high light/drought (Zhang et al., 2010, 2012; Yoshida et al., 2011a), high CO₂ (Gandin et al., 2012), low oxygen (Clifton et al., 2005), nutrient deficiency (Juszczuk et al., 2001), and bacterial infection (Spaol and Loake, 2011).

There are broad metabolite exchanges and signal communications between mitochondria and chloroplasts, and an orchestrated coordination of these two organelles is essential for plant cells (Selinski and Scheibe, 2019). Recent data showed that AOX plays a central role in coordinating signaling pathways between mitochondria and chloroplasts (Vanlerberghe et al., 2020). Analysis of plant *aox1a* mutants illustrated that AOX could protect photosynthesis from photo-damage by dissipating excess reducing power in chloroplasts (Yoshida et al., 2007, 2008, 2011b; Zhang et al., 2010, 2016). It is generally accepted that the malate/oxaloacetate (Mal/OAA) shuttle connecting chloroplasts and mitochondria is responsible for transferring excess reducing equivalents from chloroplasts to mitochondria (Noguchi and Yoshida, 2008; Taniguchi and Miyake, 2012; Zhang et al., 2012; Vishwakarma et al., 2015). Recently, photorespiration was also found to be involved in the AOX-mediated protection of photosynthesis (Li et al., 2020).

Besides providing a mitochondrial means to indirectly optimize the chloroplasts energy status, AOX could directly enter chloroplasts and regulate PETc in the thylakoid membrane (Fu et al., 2012). Overexpressing AOX2 in Arabidopsis *im* rescued the variegation phenotype of the mutant, and AOX2 was found dually targeted to mitochondria and chloroplasts. In addition, when engineered into chloroplasts, AOX1a could partially suppress the growth defect of *im* (Fu et al., 2012). These results demonstrated that both AOX2 and AOX1a could act as PQH₂ oxidase in chloroplasts, suggesting that the substrate specificity of PTOX and AOX in plants may not be as stringent as shown by *in vitro* enzyme assays (Fu et al., 2012).

Targeting peptide analysis indicated that the presence of multiple arginine and hydrophobic residues in the N-terminal region would enable a protein to be preferentially imported into mitochondria rather than into chloroplasts (Ge et al., 2014; Lee et al., 2019). All five Arabidopsis AOX members (AOX1a-1d and AOX2) fit the profile of mitochondria specifically targeted proteins, and PTOX also matches the characteristic of chloroplast targeted proteins. However, the fact that AOX2 is a dually targeted protein suggested that AOX proteins could be imported

into chloroplasts although they are predominantly present in mitochondria (Fu et al., 2012).

Taking advantage of the striking variegation phenotype of the *Arabidopsis im* mutant, we explored the functional relevance of AOXs and PTOX by overexpressing various forms of AOXs in *im*. Following the previous study which revealed AOX2 is a dually targeted protein and chloroplast-localized AOX1a could partially rescue *im* (Fu et al., 2012), this study attempts to answer the following questions: whether all AOXs could act as PQH₂ oxidase, whether elevated levels of AOXs attenuate the deficiency of electron transfer in *im*, and whether they are dually targeted proteins to mitochondria and chloroplasts. We found that all five AOXs could utilize PQH₂ as a substrate in chloroplasts, and AOX1a, AOX1b, and AOX2 could be dually targeted proteins. We concluded that AOXs could enter chloroplasts to regulate electron transfer in chloroplasts whereas mitochondria-localized AOXs do not play a significant role in compensating the PTOX deficiency in chloroplasts. This study suggested that the cellular compartmentation of proteins in plant cells might not be as strict as previously assumed, and there could be a certain plasticity for proteins to sort into different subcellular locations.

MATERIALS AND METHODS

Primers

All the primers used in this study are listed in **Supplementary Table 2**.

Plant Materials and Growth Conditions

The plants in this study included the wild type, *im*, and transgenic plants with the genetic background of *Arabidopsis thaliana* Columbia-0. Because *im* is light-sensitive, the plants were germinated and grown under low light ($\sim 20 \mu\text{mol}\cdot\text{m}^{-2}\cdot\text{s}^{-1}$) for the initial 5 days, and then transferred to normal light ($\sim 100 \mu\text{mol}\cdot\text{m}^{-2}\cdot\text{s}^{-1}$). All plants in this study were grown on soil at 23°C with a photoperiod of 16 h light/8 h dark cycle.

Constructing Transgenes and Plant Gene Transformation

Five *Arabidopsis* AOX CDS (*AOX1a*, *AOX1b*, *AOX1c*, *AOX1d*, and *AOX2*) were obtained by RT-PCR using primers listed in **Supplementary Table 2**, respectively.

For chloroplast expression, the coding sequence of five AOX mature proteins (full length AOX minus the mitochondrial targeting peptide) were fused to the *Arabidopsis* RbcS1A chloroplast targeting peptide (CTP) driven by the CaMV 35S promoter (P35S) in the binary vector pB003 (Fu et al., 2012). The resulting plasmids were respectively designated as C-mAOX1a, C-mAOX1b, C-mAOX1c, C-mAOX1d, and C-mAOX2.

For overexpressing the full length AOX proteins with their own targeting sequences, the five AOX CDS were fused to P35S in pB003, and the five resulting plasmids were named as W-AOX1a, W-AOX1b, W-AOX1c, W-AOX1d, and W-AOX2, respectively.

A cDNA fragment encoding the mature form of *Arabidopsis* PTOX (the coding sequence of PTOX minus its own targeting

peptide) was generated by RT-PCR. The amplified sequence was fused behind the coding sequences for the five AOX targeting peptide (TP) in pB003, respectively; the resulting plasmids were designated as AOX1aTP-mPTOX, AOX1bTP-mPTOX, AOX1cTP-mPTOX, AOX1dTP-mPTOX, and AOX2TP-mPTOX. The PTOX mature protein sequence was cloned into pB003 as control, in which only the initiation codon ATG was added in front of mature PTOX resulting in the plasmid ATG-mPTOX.

All constructs were confirmed by sequencing, then transferred into *Agrobacterium tumefaciens* strain GV3101 and further introduced into *im* by the floral dip method (Clough and Bent, 1998). Basta-resistant T1 transgenic plants were selected on soil by spraying 2-week-old seedlings with 150 mg/L Basta solution (Sangon Biotech, China), and verified by PCR.

RNA Extraction and RT-PCR Analysis

Total RNA was extracted from 3-week-old *Arabidopsis* leaves using the RNAPrep pure plant kit (Tiangen, China). RNA was reversely transcribed to the 1st strand cDNA using the PrimeScript II 1st strand cDNA Synthesis Kit (Takara, Japan). All the experiments above were performed according to the manufacturer's protocol. *ACTIN2* gene was used as control. PCR were performed with an initial pre-denaturation of 98°C 30 s, followed by 28 cycles of 98°C for 15 s, 55°C for 30 s, and 72°C for 1 min.

Subcellular Localization by Fluorescence Analysis of GFP-Tagged Proteins

To determine the subcellular location of AOXs with the *Arabidopsis* RbcS1A CTP, the five AOX mature CDS were respectively cloned behind the *Arabidopsis* RbcS1A CTP and inserted into pSPY-GFP (Zhang et al., 2018). The five fusion constructs were designated as C-mAOX1a-GFP, C-mAOX1b-GFP, C-mAOX1c-GFP, C-mAOX1d-GFP, and C-mAOX2-GFP, respectively.

To determine the subcellular location of AOXs with their own targeting peptides, the GFP sequence was inserted behind the AOX CDS in W-AOX1a, W-AOX1b, W-AOX1c, W-AOX1d, and W-AOX2; the resulting constructs were designated as W-AOX1a-GFP, W-AOX1b-GFP, W-AOX1c-GFP, W-AOX1d-GFP, and W-AOX2-GFP, respectively.

To determine the subcellular location of PTOX with different AOX targeting peptides, the five fragment of the AOX1aTP-mPTOX, AOX1bTP-mPTOX, AOX1cTP-mPTOX, AOX1dTP-mPTOX, and AOX2TP-mPTOX were respectively inserted before the GFP sequence in the plasmid pCAMBIA3300. The resulting constructs were designated as AOX1aTP-mPTOX-GFP, AOX1bTP-mPTOX-GFP, AOX1cTP-mPTOX-GFP, AOX1dTP-mPTOX-GFP, and AOX2TP-mPTOX-GFP.

All above constructs were introduced into the *Agrobacterium tumefaciens* GV3101 strain, and co-infiltrated with the p19 strain into *N. benthamiana* leaves for transient expression as described in Fu et al., 2012. The transfected plants were incubated at 23°C for 48–72h before taking images. Bright-field and fluorescent microscopy were performed on an Olympus Fluoview

FV1000 confocal laser scanning microscope (Olympus, Japan). The fluorescent images were taken with excitation at 488 nm and emission at 500–530 nm for detection of GFP. Mt-Mcherry were excited using 543 nm and detected in red detection channels of 570–625 nm. The chloroplast autofluorescence were excited at 594 nm and measured with an emission at 625–725 nm. *pGreen-35S:Mt-Mcherry* was used as mitochondrial marker.

Antibody Generation

Polyclonal antibodies were generated as described previously with minor modifications (Chen et al., 2000). Five AOX polyclonal antibodies were raised in rabbits against the specific and soluble coding region of each AOX expressed in *Escherichia coli* using the pGEX-4T.3 vector system (Takara, Japan). These proteins were purified by Glutathione Sepharose 4B (GE Healthcare, United States) affinity chromatography. Rabbits were immunized by serial injections of the purified specific and solubilized protein. Then, the serum were collected from immunized rabbits. Immune complexes were detected by the eECL Western Blot Kit (CWBIO, China) using a secondary antibody conjugated to horseradish peroxidase (Bioworld, United States). The chemiluminescent signals were captured with a CCD camera (Tanon 5200, China). The specific antigen peptide sequence of each AOX is listed in detail as follows:

AOX1a:ASTITLGEKTPMKEEDANQKKTENESTGGDAA
GGNNKGDKGIA;
AOX1c: SKMTFEKKKTSEEEEGSGDGVKVNQGNKG
EQLIV;
AOX1d: LSSDTSSPVSGNNQPENPIRTADGKVISTYW
GIP;
AOX2: GMSSASAMEKKDENLTVKKGQNGGGSVAVPSY
WGIETA.

Preparation of Total Leaf Proteins, Intact Chloroplast Proteins, and Immunoblotting Analysis

Total leaf proteins were extracted by grinding leaf material and resuspended in 2x SDS loading buffer [125 mM Tris-HCl, pH 6.8, 4% (w/v) SDS, 2% (v/v) 2-mercaptoethanol, 0.001% (w/v) bromophenol blue, 20% (v/v) glycerol], followed by incubation at 98°C for 5 min, centrifugation at 13,800 g for 10 min.

Intact chloroplasts were isolated using the Percoll gradient method (Perry et al., 1991; Bhuiyan et al., 2015). The 4-week-old *Arabidopsis* leaves were ground in a blender with ice-cold homogenization buffer (20 mM Tricine-KOH, pH 8.4, 450 mM sorbitol, 10 mM EDTA, pH 8.0, 10 mM NaHCO₃, and 0.1% BSA). Homogenates were then filtered through two layers of Miracloth. The filtrate was the total cell proteins, and crude chloroplasts were collected by centrifugation at 1,000 g for 10 min at 4°C. Resuspended crude chloroplasts in 1 mL of resuspension buffer (20 mM Tricine-KOH, pH 8.4, 300 mM sorbitol, 2.5 mM EDTA, and 5 mM MgCl₂) were gently overlaid on Percoll step gradients (40 and 80% v/v), and were centrifuged at 4,000 g for 20 min at 4°C. Intact chloroplasts were collected from the interface between the 40 and 80% Percoll layers with burned tips and washed once with resuspension buffer.

Immunoblotting analysis were conducted as described (Fu et al., 2012). Briefly, protein samples were electrophoresed through 12% SDS polyacrylamide gels and transferred to nitrocellulose membranes for immunoblotting analysis. The protein signals were visualized using the eECL Western Blot Kit (CWBIO, China) and captured with a CCD camera (Tanon 5200, China).

In vivo Chlorophyll Fluorescence Measurements

Chlorophyll fluorescence measurements were performed with Dual-PAM-100 fluorometer (Heinz-Walz, Germany) on intact leaves from wild-type (WT), *im*, W-AOX1b, and W-AOX2 transgenic plants grown for 7 weeks in soil. F_v'/F_m' was measured by rapid light curves. During this process, the leaves were irradiated for 30 s under different light intensities. F_v'/F_m' was calculated as $(F_m' - F_o')/F_m'$; Φ PSII was equal to $(F_m' - F)/F_m'$; 1-qP was defined as $(F_o'/F)(F_m' - F)/(F_m' - F_o')$; NPQ was calculated as $(F_m - F_m')/F_m'$. F_m is the maximum fluorescence in the dark-adapted state; F_m' is the maximum fluorescence in any light-adapted state; F_v' is the variable fluorescence equal to $(F_m' - F_o')$; F is the steady state fluorescence in the light; F_o' is the minimal fluorescence in any light-adapted state.

NPQ induction and dark kinetics measurements were performed as described previously (Fu et al., 2012). Plants were irradiated with actinic light of 1805 $\mu\text{mol m}^{-2}\text{s}^{-1}$ for 10 min following dark adaption. Relaxation data were acquired by shutting off the actinic source for an additional 5 min. During the entire time period, the fluorescence signals was superimposed with saturating 800-ms pulses of white light every 30 s.

Isolation of Thylakoid Membrane and Blue Native Gel Electrophoresis

Thylakoid membranes were isolated as described previously with minor modifications (Lima et al., 2006). For blue native gel analysis, leaves were ground with a blender in ice-cold grinding buffer and filtered through two-layers of Miracloth. The filtrate was centrifuged at 2,000 g for 5 min at 4°C, the pellet was resuspended in SH buffer (330 mM sorbitol, 50 mM HEPES, pH 8.0). Thylakoid membranes were isolated by centrifugation at 2,400 g for 2 min at 4°C. Isolated thylakoid membranes were resuspended in 50BT40G buffer (50 mM BisTris, pH 7.0, and 40% glycerol) to a final chlorophyll concentration of 1 mg mL⁻¹, and then solubilized with 1% (w/v) *n*-dodecyl- β -D-maltoside (Sigma-Aldrich, United States) for 5 min on ice. After centrifugation at 10,000 g for 10 min, the supernatant was mixed with 1/10 volume of BN sample buffer [100 mM BisTris-HCl, pH 7.0, 5% Serva blue G, 0.5 M 6-amino-*n*-caproic acid, 30% (w/v) sucrose]. Samples were loaded on a blue native gradient gel containing 5–13.5% polyacrylamide (Amresco, United States). Gel electrophoresis was performed at a constant voltage of 100 V for 6 h at 4°C.

Sequence Alignment and Phylogenetic Tree

AOXs and PTOX mature protein sequences in *Arabidopsis* were compared in multiple sequence alignment using ClustalW

program of MEGA6. The Neighbor-Joining method was used to build a phylogenetic tree with the bootstrapping value set at 1,000 replicates (Felsenstein, 1985; Saitou and Nei, 1987; Tamura et al., 2013).

Accession Numbers

The sequence data for the following Arabidopsis genes can be found in the TAIR database¹: AT3G22370 (AOX1a), AT3G22360 (AOX1b), AT3G27620 (AOX1c), At1g32350 (AOX1d), At5G64210 (AOX2), and At4G22260 (PTOX), AT3G18780 (ACTIN2), AT1G12770 (ISE1).

RESULTS

AOXs Substitute for the Function of PTOX After Targeting Into Chloroplasts

The Arabidopsis genome contains one PTOX (At4g22260) and five AOX members, including AOX1a (At3g22370), AOX1b (At3g22360), AOX1c (At3g27620), AOX1d (At1g32350), and AOX2 (At5g64210) (Saisho et al., 1997; Wang and Fu, 2016). Sequence alignment and phylogenetic analysis showed that Arabidopsis PTOX and AOXs are distantly related with 26% amino acid sequence identity (Supplementary Figure 1). Within the AOX family, AOX1a-1d are more closely related to each other, while AOX2 is distantly related to the AOX1 subfamily members. Among the four AOX1 members, AOX1b and AOX1c are the most closely related pair and evolved from a recent gene duplication event.

Although AOXs are UQH₂ oxidases and PTOX is a PQH₂ oxidase *in vitro* (Wang and Fu, 2016), AOXs could be PQH₂ oxidases *in planta*, which was illustrated by the fact that the chloroplast-localized AOX1a and AOX2 acted as PQH₂ oxidases in Arabidopsis (Fu et al., 2012). Here we further examined whether the other AOXs could function as PQH₂ oxidases in chloroplasts.

We generated constructs containing AOX coding sequences with their targeting peptides replaced by the chloroplast-specific transit peptide of RbcS1A. The resulting constructs were referred as C-mAOX1a, C-mAOX1b, C-mAOX1c, C-mAOX1d, and C-mAOX2, respectively (Figure 1A). Then we introduced these constructs into the PTOX deficient mutant (*im*), and analyzed the phenotypes of transgenic plants of the T₂ generation (Figure 1). Consistent with the previous study (Fu et al., 2012), none of the transgenic *im* plants bearing C-mAOX1a (more than 50 independent transgenic lines) showed a fully recovered WT like green phenotype, but leaf variegation was much less severe compared to *im* (Figure 1B). Transgenic *im* plants with the other C-mAOXs did not exhibit any variegation phenotype, and grew normally like WT plants (Figures 1C–F). We performed RT-PCR to examine the RNA level of AOXs in these transgenic plants and found that all transgenes are expressed well while the endogenous transcripts of all 5 AOXs are barely detectable in *im* and WT (Figure 1).

To examine whether the engineered C-mAOX proteins were successfully imported into chloroplasts under the guidance of the RbcS1A targeting peptide, we transiently expressed these recombinant C-mAOXs fused with GFP at their C-termini in *N. benthamiana*. Confocal images showed that all five C-mAOXs are targeted into chloroplasts, as illustrated by the overlay of the green fluorescence signals of GFP-tagged C-mAOXs with chlorophyll auto-fluorescence of chloroplasts (Figure 2).

Previous studies suggested that the ability to complement *im* was used as a proxy for the relative *in vivo* PQH₂ oxidase activity in chloroplasts (Fu et al., 2005, 2009, 2012). Taken together, we concluded that all 5 chloroplast-localized AOXs could act as PQH₂ oxidases and substitute for the function of PTOX to various degrees. Moreover, the PQH₂ oxidase activity of AOX1a may be weaker than those of the other four homologs *in planta* and hence not able to fully complement the defect in *im* plastids. AOX1a has presumably been optimized for UQH₂ as a substrate in mitochondrial membranes.

Overexpression of the Full Length AOX1b or AOX2 in *im* Complements Its Variegation Phenotype

It is well accepted that AOXs are mitochondrial proteins. RNAseq analysis showed that AOXs are expressed at relatively low levels. In detail, AOX1a has a slightly lower expression level (about 15 RPKM) compared to PTOX, and the other four AOX genes are barely expressed in wild type plants (Supplementary Figure 2). Mitochondrial AOXs could dissipate excess reducing power in chloroplasts and protect photosynthesis from photo-damage through the Mal/OAA shuttle (Yoshida et al., 2011b; Zhang et al., 2016). Therefore, it is possible that overexpression of AOX might reduce the variegation phenotype of *im* through the crosstalk between mitochondria and chloroplasts. The other possibility is that overexpressed AOX could overflow from mitochondria and enter chloroplasts. This scenario was previously demonstrated that when overexpression of AOX2 in *im* enabled it to enter chloroplasts and replace the function of PTOX in Arabidopsis (Fu et al., 2012).

To examine these possibilities, we overexpressed the full length AOXs in *im*, and performed analysis on T₂ generation transgenic plants (Figure 3). More specifically, *im* plants were transformed with the full-length coding sequences of all five AOXs driven by the CaMV 35S promoter (named as W-AOXs, standing for the whole sequence of AOXs, in contrast to the mature AOX sequences tested in Figures 1, 2), separately (Figure 3A). In agreement with the previous study (Fu et al., 2012), transgenic *im* plants bearing the W-AOX2 construct produced green leaves similar to WT, distinct from the striking variegation phenotype of *im* (Figure 3F). Besides W-AOX2 plants, transgenic *im* plants with W-AOX1b also showed a green leaf phenotype similar to WT (Figure 3C), indicating that AOX1b could substitute for the function of PTOX as well as AOX2. On the other hand, transgenic *im* plants of W-AOX1a, W-AOX1c, and W-AOX1d displayed a typical variegation phenotype the same as *im* (Figures 3B,D,E), suggesting that overexpression of W-AOX1a, W-AOX1c, or W-AOX1d failed to complement the

¹<https://www.arabidopsis.org>

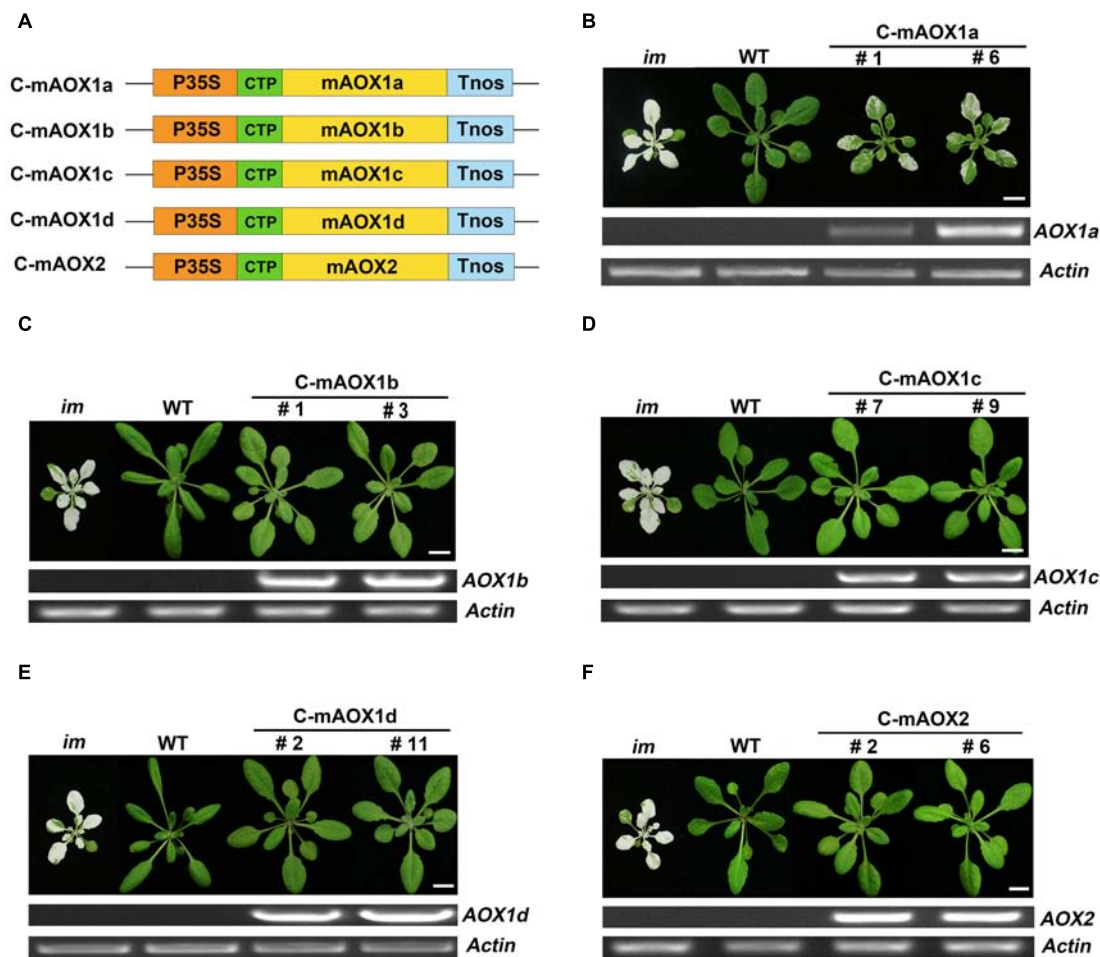


FIGURE 1 | Expression of C-mAOX constructs in *im*. **(A)** Schematic diagram of C-mAOX1a, C-mAOX1b, C-mAOX1c, C-mAOX1d, and C-mAOX2. P35S, Cauliflower Mosaic Virus 35S promoter; Tnos, terminator of nos (nopaline synthetase); CTP, chloroplast targeting sequence from *Arabidopsis thaliana* RbcS1A (Rubisco small subunit); mAOX1a, mAOX1b, mAOX1c, mAOX1d, and mAOX2 are the mature proteins (the full length AOX minus the targeting peptide). **(B–F)** Phenotypes of *im* mutant, WT, and transgenic *im* mutants carrying 35S-driven C-mAOX1a, C-mAOX1b, C-mAOX1c, C-mAOX1d, and C-mAOX2. Expression of C-mAOX in *im* was examined at the RNA level by RT-PCR. All plants were grown for 4 weeks with a photoperiod of 16 h light/8 h dark cycle under light ($\sim 100 \mu\text{mol}\cdot\text{m}^{-2}\cdot\text{s}^{-1}$) after initial low light ($\sim 20 \mu\text{mol}\cdot\text{m}^{-2}\cdot\text{s}^{-1}$) growth for 5 days as described in the “Materials and Methods” section. Actin was used as quantity control. Bars = 1 cm.

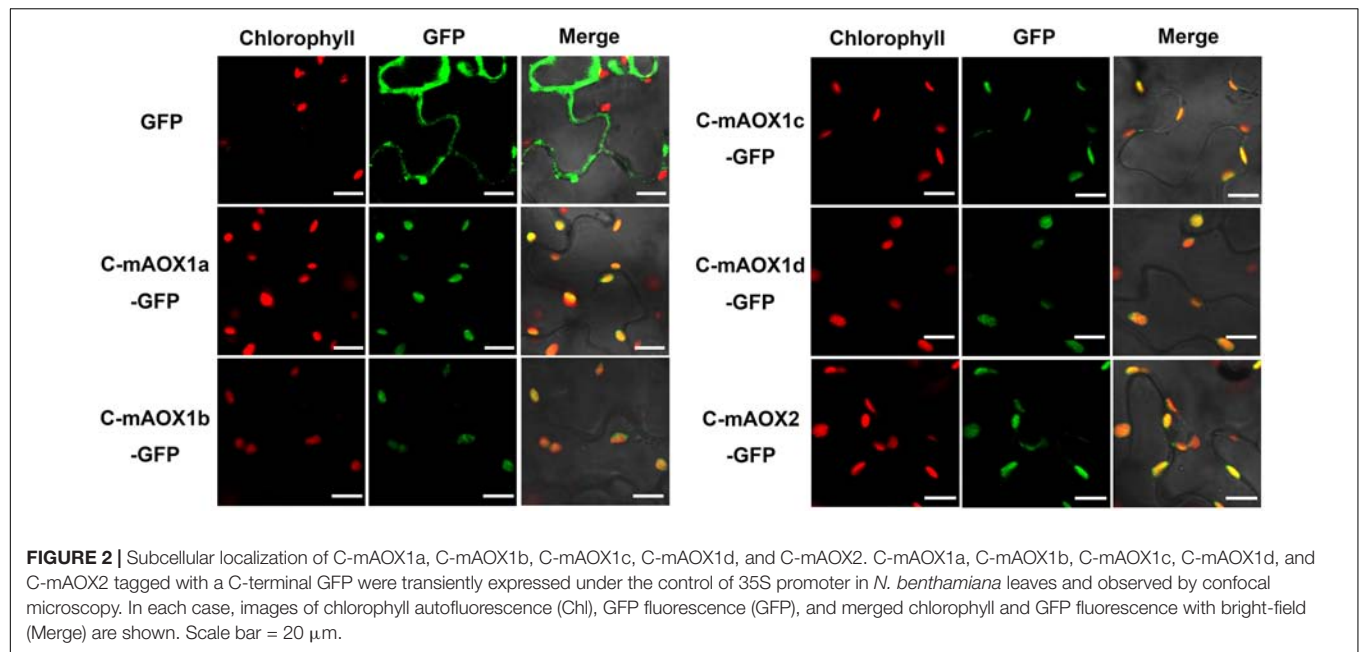
function of PTOX. This revealed remarkable differences among AOX proteins with respect to replacing the function of PTOX when they are overexpressed in *im*.

To test whether the distinct phenotypes of transgenic plants with different W-AOX constructs could be attributed to inefficiency in gene expression, we carried out immunoblotting analysis on transgenic plants with the respective AOX antibodies. Four polyclonal antibodies against AOX proteins (AOX1a, AOX1c, AOX1d, and AOX2) were raised against a specific peptide of each AOX, which was obtained from recombinant expression in *E. coli*. However, we failed to obtain a suitable antibody against AOX1b due to the difficulty to express a specific peptide of AOX1b in *E. coli*. Fortunately, the AOX1c antibody could detect AOX1b well, because of the high sequence identity (81%) between AOX1b and AOX1c. Immunoblotting assays showed that each AOX was overexpressed well in the corresponding transgenic *im* plants, in which much more

proteins were accumulated than that in non-transgenic *im* or WT (**Figure 3**), indicating that the phenotypic differences of transgenic plants do not result from different protein levels. Notably, a trace amount of AOX1a was observed in *im* and WT, while the other four AOX proteins were barely detected in *im* and WT indicating low expression levels of AOX proteins in *Arabidopsis* under normal growth conditions (**Figure 3**).

W-AOX1b and W-AOX2 Are Targeted Into Chloroplasts as Revealed by the Fluorescence Analysis of GFP-Tagged AOXs

All five AOXs are predicted to be present in mitochondria by various targeting prediction programs (**Supplementary Table 1**), and they could function as PQH₂ oxidases when targeted to chloroplasts (**Figure 1**). While overexpression of W-AOX1b and



W-AOX2 in *im* could rescue the mutant variegation phenotype, this was not observed when W-AOX1a, W-AOX1c, or W-AOX1d was overexpressed in *im* (Figure 3). This prompted us to consider that AOX1a, AOX1c, and AOX1d should be exclusively localized in mitochondria whereas AOX1b could be a mitochondria and chloroplasts dually targeted protein as AOX2. To examine this possibility, we tagged all five full-length AOXs (W-AOXs) with GFP at their C-termini, and transiently expressed these fusion proteins in *N. benthamiana*. Fluorescence image analysis showed that all five AOXs are mostly located in mitochondria as indicated by the fact that the green fluorescence signals of GFP-tagged W-AOXs overlaid well with the red fluorescence signals of Mt-Mcherry, the specific mitochondrial marker (Figure 4A). In contrast, several green fluorescence signals from GFP-tagged W-AOX1b and W-AOX2 evidently overlapped with the auto-fluorescence signals of chloroplasts (Figure 4B), indicating that, in addition to AOX2, AOX1b is also dually targeted to mitochondria and chloroplasts. With W-AOX1a, W-AOX1c, and W-AOX1d, we did not observe signals from the GFP-tagged proteins matching the auto-fluorescence signals of chloroplasts, indicating that these three AOXs are exclusively or predominantly localized in mitochondria.

W-AOX1a Is Also Targeted to Chloroplasts as Shown by Immunoblotting

To further verify the localization of AOXs in the transgenic *im* plants overexpressing W-AOXs, we purified chloroplasts by the Percoll gradient method and examined the distribution of AOXs in isolated chloroplasts by immunoblotting (Figure 5). The analysis showed that all five AOXs are barely detectable with their respective antibodies in total cell extracts or in purified chloroplast samples from *im* or WT plants (Figure 5A). However,

a remarkably high level of each AOX was observed in the total cell samples from their respective transgenic *im* plants (Figure 5A). As expected, a substantial amount of AOX1b and AOX2 was observed in the chloroplast samples from W-AOX1b and W-AOX2 transgenic plants (Figure 5A) consistent with the plant phenotypes and the fluorescence analysis of GFP-tagged W-AOX1b and W-AOX2 (Figures 3, 4). In contrast, no detectable AOX protein was observed in the chloroplast samples from transgenic *im* plants overexpressing W-AOX1c or W-AOX1d (Figure 5A), also in agreement with the phenotypes of transgenic plants and the fluorescence analysis of GFP-tagged W-AOX1c and W-AOX1d (Figures 3, 4). To our surprise, a substantial amount of AOX1a was observed in the purified chloroplast samples from transgenic *im* plants overexpressing W-AOX1a (Figure 5A), which is in striking contrast to the variegation phenotype in the W-AOX1a transgenic *im* plants (Figure 3B) and the fluorescence analysis of GFP-tagged W-AOX1a (Figure 4B).

Given the high accumulation of AOX1a in transgenic *im* plants overexpressing W-AOX1a, it is possible that the detected signals of AOX1a in chloroplasts may arise from the contamination of mitochondrial samples. In order to examine the extent of mitochondrial contamination, we included a mitochondrial specific RNA helicase, ISE1 (Stonebloom et al., 2009), in the immunoblotting titration experiments (Figure 5B). The result showed that the ISE1 signals were remarkably strong in the total cell samples of all five transgenic plants, but not detectable in their chloroplast samples, demonstrating that the purified chloroplasts were barely contaminated with mitochondria (Figure 5B). The immunoblotting assays showed that AOX1c and AOX1d are absent in the chloroplast fractions, again confirming that they are mitochondrial specific proteins. The content of AOX1a, AOX1b, and AOX2 in isolated chloroplasts was much lower than that in the total cell samples,

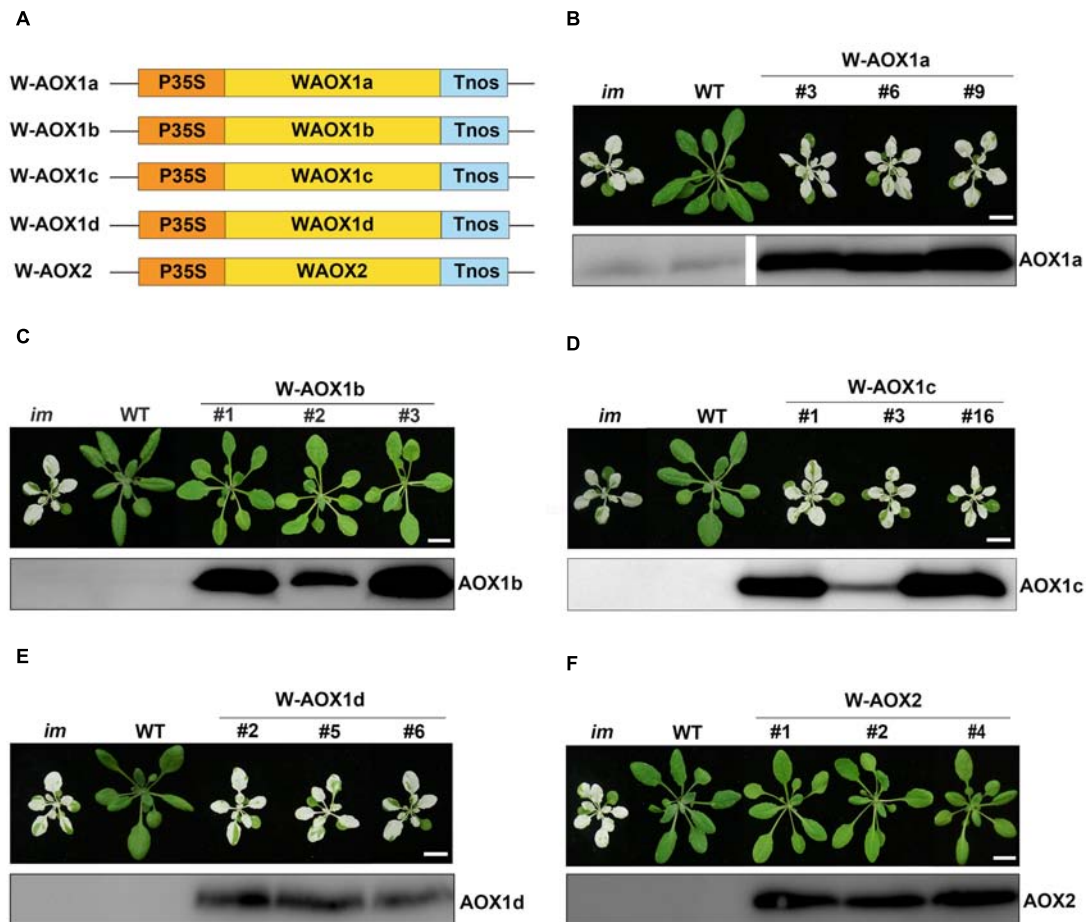


FIGURE 3 | Expression of W-AOX constructs in *im*. **(A)** Schematic diagram of W-AOX1a, W-AOX1b, W-AOX1c, W-AOX1d, and W-AOX2 constructs. P35S, Cauliflower Mosaic Virus 35S promoter; Tnos, terminator of nos (nopaline synthetase); WAOX1a, WAOX1b, WAOX1c, WAOX1d, and WAOX2 are the full length coding sequences. **(B–F)** Phenotypes of *im* mutant, WT, and three independent lines of transgenic *im* mutants carrying 35S-driven W-AOX1a, W-AOX1b, W-AOX1c, W-AOX1d, and W-AOX2. All plants were grown for 4 weeks with a photoperiod of 16 h light/8 h dark cycle under light ($\sim 100 \mu\text{mol}\cdot\text{m}^{-2}\cdot\text{s}^{-1}$) after initial low light ($\sim 20 \mu\text{mol}\cdot\text{m}^{-2}\cdot\text{s}^{-1}$) growth for 5 days as described in the “Materials and Methods” section. Total cell proteins was isolated from 10 mg of fresh leaf tissue, and subjected to 12% SDS-PAGE and probed with the corresponding AOX antibodies. Bars = 1 cm.

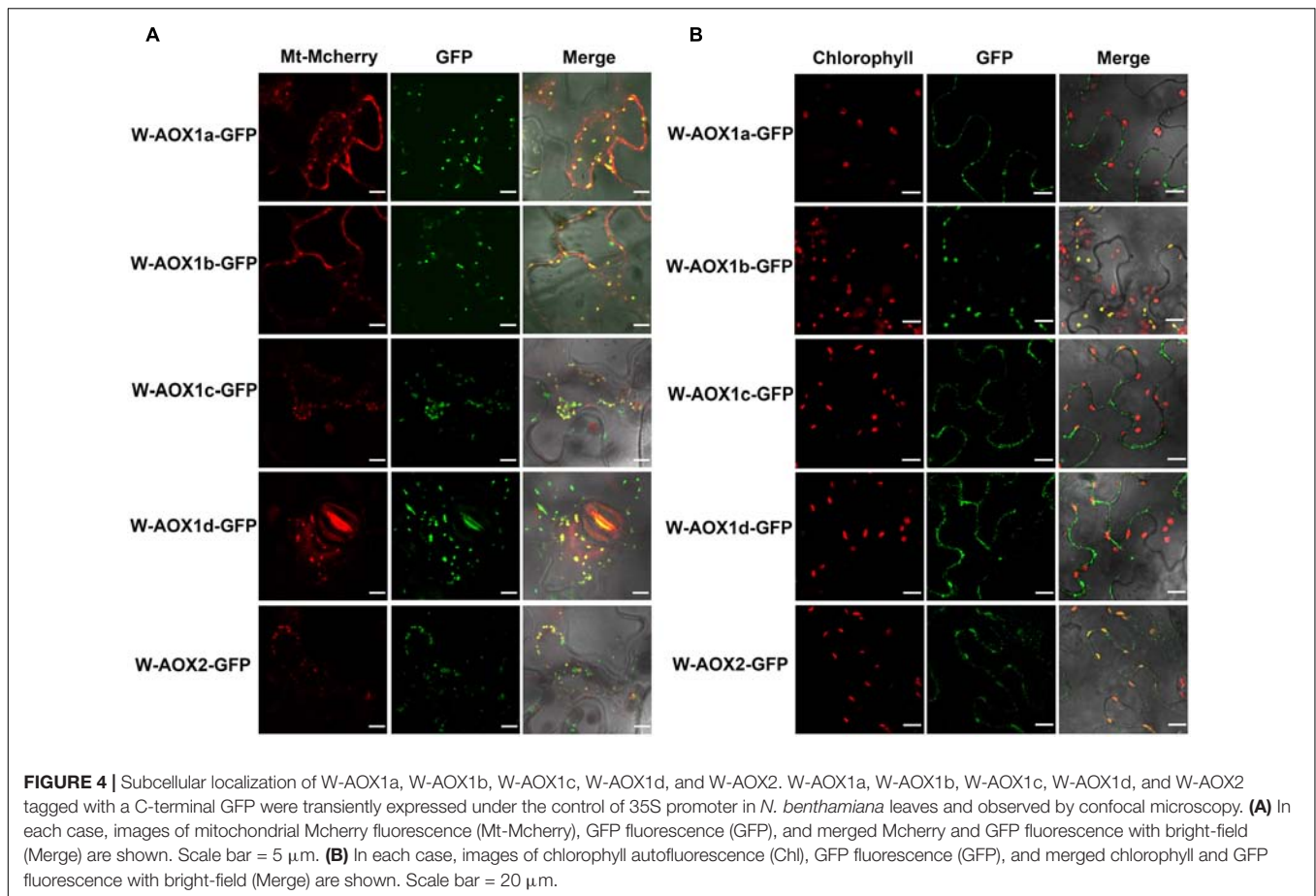
suggesting that the majority of the overexpressed AOX1a, AOX1b, and AOX2 are not present in chloroplasts, and should be normally in mitochondria. Based on the titration assays, we estimated that approximate 10% of AOX2, 4% of AOX1a and AOX1b can be sorted into chloroplasts in the respective transgenic plants (Figure 5B). This further confirmed that, AOX1a, the major AOX in plant cells, is also dually targeted to mitochondria and chloroplasts.

The immunoblotting assays showed AOX1a is a mitochondria and chloroplasts dually targeted protein, as AOX1b and AOX2. However, overexpressing W-AOX1b and W-AOX2 in *im* plants fully rescued the variegation phenotype of the mutant whereas transgenic *im* plants overexpressing W-AOX1a were as variegated as *im* (Figure 3). This phenotypic difference of transgenic plants carrying W-AOX1a, W-AOX1b, and W-AOX2 may be caused by the difference of PQH₂ oxidase activity. When targeted into chloroplasts, C-mAOX1a is only able to partially rescue PTOX function in *im* plants, in contrast to

C-mAOX1b and C-mAOX2 that fully rescue the *im* variegation phenotype (Figure 1), indicating that the PQH₂ oxidase activity of AOX1a may be very low. Therefore, although a small amount of AOX1a can enter chloroplasts, the resulting PQH₂ oxidase activity in chloroplasts is very low and not sufficient to rescue the variegation phenotype of *im*.

Targeting Peptides of AOX1a, AOX1b, and AOX2 Can Direct the Mature Form of PTOX Into Chloroplasts

The immunoblotting assays, but not the fluorescence analysis of GFP-tagged proteins, showed that W-AOX1a is a dually targeted protein in transgenic *im* plants overexpressing W-AOX1a (Figures 4, 5). The inconsistency of these two analyses could be explained by that the low amount of AOX1a present in chloroplasts cannot be detected by the fluorescence analysis. Another possibility is that some AOX proteins are mis-targeted



when overexpressed. Therefore, we think a third assay is necessary to clarify whether W-AOX1a is a dually targeted protein to mitochondria and chloroplasts.

A previous study showed that PTOX accumulates in large excess and that a trace amount of PTOX is sufficient to sustain normal chloroplast development and function (Fu et al., 2009). Therefore, the *im* mutant could be a highly sensitive tool to test whether a plant protein can be targeted into chloroplasts by examining the effect of its targeting peptide fused with the mature form of PTOX in *im* plants. If a targeting peptide directs PTOX into chloroplasts, the transgenic plants should show a green phenotype and normal growth; otherwise, the transgenic *im* plants should remain as variegated as *im*. Notably, it was confirmed in a very recent report (Sharma et al., 2019).

At first, we transformed the mature form of PTOX lacking its CTP into *im*, and found that all transgenic plants showed the same variegation phenotype as *im*, indicating that chloroplast localization is required for the function of PTOX (Figures 6A,B). Then we generated constructs with the targeting peptides of AOXs fused with the mature PTOX and introduced these constructs into *im* (Figure 6). As expected, transgenic *im* plants carrying AOX1bTP-mPTOX or AOX2TP-mPTOX showed a normal green growth, and transgenic *im* plants carrying AOX1cTP-mPTOX or AOX1dTP-mPTOX showed the same variegation phenotype as *im*. These results showed that the

targeting peptides of AOX1b and AOX2 target the mature PTOX into chloroplasts, while the targeting peptide of AOX1c or AOX1d failed to do so, implying that AOX1c and AOX1d are exclusively localized in mitochondria. Moreover, the AOX1aTP-mPTOX transgenic plants were green and grew normally as WT (Figure 6C) indicating that the targeting peptide of AOX1a can direct the mature PTOX into chloroplasts as well. To confirm these findings, we performed immunoblotting analyses on total cell protein samples and Percoll gradient-purified chloroplast samples from these transgenic plants with an antibody against PTOX. Trace amounts of PTOX were observed in the chloroplast samples from AOX1aTP-mPTOX, AOX1bTP-mPTOX, and AOX2TP-mPTOX transgenic lines, but no PTOX was detected in the chloroplast samples from ATG-mPTOX, AOX1cTP-mPTOX, or AOX1dTP-mPTOX transgenic lines (Figure 6). The phenotypic difference of transgenic *im* plants expressing W-AOX1a and AOX1aTP-mPTOX demonstrated again that the PQH₂ oxidase activity of AOX1a may be very low.

In addition, we conducted a fluorescence analysis with the transient expression system, in which the above recombinant proteins were tagged with GFP at their C-termini and transiently expressed in *N. benthamiana*. The same results were observed as with the localization analysis of GFP-tagged W-AOXs in Figure 4. The fluorescence signals analysis showed that AOX1bTP-mPTOX and AOX2TP-mPTOX were dually

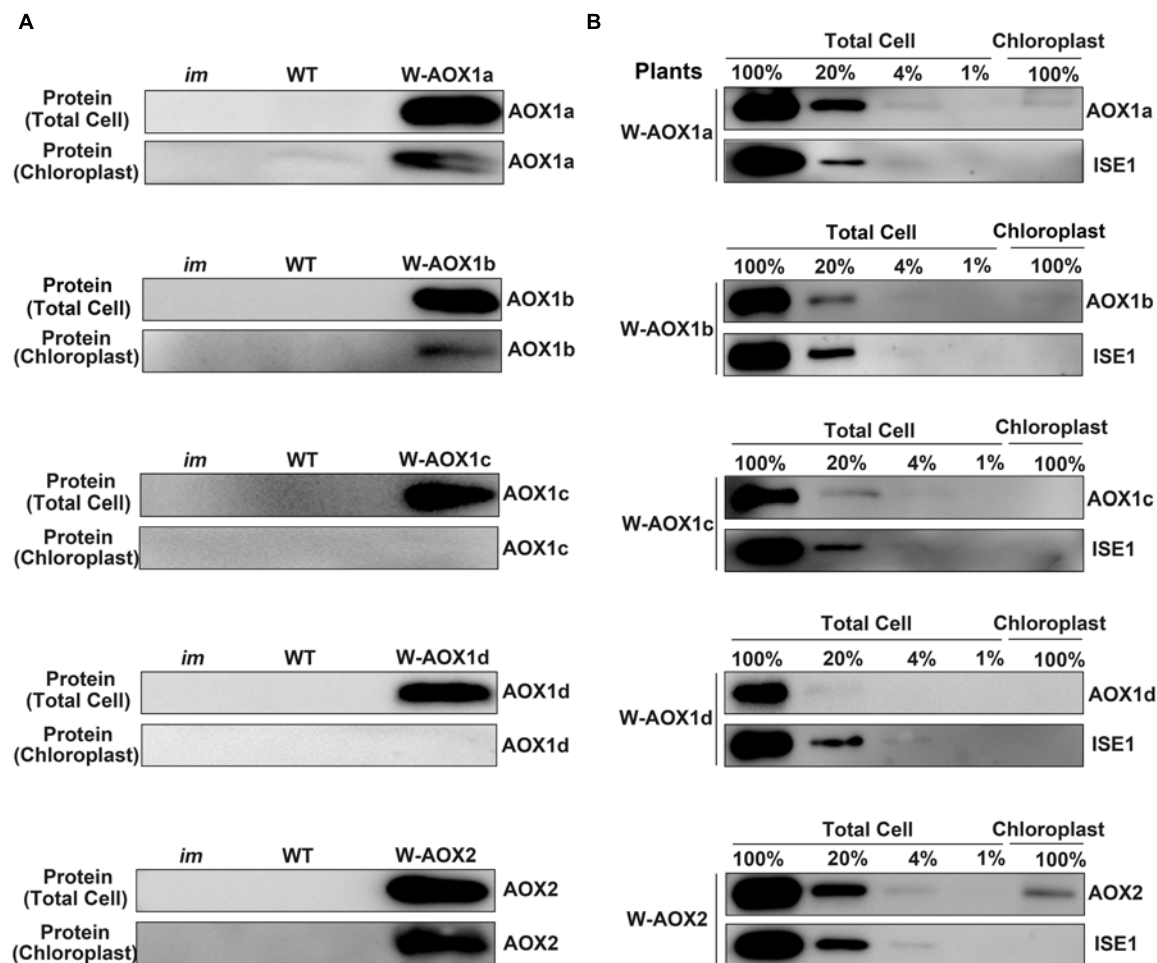


FIGURE 5 | W-AOX1a, W-AOX1b, and W-AOX2 are present in chloroplasts of the overexpression lines. **(A)** Immunoblotting analyses. Rosette leaves from 4-week-old plants as in **Figure 3** served as the source of total cell proteins and of chloroplast membranes from lysed, Percoll gradient-purified chloroplasts (designated chloroplasts). Equal protein amounts were electrophoresed through 12% SDS polyacrylamide gels, and immunoblotting analyses were performed with the corresponding AOX antibodies. **(B)** Total cell proteins or proteins from gradient purified chloroplasts were isolated from the rosette leaves of 4-week-old W-AOX1a, W-AOX1b, W-AOX1c, W-AOX1d, and W-AOX2 plants. Samples containing equal chlorophyll amounts ($2 \mu\text{g}$ chlorophyll) were electrophoresed through 12% SDS polyacrylamide gels, and immunoblotting analyses were performed with antibodies against the corresponding AOX, and ISE1, a highly expressed mitochondrial-specific protein (Stonebloom et al., 2009). The gels contained a dilution series (100, 20, 4, and 1%) of total cell proteins.

targeted proteins present in mitochondria and chloroplasts; while both AOX1cTP-mPTOX and AOX1dTP-mPTOX were exclusively localized in mitochondria (**Supplementary Figure 4**). Fluorescence signals of the GFP-tagged AOX1aTP-mPTOX barely overlapped with the auto-fluorescence of chloroplasts (**Supplementary Figure 4**), consistent with the result of **Figure 4B**, suggesting that the amount of protein entering chloroplasts could be below the detecting limit of the fluorescence analysis.

Overexpressed W-AOX1b and W-AOX2 Function Efficiently in Chloroplasts, but Differ From PTOX

Transgenic *im* plants overexpressing W-AOX1b and W-AOX2 showed a green leaf appearance, but they differed from WT

with longer and thinner leaves (**Figure 3**). We suspected that AOX1b and AOX2 cannot completely replace PTOX in chloroplasts, considering that their PQH₂ oxidase activities are lower than PTOX. We conducted *in vivo* chlorophyll fluorescence analysis to determine whether the photosynthetic capacity is compromised in transgenic *im* plants overexpressing W-AOX1b and W-AOX2. The F_v'/F_m' , which represents the maximum efficiency of PSII photochemistry under different photon flux densities, was remarkably reduced in *im* (**Figure 7**). The F_v'/F_m' values of W-AOX1b and W-AOX2 transgenic plants were similar as for WT indicating that the impaired PSII in *im* was restored by W-AOX1b and W-AOX2. ΦPSII , the quantum efficiency of PSII photochemistry at different photon flux densities (Maxwell and Johnson, 2000), in both W-AOX1b and W-AOX2 transgenic plants were slightly higher than for WT and *im* (**Figure 7**). The parameter 1-qP, which reflects the redox state of the Q_A electron

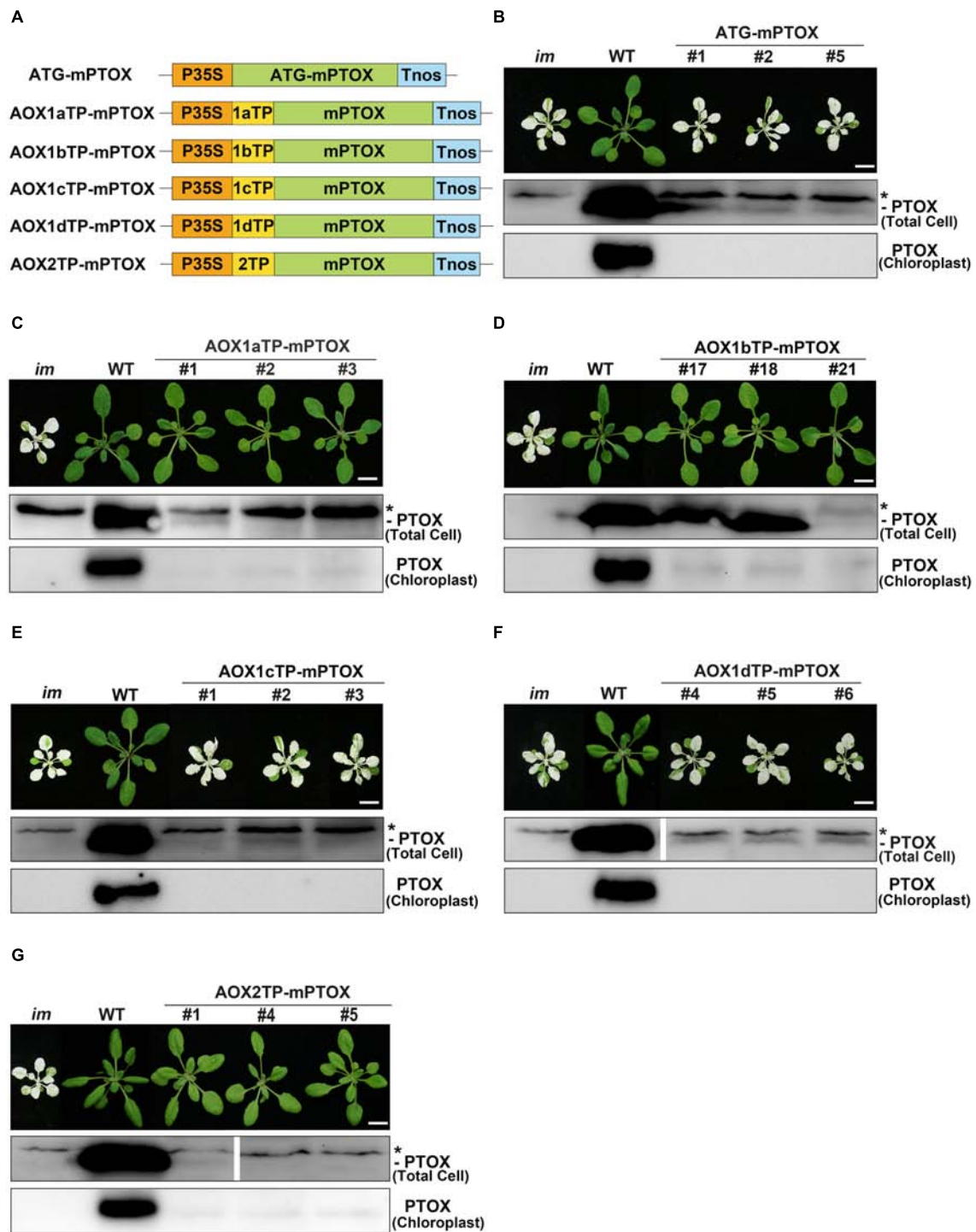


FIGURE 6 | Expression of AOXTP-mPTOX constructs in *im*. **(A)** Schematic diagram of ATG-mPTOX, AOX1aTP-mPTOX, AOX1bTP-mPTOX, AOX1cTP-mPTOX, AOX1dTP-mPTOX, and AOX2TP-mPTOX constructs. P35S, Cauliflower Mosaic Virus 35S promoter; Tnos, terminator of nos (nopaline synthetase); ATG, initiation codon; 1aTP, AOX1a targeting sequence; 1bTP, AOX1b targeting sequence; 1cTP, AOX1c targeting sequence; 1dTP, AOX1d targeting sequence; 2TP, AOX2 targeting sequence. mPTOX, mature peptide sequence of PTOX. **(B–G)** Phenotypes of *im* mutant, WT, and three independent lines of transgenic *im* mutants carrying 35S-driven ATG-mPTOX, AOX1aTP-mPTOX, AOX1bTP-mPTOX, AOX1cTP-mPTOX, AOX1dTP-mPTOX, and AOX2TP-mPTOX. All plants were grown for 4 weeks with a photoperiod of 16 h light/8 h dark cycle under light ($\sim 100 \mu\text{mol}\cdot\text{m}^{-2}\cdot\text{s}^{-1}$) after initial low light ($\sim 20 \mu\text{mol}\cdot\text{m}^{-2}\cdot\text{s}^{-1}$) growth for 5 days as described in the “Materials and Methods” section. Total cell proteins were isolated from 10 mg fresh weight of leaf tissue (Total Cell). Chloroplast proteins were isolated from pellets obtained by centrifugation of lysed, Percoll gradient-purified chloroplasts (corresponding to $2 \mu\text{g}$ of chlorophyll). The protein samples were subjected to 12% SDS-PAGE and probed with PTOX antibody. Asterisk (*) marks unspecific bands detected by an antibody against PTOX. Bars = 1 cm.

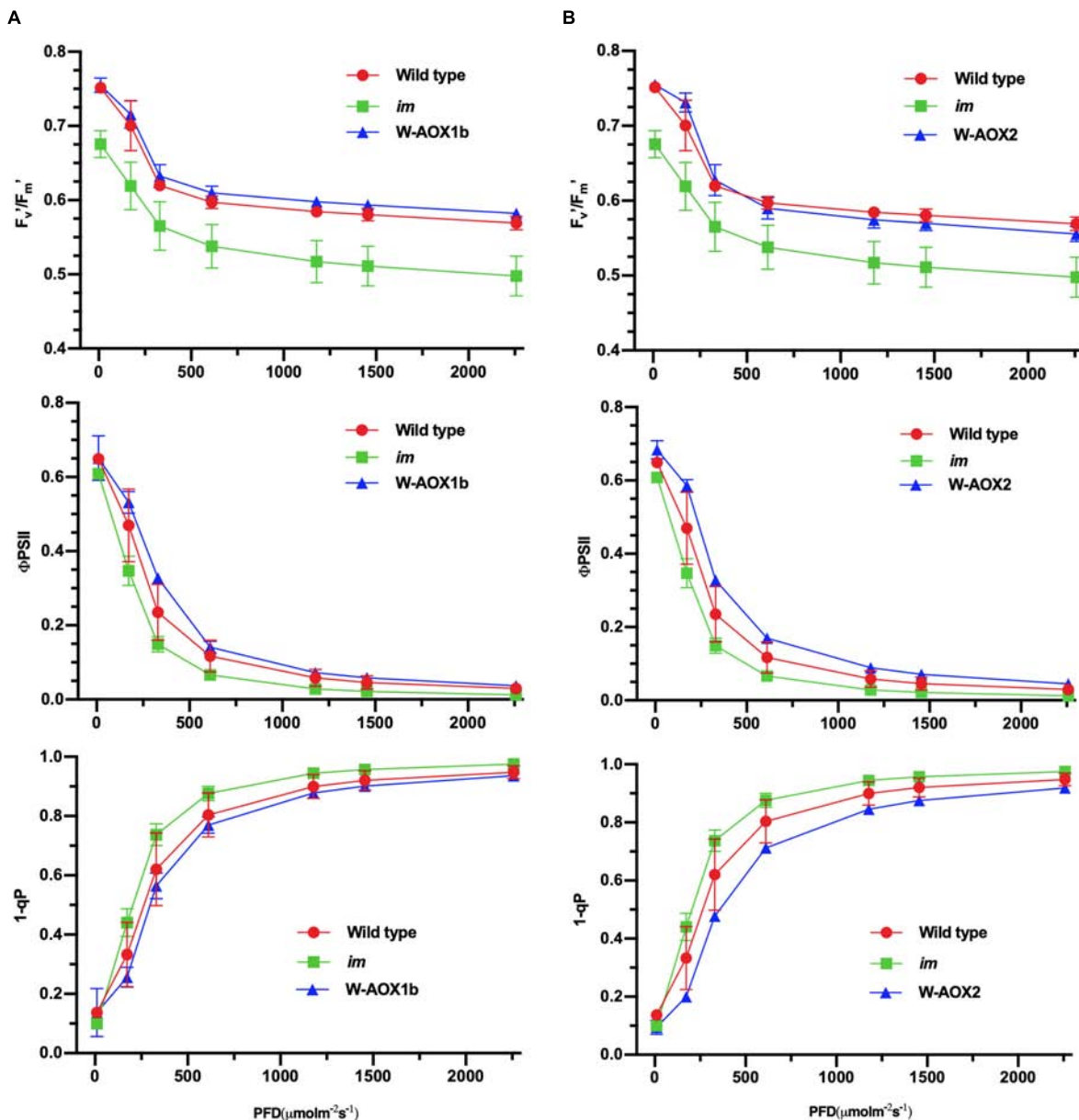


FIGURE 7 | Chlorophyll *a* fluorescence measurements. Chlorophyll fluorescence parameters were measured on intact leaves from W-AOX1b (A) and W-AOX2 (B) and wild-type and *im* grown for 7 weeks in soil under the conditions as described in the “Materials and Methods” section. The parameters included the following: F_v'/F_m' , the maximum efficiency of PSII photochemistry under different photo flux densities (PFD); Φ_{PSII} , the quantum efficiency of PSII photochemistry at different photo flux densities; $1-qP$, the redox state of the Q_A electron acceptor of PSII (Maxwell and Johnson, 2000; Müller et al., 2001).

acceptor of PSII, was lower in WT and transgenic plants than in *im* plants (Figure 7). This result indicated a more reduced PQ pool in *im*, whereas the PQ pool redox state in WT and transgenic plants is more balanced.

Non-photochemical quenching (NPQ), a measure of the ability of plants to dissipate excess light energy as heat (Müller et al., 2001), was found to be similar in *im* and W-AOX1b transgenic plants but lower than in WT (Figure 8A, left). In W-AOX2 transgenic plants, NPQ was close to that of *im* under light intensities less than $600 \mu\text{mol m}^{-2}\text{s}^{-1}$,

but similar to WT under high light intensities ($\geq 600 \mu\text{mol m}^{-2}\text{s}^{-1}$) (Figure 8A, right). This indicated that with increasing light intensity, AOX2 could dissipate excess light energy as heat more efficiently than AOX1b. The rapid induction of NPQ and the dark relaxation kinetics revealed that total NPQ is slightly higher in WT and transgenic plants than in *im* during the induction phase (Figure 8B). Taken together, most parameters were similar in the transgenic and WT plants, suggesting that steady state photosynthesis was not seriously perturbed by the presence of AOX1b and AOX2,

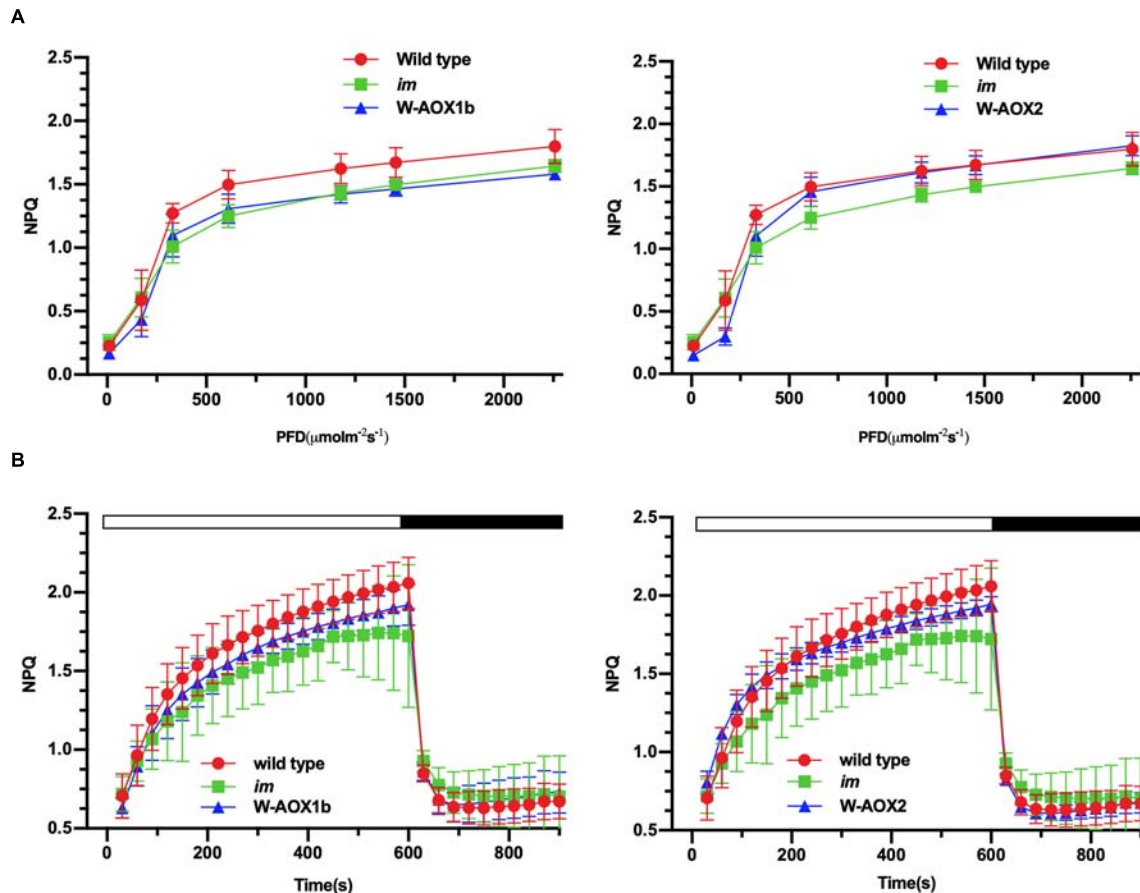


FIGURE 8 | NPQ analyses. Steady state light response NPQ (A) and rapid induction and dark relaxation NPQ kinetics (B) were measured on intact leaves from wild-type, *im*, W-AOX1b, and W-AOX2 seedlings grown for 7 weeks in soil under low light ($20 \mu\text{mol}\cdot\text{m}^{-2}\cdot\text{s}^{-1}$) for 5 days at 16-h light/8-h dark daylight cycle, and then were transferred to the normal growth condition (23°C , 16-h light/8-h dark daylight cycle, $100 \mu\text{mol}\cdot\text{m}^{-2}\cdot\text{s}^{-1}$) as described in the “Materials and Methods” section. The data represent the average \pm SD of four independent experiments.

but there were subtle differences between WT and these transgenic plants.

To investigate whether PSII assembly is affected in W-AOX1b and W-AOX2 transgenic plants, we examined the accumulation of photosynthetic complexes in thylakoid membranes by BN-PAGE. The results showed that the levels of the PSII supercomplexes (SCs) were almost the same in green tissues of *im*, WT, and both transgenic plants (Supplementary Figure 5).

DISCUSSION AND CONCLUSION

Alternative oxidase is a terminal oxidase residing in the mitochondrial inner membrane to govern the balance of carbon and energy metabolism in mitochondria. Similarly, PTOX is a plastid terminal oxidase in the thylakoid membrane to maintain the PQ pool redox balance in chloroplasts (Wang and Fu, 2016). Here, taking advantage of Arabidopsis PTOX deficient mutant, we examined the functional relevance of AOXs and PTOX.

AOXs Can Function as PQH₂ Oxidases in Chloroplasts

Chloroplast PTOX and mitochondrial AOXs originated from an ancient di-iron oxidase and diverged early during evolution even before the endosymbiotic events giving rise to mitochondria and chloroplasts (McDonald and Vanlerberghe, 2006; Nobre et al., 2016). In agreement with their long divergent history, Arabidopsis PTOX and AOXs share a very low sequence identity, about 26% (Supplementary Figure 1). In structural aspect, PTOX and AOXs have their own unique features, for instance, the dimerization domain at the N-termini of AOXs and the extra sequence at the C-terminus of PTOX (Supplementary Figure 1; Fu et al., 2005, 2009). Given the structural difference and the different substrates available in their subcellular compartment, AOXs and PTOX have developed their substrate specificities for UQH₂ and PQH₂, respectively. Indeed, *in vitro* enzyme assays showed that PTOX specifically uses PQH₂ as substrate and AOX only uses UQH₂ (Josse et al., 2003; Fu et al., 2012; Yu et al., 2014).

However, targeting AOX1b, AOX1c, AOX1d, and AOX2 to chloroplasts rescued the abnormal phenotype of *im*, whereas

targeting AOX1a to chloroplasts partially attenuated the leaf variegation of the mutant (**Figure 1**), demonstrating that all five AOXs could act as PQH₂ oxidases although to a different extent. The results from *in vitro* assays (Josse et al., 2003; Fu et al., 2012; Yu et al., 2014) led us to conclude that the PQH₂ oxidase activity of AOXs is much lower than that of PTOX. The PQH₂ oxidase activity of AOXs except AOX1a is sufficient to complement the PTOX deficiency in *im*, because only trace amounts of PTOX are normally required for normal function of chloroplasts in *Arabidopsis* (Fu et al., 2009). As the major AOX in plant mitochondria, AOX1a should have developed a high specificity for UQH₂ and possess a low PQH₂ oxidase activity compared to the other minor AOXs. This may explain why AOX1a targeted to chloroplasts only partially rescues the variegation of *im*. This result, together with the previous study (Fu et al., 2012), indicated that the plasticity of substrate preference of related enzymes in plants could be higher than expected.

Whether PTOX could act as a UQH₂ oxidase still remains unclear. The lack of obvious growth defects of AOX deficient mutants in *Arabidopsis* (Zhang et al., 2010, 2016) makes it very difficult to test the UQH₂ oxidase activity of PTOX by targeting PTOX to mitochondria of AOX deficient mutants. The *E. coli* heme-deficient mutant strain, FN102, does not grow aerobically because it lacks the UQH₂ oxidase activity of the heme-containing cytochrome pathway. However, the FN102 strain expressing AOX from *Trypanosoma brucei* could grow normally indicating that AOX could maintain respiratory electron transfer in the absence of the main cytochrome pathway chain in *E. coli* (Nihei et al., 2003). Therefore, it might be a good option to examine the UQH₂ oxidase activity of PTOX by expressing this protein in the *E. coli* FN102 strain.

AOX1a, AOX1b, and AOX2 May Be Dually Targeted Proteins in Mitochondria and Chloroplasts

Traditionally, proteins were thought to be only targeted to a single specific subcellular location. Since the pea glutathione reductase was found to be present in both mitochondria and chloroplasts in transgenic tobacco (Creissen et al., 1995), hundreds of plant proteins were identified to be targeted to multiple locations within the cell (Carrie and Small, 2013; Carrie and Whelan, 2013; Baudisch et al., 2014; Sharma et al., 2018). Currently over 100 proteins are found in both mitochondria and chloroplasts which have attracted considerable interest for their shared functions between these two energy-converting organelles. So far, the majority of identified dually targeted proteins are involved in essential common processes in mitochondria and chloroplasts, such as DNA replication, transcription, translation, and protein homeostasis (Baudisch et al., 2014; Sharma et al., 2018). The dually targeted proteins were thought to contain an ambiguous dual targeting peptide (dTP) at their N-termini which could direct passenger proteins into both chloroplasts and mitochondria (Ge et al., 2014; Sharma et al., 2018). Mitochondrial specific targeting peptides harbor multiple arginine residues and a hydrophobic sequence motif in the N-terminal region. This unique feature was

thought to convey mitochondrial specificity and avoidance of import into chloroplasts (Ge et al., 2014; Lee et al., 2019).

We observed fluorescence signals from GFP-tagged W-AOXs all overlaid well with the fluorescence signals of the mitochondrial specific dye, Mt-Mcherry (**Figure 4A**), indicating that all five AOXs are primarily located in mitochondria as expected. While a portion of signals from the GFP-tagged W-AOX1b and W-AOX2 overlapped well with auto-fluorescence of chloroplasts, this was not the case for GFP-tagged W-AOX1a (**Figure 4**). However, we did observe that overexpressed W-AOX1a, as well as W-AOX1b and W-AOX2, present in purified chloroplasts based on immunoblotting assays (**Figure 5**). To clarify the discrepancy of the results from the two different assays, we fused five AOX targeting peptides with the mature form of PTOX, and observed that the targeting peptide of AOX1a, as well as those of AOX1b and AOX2, could direct PTOX to enter chloroplasts (**Figure 6C**). Altogether, it demonstrated that AOX1a could also be targeted into chloroplasts although the amount was too small to be detected by the GFP fluorescence assay. It has been reported that some of the overexpressed proteins could be mis-targeted to wrong organelles (Lisenbee et al., 2003; Vitali et al., 2018; Zhang et al., 2019). However, we examined more than 50 independent lines of W-AOX1c and W-AOX1d transgenic *im* plants, and found that none of those lines are green. In addition, no green phenotype was found in independent lines of AOX1cTP-mPTOX and AOX1dTP-mPTOX transgenic *im* plants. All implied that the variegation suppression phenotype in transgenic lines were not likely caused by protein mis-targeting. Based on the current data and the previous results (Fu et al., 2012), we surmised that AOX1a, AOX1b, and AOX2 may be dually targeted proteins in mitochondria and chloroplasts, while AOX1c and AOX1d are specifically localized in mitochondria.

Alternative oxidase family members have been assumed to specifically reside in mitochondria (Clifton et al., 2006; Vanlerberghe, 2013). All five *Arabidopsis* AOXs are predicted to be localized in mitochondria by various subcellular targeting prediction programs (**Supplementary Table 1**). Analysis of AOX targeting peptides indicated that all contain multiple arginine residues and a hydrophobic sequence motif at the N-terminus (**Supplementary Figure 3**) fitting the profile of typical mitochondria-targeted proteins (Ge et al., 2014; Lee et al., 2019). Previously AOX1a was used as a specific mitochondrial marker to investigate whether a plant protein is targeted into mitochondria (Carrie et al., 2009).

However, the result that three AOXs (AOX1a, AOX1b, and AOX2) may be dually targeted proteins is not in agreement with the current knowledge of protein dual targeting into mitochondria and chloroplasts. Previously, a predicted specific mitochondrial protein, fumarate hydratase (FumH), was reported to be a dually targeted protein to mitochondria and chloroplasts (Baudisch et al., 2014). Together, these unexpected results suggested that the mechanisms of protein targeting into organelles are much more complex than expected, and dual targeting properties could be more abundant than anticipated.

Could AOXs Enter Chloroplasts and Function as PQH₂ Oxidase in Non-transgenic Plants?

AOX1a, AOX1b, and AOX2 may be dually targeted proteins to mitochondria and chloroplasts, and overexpression of AOX1b and AOX2 in *im* could rescue the mutant phenotype. However, the question arises whether AOX1a, AOX1b, and AOX2 could enter chloroplasts and function as PQH₂ oxidase in non-transgenic plants?

Most AOX genes are expressed at low content in plants except for AOX1a which is the most dominantly expressed isoform (Supplementary Figure 2) and expressed in all plant tissues and organs (Clifton et al., 2006). AOX1b is predominantly expressed in pollen and stamen, and AOX2 expression appears to be specific to mature seed and young inflorescences (Nakabayashi et al., 2005; Clifton et al., 2006). The transcript level of AOX1a dramatically elevates in response to multiple stress conditions. In contrast, AOX2 transcription is suppressed under most stress conditions, but remarkably induced by treatments affecting chloroplast function such as application of paraquat, cysteine, and norflurazon, suggesting a potential role for AOX2 in inter-organellar signaling between chloroplasts and mitochondria (Clifton et al., 2005). It is possible that AOX1a and AOX2 could enter chloroplasts once their expression is induced to high levels, especially under conditions where the function of chloroplasts is impaired. AOX1b and AOX2 were poorly expressed in WT plants under normal conditions (Supplementary Figure 2). We therefore suspected that they are not required for maintaining general mitochondrial functions but could play important roles under stress conditions.

Mitochondrial AOX was reported to act as a buffer pool to consume the excessive reducing power in chloroplasts through the malate/oxaloacetate shuttle (Noguchi and Yoshida, 2008; Taniguchi and Miyake, 2012). However, we found that only chloroplast-localized AOXs are able to suppress *im* variegation (Figures 1, 3). Therefore, the effects on chloroplast redox poise mediated by mitochondria-localized AOX was not pursued in this study.

The Arabidopsis *im* Mutant Can Be Used as a Tool to Examine Whether a Protein Can Be Targeted to Chloroplasts

Currently, several approaches have been established to determine the targeting specificity of proteins, including *in silico* targeting prediction, *in organelle* protein transport experiments, fluorescence analysis of GFP-tagged proteins, organelle fractionation with immunoblotting assays (Carrie and Small, 2013; Sharma et al., 2018).

The fluorescence analysis of GFP-tagged proteins is the most frequently used approach to determine the sub-cellular location of a protein. However, it is not sensitive enough to detect whether a minor part of an abundant protein is localized in different parts of the cell such as AOX1a (Figure 4). Organelle purification plus immunoblotting is a powerful method to determine whether a

protein enters a specific organelle, but it relies on the quality of subcellular fractionation and on suitable antibodies against proteins of interest.

In this study, we fused targeting peptides of AOXs with the mature form of PTOX, and found that the targeting peptide of AOX1a, as well as those of AOX1b and AOX2, could evidently direct PTOX to chloroplasts (Figure 6C). Trace amounts of PTOX are sufficient to maintain normal chloroplast development and function (Fu et al., 2009) making the *im* mutant a sensitive tool to test whether a targeting peptide could direct mature PTOX into chloroplasts. This approach had also been validated in a very recent study (Sharma et al., 2019). The *im* mutant grows well under low light and can be easily transformed. The striking variegation phenotype of the mutant enables us to examine whether a targeting peptide functions as a chloroplast transit peptide based on the phenotype of transgenic T₁ plants. If transgenic plants are green, it indicates that this is indeed the case whereas the variegation phenotype indicates that it is not (Figure 6).

DATA AVAILABILITY STATEMENT

The original contributions presented in the study are included in the article/Supplementary Material, further inquiries can be directed to the corresponding author/s.

AUTHOR CONTRIBUTIONS

AF and MX designed the research. DW, CW, CL, HS, JQ, HC, and WF performed the experiments. DW, YW, MX, FW, BL, YH, and AF analyzed the data. DW, MX, and AF wrote the manuscript with contributions and approval from all authors.

FUNDING

This work was supported by the National Natural Science Foundation of China, Nos. 32070269 and 31471261 to AF and No. 31371226 to MX, and a Shaanxi Science and Technology Project (2014KTCL02-03) to AF.

ACKNOWLEDGMENTS

We thank Dr. Danyang Wang (College of Life Sciences, Northwest University, China) for kindly providing the *pGreen-35S:Mt-Mcherry* vector, and professor Jean-David Rochaix (University of Geneva) for providing valuable suggestions during the manuscript preparation.

SUPPLEMENTARY MATERIAL

The Supplementary Material for this article can be found online at: <https://www.frontiersin.org/articles/10.3389/fpls.2021.692847/full#supplementary-material>

REFERENCES

- Abdallah, F., Salamini, F., and Leister, D. (2000). A prediction of size and evolutionary origin of the proteome of chloroplast of *Arabidopsis*. *Trends Plant Sci.* 5, 141–142. doi: 10.1016/s1360-1385(00)01574-0
- Baudisch, B., Langner, U., Garz, I., and Klösgen, R. B. (2014). The exception proves the rule? Dual targeting of nuclear-encoded proteins into endosymbiotic organelles. *New Phytol.* 201, 80–90. doi: 10.1111/nph.12482
- Bennoun, P. (2002). The present model for chlororespiration. *Photosynth. Res.* 73, 273–277. doi: 10.1023/A:1020479920622
- Bhuiyan, N. H., Friso, G., Poliakov, A., Ponnala, L., and van Wijk, K. J. (2015). MET1 is a thylakoid-associated TPR protein involved in photosystem II supercomplex formation and repair in *Arabidopsis*. *Plant Cell* 27, 262–285. doi: 10.1105/tpc.114.132787
- Blanco, N. E., Guinea-Díaz, M., Whelan, J., and Strand, Å. (2014). Interaction between plastid and mitochondrial retrograde signaling pathways during changes to plastid redox status. *Philos. Trans. R. Soc. B Biol. Sci.* 369:20130231. doi: 10.1098/rstb.2013.0231
- Carol, P., Stevenson, D., Bisabanz, C., Breitenbach, J., Sandmann, G., Mache, R., et al. (1999). Mutations in the *Arabidopsis* gene IMMUTANS cause a variegated phenotype by inactivating a chloroplast terminal oxidase associated with phytoene desaturation. *Plant Cell* 11, 57–68. doi: 10.1105/tpc.11.1.57
- Carrie, C., Kühn, K., Murcha, M. W., Duncan, O., Small, I. D., O'Toole, N., et al. (2009). Approaches to defining dual-targeted proteins in *Arabidopsis*. *Plant J.* 57, 1128–1139. doi: 10.1111/j.1365-3113X.2008.03745.x
- Carrie, C., and Small, I. (2013). A reevaluation of dual-targeting of proteins to mitochondria and chloroplasts. *Biochim. Biophys. Acta* 1833, 253–259. doi: 10.1016/j.bbamcr.2012.05.029
- Carrie, C., and Whelan, J. (2013). Widespread dual targeting of proteins in land plants: when, where, how and why. *Plant Signal. Behav.* 8:e25034. doi: 10.4161/psb.25034
- Cavalier-Smith, T. (2000). Membrane heredity and early chloroplast evolution. *Trends Plant Sci.* 5, 174–182. doi: 10.1016/s1360-1385(00)01598-3
- Chen, M., Choi, Y. D., Voytas, D. F., and Rodermeier, S. (2000). Mutations in the *Arabidopsis* VAR2 locus cause leaf variegation due to the loss of a chloroplast FtsH protease. *Plant J.* 22, 303–313. doi: 10.1046/j.1365-3113x.2000.00738.x
- Clifton, R., Lister, R., Parker, K. L., Sappl, P. G., Elhafez, D., Millar, A. H., et al. (2005). Stress-induced co-expression of alternative respiratory chain components in *Arabidopsis thaliana*. *Plant Mol. Biol.* 58, 193–212. doi: 10.1007/s11103-005-5514-7
- Clifton, R., Millar, A. H., and Whelan, J. (2006). Alternative oxidases in *Arabidopsis*: a comparative analysis of differential expression in the gene family provides new insights into function of nonphosphorylating bypasses. *Biochim. Biophys. Acta* 1757, 730–741. doi: 10.1016/j.bbmbio.2006.03.009
- Clough, S. J., and Bent, A. F. (1998). Floral dip: a simplified method for *Agrobacterium* mediated transformation of *Arabidopsis thaliana*. *Plant J.* 16, 735–743. doi: 10.1046/j.1365-3113x.1998.00343.x
- Cooley, J. W., Howitt, C. A., and Vermass, W. F. (2000). Succinate:quinol oxidoreductases in the cyanobacterium *Synechocystis* sp. strain PCC 6803: presence and function in metabolism and electron transport. *J. Bacteriol.* 182, 714–722. doi: 10.1128/jb.182.3.714-722.2000
- Creissen, G., Reynolds, H., Xue, Y., and Mullineaux, P. (1995). Simultaneous targeting of pea glutathione reductase and of a bacterial fusion protein to chloroplasts and mitochondria in transgenic tobacco. *Plant J.* 8, 167–175. doi: 10.1046/j.1365-3113x.1995.08020167.x
- Felsenstein, J. (1985). Confidence limits on phylogenies: an approach using the bootstrap. *Evolution* 39, 783–791. doi: 10.1111/j.1558-5646.1985.tb00420.x
- Finnegan, P. M., Soole, K. L., and Umbach, A. L. (2004). “Alternative mitochondrial electron transport proteins in higher plants,” in *Plant Mitochondria: From Genome to Function. Advances in Photosynthesis and Respiration* (eds D.A. Day, A.H. Millar, J. Whelan (Berlin: Springer), 163–230. doi: 10.1007/978-1-4020-2400-9_9
- Foudree, A., Putarjuna, A., Kambakam, S., Nolan, T., Fussell, J., Pogorelko, G., et al. (2012). The mechanism of variegation in immutans provides insight into chloroplast biogenesis. *Front. Plant Sci.* 3:260. doi: 10.3389/fpls.2012.00260
- Fu, A., Aluru, M., and Rodermeier, S. (2009). Conserved active site sequences in *Arabidopsis* plastid terminal oxidase (PTOX): in vitro and in planta mutagenesis studies. *J. Biol. Chem.* 284, 22625–22632. doi: 10.1074/jbc.M109.017905
- Fu, A., Liu, H., Yu, F., Kambakam, S., Luan, S., and Rodermeier, S. (2012). Alternative oxidases (AOX1a and AOX2) can functionally substitute for plastid terminal oxidase in *Arabidopsis* chloroplasts. *Plant Cell* 24, 1579–1595. doi: 10.1105/tpc.112.096701
- Fu, A., Park, S., and Rodermeier, S. (2005). Sequences required for the activity of PTOX (immutans), a plastid terminal oxidase. *J. Biol. Chem.* 280, 42489–42496. doi: 10.1074/jbc.M508940200
- Gandin, A., Duffes, C., Day, D. A., and Cousins, A. B. (2012). The absence of alternative oxidase AOX1A results in altered response of photosynthetic carbon assimilation to increasing CO₂ in *Arabidopsis thaliana*. *Plant Cell Physiol.* 53, 1627–1637. doi: 10.1093/pcp/pcs107
- Ge, C., Spänning, E., Glaser, E., and Wieslander, Å. (2014). Import determinants of organelle-specific and dual targeting peptides of mitochondria and chloroplasts in *Arabidopsis thaliana*. *Mol. Plant* 7, 121–136. doi: 10.1093/mp/sst148
- Hasan, S. S., Yamashita, E., and Cramer, W. A. (2013). Transmembrane signaling and assembly of the cytochrome b6f-lipidic charge transfer complex. *Biochim. Biophys. Acta* 1827, 1295–1308. doi: 10.1016/j.bbmbio.2013.03.002
- Josse, E. M., Alcaraz, J. P., Laboure, A. M., and Kuntz, M. (2003). In vitro characterization of a plastid terminal oxidase (PTOX). *Eur. J. Biochem.* 270, 3787–3794. doi: 10.1046/j.1432-1033.2003.03766.x
- Juszczuk, I. M., and Rychter, A. M. (2003). Alternative oxidase in higher plants. *Acta Biochim. Pol.* 50, 1257–1271.
- Juszczuk, I. M., Wagner, A. M., and Rychter, A. M. (2001). Regulation of alternative oxidase activity during phosphate deficiency in bean roots (*Phaseolus vulgaris*). *Physiol. Plant* 113, 185–192. doi: 10.1034/j.1399-3054.2001.1130205.x
- Laureau, C., Pape, R. D., Latouche, G., Moreno-Chacon, M., Finazzi, G., Kuntz, M., et al. (2013). Plastid Terminal Oxidase (PTOX) has the potential to act as a safety valve for excess excitation energy in the alpine plant species *Ranunculus glacialis* L. *Plant Cell Environ.* 36, 1296–1310. doi: 10.1111/pce.12059
- Lee, D. W., Lee, S., Lee, J., Woo, S., Razzak, A., Vitale, A., et al. (2019). Molecular mechanism of the specificity of protein import into chloroplasts and mitochondria in plant cells. *Mol. Plant* 12, 951–966. doi: 10.1016/j.molp.2019.03.003
- Leister, D. (2003). Chloroplast research in the genomic age. *Trends Genet.* 19, 47–56. doi: 10.1016/s0168-9525(02)00003-3
- Li, Y. T., Liu, M. J., Li, Y., Liu, P., Zhao, S. J., Gao, H. Y., et al. (2020). Photoprotection by mitochondrial alternative pathway is enhanced at heat but disabled at chilling. *Plant J.* 104, 403–415. doi: 10.1111/tjp.14931
- Lima, A., Lima, S., Wong, J. H., Phillips, R. S., Buchanan, B. B., and Luan, S. (2006). A redox-active FKBP-type immunophilin functions in accumulation of photosystem II supercomplex in *Arabidopsis thaliana*. *Proc. Natl. Acad. Sci. U. S. A.* 103, 12631–12636. doi: 10.1073/pnas.0605452103
- Lisenbee, C. S., Karnik, S. K., and Trelease, R. N. (2003). Overexpression and mislocalization of a tail-anchored GFP redefines the identity of peroxisomal ER. *Traffic* 4, 491–501. doi: 10.1034/j.1600-0854.2003.00107.x
- Martin, W., and Hermann, R. G. (1998). Gene transfer from organelles to nucleus: how much, what happens, and why? *Plant Physiol.* 118, 9–17. doi: 10.1104/pp.118.1.9
- Maxwell, K., and Johnson, G. N. (2000). Chlorophyll fluorescence – A practical guide. *J. Exp. Bot.* 51, 659–668. doi: 10.1093/jxb/51.345.659
- McDonald, A. E., Ivanov, A. G., Bode, R., Maxwell, D. P., Rodermeier, S. R., and Hüner, N. P. A. (2011). Flexibility in photosynthetic electron transport: the physiological role of plastoquinol terminal oxidase (PTOX). *Biochim. Biophys. Acta* 1807, 954–967. doi: 10.1016/j.bbmbio.2010.10.024
- McDonald, A. E., and Vanlerberghe, G. C. (2006). Origins, evolutionary history, and taxonomic distribution of alternative oxidase and plastoquinol terminal oxidase. *Comp. Biochem. Physiol. Part D Genomics Proteomics* 1, 357–364. doi: 10.1016/j.cbd.2006.08.001
- Møller, I. M. (2001). Plant mitochondria and oxidative stress: electron transport, NADPH turnover and metabolism of reactive oxygen species. *Annu. Rev. Plant Physiol. Plant Mol. Biol.* 52, 561–591. doi: 10.1146/annurev.arplant.52.1.561
- Mueller, S. J., and Reski, R. (2014). Evolution and communication of subcellular compartments: an integrated approach. *Plant Signal. Behav.* 9:e28993. doi: 10.4161/psb.28993

- Murakami, Y., and Toriyama, K. (2008). Enhanced high temperature tolerance in transgenic rice seedlings with elevated levels of alternative oxidase, OsAOX1a. *Plant Biotechnol.* 25, 361–364. doi: 10.5511/plantbiotechnology.25.361
- Müller, P., Li, X. P., and Niyogi, K. K. (2001). Non-photochemical quenching. A response to excess light energy. *Plant Physiol.* 125, 1558–1566. doi: 10.1104/pp.125.4.1558
- Myers, J. (1986). Photosynthetic and respiratory electron transport in a cyanobacterium. *Photosynth. Res.* 9, 135–147. doi: 10.1007/BF00029739
- Nakabayashi, K., Okamoto, M., Koshiba, T., Kamiya, Y., and Nambara, E. (2005). Genome-wide profiling of stored mRNA in *Arabidopsis thaliana* seed germination: epigenetic and genetic regulation of transcription in seed. *Plant J.* 41, 697–709. doi: 10.1111/j.1365-3113X.2005.02337.x
- Nawrocki, W. J., Tourasse, N. J., Taly, A., Rappaport, F., and Wollman, F. A. (2015). The plastid terminal oxidase: its elusive function points to multiple contributions to plastid physiology. *Annu. Rev. Plant Biol.* 66, 49–74. doi: 10.1146/annurev-arplant-043014-114744
- Nihei, C., Fukai, Y., Kawai, K., Osanai, A., Yabu, Y., Suzuki, T., et al. (2003). Purification of active recombinant trypanosome alternative oxidase. *FEBS Lett.* 538, 35–40. doi: 10.1016/s0014-5793(03)00120-0
- Nobre, T., Campos, M. D., Lucic-Mercy, E., and Arnholdt-Schmitt, B. (2016). Misannotation awareness: a tale of two gene-groups. *Front. Plant Sci.* 7:868. doi: 10.3389/fpls.2016.00868
- Noguchi, K., and Yoshida, K. (2008). Interaction between photosynthesis and respiration in illuminated leaves. *Mitochondrion* 8, 87–99. doi: 10.1016/j.mito.2007.09.003
- Okegawa, Y., Kobayash, Y., and Shikanai, T. (2010). Physiological links among alternative electron transport pathways that reduce and oxidize plastoquinone in *Arabidopsis*. *Plant J.* 63, 458–468. doi: 10.1111/j.1365-3113X.2010.04252.x
- Perry, S. E., Li, H. M., and Keegstra, K. (1991). In vitro reconstitution of protein transport into chloroplasts. *Methods Cell Biol.* 34, 327–344. doi: 10.1016/s0091-679x(08)61688-x
- Rochaix, J. (2011). Regulation of photosynthetic electron transport. *Biochim. Biophys. Acta* 1807, 375–383. doi: 10.1016/j.bbabo.2010.11.010
- Rogov, A. G., Sukhanova, E. I., Uralskaya, L. A., Aliverdieva, D. A., and Zvyagilskaya, R. A. (2014). Alternative oxidase: distribution, induction, properties, structure, regulation, and functions. *Biochemistry* 79, 1615–1634. doi: 10.1134/S0006297914130112
- Saisho, D., Nambara, E., Naito, S., Tsutsumi, N., Hirai, A., and Nakazono, M. (1997). Characterization of the gene family for alternative oxidase from *Arabidopsis thaliana*. *Plant Mol. Biol.* 35, 585–596. doi: 10.1023/a:1005818507743
- Saitou, N., and Nei, M. (1987). The neighbor-joining method: a new method for reconstructing phylogenetic trees. *Mol. Biol. Evol.* 4, 406–425. doi: 10.1093/oxfordjournals.molbev.a040454
- Schertl, P., and Braun, H. P. (2014). Respiratory electron transfer pathways in plant mitochondria. *Front. Plant Sci.* 5, 163–163. doi: 10.3389/fpls.2014.00163
- Selinski, J., and Scheibe, R. (2019). Malate valves: old shuttles with new perspectives. *Plant Biol.* 21, 21–30. doi: 10.1111/plb.12869
- Sharma, M., Bennewitz, B., and Klösigen, R. B. (2018). Rather rule than exception? How to evaluate the relevance of dual protein targeting to mitochondria and chloroplasts. *Photosynth. Res.* 138, 335–343. doi: 10.1007/s11120-018-0543-7
- Sharma, M., Kretschmer, C., Lampe, C., Stuttmann, J., and Klösigen, R. B. (2019). Targeting specificity of nuclear-encoded organelle proteins with a self-assembling split-fluorescent protein toolkit. *J. Cell Sci.* 132:jcs230839. doi: 10.1242/jcs.230839
- Spoal, S. H., and Loake, G. J. (2011). Redox-Based protein modifications: the missing link in plant immune signaling. *Curr. Opin. Plant Biol.* 14, 358–364. doi: 10.1016/j.pbi.2011.03.007
- Stepien, P., and Johnson, G. N. (2018). Plastid terminal oxidase requires translocation to the grana stacks to act as a sink for electron transport. *Proc. Natl. Acad. Sci. U. S. A.* 115, 9634–9639. doi: 10.1073/pnas.1719070115
- Stonebloom, S., Burch-Smith, T., Kim, I., Meinke, D., Mindrinos, M., and Zambryski, P. (2009). Loss of the plant DEAD-box protein ISE1 leads to defective mitochondria and increased cell-to-cell transport via plasmodesmata. *Proc. Natl. Acad. Sci. U. S. A.* 106, 17229–17234. doi: 10.1073/pnas.0909222106
- Tamiru, M., Abe, A., Utsushi, H., Yoshida, K., Takagi, H., Fujisaki, K., et al. (2013). The tillering phenotype of the rice plastid terminal oxidase (PTOX) loss-of-function mutant is associated with strigolactone deficiency. *New Phytol.* 202, 116–131. doi: 10.1111/nph.12630
- Tamura, K., Stecher, G., Peterson, D. S., Filipski, A., and Kumar, S. (2013). MEGA6: molecular Evolutionary Genetics Analysis version 6.0. *Mol. Biol. Evol.* 30, 2725–2729. doi: 10.1093/molbev/mst197
- Tan, Y. F., O'Toole, N., Taylor, N. L., and Millar, A. H. (2010). Divalent metal ions in plant mitochondria and their role in interactions with proteins and oxidative stress-induced damage to respiratory function. *Plant Physiol.* 152, 747–761. doi: 10.1104/pp.109.147942
- Taniguchi, M., and Miyake, H. (2012). Redox-shuttling between chloroplast and cytosol: integration of intra-chloroplast and extra-chloroplast metabolism. *Curr. Opin. Plant Biol.* 15, 252–260. doi: 10.1016/j.pbi.2012.01.014
- Vanlerberghe, G. C. (2013). Alternative Oxidase: A Mitochondrial Respiratory Pathway to Maintain Metabolic and Signaling Homeostasis during Abiotic and Biotic Stress in Plants. *Int. J. Mol. Sci.* 14, 6805–6847. doi: 10.3390/ijms14046805
- Vanlerberghe, G. C., Dahal, K., Alber, N. A., and Chadee, A. (2020). Photosynthesis, respiration and growth: a carbon and energy balancing act for alternative oxidase. *Mitochondrion* 52, 197–211. doi: 10.1016/j.mito.2020.04.001
- Vanlerberghe, G. C., and McIntosh, L. (1997). Alternative oxidase: from gene to function. *Annu. Rev. Plant Physiol. Plant Mol. Biol.* 48, 703–734. doi: 10.1146/annurev-arplant.48.1.703
- Vishwakarma, A., Tetali, S. D., Selinski, J., Scheibe, R., and Padmasree, K. (2015). Importance of the alternative oxidase (AOX) pathway in regulating cellular redox and ROS homeostasis to optimize photosynthesis during restriction of the cytochrome oxidase pathway in *Arabidopsis thaliana*. *Ann. Bot.* 116, 555–569. doi: 10.1093/aob/mcv122
- Vitali, D. G., Sinzel, M., Bulthuis, E. P., Kolb, A., Zabel, S., Mehlhorn, D. G., et al. (2018). The GET pathway can increase the risk of mitochondrial outer membrane proteins to be mistargeted to the ER. *J. Cell Sci.* 131:jcs211110. doi: 10.1242/jcs.211110
- Wang, D., and Fu, A. (2016). The plastid terminal oxidase is a key factor balancing the redox state of thylakoid membrane. *Enzymes* 40, 143–171. doi: 10.1016/bs.enz.2016.09.002
- Wang, H., Liang, X., Huang, J., Zhang, D., Lu, H., Liu, Z., et al. (2010). Involvement of ethylene and hydrogen peroxide in induction of alternative respiratory pathway in salt-treated *Arabidopsis* calluses. *Plant Cell Physiol.* 51, 1754–1765. doi: 10.1093/pcp/pcq134
- Wang, J., Rajakulendran, N., Amirsadeghi, S., and Vanlerberghe, G. C. (2011). Impact of mitochondrial alternative oxidase expression on the response of *Nicotiana tabacum* to cold temperature. *Physiol. Plant* 142, 339–351. doi: 10.1111/j.1399-3054.2011.01471.x
- Wu, D. Y., Wright, D. A., Wetzel, C., Voytas, D. F., and Rodermel, S. (1999). The IMMUTANS variegation locus of *Arabidopsis* defines a mitochondrial alternative oxidase homolog that functions during early chloroplast biogenesis. *Plant Cell* 11, 43–55. doi: 10.1105/tpc.11.1.43
- Yoshida, K., Terashima, I., and Noguchi, K. (2007). Up-regulation of mitochondrial alternative oxidase concomitant with chloroplast over-reduction by excess light. *Plant Cell Physiol.* 48, 606–614. doi: 10.1093/pcp/pcm033
- Yoshida, K., Watanabe, C., Kato, Y., Sakamoto, W., and Noguchi, K. (2008). Influence of chloroplastic photooxidative stress on mitochondrial alternative oxidase capacity and respiratory properties: a case study with *Arabidopsis* yellow variegated 2. *Plant Cell Physiol.* 49, 592–603. doi: 10.1093/pcp/pcn031
- Yoshida, K., Watanabe, C. K., Hachiya, T., Tholen, D., Shibata, M., Terashima, I., et al. (2011a). Distinct responses of the mitochondrial respiratory chain to long- and short-term high-light environments in *Arabidopsis thaliana*. *Plant Cell Environ.* 34, 618–628. doi: 10.1111/j.1365-3040.2010.02267.x
- Yoshida, K., Watanabe, C. K., Terashima, I., and Noguchi, K. (2011b). Physiological impact of mitochondrial alternative oxidase on photosynthesis and growth in *Arabidopsis thaliana*. *Plant Cell Environ.* 34, 1890–1899. doi: 10.1111/j.1365-3040.2011.02384.x
- Yu, Q., Feilke, K., Krieger-Liszskay, A., and Beyer, P. (2014). Functional and molecular characterization of plastid terminal oxidase from rice (*Oryza sativa*). *Biochim. Biophys. Acta* 1837, 1284–1292. doi: 10.1016/j.bbabo.2014.04.007

- Zhang, D., Chang, E., Yu, X., Chen, Y., Yang, Q., Cao, Y., et al. (2018). Molecular characterization of magnesium chelatase in Soybean [*Glycine max* (L.) Merr]. *Front. Plant Sci.* 9:720. doi: 10.3389/fpls.2018.00720
- Zhang, D. W., Xu, F., Zhang, Z. W., Chen, Y. E., Du, J. B., Jia, S. D., et al. (2010). Effects of light on cyanide-resistant respiration and alternative oxidase function in *Arabidopsis* seedlings. *Plant Cell Environ.* 33, 2121–2131. doi: 10.1111/j.1365-3040.2010.02211.x
- Zhang, D. W., Yuan, S., Xu, F., Zhu, F., Yuan, M., Ye, H. X., et al. (2016). Light intensity affects chlorophyll synthesis during greening process by metabolite signal from mitochondrial alternative oxidase in *Arabidopsis*. *Plant Cell Environ.* 39, 12–25. doi: 10.1111/pce.12438
- Zhang, E., Mohammed Al-Amily, I., Mohammed, S., Luan, C., Asplund, O., Ahmed, M., et al. (2019). Preserving Insulin Secretion in Diabetes by Inhibiting VDAC1 Overexpression and Surface Translocation in β Cells. *Cell Metab.* 29, 64–77.e6. doi: 10.1016/j.cmet.2018.09.008
- Zhang, L. T., Zhang, Z. S., Gao, H. Y., Meng, X. L., Yang, C., Liu, J. G., et al. (2012). The mitochondrial alternative oxidase pathway protects the photosynthetic apparatus against photodamage in Rumex K-1 leaves. *BMC Plant Biol.* 12:40. doi: 10.1186/1471-2229-12-40
- Zhao, S., Ye, Z., and Stanton, R. (2020). Misuse of RPKM or TPM normalization when comparing across samples and sequencing protocols. *RNA* 26, 903–909. doi: 10.1261/rna.074922.120
- Zhao, Y., Luo, L., Xu, J., Xin, P., Guo, H., Wu, J., et al. (2018). Malate transported from chloroplast to mitochondrion triggers production of ROS and PCD in *Arabidopsis thaliana*. *Cell Res.* 28, 1–14. doi: 10.1038/s41422-018-0024-8
- Conflict of Interest:** The authors declare that the research was conducted in the absence of any commercial or financial relationships that could be construed as a potential conflict of interest.
- Copyright © 2021 Wang, Wang, Li, Song, Qin, Chang, Fu, Wang, Wang, Li, Hao, Xu and Fu. This is an open-access article distributed under the terms of the Creative Commons Attribution License (CC BY). The use, distribution or reproduction in other forums is permitted, provided the original author(s) and the copyright owner(s) are credited and that the original publication in this journal is cited, in accordance with accepted academic practice. No use, distribution or reproduction is permitted which does not comply with these terms.



The Physiological Functionality of PGR5/PGRL1-Dependent Cyclic Electron Transport in Sustaining Photosynthesis

Mingzhu Ma¹, Yifei Liu^{1,2,3,4*}, Chunming Bai⁵, Yunhong Yang⁶, Zhiyu Sun¹, Xinyue Liu¹, Siwei Zhang¹, Xiaori Han^{1*} and Jean Wan Hong Yong^{3,7}

¹College of Land and Environment, National Key Engineering Laboratory for Efficient Utilization of Soil and Fertilizer Resources, Northeast China Plant Nutrition and Fertilization Scientific Observation and Research Center for Ministry of Agriculture and Rural Affairs, Key Laboratory of Protected Horticulture of Education Ministry and Liaoning Province, Shenyang Agricultural University, Shenyang, China, ²The UWA Institute of Agriculture, The University of Western Australia, Perth, WA, Australia, ³School of Biological Sciences, The University of Western Australia, Perth, WA, Australia, ⁴School of Agriculture and Environment, The University of Western Australia, Perth, WA, Australia, ⁵National Sorghum Improvement Center, Liaoning Academy of Agricultural Sciences, Shenyang, China, ⁶Professional Technology Innovation Center of Magnesium Nutrition, Yingkou Magnesite Chemical Ind Group Co., Ltd., Yingkou, China, ⁷Department of Biosystems and Technology, Swedish University of Agricultural Sciences, Alnarp, Sweden

OPEN ACCESS

Edited by:

Rebecca L. Roston,
University of Nebraska-Lincoln,
United States

Reviewed by:

Hualing Mi,
Chinese Academy of Sciences, China
Toshiharu Shikanai,
Kyoto University, Japan

*Correspondence:

Yifei Liu
yifeiliu6@hotmail.com
Xiaori Han
hanxiaori@163.com

Specialty section:

This article was submitted to
Plant Physiology,
a section of the journal
Frontiers in Plant Science

Received: 29 April 2021

Accepted: 07 June 2021

Published: 07 July 2021

Citation:

Ma M, Liu Y, Bai C, Yang Y, Sun Z,
Liu X, Zhang S, Han X and
Yong JWH (2021) The Physiological
Functionality of PGR5/PGRL1-
Dependent Cyclic Electron Transport
in Sustaining Photosynthesis.
Front. Plant Sci. 12:702196.
doi: 10.3389/fpls.2021.702196

The cyclic electron transport (CET), after the linear electron transport (LET), is another important electron transport pathway during the light reactions of photosynthesis. The proton gradient regulation 5 (PGR5)/PRG5-like photosynthetic phenotype 1 (PGRL1) and the NADH dehydrogenase-like complex pathways are linked to the CET. Recently, the regulation of CET around photosystem I (PSI) has been recognized as crucial for photosynthesis and plant growth. Here, we summarized the main biochemical processes of the PGR5/PGRL1-dependent CET pathway and its physiological significance in protecting the photosystem II and PSI, ATP/NADPH ratio maintenance, and regulating the transitions between LET and CET in order to optimize photosynthesis when encountering unfavorable conditions. A better understanding of the PGR5/PGRL1-mediated CET during photosynthesis might provide novel strategies for improving crop yield in a world facing more extreme weather events with multiple stresses affecting the plants.

Keywords: photosynthesis, cyclic electron transport, proton gradient regulation 5, PRG5-like photosynthetic phenotype 1, photoinhibition

INTRODUCTION

Life on earth depends on energy derived from the sun. Photosynthesis is the pivotal process that could harvest light energy and ultimately generate biomass using water, CO₂ and mineral nutrients. The bulk of our earth's energy resources is derived from global photosynthetic activity in either recent or ancient times (Vass et al., 2007; Liu et al., 2011; Lambers and Oliveira, 2019; Nawrocki et al., 2019). The normal operation of photosynthesis is inseparable from the participation of light energy, but any excessive high light would impact the photosystem

II (PSII), photosystem I (PSI) and the other thylakoid membrane proteins and resulting in photoinhibition and the accumulation of reactive oxygen species (ROS; Foyer and Noctor, 1999; Chaux et al., 2017; Liu, 2020). In the real world, multiple stress episodes affecting growth and development are common (Suzuki et al., 2014). Any excessive high light situation could be exacerbated further with a co-occurring high temperature (Sun et al., 2017; Lu et al., 2020), low temperature (Liu et al., 2013; Song et al., 2020; Wu et al., 2020), phosphorus deficiency (Carstensen et al., 2018; Shi et al., 2019) and drought (Wada et al., 2019). Plants have evolved several adaptations to cope with the unfavorable light situation: adjusting leaf orientation, ROS scavenging competence (Gill and Tuteja, 2010), xanthophyll cycle (Kuczyńska et al., 2020), state transitions strategy (Hepworth et al., 2021), cyclic electron transport (CET; Yadav et al., 2020) and photorespiration (Storti et al., 2019). This review summarizes the main biochemical processes of PGR5/PGRL1-dependent CET pathway. The significance of the PGR5/PGRL1-dependent CET pathway is discussed to understand how plants optimize photosynthesis under unfavorable conditions by protecting the PSII and PSI, ATP/NADPH ratio maintenance, and regulating the transitions between linear electron transport (LET) and CET.

PHOTOSYNTHETIC ELECTRON TRANSPORT

Chloroplasts convert light energy into chemical energy *via* electron transport (ET), which provides energy for the Calvin cycle and other processes. During the LET, electrons derived from water splitting in PSII are transferred *via* the cytochrome (Cyt_{b₆}f) complex, PSI and ferredoxin (Fd) to the ferredoxin-NADP reductase (FNR), which ultimately reduce NADP⁺ to NADPH, resulting in the production of NADPH (Figure 1A; Lu et al., 2020). The H⁺ enters the thylakoid lumen by the Q cycle, and the H⁺ produced by water splitting in OEC together to form the required proton motive force (*pmf*) across the thylakoid membrane (Wang et al., 2020). The *pmf*, composed of the transmembrane potential ($\Delta\psi$) and proton gradient (ΔpH), plays a key role in driving the chloroplast ATP synthase to synthesize ATP (Lapashina and Feniouk, 2018). ATP synthesis coupled with the LET is known as noncyclic photophosphorylation (NCPSP; Arnon et al., 1954, 1958). The energy derived from LET and NCPSP plays an essential role in photosynthesis and other processes. However, there would be insufficient ATP from the LET during certain multiple stress situations. Plants could compensate for the deficiency of ATP/NADPH in the LET by using the CET around the PSI (Sato et al., 2019; Ma et al., 2021), the water-water cycle (Mehler reaction; Asada et al., 1999) and the mitochondrial alternative oxidase respiration (Meng et al., 2012).

CYCLIC ELECTRON TRANSPORT

The pathway of electron transport around PSI, which recycles electrons from Fd to PQ, is called the CET, while the ATP synthesis coupled with it is called the cyclic photophosphorylation

(Bendall and Manasse, 1995). Moss and Bendall (1984) proposed that an antimycin A (AA)-sensitive enzyme is involved in the ET from Fd to PQ termed as the ferredoxin-plastoquinone reductase (FQR) with the following configuration: PSI-Fd-FQR-PQ-Cyt _{b₆}f-PSI. The discovery of a protein complex that could receive electrons from Fd and transferring electrons to PQ represented major progress in CET research. Due to the high similarity to complex I within the mitochondrial respiratory chain, it was aptly called NDH (NADH dehydrogenase-like complex; Burrows et al., 1998). The NDH pathway is the main pathway compared with PGR5 one in cyanobacteria (Miller et al., 2021). It has been reported that NDH pathway plays a crucial role at high temperature or low temperature in tobacco (Wang et al., 2006) and low-light intensity in rice (Yamori et al., 2015) and *Marchantia polymorpha* (Ueda et al., 2012). However, it is not sensitive to AA, which implied that there is possibly another FQR pathway that is sensitive to AA and regulated by Fd in CET.

The PGR5/PGRL1-Mediated CET Pathway

It was suggested that the CET around PSI helps contribute electrons to synthesize ATP: *Chlamydomonas* (Yadav et al., 2020), *Phaeodactylum* (Zhou et al., 2020), C₃ (Wang et al., 2015) and C₄ plants (Munekage et al., 2010). There are at least two CET pathways in vascular plants and *Phycophyta*: antimycin A-sensitive pathway that involves proton gradient regulation 5 (PGR5) and PGR5-like photosynthetic phenotype 1 (PGRL1), and antimycin A-insensitive NADH dehydrogenase-like (NDH) pathway (Figure 1A; Munekage et al., 2002; Huang et al., 2005; Dalcorso et al., 2008; Taira et al., 2013; Ishikawa et al., 2016). There is a high similarity between the NDH and respiratory chain proteins. Conversely, PGR5 has no homology with the mitochondrial respiratory chain proteins. In a mutant of *pgr5*, due to less influx of protons that should be from the Q cycle, the ability of non-photochemical quenching (NPQ) PSII is reduced under strong light (Yadav et al., 2020). Although PGR5 plays a key role in CET from Fd to PQ, its molecular characteristics are not sufficient to deliver all the functionality reported for FQR. Specifically, PGR5 does not contain any redox-active cysteine residues that mediates ET nor has any transmembrane domains (Yamori and Shikanai, 2016). Therefore, the role played by PGR5 in the AA-sensitive CET pathway is still unclear. It was suggested that the decrease of CET activity in *pgr5* mutants is due to its plausible role in feedback regulation (Nandha et al., 2007), and the postulated function of PGR5 is to regulate LET (Suorsa et al., 2012).

The PGRL1 was identified as another important regulator of the CET process in *Arabidopsis*. Plants lacking PGRL1 showed a decrease in CET rate and exhibiting a similar performance to the *pgr5* mutant (Dalcorso et al., 2008; Yadav et al., 2020). The regulatory role of PGR5/PGRL1-dependent CET under environmental perturbations has been studied (Wang et al., 2014; Yamori et al., 2016; Wolf et al., 2020). PGR5 is a small thylakoid protein without any known motifs that suggest its function (Munekage et al., 2002), while PGRL1 is a transmembrane protein with two transmembrane domains, and its two cysteine residues are involved in an iron cofactor binding

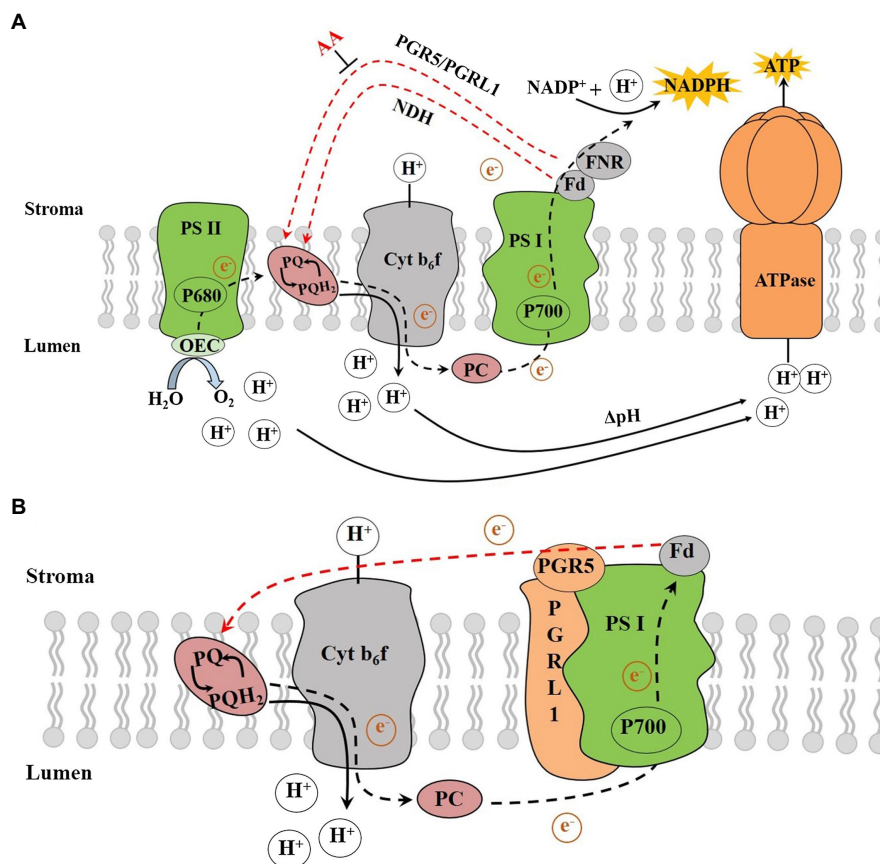


FIGURE 1 | (A) The photosynthetic electron transport chain and **(B)** The PGR5/PGRL1-dependent CET. AA, antimycin A; ATPase, ATP synthase; Cyt_b₆f, cytochrome _b₆f complex; Fd, ferredoxin; FNR, ferredoxin-NADP reductase; Lumen, thylakoid lumen; NADPH, reduced nicotinamide adenine dinucleotide phosphate; NDH, NADH dehydrogenase-like; OEC, oxygen-evolving complex; P680, pigment molecule of PSII reaction centre; P700, pigment molecule of PSI reaction centre; PC, plastocyanin; PGR5, proton gradient regulation 5; PGRL1, PRG5-like photosynthetic phenotype 1; PQ, plastoquinone; PQH₂, plastoquinol; PSI, photosystem I; PSII, photosystem II, Stroma, thylakoid stroma and ΔpH, proton gradient (adapted from Yamori and Shikanai, 2016).

(Hertle et al., 2013). The previous studies showed that the PGR5 proteins in *Arabidopsis* have low similarity to those found in cyanobacteria, excluding the coding genes of PGRL1 (Peltier et al., 2010). The double mutant of *Arabidopsis prgl1ab* showed a phenotype similar to that of *pgr5* (Dalcorso et al., 2008). In rice *pgr5* mutants, the PGRL1 protein level decreased by 50% (Nishikawa et al., 2012). Generally, the transport of electrons from Fd to PGRL1 requires the participation of PGR5 proteins, where the loss of any protein would affect the CET activity (Munekage et al., 2002; Dalcorso et al., 2008; Kono et al., 2014). Under *in vitro* conditions and when reduced Fd is present, an unknown redox reaction would catalyse the formation of disulphide bonds between cysteine residues in PGRL1 and the recombinant PGRL1 thereby reducing the analogue of PQ and quinone 2,6-dimethyl-p-benzoquinone (Hertle et al., 2013). This finding was confirmed by examining the mercaptan group of FQR (Strand et al., 2016). Shikanai (2007) speculated that PGR5 and PGRL1 proteins are important components of FQR. Subsequently, when the molecular features of PGRL1 were found to be similar to the FQR protein,

the researchers further proposed that PGRL1 could be the FQR proteins (Figure 1B; Hertle et al., 2013; Labs et al., 2016).

State Transitions and the CET

In plants, the redistribution of excitation energy between the two photosystems is modulated by reversible phosphorylation of light-harvesting complex II (LHCII) in response to light fluctuation (Allen et al., 1981; Bhatti et al., 2020). Generally, these processes are known as state transitions (Bonaventura and Myers, 1969). For *Chlamydomonas reinhardtii*, when PSII is excited, the LHCII is phosphorylated, separated from PSII and adhering to the PSI. Meanwhile, the absorbed light energy is allocated to PSI, and thereby allowing the CET to dominate; this is called state II. PSI is preferentially excited during state I during which LHCII-P is dephosphorylated, recombined with PSII, and giving priority to facilitate the LET (Finazzi et al., 2002). While it is true that CET is the main pathway of ET during state II, this does not imply that state II is a necessary condition for the

CET to operate. It was found in *C. reinhardtii* and *Arabidopsis* that the CET is not affected by the state transition (Takahashi et al., 2013). Although the CET is not related to state transition, state II is beneficial for the separation of the CET-PSI complexes (Yamori and Shikanai, 2016). The core mechanism of PGR5/PGRL1-mediated CET is similar in *C. reinhardtii* and *Arabidopsis* (Yamori and Shikanai, 2016), except for their supercomplex components related to ET. Iwai et al. (2010) identified the supercomplexes containing FNR, Fd, PGRL1, Cytb₆ and PSI in *C. reinhardtii*. In *Arabidopsis*, however, it was only confirmed that the PGRL1-PGR5 complex could interact with PSI, thus facilitating the formation of *Arabidopsis* CET supercomplex (Dalcorso et al., 2008). Although the potential CET supercomplex was not identified clearly, there were more studies to support the association of PGR5 and PGRL1 in the CET (Breyton et al., 2006; Xue et al., 2017).

THE FUNCTION OF PGR5/PGRL1-MEDIATED CET IN PLANTS

Regulating the Level of ATP and Maintaining the Balance of ATP/NADPH

The 'Proton Gradient Regulation 5' or PGR5 plays a pivotal role in proton gradient regulation. In the chloroplasts, the regulation of *pmf* must satisfy two competing physiological demands: (1) ensuring the requirements of carbon fixation for ATP and (2) decreasing the ET rate to avoid light damage under certain situations. Under relatively low light, the proportion of $\Delta\psi$ is equal to that of ΔpH . With increasing light, the proportion of ΔpH in *pmf* increases gradually. In *Arabidopsis pgr5* mutants, ΔpH accounts for about 90% of the total *pmf* at a light intensity greater than 312 $\mu\text{mol}\cdot\text{m}^{-2}\cdot\text{s}^{-1}$ (Yamamoto et al., 2016). Therefore, the size of ΔpH may be partly compensated by increasing the partitioning of ΔpH in *pmf* in *pgr5* (Yamamoto et al., 2016). To move from $\Delta\psi$ to ΔpH , some cations (mainly Mg^{2+} and K^{+}) have to be transported to the stroma via the thylakoid membrane (Kramer et al., 2003). Hind et al. (1974) indicated that the outflow of these cations could facilitate *pmf* adjusting into the ΔpH form. Besides, AtVCCN1, a voltage-dependent chloride channel, located in *Arabidopsis* thylakoid membrane can make Cl^{-} influx into the lumen during illumination and partially dissipate the $\Delta\psi$ in the lumen, thereby increasing the $\Delta pH/\Delta\psi$ ratio (Herdean et al., 2016).

Plants regulate the proportion of ATP/NADPH to meet the competing demands of metabolism and photoprotection. Thus, the regulation of the electron distribution between LET and CET is essential to maintaining optimal photosynthesis under prevailing conditions. Particularly, the PGR5/PGRL1-dependent CET plays a central role in the regulation of LET via the downregulation of the Cyt b₆f complex (Shikanai, 2014; Yamori et al., 2016). The function of CET is more relevant under conditions when the LET cannot produce sufficient ΔpH ; consequently, it is necessary to improve the ratio of ATP/NADPH by increasing the ΔpH to promote the synthesis

for more ATP (Figure 2; Yamori and Shikanai, 2016). Besides, sufficient ΔpH of thylakoid lumen contributes to the downregulation of electron transport through NPQ, preventing photodamage (Niyogi, 1999; Shikanai, 2007). Both PGR5/PGRL1 and NDH-mediated CET play a role in low light and facilitating CO_2 assimilation by providing additional ATP (Nishikawa et al., 2012). In contrast, the regulatory effect of PGR5/PGRL1 and NDH-mediated CET on ATP/NADPH is negligible in rice-growing under strong light (Yamori et al., 2015). However, strong light led to the decrease of *pmf* formation in *pgr5* mutant in *Arabidopsis* and the concomitant decrease of ATP yield, thereby disrupting the optimal ATP/NADPH balance (Kawashima et al., 2017). The stimulation of ATP/NADPH homeostasis in primary metabolism demonstrated that the energy requirement under high light is not less than that under low light (Walker et al., 2014). Hence, one might envisage that the CET should be beneficial to regulating the balance of ATP/NADPH under different light conditions. Recent studies have shown that the CET was needed to achieve a balanced ATP/NADPH ratio even under non-stress conditions in C_3 plants (Wang et al., 2015).

Inducing the NPQ and Protecting the PSII

Any excess light during photosynthesis would lead to photo-oxidative damage and reducing carbon fixation (Paredes and Quiles, 2017). The non-photochemical quenching mechanism (NPQ) plays an essential role in the photoprotection mechanism (Erickson et al., 2015). Inducing the qE component of NPQ to dissipate excessive absorbed light energy is dependent on the thylakoid lumen acidification modulated by the CET (Müller et al., 2001; Johnson et al., 2014). Under multiple stresses, electrons will preferentially reduce Fd and NADP^{+} and not O_2 , thereby avoiding oxidative damage to the photosystems caused by the excess light energy (Chow and Hope, 2004; Kukuczka et al., 2014). The previous studies have shown that NDH-mediated CET plays a significant role in rice and *M. polymorpha* under low light (Ueda et al., 2012; Yamori et al., 2015). However, in *Arabidopsis*, the deletion of the NDH gene did not alter photosynthesis significantly (Hashimoto et al., 2003). It was only when both PGR5 and NDH were mutated that the seedling has an altered phenotype (Munekage et al., 2004). Therefore, for C_3 plants, the PGR5/PGRL1 pathway is the major pathway of CET (Munekage et al., 2004; Okegawa et al., 2008; Wang et al., 2015; Okegawa and Motohashi, 2020). Recent studies have indicated that the role of CET probably varies with light intensity (Huang et al., 2015). The generation of CET-dependent *pmf* is for the synthesis of ATP under lower light (Avenson et al., 2005; Walker et al., 2014). With higher light, the acidification of thylakoid lumen is beneficial to protect PSI and PSII from photoinhibition (Takahashi et al., 2009; Tikkanen et al., 2014).

Both *pgr5* and *pgrl1* mutants in *Arabidopsis* were sensitive to abiotic stress, such as high light and extreme temperature (Munekage et al., 2002; Jin et al., 2017; Kawashima et al., 2017). When the PSII repair function of wild-type and *pgr5* mutants was inhibited, compared with wild-type plants, PSII

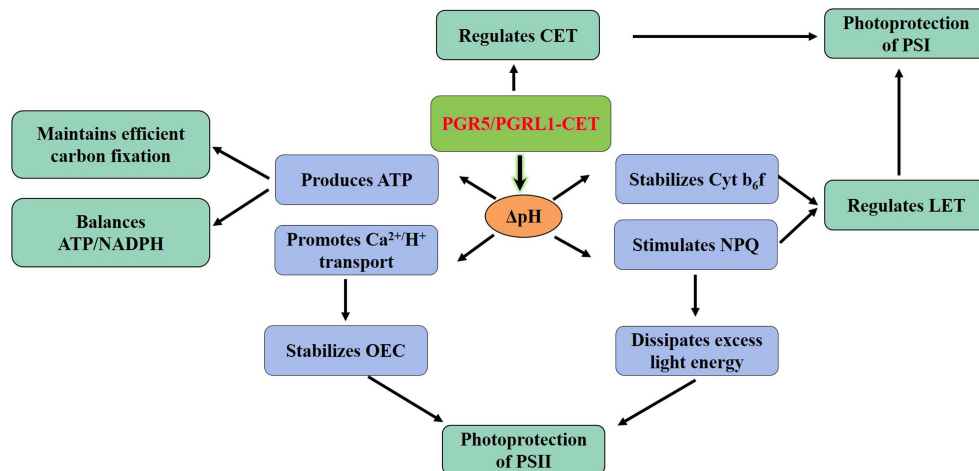


FIGURE 2 | Physiological functionality of the PGR5/PGRL1-dependent CET. The PGR5/PGRL1-mediated CET produces more ATP by increasing ΔpH to balance ATP/NADPH and meeting the requirements for efficient C fixation. Meanwhile, the increase of ΔpH would protect the PSII from photoinhibition via stimulating the NPQ and facilitating the transport of Ca^{2+}/H^{+} . ATP, adenosine triphosphate; CET, cyclic electron transport; $Cyt b_6f$, cytochrome b_6f complex; LET, linear electron transport; NADPH, reduced nicotinamide adenine dinucleotide phosphate; NPQ, non-photochemical quenching; OEC, oxygen-evolving complex; PGR5, proton gradient regulation 5; PGRL1, PRG5-like photosynthetic phenotype 1; PSI, photosystem I and PSII, photosystem II.

in *pgr5* mutants was still more sensitive to strong light (Takahashi et al., 2009), indicating that PGR5 deficiency caused photodamage to photosystems (Okegawa et al., 2010). The PSI is the likely primary target of photoinhibition, and the dynamic balance between photodamage and restoration in PSII maintains its stability (Pospisil and Tyystjarvi, 1999). Generally, the protection of PSII by CET mediated by PGR5/PGRL1 under adverse environments involves at least two different mechanisms. Firstly, the acidification of the thylakoid lumen activates NPQ to dissipate excess light energy, thereby reducing ROS production in the PSII complex (Munekage et al., 2008). Secondly, the formation of ΔpH promotes the reversed Ca^{2+}/H^{+} transport to increase the concentration of Ca^{2+} in the thylakoid lumen (Ettinger et al., 1999). As the stability of OEC depended on the level of lumen Ca^{2+} (Krieger and Weis, 1993), the acidification in the lumen would avoid the photodamage of PSII by increasing the stability of OEC (Figure 2; Takahashi et al., 2009; Huang et al., 2016). Notably, the effects of PGR5 overexpression were strikingly pleiotropic. The accumulation of PGR5 could enhance the high-light resistance of the plants, but it also markedly delayed the greening of cotyledons, thereby causing the slower seedling growth in the initial growth stage (Okegawa et al., 2007; Long et al., 2008; Sugimoto et al., 2013).

Regulating the LET and Protecting the PSI

The Fe-S clusters within the PSI complex are vulnerable to ROS when exposed to fluctuating light. In particular, PSI photodamage occurred before PSII in *pgr5* mutants (Sonoike, 2011; Suorsa et al., 2012; Kono et al., 2014, 2017). Unlike the effective and fast repair of PSII, the restoration of PSI is slower and consequently. In general, most PSI damages are considered to be almost irreversible (Zivcak et al., 2014). Gollan et al. (2017) found that PSI damage inhibited carbon fixation and other processes after high-light exposure.

Similar to its role in PSII, the protective effect of PGR5/PGRL1-mediated CET on PSI is related to the formation of ΔpH (Yamamoto and Shikanai, 2019). The CET-dependent ΔpH formation not only contributes to the synthesis of ATP but also regulates the ET via acidifying the thylakoid lumen (Shikanai, 2014, 2016; Yamori and Shikanai, 2016). The PSI acceptor-side regulation by CET sustains electron sinks downstream of PSI and preventing the over-reduction of the PSI (Munekage et al., 2002). The acidification of the thylakoid lumen downregulates the $Cyt b_6f$ complex thereby slowing down the ET from PSII towards PSI and induces the thermal dissipation of absorbed excess photon energy from the PSII antennae (Shikanai, 2016; Yamamoto and Shikanai, 2019). This is the PSI donor-side regulation by CET for PSI photoprotection (Suorsa et al., 2012). It has been reported that exogenous calcium alleviates nocturnal chilling-induced photo damage by facilitating CET, thereby enhancing the photosynthesis and biomass accumulation of peanut under low nocturnal temperature stress (Song et al., 2020; Wu et al., 2020). Additionally, plant dry weight was significantly lowered in the rice PGR5-knockdown line compared to that of WT, especially under fluctuating light (Yamori et al., 2016). Therefore, stimulating CET via artificial growth regulation might be a novel strategy to maintain sufficient photosynthetic carbon fixation and enhance yield under unfavorable conditions. Most notably, Rantala et al. (2020) indicated that both PGR5 and NDH-1 systems do not function as protective electron acceptors but mitigate the consequences of PSI inhibition and protected the remaining PSI centres by enhancing pH-dependent regulation of electron transfer from PSII to PSI.

Functional analysis showed the PSI remained fully reduced under high light in *pgr5* mutants. Interestingly, in the wild type under high light, the PSI complex was oxidized; the damage of PSI in *pgr5* was later mitigated by exogenous

application of 3-(3,4-dichlorophenyl)-1,1-dimethylurea (DCMU; inhibitor of the PSII to PSI ET; Tikkanen et al., 2010). These observations implied that the PGR5/PGRL1-mediated CET could reduce PSI damage from excessive electron flow under strong light. PGR5 and PGRL1 play crucial roles in the efficient operation of CET, whereas the maximum rate of CET is only slightly affected in *pgr5* mutants (Nandha et al., 2007). Although the CET varies slightly, the change of ATP/NADPH ratio would be sufficient to have a substantial impact on the levels of ADP, phosphatidylinositol (Pi) and NADP⁺, thus reducing the activity of PSI electron acceptor and modulating the rate of LET (Kramer et al., 2004; Avenson et al., 2005; Suorsa et al., 2016). This evidence highlighted the important role of PGR5 in regulating the LET to CET transition (Figure 2; Suorsa et al., 2016).

FUTURE OUTLOOK

Optimizing photosynthesis is an effective way to improve plant productivity. However, the variation of light and environmental conditions would often lower photosynthetic capacity and hampering electron transmission. The PGR5/PGRL1-dependent CET around PSI plays an important homeostatic role in electron transfers and thereby alleviating photoinhibition. With the recent advent of molecular techniques and sensitive analytical tools, scientists have achieved a better understanding of the PGR5/PGRL1-CET putative structure and functionality. Thus, the biological significance of the PGR5/PGRL1 pathway is better understood now although

there exist several unsolved questions: pathway initiation and interactions leading to better efficiency; the relationship between PGR5/PGRL1 and FQR and the effect of PGR5/PGRL1 expression on the PSII. Most published studies have focused on *Arabidopsis* and rice, and with less emphasis on other crops. With the availability of novel research tools, it is possible to elucidate the complex regulatory network of the PGR5/PGRL1 pathway and its role in optimizing photosynthesis under unfavorable conditions.

AUTHOR CONTRIBUTIONS

YL, MM, XH, and JY are responsible for the general overview of the opinions stated in the manuscript. YL, MM, CB, YY, ZS, XL, SZ, and JY wrote and modified the manuscript. All authors reviewed and approved the final version of the submitted manuscript.

FUNDING

This research was funded by the National Natural Science Foundation of China (project nos. 31772391 and 31301842), National Peanut Research System (project no. CARS-13-Nutrient Management), National Key Research and Development Plan (project no. 2018YFD0201001), Sheng Jing Talents Project (project no. RC170338) and China Scholarship Council Project.

REFERENCES

- Allen, J. F., Bennett, J., Steinback, K. E., and Arntzen, C. J. (1981). Chloroplast protein phosphorylation couples plastoquinone redox state to distribution of excitation energy between photosystems. *Nature* 291, 25–29. doi: 10.1038/291025a0
- Arnon, D. I., Allen, M. B., and Whatley, F. R. (1954). Photosynthesis by isolated chloroplasts. *Nature* 174, 394–396. doi: 10.1038/174394a0
- Arnon, D. I., Whatley, F. R., and Allen, M. B. (1958). Assimilatory power in photosynthesis. *Science* 127, 1026–1034. doi: 10.1126/Science.127.3305.1026
- Asada, Y., Miyake, M., Miyake, J., Kurane, R., and Tokiwa, Y. (1999). Photosynthetic accumulation of poly-(hydroxybutyrate) by cyanobacteria—the metabolism and potential for CO₂ recycling. *Int. J. Biol. Macromol.* 25, 37–42. doi: 10.1016/S0141-8130(99)00013-6
- Avenson, T. J., Cruz, J. A., Kanazawa, A., and Kramere, D. M. (2005). Regulating the proton budget of higher plant photosynthesis. *Proc. Natl. Acad. Sci. U. S. A.* 102, 9709–9713. doi: 10.1073/pnas.0503952102
- Bendall, D. S., and Manasse, R. S. (1995). Cyclic photophosphorylation and electron transport. *Biochim. Biophys. Acta. Bioenerg.* 1229, 23–38. doi: 10.1016/0005-2728(94)00195-B
- Bhatti, A. F., Choubey, R. R., Kirilovsky, D., Wientjes, E., and Amerongen, H. V. (2020). State transitions in cyanobacteria studied with picosecond fluorescence at room temperature. *Biochim. Biophys. Acta. Bioenerg.* 2020:148255. doi: 10.1016/j.bbabi.2020.148255
- Bonaventura, C., and Myers, J. (1969). Fluorescence and oxygen evolution from *Chlorella pyrenoidosa*. *Biochim. Biophys. Acta. Bioenerg.* 189, 366–383. doi: 10.1016/0005-2728(69)90168-6
- Breyton, C., Nandha, B., Johnson, G. N., Joliot, P., and Finazzi, G. (2006). Redox modulation of cyclic electron flow around photosystem I in C₃ plants. *Biochemistry* 45, 13465–13475. doi: 10.1021/bi061439s
- Burrows, P. A., Sazanov, A., Svab, Z., Maliga, P., and Nixon, P. J. (1998). Identification of a functional respiratory complex in chloroplasts through analysis of tobacco mutants containing disrupted plastid *ndh* genes. *EMBO J.* 17, 868–876. doi: 10.1093/emboj/17.4.868
- Carstensen, A., Herdean, A., Schmidt, S. B., Sharma, A., Spetea, C., Pribil, M., et al. (2018). The impacts of phosphorus deficiency on the photosynthetic electron transport chain. *Plant Physiol.* 177, 271–284. doi: 10.1104/pp.17.01624
- Chaux, F., Johnson, X., Auroy, P., Beyly-Adriano, A., Te, L., Cuiné, S., et al. (2017). PGRL1 and LHCSR3 compensate for each other in controlling photosynthesis and avoiding photosystem I photoinhibition during high light acclimation of *Chlamydomonas* cells. *Mol. Plant* 10, 216–218. doi: 10.1016/j.molp.2016.09.005
- Chow, W. S., and Hope, A. B. (2004). Electron fluxes through photosystem I in cucumber leaf discs probed by far-red light. *Photosynth. Res.* 81, 77–89. doi: 10.1023/B:PRES.0000028396.83954.36
- Dalcorso, G., Pesaresi, P., Masiero, S., Aseeva, E., Danja, S., Finazzi, G., et al. (2008). A complex containing PGRL1 and PGR5 is involved in the switch between linear and cyclic electron flow in *Arabidopsis*. *Cell* 132, 273–285. doi: 10.1016/j.cell.2007.12.028
- Erickson, E., Wakao, S., and Niyogi, K. K. (2015). Light stress and photoprotection in *Chlamydomonas reinhardtii*. *Plant J.* 82, 449–465. doi: 10.1111/tpj.12825
- Ettinger, W. F., Clear, A. M., Fanning, K. J., and Peck, M. L. (1999). Identification of a Ca²⁺/H⁺ antiporter in the plant chloroplast thylakoid membrane. *Plant Physiol.* 119, 1379–1386. doi: 10.1104/pp.119.4.1379
- Finazzi, G., Rappaport, F., Furia, A., Fleischmann, M., Rochaix, J. D., Zito, F., et al. (2002). Involvement of state transitions in the switch between linear and cyclic electron flow in *Chlamydomonas reinhardtii*. *EMBO Rep.* 3, 280–285. doi: 10.1093/embo-reports/kvf047
- Foyer, C. H., and Noctor, G. (1999). Leaves in the dark see the light. *Science* 284, 599–601. doi: 10.1126/Science.284.5414.599

- Gill, S. S., and Tuteja, N. (2010). Reactive oxygen species and antioxidant machinery in abiotic stress tolerance in crop plants. *Plant Physiol. Biochem.* 48, 909–930. doi: 10.1016/j.plaphy.2010.08.016
- Gollan, P. J., Lima-Melo, Y., Tiwari, A., Tikkanen, M., and Aro, E. M. (2017). Interaction between photosynthetic electron transport and chloroplast sinks triggers protection and signalling important for plant productivity. *Philos. Trans. R. Soc. B. Biol. Sci.* 372:20160390. doi: 10.1098/rstb.2016.0390
- Hashimoto, M., Endo, T., Peltier, G., Tasaka, M., and Shikanai, T. (2003). A nucleus-encoded factor, CRR2, is essential for the expression of chloroplast *ndhB* in *Arabidopsis*. *Plant J.* 36, 541–549. doi: 10.1046/j.1365-313X.2003.01900.x
- Hepworth, C., Wood, W. H. J., Emrich-Mills, T. Z., Proctor, M. S., Casson, S., and Johnson, M. P. (2021). Dynamic thylakoid stacking and state transitions work synergistically to avoid acceptor-side limitation of photosystem I. *Nat. Plants* 7, 87–98. doi: 10.1038/s41477-020-00828-3
- Herdean, A., Teardo, E., Nilsson, A. K., Pfeil, B. E., Johansson, O. N., Ünneper, R., et al. (2016). A voltage-dependent chloride channel fine-tunes photosynthesis in plants. *Nat. Commun.* 7:11654. doi: 10.1038/ncomms11654
- Hertle, A. P., Blunder, T., Wunder, T., Pesaresi, P., Pribil, M., Armbruster, U., et al. (2013). PGR1 is the elusive ferredoxin-plastoquinone reductase in photosynthetic cyclic electron flow. *Mol. Cell* 49, 511–523. doi: 10.1016/j.molcel.2012.11.030
- Hind, G., Nakatani, H. Y., and Izawa, S. (1974). Light-dependent redistribution of ions in suspensions of chloroplast thylakoid membranes. *Proc. Natl. Acad. Sci. U. S. A.* 71, 1484–1488. doi: 10.1073/pnas.71.4.1484
- Huang, L. S., Cobessi, D., Tung, E. Y., and Berry, E. A. (2005). Binding of the respiratory chain inhibitor antimycin to the mitochondrial bc1 complex: a new crystal structure reveals an altered intramolecular hydrogen-bonding pattern. *J. Mol. Biol.* 351, 573–597. doi: 10.1016/j.jmb.2005.05.053
- Huang, W., Yang, Y. J., Hu, H., and Zhang, S. B. (2015). Different roles of cyclic electron flow around photosystem I under sub-saturating and saturating light intensities in tobacco leaves. *Front. Plant Sci.* 6:923. doi: 10.3389/fpls.2015.00923
- Huang, W., Yang, Y. J., Hu, H., Zhang, S. B., and Cao, K. F. (2016). Evidence for the role of cyclic electron flow in photoprotection for oxygen-evolving complex. *J. Plant Physiol.* 194, 54–60. doi: 10.1016/j.jplph.2016.02.016
- Ishikawa, N., Takabayashia, A., Sato, F., and Endo, T. (2016). Accumulation of the components of cyclic electron flow around photosystem I in *C₄* plants, with respect to the requirements for ATP. *Photosynth. Res.* 129, 261–277. doi: 10.1007/s11120-016-0251-0
- Iwai, M., Takizawa, K., Tokutsu, R., Okumuro, A., Takahashi, Y., and Minagawa, J. (2010). Isolation of the elusive supercomplex that drives cyclic electron flow in photosynthesis. *Nature* 464, 1210–1213. doi: 10.1038/nature08885
- Jin, Y. J., Chen, S., Fan, X. J., Song, H., Li, X. X., Xu, J. H., et al. (2017). Diuron treatment reveals the different roles of two cyclic electron transfer pathways in photosystem II in *Arabidopsis thaliana*. *Pestic. Biochem. Physiol.* 137, 15–20. doi: 10.1016/j.pestbp.2016.09.002
- Johnson, X., Steinbeck, J., Dent, R. M., Takahashi, H., Richaud, P., Ozawa, S. I., et al. (2014). Proton gradient regulation 5-mediated cyclic electron flow under ATP- or redox-limited conditions: a study of Δ ATPase *pgr5* and Δ rbcL *pgr5* mutants in the green alga *Chlamydomonas reinhardtii*. *Plant Physiol.* 165, 438–452. doi: 10.1104/pp.113.233593
- Kawashima, R., Sato, R., Harada, K., and Masuda, S. (2017). Relative contributions of PGR5- and NDH-dependent photosystem I cyclic electron flow in the generation of a proton gradient in *Arabidopsis* chloroplasts. *Planta* 246, 1045–1050. doi: 10.1007/s00425-017-2761-1
- Kono, M., Noguchi, K., and Terashima, I. (2014). Roles of the cyclic electron flow around PSI (CET-PSI) and O_2 -dependent alternative pathways in regulation of the photosynthetic electron flow in short-term fluctuating light in *Arabidopsis thaliana*. *Plant Cell Physiol.* 55, 990–1004. doi: 10.1093/pcp/pcu033
- Kono, M., Yamori, W., Suzuki, Y., and Terashima, I. (2017). Photoprotection of PSI by far-red light against the fluctuating light-induced photoinhibition in *Arabidopsis thaliana* and field-grown plants. *Plant Cell Physiol.* 58, 35–45. doi: 10.1093/pcp/pcw215
- Kramer, D. M., Avenson, T. J., and Edwards, G. E. (2004). Dynamic flexibility in the light reactions of photosynthesis governed by both electron and proton transfer reactions. *Trends Plant Sci.* 9, 349–357. doi: 10.1016/j.tplants.2004.05.001
- Kramer, D. M., Cruz, J. A., and Kanazawa, A. (2003). Balancing the central roles of the thylakoid proton gradient. *Trends Plant Sci.* 8, 27–32. doi: 10.1016/S1360-1385(02)00010-9
- Krieger, A., and Weis, E. (1993). The role of calcium in the pH-dependent control of photosystem II. *Photosynth. Res.* 37, 117–130. doi: 10.1007/BF02187470
- Kuczynska, P., Jemioła-Rzeminska, M., Nowicka, B., Jakubowska, A., Strzalka, W., Burda, K., et al. (2020). The xanthophyll cycle in diatom *Phaeodactylum tricornutum* in response to light stress. *Plant Physiol. Biochem.* 152, 125–137. doi: 10.1016/j.plaphy.2020.04.043
- Kukuczka, B., Magneschi, L., Petroutsos, D., Steinbeck, J., Bald, T., Powikrowska, M., et al. (2014). Proton gradient regulation 5-like1-mediated cyclic electron flow is crucial for acclimation to anoxia and complementary to non-photochemical quenching in stress adaptation. *Plant Physiol.* 165, 1604–1617. doi: 10.1104/pp.114.240648
- Labs, M., Rühle, T., and Leister, D. (2016). The antimycin A-sensitive pathway of cyclic electron flow: from 1963 to 2015. *Photosynth. Res.* 129, 231–238. doi: 10.1007/s11120-016-0217-2
- Lambers, H., and Oliveira, R. S. (2019). “Photosynthesis, respiration, and long-distance transport: photosynthesis,” in *Plant Physiological Ecology* (Cham: Springer), 111–114.
- Lapashina, A. S., and Feniouk, B. A. (2018). ADP-inhibition of H^+ - F_0F_1 -ATP synthase. *Biochemistry* 83, 1141–1160. doi: 10.1134/S0006297918100012
- Liu, Y. F. (2020). Calcium chemical priming might play a significant role in relieving overnight chilling-dependent inhibition of photosynthesis in crops: a review. *Basic Clin. Pharmacol. Toxicol.* 126, 109–110. doi: 10.3389/fpls.2020.607029
- Liu, Y. F., Han, X. R., Zhan, X. M., Yang, J. F., Wang, Y. Z., Song, Q. B., et al. (2013). Regulation of calcium on peanut photosynthesis under low night temperature stress. *J. Integr. Agric.* 12, 2172–2178. doi: 10.1016/S2095-3119(13)60411-6
- Liu, Y. F., Qi, H. Y., Bai, C. M., Qi, M. F., Xu, C. Q., Hao, J. H., et al. (2011). Grafting helps improve photosynthesis and carbohydrate metabolism in leaves of muskmelon. *Int. J. Biol. Sci.* 7, 1161–1170. doi: 10.7150/ijbs.7.1161
- Long, T. A., Okegawa, Y., Shikanai, T., Schmidt, G. W., and Covert, S. F. (2008). Conserved role of proton gradient regulation 5 in the regulation of PSI cyclic electron transport. *Planta* 228, 907–918. doi: 10.1007/s00425-008-0789-y
- Lu, J., Yin, Z., Lu, T., Yang, X., Wang, F., Qi, M., et al. (2020). Cyclic electron flow modulates the linear electron flow and reactive oxygen species in tomato leaves under high temperature. *Plant Sci.* 292:110387. doi: 10.1016/j.plantsci.2019.110387
- Ma, M., Liu, Y., Bai, C., and Yong, J. W. H. (2021). The significance of chloroplast NAD(P)H dehydrogenase complex and its dependent cyclic electron transport in photosynthesis. *Front. Plant Sci.* 12:661863. doi: 10.3389/fpls.2021.661863
- Meng, X. L., Zhang, L. T., Zhang, Z. S., Gao, H. Y., and Meng, Q. W. (2012). Role of mitochondrial alternative oxidase (AOX) pathway in photoprotection in *Rumex K-1* leaves. *Chin. J. Appl. Ecol.* 23, 1803–1808. doi: 10.13287/j.1001-9332.2012.0235
- Miller, N. T., Vaughn, M. D., and Burnap, R. L. (2021). Electron flow through NDH-1 complexes is the major driver of cyclic electron flow-dependent proton pumping in cyanobacteria. *Biochim. Biophys. Acta. Bioenerg.* 1862:148354. doi: 10.1016/j.bbabi.2020.148354
- Moss, D. A., and Bendall, D. S. (1984). Cyclic electron transport in chloroplasts. The Q-cycle and the site of action of antimycin. *Biochim. Biophys. Acta. Bioenerg.* 767, 389–395. doi: 10.1016/0005-2728(84)90036-7
- Müller, P., Li, X. P., and Niyogi, K. K. (2001). Non-photochemical quenching. A response to excess light energy. *Plant Physiol.* 125, 1558–1566. doi: 10.1104/pp.125.4.1558
- Munekage, Y. N., Eymery, F., Rumeau, D., Cuiné, S., Oguri, M., Nakamura, N., et al. (2010). Elevated expression of PGR5 and NDH-H in bundle sheath chloroplasts in *C₄* flaveria species. *Plant Cell Physiol.* 51, 664–668. doi: 10.1093/pcp/pcq030
- Munekage, Y. N., Genty, B., and Peitier, G. (2008). Effect of PGR5 impairment on photosynthesis and growth in *Arabidopsis thaliana*. *Plant Cell Physiol.* 49, 1688–1698. doi: 10.1093/pcp/pcn140
- Munekage, Y., Hashimoto, M., Miyake, C., Tomizawa, K. I., Endo, T., Tasaka, M., et al. (2004). Cyclic electron flow around photosystem I is essential for photosynthesis. *Nature* 429, 579–582. doi: 10.1038/nature02598

- Munekage, Y., Hojo, M., Meurer, J., Endo, T., Tasaka, M., and Shikanai, T. (2002). PGR5 is involved in cyclic electron flow around photosystem I and is essential for photoprotection in *Arabidopsis*. *Cell* 110, 361–371. doi: 10.1016/S0092-8674(02)00867-X
- Nandha, B., Finazzi, G., Joliot, P., Hald, S., and Johnson, G. N. (2007). The role of PGR5 in the redox poisoning of photosynthetic electron transport. *Biochim. Biophys. Acta. Bioenerg.* 1767, 1252–1259. doi: 10.1016/j.bbabi.2007.07.007
- Nawrocki, W. J., Bailleul, B., Picot, D., Cardol, P., Rappaport, F., Wollman, F. A., et al. (2019). The mechanism of cyclic electron flow. *Biochim. Biophys. Acta. Bioenerg.* 1860, 433–438. doi: 10.1016/j.bbabi.2018.12.005
- Nishikawa, Y., Yamamoto, H., Okegawa, Y., Shinya, W., Nozomi, S., Yoshichika, T., et al. (2012). PGR5-dependent cyclic electron transport around PSI contributes to the redox homeostasis in chloroplasts rather than CO₂ fixation and biomass production in rice. *Plant Cell Physiol.* 53, 2117–2126. doi: 10.1093/pcp/pcs153
- Niyogi, K. K. (1999). Photoprotection revisited: genetic and molecular approaches. *Annu. Rev. Plant Biol.* 50, 333–359. doi: 10.1146/annurev.arplant.50.1.333
- Okegawa, Y., Kagawa, Y., Kobayashi, Y., and Shikanai, T. (2008). Characterization of factors affecting the activity of photosystem I cyclic electron transport in chloroplasts. *Plant Cell Physiol.* 49, 825–834. doi: 10.1093/pcp/pcn055
- Okegawa, Y., Kobayashi, Y., and Shikanai, T. (2010). Physiological links among alternative electron transport pathways that reduce and oxidize plastoquinone in *Arabidopsis*. *Plant J.* 63, 458–468. doi: 10.1111/j.1365-3113.2010.04252.x
- Okegawa, Y., Long, T. A., Iwano, M., Takayama, S., Kobayashi, Y., Covert, S. F., et al. (2007). A balanced PGR5 level is required for chloroplast development and optimum operation of cyclic electron transport around photosystem I. *Plant Cell Physiol.* 48, 462–471. doi: 10.1093/pcp/pcm116
- Okegawa, Y., and Motohashi, K. (2020). M-type thioredoxins regulate the PGR5/PGRL1-dependent pathway by forming a disulfide-linked complex with PGRL1. *Plant Cell* 32, 3866–3883. doi: 10.1105/tpc.20.00304
- Paredes, M., and Quiles, M. J. (2017). Chilling stress and hydrogen peroxide accumulation in *Chrysanthemum morifolium* and *Spathiphyllum lanceifolium*. Involvement of chlororespiration. *J. Plant Physiol.* 211, 36–41. doi: 10.1016/j.jplph.2016.11.015
- Peltier, G., Tolleter, D., Billon, E., and Cournac, L. (2010). Auxiliary electron transport pathways in chloroplasts of microalgae. *Photosynth. Res.* 106, 19–31. doi: 10.1007/s11120-010-9575-3
- Pospisil, P., and Tyystjärvi, E. (1999). Molecular mechanism of high temperature induced inhibition of acceptor side of photosystem II. *Photosynth. Res.* 62, 55–66. doi: 10.1023/A:1006369009170
- Rantala, S., Lempiäinen, T., Gerotto, C., Tiwari, A., Aro, E. M., and Tikkanen, M. (2020). PGR5 and NDH-1 systems do not function as protective electron acceptors but mitigate the consequences of PSI inhibition. *BBA-Bioenerg.* 1861:148154. doi: 10.1016/j.bbabi.2020.148154
- Sato, R., Kawashima, R., Trinh, M. D. L., Nakano, M., Nagai, T., and Masuda, S. (2019). Significance of PGR5-dependent cyclic electron flow for optimizing the rate of ATP synthesis and consumption in *Arabidopsis* chloroplasts. *Photosynth. Res.* 139, 359–365. doi: 10.1007/s11120-018-0533-9
- Shi, Q., Pang, J., Yong, J. W. H., Bai, C., Pereira, C. G., Song, Q., et al. (2019). Phosphorus-fertilisation has differential effects on leaf growth and photosynthetic capacity of *Arachis hypogaea* L. *Plant Soil* 447, 99–116. doi: 10.1007/s11104-019-04041-w
- Shikanai, T. (2007). Cyclic electron transport around photosystem I: genetic approaches. *Annu. Rev. Plant Biol.* 58, 199–217. doi: 10.1146/annurev.arplant.58.091406.110525
- Shikanai, T. (2014). Central role of cyclic electron transport around photosystem I in the regulation of photosynthesis. *Curr. Opin. Biotechnol.* 26, 25–30. doi: 10.1016/j.copbio.2013.08.012
- Shikanai, T. (2016). Regulatory network of proton motive force: contribution of cyclic electron transport around photosystem I. *Photosynth. Res.* 129, 253–260. doi: 10.1007/s11120-016-0227-0
- Song, Q. B., Liu, Y. F., Pang, J. Y., Yong, J. W. H., Chen, Y. L., Bai, C. M., et al. (2020). Supplementary calcium restores peanut (*Arachis hypogaea*) growth and photosynthetic capacity under low nocturnal temperature. *Front. Plant Sci.* 10:01637. doi: 10.3389/fpls.2019.01637
- Sonoike, K. (2011). Photoinhibition of photosystem I. *Physiol. Plant.* 142, 56–64. doi: 10.1111/j.1399-3054.2010.01437.x
- Storti, M., Alboresi, A., Gerotto, C., Aro, E. M., Finazzi, G., and Morosinotto, T. (2019). Role of cyclic and pseudo-cyclic electron transport in response to dynamic light changes in *Physcomitrella patens*. *Plant Cell Environ.* 42, 1590–1602. doi: 10.1111/pce.13493
- Strand, D. D., Fisher, N., Davis, G. A., and Kramer, D. M. (2016). Redox regulation of the antimycin A sensitive pathway of cyclic electron flow around photosystem I in higher plant thylakoids. *Biochim. Biophys. Acta. Bioenerg.* 1857, 1–6. doi:10.1016/j.bbabi.2015.07.012
- Sugimoto, K., Okegawa, Y., Tohri, A., Long, T. A., Covert, S. F., Hisabori, T., et al. (2013). A single amino acid alteration in PGR5 confers resistance to antimycin A in cyclic electron transport around PSI. *Plant Cell Physiol.* 54, 1525–1534. doi: 10.1093/pcp/ptc098
- Sun, Y., Geng, Q., Du, Y., Yang, X., and Zhail, H. (2017). Induction of cyclic electron flow around photosystem I during heat stress in grape leaves. *Plant Sci.* 256, 65–71. doi: 10.1016/j.plantsci.2016.12.004
- Suorsa, M., Järvi, S., Grieco, M., and Nurmi, M. (2012). PROTON GRADIENT REGULATIONS is essential for proper acclimation of *Arabidopsis* photosystem I to naturally and artificially fluctuating light conditions. *Plant Cell* 24, 2934–2948. doi: 10.2307/23264750
- Suorsa, M., Rossi, F., Tadini, L., Labs, M., Colombo, M., Jahns, P., et al. (2016). PGR5-PGRL1-dependent cyclic electron transport modulates linear electron transport rate in *Arabidopsis thaliana*. *Mol. Plant* 9, 271–288. doi: 10.1016/j.molp.2015.12.001
- Suzuki, N., Riveri, R. M., Shulaev, V., Blumvald, E., and Mittler, R. (2014). Abiotic and biotic stress combinations. *New Phytol.* 203, 32–43. doi: 10.1111/nph.12797
- Taira, Y., Okegawa, Y., Sugimoto, K., Abe, M., Miyoshi, H., and Shikanai, T. (2013). Antimycin A-like molecules inhibit cyclic electron transport around photosystem I in ruptured chloroplasts. *FEBS Open Bio.* 3, 406–410. doi: 10.1016/j.fob.2013.09.007
- Takahashi, H., Clowez, S., Wollman, F. A., Vallon, O., and Rappaport, F. (2013). Cyclic electron flow is redox-controlled but independent of state transition. *Nat. Commun.* 4:1954. doi: 10.1038/ncomms2954
- Takahashi, S., Milward, S. E., Fan, D. Y., Chow, W. S., and Badger, M. R. (2009). How does cyclic electron flow alleviate photoinhibition in *Arabidopsis*? *Plant Physiol.* 149, 1560–1567. doi: 10.1104/pp.108.134122
- Tikkanen, M., Grieco, M., Kangasjärvi, S., and Aro, E. M. (2010). Thylakoid protein phosphorylation in higher plant chloroplasts optimizes electron transfer under fluctuating light. *Plant Physiol.* 152, 723–735. doi: 10.1104/pp.109.150250
- Tikkanen, M., Mekala, N. R., and Aro, E. M. (2014). Photosystem II photoinhibition-repair cycle protects photosystem I from irreversible damage. *Biochim. Biophys. Acta. Bioenerg.* 1837, 210–215. doi: 10.1016/j.bbabi.2013.10.001
- Ueda, M., Kuniyoshi, T., Yamamoto, H., Sugimoto, K., Ishizaki, K., Kohchi, T., et al. (2012). Composition and physiological function of the chloroplast NADH dehydrogenase-like complex in *Marchantia polymorpha*. *Plant J.* 72, 683–693. doi: 10.1111/j.1365-3113.2012.05115.x
- Vass, I., Cser, K., and Cheregi, O. (2007). Molecular mechanisms of light stress of photosynthesis. *Ann. N. Y. Acad. Sci.* 1113, 114–122. doi: 10.1196/annals.1391.017
- Wada, S., Takagi, D., Miyake, C., Makino, A., and Suzuki, Y. (2019). Responses of the photosynthetic electron transport reactions stimulate the oxidation of the reaction center chlorophyll of photosystem I, P700, under drought and high temperatures in rice. *Int. J. Mol. Sci.* 20:2068. doi: 10.3390/ijms20092068
- Walker, B. J., Strand, D. D., Kramer, D. M., and Cousins, A. B. (2014). The response of cyclic electron flow around photosystem I to changes in photorespiration and nitrate assimilation. *Plant Physiol.* 165, 453–462. doi: 10.1104/pp.114.238238
- Wang, P., Duan, W., Takabayashi, A., Endo, T., and Mi, H. (2006). Chloroplastic NAD(P)H dehydrogenase in tobacco leaves functions in alleviation of oxidative damage caused by temperature stress. *Plant Physiol.* 141, 465–474. doi: 10.1104/pp.105.070490
- Wang, Y., He, X., Ma, W., Zhao, X., Li, B., and Tong, Y. (2014). Wheat PROTON GRADIENT REGULATION 5 is involved in tolerance to photoinhibition. *J. Integr. Agric.* 13, 1206–1215. doi: 10.1016/S2095-3119(13)60604-8
- Wang, C., Yamamoto, H., and Shikanai, T. (2015). Role of cyclic electron transport around photosystem I in regulating proton motive force. *Biochim. Biophys. Acta. Bioenerg.* 1847, 931–938. doi: 10.1016/j.bbabi.2014.11.013

- Wang, F., Yan, J., Ahammed, G. J., Wang, X., Bu, X., Xiang, H., et al. (2020). PGR5/PGRL1 and NDH mediate far-red light-induced photoprotection in response to chilling stress in tomato. *Front. Plant Sci.* 11:669. doi: 10.3389/fpls.2020.00669
- Wolf, B., Isaacson, T., Tiwari, V., Dangoor, I., Mufkadi, S., and Danon, A. (2020). Redox regulation of pgrl1 at the onset of low light intensity. *Plant J.* 103, 715–725. doi: 10.1111/tpj.14764
- Wu, D., Liu, Y., Pang, J., Yong, J. W. H., Chen, Y., Bai, C., et al. (2020). Exogenous calcium alleviates nocturnal chilling-induced feedback inhibition of photosynthesis by improving sink demand in peanut (*Arachis hypogaea*). *Front. Plant Sci.* 11:607029. doi: 10.3389/fpls.2020.607029
- Xue, X., Xu, H. M., Wu, H. Y., Shen, Y. B., Xiao, J. W., and Wan, Y. L. (2017). Research progress of cyclic electron transport in plant photosynthesis. *Plant Physiol. J.* 53, 145–158. doi: 10.13592/j.cnki.ppj.2016.0432
- Yadav, R. M., Aslam, S. M., Madireddi, S. K., Chouhan, N., and Subramanyam, R. (2020). Role of cyclic electron transport mutations pgrl1 and pgr5 in acclimation process to high light in *Chlamydomonas reinhardtii*. *Photosynth. Res.* 146, 247–258. doi: 10.1007/s11120-020-00751-w
- Yamamoto, H., and Shikanai, T. (2019). PGR5-dependent cyclic electron flow protects photosystem I under fluctuating light at donor and acceptor sides. *Plant Physiol.* 179, 588–600. doi: 10.1104/pp.18.01343
- Yamamoto, H., Takahashi, S., Badger, M. R., and Shikanai, T. (2016). Artificial remodelling of alternative electron flow by flavodiiron proteins in *Arabidopsis*. *Nat. Plants.* 2:16012. doi: 10.1038/nplants.2016.12
- Yamori, W., Makino, A., and Shikanai, T. (2016). A physiological role of cyclic electron transport around photosystem I in sustaining photosynthesis under fluctuating light in rice. *Sci. Rep.* 6:20147. doi: 10.1038/srep20147
- Yamori, W., and Shikanai, T. (2016). Physiological functions of cyclic electron transport around photosystem I in sustaining photosynthesis and plant growth. *Annu. Rev. Plant Biol.* 67, 81–106. doi: 10.1146/annurev-arplant-043015-112002
- Yamori, W., Shikanai, T., and Makino, A. (2015). Photosystem I cyclic electron flow via chloroplast NADH dehydrogenase-like complex performs a physiological role for photosynthesis at low light. *Sci. Rep.* 5:13908. doi: 10.1038/srep13908
- Zhou, L., Gao, S., Wu, S., Han, D., Wang, H., Gu, W., et al. (2020). PGRL1 overexpression in *Phaeodactylum tricornutum* inhibits growth and reduces apparent PSII activity. *Plant J.* 103, 1850–1857. doi: 10.1111/tpj.14872
- Zivcak, M., Kalaji, H. M., Shao, H. B., Olsovska, K., and Brestic, M. (2014). Photosynthetic proton and electron transport in wheat leaves under prolonged moderate drought stress. *J. Photoch. Photobiol. B.* 137, 107–115. doi: 10.1016/j.jphotobiol.2014.01.007

Conflict of Interest: YY was employed by the company Yingkou Magnesite Chemical Ind Group Co. Ltd.

The remaining authors declare that the research was conducted in the absence of any commercial or financial relationships that could be construed as a potential conflict of interest.

Copyright © 2021 Ma, Liu, Bai, Yang, Sun, Liu, Zhang, Han and Yong. This is an open-access article distributed under the terms of the Creative Commons Attribution License (CC BY). The use, distribution or reproduction in other forums is permitted, provided the original author(s) and the copyright owner(s) are credited and that the original publication in this journal is cited, in accordance with accepted academic practice. No use, distribution or reproduction is permitted which does not comply with these terms.



How to Measure Grana – Ultrastructural Features of Thylakoid Membranes of Plant Chloroplasts

Radosław Mazur¹, Agnieszka Mostowska² and Łucja Kowalewska^{2*}

¹Department of Metabolic Regulation, Institute of Biochemistry, Faculty of Biology, University of Warsaw, Warsaw, Poland,

²Department of Plant Anatomy and Cytology, Institute of Plant Experimental Biology and Biotechnology, Faculty of Biology, University of Warsaw, Warsaw, Poland

OPEN ACCESS

Edited by:

Rebecca L. Roston,
University of Nebraska-Lincoln,
United States

Reviewed by:

Rajagopal Subramanyam,
University of Hyderabad,
India

Gadi Schuster,
Technion Israel Institute of
Technology, Israel

*Correspondence:

Łucja Kowalewska
lucja.kowalewska@uw.edu.pl

Specialty section:

This article was submitted to
Plant Physiology,
a section of the journal
Frontiers in Plant Science

Received: 09 August 2021

Accepted: 09 September 2021

Published: 06 October 2021

Citation:

Mazur R, Mostowska A and
Kowalewska Ł (2021) How to
Measure Grana – Ultrastructural
Features of Thylakoid Membranes of
Plant Chloroplasts.
Front. Plant Sci. 12:756009.
doi: 10.3389/fpls.2021.756009

Granum is a basic structural unit of the thylakoid membrane network of plant chloroplasts. It is composed of multiple flattened membranes forming a stacked arrangement of a cylindrical shape. Grana membranes are composed of lipids and tightly packed pigment-protein complexes whose primary role is the catalysis of photosynthetic light reactions. These membranes are highly dynamic structures capable of adapting to changing environmental conditions by fine-tuning photochemical efficiency, manifested by the structural reorganization of grana stacks. Due to a nanometer length scale of the structural granum features, the application of high-resolution electron microscopic techniques is essential for a detailed analysis of the granum architecture. This mini-review overviews recent approaches to quantitative grana structure analyses from electron microscopy data, highlighting the basic manual measurements and semi-automated workflows. We outline and define structural parameters used by different authors, for instance, granum height and diameter, thylakoid thickness, end-membrane length, Stacking Repeat Distance, and Granum Lateral Irregularity. This article also presents insights into efficient and effective measurements of grana stacks visualized on 2D micrographs. The information on how to correctly interpret obtained data, taking into account the 3D nature of grana stacks projected onto 2D space of electron micrograph, is also given. Grana ultrastructural observations reveal key features of this intriguing membrane arrangement, broadening our knowledge of the thylakoid network's remarkable plasticity.

Keywords: chloroplast, grana, granum stack, measurements, thylakoid membranes, transmission electron microscopy, ultrastructure

GRANA AS BASIC STRUCTURAL UNITS OF THE CHLOROPLAST THYLAKOID NETWORK IN PLANTS

Grana are essential structural features of the chloroplast thylakoid network, which are specific for plants. They are both confined structures characterized by a distinct molecular composition and, simultaneously, continuous elements of intertwined stroma-grana thylakoid network. Other photosynthetic organisms do not have a clear division between stacked grana and loosely arranged stroma thylakoid (ST) domains. Cyanobacteria possess unstacked photosynthetic membranes forming fascicular, radial, or parallel arrangements (Mareš et al., 2019). Similarly,

red algae also do not exhibit thylakoid stacking, while brown algae and diatoms contain appressed membranes grouped by 2 or 3 (Bertrand, 2010). In green algae, the thylakoid membranes are organized into clearly differentiated stacked and unstacked regions but without highly structured multiple membrane layers characteristic for plant grana (Engel et al., 2015). Some authors describe thylakoid membrane stacks of late branching green algae taxa *Coleochaetales* and *Charales* as grana; however, based on the widely accepted evolutionary hypothesis, grana evolved after land colonization and therefore, are unique for plants (Gunning and Schwartz, 1999; Larkum and Veski, 2003; Mullineaux, 2005). It is worth noticing that although thylakoid membranes of different plant groups, from Bryophytes to Angiosperms, show high variability of photosynthetic complexes supramolecular organization, their grana exhibit similar nanomorphology (Chen et al., 2018b).

From the structural point of view, grana might be described as stacks of discoidal-shaped thylakoids; however, such a general definition is insufficient for detailed qualitative and quantitative analysis of grana structure. A single granum stack is usually composed of 5–25 thylakoid layers with diameters between 300 and 550 nm. The model granum structure is built by thylakoid membranes with the same diameter forming a perfect cylindrical shape. However, in most plant species and specific environmental conditions, the grana structures are highly irregular – with a variable diameter of thylakoid layers and their shift in the lateral plane (Figure 1A). It is difficult to structurally distinguish the individual grana stacks with high confidence; therefore, a precise procedure formulation is required (see “Grana Ultrastructural Parameters”).

General granum definition also does not determine the boundary of the granum in the vertical plane. No limit of the maximal granum height exists; many plant species, especially shade-grown ones, can form grana composed of over 50 layers (Anderson et al., 1973; Chow et al., 2005). Nonetheless, the minimal number of stacked layers that can be considered granum is questionable. The granum stack is built of its core, margins, and end-membranes (Figure 1B). These components are characterized by the specific lipid–pigment–protein composition (reviewed in Ruban and Johnson, 2015; Koochak et al., 2019). The boundary of the granum in the lateral plane is set by highly curved membrane regions called grana margins, with peripheries called “curvature domains” that can be biochemically separated (Trotta et al., 2019). Some authors propose a more strict definition of grana margins based on biochemical studies, describing them as an interface between appressed and non-appressed regions only (Rantala et al., 2020). Thylakoids resemble flattened vesicles; they are composed of two membranes and an inner aqueous compartment called “lumen.” Neighboring thylakoids in the stack are partitioned by a thin layer of stroma compartment called “stromal gap,” “interthylakoid stromal space,” or “partition gap” (Figure 1C). In the case of core thylakoids, both membranes are identical, while grana end-thylakoids have a heterogeneous architecture; the inner membrane is similar to that of the core thylakoids and the outer one to the ST membrane (Anderson et al., 2012). Considering all this, the lowest granum stack, which contains

all types of structural components, has to be built by at least three thylakoid layers. Already in early ultrastructural studies, the two-layer membrane stacks were described as “membrane overlaps” pointing to a different structural assignment of such arrangements (Gunning and Steer, 1975; Figure 1D).

An accurate understanding of the granum structure enables the determination of reliable measuring protocols necessary to provide comparable results obtained by different researchers. Detailed analysis of grana structure provides important information about the thylakoid membrane remodeling forced by plant ontogenesis (Kowalewska et al., 2016; Armarego-Marriott et al., 2019; Pipitone et al., 2021), light intensity and quality (Rozak et al., 2002; Yamamoto et al., 2014; Demmig-Adams et al., 2015; Schumann et al., 2017; Flannery et al., 2021), and other environmental factors (Fq et al., 2012; Jiang et al., 2017; Chen et al., 2018a; Zechmann, 2019; Mazur et al., 2020). However, structural analysis indirectly indicates the organization and efficiency of the photosynthetic light reaction machinery (Pribil et al., 2018; Mazur et al., 2019; Wood et al., 2019; Hepworth et al., 2021) and photonic effects in the thylakoid network (Capretti et al., 2019).

Structural grana analysis using mutants with an aberrant composition of thylakoids is particularly helpful in understanding the role of lipid–pigment–protein components in the self-organization of different membrane shapes, such as curved, flat, and stacked regions (Fristedt et al., 2009; Armbruster et al., 2013; Mazur et al., 2019; Bykowski et al., 2021; Gupta et al., 2021; Raven, 2021). A necessary condition, though not sufficient, to define a given chloroplast-localized structure as granum is membrane stacking. The balance between attractive van der Waals forces, repulsive electrostatic and hydrostructural forces was described as crucial for maintaining grana stacking. The abundance, stability, and surface charge of thylakoid membrane components mainly mediate such balance (Puthiyaveetil et al., 2017).

Several thylakoid membrane components have been recognized to play a crucial role in the fine-tuning of grana structure. Numerous studies showed that changes in the ratio of antenna light-harvesting complexes (LHCII) and core proteins of photosystem II (PSII) induce grana size remodeling. Depletion of chloroplast-encoded PSII subunits caused the formation of “super-grana” containing dozens of membranes (Belgio et al., 2015), while lack of Lhcb1 and Lhcb2 antenna proteins resulted in a significant decrease in grana height (Andersson et al., 2003; Anderson et al., 2012; Pietrzykowska et al., 2014; Nicol et al., 2019). Small grana size is also typical for the *chlorina* mutants, characterized by reduced chlorophyll *b* content (e.g., Kim et al., 2009). Tuning of grana structure was also linked with posttranslational modifications of photosynthetic proteins, e.g., increased polyamination of Lhcb, resulting from overexpression of plastidial transglutaminase, caused the formation of extremely high grana stacks (Ioannidis et al., 2009; Ioannidis et al., 2012). In contrast, decreased acetylation of photosynthetic proteins (*Arabidopsis nsi* mutant) induced the formation of lower stacks compared with wild-type plants (Koskela et al., 2018),

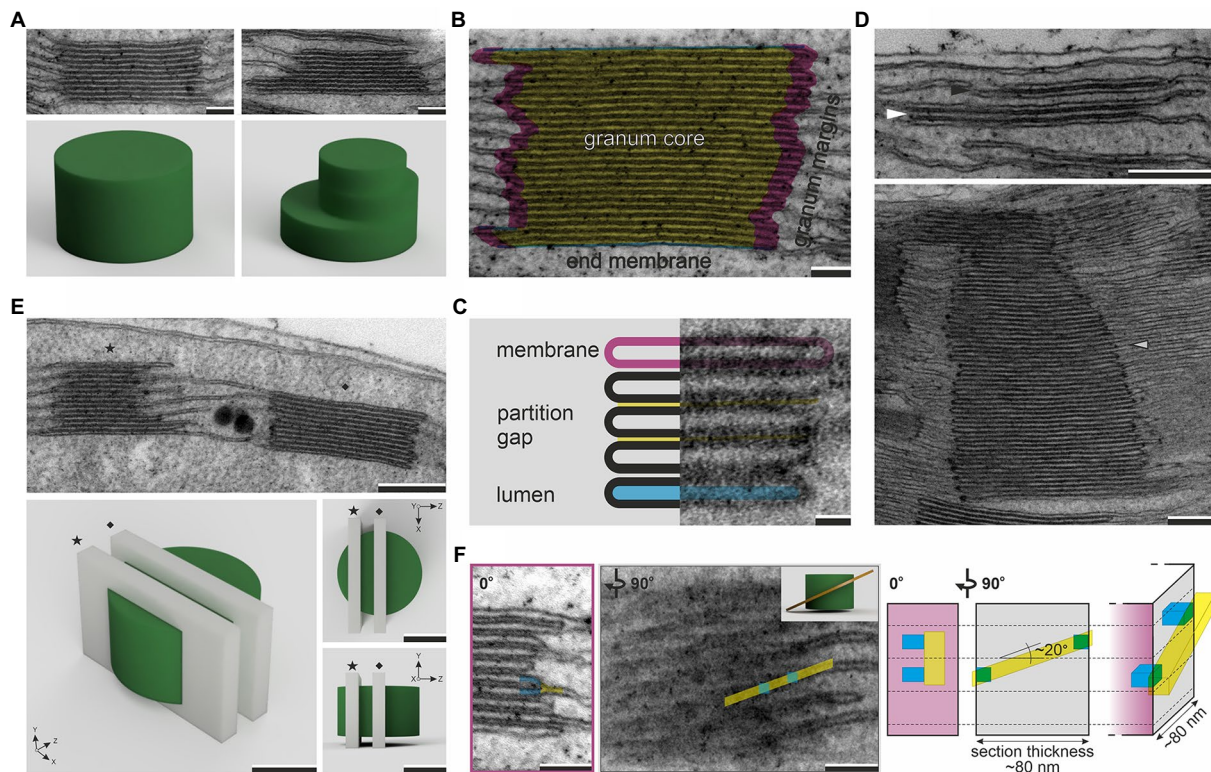


FIGURE 1 | Electron micrographs of regular (left column) and irregular (right column) grana structures with corresponding 3D models showing the hypothetical spatial representation of visualized stacks (**A**). Three main ultrastructural components of granum stack – granum core (yellow), granum margins (pink), and end membranes (blue; **B**). Basic compartments of stacked thylakoids – membrane (pink), partition gap (yellow), and lumen (blue; **C**). Electron micrographs showing two-layer thylakoid membrane stack, i.e., “membrane overlap” (black arrowhead), the lowest possible granum built by three thylakoid layers (white arrowhead), and extremely high granum stack composed of over 70 thylakoid layers (gray arrowhead; **D**). Electron micrograph and corresponding 3D models showing two different z-axis planes (star – tangential cut, diamond – central cut) of random granum sectioning; note that section planes (light gray cuboids) visible on 3D granum renders (green) represent 70-nm-thick ultrathin sections (**E**). Electron micrographs showing connection of neighboring grana thylakoids through stroma thylakoid (yellow) in the granum marginal region (blue) as visualized from two different angles (inset in the right corner of the second image presents a simplified 3D model of helical grana-stroma thylakoid arrangement); right side of the panel shows a scheme of the connection region visible in the perspective view and two orientations corresponding to presented micrographs; for ultrathin section with thickness between 70 and 90 nm and angle of stroma thylakoid staggering $\sim 20^\circ$, connection of two neighboring grana thylakoid layers can be observed in one section and visible as a fork-like structure on the sample projection (transmission electron microscopy (TEM) image; **F**). Note that various angles of granum section showed in panels (**E**) and (**F**) are presented on different grana stacks; electron micrographs were obtained from fully developed chloroplasts of *Arabidopsis thaliana* (**A–F**, with the exception of the lower image in panel **D**) and *Ficus elastica* (lower image on panel **D**); scale bar = 100 nm (**A,B,F**), 20 nm (**C**), 250 nm (**D,E**).

and lack of PSII core protein phosphorylation (*Arabidopsis stn8*, *stn7stn8* mutants) resulted in increased grana diameter (Fristedt et al., 2009).

Moreover, a family of structural membrane proteins – CURVATURE THYLAKOID 1 (CURT1), were recognized to mediate the diameter of grana stacks in a dosage-dependent manner and facilitate membrane curvature at the grana margins (Armbruster et al., 2013; Pribil et al., 2018). The grana-localized REDUCED INDUCTION OF NON-PHOTOCHEMICAL QUENCHING (RIQ) proteins regulate the grana height and probably link the grana structure with the organization of LHCII (Yokoyama et al., 2016). All acyl lipid components of thylakoid membranes were proved to be important in maintaining proper grana sizes; however, only monogalactosyldiacylglycerol role in the formation of helical grana arrangements was shown (Yu and Benning, 2003; Mazur et al., 2019). We have also recently presented that increased

lutein to carotene ratio causing membrane rigidification results in hampered grana membrane folding (Bykowski et al., 2021). In all of these studies, ultrastructural transmission electron microscopy (TEM) analysis was essential to understand structural role of particular membrane components in the grana self-organization process.

METHODS USED IN THE VISUALIZATION OF GRANUM MORPHOLOGY AND THEIR LIMITATIONS

Efficient measurements of grana structural parameters require high-quality visualization of the thylakoid network. The catalog of suitable microscopy methods is limited due to the dimensions

of the grana stacks. In general, these methods can be divided into two groups (i) enabling *in vivo* analysis but with lower resolution, and (ii) high-resolution methods requiring sample fixation.

In vivo methods are mainly based on the detection of chlorophyll autofluorescence (reviewed in Kowalewska et al., 2019). Their advantage lies in the precise tracking of membrane remodeling triggered by different factors. Still, they fail in detailed grana visualization at the level of particular thylakoid layers. Typical grana structural parameters obtained using an *in vivo* approach are granum diameter (Uwada et al., 2017; Wood et al., 2019; Hepworth et al., 2021), also defined as full-width at half-maximum fluorescence intensity of the fluorescent spots (grana; Herbstova et al., 2012; Iwai et al., 2018; Wood et al., 2018; Flannery et al., 2021), and parameters describing the whole network. These parameters include: the number of grana stacks per chloroplast (Wood et al., 2018, 2019; Mazur et al., 2019), their distribution (Herbstova et al., 2012; Chen et al., 2014), and average grana sizes determined indirectly by the surface/volume ratio for 3D models of chlorophyll fluorescence (Bykowski et al., 2021).

High-resolution TEM, although requiring sample fixation, remains the most favored method to study the grana morphology due to the nanometer length scale of the grana structural details. The thylakoid ultrastructure might also be assessed using small-angle scattering methods that enable a noninvasive analysis of high volume samples (Ünnep et al., 2017; Jakubauskas et al., 2019; Ünnep et al., 2020; Zsiros et al., 2020; Jakubauskas et al., 2021). Only periodic membrane attributes can be registered, while no information on grana diameter or details of membrane connections could be revealed. TEM, however, gives access to a broader range of grana structural parameters defined and described in “**Grana Ultrastructural Parameters**” of this mini-review.

Regardless of the numerous advantages of the TEM method in the grana structure studies, particular sample preparation conditions should be considered for a reliable analysis. Due to the relatively small area of TEM analysis, it is essential to control the region of sampling. Chloroplasts of the leaf mesophyll of mono- and dicotyledonous plants do not form a uniform group of organelles. Their thylakoid network is characterized by different structural parameters depending on the leaf age and cell position within the leaf blade (Avramova et al., 2015; Gugel and Soll, 2016). Similarly, a unified time of sample collection is also essential. Suppose sampling throughout the light-dark cycle is not required. In that case, the most favorable time for sample fixation is at the end of the dark phase when the starch grains are, in most cases, degraded, enabling proper observation of the thylakoid network. This approach applies both for samples fixed using chemical and cryo-protocols. High-pressure freezing combined with the freeze-substitution method is particularly susceptible to starch grains whose presence during the procedure leads to the local thylakoid swelling near starch deposits (McDonald, 2014; Armarego-Marriott et al., 2019).

INTERPRETATION OF A 3D GRANA STRUCTURE PROJECTED ONTO 2D SPACE

Although electron microscopy techniques enable a volumetric analysis of samples (electron tomography, serial block-face scanning electron microscopy, or focus ion beam scanning electron microscopy), these techniques are time- and money-consuming. For instance, visualization of the 3D structure of granum using electron tomography requires a multistep procedure composed of data acquisition, alignment, reconstruction, segmentation, and visualization (reviewed in Daum and Kuhlbrandt, 2011; Otegui and Pennington, 2018; Staehelin and Paolillo, 2020). Such extensive workflow limits the possibility of obtaining large data sets and, therefore, reliable quantitative analysis of particular structural parameters. In contrast, 2D TEM analysis is more accessible for researchers and enables the creation of relatively large data sets. However, it is essential to acknowledge that 2D analysis of 3D objects with complicated spatial structures is not straightforward, and the random nature of sample cutting has to be taken into account. The analysis of granum diameter on 2D sections is prone to chord error. It cannot be established whether the observed section shows the diameter or any other chord of the discoidal granum (**Figure 1E**). Therefore, large values of standard deviation are typical for the granum diameter measurements, which points to the necessity of analyzing big data sets for reliable comparison between samples. Another common issue in proper analysis of 2D grana images is related to the interpretation of the structure of grana-stroma thylakoid connections. In these regions, some authors show “fork-like connections” of ST with two neighboring layers of grana stack (fret-like protrusions) using 2D TEM projections (Shimoni et al., 2005; Koochak et al., 2019). However, it should be stressed that such structures are most probably only local phenomena in the *z*-axis of the specimen, which, for 3D models, are parts of STs staggering between granum layers forming pseudo-helical arrangement in the nearest stack surrounding (Mustárdy et al., 2008; Austin and Staehelin, 2011; Kowalewska et al., 2016; Bussi et al., 2019). The typical ultrathin section is 70–90 nm thick; if the granum-connected ST membrane shifts at an angle of around 20° (Austin and Staehelin, 2011; Bussi et al., 2019), membrane staggering between two neighboring layers might be observed within one specimen (for details see **Figure 1F**). TEM images are projections of the visualized sample; therefore, it is impossible to establish the membrane’s *z*-axis position inside the sample, and the risk of misinterpretation is significant.

GRANA ULTRASTRUCTURAL PARAMETERS

The first measurements of grana ultrastructural parameters were performed, *in situ*, with the help of mechanical instruments – curvometers on printed electron micrographs of chloroplasts (similarly to measurements on maps). The length of grana

and stroma thylakoids was measured per randomly chosen unit area ($1\ \mu\text{m}^2$) of each chloroplast cross section. The number of thylakoids per granum was also determined (e.g., Brangeon, 1973; Mostowska, 1986). Such basic parameters are also frequently assessed in current microscopy studies using digital micrographs and image analysis software of choice, followed by different approaches in data presentation and appropriate statistical analyses (e.g., Rozak et al., 2002; Anderson et al., 2012; Pietrzykowska et al., 2014; Pribil et al., 2018; Wood et al., 2018; Nicol et al., 2019; Li et al., 2020).

Several structural parameters describe the vertical direction of the granum ultrastructure. The most basic one is the granum height. It is established by measuring the distance between the top and bottom layers of the granum end-membranes. Such distance has to be measured perpendicular to the granum lateral plane (**Figure 2A**). Significant variability in the granum height was registered in plants exposed to different light conditions and connected to the proportion between PSII core and antennae complexes (reviewed in Allen and Forsberg, 2001; Waters and Langdale, 2009; Anderson et al., 2012). The granum height might also be affected by modified physical properties of thylakoid membranes forced by changes in their pigment-protein composition, influencing membrane folding capabilities (Bykowski et al., 2021). Moreover, significant changes in the height of granum stacks were observed in the second phase of the chloroplast biogenesis in different plant species, together with the accumulation of associated photosynthetic proteins and capacity (Armarego-Marriott et al., 2019; Pipitone et al., 2021). In the most general approach, height in the middle of the granum diameter is obtained; however, if the thylakoid thickness is not constant throughout the diameter of the stack, additional measurements have to be taken (for details, see **Figure 2A**). Such analysis enabled, e.g., observation of swelling and/or bending of the grana marginal regions in plants exposed to high-light conditions to empower more efficient D1 protein turnover (Herbstova et al., 2012; Yoshioka-Nishimura et al., 2014; Kirchhoff, 2019).

Measurement of height combined with the counting of the thylakoid layers that build a particular granum stack enables calculation of the so-called Stacking Repeat Distance (SRD), also named “Repeat Distance,” which represents the average thickness of the thylakoid with the neighboring partition gap (**Figure 2B**). SRD might also be measured directly through manual or semi-automated segmentation of particular granum elements (membrane, lumen, and partition gap) using high magnifications. Various semi-automated approaches based on pixel gradient and power spectrum analyses were applied by different authors (Kirchhoff et al., 2011; Tsabari et al., 2015; Wood et al., 2018; Li et al., 2020; for details, see **Figure 2B**). It should be noted that all detailed analyses of granum layers require high-quality images of grana stacks cut parallelly to the vertical granum direction (**Figure 2C**). The analysis of SRD and sizes of particular granum elements is frequently assessed in studies on the influence of light on the thylakoid ion transport resulting in significant changes in, e.g., lumen or partition gap sizes due to water diffusion and changes in repulsive/attractive forces, respectively (Kim et al., 2005; Puthiyaveetil et al., 2017).

The granum lateral (horizontal) plane analysis requires a precise definition of the granum stack boundary. Due to the high variability of grana architecture in the lateral plane, identifying a single granum stack should be justified each time. For instance, it might be assumed that a single granum stack is characterized by (i) common height, which is shared by all stacked membranes building a particular stack, and (ii) shifted regions which are built by at least three stacked membranes (**Figure 2D**). In such conditions, membrane overlaps connecting neighboring grana are not considered part of these stacks. Therefore, complicated connections of stacked membranes can be quite easily identified for a reliable analysis (**Figure 2D**). As a consequence of irregular membrane stacks, the granum diameter established in a single measurement of a layer placed in the middle of the granum should be considered as an oversimplification in most cases. Since a granum stack can be built of layers with significantly different diameters (see examples in **Figure 1A**), a more precise analysis should be provided, where every layer of the granum stack is measured separately, and the average granum diameter is calculated. Calculations of grana diameters were used to understand the connection between the thylakoid structure and the balance between linear and cyclic electron transport (Wood et al., 2018). Diameter measurements were helpful in the establishment of the structural role of CURT1A proteins (Armbruster et al., 2013) and also, e.g., in deciphering the influence of defective PSII core protein phosphorylation on lateral migration of D1 and FtsH proteins between the membrane domains (Khatoon et al., 2009; Puthiyaveetil et al., 2014).

From the diameter values of all membranes building a single granum, a parameter reflecting irregularity of the particular stack called “Granum Lateral Irregularity” (GLI) can be calculated. GLI is defined as the coefficient of variation (the ratio of the standard deviation to the mean) of membrane diameters within the granum (Kowalewska et al., 2016). The minimal GLI value of 0 is reached by grana stacks built of membranes with the same diameter; the higher variability in granum thylakoid diameters, the higher the GLI value (**Figure 2E**). GLI as a relative variation gives a good measure of irregularity since the chord error of grana thylakoid diameter is minimized. GLI parameter, however, does not consider the shifting of membranes in the lateral plane. Therefore, we introduce a new parameter that covers this issue giving information about the irregularity of the granum cross section. “Granum Cross-Sectional Irregularity” (GSI) is calculated by comparing the granum cross-sectional area and rectangle area with the same perimeter and height as the granum cross section (**Figure 2F**). This approach allows identifying irregular grana whose GLI value is close to 0, while membrane shifting in the lateral plane is significant (**Figure 2F**). Irregular granum arrangement also results in a substantial increase in the ratio of the granum end-membranes to the total stacked membranes; the more irregular granum, the higher the ratio (**Figure 2G**). Although the height and diameter of grana stacks significantly increase during the initial stages of chloroplast biogenesis, it was established that granum irregularity decreases during this process, indicating an organized structural pathway of grana maturation (Kowalewska et al., 2016). However, the influence of grana structural irregularity on the thylakoid network

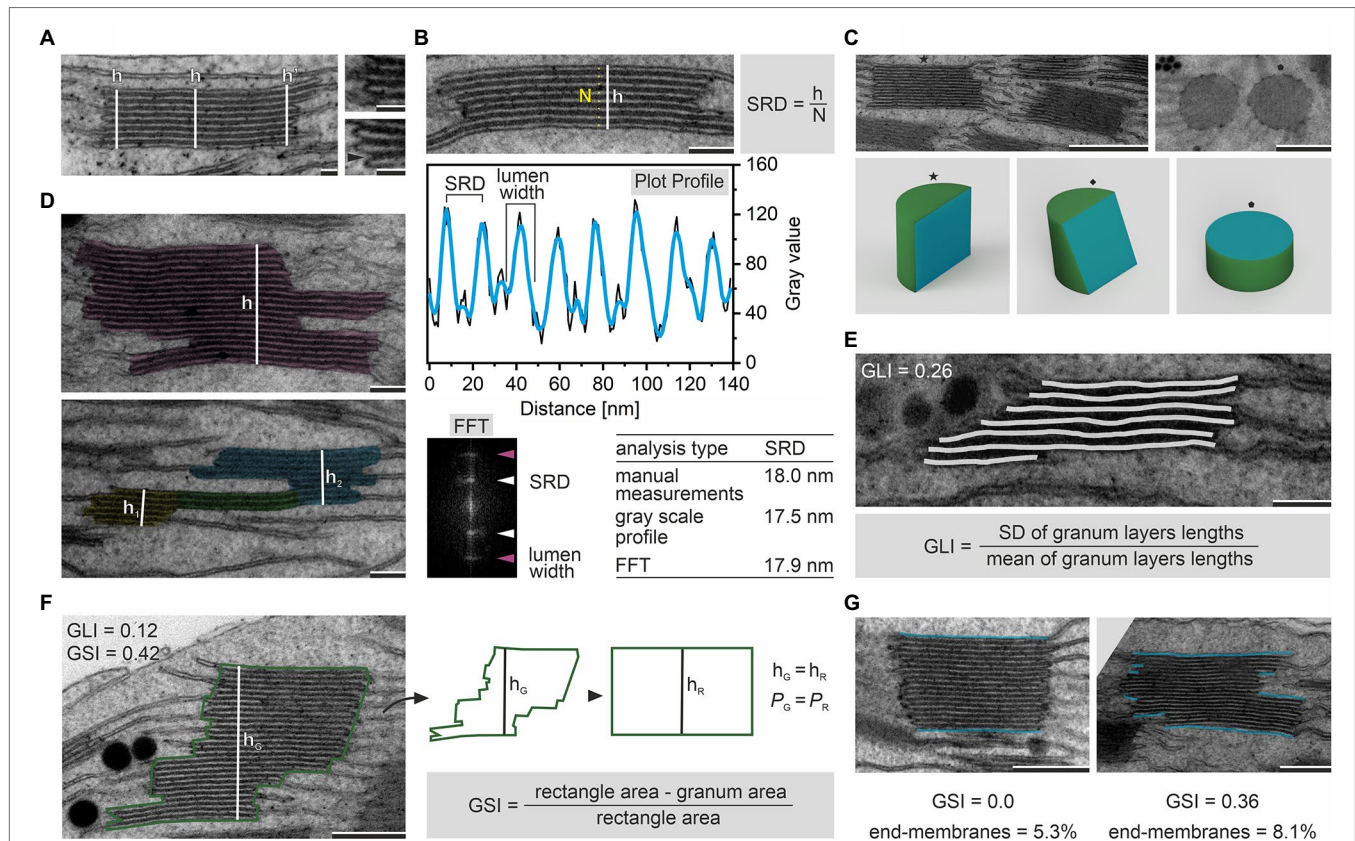


FIGURE 2 | Determination of grana height (h) by measurements in central and marginal region of the stack; the upper inset shows typical marginal region, the lower inset presents membrane bending in the grana margin resulting in the local increase in stack height; note that such local increase might also be registered in the case of the lumen margin swelling (A). Various image-analysis approaches used to calculate the Stacking Repeat Distance (SRD) parameter; the manual method requires measurement of the grana height (h), thylakoid layers counting (N), and application of the given formula; semiautomated approach is based on the analysis of gray scale intensity profile obtained using, e.g., ImageJ Plot Profile function on the manually marked region (gray – raw data, blue – plot smoothed using Savitzky–Golay filter); Fast Fourier Transformation (FFT) analysis of grana periodicity enabling single-step automated SRD calculation; note that all calculated SRD values presented in the table were obtained by the analysis of the grana micrograph showed in the upper part of this panel (B). Appearance of grana ultrastructure depends on the angle of grana section; cutting planes (blue) are presented on simplified rendered grana 3D models (star – parallel cut, diamond – shifted cut, pentagon – top cut); note that only sections parallel to the vertical grana axis enable reliable analyses of SRD parameter (C). Exemplary images showing irregular membrane stack (pink) having one common height (h ; upper micrograph) and membrane stack composed of two distinct sections (yellow, blue) of different heights (h_1 , h_2) connected by a three-layer sector (green; lower micrograph); note that according to the definition used in this manuscript membrane stacks with one common height only are in the single grana category (D). Marking of grana thylakoid lengths (light gray) on an exemplary grana micrograph; these values are necessary to calculate the Grana Lateral Irregularity (GLI) according to the provided formula; note that GLI value given in the upper left corner was calculated from the presented image (E). Marking of the grana height (h_G , white) and the perimeter (P_G , green); these values are necessary to calculate the cross-sectional grana area and also area of the rectangle having identical height and perimeter as the measured grana; both area values are necessary to calculate the Grana Cross-Sectional Irregularity (GSI) according to the provided formula; note that GSI and GLI can be significantly different in one grana stack (F). Images of two grana stacks with different GSI values and the end-membrane region marked (blue); higher value of GSI parameter corresponds to an increase in the ratio of the end-membrane length to the total membrane length within particular grana (expressed in %; G). Note that various angles of grana sections showed in panel (C) are presented on different grana stacks; electron micrographs were obtained from fully developed chloroplasts of *Arabidopsis thaliana* (left images on A and C; B, D, E; right image on G) and *Pisum sativum* (insets on A; right image on C; F; left image on G); scale bar = 50 nm (A), 100 nm (B, D, E), 250 nm (F, G), 500 nm (C). Ultrastructural features of grana were calculated with the help of ImageJ software (Abramoff et al., 2004).

structural reorganization in different conditions is entirely unknown and requires further investigation.

PERSPECTIVES

Although the whole thylakoid network of a single chloroplast forms a continuous arrangement, the grana stacks are structurally isolated units whose architecture, resulting from a plethora of

interactions between membrane components, might be analyzed quantitatively and qualitatively. Recently, a growing number of studies have shown that the grana nano-morphology itself is a significant factor regulating light harvesting and electron transfer (reviewed in Johnson and Wientjes, 2020). For instance, data derived from quantitative analysis of microscopy images were used to simulate plastocyanin diffusion between stacked and unstacked thylakoid domains. It was shown that a specific range of observed grana diameters results from the optimization

of electron transport limited by efficient diffusion of this long-range electron carrier (Hohner et al., 2020). The establishment of a direct role of grana stacks in the efficient performance of photosynthesis has been a subject of many studies, but reasons for the formation of such distinct membrane structures is still under debate (reviewed in Mullineaux, 2005; Anderson et al., 2008; Nevo et al., 2012; Puthiyaveetil et al., 2016; Lambrev and Akhtar, 2019; Moazzami Gudarzi et al., 2021; Müh et al., 2021). An ultrastructure-focused approach adds another dimension to grana function studies, which earlier has been mainly investigated and conceptualized at the level of protein–protein and protein–lipid interactions (reviewed in Johnson and Wientjes, 2020).

In this mini-review, we focused on the use of 2D TEM for quantitative analysis of grana structure. So far, such measurements are mainly executed using manual methods. They are time-consuming and also susceptible to the “human eye” bias, which only partially might be reduced by blinded experiments. The rapid development of machine learning in analyzing different microscopy data (Rawat and Wang, 2017) points to the possibility of applying fully automated protocols for obtaining grana structural parameters. Furthermore, the advantages of the electron microscopy methods *per se* can bring the structural analysis of the thylakoid network to a higher level. Recently developed techniques called jointly “*in situ* liquid cell TEM” could, in the future, enable *in vivo* analysis of the thylakoid network nano-morphology (Pu et al., 2020). On the other hand, a similar goal could be achieved by further developing the 3D structural illumination microscopy method to *in vivo* visualize single layers of grana stacks (Chen et al., 2014). Finally, the advancement in the structural analysis of chloroplast thylakoids should also

be extended to the region of STs. Their (i) distinctive role in the light phase of photosynthesis, (ii) complicated and highly organized spatial structure (Bussi et al., 2019), and (iii) possible rearrangements in different genotypes (e.g., Armbruster et al., 2013) point to the importance of detailed structural studies of these thylakoid compartments. However, due to the different architecture of grana and stroma thylakoids, such studies will require the introduction of appropriate structural parameters and new measuring protocols that will consider the complex spatial arrangement of the stroma thylakoids.

AUTHOR CONTRIBUTIONS

ŁK and RM provided a conception of the manuscript and prepared figures. ŁK, RM, and AM wrote and edited the manuscript. ŁK provided microscopy images. All authors contributed to the article and approved the submitted version.

FUNDING

ŁK acknowledges funding from the National Science Centre, Poland, under grant number 2019/35/D/NZ3/03904.

ACKNOWLEDGMENTS

Transmission electron microscopy images were performed in the Laboratory of Electron Microscopy, Nencki Institute of Experimental Biology of PAS, Warsaw, Poland.

REFERENCES

- Abramoff, M. D., Magalhães, P. J., and Ram, S. J. (2004). Image processing with ImageJ. *Biophoton. Int.* 11, 36–42.
- Allen, J. F., and Forsberg, J. (2001). Molecular recognition in thylakoid structure and function. *Trends Plant Sci.* 6, 317–326. doi: 10.1016/S1360-1385(01)02010-6
- Anderson, J. M., Chow, W. S., and De Las, R. J. (2008). Dynamic flexibility in the structure and function of photosystem II in higher plant thylakoid membranes: the grana enigma. *Photosynth. Res.* 98, 575–587. doi: 10.1007/s11220-008-9381-3
- Anderson, J. M., Goodchild, D. J., and Boardman, N. K. (1973). Composition of the photosystems and chloroplast structure in extreme shade plants. *Biochim. Biophys. Acta Bioenerg.* 325, 573–585. doi: 10.1016/0005-2728(73)90217-X
- Anderson, J. M., Horton, P., Kim, E. H., and Chow, W. S. (2012). Towards elucidation of dynamic structural changes of plant thylakoid architecture. *Philos. Trans. R. Soc. Lond. Ser. B Biol. Sci.* 367, 3515–3524. doi: 10.1098/rstb.2012.0373
- Andersson, J., Wentworth, M., Walters, R. G., Howard, C. A., Ruban, A. V., Horton, P., et al. (2003). Absence of the Lhcb1 and Lhcb2 proteins of the light-harvesting complex of photosystem II – effects on photosynthesis, grana stacking and fitness. *Plant J.* 35, 350–361. doi: 10.1046/j.1365-3113x.2003.01811.x
- Armarego-Marriott, T., Kowalewska, L., Burgos, A., Fischer, A., Thiele, W., Erban, A., et al. (2019). Highly resolved systems biology to dissect the etioplast-to-chloroplast transition in tobacco leaves. *Plant Physiol.* 180, 654–681. doi: 10.1104/pp.18.01432
- Armbruster, U., Labs, M., Pribil, M., Viola, S., Xu, W., Scharfenberg, M., et al. (2013). *Arabidopsis* CURVATURE THYLAKOID1 proteins modify
- THYLAKOID architecture by inducing membrane curvature. *Plant Cell* 25, 2661–2678. doi: 10.1105/tpc.113.113118
- Austin, J. R., and Staehelin, L. A. (2011). Three-dimensional architecture of grana and stroma thylakoids of higher plants as determined by electron tomography. *Plant Physiol.* 155, 1601–1611. doi: 10.1104/pp.110.170647
- Avramova, V., Sprangers, K., and Beemster, G. (2015). The maize leaf: another perspective on growth regulation. *Trends Plant Sci.* 20, 787–797. doi: 10.1016/j.tplants.2015.09.002
- Belgio, E., Ungerer, P., and Ruban, A. V. (2015). Light-harvesting superstructures of green plant chloroplasts lacking photosystems. *Plant Cell Environ.* 38, 2035–2047. doi: 10.1111/pce.12528
- Bertrand, M. (2010). Carotenoid biosynthesis in diatoms. *Photosynth. Res.* 106, 89–102. doi: 10.1007/s11220-010-9589-x
- Brangeon, J. (1973). Compared ontogeny of the two types of chloroplasts of *Zea mays*. *J. Microsc.* 16, 233–242.
- Bussi, Y., Shimoni, E., Weiner, A., Kapon, R., Charuvi, D., Nevo, R., et al. (2019). Fundamental helical geometry consolidates the plant photosynthetic membrane. *Proc. Natl. Acad. Sci. U. S. A.* 116, 22366–22375. doi: 10.1073/pnas.1905994116
- Bykowski, M., Mazur, R., Wójtowicz, J., Suski, S., Garstka, M., Mostowska, A., et al. (2021). Too rigid to fold: carotenoid-dependent decrease in thylakoid fluidity hampers the formation of chloroplast grana. *Plant Physiol.* 185, 210–227. doi: 10.1093/plphys/kiab009
- Capretti, A., Ringsmuth, A. K., van Velzen, J. F., Rosnik, A., Croce, R., and Gregorkiewicz, T. (2019). Nanophotonics of higher-plant photosynthetic membranes. *Light Sci. Appl.* 8.5. doi: 10.1038/s41377-018-0116-8
- Chen, Y. E., Su, Y. Q., Mao, H. T., Wu, N., Zhu, F., Yuan, M., et al. (2018b). Terrestrial plants evolve highly assembled photosystem complexes in adaptation to light shifts. *Front. Plant Sci.* 9:1811. doi: 10.3389/fpls.2018.01811

- Chen, D., Wang, S., Qi, L., Yin, L., and Deng, X. (2018a). Galactolipid remodeling is involved in drought-induced leaf senescence in maize. *Environ. Exp. Bot.* 150, 57–68. doi: 10.1016/j.envexpbot.2018.02.017
- Chen, M.-Y., Zhuo, G.-Y., Chen, K.-C., Wu, P.-C., Hsieh, T.-Y., Liu, T.-M., et al. (2014). Multiphoton imaging to identify grana, stroma thylakoid, and starch inside an intact leaf. *BMC Plant Biol.* 14:175. doi: 10.1186/1471-2229-14-175
- Chow, W. S., Kim, E.-H., Horton, P., and Anderson, J. M. (2005). Granal stacking of thylakoid membranes in higher plant chloroplasts: the physicochemical forces at work and the functional consequences that ensue. *Photochem. Photobiol. Sci.* 4, 1081–1090. doi: 10.1039/b507310n
- Daum, B., and Kuhlbrandt, W. (2011). Electron tomography of plant thylakoid membranes. *J. Exp. Bot.* 62, 2393–2402. doi: 10.1093/jxb/err034
- Demmig-Adams, B., Muller, O., Stewart, J. J., Cohu, C. M., and Adams, W. W. (2015). Chloroplast thylakoid structure in evergreen leaves employing strong thermal energy dissipation. *J. Photochem. Photobiol. B* 152, 357–366. doi: 10.1016/j.jphotobiol.2015.03.014
- Engel, B. D., Schaffer, M., Kuhn Cuellar, L., Villa, E., Plitzko, J. M., and Baumeister, W. (2015). Native architecture of the *Chlamydomonas* chloroplast revealed by in situ cryo-electron tomography. *elife* 4:e04889. doi: 10.7554/eLife.04889
- Flannery, S. E., Hepworth, C., Wood, W. H. J., Pastorelli, F., Hunter, C. N., Dickman, M. J., et al. (2021). Developmental acclimation of the thylakoid proteome to light intensity in *Arabidopsis*. *Plant J.* 105, 223–244. doi: 10.1111/tpl.15053
- Fq, D. Y. H., Yang, X. F., Chen, S. T., Wang, Y. T., Li, J. K., Shen, Q., et al. (2012). Downregulation of chloroplast RPS1 negatively modulates nuclear heat-responsive expression of HsfA2 and its target genes in *Arabidopsis*. *PLoS Genet.* 8:e1002669. doi: 10.1371/journal.pgen.1002669
- Fristedt, R., Willig, A., Granath, P., Crevecoeur, M., Rochaix, J. D., and Vener, A. V. (2009). Phosphorylation of photosystem II controls functional macroscopic folding of photosynthetic membranes in *Arabidopsis*. *Plant Cell* 21, 3950–3964. doi: 10.1105/tpc.109.069435
- Gugel, I. L., and Soll, J. (2016). Chloroplast differentiation in the growing leaves of *Arabidopsis thaliana*. *Protoplasma* 254, 1857–1866. doi: 10.1007/s00709-016-1057-9
- Gunning, B. E. S., and Schwartz, O. M. (1999). Confocal microscopy of thylakoid autofluorescence in relation to origin of grana and phylogeny in the green algae. *Funct. Plant Biol.* 26, 695–708. doi: 10.1071/PP99076
- Gunning, B. E. S., and Steer, M. W. (1975). *Ultrastructure and the Biology of Plant Cell*. London: Edward Arnold.
- Gupta, T. K., Klumpe, S., Gries, K., Heinz, S., Wietrzynski, W., Ohnishi, N., et al. (2021). Structural basis for VIPP1 oligomerization and maintenance of thylakoid membrane integrity. *Cell* 184, 3643–3659. doi: 10.1016/j.cell.2021.05.011
- Hepworth, C., Wood, W. H. J., Emrich-Mills, T. Z., Proctor, M. S., Casson, S., and Johnson, M. P. (2021). Dynamic thylakoid stacking and state transitions work synergistically to avoid acceptor-side limitation of photosystem I. *Nat. Plants* 7, 87–98. doi: 10.1038/s41477-020-00828-3
- Herbstová, M., Tietz, S., Kinzel, C., Turkina, M. V., and Kirchhoff, H. (2012). Architectural switch in plant photosynthetic membranes induced by light stress. *Proc. Natl. Acad. Sci. U. S. A.* 109, 20130–20135. doi: 10.1073/pnas.1214265109
- Hohner, R., Pribil, M., Herbstová, M., Lopez, L. S., Kunz, H. H., Li, M., et al. (2020). Plastocyanin is the long-range electron carrier between photosystem II and photosystem I in plants. *Proc. Natl. Acad. Sci. U. S. A.* 117, 15354–15362. doi: 10.1073/pnas.2005832117
- Ioannidis, N. E., Lopera, O., Santos, M., Torne, J. M., and Kotzabasis, K. (2012). Role of plastid transglutaminase in LHCII polyamination and thylakoid electron and proton flow. *PLoS One* 7:e41979. doi: 10.1371/journal.pone.0041979
- Ioannidis, N. E., Ortigosa, S. M., Veramendi, J., Pinto-Marijuan, M., Fleck, I., Carvajal, P., et al. (2009). Remodeling of tobacco thylakoids by over-expression of maize plastidial transglutaminase. *Biochim. Biophys. Acta* 1787, 1215–1222. doi: 10.1016/j.bbabo.2009.05.014
- Iwai, M., Roth, M. S., and Niyogi, K. K. (2018). Subdiffraction-resolution live-cell imaging for visualizing thylakoid membranes. *Plant J.* 96, 233–243. doi: 10.1111/tpl.14021
- Jakubauskas, D., Kowalewska, L., Sokolova, A. V., Garvey, C. J., Mortensen, K., Jensen, P. E., et al. (2019). Ultrastructural modeling of small angle scattering from photosynthetic membranes. *Sci. Rep.* 9:19405. doi: 10.1038/s41598-019-55423-0
- Jakubauskas, D., Mortensen, K., Jensen, P. E., and Kirkensgaard, J. (2021). Small-angle x-ray and neutron scattering on photosynthetic membranes. *Front. Chem.* 9:631370. doi: 10.3389/fchem.2021.631370
- Jiang, C., Zu, C., Lu, D., Zheng, Q., Shen, J., Wang, H., et al. (2017). Effect of exogenous selenium supply on photosynthesis, Na⁺ accumulation and antioxidative capacity of maize (*Zea mays* L.) under salinity stress. *Sci. Rep.* 7:42039. doi: 10.1038/srep42039
- Johnson, M. P., and Wientjes, E. (2020). The relevance of dynamic thylakoid organisation to photosynthetic regulation. *Biochim. Biophys. Acta Bioenerg.* 1861:148039. doi: 10.1016/j.bbabo.2019.06.011
- Khatoun, M., Inagawa, K., Pospisil, P., Yamashita, A., Yoshioka, M., Lundin, B., et al. (2009). Quality control of photosystem II: thylakoid unstacking is necessary to avoid further damage to the D1 protein and to facilitate D1 degradation under light stress in spinach thylakoids. *J. Biol. Chem.* 284, 25343–25352. doi: 10.1074/jbc.M109.007740
- Kim, E. H., Chow, W. S., Horton, P., and Anderson, J. M. (2005). Entropy-assisted stacking of thylakoid membranes. *Biochim. Biophys. Acta* 1708, 187–195. doi: 10.1016/j.bbabo.2005.03.011
- Kim, E. H., Li, X. P., Razeghifard, R., Anderson, J. M., Niyogi, K. K., Pogson, B. J., et al. (2009). The multiple roles of light-harvesting chlorophyll a/b-protein complexes define structure and optimize function of *Arabidopsis* chloroplasts: a study using two chlorophyll b-less mutants. *Biochim. Biophys. Acta* 1787, 973–984. doi: 10.1016/j.bbabo.2009.04.009
- Kirchhoff, H. (2019). Chloroplast ultrastructure in plants. *New Phytol.* 223, 565–574. doi: 10.1111/nph.15730
- Kirchhoff, H., Hall, C., Wood, M., Herbstová, M., Tsbari, O., Nevo, R., et al. (2011). Dynamic control of protein diffusion within the granal thylakoid lumen. *Proc. Natl. Acad. Sci. U. S. A.* 108, 20248–20253. doi: 10.1073/pnas.1104141109
- Koochak, H., Puthiyaveetil, S., Mullendore, D. L., Li, M., and Kirchhoff, H. (2019). The structural and functional domains of plant thylakoid membranes. *Plant J.* 97, 412–429. doi: 10.1111/tpl.14127
- Koskela, M. M., Brunje, A., Ivanauskaitė, A., Grabsztunowicz, M., Lassowskai, I., Neumann, U., et al. (2018). Chloroplast acetyltransferase NSI is required for state transitions in *Arabidopsis thaliana*. *Plant Cell* 30, 1695–1709. doi: 10.1105/tpc.18.00155
- Kowalewska, L., Bykowski, M., and Mostowska, A. (2019). Spatial organization of thylakoid network in higher plants. *Bot. Lett.* 166, 326–343. doi: 10.1080/23818107.2019.1619195
- Kowalewska, L., Mazur, R., Suski, S., Garstka, M., and Mostowska, A. (2016). Three-dimensional visualization of the tubular-lamellar transformation of the internal plastid membrane network during runner bean chloroplast biogenesis. *Plant Cell* 28, 875–891. doi: 10.1105/tpc.15.01053
- Lambrev, P. H., and Akhtar, P. (2019). Macroorganisation and flexibility of thylakoid membranes. *Biochem. J.* 476, 2981–3018. doi: 10.1042/BCJ20190080
- Larkum, A. W. D., and Vesik, M. (2003). “Algal plastids: their fine structure and properties,” in *Photosynthesis in Algae*. eds. A. W. D. Larkum, S. Douglas and J. A. Raven (Dordrecht: Springer), 11–28.
- Li, M., Mukhopadhyay, R., Svoboda, V., Oung, H. M. O., Mullendore, D. L., and Kirchhoff, H. (2020). Measuring the dynamic response of the thylakoid architecture in plant leaves by electron microscopy. *Plant Direct* 4:e00280. doi: 10.1002/pld3.280
- Mareš, J., Strunecký, O., Bučinská, L., and Wiedermannová, J. (2019). Evolutionary patterns of thylakoid architecture in cyanobacteria. *Front. Microbiol.* 10:277. doi: 10.3389/fmicb.2019.00277
- Mazur, R., Gieczewska, K., Kowalewska, L., Kuta, A., Proboszcz, M., Gruszecki, W. I., et al. (2020). Specific composition of lipid phases allows retaining an optimal thylakoid membrane fluidity in plant response to low-temperature treatment. *Front. Plant Sci.* 11:723. doi: 10.3389/fpls.2020.00723
- Mazur, R., Mostowska, A., Szach, J., Gieczewska, K., Wojtowicz, J., Bednarska, K., et al. (2019). Galactolipid deficiency disturbs spatial arrangement of the thylakoid network in *Arabidopsis thaliana* plants. *J. Exp. Bot.* 70, 4689–4704. doi: 10.1093/jxb/erz219
- McDonald, K. L. (2014). Out with the old and in with the new: rapid specimen preparation procedures for electron microscopy of sectioned biological material. *Protoplasma* 251, 429–448. doi: 10.1007/s00709-013-0575-y

- Moazzami Gudarzi, M., Aboutaleb, S. H., and Satalov, A. (2021). Is the debate over grana stacking formation finally solved? *Nat. Plants* 7, 277–278. doi: 10.1038/s41477-021-00880-7
- Mostowska, A. (1986). Thylakoid and grana formation during the development of pea chloroplasts, illuminated by white, red, and blue low intensity light. *Protoplasma* 134, 88–94. doi: 10.1007/BF01275706
- Müh, F., van Oort, B., Puthiyaveetil, S., and Kirchhoff, H. (2021). Reply to: is the debate over grana stacking formation finally solved? *Nat. Plants* 7, 279–281. doi: 10.1038/s41477-021-00881-6
- Mullineaux, C. W. (2005). Function and evolution of grana. *Trends Plant Sci.* 10, 521–525. doi: 10.1016/j.tplants.2005.09.001
- Mustárdy, L., Buttle, K., Steinbach, G., and Garab, G. (2008). The three-dimensional network of the thylakoid membranes in plants: quasi-helical model of the granum-stroma assembly. *Plant Cell* 20, 2552–2557. doi: 10.1105/tpc.108.059147
- Nevo, R., Charuvi, D., Tsabari, O., and Reich, Z. (2012). Composition, architecture and dynamics of the photosynthetic apparatus in higher plants. *Plant J.* 70, 157–176. doi: 10.1111/j.1365-3113.2011.04876.x
- Nicol, L., Nawrocki, W. J., and Croce, R. (2019). Disentangling the sites of non-photochemical quenching in vascular plants. *Nat. Plants* 5, 1177–1183. doi: 10.1038/s41477-019-0526-5
- Otegui, M. S., and Pennington, J. G. (2018). Electron tomography in plant cell biology. *Microscopy* 68, 69–79. doi: 10.1093/jmicro/dfy133
- Pietrzykowska, M., Suorsa, M., Semchonok, D. A., Tikkanen, M., Boekema, E. J., Aro, E. M., et al. (2014). The light-harvesting chlorophyll a/b binding proteins Lhcb1 and Lhcb2 play complementary roles during state transitions in *Arabidopsis*. *Plant Cell* 26, 3646–3660. doi: 10.1105/tpc.114.127373
- Pipitone, R., Eicke, S., Pfister, B., Glauser, G., Falconet, D., Uwizye, C., et al. (2021). A multifaceted analysis reveals two distinct phases of chloroplast biogenesis during de-etiolation in *Arabidopsis*. *elife* 10:e62709. doi: 10.7554/eLife.62709
- Pribil, M., Sandoval-Ibáñez, O., Xu, W., Sharma, A., Labs, M., Liu, Q., et al. (2018). Fine-tuning of photosynthesis requires CURVATURE THYLAKOID1-mediated THYLAKOID plasticity. *Plant Physiol.* 176, 2351–2364. doi: 10.1104/pp.17.00863
- Pu, S., Gong, C., and Robertson, A. W. (2020). Liquid cell transmission electron microscopy and its applications. *R. Soc. Open Sci.* 7:191204. doi: 10.1098/rsos.191204
- Puthiyaveetil, S., Kirchhoff, H., and Höhnner, R. (2016). “Structural and functional dynamics of the thylakoid membrane system,” in *Chloroplasts: Current Research and Future Trends*. ed. H. Kirchhoff (Poole, UK: Caister Academic Press), 59–88.
- Puthiyaveetil, S., Tsabari, O., Lowry, T., Lenhert, S., Lewis, R. R., Reich, Z., et al. (2014). Compartmentalization of the protein repair machinery in photosynthetic membranes. *Proc. Natl. Acad. Sci. U. S. A.* 111, 15839–15844. doi: 10.1073/pnas.1413739111
- Puthiyaveetil, S., van Oort, B., and Kirchhoff, H. (2017). Surface charge dynamics in photosynthetic membranes and the structural consequences. *Nat. Plants* 3:17020. doi: 10.1038/nplants.2017.20
- Rantala, M., Rantala, S., and Aro, E.-M. (2020). Composition, phosphorylation and dynamic organization of photosynthetic protein complexes in plant thylakoid membrane. *Photochem. Photobiol. Sci.* 19, 604–619. doi: 10.1039/D0PP00025F
- Raven, J. A. (2021). Determinants, and implications, of the shape and size of thylakoids and cristae. *J. Plant Physiol.* 257:153342. doi: 10.1016/j.jplph.2020.153342
- Rawat, W., and Wang, Z. (2017). Deep convolutional neural networks for image classification: a comprehensive review. *Neural Comput.* 29, 2352–2449. doi: 10.1162/neco_a_00990
- Rozak, P. R., Seiser, R. M., Wacholtz, W. F., and Wise, R. R. (2002). Rapid, reversible alterations in spinach thylakoid appression upon changes in light intensity. *Plant Cell Environ.* 25, 421–429. doi: 10.1046/j.0016-8025.2001.00823.x
- Ruban, A. V., and Johnson, M. P. (2015). Visualizing the dynamic structure of the plant photosynthetic membrane. *Nat. Plants* 1:15161. doi: 10.1038/nplants.2015.161
- Schumann, T., Paul, S., Melzer, M., Dormann, P., and Jahns, P. (2017). Plant growth under natural light conditions provides highly flexible short-term acclimation properties toward high light stress. *Front. Plant Sci.* 8:681. doi: 10.3389/fpls.2017.00681
- Shimoni, E., Rav-Hon, O., Ohad, I., Brumfeld, V., and Reich, Z. (2005). Three-dimensional organization of higher-plant chloroplast thylakoid membranes revealed by electron tomography. *Plant Cell* 17, 2580–2586. doi: 10.1105/tpc.105.035030
- Staelhelin, L. A., and Paolillo, D. J. (2020). A brief history of how microscopic studies led to the elucidation of the 3D architecture and macromolecular organization of higher plant thylakoids. *Photosynth. Res.* 145, 237–258. doi: 10.1007/s11120-020-00782-3
- Trotta, A., Bajwa, A. A., Mancini, I., Paakkari, V., Pribil, M., and Aro, E. M. (2019). The role of phosphorylation dynamics of CURVATURE THYLAKOID 1B in plant thylakoid membranes. *Plant Physiol.* 181, 1615–1631. doi: 10.1104/pp.19.00942
- Tsabari, O., Nevo, R., Meir, S., Carrillo, L. R., Kramer, D. M., and Reich, Z. (2015). Differential effects of ambient or diminished CO₂ and O₂ levels on thylakoid membrane structure in light-stressed plants. *Plant J.* 81, 884–894. doi: 10.1111/tpj.12774
- Ünnep, R., Paul, S., Zsiros, O., Kovács, L., Székely, N. K., Steinbach, G., et al. (2020). Thylakoid membrane reorganizations revealed by small-angle neutron scattering of *Monstera deliciosa* leaves associated with non-photochemical quenching. *Open Biol.* 10:200144. doi: 10.1098/rsob.200144
- Ünnep, R., Zsiros, O., Hörcsik, Z., Markó, M., Jajoo, A., Kohlbrecher, J., et al. (2017). Low-pH induced reversible reorganizations of chloroplast thylakoid membranes – as revealed by small-angle neutron scattering. *Biochim. Biophys. Acta Bioenerg.* 1858, 360–365. doi: 10.1016/j.bbabi.2017.02.010
- Uwada, T., Huang, L.-T., Hee, P.-Y., Usman, A., and Masuhara, H. (2017). Size-dependent optical properties of grana inside chloroplast of plant cells. *J. Phys. Chem. B* 121, 915–922. doi: 10.1021/acs.jpcc.6b10204
- Waters, M. T., and Langdale, J. A. (2009). The making of a chloroplast. *EMBO J.* 28, 2861–2873. doi: 10.1038/emboj.2009.264
- Wood, W. H. J., Barnett, S. F. H., Flannery, S., Hunter, C. N., and Johnson, M. P. (2019). Dynamic thylakoid stacking is regulated by LHCII phosphorylation but not its interaction with PSI. *Plant Physiol.* 180, 2152–2166. doi: 10.1104/pp.19.00503
- Wood, W. H. J., MacGregor-Chatwin, C., Barnett, S. F. H., Mayneord, G. E., Huang, X., Hobbs, J. K., et al. (2018). Dynamic thylakoid stacking regulates the balance between linear and cyclic photosynthetic electron transfer. *Nat. Plants* 4, 116–127. doi: 10.1038/s41477-017-0092-7
- Yamamoto, Y., Kai, S., Ohnishi, A., Tsumura, N., Ishikawa, T., Hori, H., et al. (2014). Quality control of PSII: behavior of PSII in the highly crowded grana thylakoids under excessive light. *Plant Cell Physiol.* 55, 1206–1215. doi: 10.1093/pcp/pcu043
- Yokoyama, R., Yamamoto, H., Kondo, M., Takeda, S., Ifuku, K., Fukao, Y., et al. (2016). Grana-localized proteins, RIQ1 and RIQ2, affect the organization of light-harvesting complex II and grana stacking in *Arabidopsis*. *Plant Cell* 28, 2261–2275. doi: 10.1105/tpc.16.00296
- Yoshioka-Nishimura, M., Nanba, D., Takaki, T., Ohba, C., Tsumura, N., Morita, N., et al. (2014). Quality control of photosystem II: direct imaging of the changes in the thylakoid structure and distribution of FtsH proteases in spinach chloroplasts under light stress. *Plant Cell Physiol.* 55, 1255–1265. doi: 10.1093/pcp/pcu079
- Yu, B., and Benning, C. (2003). Anionic lipids are required for chloroplast structure and function in *Arabidopsis*. *Plant J.* 36, 762–770. doi: 10.1046/j.1365-3113.2003.01918.x
- Zechmann, B. (2019). Ultrastructure of plastids serves as reliable abiotic and biotic stress marker. *PLoS One* 14:e0214811. doi: 10.1371/journal.pone.0214811
- Zsiros, O., Ünnep, R., Nagy, G., Almásy, L., Patai, R., Székely, N. K., et al. (2020). Role of protein-water interface in the stacking interactions of granum thylakoid membranes – as revealed by the effects of Hofmeister salts. *Front. Plant Sci.* 11:1257. doi: 10.3389/fpls.2020.01257

Conflict of Interest: The authors declare that the research was conducted in the absence of any commercial or financial relationships that could be construed as a potential conflict of interest.

Publisher's Note: All claims expressed in this article are solely those of the authors and do not necessarily represent those of their affiliated organizations, or those of the publisher, the editors and the reviewers. Any product that may be evaluated in this article, or claim that may be made by its manufacturer, is not guaranteed or endorsed by the publisher.

Copyright © 2021 Mazur, Mostowska and Kowalewska. This is an open-access article distributed under the terms of the Creative Commons Attribution License (CC BY). The use, distribution or reproduction in other forums is permitted, provided the original author(s) and the copyright owner(s) are credited and that the original publication in this journal is cited, in accordance with accepted academic practice. No use, distribution or reproduction is permitted which does not comply with these terms.



A Novel Chloroplast Protein RNA Processing 8 Is Required for the Expression of Chloroplast Genes and Chloroplast Development in *Arabidopsis thaliana*

Mengmeng Kong¹, Yaozong Wu¹, Ziyuan Wang², Wantong Qu², Yixin Lan¹, Xin Chen¹, Yanyun Liu¹, Perveen Shahnaz¹, Zhongnan Yang², Qingbo Yu^{2*} and Hualing Mi^{1*}

¹ National Key Laboratory of Plant Molecular Genetics, CAS Center for Excellence in Molecular Plant Sciences, Shanghai Institute of Plant Physiology and Ecology, Chinese Academy of Sciences, Shanghai, China, ² Shanghai Key Laboratory of Plant Molecular Sciences, College of Life Sciences, Shanghai Normal University, Shanghai, China

OPEN ACCESS

Edited by:

Yan Lu,
Western Michigan University,
United States

Reviewed by:

Honglei Jin,
Guangzhou University of Chinese
Medicine, China
Dawei Zhang,
Sichuan University, China

*Correspondence:

Qingbo Yu
yuqing9860@shnu.edu.cn
Hualing Mi
hlmi@cmeps.ac.cn

Specialty section:

This article was submitted to
Plant Physiology,
a section of the journal
Frontiers in Plant Science

Received: 27 April 2021

Accepted: 03 November 2021

Published: 09 December 2021

Citation:

Kong M, Wu Y, Wang Z, Qu W,
Lan Y, Chen X, Liu Y, Shahnaz P,
Yang Z, Yu Q and Mi H (2021) A Novel
Chloroplast Protein RNA Processing 8
Is Required for the Expression
of Chloroplast Genes and Chloroplast
Development in *Arabidopsis thaliana*.
Front. Plant Sci. 12:700975.
doi: 10.3389/fpls.2021.700975

Chloroplast development involves the coordinated expression of both plastids- and nuclear-encoded genes in higher plants. However, the underlying mechanism still remains largely unknown. In this study, we isolated and characterized an *Arabidopsis* mutant with an albino lethality phenotype named *RNA processing 8* (*rp8*). Genetic complementation analysis demonstrated that the gene *AT4G37920* (*RP8*) was responsible for the mutated phenotype. The *RP8* gene was strongly expressed in photosynthetic tissues at both transcription and translation protein levels. The *RP8* protein is localized in the chloroplast and associated with the thylakoid. Disruption of the *RP8* gene led to a defect in the accumulation of the *rpoA* mature transcript, which reduced the level of the RpoA protein, and affected the transcription of PEP-dependent genes. The abundance of the chloroplast rRNA, including 23S, 16S, 4.5S, and 5S rRNA, were reduced in the *rp8* mutant, respectively, and the amounts of chloroplast ribosome proteins, such as, PRPS1(uS1c), PRPS5(uS5c), PRPL2 (uL2c), and PRPL4 (uL4c), were substantially decreased in the *rp8* mutant, which indicated that knockout of *RP8* seriously affected chloroplast translational machinery. Accordingly, the accumulation of photosynthetic proteins was seriously reduced. Taken together, these results indicate that the *RP8* protein plays an important regulatory role in the *rpoA* transcript processing, which is required for the expression of chloroplast genes and chloroplast development in *Arabidopsis*.

Keywords: *Arabidopsis*, chloroplast, plastid-encoded RNA polymerase, RpoA, RNA processing 8

INTRODUCTION

In higher plants, the chloroplast is a kind of semi-autonomous organelle that originated from a free-living cyanobacterium and has retained a reduced genome during the evolutionary process (Raven and Allen, 2003). Chloroplasts as the typical plastids in leaf mesophyll cells develop from proplastids (Valkov et al., 2009). It is estimated that over 3,000 proteins exist in the chloroplast (Sato et al., 1999; Leister, 2003). However, most of the chloroplast proteins are encoded by the nuclear genes and imported from the cytosol (Inaba and Schnell, 2008). The chloroplast genome only encodes 120–130 genes that primarily participate in photosynthesis, plastid transcription, and

translation processes (Daniell et al., 2016). Thus, chloroplast development involves the coordinated expression of both plastids- and nuclear-encoded genes (Leister, 2003; Lopez-Juez and Pyke, 2005).

Chloroplast genes are organized as operons which are transcribed as polycistronic units by two RNA polymerases, namely, a nuclear-encoded phage-type RNA polymerase (NEP) and a plastid-encoded bacterial-type RNA polymerase (PEP) (Pfalz and Pfannschmidt, 2013; Yu et al., 2014a; Pfannschmidt et al., 2015). NEP is involved in the transcription of housekeeping genes when plant cells establish the plastid transcription system during the early stage of chloroplast development. While, PEP is responsible for the transcription of photosynthetic-related genes (Pfalz and Pfannschmidt, 2013; Chi et al., 2015). In the chloroplast, the PEP complex represents a major RNA polymerase activity; over 80% of all primary chloroplast genes are transcribed by PEP in mature green leaves (Zhelyazkova et al., 2012). Although the core subunits of the PEP enzyme (α , β , β' , and β'') are encoded by plastid-encoded genes *rpoA*, *rpoB*, *rpoC1*, *rpoC2*, respectively, numerous nuclear-encoded accessory proteins have been identified from the PEP complex in recent years (Pfalz et al., 2006; Yu et al., 2014a), which play important regulatory roles in maintaining PEP transcriptional activity. For example, sigma factors that are encoded by the nuclear genome confer promoter recognition for PEP-dependent transcription (Schweer et al., 2006, 2010). In addition, 12 nucleus-encoded regulatory proteins called PEP-associated proteins (PAPs) have been identified by precise biochemical techniques, which are tightly associated with the PEP core subunits (Steiner et al., 2011; Pfalz and Pfannschmidt, 2013). They perform specific functions in the PEP complex, including protecting chloroplast nucleoids from superoxide anion radicals and redox reactions (Pfalz et al., 2006; Arsova et al., 2010; Pfalz and Pfannschmidt, 2013). pTAC10/PAP3 which co-migrates with RpoB can be phosphorylated by chloroplast-targeted casein kinase 2 (cpCK2) to regulate the transcription of plastid genes (Yu et al., 2018). TAC7/PAP12 interacts with FLN1, TAC10/PAP3, TAC12/PAP5, and TAC14/PAP7, regulating chloroplast gene expression (Yu et al., 2013). Interestingly, *paps* knockout mutants always exhibit an albino or pale-green phenotype with impaired transcription of PEP-dependent genes, suggesting that loss of PAPs protein have affected the activity of the PEP complex (Pfalz et al., 2006; Arsova et al., 2010; Gao et al., 2011; Steiner et al., 2011; Yu et al., 2013).

Chloroplast gene expression is regulated at various levels including transcription, RNA metabolism, and translation (Pfannschmidt and Liere, 2005; del Campo, 2009). After chloroplast transcript precursor is produced, it undergoes post-transcriptional processes including exo- and endo-ribonuclease cleavage, RNA splicing, and editing (Bollenbach et al., 2005). Numerous nuclear-encoded chloroplast ribonucleases (RNases) in *Arabidopsis* have been verified to be involved in RNA processing and degradation (MacIntosh and Castandet, 2020), such as exoribonucleases PNPase, RNase R, and RNR1 (Bollenbach et al., 2005; Germain et al., 2011, 2012), endoribonuclease RNase E (Mudd et al., 2008; Walter et al., 2010), CSP41a and CSP41b (Beligni and Mayfield, 2008; Chevalier et al., 2015). Also, the pentatricopeptide repeat (PPR)

protein family has been found to be involved in different aspects of RNA metabolism in chloroplasts, including RNA transcription and stability, RNA editing, RNA maturation, RNA translation, and RNA splicing (Schmitz-Linneweber and Small, 2008; Zoschke et al., 2016; Wang et al., 2021). For example, PDM1 is involved in the processing of *rpoA* through association with the polycistronic mRNA in *Arabidopsis* (Wu and Zhang, 2010; Zhang et al., 2015). Additionally, the PDM1 protein is also involved in plastid RNA editing events (Pyo et al., 2013; Zhang et al., 2015). *Arabidopsis* YS1 is required for editing *rpoB* transcripts (Zhou et al., 2009). OTP70 is involved in splicing of the *rpoC1* transcript, which causes a typical PEP-deficient phenotype (Chateigner-Boutin et al., 2011). CLB19 is required for editing the *rpoA* transcript (Chateigner-Boutin et al., 2008). OsPPR16 is responsible for the editing of *rpoB* in rice, knockout of *OsPPR16* leads to impaired accumulation of the RpoB protein and reduced expression of PEP-dependent genes (Huang et al., 2020). These mutants with defects in chloroplast gene expression show pigment defects and even embryonic lethal phenotypes (Pfalz et al., 2006; Arsova et al., 2010; Chateigner-Boutin et al., 2011; Aryamanesh et al., 2017; Wang et al., 2020). Therefore, chloroplast function maintenance requires the coordinated expression of chloroplast genes, which is important for plant growth and development.

Screening mutants with pigmentation deficient phenotypes is a powerful reverse genetic approach to identify essential genes for chloroplast development. In the past years, several independent research groups have undertaken large-scale genetic screening of the pigmentation deficient mutants and identified a series of nuclear genes essential for chloroplast development (Ajjawi et al., 2010; Myouga et al., 2010). Nevertheless, these findings are still far from a complete understanding of chloroplast development. It is necessary to continue to screen more *Arabidopsis* mutants and identify the corresponding mutated genes, which could provide additional insights into chloroplast biogenesis. In this study, we isolated a novel mutant with an albino lethal phenotype named *RNA processing 8 (rp8)* in *Arabidopsis* by using T-DNA mutant screening. The *RP8* gene, highly expressed at the seedling stage, encodes a chloroplast-targeted protein. In the *rp8* mutant, the transcription levels of PEP-dependent chloroplast genes are decreased. We subsequently found that the mature transcripts of *rpoA* decreased, which is considered to be the main reason for the deficient transcription of PEP-dependent genes in the *rp8* mutant. These results suggested that *RP8* is required for the accumulation of PEP complexes and is involved in chloroplast RNA metabolism. This work would provide a prospect for understanding the role of *RP8* in chloroplast RNA metabolism in *Arabidopsis thaliana*.

MATERIALS AND METHODS

Plant Materials and Growth Conditions

Arabidopsis thaliana ecotype Columbia [wild type (WT)] was used in this study. The T-DNA insertion line (SALK_080811) was obtained from Arabidopsis Biological Resource Center (ABRC, Ohio State University). The T-DNA insertion site was identified

by PCR amplification with the T-DNA left border primer LB3 and the gene-specific primers, Left Primer (LP) and Right Primer (RP). For laboratory work, surface-sterilized seeds were sown on Murashige and Skoog (MS) medium supplemented with 2% sucrose and 0.8% (w/v) agar. Plants were grown at 22°C under 16 h light/8 h dark conditions at 30 $\mu\text{mol photons m}^{-2}\text{s}^{-1}$.

Nucleic Acid Isolation, cDNA Synthesis, RT-PCR, qRT-PCR, and Northern Blot Analysis

For genomic DNA isolation, samples were homogenized in extraction buffer [200 mM Tris-HCl, pH 7.5; 25 mM NaCl; 25 mM EDTA; 0.5% (w/v) SDS], then the homogenate was extracted through phenol/chloroform. After centrifugation, DNA was precipitated from the supernatant by adding cold isopropyl alcohol. After washing with 70% (v/v) ethanol, the DNA was rehydrated in distilled water. For total RNA extraction, a commercial RNAiso Plus kit (Takara, Otsu, Japan) was used in accordance with the manufacturer's instructions. Briefly, 2-week-old plants were homogenized in liquid nitrogen, then the homogenate was lysed in the appropriate amount of RNAiso Plus buffer. The mixture was incubated for 5 min at room temperature, then centrifuged at 12,000 rpm for 5 min at 4°C. The supernatant was collected into a new microtube and treated with chloroform. After centrifugation at 12,000 rpm for 15 min at 4°C, an equal volume of isopropanol was added to the supernatant. The pellet was recovered after centrifugation at 15,000 rpm for 10 min at 4°C and dissolved in distilled RNase-free water. Total RNA samples (2–5 μg) were used as templates for the synthesis of the first-strand cDNA with a PrimeScriptTM RT Reagent Kit with gDNA Eraser (Takara, Otsu, Japan), according to the manufacturer's instructions. RT-PCR reactions were performed with specific primers for *RP8*. *Actin2* gene (At3g18780) was used as an internal positive control. Quantitative PCR was performed using the SYBR Green PCR amplification mixture on a StepOnePlusTM Real-Time PCR System (Applied Biosystems, United States). Specific amplification has been confirmed by melting curve analysis. Three biological repeats were performed independently and each sample was operated in triplicate. For Northern blot analysis, equal amounts of total RNA (10 μg) were transferred to positively charged nylon membranes (Roche, Switzerland) after formamide denaturing agarose gel electrophoresis and was further probed with digoxigenin (DIG)-labeled nucleic acid probes (Roche, Switzerland). The probes were synthesized with a PCR DIG synthesis mix (Roche)¹ with the specific primers listed in **Supplementary Table 1**. Both hybridization and chemiluminescence detection was carried out, according to the Roche manual.

Complementation Analysis

As for the genomic complementation analysis, the 2.9 kb full-length genomic fragment of *At4g37920* was amplified using high-fidelity KOD plus polymerase (TOYOBO, Japan)² with

the gene-specific primers listed in **Supplementary Table 1**, and sub-cloned into a binary vector pCambia1301. The construct was introduced into heterozygotes mediated by *Agrobacterium tumefaciens* strain using floral dip transformation as described (Clough and Bent, 1998). Transgenic plants were screened on MS medium with 80 mg L⁻¹ hygromycin B (Roche). The genomic backgrounds of these hygromycin-resistant transformants were further analyzed with the specific primers listed in **Supplementary Table 1**.

Transmission Electron Microscopy

Leaf segments were fixed with 2.5% glutaraldehyde in phosphate buffer (pH 7.2) for 24 h at 4°C and washed three times with the same buffer. The tissues were postfixed overnight in 1% OsO₄ at 4°C. The fixed samples were dehydrated through a series of ethanol solutions, infiltrated with a series of epoxy resin in epoxy propane, and embedded in Epon 812 resin. Ultrathin sections were cut with a diamond knife and mounted onto copper grids. Then, the samples were stained with 2% uranyl acetate for 10 min followed by lead citrate for 2 min and observed with a transmission electron microscope (Phillips CM120).

Fluorescence Microscopy

To construct p35S:RP8-GFP, a 297-bp coding fragment containing the transit peptide was amplified using specific primers and cloned into the *XhoI* and *SpeI* sites of the GFP vector. GFP was transiently expressed in protoplasts of *N. benthamiana* using polyethylene glycol protocol (Lyznik et al., 1991). The GFP fluorescence (green) and chloroplast autofluorescence (red) of *N. benthamiana* protoplasts were imaged using a confocal laser scanning microscope (Zeiss LSM500). The filter sets used were BP505-545 (excitation 488 nm; emission 505-545 nm) and LP585 (excitation 488 nm; emission 585 nm) to detect GFP and the chlorophyll autofluorescence.

Protein Extraction and Immunoblot Analysis

Total proteins were extracted from 2-week-old plants, according to the method described (Yu et al., 2011). Different samples were quantified by Protein Assay (Bio-Rad, United States). A total of 30 μg of protein was loaded per lane and separated by 12–15% sodium dodecyl sulfate-polyacrylamide gel electrophoresis (SDS-PAGE). After electrophoresis, proteins were transferred onto a 45 μm PVDF membrane (Millipore, United States) and incubated with antibodies against chloroplast proteins (Agrisera, Sweden).³ Signals were identified by an ECL plus Immunoblot detection system (GE) following the manufacturer's instructions.

Expression and Purification of the Recombinant RP8 Protein

The coding sequence for the RP8 protein without the N-terminal putative transit peptide was amplified with the KOD plus polymerase (TOYOBO, Japan)² with gene-specific primers listed in **Supplementary Table 1** and subcloned into

¹<http://www.roche.com>

²<http://www.toyobo-global.com/>

³<http://www.agrisera.com>

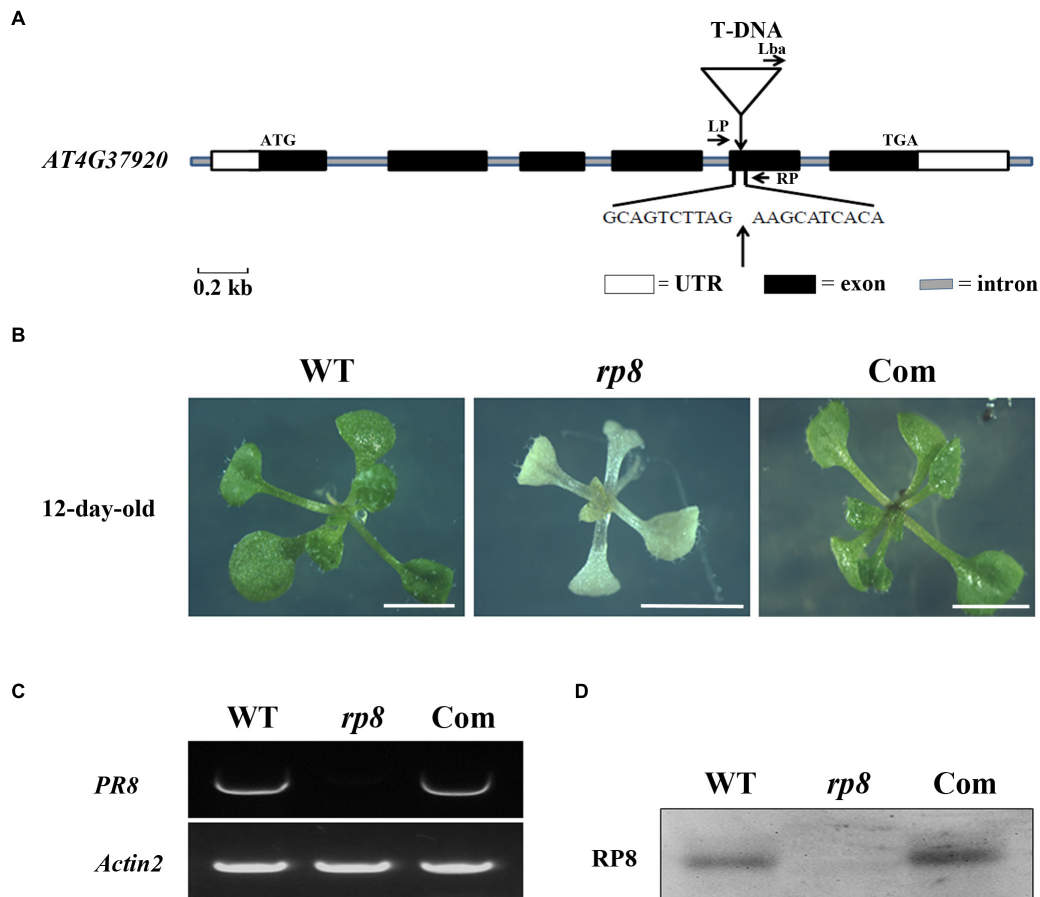


FIGURE 1 | Identification and characterization of the *rp8* mutant. **(A)** Schematic representation of the *RP8* gene and the T-DNA insertion. Black boxes represent exons, lines represent introns, and white boxes represent the start and stop regions. The white triangle shows the T-DNA insertion site in the fifth exon of At4g37920. **(B)** Phenotypes of 12-day-old wild-type (WT), *rp8* mutant, and complementation plant (Com). All plants are grown on MS medium containing 2% sucrose under light intensity at $30 \mu\text{mol m}^{-2} \text{s}^{-1}$. Bars = 0.5 cm. **(C)** RT-PCR analysis of the *RP8* gene expression in WT, *rp8* mutant, and complementation plants. *Actin2* was used as an internal control. **(D)** Immunoblot analysis of the RP8 protein in WT, *rp8* mutant, and complementation plants. Each lane was loaded with 30 μg total proteins.

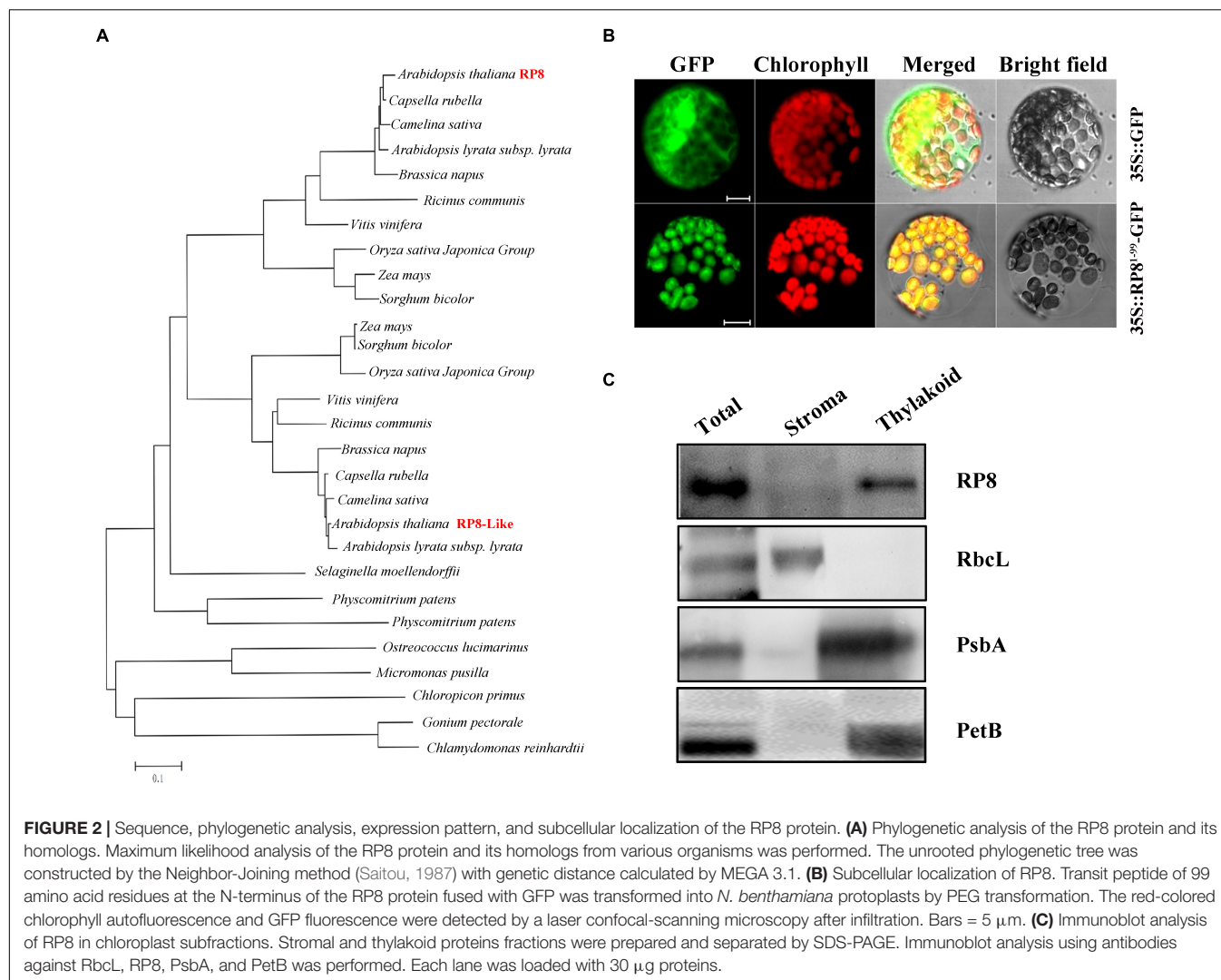
pET51b vector, in frame with a $6 \times \text{His}$ tag at C-terminus. The RP8 protein was overexpressed in the *Escherichia coli* BL21 (DE3) strain. When it was grown to $\text{OD}_{600} = 0.6$, 100 mM isopropyl- β -D-thiogalactopyranoside was added. Then, the *E. coli* was cultured at 16°C for 12 h to induce the recombinant protein. All protein purification steps were carried out as described in a study by Sun et al. (2019). The 5 mg purified RP8 protein was sent to Shanghai Orizymes Biotech Company, Shanghai, China to make an antibody of RP8.

RESULTS

Isolation and Phenotypic Characterization of the *rp8* Knockout Line

To identify novel nuclear-encoding factors essential for chloroplast development, we screened pigment-deficient

mutants of T-DNA insertional lines from the Arabidopsis Biological Resource Center, ABRC. Among the obtained mutant lines, an albino mutant from SALK_080811 with seedling lethal phenotype was characterized and subsequently named as *rp8* (RNA Processing 8). PCR sequencing confirmed that the T-DNA was inserted into the fifth exon of the locus, At4g37920 (Figure 1A) as claimed in the SALK database. Genetic analysis revealed that the progenies from heterozygous segregated approximately at a 3:1 ratio, indicating that the mutant was caused by a single recessive mutation. When cultivated on sucrose-supplemented medium under low light conditions at $30 \mu\text{mol photons m}^{-2} \text{s}^{-1}$, homozygous lines still showed an albino phenotype which only can survive for approximately 3 weeks with six to eight leaves (Figure 1B). Examination of young siliques of the heterozygous line also showed that approximately 25% of developing ovules were white (Supplementary Figure 1). RT-PCR results showed that no transcript of the *RP8* gene was detected in the *rp8* mutant, while it was present in



the wild type (Figure 1C). Further immunoblot analysis showed that the corresponding size of 43 kDa protein was not detected in the *rp8* mutant, but clearly present in the wild type (Figure 1D).

To further confirm whether the knockout of the *At4g37920* locus is responsible for the albino phenotype, we performed the genetic complementation analysis. We cloned a full-length genomic fragment of the *At4g37920* gene, then transformed it into the heterozygous lines through *Agrobacterium* transformation. We obtained more than seven independent transgenic complementation lines with *RP8* genotype but showed the wild-type phenotype (Figure 1B). RT-PCR analysis detected the full-length transcript of the *RP8* gene in these complementation lines and a specific 43 kDa protein could also be detected by immunoblot analysis as in wild type (Figures 1C,D). Taken together, these results demonstrated the albino mutant was due to the knockout of the *At4g37920* locus which is essential for photoautotrophic growth and plant viability in *Arabidopsis*.

RP8 Encodes a Novel Chloroplast-Localized Unknown Protein in *Arabidopsis*

The genome locus *At4g37920* encodes a 427-aa-long protein with a predicted molecular mass of 48.7 kDa. It was annotated as an endoribonuclease E-like protein (RNase E-like) in the TAIR database.⁴ Nevertheless, alignment analysis revealed no significant similarity between the RP8 and RNase E proteins, and conserved domain analysis also showed no known information in the currently available database (see text footnote 5). This analysis indicated that *RP8* encoded an unknown protein, and it does not belong to the endoribonuclease E-like family. Sequence searching of the PPDB database identified that one homologous of RP8, RP8-like protein (AT1G36320), is probably located in the chloroplast of *Arabidopsis*. They share 41% identity and 67% similarity at the amino acid level⁵ (Supplementary Figure 2).

⁴<https://www.arabidopsis.org/>

⁵<http://ppdb.tc.cornell.edu/dbsearch/gene.aspx?acc=AT1G36320>

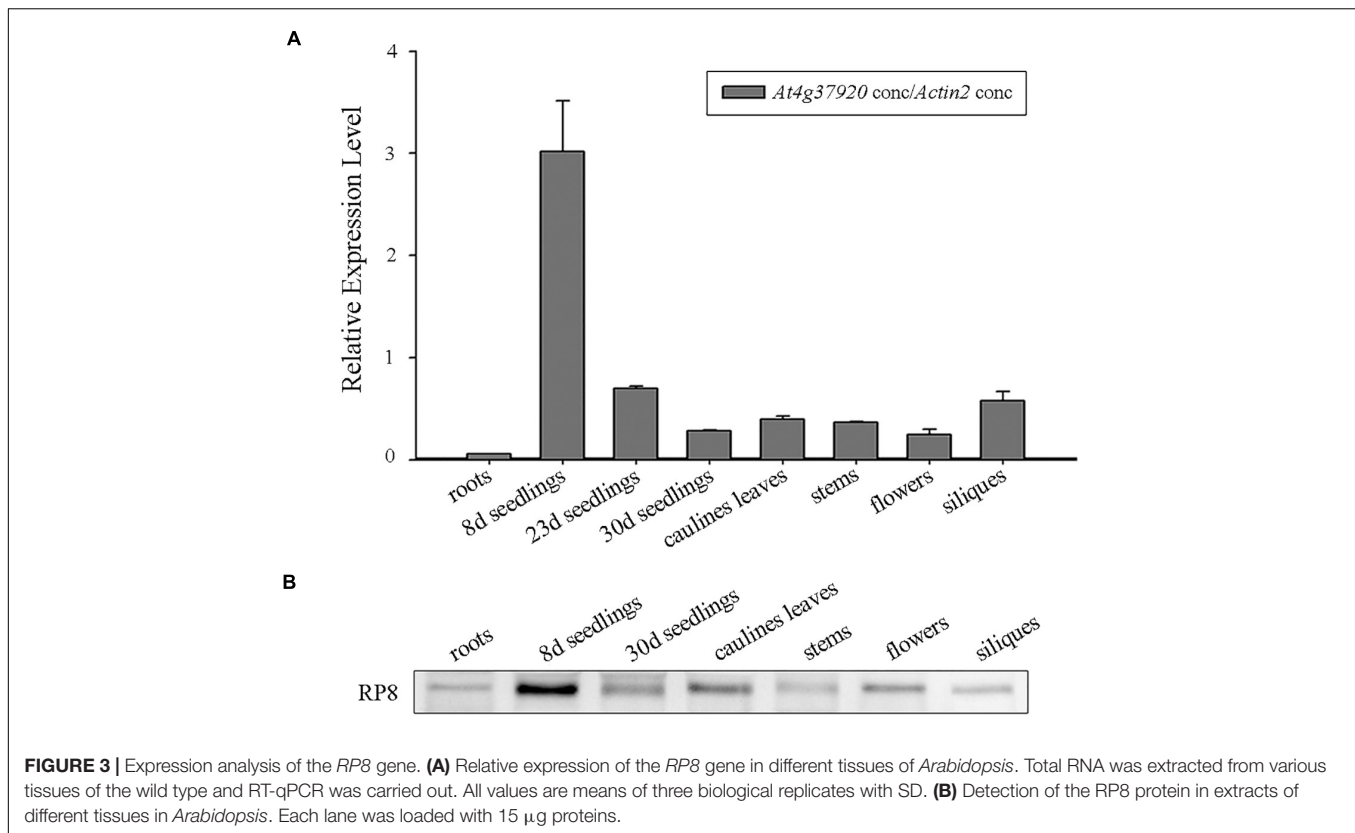


FIGURE 3 | Expression analysis of the *RP8* gene. **(A)** Relative expression of the *RP8* gene in different tissues of *Arabidopsis*. Total RNA was extracted from various tissues of the wild type and RT-qPCR was carried out. All values are means of three biological replicates with SD. **(B)** Detection of the *RP8* protein in extracts of different tissues in *Arabidopsis*. Each lane was loaded with 15 μ g proteins.

No obvious functional domain or motif was predicted in either *RP8* or the *RP8*-like protein by any available bioinformatic tools. The BLASTP searching database in the NCBI website revealed that *RP8* and the *RP8*-like protein are present in both dicotyledons and monocotyledons, such as *Camelin sativa*, *Brassica napus*, *Capsella rubella*, *Ricinus communis* and *Oryza*, *Sorghum bicolor*, *Zea mays*, and *Physcomitrium patens*. But only *RP8*-like homologous proteins are found in the species including *Selaginella moellendorffii*, moss, and a green alga. No homologous protein is detected in bacteria (**Figure 2A**). These data suggested that *RP8* and its homologous proteins are widely present in green plants, which probably originated from green alga.

Both the TargetP⁶ (Emanuelsson et al., 2000) and Predator software predicted that the *RP8* protein contains a putative chloroplast trans-peptide at the N-terminal region. To further confirm the subcellular localization of *RP8*, we constructed the coding sequence of the N-terminal 99-amino acid fused to a green fluorescent protein (GFP) under the control of the cauliflower mosaic virus 35S promoter. The plasmid containing the chimeric gene was transformed into the protoplasts of *N. benthamiana* through a polyethylene glycol (PEG)-mediated transformation method. Transient expression of the fusion protein was then examined by a confocal laser-scanning microscope. Our results showed that the green fluorescence of the chimeric protein was co-localized with chlorophyll autofluorescence (**Figure 2B**). By contrast, the fluorescence from free GFP protein was present

ubiquitously in the cytoplasm. These data suggested that the N-terminal region functions as a trans-peptide that is able to target the *RP8* protein to the chloroplast exclusively. Thus, the *RP8* protein is localized in the chloroplast. To further demonstrate its location in the chloroplast, the stroma and thylakoid fractions were separated and immunoblot analysis using antibodies against corresponding marker proteins of stroma (RbcL) and thylakoid (PsbA and PetB) were performed. These results indicated that *RP8* is associated with the thylakoid membranes (**Figure 2C**). Taken together, we concluded that *RP8* is a chloroplast-localized protein associated with the thylakoid membranes in *Arabidopsis*.

Expression of the *RP8* Gene in *Arabidopsis*

We examined the expression of the *RP8* gene using the publicly available microarray data and Genevestigator v3 (Zimmermann et al., 2004). The developmental expression analysis revealed that the *RP8* gene is highly expressed in seedlings, leaves, and flowers (**Supplementary Figure 3**). The anatomical expression analysis showed a higher expression of the *RP8* gene in juvenile leaves compared with other tissues, suggesting that *RP8* plays an important role during the early stage of chloroplast development (**Supplementary Figure 3**). To investigate the expression pattern of the *RP8* gene, total RNA was extracted from various tissues of the wild type, quantitative reverse transcription RT-qPCR analysis was performed. Our results showed that the *RP8* gene

⁶<http://www.cbs.dtu.dk/services/TargetP/>

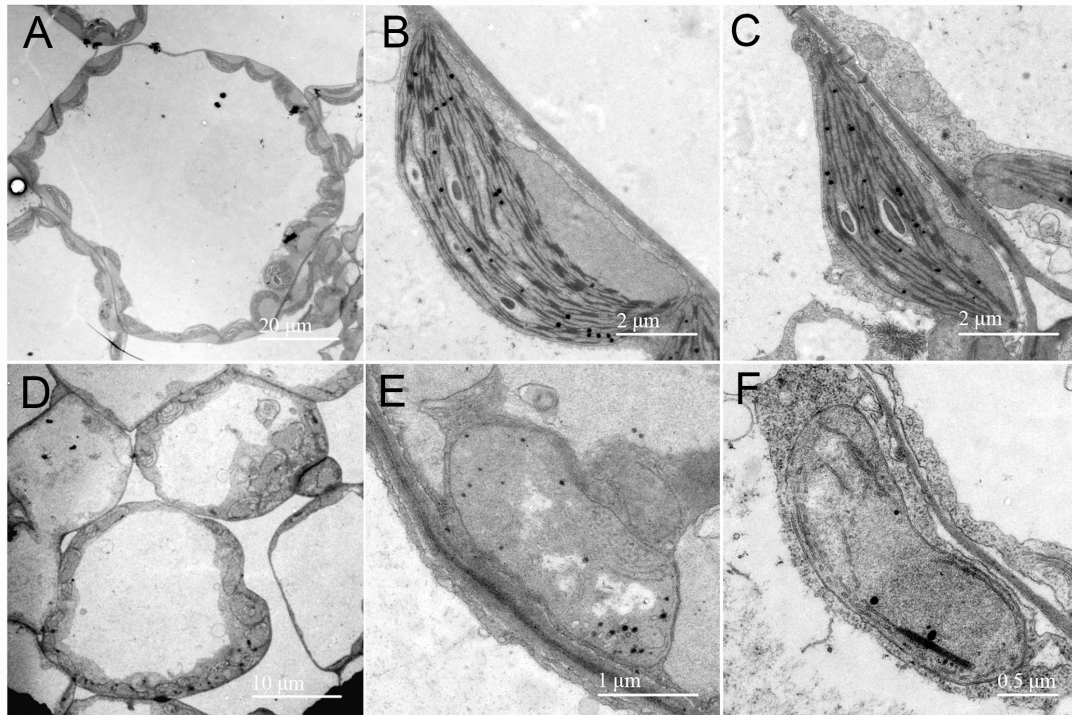


FIGURE 4 | Chloroplast ultrastructure observation in the wild type and the *rp8* mutant. Transmission electron micrographs of chloroplasts in leaves from the 12-day-old wild type (**A–C**) and the *rp8* mutant (**D–F**) grown under low light intensity at $30 \mu\text{mol photons m}^{-2} \text{s}^{-1}$. (**A,D**) Are the overview of mesophyll cell chloroplasts. (**B,E**) Are chloroplasts of cotyledons, (**C,F**) Are chloroplasts of true leaves. Scale bars are indicated.

was expressed in leaves, stems, flowers, siliques, and especially high in 8-day-old seedlings. In contrast, the *RP8* transcript in roots was barely detected. This result suggests that the *RP8* gene is widely expressed in photosynthetic tissues (**Figure 3A**). We also used an antibody against RP8 to confirm its accumulation in different plant tissues. As **Figure 3B** showed, the RP8 protein accumulated highly in the 8-day-old seedlings, which is consistent with the transcript levels. Unexpectedly, the RP8 protein can still accumulate in roots, although transcripts of RP8 were barely detected in roots. Taken together, our data showed that the *RP8* gene is strongly expressed in photosynthetic tissues at both transcription and protein levels.

Defects in Chloroplast Development in the *rp8* Mutant

To examine the development status of the chloroplast in the *rp8* mutant, we observed the chloroplast from 2-week-old seedlings by transmission electron microscopy (TEM). In the wild type, the chloroplast contains a well-organized stroma and stacked grana thylakoids in both cotyledons and true leaves (**Figures 4A–C**). In contrast, the thylakoids were nearly absent in the cotyledons of the *rp8* mutant, and only a few thylakoid lamellae can be observed from its true leaves (**Figures 4D–F**). These observations indicated that chloroplast development in the *rp8* mutant was seriously arrested at the early stage and that RP8 is essential for thylakoid formation and chloroplast development in *Arabidopsis*. We also

investigated the accumulation of photosynthetic-related proteins in the *rp8* mutant. These proteins, including three components of PSII complex (PsbA, PsbD, and OEC33), two components of PSI (PsaB and PsaD), one component of *cyb6/f* complex (PetA), two ATP synthase subunits (AtpB and AtpF), one subunit of light-harvest complex and chlorophyll a/b-binding protein (Lhcb1), and the large subunit of rubisco (RbcL), were checked using their corresponding antibodies. Our results showed that the amounts of AtpB and RbcL were reduced in the *rp8* mutant (**Figure 5** and **Supplementary Figure 5**). PsbA, PsbD, OEC33, PsaB, PsaD, and Lhcb1 are barely detected in the *rp8* mutant, although these proteins can be detected in the wild type. These results indicate that components of photosynthetic complexes were seriously reduced in the *rp8* mutant. Altogether, these results prove that the accumulation of photosynthetic proteins and the development of chloroplasts were seriously blocked in the *rp8* mutant.

Expression of Chloroplast-Associated Genes in the *rp8* Mutant

Because numerous nucleus-encoded genes regulate chloroplast gene expression (Zhou et al., 2009; Chateigner-Boutin et al., 2011; Gao et al., 2011; Yu et al., 2013; Huang et al., 2018; Wang et al., 2020), we - want to check the putative role of RP8 in chloroplast RNA metabolism by investigating chloroplast transcript profiles in the *rp8* mutant by Northern blot. The *psaA*, *psbA*, *psbB*, *petB*, and *rbcl* genes were chosen because they are

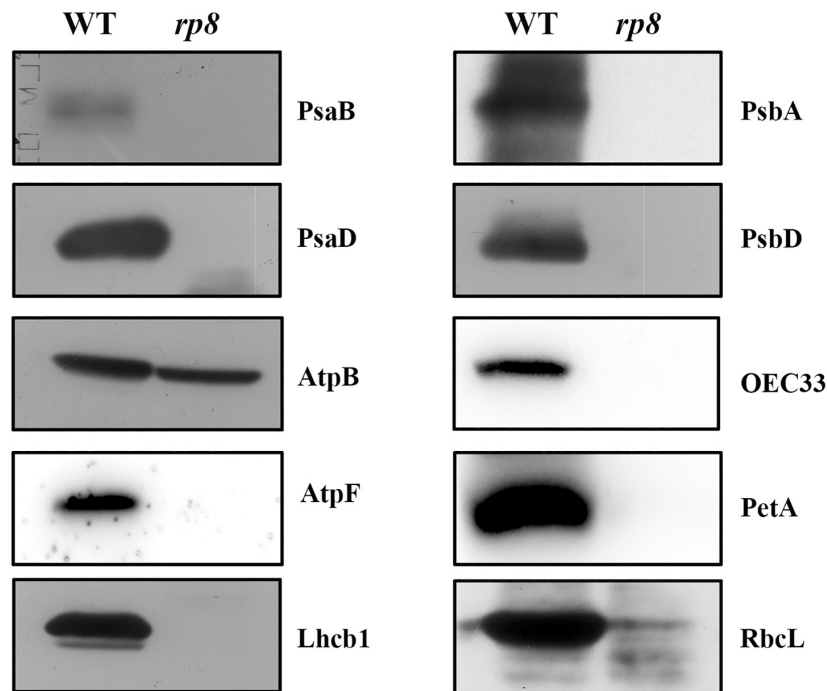


FIGURE 5 | Accumulation of photosynthetic proteins in the wild type and the *rp8* mutant. Immunoblot analysis of photosynthetic proteins PsbA, PsbD, AtpB, AtpF, Lhcb1, PsbA, PsbD, OEC33, PetA, and RbcL from the wild type (WT) and the *rp8* mutant using the corresponding antibodies, respectively. Each lane was loaded with 30 μ g total proteins.

PEP-dependent (class I). The *rps11*, *rpoA*, *rpoB*, and *rpoC2* were chosen because they are NEP-dependent (class III). The *atpB* and *clpP* were chosen because they are both PEP and NEP-dependent (class II) (Hajdukiewicz et al., 1997). As for those PEP-dependent chloroplast transcripts, their accumulations were seriously reduced in the *rp8* mutant compared with those of the wild type (Figure 6A). In contrast, the accumulations of NEP-dependent transcripts (*rps11*, *rpoB*, *rpoC2*) were increased in the *rp8* mutant (Figure 6B). As for the *atpB* operon, 2.6- and 2.0-kb transcripts are transcribed by PEP (σ dependent) and NEP, respectively (Schweer et al., 2006). In the *rp8* mutant, the 2.6-kb transcripts observed in the wild-type plant are not transcribed, whereas a novel 4.8-kb transcript transcribed by NEP was detected in the *rp8* mutant (Figure 6C). We also checked the transcripts of two nucleus genes *Lhcb1* and *AtpC1*, and no significant alteration was detected between the *rp8* mutant and the wild type (Figure 6D). This expression pattern is similar to other PEP-deficient mutants that have been reported earlier (Pfalz et al., 2006; Gao et al., 2011; Yu et al., 2013). Thus, our data showed that the null mutation of *RP8* affected the proper expression of chloroplast genes, resulting in reduced amounts of PEP-dependent chloroplast transcripts.

Noticeably, the *rpoA* gene encoding the alpha subunit of the PEP complex was transcribed by NEP. Here, we found that the number of mature transcripts of *rpoA* (about 990 nt) was clearly decreased in the *rp8* mutant. In contrast, no obvious difference in the processing of the *rps11* transcript located in the *rpoA* polycistron was observed between the wild type and the *rp8*

mutant. Since the accumulation of mature transcripts of *rpoA* was decreased in the *rp8* mutant, we further checked whether the level of the RpoA protein was affected. Immunoblot analysis showed that the protein level of RpoA in the mutant was dramatically reduced by 50% (Figure 6F). This result suggests that the defective *rpoA* polycistronic processing affects the accumulation of the RpoA protein. Similarly, we investigated the accumulation of another core protein of the PEP complex, RpoB, in the *rp8* mutant. Our data showed that the RpoB protein level was also dramatically reduced by 25% in the *rp8* mutant (Figure 6G). Taken together, our data suggested that the *RP8* deletion affects the processing of *rpoA* transcripts, which resulted in the defective accumulation of the PEP core complex and impaired expression of PEP-dependent chloroplast genes at the early growth stage.

Ribosomal RNAs and Proteins Were Substantially Reduced in the Chloroplast of the *rp8* Mutant

Ribonucleic acid processing 8 (RP8) is associated with thylakoids, as translationally active ribosomes are (Zoschke and Barkan, 2015). In the *rp8* mutant, accumulation of both alpha- and beta-PEP subunits (RpoA and RpoB) are affected (Figures 6F,G), and photosynthetic membrane proteins are barely detected (Figure 5). We further checked the possibility of *RP8* interference with translation. First, we checked the accumulation of chloroplast rRNAs in the *rp8* mutant compared with that of the wild type. Northern blot analysis showed that the

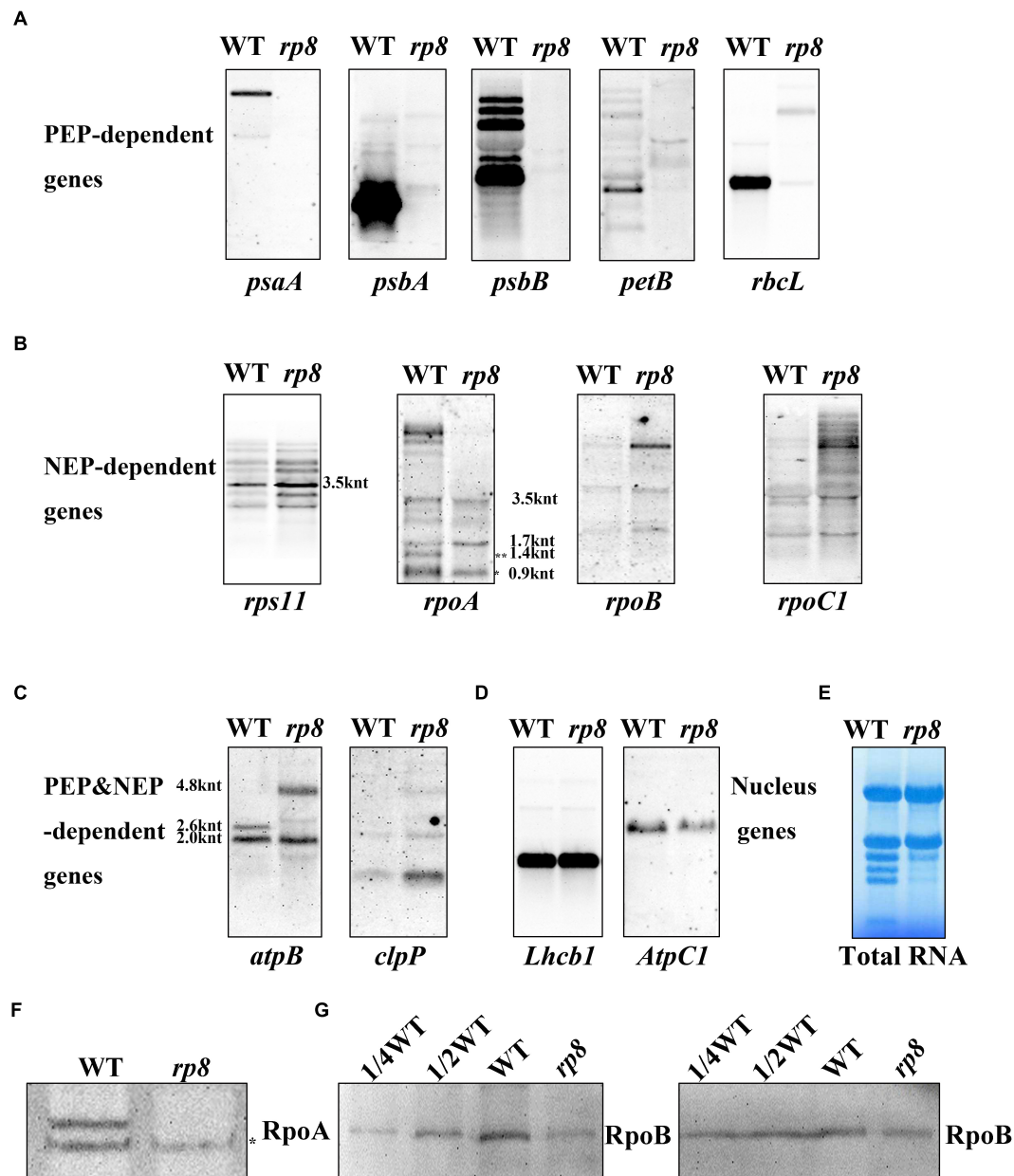


FIGURE 6 | Northern blot analysis of chloroplast-associated genes in the wild type (WT) and the *rp8* mutant. **(A)** Steady-state levels of PEP-dependent transcripts, *psaA*, *psbA*, *psbB*, *petB*, and *rbcL*. **(B)** Steady-state levels of NEP-dependent transcripts (*rps11*, *rpoA*, *rpoB*, and *rpoC1*). * Indicates the mature transcripts of *rpoA* (990 nt), ** indicates the 1.4 knt transcript as described in Zhang et al. (2015). The sizes of the transcripts were indicated according to Wu and Zhang (2010). **(C)** Steady-state levels of chloroplast transcripts that are both PEP- and NEP-dependent (*atpB* and *clpP*). As for the *atpB* transcripts, 4.8, 2.6, and 2.0 knt transcripts are indicated. **(D)** Steady-state levels of two nucleus genes (*Lhcb1* and *AtpC1*). **(E)** Methylene blue staining of total RNA for loading control. About 10 μ g total RNA was transferred to a nylon membrane after electrophoresis, then probed with DIG-labeled probes. **(F)** Immunoblot analysis of RpoA with the antibody described in Zhang et al. (2018) (*represents the specific band for the RpoA protein). **(G)** Immunoblot analysis of RpoB protein levels in the wild type (WT) and the *rp8* mutant. Total proteins from the WT samples were loaded with three different concentrations (7.5, 15, and 30 μ g), and total proteins from the mutant samples were loaded with 30 μ g, respectively. *Arabidopsis* mutant *ptac10* with a decreased RpoB protein level was used as a control (Chang et al., 2017; Yu et al., 2018).

abundance of the chloroplast rRNA, including 23S, 16S, 4.5S, and 5S rRNA, was severely decreased in the *rp8* mutant (Figure 7A). Second, we checked the amount of chloroplast ribosome proteins in the *rp8* mutant. Our immunoblot analysis showed that the amounts of chloroplast ribosome proteins,

including PRPS1 (uS1c), PRPS5(uS5c), PRPL2 (uL2c), and PRPL4 (uL4c), were substantially reduced in the *rp8* mutant (Figure 7B), compared with those in the wild type. These data showed that knockout of RP8 seriously affected chloroplast translational machinery.

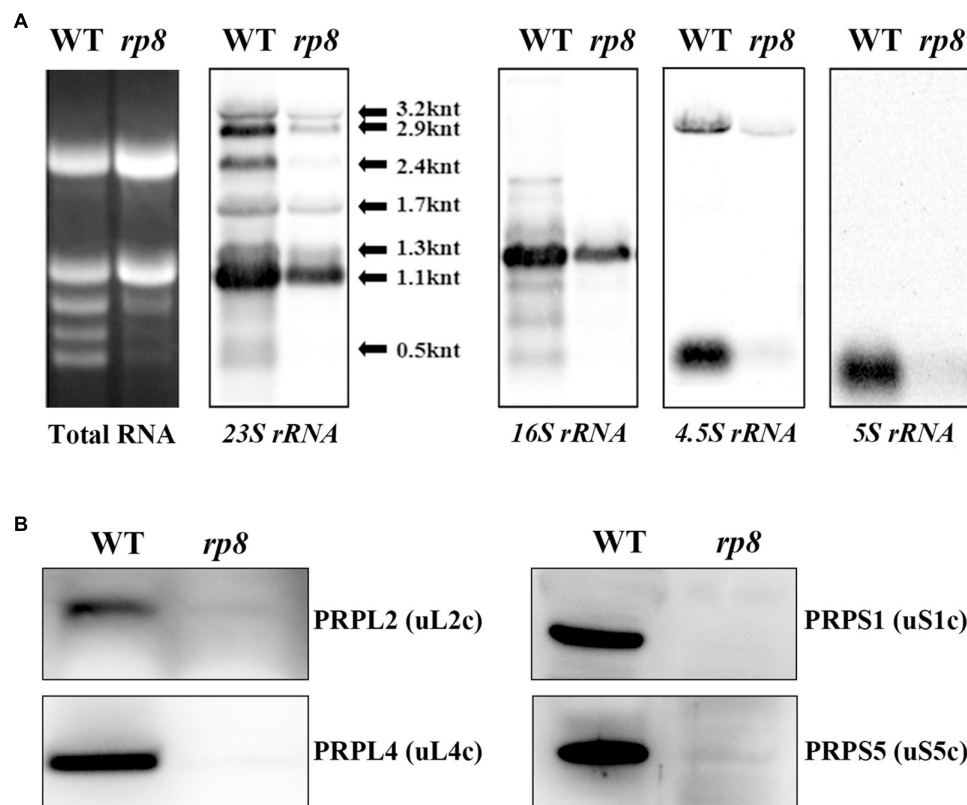


FIGURE 7 | Analysis of chloroplast ribosomes in the wild type (WT) and the *rp8* mutant. **(A)** Total RNA in the WT and the *rp8* mutant and Northern blot analysis of chloroplast-encoded rRNAs. **(B)** Immunoblot analysis of chloroplast ribosomal proteins PRPS1 (uS1c), PRPS5 (uS5c), PRPL2 (uL2c), and PRPL4 (uL4c) in the WT and the *rp8* mutant. Each lane was loaded with 30 μ g total proteins.

DISCUSSION

In this study, we characterized a pigmentation-deficient mutant *rp8* in detail. Our data demonstrated that the chloroplast-localized RP8 protein is required for the maturation of the polycistronic *rpoA* transcript, which is essential for PEP function and chloroplast development. Our work would enrich the knowledge in chloroplast gene expression and chloroplast development.

In higher plants, chloroplasts come from proplastids which are small undifferentiated plastids lacking pigments or internal membrane structures. This process is often accompanied by the highly coordinated expression of plastid- and nuclear-encoded genes (Shiina et al., 2005), which is necessary to maintain chloroplast function. Since most chloroplast proteins are nuclear-encoded, many nuclear genes mutations result in a defect in chloroplast development and albino lethal phenotype (Pfalz et al., 2006; Arsova et al., 2010; Gao et al., 2011; Yu et al., 2013; Wang et al., 2020). Although RP8 encoded by the At4g37920 gene in *Arabidopsis* is annotated as an RNase E-like protein, no further evidence supported this annotation at present. The albino lethal phenotype of the *rp8* mutant may result from the arrested chloroplast development since they have poorly developed abnormal chloroplast with a few thylakoids lamella (Figure 4). Accordingly, the accumulation of thylakoid proteins

in the *rp8* mutant was substantially reduced (Figure 5). Genetic complementation analysis confirmed that the loss of function of the *RP8* gene is required for the mutant phenotype. Consistent with the transcription level of the *RP8* gene, the RP8 protein is highly expressed at the seedling stage, suggesting an essential role for the RP8 protein in chloroplast development (Figure 3). Although the transcript level of RP8 in roots was low, the RP8 protein can still accumulate in roots, and its abundance is no different from that in stems, flowers, and siliques. There may exist a distinct regulator at the expression level of the *RP8* gene in these tissues.

Phylogenetic analysis showed that the RP8 protein probably originated from the green alga, not from cyanobacteria (Figure 2A). Both RP8 and the RP8-like protein are present in higher plants but only RP8-like proteins exist in a green alga, indicating gene duplication probably happened during the evolution of organisms from ocean to land. Although the RP8 protein shares high identity with the RP8-like protein (Supplementary Figure 2), the pleiotropic phenotype of the *rp8* mutant strongly suggested its distinct function in chloroplasts of higher plants, which also highlighted the importance of the RP8 protein family during chloroplast development. In *Arabidopsis* chloroplasts, the existence of RP8 and its paralogous proteins appear not to be occasional. For example, MRL7 and MRL7-L are two homologous chloroplast proteins that play essential

but non-redundant roles (Qiao et al., 2011). Both MRL7 and MRL7-L are present in embryophytes, but MRL7-L is absent in lower plants (Qiao et al., 2011; Yu et al., 2011, 2014b). Although both MRL7 and MRL7-L are involved in regulating chloroplast gene expression, knockout of either of them results in an albino phenotype (Qiao et al., 2011), indicating the functional diversification of MRL7 and MRL7-L in chloroplasts.

Chloroplast gene expression is required for the development of chloroplast in higher plants. Loss-of-function mutation genes encoding subunits of chloroplast RNA polymerase and their regulatory proteins always impaired chloroplast gene expression and further resulted in arrested chloroplast development (Pfalz et al., 2006; Gao et al., 2011; Yu et al., 2013). In this work, we investigated the expression profiles of chloroplast genes in the *rp8* mutant. Northern blot results showed that the *rp8* mutant displayed seriously reduced levels of chloroplast-encoded photosynthetic genes transcribed by PEP, but the transcript levels of NEP-dependent genes, *rpoB*, *rpoC1* were increased (Figures 6A–C). The increased levels of NEP-dependent chloroplast gene expression in the mutant might be due to a feedback regulatory mediated by tRNA^{Glu} (Hanaoka et al., 2005). This expressional pattern of chloroplast transcripts in the *rp8* mutant resembles those of *paps* mutants and Δ *rpo* mutants (Pfalz et al., 2006; Ajjawi et al., 2010; Myouga et al., 2010; Gao et al., 2011; Yu et al., 2013; Chang et al., 2017; Liebers et al., 2018). These results suggest that RP8 probably plays an important regulatory role in chloroplast gene expression. Nevertheless, no evidence showed that the RP8 protein is a component of the PEP complex, like PAPs proteins (Pfalz et al., 2006; Steiner et al., 2011). It was noticeable that the mature transcript of *rpoA* (990 nt) located in the *L23-L2-S19-L22-S3-L16-L14-S8-L36-S11-rpoA* polycistron was decreased in the *rp8* mutant. But the transcripts of *rps11* in the same polycistron upstream of *rpoA* were not affected (Figure 6B), indicating that RP8 may specifically be involved in the processing of *rpoA* transcripts. In addition, we checked the effects of the *rp8* mutation on the intron splicing of chloroplast genes. There are no obvious abnormal chloroplast pre-mRNA splicing events found in the *rp8* mutant (Supplementary Figure 4), suggesting that RP8 may be specifically involved in the processing of the *rpoA* polycistron in chloroplasts. Like the *opt70* mutant in *Arabidopsis*, interrupting the processing of the *rpoC1* transcript which encodes the β' core subunit of the PEP complex impaired the PEP activity and led to the defective chloroplast development (Chateigner-Boutin et al., 2011). Our data suggested that reduced *rpoA* transcripts affected the accumulation of the RpoA protein in the *rp8* mutant, which may result in decreased accumulation of the PEP complex and subsequently affect the expression of PEP-dependent chloroplast genes (Figure 6).

Interestingly, we found some other nuclear-encoded proteins associated with the *rpoA* transcript in *Arabidopsis*, which leads to a lower accumulation level of the RpoA protein and reduced transcription of PEP-dependent genes. For example, mTERF6 is directly associated with a 3'-end sequence of the *rpoA* polycistron and is involved in the transcription termination of the *rpoA* polycistron (Zhang et al., 2018). The PDM1 protein is involved in the processing of *rpoA* transcripts by

associating with the intergenic sequence of *S11-rpoA*, which is important for post-transcriptional regulation in chloroplasts (Wu and Zhang, 2010; Yin et al., 2012; Pyo et al., 2013; Zhang et al., 2015). It further suggested that PDM1 is a hub protein; it can recruit various functional proteins which are responsible for different post-transcriptional processing (Yin et al., 2012; Zhang et al., 2015). So it is reasonable for us to speculate that the RP8 protein may be recruited by some *rpoA*-associated proteins to assist related processes during *rpoA* transcript processing. Of course, this assumption still needs to be further investigated in the future. Additionally, RP8 is associated with thylakoids (Figure 2C), as translationally active ribosomes (Zoschke and Barkan, 2015). We found that both chloroplast rRNAs and chloroplast ribosomal proteins were significantly decreased in the *rp8* mutant (Figure 7), which suggested that the function of RP8 might be related to chloroplast translation. We cannot exclude the possibility that the reduction of chloroplast rRNAs and chloroplast ribosomal proteins is due to the pleiotropic effects of the RP8 mutation.

DATA AVAILABILITY STATEMENT

The datasets presented in this study can be found in online repositories. The names of the repository/repositories and accession number(s) can be found in the article/Supplementary Material.

AUTHOR CONTRIBUTIONS

MK, QY, and HM designed the experiments and wrote the manuscript. MK, YW, ZW, and WQ performed the experiments. YXL, XC, and YYL analyzed the data. PS and ZY analyzed the data and revised the manuscript. All authors contributed to the article and approved the submitted version.

FUNDING

This work was supported by funds from the Funding for Synthesis Biology (2019YFA0904602), the Strategic Priority Research Program of CAS (XDB27020106), and the National Natural Science Foundation of China (31970255).

ACKNOWLEDGMENTS

We thank Dr. Weihua Huang (Shanghai Normal University) for providing the primers for chloroplast gene-splicing analysis.

SUPPLEMENTARY MATERIAL

The Supplementary Material for this article can be found online at: <https://www.frontiersin.org/articles/10.3389/fpls.2021.700975/full#supplementary-material>

Supplementary Figure 1 | The seedling-lethal phenotype of the *rp8* mutant.

Supplementary Figure 2 | Protein alignment analysis between RP8 and RP8-like Protein (AT1G36320).

Supplementary Figure 3 | Different stages of development and tissue expression of the *RP8* gene, according to publicly available Affymetrix GeneChip microarray data.

Supplementary Figure 4 | RT-PCR analysis of intron splicing of chloroplast genes in the wild type and the *rp8* mutant.

Supplementary Figure 5 | Coomassie brilliant blue staining for the wild type and the *rp8* mutant.

REFERENCES

- Ajjawi, I., Lu, Y., Savage, L. J., Bell, S. M., and Last, R. L. (2010). Large-scale reverse genetics in *Arabidopsis*: case studies from the Chloroplast 2010 Project. *Plant Physiol.* 152, 529–540. doi: 10.1104/pp.109.148494
- Arsova, B., Hoja, U., Wimmelbacher, M., Greiner, E., Ustün, S., Melzer, M., et al. (2010). Plastidial thioredoxin z interacts with two fructokinase-like proteins in a thiol-dependent manner: evidence for an essential role in chloroplast development in *Arabidopsis* and *Nicotiana benthamiana*. *Plant Cell* 22, 1498–1515. doi: 10.1105/tpc.109.071001
- Aryamanesh, N., Ruwe, H., Sanglard, L. V., Eshraghi, L., Bussell, J. D., Howell, K. A., et al. (2017). The pentatricopeptide repeat protein EMB2654 is essential for trans-splicing of a chloroplast small ribosomal subunit transcript. *Plant Physiol.* 173, 1164–1176. doi: 10.1104/pp.16.01840
- Beligni, M. V., and Mayfield, S. P. (2008). *Arabidopsis thaliana* mutants reveal a role for CSP41a and CSP41b, two ribosome-associated endonucleases in chloroplast ribosomal RNA metabolism. *Plant Mol. Biol.* 67, 389–401. doi: 10.1007/s11103-008-9328-2
- Bollenbach, T. J., Lange, H., Gutierrez, R., Erhardt, M., Stern, D. B., and Gagliardi, D. (2005). RNRI, a 3′-5′ exoribonuclease belonging to the RNR superfamily, catalyzes 3′ maturation of chloroplast ribosomal RNAs in *Arabidopsis thaliana*. *Nucleic Acids Res.* 33, 2751–2763. doi: 10.1093/nar/gki576
- Chang, S. H., Lee, S., Um, T. Y., Kim, J. K., Do, C. Y., and Jang, G. (2017). pTAC10, a key subunit of plastid-encoded RNA polymerase, promotes chloroplast development. *Plant Physiol.* 174, 435–449. doi: 10.1104/pp.17.00248
- Chateigner-Boutin, A. L., des Francs-Small, C. C., Delannoy, E., Kahlau, S., Tanz, S. K., de Longevialle, A. F., et al. (2011). OTP70 is a pentatricopeptide repeat protein of the E subgroup involved in splicing of the plastid transcript *rpoC1*. *Plant J.* 65, 532–542. doi: 10.1111/j.1365-313X.2010.04441.x
- Chateigner-Boutin, A. L., Ramos-Vega, M., Guevara-García, A., Andrés, C., de la Luz Gutiérrez-Nava, M., Cantero, A., et al. (2008). CLB19, a pentatricopeptide repeat protein required for editing of *rpoA* and *clpP* chloroplast transcripts. *Plant J.* 56, 590–602. doi: 10.1111/j.1365-313X.2008.03634.x
- Chevalier, F., Gulam, M. M., Rondet, D., Pfannschmidt, T., Merendino, L., and Lerbs-Mache, S. (2015). Characterization of the *psbH* precursor RNAs reveals a precise endoribonuclease cleavage site in the *psbT/psbH* intergenic region that is dependent on *psbN* gene expression. *Plant Mol. Biol.* 88, 357–367. doi: 10.1007/s11103-015-0325-y
- Chi, W., He, B., Mao, J., Jiang, J., and Zhang, L. (2015). Plastid sigma factors: Their individual functions and regulation in transcription. *Biochim. Biophys. Acta* 1847, 770–778. doi: 10.1016/j.bbabi.2015.01.001
- Clough, S. J., and Bent, A. F. (1998). Floral dip: a simplified method for *Agrobacterium*-mediated transformation of *Arabidopsis thaliana*. *Plant J.* 16, 735–743. doi: 10.1046/j.1365-313X.1998.00343.x
- Daniell, H., Lin, C. S., Yu, M., and Chang, W. J. (2016). Chloroplast genomes: diversity, evolution, and applications in genetic engineering. *Genome Biol.* 17:134. doi: 10.1186/s13059-016-1004-2
- del Campo, E. M. (2009). Post-transcriptional control of chloroplast gene expression. *Gene Regul. Syst. Biol.* 3, 31–47. doi: 10.4137/grsb.s2080
- Emanuelsson, O., Nielsen, H., Brunak, S., and von Heijne, G. (2000). Predicting subcellular localization of proteins based on their N-terminal amino acid sequence. *J. Mol. Biol.* 300, 1005–1016. doi: 10.1006/jmbi.2000.3903
- Gao, Z. P., Yu, Q. B., Zhao, T. T., Ma, Q., Chen, G. X., and Yang, Z. N. (2011). A functional component of the transcriptionally active chromosome complex, *Arabidopsis* pTAC14, interacts with pTAC12/HEMERA and regulates plastid gene expression. *Plant Physiol.* 157, 1733–1745. doi: 10.1104/pp.111.184762
- Germain, A., Herlich, S., Larom, S., Kim, S. H., Schuster, G., and Stern, D. B. (2011). Mutational analysis of *Arabidopsis* chloroplast polynucleotide phosphorylase reveals roles for both RNase PH core domains in polyadenylation, RNA 3′-end maturation and intron degradation. *Plant J.* 67, 381–394. doi: 10.1111/j.1365-313X.2011.04601.x
- Germain, A., Kim, S. H., Gutierrez, R., and Stern, D. B. (2012). Ribonuclease II preserves chloroplast RNA homeostasis by increasing mRNA decay rates, and cooperates with polynucleotide phosphorylase in 3′ end maturation. *Plant J.* 72, 960–971. doi: 10.1111/tpj.12006
- Hajdukiewicz, P. T., Allison, L. A., and Maliga, P. (1997). The two RNA polymerases encoded by the nuclear and the plastid compartments transcribe distinct groups of genes in tobacco plastids. *EMBO J.* 16, 4041–4048. doi: 10.1093/emboj/16.13.4041
- Hanaoka, M., Kanamaru, K., Fujiwara, M., Takahashi, H., and Tanaka, K. (2005). Glutamyl-tRNA mediates a switch in RNA polymerase use during chloroplast. *EMBO Rep.* 6, 545–550. doi: 10.1038/sj.embor.7400411
- Huang, W., Zhang, Y., Shen, L., Fang, Q., Liu, Q., Gong, C., et al. (2020). Accumulation of the RNA polymerase subunit *RpoB* depends on RNA editing by OsPPR16 and affects chloroplast development during early leaf development in rice. *New Phytol.* 228, 1401–1416. doi: 10.1111/nph.16769
- Huang, W., Zhu, Y., Wu, W., Li, X., Zhang, D., Yin, P., et al. (2018). The Pentatricopeptide Repeat Protein SOT5/EMB2279 is required for plastid *rpl2* and *trnK* intron splicing. *Plant Physiol.* 177, 684–697. doi: 10.1104/pp.18.00406
- Inaba, T., and Schnell, D. J. (2008). Protein trafficking to plastids: one theme, many variations. *Biochem. J.* 413, 15–28. doi: 10.1042/BJ20080490
- Leister, D. (2003). Chloroplast research in the genomic age. *Trends Genet.* 19, 47–56. doi: 10.1016/s0168-9525(02)00003-3
- Liebers, M., Chevalier, F., Blanvillain, R., and Pfannschmidt, T. (2018). PAP genes are tissue- and cell-specific markers of chloroplast development. *Planta* 248, 629–646. doi: 10.1007/s00425-018-2924-8
- Lopez-Juez, E., and Pyke, K. A. (2005). Plastids unleashed: Their development and their integration in plant development. *Int. J. Dev. Biol.* 49, 557–577. doi: 10.1387/ijdb.051997el
- Lyznik, L. A., Peng, J. Y., and Hodges, T. K. (1991). Simplified procedure for transient transformation of plant protoplasts using polyethylene glycol treatment. *Biotechniques* 10, 294–300.
- MacIntosh, G. C., and Castandet, B. (2020). Organellar and Secretory Ribonucleases: Major Players in Plant RNA Homeostasis. *Plant Physiol.* 183, 1438–1452. doi: 10.1104/pp.20.00076
- Mudd, E. A., Sullivan, S., Gisby, M. F., Mironov, A., Kwon, C. S., Chung, W. I., et al. (2008). A 125 kDa RNase E/G-like protein is present in plastids and is essential for chloroplast development and autotrophic growth in *Arabidopsis*. *J. Exp. Bot.* 59, 2597–2610. doi: 10.1093/jxb/ern126
- Myouga, F., Akiyama, K., Motohashi, R., Kuromori, T., Ito, T., Iizumi, H., et al. (2010). The Chloroplast Function Database: a large-scale collection of *Arabidopsis* Ds/Spm- or T-DNA-tagged homozygous lines for nuclear-encoded chloroplast proteins, and their systematic phenotype analysis. *Plant J.* 61, 529–542. doi: 10.1111/j.1365-313X.2009.04074.x
- Pfalz, J., and Pfannschmidt, T. (2013). Essential nucleoid proteins in early chloroplast development. *Trends Plant Sci.* 18, 186–194. doi: 10.1016/j.tplants.2012.11.003
- Pfalz, J., Liere, K., Kandlbinder, A., Dietz, J., and Oelmüller, R. (2006). pTAC2, -6, and -12 are components of the transcriptionally active plastid chromosome that are required for plastid gene expression. *Plant Cell* 18, 176–197. doi: 10.1105/tpc.105.036392
- Pfannschmidt, T., and Liere, K. (2005). Redox regulation and modification of proteins controlling chloroplast gene expression. *Antioxid. Redox. Signal.* 7, 607–618. doi: 10.1089/ars.2005.7.607
- Pfannschmidt, T., Blanvillain, R., Merendino, L., Courtis, F., Chevalier, F., Liebers, M., et al. (2015). Plastid RNA polymerases: orchestration of enzymes with different evolutionary origins controls chloroplast biogenesis during the plant life cycle. *J. Exp. Bot.* 66, 6957–6973. doi: 10.1093/jxb/erv415

- Pyo, Y. J., Kwon, K. C., Kim, A., and Cho, M. H. (2013). Seedling lethal1, a pentatricopeptide repeat protein lacking an E/E+ or DYW domain in *Arabidopsis*, is involved in plastid gene expression and early chloroplast development. *Plant Physiol.* 163, 1844–1858. doi: 10.1104/pp.113.227199
- Qiao, J., Ma, C., Wimmelbacher, M., Bornke, F., and Luo, M. (2011). Two novel proteins, MRL7 and its paralog MRL7-L, have essential but functionally distinct roles in chloroplast development and are involved in plastid gene expression regulation in *Arabidopsis*. *Plant Cell Physiol.* 52, 1017–1030. doi: 10.1093/pcp/pcr054
- Raven, J. A., and Allen, J. F. (2003). Genomics and chloroplast evolution: what did cyanobacteria do for plants? *Genome Biol.* 4:209. doi: 10.1186/gb-2003-4-3-209
- Saitou, N. (1987). The neighbor-joining method: a new method for reconstructing phylogenetic tree. *Mol. Biol. Evol.* 4:406. doi: 10.1093/oxfordjournals.molbev.a040454
- Sato, S., Nakamura, Y., Kaneko, T., Asamizu, E., and Tabata, S. (1999). Complete structure of the chloroplast genome of *Arabidopsis thaliana*. *DNA Res.* 6, 283–290. doi: 10.1093/dnares/6.5.283
- Schmitz-Linneweber, C., and Small, I. (2008). Pentatricopeptide repeat proteins: a socket set for organelle gene expression. *Trends Plant Sci.* 13, 1360–1385. doi: 10.1016/j.tplants.2008.10.001
- Schweer, J., Loschelder, H., and Link, G. (2006). A promoter switch that can rescue a plant sigma factor mutant. *FEBS Lett.* 580, 6617–6622. doi: 10.1016/j.febslet.2006.11.010
- Schweer, J., Türkeri, H., Kolpack, A., and Link, G. (2010). Role and regulation of plastid sigma factors and their functional interactors during chloroplast transcription—recent lessons from *Arabidopsis thaliana*. *Eur. J. Cell Biol.* 89, 940–946. doi: 10.1016/j.ejcb.2010.06.016
- Shiina, T., Tsunoyama, Y., Nakahira, Y., and Khan, M. S. (2005). Plastid RNA polymerases, promoters, and transcription regulators in higher plants. *Int. Rev. Cytol.* 244, 1–68. doi: 10.1016/S0074-7696(05)44001-2
- Steiner, S., Schröter, Y., Pfalz, J., and Pfannschmidt, T. (2011). Identification of essential subunits in the plastid-encoded RNA polymerase complex reveals building blocks for proper plastid development. *Plan Physiol.* 157, 1043–1055. doi: 10.1104/pp.111.184515
- Sun, N., Han, X., Xu, M., Kaplan, A., Espie, G. S., and Mi, H. (2019). A thylakoid-located carbonic anhydrase regulates CO₂ uptake in the cyanobacterium *Synechocystis* sp. *New Phytol.* 222, 206–217. doi: 10.1111/nph.15575
- Valkov, V. T., Scotti, N., Kahlau, S., Maclean, D., Grillo, S., Gray, J. C., et al. (2009). Genome-wide analysis of plastid gene expression in potato leaf chloroplasts and tuber amyloplasts: transcriptional and posttranscriptional control. *Plant Physiol.* 150, 2030–2044.
- Walter, M., Piepenburg, K., Schöttler, M. A., Petersen, K., Kahlau, S., Tiller, N., et al. (2010). Knockout of the plastid RNase E leads to defective RNA processing and chloroplast ribosome deficiency. *Plant J.* 64, 851–863. doi: 10.1111/j.1365-313X.2010.04377.x
- Wang, X. W., An, Y. Q., Xu, P., and Xiao, J. W. (2021). Functioning of PPR Proteins in Organelle RNA Metabolism and Chloroplast Biogenesis. *Front. Plant Sci.* 12:627501. doi: 10.3389/fpls.2021.627501
- Wang, X., Zhao, L., Man, Y., Li, X., Wang, L., and Xiao, J. (2020). PDM4, a pentatricopeptide repeat protein, affects chloroplast gene expression and chloroplast development in *Arabidopsis thaliana*. *Front. Plant Sci.* 11:1198. doi: 10.3389/fpls.2020.01198
- Wu, H., and Zhang, L. X. (2010). The PPR protein PDM1 is involved in the processing of *rpoA* pre-mRNA in *Arabidopsis thaliana*. *Chinese Sci. Bull.* 30, 3485–3489. doi: 10.1007/s11434-010-4040-4
- Yin, Q. Q., Cui, Y. L., Zhang, G. R., Zhang, H. D., Wang, X. M., and Yang, Z. N. (2012). The *Arabidopsis* pentatricopeptide repeat protein PDM1 is associated with the intergenic sequence of *S11-rpoA* for *rpoA* monocistronic RNA cleavage. *Chinese Sci. Bull.* 57, 3452–3459. doi: 10.1007/s11434-012-5278-9
- Yu, F., Park, S. S., Liu, X., Foudree, A., Fu, A., Powikrowska, M., et al. (2011). SUPPRESSOR OF VARIEGATION4, a new var2 suppressor locus, encodes a pioneer protein that is required for chloroplast biogenesis. *Mol. Plant.* 4, 229–240. doi: 10.1093/mp/ssq074
- Yu, Q. B., Huang, C., and Yang, Z. N. (2014a). Nuclear-encoded factors associated with the chloroplast transcription machinery of higher plants. *Front. Plant Sci.* 5:316. doi: 10.3389/fpls.2014.00316
- Yu, Q. B., Lu, Y., Ma, Q., Zhao, T. T., Huang, C., Zhao, H. F., et al. (2013). TAC7, an essential component of the plastid transcriptionally active chromosome complex, interacts with FLN1, TAC10, TAC12 and TAC14 to regulate chloroplast gene expression in *Arabidopsis thaliana*. *Physiol. Plant.* 148, 408–421. doi: 10.1111/j.1399-3054.2012.01718.x
- Yu, Q. B., Ma, Q., Kong, M. M., Zhao, T. T., Zhang, X. L., Zhou, Q., et al. (2014b). AtECB1/MRL7, a thioredoxin-like fold protein with disulfide reductase activity, regulates chloroplast gene expression and chloroplast biogenesis in *Arabidopsis thaliana*. *Mol. Plant.* 7, 206–217. doi: 10.1093/mp/ss t092
- Yu, Q. B., Zhao, T. T., Ye, L. S., Cheng, L., Wu, Y. Q., Huang, C., et al. (2018). pTAC10, an S1-domain-containing component of the transcriptionally active chromosome complex, is essential for plastid gene expression in *Arabidopsis thaliana* and is phosphorylated by chloroplast-targeted casein kinase II. *Photosynth Res.* 137, 69–83. doi: 10.1007/s11220-018-0479-y
- Zhang, H. D., Cui, Y. L., Huang, C., Yin, Q. Q., Qin, X. M., Xu, T., et al. (2015). PPR protein PDM1/SEL1 is involved in RNA editing and splicing of plastid genes in *Arabidopsis thaliana*. *Photosynth Res.* 126, 311–321. doi: 10.1007/s11220-015-0171-4
- Zhang, Y., Cui, Y. L., Zhang, X. L., Yu, Q. B., Wang, X., Yuan, X. B., et al. (2018). A nuclear-encoded protein, mTERF6, mediates transcription termination of *rpoA* polycistron for plastid-encoded RNA polymerase-dependent chloroplast gene expression and chloroplast development. *Sci. Rep.* 8:11929. doi: 10.1038/s41598-018-30166-6
- Zhelyazkova, P., Sharma, C. M., Förstner, K. U., Liere, K., Vogel, J., and Börner, T. (2012). The primary transcriptome of barley chloroplasts: numerous noncoding RNAs and the dominating role of the plastid-encoded RNA polymerase. *Plant Cell* 24, 123–136. doi: 10.1105/tpc.111.089441
- Zhou, W., Cheng, Y., Yap, A., Chateigner-Boutin, A. L., Delannoy, E., Hammani, K., et al. (2009). The *Arabidopsis* gene YS1 encoding a DYW protein is required for editing of *rpoB* transcripts and the rapid development of chloroplasts during early growth. *Plant J.* 58, 82–96. doi: 10.1111/j.1365-313X.2008.03766.x
- Zimmermann, P., Hirsch-Hoffmann, M., Hennig, L., and Gruissem, W. (2004). GENEVESTIGATOR. *Arabidopsis* microarray database and analysis toolbox. *Plant Physiol.* 136, 2621–2632. doi: 10.1104/pp.104.046367
- Zoschke, R., and Barkan, A. (2015). Genome-wide analysis of thylakoid-bound ribosomes in maize reveals principles of cotranslational targeting to the thylakoid membrane. *Proc. Natl. Acad. Sci. U.S.A.* 112, 1678–1687. doi: 10.1073/pnas.1424655112
- Zoschke, R., Watkins, K. P., Miranda, R. G., and Barkan, A. (2016). The PPR-SMR protein PPR53 enhances the stability and translation of specific chloroplast RNAs in maize. *Plant J.* 85, 594–606. doi: 10.1111/tpj.13093

Conflict of Interest: The authors declare that the research was conducted in the absence of any commercial or financial relationships that could be construed as a potential conflict of interest.

Publisher's Note: All claims expressed in this article are solely those of the authors and do not necessarily represent those of their affiliated organizations, or those of the publisher, the editors and the reviewers. Any product that may be evaluated in this article, or claim that may be made by its manufacturer, is not guaranteed or endorsed by the publisher.

Copyright © 2021 Kong, Wu, Wang, Qu, Lan, Chen, Liu, Shahnaz, Yang, Yu and Mi. This is an open-access article distributed under the terms of the Creative Commons Attribution License (CC BY). The use, distribution or reproduction in other forums is permitted, provided the original author(s) and the copyright owner(s) are credited and that the original publication in this journal is cited, in accordance with accepted academic practice. No use, distribution or reproduction is permitted which does not comply with these terms.



Molecular Characterization of Mg-Chelatase CHL Subunit in Pea (*Pisum sativum* L.)

Cai-jun Wu^{††}, Jie Wang^{††}, Jun Zhu¹, Jing Ren¹, You-xin Yang¹, Tao Luo², Lu-xi Xu¹, Qing-hong Zhou¹, Xu-feng Xiao¹, Yu-xin Zhou¹ and Sha Luo^{1*}

¹ Department of Horticulture, College of Agronomy, Jiangxi Agricultural University, Nanchang, China, ² Institute of Life Science and School of Life Sciences, Nanchang University, Nanchang, China

OPEN ACCESS

Edited by:

Alistair McCormick,
University of Edinburgh,
United Kingdom

Reviewed by:

Yan Lu,
Western Michigan University,
United States
Robert Drant Willows,
Macquarie University, Australia

*Correspondence:

Sha Luo
luosha@jxau.edu.cn

^{††} These authors have contributed
equally to this work

Specialty section:

This article was submitted to
Plant Physiology,
a section of the journal
Frontiers in Plant Science

Received: 24 November 2021

Accepted: 03 January 2022

Published: 25 January 2022

Citation:

Wu C-j, Wang J, Zhu J, Ren J,
Yang Y-x, Luo T, Xu L-x, Zhou Q-h,
Xiao X-f, Zhou Y-x and Luo S (2022)
Molecular Characterization
of Mg-Chelatase CHL Subunit in Pea
(*Pisum sativum* L.).
Front. Plant Sci. 13:821683.
doi: 10.3389/fpls.2022.821683

As a rate-limiting enzyme for chlorophyll biosynthesis, Mg-chelatase is a promising target for improving photosynthetic efficiency. It consists of CHLH, CHLD, and CHL subunits. In pea (*Pisum sativum* L.), two putative CHL genes (*PsCHL1* and *PsCHL2*) were revealed recently by the whole genome sequencing, but their molecular features are not fully characterized. In this study, *PsCHL1* and *PsCHL2* cDNAs were identified by PCR-based cloning and sequencing. Phylogenetic analysis showed that *PsCHL*s were derived from an ancient duplication in legumes. Both *PsCHL*s were more highly expressed in leaves than in other organs and downregulated by abscisic acid and heat treatments, while *PsCHL1* was more highly expressed than *PsCHL2*. *PsCHL1* and *PsCHL2* encode 422- and 417-amino acid proteins, respectively, which shared 82% amino acid identity and were located in chloroplasts. Plants with a silenced *PsCHL1* closely resembled *PsCHL1* and *PsCHL2* double-silenced plants, as both exhibited yellow leaves with barely detectable Mg-chelatase activity and chlorophyll content. Furthermore, plants with a silenced *PsCHL2* showed no obvious phenotype. In addition, the N-terminal fragment of *PsCHL1* (*PsCHL1N*, Val63-Cys191) and the middle fragment of *PsCHL1* (*PsCHL1M*, Gly192-Ser336) mediated the formation of homodimers and the interaction with CHLD, respectively, while active *PsCHL1* was only achieved by combining *PsCHL1N*, *PsCHL1M*, and the C-terminal fragment of *PsCHL1* (Ser337-Ser422). Taken together, *PsCHL1* is the key CHL subunit, and its peptide fragments are essential for maintaining Mg-chelatase activity, which can be used to improve photosynthetic efficiency by manipulating Mg-chelatase in pea.

Keywords: chlorophyll synthesis, Mg-chelatase CHL subunit, photosynthesis, *Pisum sativum*, protein-protein interaction, virus-induced gene silencing

INTRODUCTION

Pea (*Pisum sativum* L.) is the second most important legume crop in the world and produces high protein feed for animal and human nutrition (Kreplak et al., 2019). It is also a valuable source of mineral nutrients, complex starch, several vitamins, antioxidants, and fiber, which are fairly low in calories and demonstrate health benefits (Guillon and Champ, 2003; Dahl et al., 2012; Tayade, 2019). The growth of the demand for peas accompanies with the increasing world population,

mainly in developing regions. To meet the growing need for peas, yield and quality must be improved at a higher rate than before by agricultural approaches.

There is a direct cause-effect relationship between crop production and photosynthesis (Moss and Musgrave, 1971), and many efforts have been made to achieve greater yield by improving photosynthetic efficiency (Zhu et al., 2010; Long et al., 2015). Various factors can affect photosynthetic efficiency, and chlorophyll content is essential (Croce and van Amerongen, 2014). The chlorophyll biosynthesis pathway is the Mg^{2+} branch of the tetrapyrrole biosynthetic pathway, which is catalyzed by a heterotrimeric enzyme, Mg-chelatase, composed of CHLI (36–46 kDa), CHLD (60–87 kDa), and CHLH (120–155 kDa) subunits (Masuda, 2008). The catalytic properties of plant Mg-chelatase were first revealed in pea (Walker and Weinstein, 1994; Guo et al., 1998). The enzymatic reaction includes at least two steps, an activation step, and an insertion step, which requires the hydrolysis of ATP. The CHLI subunit is the main subunit responsible for the hydrolysis of ATP in the process of enzymatic reactions (Jensen et al., 1999; Reid et al., 2003) and is essential for maintaining the CHLI-CHLD-Mg-ATP complex (Lake et al., 2004; Luo et al., 2013). It is the only reported subunit modulated by redox regulation *via* the chloroplast thioredoxin system (Ikegami et al., 2007; Luo et al., 2012; Perez-Ruiz et al., 2014). In addition, it is also involved in chloroplast reactive oxygen species homeostasis and Ca^{2+} signaling in pea (Luo et al., 2016). As a key regulatory point of chlorophyll biosynthesis, the CHLI subunit might be the primary target to engineer at a molecular level. The CHLI subunit belongs to the ATPase associated with various cellular activities (AAA+) superfamily^{13,14}. It possesses characteristic motifs involved in ATP binding such as Walker A and B (W-A and W-B) motifs, sensors 1 and 2 (S-1 and S-2) motifs, presensor I and II (PS-I and II) insert, and arginine finger (ARG-finger) motif (Reid et al., 2003; Lake et al., 2004). It is reported that the mutations in PS-II insert and S-2 motif as well as the mutations between the S-1 motif and the ARG-finger motif could abolish the function of Mg-chelatase in plant (Zhang et al., 2006; Campbell et al., 2014; Gao et al., 2016; Du et al., 2018; Mao et al., 2018). However, the peptide fragments of the CHLI responsible for protein-protein interaction and ATPase activity are unclear.

Interestingly, sequence data in the National Center for Biotechnology Information (NCBI) database¹ revealed that there is more than one *CHLI* gene in the genomes of most dicots and some algae (Rissler et al., 2002; Huang and Li, 2009; Brzezowski et al., 2016; Sawicki et al., 2017; Zhang et al., 2018). However, the functions of different *CHLI* genes have been only studied in *Chlamydomonas reinhardtii* and *Arabidopsis thaliana*, and conflicting results have been reported (Rissler et al., 2002; Apchelimov et al., 2007; Kobayashi et al., 2008; Huang and Li, 2009; Brzezowski et al., 2016; Sawicki et al., 2017). Rissler et al. (2002) reported that *Arabidopsis* AtCHLI2 supports only limited chlorophyll synthesis and Apchelimov et al. (2007) proposed that AtCHLI2 is not functional in the Mg-chelatase complex, while Kobayashi et al. (2008) revealed that AtCHLI2 contributes

to the assembly of the Mg-chelatase complex and Huang et al. showed that AtCHLI2 can substitute for AtCHLI1 (Huang and Li, 2009). In *C. reinhardtii*, Brzezowski et al. (2016) found that CrCHLI2 cannot substitute for CrCHLI1, but Sawicki et al. (2017) demonstrated that CrCHLI2 stimulates Mg-chelatase activity in chlorophyll synthesis. In our previous study, the whole genome data of pea were not available at that time, thus, *CHLI* was silenced in pea by virus-induced gene silencing (VIGS) using a partial *CHLI* sequence obtained by a homology-based cloning method, demonstrating the essential role of pea CHLI in Mg-chelatase activity and chlorophyll biosynthesis (Luo et al., 2013). By searching the pea genome-wide database released in 2019² (Kreplak et al., 2019), the sequence used for silencing pea *CHLI* in our previous study (Luo et al., 2013) matched two different genes (Psat1g200160 and Psat7g118680), suggesting that there are two *CHLI* genes in pea and both of them were silenced in our previous study (Luo et al., 2013). To further explore whether these two genes encoded CHLI subunits and what roles they played in chlorophyll biosynthesis, the present study characterized them at transcriptional and protein levels and identified the peptide fragments of CHLI responsible for protein-protein interactions and enzyme activity, which may provide the primary targets to improve photosynthetic efficiency in pea.

MATERIALS AND METHODS

Plant Material and Growth Conditions

Pea (*P. sativum* ‘Torsdag’; JI992) seeds were cleaned and soaked in tap water for 24 h and germinated on moist filter paper in the dark for 2 days before being planted in soil. Plants were grown in growth chambers (22°C, 65% relative humidity, 250 $\mu\text{mol m}^{-2} \text{s}^{-1}$, 16/8 h light/dark photoperiod).

Cloning of PsCHLI cDNA Sequences

A $\lambda\text{gt}11$ cDNA library, representing the leaf mRNA of a 7-day-old pea (Clontech Laboratories, Inc., Mountain View, CA, United States), was screened using polymerase chain reaction (PCR) as previously described (Alfandari and Darribère, 1994), with primers (Ls-PsCHLI-F/R, **Supplementary Table 1**) designed according to the conserved sequence of the *CHLI* genes in the legume family. The inserted fragments in the PCR-positive clones were characterized by DNA sequencing with the $\lambda\text{gt}11$ insertion checking primers (ICP-F/R, **Supplementary Table 1**) and were screened by the Basic Local Alignment Search Tool³ to confirm whether the clones contained *PsCHLIs*. The positive clones containing *PsCHLIs* were assembled by sequence similarity to obtain the longest sequences for *PsCHLIs*, which were finally verified by reverse transcription-PCR (RT-PCR) from JI992 leaf tissues and DNA sequencing with checking and sequencing primers for *PsCHLIs* (PsCHLI1-F/R and PsCHLI2-F/R, **Supplementary Table 1**).

¹<http://www.ncbi.nlm.nih.gov/genbank>

²<https://urgi.versailles.inra.fr/blast/>

³<https://blast.ncbi.nlm.nih.gov/>

Phylogenetic Analysis

Amino acid sequences of the Mg-chelatase CHLI subunit homologs were obtained from the NCBI database (see text footnote 1), aligned using ClustalX software v2.1,⁴ and refined using GeneDoc software v2.7.⁵ A neighbor-joining (NJ) tree was constructed based on 1,000 bootstrap replications using MEGA 6.0.⁶

Promoter Analysis

The 1,500 bp region upstream of the translation start codon ATG of *PsCHLI1* and *PsCHLI2* was obtained from *P. sativum* v1a banks and the 1,500 bp region upstream of the translation start codon ATG of Arabidopsis *AtCHLI1* and *AtCHLI2* was obtained from NCBI database. The sequences were analyzed to study the regulatory elements in the promoter regions of each gene using the online program PlantCARE⁷ (Lescot et al., 2002). Since the CAAT box is a proximal promoter element, the predicted CAAT boxes were counted in the 400 bp region upstream of the genes.

Gene Expression Analysis

For examination of the expression of *PsCHLI1* and *PsCHLI2* in different organs, RNA was extracted from organs at different developmental stages. The roots, leaves, and stems were harvested from 1-week-old seedlings. The flowers were sampled from flowering plants (45 days old). Young pods (3–4 cm long) and immature seeds were sampled from 60-day-old plants. Each organ sample was collected from at least four plants and mixed for RNA isolation. Three biological replicates were performed.

Sterilized pea seeds were germinated on moist filter paper in the dark for 2 days and then transferred into growth chambers (22°C, 65% relative humidity, 250 $\mu\text{mol m}^{-2} \text{s}^{-1}$, 16/8 h light (8:00–24:00)/dark photoperiod) for 7 days. Then, the leaves were collected from the seedlings at different time points [8:00 (light on), 12:00, 16:00, 20:00, 24:00 (light off), 4:00] to examine the expression of *PsCHLI1* and *PsCHLI2* under the diurnal changes. For each time point, leaves from at least four plants were collected and mixed for RNA isolation at once, and three biological replicates were performed. For sample collection during dark hours, samples were immediately collected without exposure to light.

Pea seedlings were grown in the dark for 7 days and illuminated for 2, 4, 8, 16, and 24 h. For each irradiation time, leaves from at least four plants were collected and mixed for RNA isolation at once, and three biological replicates were performed. RNA was extracted for examining the expression of *PsCHLI1* and *PsCHLI2* in response to light.

To examine the expression of *PsCHLI1* and *PsCHLI2* following hormone and stress treatments, sterilized pea seeds were germinated on moist filter paper in the dark for 2 days and then transferred into growth chambers (22°C, 65% relative humidity, 250 $\mu\text{mol m}^{-2} \text{s}^{-1}$, 16/8 h light/dark photoperiod) for 7 days. The seedlings were then transferred into ABA (0.1 mM), NaCl

(300 mM), and PEG6000 (20%, w/v) solutions for 24 h at 22°C. For heat treatment, the seedlings were grown in water for 24 h at 37°C. Seedlings grown in water at 22°C were used as a control. For each treatment, leaves from at least four plants were collected and mixed for RNA isolation at once, and three biological replicates were performed.

Furthermore, RNA was extracted from the top and premature leaves of VIGS plants at 14 days after infiltration (dpi) at 12:00.

The total RNA was extracted from 20 to 40 mg of samples using TRIzol® Reagent (Thermo Fisher Scientific, Waltham, MA, United States) according to the manufacturer's instructions. Quantitative real-time (qPCR) was performed as previously described (Luo et al., 2013). The primers used in the qPCR amplification are described in **Supplementary Table 1**. The $2^{-\Delta\Delta C_t}$ method was used to calculate relative expression. The transcript levels were quantitatively normalized to the transcript level of pea *EF-1 α* (GenBank: X96555), which encodes the elongation factor 1- α .

The transcriptional level between *PsCHLI1* and *PsCHLI2* was also compared by RNA-seq using pea leaves. Each leaf sample was collected from at least four 1-week-old plants and mixed for RNA isolation at once. Three biological replicates were performed. For each biological replicate, 1 μg leaf total RNA was used to generate sequencing libraries by NEBNext® Ultra™ II RNA Library Prep Kit for Illumina® (New England Biolabs Inc., Ipswich, MA, United States) following the manufacturer's recommendations. The library preparations were sequenced on an Illumina platform, and paired-end reads were generated. The raw reads were further processed with an online bioinformatic pipeline tool, BMKCloud.⁸ Raw data (raw reads) in the fastq format was first processed through in-house perl scripts and then adapter, ploy-N, and low-quality reads were removed to obtain clean data (clean reads). The clean reads were then mapped to the pea genome sequence using HISAT2 v2.2.1 software⁹ (Kim et al., 2019). Only reads with a perfect match or one mismatch were further analyzed and annotated based on the pea genome. Gene expression levels were estimated by fragments per kilobase of transcript per million fragments mapped.

Subcellular Localization

The coding sequences of *PsCHLI1* and *PsCHLI2* were synthesized through DNA synthesis (Genscript Biotech Corporation, Nanjing, China) and cloned into the pM999 vector (C-terminal fused YFP). The resulting plasmids (pM999-*PsCHLI1* and pM999-*PsCHLI2*) and pM999 empty vector were transformed into pea protoplasts according to our previously reported method (Luo et al., 2018). The transformed pea protoplasts were incubated in the dark for 24 h, and images were captured with a laser confocal microscope (TCS SP2; Leica).

Virus-Induced Gene Silencing Assay

The 1–184 bp and 1,358–1,504 bp *PsCHLI1* cDNA and the 1–99 bp and 1,297–1,577 bp *PsCHLI2* cDNA sequences were synthesized through DNA synthesis (Genscript Biotech

⁴<https://clustalx.software.informer.com/2.1>

⁵<https://genedoc.software.informer.com>

⁶<https://www.megasoftware.net/>

⁷<https://bioinformatics.psb.ugent.be/webtools/plantcare/html/>

⁸www.biocloud.net

⁹<https://daehwankimlab.github.io/hisat2/download/>

Corporation) and inserted into a VIGS vector, pCAPE2, resulting in the plasmids: pCAPE2-PsCHLI1 and pCAPE2-PsCHLI2 (Supplementary Figure 1). The VIGS assay was performed as follows: the pCAPE1 plasmid was co-inoculated with pCAPE2-PsCHLI1, pCAPE2-PsCHLI2, the previously constructed pCAPE2-PsCHLI (Luo et al., 2013), and pCAPE2-GFP (negative control) (Luo et al., 2013) into *P. sativum* (cv. Torsdag; J1992) plants through *Agrobacterium* infiltration. The infected plants were grown in growth chambers (22°C, 65% relative humidity, 250 $\mu\text{mol m}^{-2} \text{s}^{-1}$, 16/8 h light/dark photoperiod).

Determination of Chlorophyll Content

The total chlorophyll (chlorophyll, a + b) was extracted with 100% acetone, and the concentration was determined spectrophotometrically according to our previous study (Luo et al., 2016).

Construction of the Plasmids for Y2H Assay, Glutathione S Transferase Pull-Down Assay, and Prokaryotic Expression

The cDNA fragments encoding PsCHLI1N, PsCHLI1M, PsCHLI1C, PsCHLI1N plus PsCHLI1M (PsCHLI1NM), PsCHLI1M plus PsCHLI1C (PsCHLI1MC), and PsCHLI1N plus PsCHLI1M plus PsCHLI1C (PsCHLI1NMC), as well as PsCHLI2, and the PsCHLD subunit minus the cTPs, were generated through RT-PCR using the primers described in Supplementary Table 1. The cDNA fragments were then inserted into the prey vector, pGADT7, bait vector, pGBKT7, and prokaryotic expression vectors, pGEX6P-1 (GST tag) and pET-28a (6 \times histidine tag, His tag), without disturbing the open reading frame, resulting in the following plasmids: pGADT7-PsCHLI1N, pGADT7-PsCHLI1M, pGADT7-PsCHLI1C, pGADT7-PsCHLI1NM, pGADT7-PsCHLI1MC, pGADT7-PsCHLI1NMC, pGADT7-PsCHLI2, pGEX6P-1-PsCHLI1N, pGEX6P-1-PsCHLI1M, pGEX6P-1-PsCHLI1C, pGEX6P-1-PsCHLI1NM, pGEX6P-1-PsCHLI1MC, pGEX6P-1-PsCHLI1NMC, pGBKT7-PsCHLI1NMC, pGBKT7-PsCHLI2, pET-28a-PsCHLI1NMC, pET-28a-PsCHLI2, pGBKT7-PsCHLD, and pET-28a-PsCHLD.

Y2H Assay

Saccharomyces cerevisiae strain AH109 was co-transformed with both bait and prey plasmids using the lithium acetate method according to the manufacturer's protocol (Clontech, protocol PT3247-1). The transformants were first selected on Synthetic Dropout (SD/-Leu/-Trp) and scraped onto high-stringency quadruple-dropout media (SD/-Leu/-Trp/-His/-Ade) supplemented with 40 mg/L X-a-Gal to screen the interactions.

Glutathione S Transferase Pull-Down Assay

Escherichia coli strain BL21 was co-transformed with both GST-tagged and His-tagged prokaryotic expression plasmids by electroporation. The expression of recombinant proteins was performed according to our previously published paper (Luo

et al., 2018). The GST tag fused proteins and their interacting proteins in the cell lysates were pulled down by glutathione agarose (Thermo Fisher Scientific, Waltham, MA, United States), and detected by western blot using an anti-His tag antibody (Abcam PLC, Cambridge, MA, United States) and an anti-CHLD antibody (Luo et al., 2013).

Measurement of ATPase and Mg-Chelatase Activity

The expression of GST-tagged prokaryotic expression plasmids was performed as described previously (Luo et al., 2018). The recombinant proteins were purified using glutathione agarose (Thermo Fisher Scientific), and the GST tag was removed by PreScission Protease (Thermo Fisher Scientific) according to the user manual. The ATPase activity of recombinant PsCHLI1N, PsCHLI1M, PsCHLI1C, PsCHLI1NM, PsCHLI1MC, and PsCHLI1NMC was measured as previously described (Luo et al., 2012). The activity of Mg-chelatase reconstituted by the different domains of the pea CHLI subunit and the recombinant rice CHLD, CHLH, and GUN4 proteins, expressed and purified using the previously published plasmids (Zhou et al., 2012), was performed as previously described (Luo et al., 2018). Mg-chelatase activity in the VIGS plants was determined by a stopped fluorometric assay as described by Guo et al. (1998).

Statistical Analyses

Data are expressed as the means \pm S.E.M. The differences between the controls and samples were assessed with one-way analysis of variance and the Dunnett's test. Statistically significant differences were determined at $P < 0.05$ by the statistical software GraphPad Prism (version 5.01).

RESULTS

Two CHLI Subunits Were Identified in Pea

cDNA encoding the CHLI subunit was identified by PCR-based screening of the pea leaf *λgt11* cDNA library with primers designed according to the conserved sequence of the CHLI coding sequence in the legume family. Two different cDNAs were identified and verified by reverse transcription-polymerase chain reaction from J1992 leaf tissues and DNA sequencing. The 1,513-bp cDNA was named *PsCHLI1* (GenBank: JN198382), which contained a 104-bp-long 5'-untranslated region, 140-bp-long 3'-untranslated region, and 1,269-bp-long coding sequence. The 1,577-bp cDNA was named *PsCHLI2* (GenBank: MN128704), containing a 41-bp-long 5'-untranslated region, 282-bp-long 3'-untranslated region, and a 1,254-bp-long coding sequence.

After searching the pea genome-wide database (see text footnote 2) for *PsCHLI1* and *PsCHLI2* cDNA, the *PsCHLI1* and *PsCHLI2* genes were found to be located on chromosomes 1 (Psat1g200160.1, chr1LG6: 350733206-350736270) and 7 (Psat7g118680.1, chr7LG7: 195953907-195956035), respectively (Supplementary Figure 2). Both *PsCHLI* genes contained three

exons and two introns and same lengths of exon 2 and the coding sequence in exon 3 (**Supplementary Figure 2**). *PsCHLI1* had longer introns and five-prime (5') and three-prime (3') untranslated regions than *PsCHLI2* (**Supplementary Figure 2**).

Both *PsCHLI1* and *PsCHLI2* encode ~46 kDa polypeptides with 422 and 417 amino acid residues (aa), respectively, which are similar in molecular mass to their corresponding homologs identified in other plant species (**Supplementary Figure 3**). *PsCHLI1* and *PsCHLI2* are highly similar, sharing 82% amino acid identity (**Supplementary Figure 3**). Alignment of the *PsCHLI*s to their orthologs from different species showed that the numbering of secondary structure elements in *PsCHLI*s follows the convention for AAA + proteins containing Walker A and B motifs (W-A and W-B). W-A, W-B, presensor I (PS-I) insert, helix2 insert (H2-insert), arginine finger (ARG-finger), and sensors 1 and 2 (S-1 and S-2) were conserved in *PsCHLI1* and *PsCHLI2* (**Supplementary Figure 3**).

PsCHLI1 and PsCHLI2 Were Derived From an Ancient Duplication in Legumes

Using the neighbor-joining (NJ) method, a bootstrap consensus tree was constructed on the basis of 33 aligned CHLI amino acid sequences from 19 higher plant species, comprising 14 dicotyledons (*P. sativum*, *Glycine max*, *Phaseolus vulgaris*, *Vigna radiata*, *Cajanus cajan*, *Medicago truncatula*, *Cicer arietinum*, *Arachis hypogaea*, *Lotus japonicus*, *Ricinus communis*, *Gossypium arboreum*, *Vitis vinifera*, *Populus trichocarpa*, and *A. thaliana*) and 5 monocotyledons (*Hordeum vulgare*, *Brachypodium distachyon*, *Oryza sativa*, *Z. mays*, and *Sorghum bicolor*) to investigate the evolution history of the plant CHLI subunit. The sequences of *CHLI*s were clustered into dicot and monocot clades and subsequently diverged by family (**Figure 1**). The legume CHLI homologs were sub-grouped into two clades. One clade contains *A. hypogaea* which encodes two recently duplicated *CHLI*s (**Figure 1**). Another clade contains *P. sativum*, *Glycine max*, *Phaseolus vulgaris*, *Vigna radiata*, *Cajanus cajan*, *Medicago truncatula*, *Cicer arietinum*, and *Lotus japonicus* (**Figure 1**). Interestingly, the same species in this clade were divided into two subclades except *L. japonicus* that encodes only one CHLI (**Figure 1**), indicating that *CHLI*s in *P. sativum*, *Glycine max*, *Phaseolus vulgaris*, *Vigna radiata*, *Cajanus cajan*, *Medicago truncatula*, and *Cicer arietinum* were derived from an ancient duplication and maintenance of the duplicated genes. In addition, *CHLI*s in *Glycine max* and *Medicago truncatula* apparently experienced the recent duplications (**Figure 1**).

Regulatory Elements in the Promoter Regions of PsCHLI1 and PsCHLI2

More regulatory elements in promoter regions were predicted in the upstream region of *PsCHLI1* compared with that of *PsCHLI2* (54 vs. 29, **Supplementary Table 2**), especially for the CAAT box (13 vs. 2, **Supplementary Table 2**). Among *cis*-acting regulatory motifs, 12 and 7 light responsive elements, 21 and 10 hormone responsive elements, and 8 and 10 stress responsive elements were predicted in the promoter regions of *PsCHLI1* and *PsCHLI2*, respectively (**Supplementary Table 2**).

PsCHLI1 and PsCHLI2 Show Different Expression Profiles

To study the role of *PsCHLI*s in chlorophyll biosynthesis, the expression profiles of their encoding genes were examined through qPCR. The amplification efficiencies of the primers for *PsCHLI1*, *PsCHLI2*, and *EF-1 α* (reference gene) were 105.62, 107.77, and 99.52%, respectively (**Supplementary Figure 4**), indicating that the primers were effective for qPCR. The transcription level of *PsCHLI1* and *PsCHLI2* was investigated in roots, stems, leaves, flowers, pods, and immature seeds. The results revealed that *PsCHLI1* was most highly expressed in leaves but at a low level in stems, flowers, and pods, and an almost negligible level in roots and immature seeds (**Figure 2A**). The expression level of *PsCHLI2* was about twofold higher in leaves than in other organs (**Figure 2B**).

Since the amplification efficiencies of the primers for *PsCHLI1* and *PsCHLI2* were quite similar (**Supplementary Figure 4**), the expression level of *PsCHLI1* and *PsCHLI2* were compared by qPCR. *PsCHLI1* was more highly expressed than *PsCHLI2* in leaves (61.81 vs. 1.00, **Figure 2C**). This was confirmed by RNA sequencing (RNA-seq) using pea leaves (**Figure 2D** and **Supplementary Table 3**).

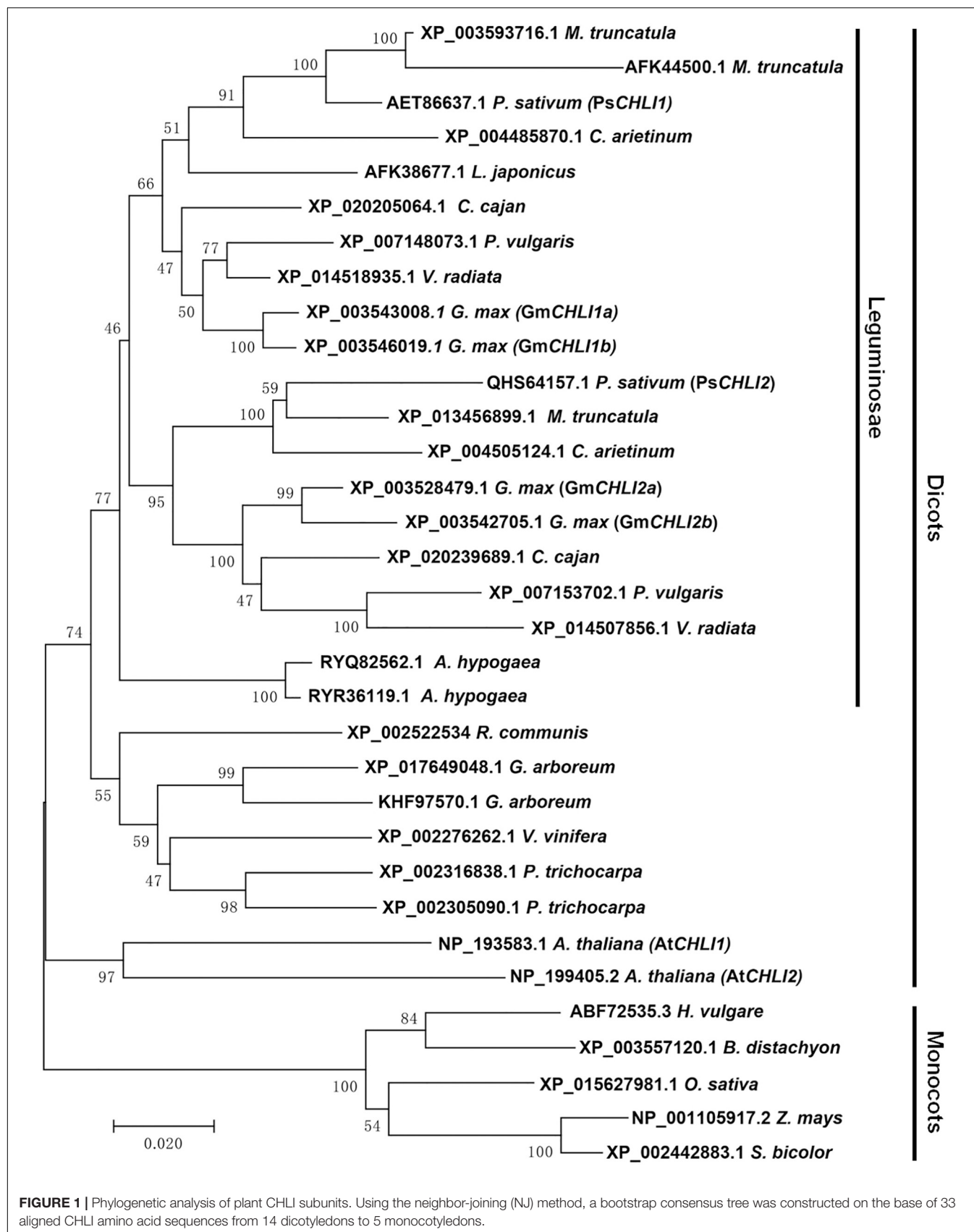
In addition, the transcription level of *PsCHLI1* showed diurnal changes (**Figures 2E,F**). When the light was on at 8:00, *PsCHLI1* was expressed at the lowest level and then its transcripts reached the highest level at 12:00, decreased at 16:00, returned to an equivalent level as that of 8:00 at 20:00, and increased at 24:00 when the light was off (**Figure 2E**). Subsequently, *PsCHLI1* was downregulated at 4:00 and to the lowest level at 8:00 (**Figure 2E**). In contrast, expression of *PsCHLI2* was relatively steady in different time points (**Figure 2F**). The expression profiles of *PsCHLI1* and *PsCHLI2* responding to light were also examined. The results showed that the expression of *PsCHLI1* was upregulated gradually from 4 to 24 h illumination (**Figure 2G**), while the expression of *PsCHLI2* was upregulated at 16 and 24 h illumination (**Figure 2H**).

We also examined the expression of *PsCHLI1* and *PsCHLI2* responding to abscisic acid (ABA) and abiotic stresses (heat, salt, and drought) by the qPCR. The results showed that *PsCHLI1* was significantly downregulated following ABA, heat, salt, and drought treatments ($P < 0.05$, **Figure 2I**) and *PsCHLI2* was only significantly downregulated following ABA and heat treatments ($P < 0.05$, **Figure 2J**).

PsCHLI1 and PsCHLI2 Are Both Located in Pea Chloroplasts

The putative chloroplast transit peptides (cTPs) were predicted at the N-terminus of *PsCHLI1* (1-62 aa) and *PsCHLI2* (1-34 aa) by ChloroP v1.1¹⁰ (**Supplementary Figure 3**). To confirm their subcellular localization, yellow fluorescent fusion proteins were generated by fusing yellow fluorescent protein (YFP) to the C terminus of full-length *PsCHLI1* and *PsCHLI2*. These fusion proteins and the YFP were transiently expressed in pea leaf protoplasts and observed by confocal laser scanning

¹⁰<http://www.cbs.dtu.dk/services/ChloroP/>



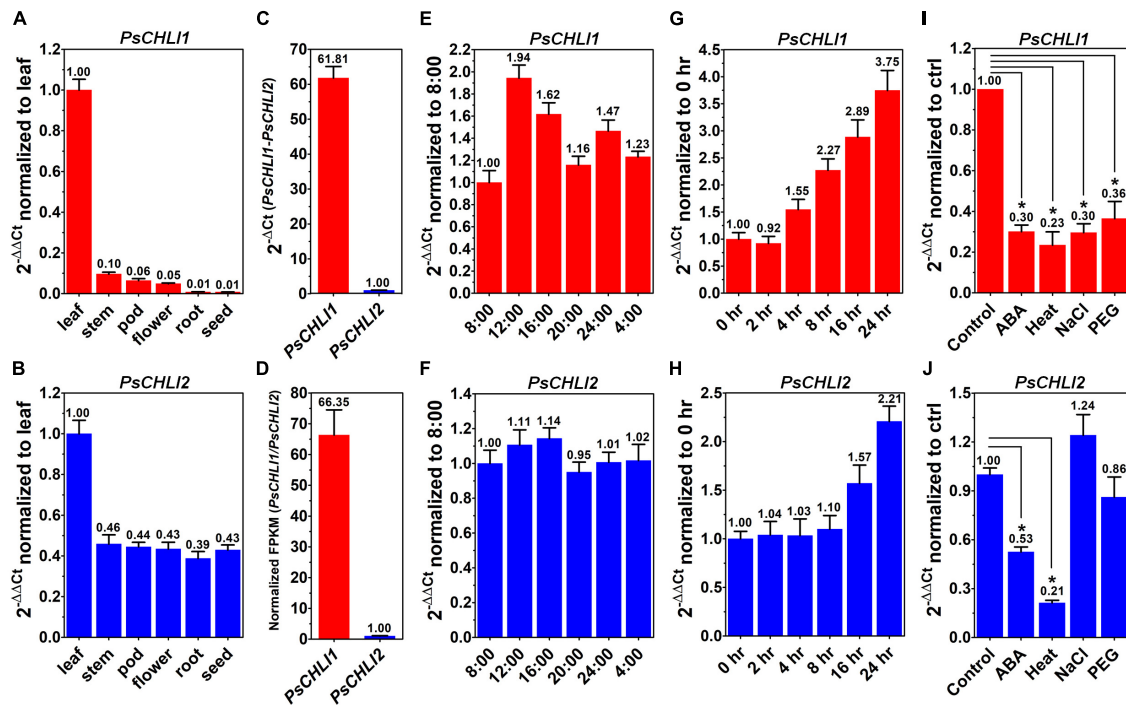


FIGURE 2 | Expression profiles of *PsCHLI1* and *PsCHLI2*. The expression of *PsCHLI1* and *PsCHLI2* in different organs (A,B), time points (E,F), irradiation times (G,H), abscisic acid (ABA, I,J), and abiotic stresses (heat, NaCl, and PEG6000, I,J) were examined by quantitative real-time PCR (qPCR). The expression level of *PsCHLI1* and *PsCHLI2* was compared by qPCR (C) and RNA sequencing (D). The $2^{-\Delta\Delta Ct}$ method was used to calculate the relative expression for qPCR. The transcript levels were quantitatively normalized to the transcript level of pea *EF-1 α* . Gene expression levels for RNA sequencing were estimated by fragments per kilobase of transcript per million fragments mapped (FPKM). Error bars indicate the standard error of the mean (SEM) from three biological replicates, * $P < 0.05$, one-way analysis of variance.

microscopy. The results showed that YFP fluorescence was only visualized in the chloroplasts of the protoplasts that transiently expressed YFP-fused *PsCHLI1* and *PsCHLI2* (Figure 3), indicating that *PsCHLI1* and *PsCHLI2* are both located in pea chloroplasts.

PsCHLI1, but Not PsCHLI2, Is Essential for Chlorophyll Biosynthesis in Pea

Although *PsCHLI1* and *PsCHLI2* have high sequence similarity and are both located in pea chloroplasts, their expression profiles suggest different roles for the *PsCHLIs* in chlorophyll biosynthesis. To study the roles of *PsCHLI1* and *PsCHLI2* in chlorophyll biosynthesis, the 5'- and 3'-end sequences of *PsCHLI1* and *PsCHLI2*, which have low identity, were selected as the targets for a VIGS assay to specifically silence *PsCHLI1* and *PsCHLI2* in pea (Supplementary Figure 1). As a control, the VIGS-GFP and VIGS-*PsCHLI* plants described in our previous study (Luo et al., 2013) were used (Figures 4A,B and Supplementary Figure 5). The phenotype of *PsCHLI1* silenced (VIGS-*PsCHLI1*) plants resembled VIGS-*PsCHLI* plants (in which both *PsCHLI1* and *PsCHLI2* were targeted for silencing), demonstrating three types of leaves, including fully yellow leaves (fy), yellow sectors from mosaic leaves (y/m), and green sectors from mosaic leaves (g/m) (Figures 4B,C

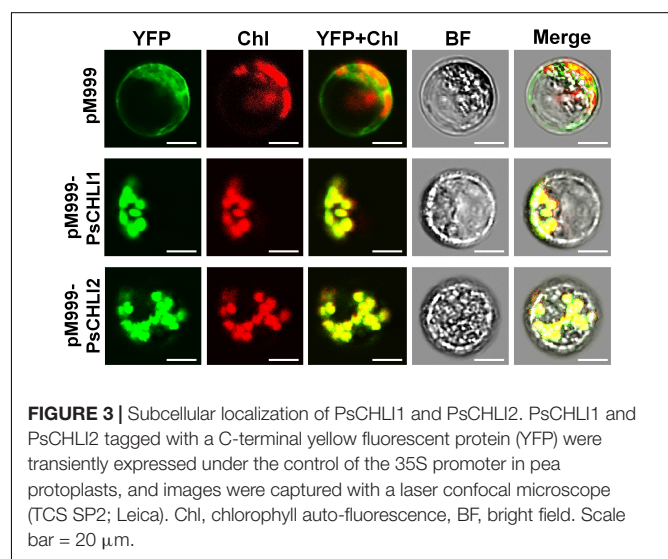


FIGURE 3 | Subcellular localization of *PsCHLI1* and *PsCHLI2*. *PsCHLI1* and *PsCHLI2* tagged with a C-terminal yellow fluorescent protein (YFP) were transiently expressed under the control of the 35S promoter in pea protoplasts, and images were captured with a laser confocal microscope (TCS SP2; Leica). Chl, chlorophyll auto-fluorescence, BF, bright field. Scale bar = 20 μ m.

and Supplementary Figure 5), while *PsCHLI2* silenced (VIGS-*PsCHLI2*) plants showed no phenotype compared with VIGS-GFP plants (Figure 4D and Supplementary Figure 5). *PsCHLI1* in VIGS-*PsCHLI1* plants and *PsCHLI2* in VIGS-*PsCHLI2* plants, as well as *PsCHLI1* and *PsCHLI2* in VIGS-*PsCHLI* plants, were

silenced by more than 90% (**Figure 4E**), while neither silencing *PsCHLI1* nor *PsCHLI2* changed the transcriptional level of the other *PsCHLI* homologs (**Figure 4E**). In addition, to examine the protein level of *PsCHLI1* and *PsCHLI2* in the VIGS plants, western blot was performed using a previously verified anti-Arabidopsis CHLI1 antibody (Luo et al., 2013). This antibody recognized both the recombinant *PsCHLI1* and *PsCHLI2* and overexpressed them in *E. coli* due to the high similarity in amino acids between *PsCHLI1* and *PsCHLI2* (**Supplementary Figure 6**). The target bands that showed equivalent intensity and matched the predicted molecular weight of *PsCHLI*s were detected in VIGS-GFP and VIGS-*PsCHLI2* plants (**Figure 4F**). In contrast, neither *PsCHLI1* nor *PsCHLI2* were detected in the leaves of both VIGS-*PsCHLI1* and VIGS-*PsCHLI* plants (**Figure 4F**). Furthermore, Mg-chelatase activity and chlorophyll content were hardly detectable in the yellow leaf of both VIGS-*PsCHLI* and VIGS-*PsCHLI1* plants, while they were not affected in green leaves of VIGS-*PsCHLI2* plants compared with VIGS-GFP control plants (**Figures 4G,H**). The development of flowers, pods, and seeds was not affected in either VIGS-*PsCHLI1* or VIGS-*PsCHLI2* plants, which was consistent with our reported phenotype for VIGS-*PsCHLI* plants (Luo et al., 2013). The yield of pods and seeds from the VIGS-*PsCHLI2* plant is equivalent to that in VIGS-GFP plants. However, both VIGS-*PsCHLI* and VIGS-*PsCHLI1* plants died earlier than VIGS-GFP plants, and thus fewer pods and seeds were harvested from both VIGS-*PsCHLI* and VIGS-*PsCHLI1* plants than VIGS-GFP plants.

The N-Terminal Fragment of *PsCHLI1* Mediates the Formation of *PsCHLI1* Dimers, and the Middle Fragment of *PsCHLI1* Is Involved in the Interaction With *PsCHLD*

Previous studies have demonstrated that the interactions between subunits are essential for maintaining Mg-chelatase activity (Masuda, 2008). The present study showed that *PsCHLI1* is the predominant CHLI subunit in pea leaves and is essential for chlorophyll biosynthesis in pea. Therefore, the role of *PsCHLI1* in subunit-subunit interactions was further explored. According to the structure-based alignment of the amino acid sequences of CHLI/BchI (**Supplementary Figure 3**), *PsCHLI1* (minus the chloroplast transit peptide) was characterized into three peptide fragments: the N-terminal fragment (*PsCHLI1N*, Val63 to Cys191), containing an ATP/GTP binding motif A (Walker A) and an α 1- β 2- β hairpin motif; the C-terminal fragment (*PsCHLI1C*, Ser337 to Ser422), possessing four α helices and the sensor 2 region (S2); and the middle fragment (*PsCHLI1M*, Gly192 to Ser336), linking *PsCHLI1N* and *PsCHLI1C*, which includes three insertions into the core AAA topology (H2-insert, PSI-insert and PSII insert), ATP/GTP binding motif B (Walker B), sensor 1 region (S1), and ARG-finger (**Figure 5A** and **Supplementary Figure 3**). A yeast two-hybrid (Y2H) assay was performed to explore the role of the above *PsCHLI1* fragments in mediating the interactions between *PsCHLI1* and *PsCHLI1* or *PsCHLD*. The results showed that *PsCHLI1N* interacted with *PsCHLI1* but

not *PsCHLD* (**Figure 5B**), while *PsCHLI1M* interacted with *PsCHLD* but not *PsCHLI1* (**Figure 5B**). Notably, if *PsCHLI1N* fused with *PsCHLI1M* (*PsCHLI1NM*), homodimerization and an interaction with *PsCHLD* were both observed (**Figure 5B**). However, *PsCHLI1C* did not interact with *PsCHLI1* or *PsCHLD* (**Figure 5B**). The interaction with *PsCHLD* was observed only when *PsCHLI1C* was fused with *PsCHLI1M* (*PsCHLI1MC*) (**Figure 5B**). Furthermore, a glutathione S transferase (GST) pull-down assay was performed to confirm the results of the Y2H assay. For this purpose, GST tag-fused *PsCHLI1* was co-expressed with His tag-fused *PsCHLI1* or *PsCHLD* in *E. coli* and pulled down by glutathione agarose. In the negative control, neither His-tagged *PsCHLI1* nor *PsCHLD* were pulled down by GST itself (**Figure 5C**). His-tagged *PsCHLI1* was pulled down by GST-tagged *PsCHLI1NMC*, *PsCHLI1N*, and *PsCHLI1NM* (**Figure 5C**), and the His-tagged *PsCHLD* interacted with GST-tagged *PsCHLI1NMC*, *PsCHLI1NM*, *PsCHLI1M*, and *PsCHLI1MC* (**Figure 5C**), consistent with the results from the Y2H assay. In addition, whether *PsCHLI2* can form homodimers and interact with *PsCHLI1* or *PsCHLD* were also examined by Y2H assay. The result showed that *PsCHLI2* can also form homodimer and interact with *PsCHLI1* and *PsCHLD* (**Supplementary Figure 7**).

All Three Peptide Fragments of *PsCHLI1* Are Essential for Maintaining the Enzyme Activity of *PsCHLI1*

To study the role of the three peptide fragments of *PsCHLI1* in maintaining the activities of ATPase and Mg-chelatase, the truncated *PsCHLI1* recombinant proteins were purified and expressed in *E. coli* (**Supplementary Figure 8**). Although *PsCHLI1N* mediated the formation of the homodimer of the CHLI subunit, it showed no significant ATPase or Mg-chelatase activity compared with the negative control (GST protein itself) ($P > 0.05$, **Figure 6**). Similar to *PsCHLI1N*, the action of *PsCHLI1M* in mediating the interaction between *PsCHLI1* and *PsCHLD* was not sufficient to maintain the activity of ATPase and Mg-chelatase (**Figure 6**). *PsCHLI1C* had no ATPase or Mg-chelatase activity since it did not interact with *PsCHLI1* and *PsCHLD* (**Figure 6**). *PsCHLI1NM* was also inactive, although this protein could interact with both *PsCHLI1* and *PsCHLD* (**Figure 6**). Only the combination of the three peptide fragments of *PsCHLI1* (*PsCHLI1NMC*) was essential for maintaining ATPase activity and reconstituting active Mg-chelatase *in vitro* (**Figure 6**).

DISCUSSION

Different Expression Level Between Duplicated *CHLI*s May Be Related to Their Divergent Gene Duplication Pattern

Phylogenetic analysis showed that duplicated *CHLI*s in dicots could be derived from an ancient gene duplication and/or a recent gene duplication (**Figure 1**). In pea, the duplicated *CHLI*s (*PsCHLI1* and *PsCHLI2*) originated from an ancient

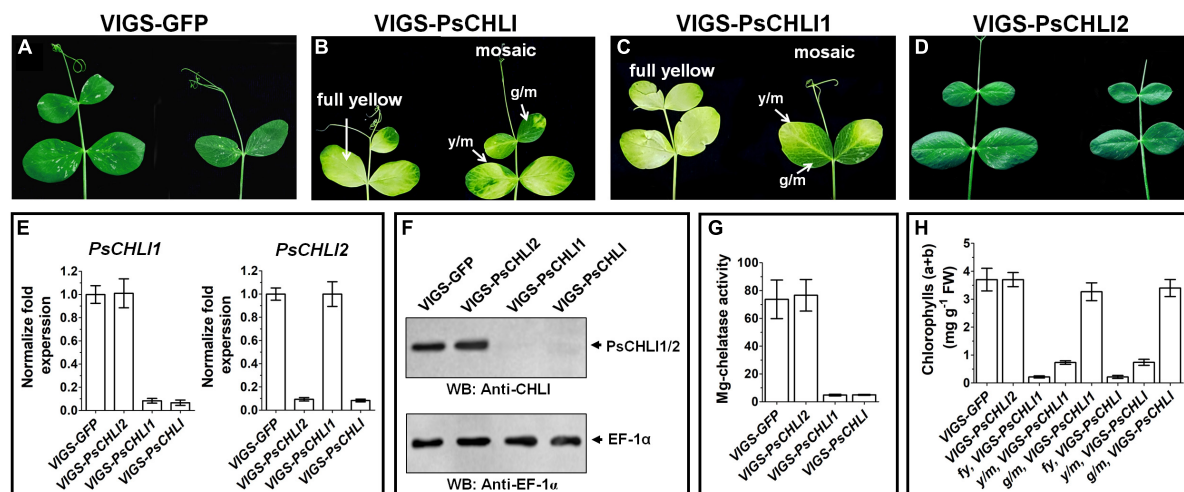


FIGURE 4 | Phenotypes of virus-induced gene silencing (VIGS) plants. *PsCHLI1* and *PsCHLI2* were silenced in pea by a VIGS method. VIGS-GFP plants represented a negative control for the effect of virus infection (A). VIGS-PsCHLI plants, described in our previous study (Luo et al., 2013), were used as a positive control (B). VIGS-PsCHLI1 plants showed yellow leaves. Three types of leaf phenotypes are shown: fully yellow leaves; y/m, yellow sectors from mosaic leaves; g/m, green sectors from mosaic leaves (C). Leaves of VIGS-PsCHLI2 plants resembled those in VIGS-GFP control plants (D). The expression of *PsCHLI1* and *PsCHLI2* in VIGS plants was measured by quantitative real-time PCR. The $2^{-\Delta\Delta Ct}$ method was used to calculate the relative expression. The transcript levels were quantitatively normalized to the transcript level of pea *EF-1 α* (E). The protein level of *PsCHLI1* and *PsCHLI2* in VIGS plants was measured by western blot. EF-1 α was used as a loading control (F). Mg-chelatase activity (G) and chlorophyll content (H) were also examined in VIGS plants. All plants had three independent infiltrations and were observed 3 weeks after infiltration. Error bars indicate the SEM from at least six VIGS plants in three independent infiltrations.

duplication (Figure 1) and they differ greatly in their expression level (Figure 2). In Arabidopsis, *AtCHLI1* and *AtCHLI2* were derived from a recent duplication (Figure 1) and *AtCHLI2* was not expressed much lower than *AtCHLI1* (Rissler et al., 2002; Huang and Li, 2009). In addition, the *CHLIs* in soybean experienced both ancient and recent gene duplications, resulting in four *CHLIs* (*GmCHLI1a*, *GmCHLI1b*, *GmCHLI2a*, and *GmCHLI2b*, Figure 1). The two *GmCHLI1* paralogs were more highly expressed than the two *GmCHLI2* paralogs, while there was no obvious difference in expression between *GmCHLI1a* and *GmCHLI1b* or between *GmCHLI2a* and *GmCHLI2b* (Li et al., 2016). These results suggested that the *CHLI* paralogs derived from the ancient gene duplication differ greatly in their expression level, while the expression level of *CHLI* paralogs derived from the recent gene duplication shows no obvious difference. A recent study in soybean indicated that the number of the CAAT box (important for the sufficient transcription of the downstream gene) in proximal promoter of *CHLI* paralogs is positively correlated with their transcription levels (Zhang et al., 2018). This phenomenon is also present in pea and Arabidopsis (Supplementary Table 2). These results implied that the changes of promoter regions in *CHLI* duplicated pairs may affect their expression levels during evolution.

Only One Copy of Duplicated *PsCHLIs* Acts as Mg-Chelatase CHLI Subunit Due to Non-functionalization at the Expression Level in Pea

Duplicate gene pairs may experience a potential fate that loss-of-function mutations in the coding region and/or the

destruction in the regulatory regions of one duplicate led to non-functionalization by losing gene function and/or gene expression (Force et al., 1999). The present study found that *PsCHLI1* was more highly expressed than *PsCHLI2* at both transcriptional and protein levels, suggesting that adequate *PsCHLI1* but few *PsCHLI2* proteins were present in pea leaves. Although *PsCHLI2* could form a homodimer and interacted with *PsCHLI1* and *PsCHLD* and had similar ATPase and reconstituted Mg-chelatase activities to *PsCHLI1* *in vitro* (Supplementary Figure 7), the low expression of *PsCHLI2* resulted in few proteins in pea leaves and silencing *PsCHLI2* in pea did not affect leaf Mg-chelatase activity. In addition, pea plants with a silenced *PsCHLI1* had undetectable Mg-chelatase activity in leaves. These results suggested that *PsCHLI2* probably experienced non-functionalization at the expression level and only *PsCHLI1* acted as the key CHLI subunit of Mg-chelatase in pea leaves. Previous studies in Arabidopsis and soybean demonstrated that two copies of duplicated pair of *CHLI* derived from a recent gene duplication showed no or slightly obvious difference at the expression level and participated in chlorophyll synthesis (Huang and Li, 2009; Zhang et al., 2018). In this study, our findings provided a new information about the divergence of *CHLIs* in plants apart from the results in Arabidopsis and soybean. To our knowledge, it is the first to investigate the function of a duplicated pair of *CHLI* originating from an ancient gene duplication.

Roles of *PsCHLI1* Motifs in Mg-Chelatase

CHLI is essential for both activation and insertion steps in the enzymatic reaction of Mg-chelatase (Masuda, 2008). In the

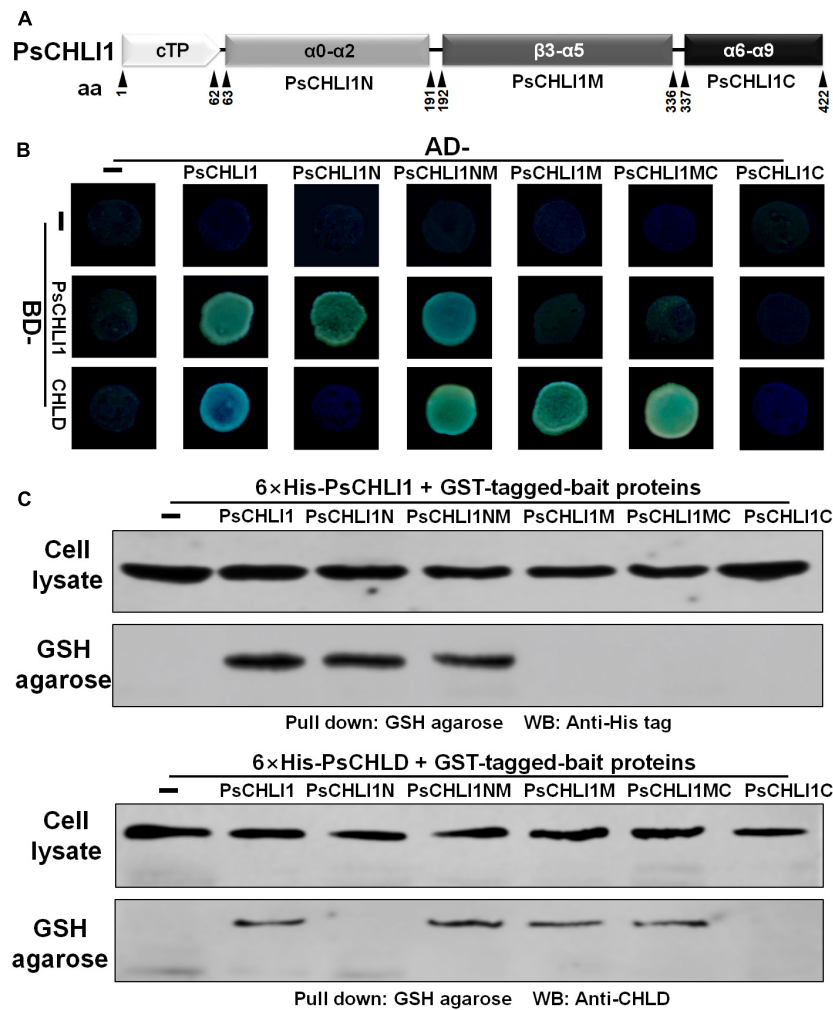


FIGURE 5 | Peptide fragments of PsCHLI1 for protein-protein interactions. **(A)** Four peptide fragments of PsCHLI1. The amino acid positions (aa) are indicated below the elements. Secondary structure elements in the different peptide fragments are shown in the boxes. α , α -helices; β , β -sheets. The interactions between PsCHLI1 or PsCHLD and the different fragments of PsCHLI1 were determined by the yeast two-hybrid assay **(B)** and glutathione S transferase (GST) pull-down assay **(C)**. cTP, chloroplast transit peptide; PsCHLI1N, the N-terminal fragment of PsCHLI1; PsCHLI1M, the middle fragment of PsCHLI1; PsCHLI1C, the C-terminal fragment of PsCHLI1; PsCHLI1NM, PsCHLI1N fused with PsCHLI1M; PsCHLI1MC, PsCHLI1M fused with PsCHLI1C; GSH, glutathione.

activation step, six CHLIs are assembled into a hexameric ring structure and interact with the hexameric ring of CHLD to form a CHLIs-CHLDs-Mg-ATP complex for the insertion step, in which CHLI hydrolyzes ATP to provide energy (Lake et al., 2004; Masuda, 2008; Luo et al., 2013). In this study, the PsCHLI2 protein was undetectable in pea leaves by western blot and silencing *PsCHLI2* in pea plants did not affect the Mg-chelatase activity and the chlorophyll content. These results indicated PsCHLI2 is not functional in the Mg-chelatase complex. It is proposed that only PsCHLI1 participates in the assembly of the hexameric CHLI ring structure and interacting with PsCHLD in pea leaves. Therefore, the peptide fragments of the PsCHLI1 responsible for protein-protein interaction and enzyme activity were characterized. The present study found that AAA modules were conserved in PsCHLI1. The Walker A motif in the PsCHLI1N was responsible for CHLI dimerization that is

important for the assemble of the ring structure. Three PsCHLI1 homodimers form a hexameric ring structure. The Walker B and sensor 1 motifs in the PsCHLI1M were involved in the interaction between CHLI and CHLD. Although PsCHLI1NM, containing the above motifs, mediated protein interactions, it had no ATPase or Mg-chelatase activity. These results indicated that PsCHLI1C was also required for maintaining enzyme activity, although it was not involved in protein-protein interactions. The sensor 2 motifs (also called sensor arginine, S-2, arginine₃₆₁) located in the PsCHLI1C have been reported to be vital for ATPase activity (Mao et al., 2018). Although the motifs of AAA modules in PsCHLI1 were involved in different steps of enzymatic reaction, they were essential for the function of CHLI. In addition, other motifs in PsCHLI1 may also take part in maintaining Mg-chelatase activity. The point mutations in amino acids, including glycine, arginine, glutamine, and aspartate

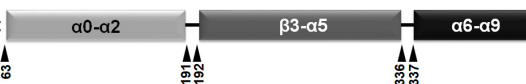
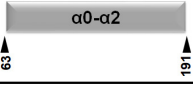
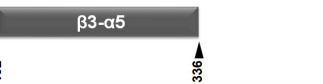




PsCHLI1NMC		ATPase activity (nmol phosphate h ⁻¹)	Mg chelatase activity (pmol Mg deuterio 30 min ⁻¹)
		24.92 ± 1.19	44.10 ± 5.46
PsCHLI1N		1.26 ± 0.32	0.09 ± 0.06
PsCHLI1M		1.89 ± 0.18	0.12 ± 0.09
PsCHLI1NM		1.59 ± 0.33	0.10 ± 0.05
PsCHLI1MC		1.78 ± 0.21	0.10 ± 0.05
PsCHLI1C		1.71 ± 0.12	0.08 ± 0.07
GST		1.19 ± 0.45	0.08 ± 0.06

FIGURE 6 | Peptide fragments of PsCHLI1 for enzyme activity. The different fragments of 1 μ M PsCHLI1 and GST purified from *E. coli* were used to determine ATPase activity by the Malachite Green colorimetric assay. The different fragments of 0.2 μ M PsCHLI1 and GST purified from *E. coli* were combined with recombinant rice CHLD (0.05 μ M), CHLH (0.5 μ M), and GUN4 (0.5 μ M) proteins to reconstitute the Mg-chelatase activity *in vitro* by a stopped fluorometric assay. Data represent the mean \pm S.E.M of nine replications from three independent assays. Differences between the GST group and groups of the PsCHLI1 fragments were assessed with analysis of variance. Secondary structure elements in the different peptide fragments are shown in the boxes. α , α -helices; β , β -sheets.

between the sensor 1 motif and the ARG-finger motif, and arginine in the PS-II insert, could abolish the function of Mg-chelatase in cucumber (Gao et al., 2016), soybean (Campbell et al., 2014; Du et al., 2018), and rice (Zhang et al., 2006). These residues are conserved in PsCHLI1M (glycine₂₇₁, arginine₂₇₄, glutamine₂₇₆, aspartate₂₇₉, and arginine₃₁₄), indicating their roles in the interaction with CHLD. In addition, our previous study showed that cysteines in PsCHLI1N (cysteine₁₀₀ and cysteine₁₉₁) and PsCHLI1C (cysteine₃₅₂ and cysteine₃₉₄) can be redox-regulated and are important for the ATPase activity of CHLI and Mg-chelatase (Luo et al., 2012). Taken together, all AAA modules in PsCHLI1 are essential for maintaining the ATPase activity of CHLI and reconstituting active Mg-chelatase.

DATA AVAILABILITY STATEMENT

The datasets presented in this study can be found in online repositories. The names of the repository/repositories and accession number(s) can be found below: <https://www.ncbi.nlm.nih.gov/>, PRJNA752108.

AUTHOR CONTRIBUTIONS

C-JW and SL designed the experiments. JZ and TL cloned the pea *CHLI* cDNA and did sequence analyses and performed the yeast two-hybrid assay. JW and JR performed the quantitative

real-time PCR. JW constructed the plasmids. C-JW and Y-XZ conducted the subcellular localization. Q-HZ determined the chlorophyll content. JW and L-XX measured the enzyme activity. SL performed the virus-induced gene silencing assay. TL and SL conducted the GST pull-down assay. Y-XY and SL performed phylogeny analysis. X-FX, TL, and SL analyzed the data, interpreted the results, and wrote the manuscript. All authors read and approved the final manuscript.

FUNDING

This work was supported by the National Natural Science Foundation of China (Grant No. 31860053) and the Natural Science Foundation of Jiangxi Province, China (Grant No. 20181BAB214013).

ACKNOWLEDGMENTS

The authors are grateful for the helpful assistances of RNA-Seq from Biomarker Technologies Corporation (Beijing, China).

SUPPLEMENTARY MATERIAL

The Supplementary Material for this article can be found online at: <https://www.frontiersin.org/articles/10.3389/fpls.2022.821683/full#supplementary-material>

REFERENCES

- Alfandari, D., and Darribère, T. (1994). A simple PCR method for screening cDNA libraries. *Genome Res.* 4, 46–49. doi: 10.1101/gr.4.1.46
- Apchelimov, A. A., Soldatova, O. P., Ezhova, T. A., Grimm, B., and Shestakov, S. V. (2007). The analysis of the ChlI 1 and ChlI 2 genes using acifluorfen-resistant mutant of *Arabidopsis thaliana*. *Planta* 225, 935–943. doi: 10.1007/s00425-006-0390-1
- Brzezowski, P., Sharifi, M. N., Dent, R. M., Morhard, M. K., Niyogi, K. K., and Grimm, B. (2016). Mg chelatase in chlorophyll synthesis and retrograde signaling in *Chlamydomonas reinhardtii*: CHLI2 cannot substitute for CHLI1. *J. Exp. Bot.* 67, 3925–3938. doi: 10.1093/jxb/erw004
- Campbell, B. W., Mani, D., Curtin, S. J., Slaterry, R. A., Michno, J.-M., Ort, D. R., et al. (2014). Identical substitutions in magnesium chelatase paralogs result in chlorophyll-deficient soybean mutants. *G3 (Bethesda)* 5, 123–131. doi: 10.1534/g3.114.015255
- Croce, R., and van Amerongen, H. (2014). Natural strategies for photosynthetic light harvesting. *Nat. Chem. Biol.* 10, 492–501. doi: 10.1038/nchembio.1555
- Dahl, W. J., Foster, L. M., and Tyler, R. T. (2012). Review of the health benefits of peas (*Pisum sativum* L.). *Br. J. Nutr.* 108, S3–S10. doi: 10.1017/S0007114512000852
- Du, H., Qi, M., Cui, X., Cui, Y., Yang, H., Zhang, J., et al. (2018). Proteomic and functional analysis of soybean chlorophyll-deficient mutant cd1 and the underlying gene encoding the CHLI subunit of Mg-chelatase. *Mol. Breed.* 38:71. doi: 10.1007/s11032-018-0819-9
- Force, A., Lynch, M., Pickett, F. B., Amores, A., Yan, Y. I., and Postlethwait, J. (1999). Preservation of duplicate genes by complementary, degenerative mutations. *Genetics* 151, 1531–1545. doi: 10.1093/genetics/151.4.1531
- Gao, M., Hu, L., Li, Y., and Weng, Y. (2016). The chlorophyll-deficient golden leaf mutation in cucumber is due to a single nucleotide substitution in CsChlI for magnesium chelatase I subunit. *Theor. Appl. Genet.* 129, 1961–1973. doi: 10.1007/s00122-016-2752-9
- Guillon, F., and Champ, M. (2003). Carbohydrate fractions of legumes: uses in human nutrition and potential for health. *Br. J. Nutr.* 88(Suppl. 3), S293–S306. doi: 10.1079/BJN2002720
- Guo, R., Luo, M., and Weinstein, J. D. (1998). Magnesium-chelatase from developing pea leaves. *Plant Physiol.* 116, 605–615. doi: 10.1104/pp.116.2.605
- Huang, Y.-S., and Li, H.-M. (2009). *Arabidopsis* CHLI2 can substitute for CHLI1. *Plant Physiol.* 150, 636–645. doi: 10.1104/pp.109.13.5368
- Ikegami, A., Yoshimura, N., Motohashi, K., Takahashi, S., Romano, P. G. N., Hisabori, T., et al. (2007). The CHLI1 subunit of *Arabidopsis thaliana* magnesium chelatase is a target protein of the chloroplast thioredoxin. *J. Biol. Chem.* 282, 19282–19291. doi: 10.1074/jbc.M7033.24200
- Jensen, P. E., Gibson, L. C., and Hunter, C. N. (1999). ATPase activity associated with the magnesium-protoporphyrin IX chelatase enzyme of *Synechocystis PCC6803*: evidence for ATP hydrolysis during Mg²⁺ insertion, and the MgATP-dependent interaction of the ChlI and ChlD subunits. *Biochem. J.* 339, 127–134.
- Kim, D., Paggi, J. M., Park, C., Bennett, C., and Salzberg, S. L. (2019). Graph-based genome alignment and genotyping with HISAT2 and HISAT-genotype. *Nat. Biotechnol.* 37, 907–915. doi: 10.1038/s41587-019-0201-4
- Kobayashi, K., Mochizuki, N., Yoshimura, N., Motohashi, K., Hisabori, T., and Masuda, T. (2008). Functional analysis of *Arabidopsis thaliana* isoforms of the Mg-chelatase CHLI subunit. *Photochem. Photobiol. Sci.* 7, 1188–1195. doi: 10.1039/b802604c
- Kreplak, J., Madoui, M.-A., Cápál, P., Novák, P., Labadie, K., Aubert, G., et al. (2019). A reference genome for pea provides insight into legume genome evolution. *Nat. Genet.* 51, 1411–1422. doi: 10.1038/s41588-019-0480-1
- Lake, V., Olsson, U., Willows, R. D., and Hansson, M. (2004). ATPase activity of magnesium chelatase subunit I is required to maintain subunit D in vivo. *Eur. J. Biochem.* 271, 2182–2188. doi: 10.1111/j.1432-1033.2004.04143.x
- Lescot, M., Déhais, P., Thijs, G., Marchal, K., Moreau, Y., Van de Peer, Y., et al. (2002). PlantCARE, a database of plant cis-acting regulatory elements and a portal to tools for in silico analysis of promoter sequences. *Nucleic Acids Res.* 30, 325–327. doi: 10.1093/nar/30.1.325
- Li, Q., Fang, C., Duan, Z., Liu, Y., Qin, H., Zhang, J., et al. (2016). Functional conservation and divergence of GmCHLI genes in polyploid soybean. *Plant J.* 88, 584–596. doi: 10.1111/tjp.13282
- Long, S. P., Marshall-Colon, A., and Zhu, X. G. (2015). Meeting the global food demand of the future by engineering crop photosynthesis and yield potential. *Cell* 161, 56–66. doi: 10.1016/j.cell.2015.03.019
- Luo, S., Luo, T., Liu, Y., Li, Z., Fan, S., and Wu, C. (2018). N-terminus plus linker domain of Mg-chelatase D subunit is essential for Mg-chelatase activity in *Oryza sativa*. *Biochem. Biophys. Res. Commun.* 497, 749–755. doi: 10.1016/j.bbrc.2018.02.146
- Luo, S., Luo, T., Peng, P., Li, Y., and Li, X. (2016). Disturbance of chlorophyll biosynthesis at Mg branch affects the chloroplast ROS homeostasis and Ca²⁺ signaling in *Pisum sativum*. *Plant Cell Tissue Organ. Cult.* 127, 729–737. doi: 10.1007/s11240-016-1008-3
- Luo, T., Fan, T., Liu, Y., Rothbart, M., Yu, J., Zhou, S., et al. (2012). Thioredoxin redox regulates ATPase activity of magnesium chelatase CHLI subunit and modulates redox-mediated signaling in tetrapyrrole biosynthesis and homeostasis of reactive oxygen species in pea plants. *Plant Physiol.* 159, 118–130. doi: 10.1104/pp.112.19.5446
- Luo, T., Luo, S., Araújo, W. L., Schlicke, H., Rothbart, M., Yu, J., et al. (2013). Virus-induced gene silencing of pea CHLI and CHLD affects tetrapyrrole biosynthesis, chloroplast development and the primary metabolic network. *Plant Physiol. Biochem.* 65, 17–26. doi: 10.1016/j.plaphy.2013.01.006
- Mao, G., Ma, Q., Wei, H., Su, J., Wang, H., Ma, Q., et al. (2018). Fine mapping and candidate gene analysis of the virescent gene vlin Upland cotton (*Gossypium hirsutum*). *Mol. Gen. Genet.* 293, 249–264. doi: 10.1007/s00438-017-1383-4
- Masuda, T. (2008). Recent overview of the Mg branch of the tetrapyrrole biosynthesis leading to chlorophylls. *Photosynth. Res.* 96, 121–143. doi: 10.1007/s1120-008-9291-4
- Moss, D. N., and Musgrave, R. B. (1971). “Photosynthesis and crop production,” in *Advances in Agronomy*, ed. N. C. Brady (Cambridge, MA: Academic Press), 317–336. doi: 10.1016/s0065-2113(08)60155-8
- Perez-Ruiz, J. M., Guinea, M., Puerto-Galan, L., and Cejudo, F. J. (2014). NADPH thioredoxin reductase C is involved in redox regulation of the Mg-chelatase I subunit in *Arabidopsis thaliana* chloroplasts. *Mol. Plant* 7, 1252–1255. doi: 10.1093/mp/ssu032
- Reid, J. D., Siebert, C. A., Bullough, P. A., and Hunter, C. N. (2003). The ATPase activity of the ChlI subunit of magnesium chelatase and formation of a heptameric AAA+ ring. *Biochemistry* 42, 6912–6920. doi: 10.1021/bi034082q
- Rissler, H. M., Collakova, E., DellaPenna, D., Whelan, J., and Pogson, B. J. (2002). Chlorophyll biosynthesis. expression of a second Chl I Gene of magnesium chelatase in *Arabidopsis* supports only limited chlorophyll synthesis. *Plant Physiol.* 128, 770–779. doi: 10.1104/pp.010625
- Sawicki, A., Zhou, S., Kwiatkowski, K., Luo, M., and Willows, R. D. (2017). 1-N-histidine phosphorylation of ChlD by the AAA+ ChlI2 stimulates magnesium chelatase activity in chlorophyll synthesis. *Biochem. J.* 474, 2095–2105. doi: 10.1042/bj2990277
- Tayade, R. (2019). Insight into the prospects for the improvement of seed starch in legume seeds – A review. *Plant Sci.* 10:1213. doi: 10.3389/fpls.2019.01213
- Walker, C. J., and Weinstein, J. D. (1994). The magnesium-insertion step of chlorophyll biosynthesis is a two-stage reaction. *Biochem. J.* 299(Pt 1), 277–284. doi: 10.1042/bj2990277
- Zhang, D., Chang, E., Yu, X., Chen, Y., Yang, Q., Cao, Y., et al. (2018). Molecular characterization of magnesium chelatase in soybean [*Glycine max* (L.) Merr.]. *Front. Plant Sci.* 9:720. doi: 10.3389/fpls.2018.00720
- Zhang, H., Li, J., Yoo, J.-H., Yoo, S.-C., Cho, S.-H., Koh, H.-J., et al. (2006). Rice chlorina-1 and chlorina-9 encode ChlD and ChlI subunits of Mg-chelatase, a

- key enzyme for chlorophyll synthesis and chloroplast development. *Plant Mol. Biol.* 62, 325–337. doi: 10.1007/s11103-006-9024-z
- Zhou, S., Sawicki, A., Willows, R. D., and Luo, M. (2012). C-terminal residues of *Oryza sativa* GUN4 are required for the activation of the ChlH subunit of magnesium chelatase in chlorophyll synthesis. *FEBS Lett.* 586, 205–210. doi: 10.1016/j.febslet.2011.12.026
- Zhu, X. G., Long, S. P., and Ort, D. R. (2010). Improving photosynthetic efficiency for greater yield. *Annu. Rev. Plant Physiol.* 61, 235–261. doi: 10.1146/annurev-arplant-042809-112206

Conflict of Interest: The authors declare that the research was conducted in the absence of any commercial or financial relationships that could be construed as a potential conflict of interest.

Publisher's Note: All claims expressed in this article are solely those of the authors and do not necessarily represent those of their affiliated organizations, or those of the publisher, the editors and the reviewers. Any product that may be evaluated in this article, or claim that may be made by its manufacturer, is not guaranteed or endorsed by the publisher.

Copyright © 2022 Wu, Wang, Zhu, Ren, Yang, Luo, Xu, Zhou, Xiao, Zhou and Luo. This is an open-access article distributed under the terms of the Creative Commons Attribution License (CC BY). The use, distribution or reproduction in other forums is permitted, provided the original author(s) and the copyright owner(s) are credited and that the original publication in this journal is cited, in accordance with accepted academic practice. No use, distribution or reproduction is permitted which does not comply with these terms.



Stromal Protein Chloroplast Development and Biogenesis1 Is Essential for Chloroplast Development and Biogenesis in *Arabidopsis thaliana*

Weijie Chen^{1†}, Jingang Huang^{1†}, Shiwei Chen¹, Lin Zhang¹, Jean-David Rochaix², Lianwei Peng¹ and Qiang Xin^{1*}

¹Shanghai Key Laboratory of Plant Molecular Sciences, College of Life Sciences, Shanghai Normal University, Shanghai, China, ²Departments of Molecular Biology and Plant Biology, University of Geneva, Geneva, Switzerland

OPEN ACCESS

Edited by:

Hongbo Gao,
Beijing Forestry University, China

Reviewed by:

Peng Wang,
Humboldt University of Berlin,
Germany
Hongbin Wang,
Guangzhou University of Chinese
Medicine, China

*Correspondence:

Qiang Xin
xinqiang0327@shnu.edu.cn

[†]These authors have contributed
equally to this work

Specialty section:

This article was submitted to
Plant Physiology,
a section of the journal
Frontiers in Plant Science

Received: 15 November 2021

Accepted: 17 January 2022

Published: 10 February 2022

Citation:

Chen W, Huang J, Chen S, Zhang L,
Rochaix J-D, Peng L and
Xin Q (2022) Stromal Protein
Chloroplast Development and
Biogenesis1 Is Essential for
Chloroplast Development and
Biogenesis in *Arabidopsis thaliana*.
Front. Plant Sci. 13:815859.
doi: 10.3389/fpls.2022.815859

Although numerous studies have been carried out on chloroplast development and biogenesis, the underlying regulatory mechanisms are still largely elusive. Here, we characterized a chloroplast stromal protein Chloroplast Development and Biogenesis1 (CDB1). The knockout *cdb1* mutant exhibits a seedling-lethal and ivory leaf phenotype. Immunoblot and RNA blot analyses show that accumulation of chloroplast ribosomes is compromised in *cdb1*, resulting in an almost complete loss of plastid-encoded proteins including the core subunits of the plastid-encoded RNA polymerase (PEP) RpoB and RpoC2, and therefore in impaired PEP activity. Orthologs of CDB1 are found in green algae and land plants. Moreover, a protein shows high similarity with CDB1, designated as CDB1-Like (CDB1L), is present in angiosperms. Absence of CDB1L results in impaired embryo development. While CDB1 is specifically located in the chloroplast stroma, CDB1L is localized in both chloroplasts and mitochondria in *Arabidopsis*. Thus, our results demonstrate that CDB1 is indispensable for chloroplast development and biogenesis through its involvement in chloroplast ribosome assembly whereas CDB1L may fulfill a similar function in both mitochondria and chloroplasts.

Keywords: chloroplast, ribosome, mitochondria, CDB1, CDB1L

INTRODUCTION

Chloroplasts are the sites of photosynthesis in eukaryotic cells and arose from a cyanobacterium-like ancestor through endosymbiosis. In higher plants, light triggers chloroplast development from undifferentiated small organelles called proplastids in meristematic cells (Pogson and Albrecht, 2011). During differentiation and biogenesis, chloroplasts transcribe their own genome into mRNAs for protein synthesis. These proteins are essential for the development of functional chloroplasts (Sakamoto et al., 2008). Chloroplast genomes of green plants comprise ~120 genes encoding the components of the gene expression system (RNA polymerase core subunits, ribosomal proteins, tRNAs, and rRNAs), subunits of the photosynthetic machinery [Rubisco,

photosystem I and II (PSI and PSII), cytochrome *b₆f* complex (Cyt *b₆f*), ATP synthase, and NAD(P)H dehydrogenase-like (NDH) complex] as well as some other proteins involved in various metabolic processes in chloroplasts (Dobrogojski et al., 2020). In addition to the plastid-encoded proteins, chloroplasts also contain ~3,000 nucleus-encoded proteins which are synthesized on cytosolic ribosomes and then imported into chloroplasts (Friso et al., 2004; Heazlewood et al., 2006). Thus, chloroplast development and biogenesis require tight coordination of plastid and nuclear gene expression.

Chloroplast transcription involves the interplay of two types of RNA polymerases: nuclear-encoded phage-type RNA polymerase (NEP) and plastid-encoded bacterial-type RNA polymerase (PEP; Shiina et al., 2005; Börner et al., 2015). In *Arabidopsis*, NEP is encoded by the nuclear genes *RpoTp* and *RpoTmp*, and is essential for transcription of the plastid PEP transcription machinery including *rpoA* and *rpoB-C1-C2* as well as some plastid housekeeping genes (Steiner et al., 2011; Pfalz and Pfannschmidt, 2013). Plastid genes involved in photosynthesis are primarily transcribed by the PEP transcription machinery (Swiatecka-Hagenbruch et al., 2007; Liere et al., 2011). PEP is composed of four catalytic core subunits (α , β , β' , and β''), which are encoded by *rpoA*, *rpoB*, *rpoC1*, and *rpoC2*, respectively. Besides its four core subunits, PEP activity is also regulated by at least 12 PEP-associated proteins (PAPs; Pfalz and Pfannschmidt, 2013). Intriguingly, most mutants of these PEP complex subunits display an albino/ivory leaf phenotype with arrested plastid development and strongly decreased expression of PEP-dependent genes (Pfalz and Pfannschmidt, 2013).

Translation in chloroplasts is performed by prokaryotic-type 70S ribosomes composed of a large 50S and a small 30S subunit. Biochemical analysis showed that, in spinach, the 50S subunit contains 23S, 5S, and 4.5S rRNA as well as 33 ribosomal proteins whereas the 30S subunit consists of 16S rRNA and 25 ribosomal proteins (Manuell et al., 2007; Graf et al., 2016; Perez Boerema et al., 2018). Because of their common origin, chloroplast and bacterial ribosomes exhibit some conserved structural and functional features such as the mRNA decoding (30S small subunit) and the peptide bond synthesis (50S large subunit) functions (Manuell et al., 2007; Sharma et al., 2007). Besides the classical ribosomal proteins which have orthologs in *Escherichia coli*, five plastid-specific ribosomal proteins (PSRPs) with essential functional roles were also found in plant plastid ribosomes (Sharma et al., 2010; Tiller et al., 2012). Although the overall structural organization of chloroplast ribosomes has been characterized, little is known about the molecular mechanisms underlying their assembly.

Ribosome biogenesis is a complicated process that comprises the transcription of a large pre-rRNA precursor, its processing and folding and the assembly of the ribosomal proteins with the mature rRNAs (Shajani et al., 2011; Weis et al., 2015). So far, a dozen of factors appears to be required for the maturation of rRNAs in chloroplasts, such as RNase R homolog 1 (RNR1) which is involved in the maturation of 23S, 16S, and 5S rRNAs (Bollenbach et al., 2005). Loss of endonucleases RNase E in *Arabidopsis* causes defective rRNA processing and subsequent

plastid ribosome deficiency (Schein et al., 2008; Walter et al., 2010). The DEAD-box RNA helicases RH22 and RH39 function in the assembly of the 50S ribosomal subunit and 23S rRNA processing, respectively (Nishimura et al., 2010; Chi et al., 2012). A conserved protein with an unknown functional DUF177 domain is specifically required for the accumulation of 23S rRNA (Yang et al., 2016). In addition to the factors required for chloroplast rRNA maturation, there are many factors involved in the biogenesis of chloroplast ribosomes. For example, ObgC is a GTPase that associates with chloroplast 50S ribosomal subunits through 23S rRNA (Bang et al., 2012). Pro-rich protein CGL20 is also required for the assembly of the 50S ribosomal subunit (Reiter et al., 2020).

Here, we have characterized an *Arabidopsis* mutant that displays an ivory leaf phenotype with arrested chloroplast development. We designated this mutant *chloroplast development and biogenesis1* (*cdb1*). The *CDB1* gene encodes a protein with unknown function that is targeted to the chloroplast stroma. Loss of *CDB1* leads to defects in accumulation of plastid-encoded proteins, including chloroplast ribosomes. These data suggest that *CDB1* is indispensable for chloroplast development through its involvement in chloroplast ribosome assembly. We also provide evidence that the paralog of *CDB1*, *CDB1-Like* (*CDB1L*), is located both in chloroplasts and mitochondria and essential for embryo development in *Arabidopsis*.

MATERIALS AND METHODS

Plant Material and Growth Conditions

Mutants of *cdb1* (SALK_080811C) and *cdb1l* (GK-844F05) were obtained from the Nottingham *Arabidopsis* Stock Center (NASC). The T-DNA insertions were confirmed by PCR analysis and subsequent sequencing with the primers *CDB1*-TF and *CDB1*-TR, *CDB1L*-TF, and *CDB1L*-TR (for all primer sequences, see **Supplementary Table 3**), respectively. Seeds were planted in Murashige and Skoog (MS) culture medium (pH 5.8) with 3% sucrose and 0.7% agar at 4°C in the dark for 48 h. Then the plants were cultured under long-day conditions (16 h-light/8 h-dark) at 23°C with an irradiance of 50 $\mu\text{mol photons m}^{-2}\text{s}^{-1}$ for 3–4 weeks. For complementation of the mutants, genomic sequences of *CDB1* (AT4G37920) and *CDB1L* (AT1G36320) plus the upstream promoters were cloned into pCambia1301 to produce transgenic lines. The genomic sequence of *CDB1* was fused with the HA tag and cloned into the pCambia1301 vector to generate *CDB1*-HA transgenic plants. All the above vectors were transferred into *Agrobacterium tumefaciens* strain GV3101 and then introduced into *Arabidopsis* by the floral-dip method (Clough and Bent, 1998).

Transmission Electron Microscopy

Leaves from 2-week-old plants grown on MS medium with 3% sucrose were fixed with 2.5% glutaraldehyde in phosphate buffer (pH 7.2) for 24 h at 4°C. After washing three times with the same buffer, the fixed samples were dehydrated with a series of ethanol solutions (15, 30, 50, 70, 80, 90, and 100%). Then, the dehydrated samples were infiltrated with a series of

epoxy resin in epoxy propane (25, 50, 75, and 100%), and embedded in Epon 812 resin. The samples were cut through an ultramicrotome, and images were taken with a transmission electron microscope (Phillips CM120).

Subcellular Localization of Green Fluorescent Protein

To study the subcellular location of CDB1 and CDB1L, full cDNA sequences of *CDB1* and *CDB1L* were cloned into the pBI221-GFP vector. The chloroplast localization control RbcS-GFP was constructed as described previously (Zhang et al., 2018). The constructs were transformed into *Arabidopsis* protoplasts by PEG-mediated protoplast transformation. The mitochondrial marker MitoTracker Red CMXRos at a final concentration of 100 nM was incubated with the protoplasts for 15 min in the dark and washed twice before imaging. GFP signals were captured by confocal laser scanning microscopy (LSM 780, Zeiss). The experiment was repeated twice independently with similar results.

Antibody Production and Antibody Source

Sequences encoding the mature CDB1 and CDB1L proteins were amplified and cloned into the pET-28a expression vector (Merck Millipore) to express the recombinant proteins in the *E. coli* strain BL21 (DE3) in the presence of 0.5 mM IPTG. Recombinant proteins were purified using Ni-NTA agarose (Qiagen) and used to produce rabbit polyclonal antiserum (PhytoAB). Antiserum was employed in dilutions of 1:1,000. For examination of the specificity of CDB1 and CDB1L antibodies, immunoblots were performed using the recombinant CDB1 and CDB1L proteins. No cross reaction between the two proteins was detected when as much as 8 ng of recombinant CDB1 and CDB1L proteins was loaded (**Supplementary Figure 3**), indicating the specificity of these two antibodies.

Antibodies against HA tag (PhytoAB, PHY5011), D1 (PhytoAB, PHY0057), D2 (PhytoAB, PHY0323), LHCII (made in our lab), PetA (PhytoAB, PHY0321), PetC (PhytoAB, PHY0163), PetD (PhytoAB, PHY0354), PsaA (PhytoAB, PHY0342), PsaD (PhytoAB, PHY0343), CF₁γ (PhytoAB, PHY0161), CF₁ε (PhytoAB, PHY0315), RbcL (PhytoAB, PHY0066), phosphoglycerate kinase (PGK1; PhytoAB, PHY0405), ribulose phosphate epimerase (RPE; PhytoAB, PHY0616), RpoB (PhytoAB, PHY1700), RpoC2 (PhytoAB, PHY0382), RPS2 (PhytoAB, PHY0427), RPS4 (PhytoAB, PHY0428), PSRP2 (PhytoAB, PHY0420), RPL1 (PhytoAB, PHY0421), RPL6 (PhytoAB, PHY0411), RPL10 (PhytoAB, PHY0423), RPL11 (PhytoAB, PHY0413), and RPL18 (PhytoAB, PHY0414) were purchased from a commercial supplier and used at a 1:1,000 dilution.

Protein Isolation and Immunoblot Analysis

Chloroplast stromal proteins and thylakoid membranes were extracted from 4-week-old plants. Intact chloroplasts were isolated using isolation buffer (0.33 M sorbitol and 20 mM HEPES/KOH, pH 7.6) and then osmotically ruptured in 20 mM HEPES/KOH (pH 7.6; Zhang et al., 2018). To separate the thylakoid

membranes and stromal proteins, the ruptured chloroplasts were centrifuged at 12,000 × g for 10 min at 4°C. Clear supernatant containing stromal proteins was quantified with a Protein Assay Kit (Bio-Rad Laboratories), and the pellet containing thylakoid membrane was solubilized in 20 mM HEPES/KOH (pH 7.6). Both stromal and thylakoid proteins were solubilized in 2 × sample buffer (50 mM Tris-HCl, pH 6.8, 5% SDS, 20% glycerol, 8 M urea, 5% 2-mercaptoethanol, and 1% bromophenol blue).

Mitochondria were isolated as previously described (Sweetlove et al., 2007). Four week-old WT plants were fully homogenized in isolation buffer (0.3 M sucrose, 5 mM tetrasodium pyrophosphate, 10 mM KH₂PO₄, pH 7.5, 2 mM EDTA, 1% PVP40, 1% BSA, 5 mM cysteine, and 20 mM ascorbic acid), filtered through Miracloth, and then centrifuged at 5,000 × g for 10 min at 4°C. The supernatant was collected and centrifuged at 20,000 × g for 10 min at 4°C. The pellet containing crude mitochondria was resuspended in buffer with 0.3 M sucrose, 1 mM EGTA, and 10 mM MOPS/KOH, pH 7.2 and further centrifuged through a Percoll density gradient consisting of 18, 25, and 50% Percoll solution at 40,000 × g for 55 min at 4°C. Intact mitochondria at the 25%–50% Percoll interface were collected. Protein concentration was determined using a DC Protein Assay kit (BioRad, 5000116). Mitochondrial proteins were solubilized in 2 × sample buffer.

Protein samples were separated by SDS-PAGE and transferred to nitrocellulose membranes. The membrane was incubated with specific antibodies, and then the signals were detected by the LuminoGraph WSE-6100 (ATTO Technology).

RNA Sequencing and Differential Gene Expression Analysis

Total RNA was extracted from WT and *cdb1* leaves using Trizol reagent kit (Invitrogen, Carlsbad, CA, United States), and rRNAs were removed by Ribo-ZeroTM Magnetic Kit (Epicentre, Madison, WI, United States) to retain mRNAs and other RNAs. Enriched RNAs were fragmented and reverse transcribed into cDNA with random primers. Second-strand cDNA was synthesized, end repaired, and ligated to Illumina sequencing adapters using NEB#7490 kit (NEB E7490L, New England Biolabs). The ligation products of 300–500 bp were selected by agarose gel electrophoresis, PCR amplified, and sequenced using Illumina HiSeq2500 (Gene Denovo Biotechnology Co. Ltd.).

Raw Reads were filtered by fastp (version 0.18.0) to get high quality clean reads (Chen et al., 2018). Clean reads were mapped to the *Arabidopsis* reference genome (TAIR10) using HISAT2.2.4 (Kim et al., 2019) and then sorted according to chromosome and physical position of the reference genome by samtools (Li et al., 2009). Reads were counted by featureCounts in Rsubread (version: 2.2.6) R package and normalized to get Transcripts Per Kilobase of exon model per Million mapped reads (TPM) and trimmed mean of M value (TMM; Liao et al., 2019). Differentially expressed genes (DEGs) were analyzed using DESeq2 (version: 1.28.1) applying a $|\log_2(FC)| > 1$ and an adjusted $p < .05$ parameters (Love et al., 2014). Gene Ontology (GO) enrichment analysis for DEGs was performed using

clusterProfiler package (Wu et al., 2021). A false discovery rate (FDR) of <0.05 was considered for threshold.

The RNA-seq data have been uploaded in the NCBI Sequence Read Archive under accession number PRJNA781386.

RNA Blot Analysis

Total RNA of WT and *cdb1* was extracted from 4-week-old *Arabidopsis* plants using Trizol reagent (Thermo Fisher Scientific). The rRNAs were detected by ethidium bromide staining. A total of 5 µg RNA of WT and *cdb1* samples were separated by electrophoresis on 1.4% (w/v) agarose-formaldehyde gels and subsequently blotted onto a nylon membrane (GE Healthcare). RNA was fixed on the nylon membrane by UV irradiation (UVP Hybridizer Oven). The membrane was hybridized with the specific probes labeled with digoxigenin, and the signals were visualized by the LuminoGraph WSE-6100 (ATTO Technology). Primers used to generate probes for the chloroplast *rrn* operons are shown in **Supplementary Table 3**.

Other Methods

Chlorophyll fluorescence was measured using the MAXI version of the Imaging-PAM M-Series chlorophyll fluorescence system with default settings. Before measurement, the plants were kept in the dark for 20 min. Protein alignment and evolutionary tree were produced using MEGA6 (Tamura et al., 2013).

RESULTS

Arabidopsis cdb1 Mutant Exhibits an Ivory Phenotype

In recent years, many mutants with albino or ivory phenotype were reported. Analysis of these mutants by transmission electron microscopy revealed defects in plastid development and biogenesis as for *pdm4* and several *pTAC* mutants (Pfalz et al., 2006; Wang et al., 2020). To further investigate the underlying mechanisms of chloroplast development and biogenesis, we characterized a T-DNA insertion mutant (SALK_080811C) with an ivory phenotype (**Figures 1A,B**). PCR product sequencing showed that the T-DNA was inserted in the sixth exon of *AT4G37920* (**Figure 1A**). This mutant could grow on MS medium supplemented with 3% sucrose but could not survive photoautotrophically when transplanted in soil. The leaves of this mutant display an ivory phenotype (**Figure 1B**). By transmission electron microscopy observation, we found that, unlike the chloroplasts in WT with well-organized thylakoid membranes, the plastids of this mutant did not exhibit organized membrane structures (**Figure 1C**). These results indicate that chloroplast development and biogenesis is arrested. Accordingly, we named this mutant *cdb1*.

Chlorophyll fluorescence of WT and *cdb1* plants grown on MS medium was analyzed. In WT, the minimal fluorescence (F_0) and the maximal fluorescence (F_m) were 0.17 ± 0.01 and 0.75 ± 0.01 , respectively. The maximum quantum efficiency of PSII (F_v/F_m) was 0.77 ± 0.01 . Consistent with the ivory phenotype of *cdb1*, almost no chlorophyll fluorescence was detected in the *cdb1* mutant as F_0

and F_m were 0.069 ± 0.020 and 0.086 ± 0.020 , respectively (**Figure 1B**). The value of F_v/F_m is close to 0, indicating no PSII activity in *cdb1*.

To confirm that the ivory leaf phenotype was due to the disruption of *CDB1* in *cdb1*, we complemented the mutants with the genomic gene sequence including its native promoter (*CDB1-COM*) and the full-length coding region of *CDB1* fused to the HA tag at its C terminus (*CDB1-HA*). The *CDB1-COM* and *CDB1-HA* complemented plants displayed a phenotype similar to WT and the ivory leaf and fluorescence emission defects were all rescued (**Figure 1B**). A specific antibody raised against CDB1 was used to detect the CDB1 protein by immunoblotting using a total protein extract from 4-week-old leaves of WT, *CDB1-HA*, and *CDB1-COM* plants (**Figure 1D**). The *CDB1* gene encodes a 48.73 kDa protein with a predicted chloroplast transit peptide (cTP). A signal corresponding to a molecular mass of about 42 kDa was detected consistent with the predicted molecular mass of CDB1 without cTP (**Figure 1D**). CDB1-HA fusion protein was detected in the *CDB1-HA* complemented plants with a slightly larger molecular mass than the native CDB1 protein (**Figure 1D**). CDB1 was absent in the *cdb1* mutant due to the T-DNA insertion in *AT4G37920*. These results indicate that *cdb1* is a null mutation and *CDB1* is responsible for chlorophyll accumulation and chloroplast development.

Chloroplast Protein Accumulation in *cdb1*

Since the *cdb1* mutant showed an ivory phenotype, it was necessary to investigate chloroplast protein accumulation *in vivo*. Total protein from 3-week-old leaves of WT and *cdb1* was isolated and tested by immunoblot analysis using antibodies against subunits of the major photosynthetic complexes. Accumulation of thylakoid membrane proteins, including D1, D2, and LHCII of the PSII complex, PetA (Cyt *f*) and PetD of Cyt *b₆f*, and PsaA and PsaD of PSI were all undetectable in the *cdb1* mutant and only trace amounts of CF₁γ and CF₁ε of ATP synthase and PetC of Cyt *b₆f* were detected (**Figure 2**). Abundance of three enzymes involved in the photosynthetic carbon reduction Calvin cycle was also analyzed (**Figure 2**). While a trace amount of plastid-encoded RuBisCO large subunit (RbcL) was detected in the *cdb1* mutant, the levels of the nuclear-encoded PGK1 and RPE were comparable in the mutant to those of WT (**Figure 2**).

These results indicate that all plastid-encoded proteins analyzed do not accumulate or are only present in tiny amounts in *cdb1* as shown for D1, D2, PetA, PsaA, CF₁ε, and RbcL. Nucleus-encoded chloroplast proteins whose stable accumulation is independent of the presence of other plastid-encoded proteins were present in normal amounts in the *cdb1* mutant as seen for PGK1 and RPE. These results agree with earlier studies showing that the stable accumulation of proteins belonging to a photosynthetic complex depends on the presence of all core subunits and especially on those that are plastid-encoded (Naver et al., 2001; Peng et al., 2006). Therefore, a possible explanation for the immunoblot results of *cdb1* is that synthesis of all plastid-encoded proteins is blocked in *cdb1* resulting not only in the absence of these proteins but also of their nucleus-encoded partner proteins of the same photosynthetic complex. In contrast, other nucleus-encoded chloroplast proteins such as PGK1 and RPE are unaffected in *cdb1* (**Figure 2**).

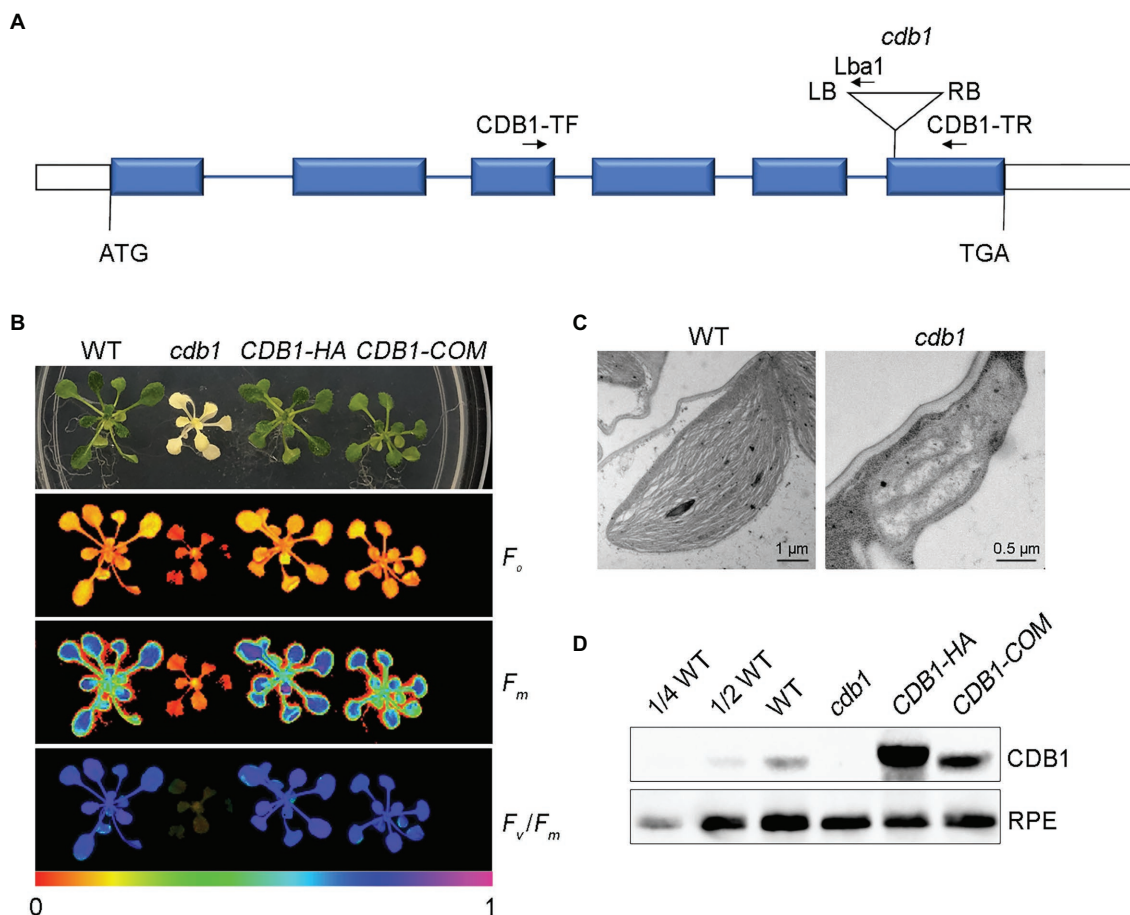


FIGURE 1 | Characterization of the *cdb1* mutant. **(A)** Scheme of the structure of the *Chloroplast Development and Biogenesis1* (*CDB1*) gene with the T-DNA insertion. The six blue boxes indicate exons. 5' and 3' UTRs are shown as white boxes and introns as black lines. The T-DNA insertion is indicated by a triangle. The forward (*CDB1*-TF) and reverse primers (*CDB1*-TR and *Lba1*) used for PCR analysis are indicated with arrows. **(B)** Chlorophyll fluorescence images of 4-week-old WT (wild-type), *cdb1* and complemented plants *CDB1*-HA and *CDB1*-COM. The minimal fluorescence (F_0), the maximal fluorescence (F_m) and F_v/F_m of WT, *cdb1* and two complemented plants were measured by Imaging-PAM. Fluorescence was visualized using a pseudocolor index from red (0) to purple (1) as indicated at the bottom. **(C)** Transmission electron micrographs of chloroplasts in leaves from 2-week-old WT and *cdb1* mutant. Scale bars are indicated. **(D)** Protein accumulation of CDB1 in total protein extracts from 4-week-old leaves of WT, *cdb1* and complemented plants *CDB1*-HA and *CDB1*-COM. Immunoblotting was performed with a CDB1-specific antibody. An antibody specific for ribulose phosphate epimerase (RPE) was used as loading control.

RNA-Seq Analysis of the *cdb1* Mutant

To determine the function of CDB1 in chloroplast development, we carried out an RNA-seq analysis on 4-week-old leaves of *cdb1* and WT. Transcriptional profiles of nucleus- and chloroplast-encoded genes were compared using RNA-seq. A total of 3,515 genes were differentially expressed more than 2-fold in *cdb1* compared to WT (**Figure 3A**). They include 1,395 upregulated and 2,120 downregulated genes (**Figure 3A**). Gene Ontology (GO) analysis revealed that a large proportion of the DEGs are related to the nucleus and chloroplast (**Figure 3B**). Among 618 DEGs related to the chloroplast (GO:0009507), 272 nuclear and 30 chloroplast DEGs are upregulated whereas 296 nuclear and 18 chloroplast DEGs are downregulated (**Supplementary Figure 1**).

The plastid genes can be divided into three classes according to which plastid RNA polymerase transcribes them. Class I and III are transcribed by the PEP and NEP, respectively.

Transcription of class II depends on both PEP and NEP. RNA-seq results showed that expression of class I genes (e.g., *psbA*, *psbH*, *petB*, *petD*, *ndhA*, and *rbcl*) was significantly reduced whereas expression of Class III genes (e.g., *accD*, *rpoA*, *rpoB*, *rpoC1*, *rpoC2*, and *ycf2*) and most of Class II genes (e.g., *atpI*, *rps16*, *clpP*, and *ycf1*) was greatly upregulated (**Figure 3C**; **Supplementary Table 1**). The upregulated NEP-dependent Class III genes and the differentially expressed nuclear genes of chloroplast proteins may possibly participate in a compensating response to the decreased expression of Class I genes. These results suggest that transcription of the PEP-dependent genes is impaired in the absence of CDB1. Immunoblot analysis showed that the core subunits of the PEP complex RpoB is undetectable and RpoC2 is only present in a tiny amount in *cdb1* (**Figure 3D**), indicating that absence of the functional PEP complex is responsible for the impaired transcription of the PEP-dependent genes in *cdb1*.

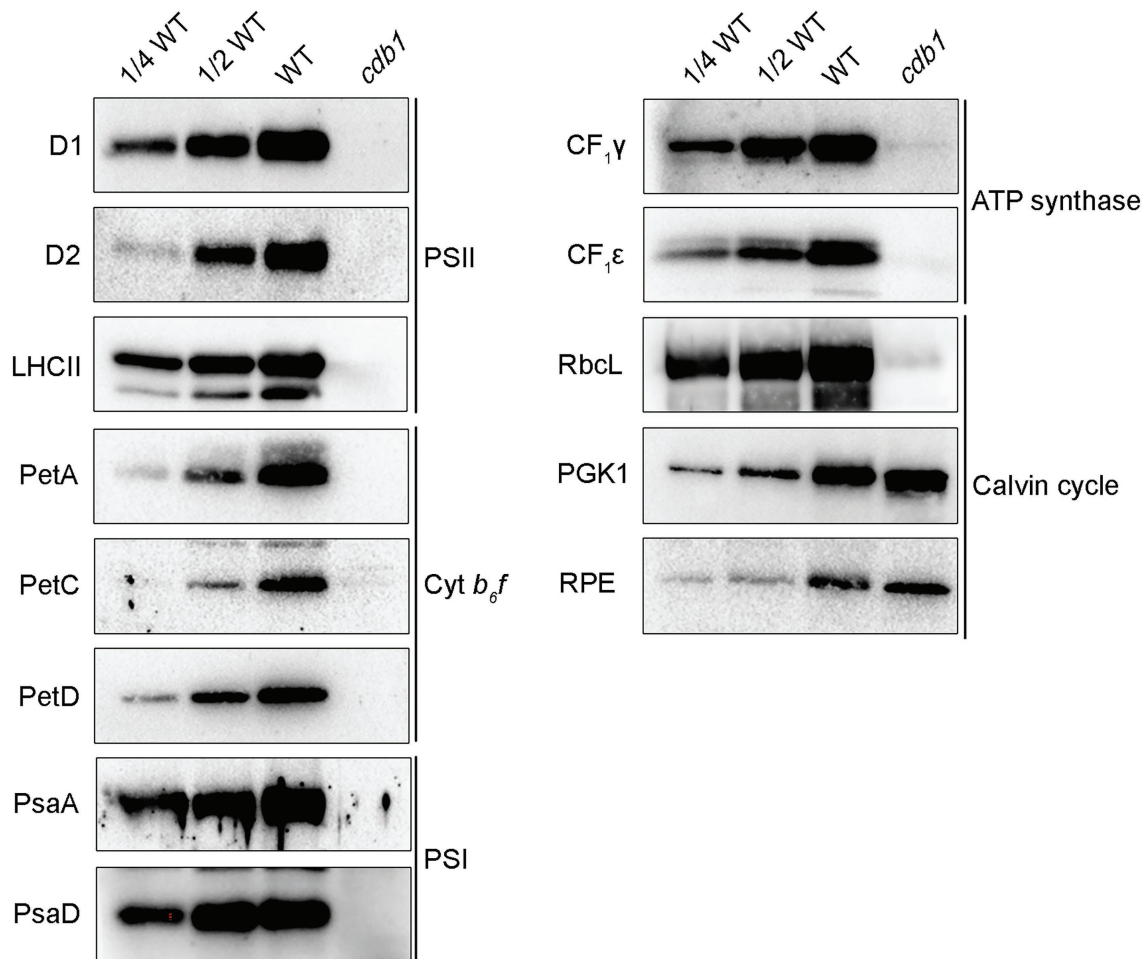


FIGURE 2 | Comparative analysis of subunits of photosynthetic complexes from WT and *cdb1*. Total protein isolated from 3-week-old WT and *cdb1* plants was analyzed by immunoblotting with antibodies against representative subunits of the multiprotein complexes of the thylakoid membrane: D1, D2, and LHCII from photosystem II (PSII), PetA, PetC, and PetD from Cyt *b₆f*, PsaA and PsaD from PSI, CF₁γ, and CF₁ε from ATP synthase. Antibodies against RbcL, phosphoglycerate kinase (PGK1), and RPE were used as representative components of the Calvin cycle.

Decreased Accumulation of Chloroplast Ribosomes in *cdb1*

Although drastic reductions of RpoB and RpoC2 were observed in *cdb1*, the levels of their mRNAs are higher in *cdb1* than in WT (Figures 3C,D). This observation implies that translation of *rpoB* and *rpoC2* by ribosomes or assembly of the PEP complex is impaired in *cdb1*. To address the possible role of CDB1 in chloroplast ribosome accumulation, we examined the levels of chloroplast ribosomal proteins and rRNA in *cdb1* and WT. Immunoblot analysis showed that the amount of 30S ribosomal protein RPS2, RPS4, and PSRP2 and 50S ribosomal subunits RPL1, RPL6, RPL10, RPL11, and RPL18 are barely detectable or greatly reduced in *cdb1* (Figure 4A). Chloroplast rRNAs are transcribed from a single transcription unit that includes the 16S, 23S, 4.5S, and 5S *rrn* genes (Figure 4B). The RNA precursors are then processed to produce mature 16S, 23S, 4.5S, and 5S rRNA (Figure 4B). RNA blotting revealed that the amounts of 1.5-kb 16S, 1.1 and 1.3-kb 23S, 0.1-kb 4.5S, and 0.12-kb

5S mature rRNAs are all drastically reduced (Figure 4C). These results indicate that accumulation of chloroplast ribosomes is impaired in *cdb1*, and explains why accumulation of the chloroplast-encoded proteins is reduced in *cdb1* (Figure 2). Taken together, we propose that CDB1 is essential for the assembly of chloroplast ribosomes.

Molecular Characterization of the CDB1 Protein

The CDB1 gene consists of six exons separated by five introns. It encodes a 427-amino acid protein with an unknown function. SMART search-based analysis¹ and the annotation of The Plant Proteome Database (PPDB)² suggest that CDB1 contains a putative cTP at its N-terminus (1–62 aa) and a predicated coiled-coil domain (135–168 aa; Figure 5A). No other assigned functional motif was found in CDB1.

¹<http://smart.embl-heidelberg.de/>

²<http://ppdb.tc.cornell.edu/>

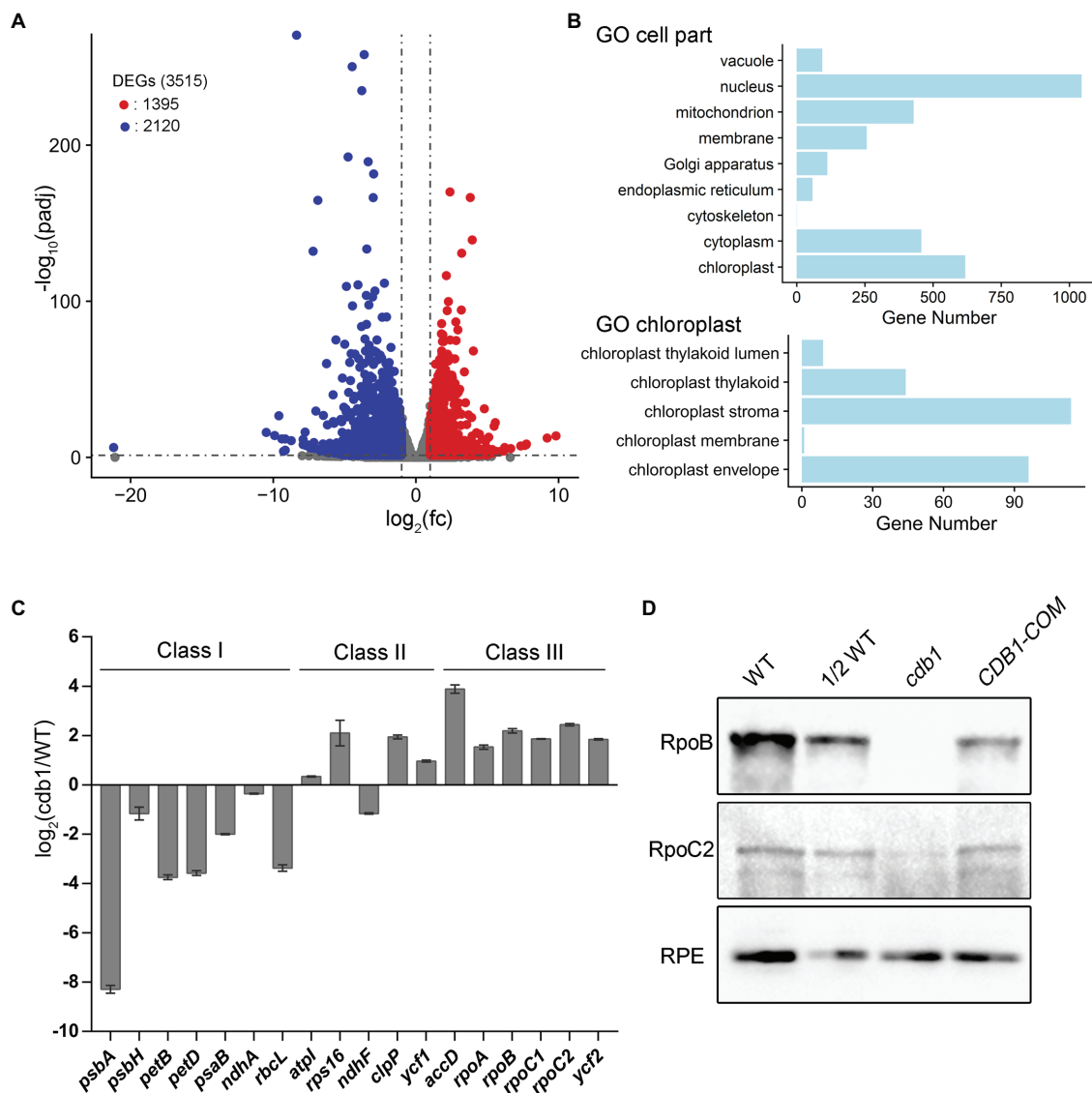


FIGURE 3 | Transcriptome analysis of WT and *cdB1* plants. **(A)** Volcano plot showing the differentially expressed genes (DEGs) in WT and *cdB1* [$p_{\text{adj}} < 0.05$, fold change (fc) > 2]. Total RNA was extracted from 4-week-old leaves of *cdB1* and WT. The constructed cDNA library was sequenced using Illumina HiSeq 2,500. DEGs were identified by DESeq2 according to the parameter of fold change > 2 and adjusted p value below 0.05. Volcano plot was generated by R package ggplot2. Down- and upregulated genes are indicated by blue and red dots, respectively. Three biological replicates of WT and *cdB1* were used for RNA-seq experiment. **(B)** Diagram showing gene numbers relative to “cell part” and “chloroplast” in Gene Ontology (GO) enrichment of DEGs in *cdB1* vs. WT. GO enrichment of DEGs was performed using clusterProfiler. **(C)** Plastid gene transcript levels. Differential expression of plastid genes in *cdB1* vs. WT is represented according to the RNA-seq data. The representative plastid genes include Class I genes (*psbA*, *psbH*, *petB*, *petD*, *psaB*, *ndhA*, and *rbcl*), Class II genes (*atpl*, *rps16*, *ndhF*, *clpP*, and *ycf1*), and Class III genes (*accD*, *rpoA*, *rpoB*, *rpoC1*, *rpoC2*, and *ycf2*). $\log_2[\text{fold change}(\text{cdB1/WT})] \pm \text{SD}$ values are from three biological replicates. **(D)** Immunoblot analysis of RpoB and RpoC2. Total protein isolated from 3-week-old WT, *cdB1* and CDB1-COM were hybridized with antibodies against RpoB and RpoC2. RPE was used as a loading control.

To determine the subcellular localization of CDB1, a construct containing 35S:CDB1-GFP was transformed into *Arabidopsis* protoplasts. Strong GFP signals were exclusively detected in chloroplasts with CDB1-GFP and they closely merged with chlorophyll autofluorescence (Figure 5B). Besides, the fluorescent signals of CDB1-GFP were similar to those from RbcS-GFP, the small subunit of ribulose-1, 5-bisphosphate carboxylase

(RbcS) fused to GFP (Figure 5B). These results indicate that CDB1 is a chloroplast protein, consistent with the presence of cTP at its N-terminus (Figure 5A). To investigate its precise localization, immunoblots were performed using chloroplast stroma and thylakoids isolated from WT and CDB1-HA complemented plants. The results show that CDB1 and HA-tagged CDB1 are localized in the chloroplast stroma (Figure 5C).

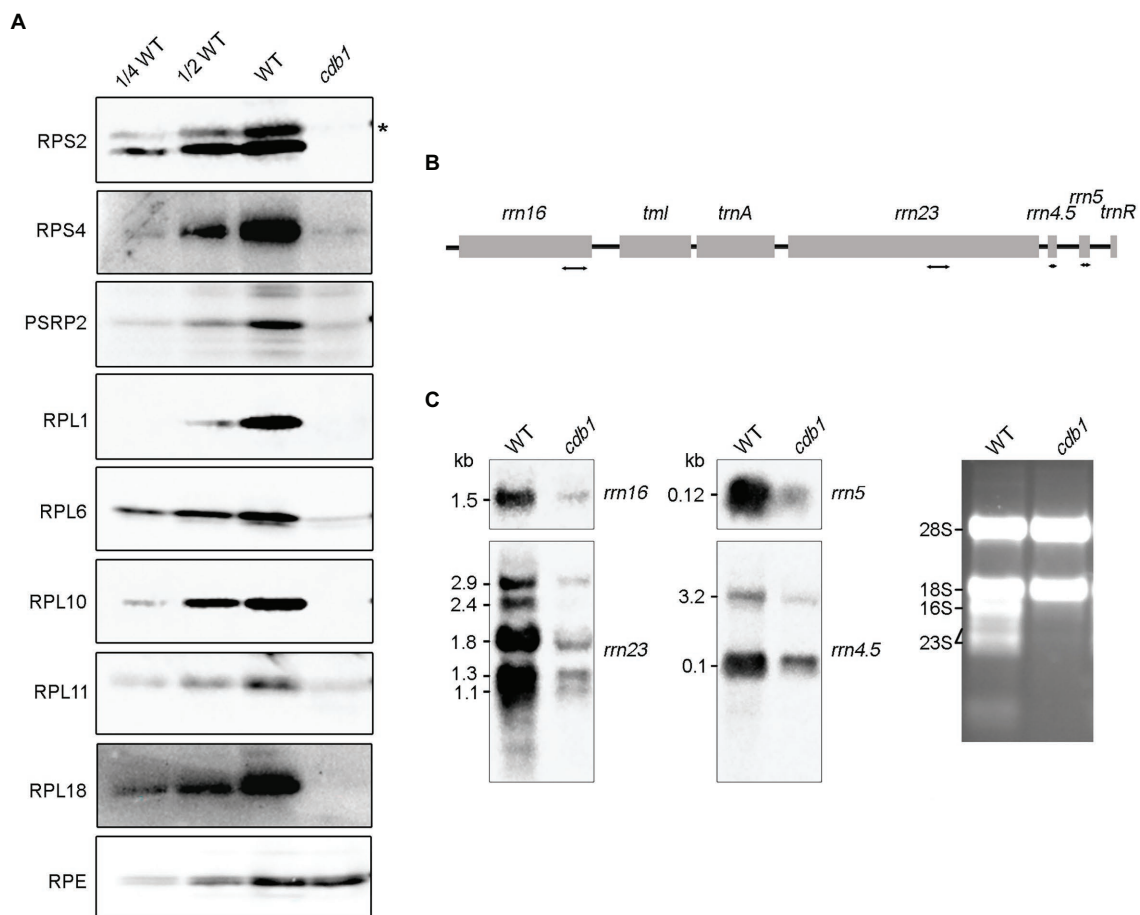


FIGURE 4 | Accumulation of chloroplast ribosomes in WT and *cdb1* plants. **(A)** Immunoblot analysis of representative 50S and 30S ribosomal subunit proteins. Total protein isolated from 3-week-old WT and *cdb1* plants was analyzed by immunoblotting with antibodies against RPS2, RPS4, PSRP2, RPL1, RPL6, RPL10, RPL11, and RPL18. RPE was used as a loading control. Black asterisk indicates the authentic protein. **(B)** Scheme of the chloroplast *rrn* operon with the four probes used for the RNA blots. The four probes for *rrn16*, *rrn23*, *rrn4.5*, and *rrn5* are marked by double-arrow lines under the chloroplast *rrn* operon. **(C)** Accumulation of rRNA in WT and *cdb1*. Total RNA from leaves of 3-week-old WT and *cdb1* was subjected to RNA blot analysis with specific probes against 16S, 23S, 4.5S, and 5S. Sizes of the distinct forms of the rRNA species are indicated on the left; rRNAs of WT and *cdb1* stained with ethidium bromide were used as loading control.

Evolution and Structural Analyses of CDB1 in Photosynthetic Viridiplantae

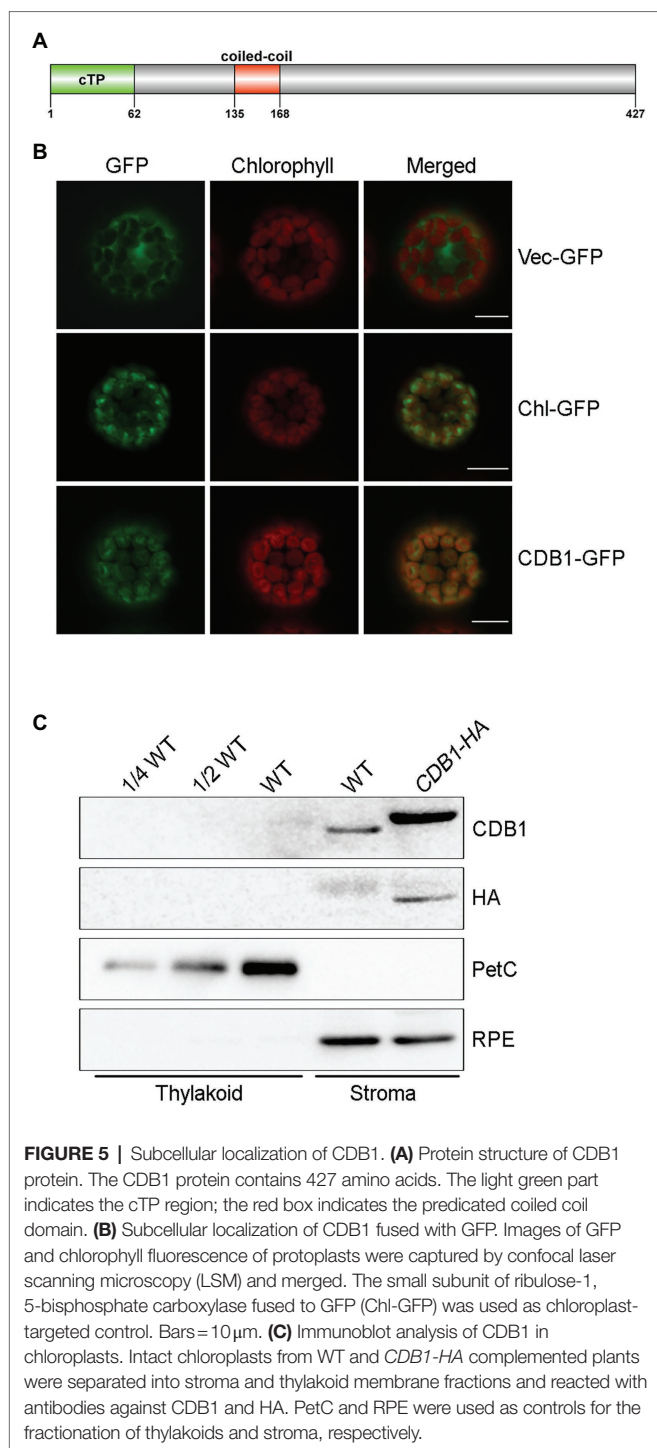
To explore the phylogenetic evolution of CDB1, its homologs were searched using BLAST-P against the NCBI database.³ Putative orthologs and paralogs were found in most photosynthetic eukaryotes (land plants and green algae) with a high conservation across the entire protein sequence except for the cTP region (Supplementary Figure 2). No homolog of CDB1 was found in cyanobacteria. A neighbor-joining phylogenetic tree for CDB1 homologs was constructed, containing 19 genes from 10 sequenced species representing green algae and land plants (Figure 6). Both green alga *Chlamydomonas reinhardtii* and the lycophyte *Selaginella moellendorffii* have one homolog of CDB1. A total of three homologous sequences

were found in the moss *Physcomitrella patens*. No homologs were found in gymnosperms probably due to the incomplete genome information. Interestingly, besides CDB1, a second CDB1-related protein, designated as CDB1L, was found from both monocot and dicot plants. The mature *Arabidopsis* CDB1 and CDB1L proteins share 41.5% amino acid sequence identity (Figure 7). These imply that CDB1 proteins originated from green alga and were resolved into two clades in angiosperms during evolution.

The elucidation of the function of CDB1 remains challenging because no homolog or similar domain was characterized in previous reports. To gain insights into this question, the three-dimensional structure of *Arabidopsis* CDB1 was predicted by AlphaFold2⁴ (Jumper et al., 2021; Figure 7A). The predicted structure of mature CDB1 contains two very short β -sheets

³<http://blast.ncbi.nlm.nih.gov>

⁴<https://www.alphafold.ebi.ac.uk/>



(β 1 and β 2) and a total of 17 helical structures, including 14 α -helices (α 3–17) and three 3_{10} -helices (Figures 7A,C). Based on the sequence identity to CDB1 homologs (Supplementary Figure 2), the evolutionary conservation scores were mapped onto the *Arabidopsis* CDB1 structure using the ConSurf server. The results show that the conserved residues in the CDB1 protein family are clustered in the secondary structure elements of mature *Arabidopsis* CDB1 (Figure 7B;

Supplementary Figure 2). This suggests that the members of the CDB1 protein family might have similar biological functions.

Functional Analysis of CDB1L in *Arabidopsis*

To investigate the functions of the *CDB1* paralog which was designated as *CDB1L* in *Arabidopsis*, the *cdb1l* (GK-844F05) mutant was obtained. Sequencing of PCR products showed that the T-DNA was inserted into the sixth exon of the *CDB1L* (Figure 8A). Because we were unable to obtain *cdb1l* homozygous mutants, we determined the segregation ratio of heterozygous to WT phenotype in the progeny of *cdb1l* heterozygous plants and found that it was close to 2:1 (Supplementary Table 2). Thus, it is likely that homozygous lethality occurs during embryo development of *cdb1l* homozygous seeds. To test this possibility, we examined the seeds in developing siliques from the *cdb1l* heterozygous plants. A deficiency in endosperm or embryo development of some seeds was detected in these plants (Figure 8B). Some of the affected seeds gave rise to intact seeds but they were pale and became withered at a later stage of development (Figure 8B). It is interesting that some seeds of the *cdb1* heterozygous plants also exhibit a pale color (Figure 8B). These seeds are likely to be the *cdb1* homozygous seeds defective in chloroplast biogenesis.

To confirm that the seed abortion phenotype was due to the disruption of *CDB1L*, we complemented the *cdb1l* heterozygous mutant with the full-length genomic *CDB1L* sequence driven by its authentic promoter. As shown in Figure 8B, the complemented plants (*CDB1L-COM*) produced well-developed seeds similar to WT, confirming that the aborted seeds in the *cdb1l* heterozygous mutants resulted from the disruption of *CDB1L*.

To determine the subcellular localization of CDB1L, a construct containing its coding region fused with GFP at the C-terminus was transformed into *Arabidopsis*. The CDB1L-GFP signal co-localized with chlorophyll (Figure 8C), suggesting that CDB1L is localized in chloroplasts. However, some of the CDB1L-GFP signals were also found outside chloroplasts and co-localized with mito-tracker red, indicating that CDB1L is also localized in mitochondria (Figure 8C). To further confirm the location of CDB1L, a specific antibody against CDB1L was raised to detect CDB1L accumulation in chloroplasts and mitochondria (Figures 8D,E; Supplementary Figure 3). The stroma and thylakoid fractions of chloroplasts isolated from WT leaves were used for immunoblot analysis. The results showed that CDB1L is localized in the chloroplast stroma (Figure 8D). These results are consistent with the localization of CDB1L-GFP (Figure 8C) and the detection of CDB1L in chloroplasts by mass spectrometry (The Plant Proteome Database).⁵

Analysis of proteins from purified mitochondria showed that CDB1L is also present in mitochondria. However, the molecular mass of mitochondrial-localized CDB1L is slightly less than that of chloroplast-localized CDB1L (Figure 8E). This might be due to the different length of the transit peptide in CDB1L, which is removed after entering into

⁵<http://ppdb.tc.cornell.edu/dbsearch/gene.aspx?id=3387>

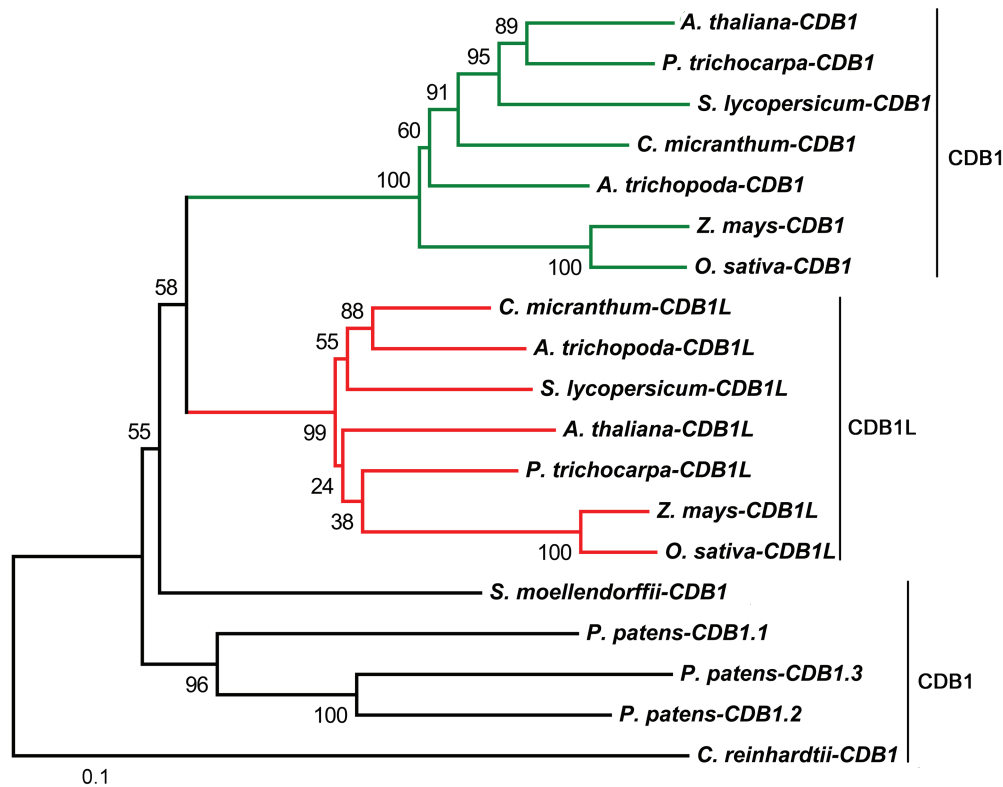


FIGURE 6 | Phylogenetic tree of CDB1 homologs. Nineteen proteins of the CDB1 family were selected to infer the evolutionary history using the Neighbor-Joining method, with bootstrap values (%) from 1,000 replicates. Numbers at branches are percentage of replicate trees in the bootstrap test. The scale bar indicates the units of the number of amino acid substitutions per site. All the analyses were conducted in MEGA6. Alignments of all 19 sequences based on identity/similarity and structural properties are shown in **Supplementary Figure 2**.

chloroplasts and mitochondria. No CDB1 signal was found in the mitochondrial samples (**Figure 8E**), indicating that CDB1 is not a mitochondrial protein but specifically localized in chloroplasts (**Figure 5**). In summary, these results indicate that the CDB1L protein has a dual localization in chloroplasts and mitochondria. Loss of CDB1L leads to a deficiency of seed development in *Arabidopsis*.

DISCUSSION

Chloroplast development is a programmed and complicated process regulated by numerous nuclear and chloroplast genes (Pogson and Albrecht, 2011). Previous studies have identified many nuclear factors that are involved in the regulatory mechanisms of chloroplast development. Here, we report the existence of a novel chloroplast stromal protein CDB1 that is essential for chloroplast development and biogenesis. Absence of CDB1 leads to an ivory seedling phenotype of *Arabidopsis* and the seedlings cannot survive autotrophically in the soil (**Figure 1**). Consistent with its ivory and chlorophyll fluorescence phenotype, the *cdb1* mutant is defective in the accumulation of thylakoid protein complexes and RuBisCO complex in the chloroplast stroma (**Figure 2**). These results

suggest that CDB1 is essential for chloroplast development and plant growth.

RNA-seq analysis revealed that plastid gene expression was dramatically altered in *cdb1* leaves (**Supplementary Figure 1**). Transcript levels of PEP-dependent genes were all decreased (Class I genes, including *psbA*, *psbH*, *petB*, *petD*, *psaB*, and *rbcL*); on the contrary, those of NEP-dependent genes were unchanged or even increased (Class III genes, including *rpoA*, *rpoB*, *rpoC1*, *rpoC2*, *clpP*, *ycf1*, and *ycf2*; **Figure 3C**). These results indicate that *cdb1* mutant is severely impaired in PEP activity. A similar molecular phenotype has been observed in mutants lacking PEP components or regulatory factors, such as *ptac2/ptac6/ptac12/ptac14* (Pfalz et al., 2006; Gao et al., 2012), *sig6* (Loschelder et al., 2006; Chi et al., 2010); PPR genes, such as *pdm2*, *pdm3*, and *pdm4* (Du et al., 2017; Zhang et al., 2017; Wang et al., 2020); and some other factors, such as *ys1* (Zhou et al., 2009), *clb19* (Chateigner-Boutin et al., 2008), and *dg1* (Chi et al., 2008). In contrast to these mutants, however, the *cdb1* mutant accumulates no RpoB and only a trace amount of RpoC2 (**Figure 3D**), indicating the impaired formation of the PEP complex. Because the expression levels of the genes encoding the core PEP subunits (*rpoA*, *rpoB*, *rpoC1*, and *rpoC2*) are highly increased in *cdb1* (**Figure 3C**;

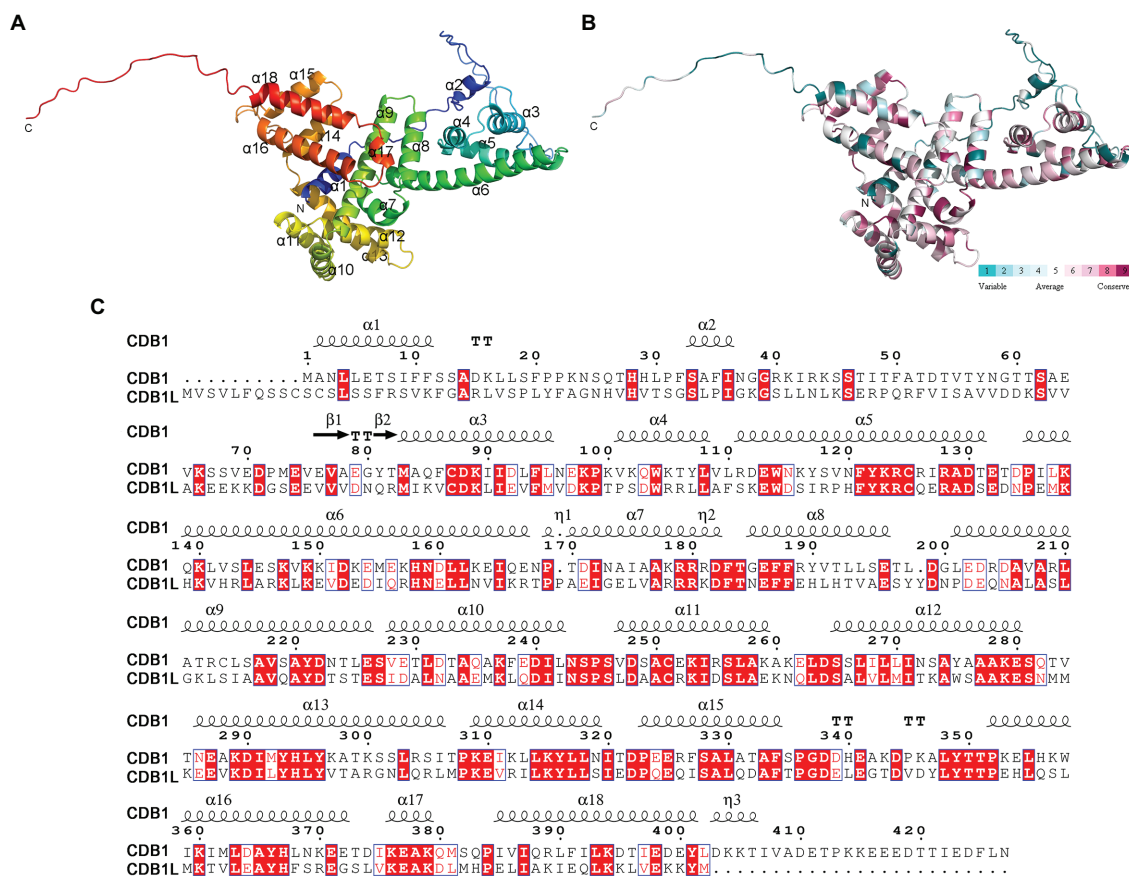


FIGURE 7 | Overall structure of CDB1. **(A)** Crystal structure of CDB1 predicted by AlphaFold2. The α -helices and N, C-terminus are indicated. **(B)** Surface conservation analysis of CDB1 using ConSurf web server. The cartoon structure of CDB1 was colored according to the conservation score from the 19 CDB1 family homologs. **(C)** Sequence alignment of CDB1 and CDB1L from *Arabidopsis*. Secondary structure elements above the alignment were generated using ESPript (<https://esprict.ibcp.fr>). Numbers indicate the original amino acid positions in CDB1. Highly conserved residues are represented by white letters with a red background.

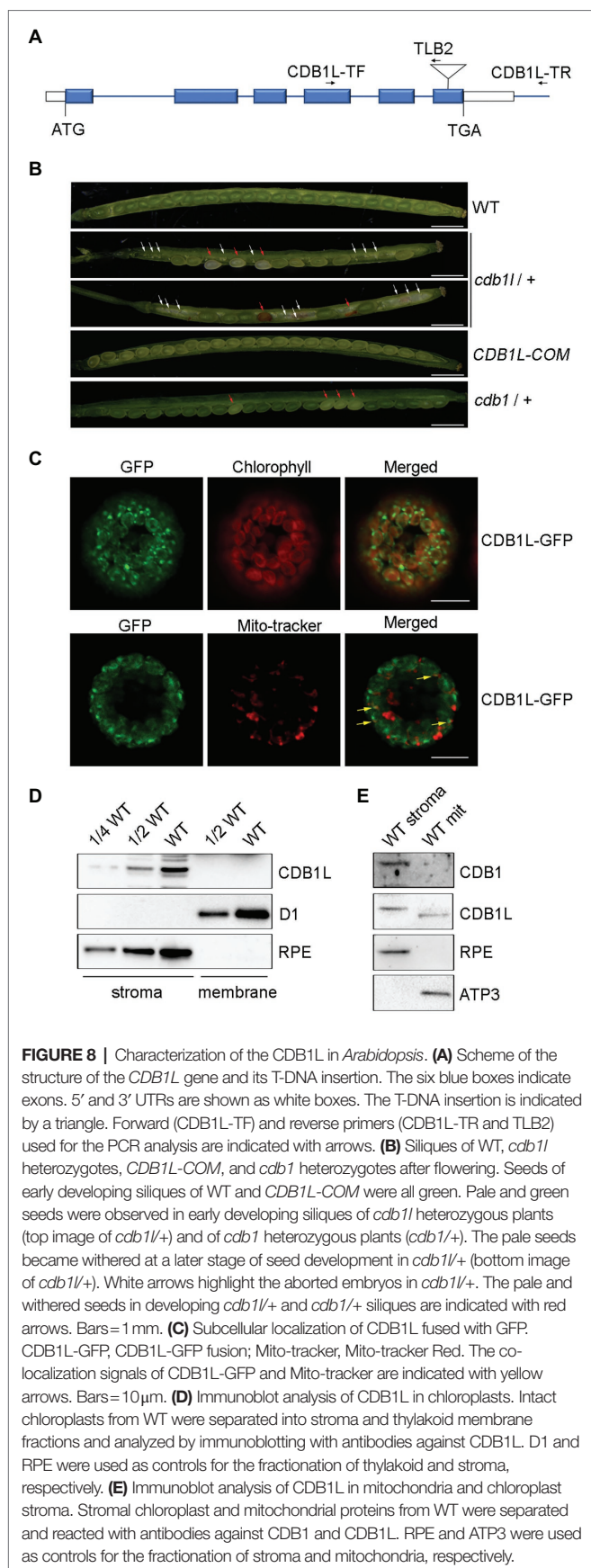
Supplementary Figure 1), it is likely that the translation of the PEP subunits or assembly of the PEP complex is impaired in the chloroplasts of *cdb1*.

Further immunoblot and RNA analysis showed that the accumulation of proteins of the 30S and 50S ribosomal subunits as well as ribosomal rRNAs (16S, 23S, 4.5S, and 5S) is dramatically decreased in *cdb1* (Figure 4). These results imply that chloroplast ribosomes cannot assemble in this mutant. This conclusion could also be confirmed by the analysis of the levels of chloroplast proteins. Plastid-encoded proteins (such as D1, D2, PetA, PsaA, CF₁ ϵ , and RbcL) and nucleus-encoded chloroplast proteins (such as PetC, PsaD, and CF₁ γ) which together with their plastid-encode partner proteins form stable complexes are absent or barely detectable in *cdb1* (Figure 2). In contrast, nucleus-encoded chloroplast proteins which do not assemble in complexes with other plastid-encoded proteins accumulate normally in the mutant (Figure 2). We therefore conclude that the absence of CDB1 compromises chloroplast ribosome assembly, which in turn affects the translation of plastid-encoded mRNAs, notably those of the PEP complex and

ultimately impairs chloroplast development during the early stages of seedling growth.

RNA-seq data revealed that almost all chloroplast ribosomal protein genes were upregulated in the *cdb1* mutant except *rps14*, a plastid gene encoding a 30S ribosomal subunit (Supplementary Figure 1). The level of *rps14* transcript in *cdb1* was reduced to ~1/4 of wild type (Supplementary Figure 1). However, this moderate reduction in *rps14* mRNA is unlikely to be the direct reason for the severe deficiency in accumulation of chloroplast ribosomes. Previous studies demonstrated that RPS14 could also be transcribed to some extent in PEP-deficient mutants (Legen et al., 2002), and reduction of *rps14* transcript can be explained by the absence of the PEP complex. Hence, we propose that CDB1 participates in chloroplast ribosome biogenesis. It may function as a molecular chaperone to assist chloroplast ribosome assembly or maintain the structural stability of ribosomes during their biogenesis. It is also possible that CDB1 is involved in the maturation of the chloroplast rRNAs.

Phylogenetic analysis revealed that the CDB1 paralog CDB1L is present in angiosperms (Figure 6). Knockout of CDB1L



results in embryo abortion (**Figure 8B**). Subcellular localization indicated that CDB1L is dually localized in chloroplasts and mitochondria (**Figures 8C–E**). The sequence and structural similarity of CDB1L and CDB1 indicates that mitochondria-localized CDB1L may perform a similar function during mitochondrial ribosome biogenesis. Previous reports have confirmed that loss of mitochondrial function usually results in arrested embryo development as observed in mutants deficient in Atp11 and Atp12 that are essential for mitochondrial ATP synthase assembly (Duan et al., 2020) and in AARS proteins that are required for translation in mitochondria (Berg et al., 2005). In *cdb11* heterozygous plants, some of the seeds can mature but they have a pale color (**Figure 8B**). Similar seeds were also found in the *cdb1* heterozygous plants (**Figure 8B**), as well as in the *pmd1*, *pmd2*, *pmd3*, and *pmd4* mutants, in which chloroplast PEP activity is impaired and chloroplast development and biogenesis is arrested (Pyo et al., 2013; Du et al., 2017; Zhang et al., 2017; Wang et al., 2020). These observations suggest that chloroplast development is affected in the pale seeds of *cdb1* and *cdb11* heterozygous plants. It is possible that chloroplast-localized CDB1L plays an essential role during chloroplast biogenesis and this function cannot be complemented by its CDB1 paralog.

Phylogenetic tree analysis showed that CDB1 homologs can be found in most photosynthetic eukaryotes from green algae to land plants (**Figure 6**). The conserved residues in the CDB1 family proteins could be clustered to the secondary structure elements of the CDB1 protein structure predicted by AlphaFold2 (**Supplementary Figure 2**), suggesting that the CDB1 family proteins might have similar biological functions. Interestingly, homologs in angiosperms were further resolved into two clades, containing CDB1 and CDB1L, respectively. The phylogenetic tree showed that CDB1 proteins from lower photosynthetic Viridiplantae are closer to CDB1L than to CDB1 in angiosperms (**Figure 6**). This suggests that CDB1L proteins originated from green alga and that the CDB1 proteins in monocot and dicot plants probably evolved through gene duplication during the emergence of angiosperms, where they have assumed new functions in chloroplast ribosome biogenesis. The dual-localized CDB1L proteins in angiosperms may have a similar role as CDB1 from lower photosynthetic Viridiplantae, and operate both in chloroplasts and mitochondria.

DATA AVAILABILITY STATEMENT

The original contributions presented in the study are publicly available. This data can be found here: National Center for Biotechnology Information (NCBI) BioProject database under accession number PRJNA781386.

AUTHOR CONTRIBUTIONS

QX conceived the study and designed experiments and produced the figures. WC, JH, and SC performed experiments. WC, JH, SC, LZ, J-DR, LP, and QX analyzed the data. QX, J-DR, and

LP wrote the manuscript. QX and LP supervised the whole study. All authors contributed to the article and approved the submitted version.

FUNDING

This work was supported by the fund of Shanghai Engineering Research Center of Plant Germplasm Resources (17DZ2252700).

ACKNOWLEDGMENTS

We thank the Nottingham *Arabidopsis* Stock Center (NASC) for providing the mutant seeds.

SUPPLEMENTARY MATERIAL

The Supplementary Material for this article can be found online at: <https://www.frontiersin.org/articles/10.3389/fpls.2022.815859/full#supplementary-material>

REFERENCES

- Bang, W. Y., Chen, J., Jeong, I. S., Kim, S. W., Kim, C. W., Jung, H. S., et al. (2012). Functional characterization of OgcC in ribosome biogenesis during chloroplast development. *Plant J.* 71, 122–134. doi: 10.1111/j.1365-313X.2012.04976.x
- Berg, M., Rogers, R., Muralla, R., and Meinke, D. (2005). Requirement of aminoacyl-tRNA synthetases for gametogenesis and embryo development in *Arabidopsis*. *Plant J.* 44, 866–878. doi: 10.1111/j.1365-313X.2005.02580.x
- Bollenbach, T. J., Lange, H., Gutierrez, R., Erhardt, M., Stern, D. B., and Gagliardi, D. (2005). RNR1, a 3'-5' exoribonuclease belonging to the RNR superfamily, catalyzes 3' maturation of chloroplast ribosomal RNAs in *Arabidopsis thaliana*. *Nucleic Acids Res.* 33, 2751–2763. doi: 10.1093/nar/gki576
- Börner, T., Aleynikova, A. Y., Zubo, Y. O., and Kusnetsov, V. V. (2015). Chloroplast RNA polymerases: role in chloroplast biogenesis. *BBA-Bioenergetics* 1847, 761–769. doi: 10.1016/j.bbabi.2015.02.004
- Chateigner-Boutin, A.-L., Ramos-Vega, M., Guevara-García, A., Andrés, C., De La Luz Gutiérrez-Nava, M., Cantero, A., et al. (2008). CLB19, a pentatricopeptide repeat protein required for editing of *rpoA* and *clpP* chloroplast transcripts. *Plant J.* 56, 590–602. doi: 10.1111/j.1365-313X.2008.03634.x
- Chen, S., Zhou, Y., Chen, Y., and Gu, J. (2018). Fastp: an ultra-fast all-in-one FASTQ preprocessor. *Bioinformatics* 34, i884–i890. doi: 10.1093/bioinformatics/bty560
- Chi, W., He, B., Mao, J., Li, Q., Ma, J., Ji, D., et al. (2012). The function of RH22, a DEAD RNA helicase, in the biogenesis of the 50S ribosomal subunits of *Arabidopsis* chloroplasts. *Plant Physiol.* 158, 693–707. doi: 10.1104/pp.111.186775
- Chi, W., Ma, J., Zhang, D., Guo, J., Chen, F., Lu, C., et al. (2008). The pentatricopeptide repeat protein DELAYED GREENING1 is involved in the regulation of early chloroplast development and chloroplast gene expression in *Arabidopsis*. *Plant Physiol.* 147, 573–584. doi: 10.1104/pp.108.116194
- Chi, W., Mao, J., Li, Q., Ji, D., Zou, M., Lu, C., et al. (2010). Interaction of the pentatricopeptide-repeat protein DELAYED GREENING 1 with sigma factor SIG6 in the regulation of chloroplast gene expression in *Arabidopsis* cotyledons. *Plant J.* 64, 14–25. doi: 10.1111/j.1365-313X.2010.04304.x
- Clough, S. J., and Bent, A. F. (1998). Floral dip: a simplified method for agrobacterium-mediated transformation of *Arabidopsis thaliana*. *Plant J.* 16, 735–743. doi: 10.1046/j.1365-313x.1998.00343.x
- Dobrogojski, J., Adamiec, M., and Luciński, R. (2020). The chloroplast genome: a review. *Acta Physiol. Plant* 42:98. doi: 10.1007/s11738-020-03089-x
- Du, L., Zhang, J., Qu, S., Zhao, Y., Su, B., Lv, X., et al. (2017). The pentatricopeptide repeat protein pigment-defective Mutant2 is involved in the regulation of chloroplast development and chloroplast gene expression in *Arabidopsis*. *Plant Cell Physiol.* 58, 747–759. doi: 10.1093/pcp/pcx004
- Duan, Z., Li, K., Zhang, L., Che, L., Lu, L., Rochaix, J.-D., et al. (2020). F-type ATP synthase assembly factors Atp11 and Atp12 in *Arabidopsis*. *Front. Plant Sci.* 11:522753. doi: 10.3389/fpls.2020.522753
- Friso, G., Giacomelli, L., Ytterberg, A. J., Peltier, J.-B., Rudella, A., Sun, Q., et al. (2004). In-depth analysis of the thylakoid membrane proteome of *Arabidopsis thaliana* chloroplasts: new proteins, new functions, and a plastid proteome database. *Plant Cell* 16, 478–499. doi: 10.1105/tpc.017814
- Gao, Z. P., Chen, G. X., and Yang, Z. N. (2012). Regulatory role of *Arabidopsis* pTAC14 in chloroplast development and plastid gene expression. *Plant Signal. Behav.* 7, 1354–1356. doi: 10.4161/psb.21618
- Graf, M., Arenz, S., Huter, P., Dönhöfer, A., Nováček, J., and Wilson, D. N. (2016). Cryo-EM structure of the spinach chloroplast ribosome reveals the location of plastid-specific ribosomal proteins and extensions. *Nucleic Acids Res.* 45, gkw1272–gkw2896. doi: 10.1093/nar/gkw1272
- Heazlewood, J. L., Verboom, R. E., Tonti-Filippini, J., Small, I., and Millar, A. H. (2006). SUBA: the *Arabidopsis* subcellular database. *Nucleic Acids Res.* 35, D213–D218. doi: 10.1093/nar/gkl863
- Jumper, J., Evans, R., Pritzel, A., Green, T., Figurnov, M., Ronneberger, O., et al. (2021). Highly accurate protein structure prediction with AlphaFold. *Nature* 596, 583–589. doi: 10.1038/s41586-021-03819-2
- Kim, D., Paggi, J. M., Park, C., Bennett, C., and Salzberg, S. L. (2019). Graph-based genome alignment and genotyping with HISAT2 and HISAT-genotype. *Nat. Biotechnol.* 37, 907–915. doi: 10.1038/s41587-019-0201-4
- Legen, J., Kemp, S., Krause, K., Profanter, B., Herrmann, R. G., and Maier, R. M. (2002). Comparative analysis of plastid transcription profiles of entire plastid chromosomes from tobacco attributed to wild-type and PEP-deficient transcription machineries. *Plant J.* 31, 171–188. doi: 10.1046/j.1365-313X.2002.01349.x
- Li, H., Handsaker, B., Wysoker, A., Fennell, T., Ruan, J., Homer, N., et al. (2009). The sequence alignment/map format and SAMtools. *Bioinformatics* 25, 2078–2079. doi: 10.1093/bioinformatics/btp352
- Liao, Y., Smyth, G. K., and Shi, W. (2019). The R package Rsubread is easier, faster, cheaper and better for alignment and quantification of RNA sequencing reads. *Nucleic Acids Res.* 47:e47. doi: 10.1093/nar/gkz114

Supplementary Figure 1 | Transcript levels of all sequenced plastid genes. Differential expression of plastid-encoded genes in *cdb1* vs. WT is represented according to the RNA-seq data. The $\log_2[\text{fold change}(\text{cdb1}/\text{WT})] \pm \text{SD}$ values are from the three biological replicates.

Supplementary Figure 2 | Sequences of CDB1 family proteins from *Arabidopsis thaliana* (CDB1: AT4G37920; CDB1L: AT1G36320), *Populus trichocarpa* (CDB1: XP_024461654.1; CDB1L: XP_024450195.1), *Solanum lycopersicum* (CDB1: XP_004231977.1; CDB1L: XP_004237860.1), *Cinnamomum micranthum f. kanehirae* (CDB1: RWR82510.1; CDB1L: RWR94545.1), *Amborella trichopoda* (CDB1: XP_006856624.2; CDB1L: XP_020521452.1), *Zea mays* (CDB1: NP_001144269.1; CDB1L: NP_001358639.1), *Oryza sativa Japonica* (CDB1: XP_015623683.1; CDB1L: XP_015622979.1), *Physcomitrella patens* (CDB1.1: XP_024388931.1; CDB1.2: XP_024392048.1; and CDB1.3: XP_024372527.1), *Selaginella moellendorffii* (CDB1: XP_002962701.2), and *Chlamydomonas reinhardtii* (CDB1: PNW69832.1). Secondary structure elements above the alignment were generated by ESPript (<https://esprict.ibcp.fr>). Numbers indicate the original amino acid positions in CDB1. Highly conserved residues are represented in white letters with red background.

Supplementary Figure 3 | Test of CDB1 and CDB1L antibodies. Mature CDB1 (corresponding to amino acids 63–427 of CDB1) and CDB1L (corresponding to amino acids 13–414 of CDB1L) were used to raise antibodies in rabbits. Recombinant protein of CDB1 and CDB1L (8ng) was separated by SDS-PAGE and detected with antibodies against CDB1 (left) and CDB1L (right), respectively. Recombinant proteins with predicted molecular mass are indicated with arrows.

- Liere, K., Weihe, A., and Börner, T. (2011). The transcription machineries of plant mitochondria and chloroplasts: composition, function, and regulation. *J. Plant Physiol.* 168, 1345–1360. doi: 10.1016/j.jplph.2011.01.005
- Loschelder, H., Schweer, J., Link, B., and Link, G. (2006). Dual temporal role of plastid sigma factor 6 in *Arabidopsis* development. *Plant Physiol.* 142, 642–650. doi: 10.1104/pp.106.085878
- Love, M. I., Huber, W., and Anders, S. (2014). Moderated estimation of fold change and dispersion for RNA-seq data with DESeq2. *Genome Biol.* 15:550. doi: 10.1186/s13059-014-0550-8
- Manuell, A. L., Quispe, J., and Mayfield, S. P. (2007). Structure of the chloroplast ribosome: novel domains for translation regulation. *PLoS Biol.* 5:e209. doi: 10.1371/journal.pbio.0050209
- Naver, H., Boudreau, E., and Rochaix, J.-D. (2001). Functional studies of Ycf3: its role in assembly of photosystem I and interactions with some of its subunits. *Plant Cell* 13, 2731–2745. doi: 10.1105/tpc.010253
- Nishimura, K., Ashida, H., Ogawa, T., and Yokota, A. (2010). A DEAD box protein is required for formation of a hidden break in *Arabidopsis* chloroplast 23S rRNA. *Plant J.* 63, 766–777. doi: 10.1111/j.1365-313X.2010.04276.x
- Peng, L., Ma, J., Chi, W., Guo, J., Zhu, S., Lu, Q., et al. (2006). LOW PSII ACCUMULATION1 is involved in efficient assembly of photosystem II in *Arabidopsis thaliana*. *Plant Cell* 18, 955–969. doi: 10.1105/tpc.105.037689
- Perez Boerema, A., Aibara, S., Paul, B., Tobiasson, V., Kimanius, D., Forsberg, B. O., et al. (2018). Structure of the chloroplast ribosome with chl-RRF and hibernation-promoting factor. *Nat. Plants* 4, 212–217. doi: 10.1038/s41477-018-0129-6
- Pfalz, J., Liere, K., Kandlbinder, A., Dietz, K.-J., and Oelmüller, R. (2006). pTAC2, –6, and –12 are components of the transcriptionally active plastid chromosome that are required for plastid gene expression. *Plant Cell* 18, 176–197. doi: 10.1105/tpc.105.036392
- Pfalz, J., and Pfannschmidt, T. (2013). Essential nucleoid proteins in early chloroplast development. *Trends Plant Sci.* 18, 186–194. doi: 10.1016/j.tplants.2012.11.003
- Pogson, B. J., and Albrecht, V. (2011). Genetic dissection of chloroplast biogenesis and development: an overview. *Plant Physiol.* 155, 1545–1551. doi: 10.1104/pp.110.170365
- Pyo, Y. J., Kwon, K.-C., Kim, A., and Cho, M. H. (2013). Seedling Lethal1, a pentatricopeptide repeat protein lacking an E/E+ or DYW domain in *Arabidopsis*, is involved in plastid gene expression and early chloroplast development. *Plant Physiol.* 163, 1844–1858. doi: 10.1104/pp.113.227199
- Reiter, B., Vamvaka, E., Marino, G., Kleine, T., Jahns, P., Bolle, C., et al. (2020). The *Arabidopsis* protein CGL20 is required for plastid 50S ribosome biogenesis. *Plant Physiol.* 182, 1222–1238. doi: 10.1104/pp.19.01502
- Sakamoto, W., Miyagishima, S.-Y., and Jarvis, P. (2008). Chloroplast biogenesis: control of plastid development, protein import, division and inheritance. *Arabidopsis Book* 6:e0110. doi: 10.1199/tab.0110
- Schein, A., Sheffy-Levin, S., Glaser, F., and Schuster, G. (2008). The RNase E/G-type endoribonuclease of higher plants is located in the chloroplast and cleaves RNA similarly to the *E. coli* enzyme. *RNA* 14, 1057–1068. doi: 10.1261/rna.907608
- Shajani, Z., Sykes, M. T., and Williamson, J. R. (2011). Assembly of bacterial ribosomes. *Annu. Rev. Biochem.* 80, 501–526. doi: 10.1146/annurev-biochem-062608-160432
- Sharma, M. R., Dönhöfer, A., Barat, C., Marquez, V., Datta, P. P., Fucini, P., et al. (2010). PSRP1 is not a ribosomal protein, but a ribosome-binding factor that is recycled by the ribosome-recycling factor (RRF) and elongation factor G (EF-G) 2. *J. Biol. Chem.* 285, 4006–4014. doi: 10.1074/jbc.M109.062299
- Sharma, M. R., Wilson, D. N., Datta, P. P., Barat, C., Schlutzen, F., Fucini, P., et al. (2007). Cryo-EM study of the spinach chloroplast ribosome reveals the structural and functional roles of plastid-specific ribosomal proteins. *Proc. Natl. Acad. Sci. U. S. A.* 104, 19315–19320. doi: 10.1073/pnas.0709856104
- Shiina, T., Tsunoyama, Y., Nakahira, Y., and Khan, M. S. (2005). Plastid RNA polymerases, promoters, and transcription regulators in higher plants. *Int. Rev. Cytol.* 244, 1–68. doi: 10.1016/S0074-7696(05)44001-2
- Steiner, S., Schröter, Y., Pfalz, J., and Pfannschmidt, T. (2011). Identification of essential subunits in the plastid-encoded RNA polymerase complex reveals building blocks for proper plastid development. *Plant Physiol.* 157, 1043–1055. doi: 10.1104/pp.111.184515
- Sweetlove, L. J., Taylor, N. L., and Leaver, C. J. (2007). Isolation of intact, functional mitochondria from the model plant *Arabidopsis thaliana*. *Methods Mol. Biol.* 372, 125–136. doi: 10.1007/978-1-59745-365-3_9
- Swiatecka-Hagenbruch, M., Liere, K., and Börner, T. (2007). High diversity of plastidial promoters in *Arabidopsis thaliana*. *Mol. Gen. Genomics* 277, 725–734. doi: 10.1007/s00438-007-0222-4
- Tamura, K., Stecher, G., Peterson, D., Filipowski, A., and Kumar, S. (2013). MEGA6: molecular evolutionary genetics analysis version 6.0. *Mol. Biol. Evol.* 30, 2725–2729. doi: 10.1093/molbev/mst197
- Tiller, N., Weingartner, M., Thiele, W., Maximova, E., Schöttler, M. A., and Bock, R. (2012). The plastid-specific ribosomal proteins of *Arabidopsis thaliana* can be divided into non-essential proteins and genuine ribosomal proteins. *Plant J.* 69, 302–316. doi: 10.1111/j.1365-313X.2011.04791.x
- Walter, M., Piepenburg, K., Schöttler, M. A., Petersen, K., Kahlau, S., Tiller, N., et al. (2010). Knockout of the plastid RNase E leads to defective RNA processing and chloroplast ribosome deficiency. *Plant J.* 64, 851–863. doi: 10.1111/j.1365-313X.2010.04377.x
- Wang, X., Zhao, L., Man, Y., Li, X., Wang, L., and Xiao, J. (2020). PDM4, a pentatricopeptide repeat protein, affects chloroplast gene expression and chloroplast development in *Arabidopsis thaliana*. *Front. Plant Sci.* 11:1198. doi: 10.3389/fpls.2020.01198
- Weis, B. L., Kovacevic, J., Missbach, S., and Schleiff, E. (2015). Plant-specific features of ribosome biogenesis. *Trends Plant Sci.* 20, 729–740. doi: 10.1016/j.tplants.2015.07.003
- Wu, T., Hu, E., Xu, S., Chen, M., Guo, P., Dai, Z., et al. (2021). clusterProfiler 4.0: A universal enrichment tool for interpreting omics data. *Innovations* 2:100141. doi: 10.1016/j.xinn.2021.100141
- Yang, J., Suzuki, M., and McCarty, D. R. (2016). Essential role of conserved DUF177A protein in plastid 23S rRNA accumulation and plant embryogenesis. *J. Exp. Bot.* 67, 5447–5460. doi: 10.1093/jxb/erw311
- Zhang, L., Pu, H., Duan, Z., Li, Y., Liu, B., Zhang, Q., et al. (2018). Nucleus-encoded protein BFA1 promotes efficient assembly of the chloroplast ATP synthase coupling factor 1. *Plant Cell* 30, 1770–1788. doi: 10.1105/tpc.18.00075
- Zhang, J., Xiao, J., Li, Y., Su, B., Xu, H., Shan, X., et al. (2017). PDM3, a pentatricopeptide repeat-containing protein, affects chloroplast development. *J. Exp. Bot.* 68, 5615–5627. doi: 10.1093/jxb/erx360
- Zhou, W., Cheng, Y., Yap, A., Chateigner-Boutin, A.-L., Delannoy, E., Hammani, K., et al. (2009). The *Arabidopsis* gene YS1 encoding a DYW protein is required for editing of *rpoB* transcripts and the rapid development of chloroplasts during early growth. *Plant J.* 58, 82–96. doi: 10.1111/j.1365-313X.2008.03766.x

Conflict of Interest: The authors declare that the research was conducted in the absence of any commercial or financial relationships that could be construed as a potential conflict of interest.

Publisher's Note: All claims expressed in this article are solely those of the authors and do not necessarily represent those of their affiliated organizations, or those of the publisher, the editors and the reviewers. Any product that may be evaluated in this article, or claim that may be made by its manufacturer, is not guaranteed or endorsed by the publisher.

Copyright © 2022 Chen, Huang, Chen, Zhang, Rochaix, Peng and Xin. This is an open-access article distributed under the terms of the Creative Commons Attribution License (CC BY). The use, distribution or reproduction in other forums is permitted, provided the original author(s) and the copyright owner(s) are credited and that the original publication in this journal is cited, in accordance with accepted academic practice. No use, distribution or reproduction is permitted which does not comply with these terms.



Rubredoxin 1 Is Required for Formation of the Functional Photosystem II Core Complex in *Arabidopsis thaliana*

Liping Che^{1†}, Han Meng^{2†}, Junxiang Ruan¹, Lianwei Peng² and Lin Zhang^{2*}

¹ School of Environmental and Geographical Sciences, Shanghai Normal University, Shanghai, China, ² Shanghai Key Laboratory of Plant Molecular Sciences, College of Life Sciences, Shanghai Normal University, Shanghai, China

OPEN ACCESS

Edited by:

Alistair McCormick,
University of Edinburgh,
United Kingdom

Reviewed by:

Julian Eaton-Rye,
University of Otago, New Zealand
Josef Komenda,
Academy of Sciences of the Czech
Republic (ASCR), Czechia

*Correspondence:

Lin Zhang
zhanglin2017@shnu.edu.cn

[†] These authors have contributed
equally to this work and share first
authorship

Specialty section:

This article was submitted to
Plant Physiology,
a section of the journal
Frontiers in Plant Science

Received: 29 November 2021

Accepted: 13 January 2022

Published: 23 February 2022

Citation:

Che L, Meng H, Ruan J, Peng L
and Zhang L (2022) Rubredoxin 1 Is
Required for Formation of the
Functional Photosystem II Core
Complex in *Arabidopsis thaliana*.
Front. Plant Sci. 13:824358.
doi: 10.3389/fpls.2022.824358

Chloroplast thylakoid protein rubredoxin 1 (RBD1) in *Chlamydomonas* and its cyanobacterial homolog RubA contain a rubredoxin domain. These proteins have been proposed to participate in the assembly of photosystem II (PSII) at early stages. However, the effects of inactivation of RBD1 on PSII assembly in higher plants are largely unclear. Here, we characterized an *Arabidopsis rbd1* mutant in detail. A drastic reduction of intact PSII complex but relatively higher levels of assembly intermediates including PSII RC, pre-CP47, and pre-CP43 were found in *rbd1*. Polysome association and ribosome profiling revealed that ribosome recruitment of *psbA* mRNA is specifically reduced. Consistently, *in vivo* protein pulse-chase labeling showed that the rate of D1/pD1 synthesis is significantly reduced in *rbd1* compared with WT. Moreover, newly synthesized mature D1 and pD1/D2 can assemble into the PSII reaction center (RC) complex but further formation of larger PSII complexes is nearly totally blocked in *rbd1*. Our data imply that RBD1 is not only required for the formation of a functional PSII core complex during the early stages of PSII assembly but may also be involved in the translation of D1 in higher plants.

Keywords: rubredoxin, photosystem II, reaction center, *psbA*, ribosome profiling, *Arabidopsis thaliana*

INTRODUCTION

Photosystem II (PSII) is the primary pigment-protein complex in the photosynthetic electron transport chain in oxygenic organisms. PSII harvests light energy to split water resulting in the release of oxygen and electrons that are transferred from water to plastoquinone in cyanobacteria, algae, and plants. PSII drives oxygenic photosynthesis together with PSI (Photosystem I), Cyt *b₆f* (Cytochrome *b₆f*), and ATP synthase, and provides energy and oxygen for most living organisms on earth (Nelson and Junge, 2015; Shen, 2015). In higher plants, PSII is composed of the PSII reaction center (RC), CP43 and CP47, the oxygen-evolving complex (OEC), and LHClI as well as several small subunits with a low molecular mass. PSII RC is the minimum unit for the primary photochemical reaction and is composed of the subunits D1, D2, PsbI, and two subunits of cytochrome *b₅₅₉* (PsbE and PsbF) (Nelson and Yocum, 2006). The D1 and D2 proteins form a heterodimer and bind the basal redox components required for PSII electron transport such as P680, pheophytin, non-heme iron and quinone (Umena et al., 2011). CP43 and CP47 are peripheral core antenna subunits attached to the PSII RC. They function in energy transfer from

light harvesting complex (LHCII) to the PSII reaction center. As the catalytic site for water splitting, OEC is composed of one Ca atom, four Mn atoms, and five oxygen atoms (Mn_4CaO_5 cluster). Seven amino acid residues from D1 and CP43 provide ligands to OEC (Umena et al., 2011; Shen, 2015). PsbO, PsbP, and PsbQ are attached to the lumen side of PSII. Together with CP43, these proteins provide protection and contribute to access channels for substrate and products during water oxidation. LHCII proteins bind to PSII forming the PSII-LHCII complex which in turn forms PSII-LHCII supercomplexes in the thylakoid membrane.

Assembly of PSII in chloroplasts occurs in a stepwise manner (Baena-González and Aro, 2002; Rokka et al., 2005; Mulo et al., 2008; Nixon et al., 2010; Komenda et al., 2012; Lyska et al., 2013; Nickelsen and Rengstl, 2013). First, the precursor of D1 (pD1) is co-translationally assembled into the D2-Cyt b_{559} receptor complex to form the PSII RC with the PsbI subunit. The C-terminal 9–13 residues of pD1 are subsequently removed by the CtpA enzyme to form functional D1 protein (Che et al., 2013). Second, CP47 is integrated into the RC to form the CP47-RC complex. The chloroplast-encoded proteins PsbH, PsbM, PsbTc, and the nucleus-encoded protein PsbR are assembled into the CP47-RC complex to form CP43-less PSII. In the next step, CP43 and other subunits are integrated to form the PSII monomer. Finally, the PsbO, PsbP, and PsbQ subunits associate with the PSII monomer and form supercomplexes with LHCII eventually with the help of PsbJ and PsbZ (Rokka et al., 2005).

More than a dozen PSII assembly factors are required for the PSII assembly at various steps in higher plants. For the biogenesis of the PSII RC complex, several facilitating factors are involved in particular steps such as *psbA* translation, pD1 processing, and assembly of the complex. HCF173 is a protein weakly related to short-chain dehydrogenases/reductases. It forms a high molecular weight complex that both facilitates translational initiation of D1 and stabilizes the *psbA* mRNA (Schult et al., 2007). After translation, the nine residue C-terminal tail of pD1 is cleaved by the lumen-localized C-terminal processing protease CtpA (Che et al., 2013). Two One-Helix-Proteins OHP1 and OHP2 as well as the HCF244 protein form a complex essential for the formation of the PSII RC complex. Formation of the OHP1/OHP2/HCF244 complex is likely required for the efficient recruitment of ribosomes with *psbA* mRNA encoding D1 and also for the delivery of chlorophyll and/or other cofactors to the D1/D2 heterodimer (Beck et al., 2017; Hey and Grimm, 2018; Li et al., 2018; Myouga et al., 2018; Chotewutmontri et al., 2020). In addition, thylakoid lumen protein HCF136 is essential for PSII RC formation (Meurer et al., 1998; Plücker et al., 2002). YCF48, the ortholog of HCF136 in cyanobacteria and red algae, is a seven-bladed beta-propeller that promotes efficient incorporation of D1 into the PSII RC complex by interacting with newly synthesized pD1 on the thylakoid lumen side (Komenda et al., 2008; Yu et al., 2018). Chloroplast-encoded PsbN is not a PSII subunit but rather acts as a molecular chaperone required in the early phase of PSII RC formation (Torabi et al., 2014).

Rubredoxins are iron-containing proteins in which one iron atom is coordinated by four cysteine residues, and they participate in electron transfer reactions (Lovenberg and

Sobel, 1965; Adman et al., 1975). RBD1 (Rubredoxin 1) from *Chlamydomonas* and its ortholog from cyanobacteria RubA contain one rubredoxin domain and one transmembrane domain. Loss of RBD1 in photosynthetic eukaryotes impacts the functional accumulation of PSII (Calderon et al., 2013). Further studies demonstrated that they may participate in PSII RC formation by participating together with cyt b_{559} to protect PSII assembly intermediates from photooxidation or maintaining PSII co-factors in a suitable redox state to prevent photodamage (García-Cerdán et al., 2019; Kiss et al., 2019).

In this study, we characterized the *rbd1* mutant of *Arabidopsis*. We demonstrate that ribosome recruitment of *psbA* mRNA encoding the D1 protein is specifically reduced in *rbd1*, suggesting that RBD1 may act as a regulatory factor involving D1 translation. The PSII reaction center accumulates in higher amounts in *rbd1* but further association with other PSII assembly intermediates to form the larger PSII complex and supercomplexes is nearly totally blocked. These data imply that *Arabidopsis* RBD1, similarly to the orthologs found in *Chlamydomonas* and cyanobacteria, exerts a role in the formation of a functional PSII core complex during the early stages of PSII assembly.

MATERIALS AND METHODS

Plant Materials and Growth Conditions

The T-DNA insertion mutant *rbd1* (WiscDsLoxHs187_05C) was obtained from Nottingham Arabidopsis Stock Center (NASC). Position of the T-DNA insertion in *rbd1* was confirmed by PCR using primers in **Supplementary Table 1** and subsequent sequencing of the PCR products. Wild type (Columbia, Col-0), *rbd1*, and *rbd1*-com plants were grown on Murashige and Skoog (MS) basal medium containing 3% sucrose and 0.05% (w/v) MES (2-morpholinoethanesulfonic acid) (pH 5.8) under a 16-h photoperiod with 50 $\mu\text{mol photons m}^{-2} \text{ s}^{-1}$ at 23°C in a greenhouse.

For complementation analysis, a genomic DNA fragment containing *RBD1* and its promoter (750 bp upstream of transcription initiation site) was amplified by PCR using primers RBD1-1301-F and RBD1-1301-R (**Supplementary Table 1**). PCR products were then cloned into the pCAMBIA1301 vector. The resulting vector was then transferred into *Agrobacterium tumefaciens* C58C and transformed into heterozygous *rbd1* plants by the floral dipping method (Clough and Bent, 1998).

Chlorophyll Fluorescence Analysis

Images of chlorophyll *a* fluorescence were captured with a MAXI-IMAGING-PAM chlorophyll fluorometer (Walz, Germany) with default parameters. Plants were first kept in darkness for 20 min and the minimum fluorescence (F_0) was measured by turning on the measuring light (ML). Maximum fluorescence (F_m) was then determined with a saturating pulse (SP). The maximum quantum yield of PSII was calculated as $F_v/F_m = (F_m - F_0)/F_m$. Images of F_0 and F_v/F_m were displayed using a false color scale from 0 to 1.

Transients of Chlorophyll *a* fluorescence were monitored using a PAM-2500 chlorophyll fluorometer (Walz, Germany).

Plants were dark adapted for 20 min. Then F_o and F_m were determined with the measuring light (ML, red light, intensity 2) or a saturating pulse (SP, red light, intensity 10, 0.6 s), respectively. Then, the leaves were illuminated with actinic light (AL, red light, $64 \mu\text{mol photons m}^{-2} \text{ s}^{-1}$) for 4 min and the steady-state fluorescence (F_t) was recorded.

Antibody Generation and Resources

The sequence encoding the soluble part of RBD1 protein (amino acid residues 13–174) was amplified by PCR from cDNA with primers of RBD1-ab-F and RBD1-ab-R (Supplementary Table 1). The PCR products were cloned into the pET28a expression vector (Novagen, United States) by double enzyme digestion and the reconstructed vector was transformed into *E. coli* Rosetta competent cells for expression of the recombinant protein. After induction with 0.5 mM IPTG for 4 h at 37°C , the cells were harvested and recombinant protein was purified from the supernatant on a Ni-NTA agarose column (Qiagen). Polyclonal antibody against RBD1 was raised in rabbits.

Antibodies of D1 (PHY0057, 1:2,000), D2 (PHY0060, 1:2,000), CP43 (PHY0318, 1:5,000), CP47 (PHY0319, 1:2,000), PsbE (PHY0506A, 1:5,000), PsbI (PHY0132A, 1:1,000), PsbO (PHY0344, 1:2,000), PsbA (PHY0342, 1:2,000), PsbD (PHY0343, 1:5,000), Cyt b_6 (PHY0020S, 1:1,000), CF $_1$ γ (PHY0313, 1:1,000), CF $_1$ ϵ (PHY0314, 1:1,000), and SBPase (PHY0410S, 1:1,000) were obtained from PhytoAB.

Isolation of Thylakoid Membranes, BN/2D-PAGE, and Tricine-SDS-PAGE

Chloroplast thylakoids were isolated according to Zhang et al. (2016). Briefly, leaves of 4-week-old plants grown on MS medium were homogenized in isolation buffer I (0.33 M sorbitol, 30 mM Tricine/KOH, pH 8.4, 10 mM NaHCO_3 , 5 mM EGTA, 5 mM EDTA), and the homogenate was filtered through three layers of Miracloth (Calbiochem, United States). After centrifugation at 4,200 g for 5 min at 4°C and resuspension in isolation buffer II (0.3 M sorbitol, 20 mM Hepes-KOH, pH 7.6, 5 mM MgCl_2 , 2.5 mM EDTA), intact chloroplasts were osmotically ruptured in lysis buffer (5 mM MgCl_2 , 2.5 mM EDTA, 20 mM Hepes-KOH, pH 7.6). Thylakoid membranes were separated by centrifugation at 10,000 g for 2 min at 4°C .

BN-PAGE, SDS-urea-PAGE, and immunoblot analysis were performed as previously described (Zhang et al., 2016). For 2D/SDS-PAGE, excised BN-PAGE strips were incubated with $2 \times$ SDS sample buffer (50 mM Tris-HCl, pH 6.8, 8 M urea, 5% SDS, 20% glycerol, 5% β -mercaptoethanol, 1% bromophenol blue) for 30 min at 25°C and layered onto denaturing 15% SDS-urea-PAGE gels. For Tricine-SDS-PAGE, samples were solubilized in $4 \times$ Tricine sample buffer (12% SDS, 6% β -mercaptoethanol, 30% glycerol, 150 mM Tris-HCl, pH 7.0, 0.05% Coomassie Brilliant Blue G250) and separated on 10/16% step-gradient Tricine-SDS gels. For immunoblot analysis, proteins separated by SDS-urea-PAGE or Tricine-SDS-PAGE were transferred to nitrocellulose membranes (GE Healthcare, United States) and incubated with various antibodies.

Signals were captured with a WSE-6200 LuminoGraph II Chemiluminescence Imaging system (ATTO Technology, Japan).

Nucleic Acid Analysis

Arabidopsis crude DNA was extracted from leaves through shock crushing with DNA extraction buffer (0.2 M Tris-HCl, pH 8.0; 12.5 mM EDTA, 0.25 M NaCl, 0.5% SDS), and the DNA was precipitated with ethanol and centrifuged at 13,500 g for 10 min at room temperature. The DNA was solubilized and subjected to PCR analysis. RNA gel blot analysis was performed according to Zhang et al. (2018). Total RNA was extracted from the leaves of 4-week-old plants with liquid nitrogen using TRIzol reagent (Invitrogen, United States). Equal amounts of total RNA were separated by formamide denaturing agarose gel electrophoresis and transferred to a nylon membrane (GE Healthcare, United States). RNA was detected using nucleic acid probes labeled with digoxigenin (DIG, Roche, Switzerland).

Polysome association analysis was performed according to our previous studies (Zhang et al., 2018). Leaves of 4-week-old plants were ground in liquid nitrogen, and polysomes were extracted with polysome extraction buffer (0.2 M Tris-HCl, pH 9.0, 0.2 M Sucrose, 0.2 M KCl, 35 mM MgCl_2 , 25 mM EGTA, 1% [v/v] Triton X-100, 2% [v/v] polyoxyethylene-10-tridecyl ether, 0.5 mg mL^{-1} heparin, 0.1 M 2-mercaptoethanol, 0.1 mg mL^{-1} chloramphenicol, 25 $\mu\text{g mL}^{-1}$ cycloheximide). After centrifugation at 20,000 g for 5 min at 4°C , the supernatants were further solubilized with 0.5% (w/v) sodium deoxycholate. Unresolved membrane was removed by centrifugation at 20,000 g for 15 min at 4°C , and the supernatants were subsequently layered on 15–55% sucrose gradients. After centrifugation at 237,000 g in the SW55 rotor for 65 min at 4°C , each gradient was divided into 10 0.5-mL fractions and proteins associated with RNA were denatured with 0.5% (w/v) SDS and 20 mM EDTA, and then RNA was extracted with acid phenol/chloroform/isoamyl alcohol (25:24:1). The RNA associated with polysomes was precipitated with 95% ethanol at room temperature and solubilized in DEPC-treated water. The samples were subjected to RNA gel blot analysis.

In vivo Labeling and Chasing of Chloroplast Proteins

Chloroplast proteins labeling and chasing analysis was performed as previously described (Zhang et al., 2018). Labeled proteins were fractionated by SDS-urea-PAGE or 2D BN/SDS-PAGE, and signals were detected by autoradiography.

Ribosome Profiling and RNA-Seq

The ribosomal profiling analysis was performed by Gene Denovo Biotechnology Co., (Guangzhou, China) according to Ingolia et al. (2012) with modifications. Leaves of 4-week-old mutants and WT plants were ground to powder in liquid nitrogen and then dissolved in lysis buffer (20 mM Tris HCl pH 8.0, 1.5 mM MgCl_2 , 140 mM KCl, 100 $\mu\text{g mL}^{-1}$ chloramphenicol, 100 mg mL^{-1} cycloheximide, 1% Triton-X-100). After centrifugation at 20,000 g for 10 min at 4°C , the supernatant was treated with RNase I (NEB, United States) and DNase I (NEB, United States)

at room temperature for 45 min to degrade DNA and unprotected RNA. Nuclease digestion was stopped by adding RNase inhibitor (SUPERase•In; Ambion, United States). Then, digested RNAs were separated by size exclusion columns (illustra MicroSpin S-400 HR Columns; GE Healthcare) and SDS was added to the elution at a final concentration of 1% to denature RNA-associated proteins. RNAs with a size greater than 17 nt were isolated with RNA Clean and Concentrator-25 kit (Zymo Research, United States). rRNA was removed as reported previously (Morlan et al., 2012), and RNAs were further purified using magnetic beads (Vazyme, China).

Ribo-seq libraries were prepared with NEBNext Multiple Small RNA Library Prep Set for Illumina (NEB, United States) according to the user manual. PCR products with DNA fragments at 140–160 bp (representing insert sizes of 18–35 bp) were enriched to generate a cDNA library and sequenced with Illumina HiSeq™ X10 (Gene Denovo Biotechnology Co., China).

Read processing, alignment, and analysis were carried out according to Chotewutmontri and Barkan (2018). Reads counts in the open reading frame (ORF) of coding genes were calculated by software RSEM, and gene expression level was normalized by using RPKM (Reads Per Kilobase of transcript per Million mapped reads) method. Read counts and RPKM values for chloroplast genes are summarized in **Supplementary Table 2**. Distribution of ribosome footprints along the ORF was normalized by the sum of the total read counts.

The raw data of ribosome profiling reported in this paper have been deposited in the GenBank (NCBI) Sequence Read Archive (SRA) with accession number PRJNA785666¹.

Accession Numbers

The sequences data in this assay obtain from the Arabidopsis Information Resource or GenBank/EMBL databases under the following accession numbers: AtRBD1 (AT1G54500, *Arabidopsis thaliana*), CrRBD1 (Cre07.g315150.t1.2, *Chlamydomonas reinhardtii*), and SyRubA (slr2033, *Synechocystis* sp. PCC 6803).

RESULTS

The *rbd1* Mutant Is Defective in Growth and PSII Function

To investigate the function of RBD1 in higher plants, the T-DNA insertion Arabidopsis mutant *rbd1* was obtained from NASC (Nottingham Arabidopsis Stock Center). As reported previously, the *rbd1* mutant cannot grow photoautotrophically on soil and exhibits a yellow-green leaf phenotype when grown on Murashige and Skoog (MS) medium (**Figure 1A**, Calderon et al., 2013). Chlorophyll *a* fluorescence imaging and fluorescence transients showed that the minimum chlorophyll *a* fluorescence (F_o) is increased and the variable fluorescence (F_v) decreased in *rbd1*, resulting in a reduced maximum quantum yield of PSII (F_v/F_m) (**Figures 1A,B**). These results indicate that the PSII activity is reduced in the *rbd1* mutant.

The *RBD1* gene of Arabidopsis does not contain introns (**Figure 1C**). Sequencing of the PCR products showed that the T-DNA was inserted into the coding region of *RBD1*, resulting in a complete loss of RBD1 protein in thylakoids (**Figure 1D**). Introduction of the genomic *RBD1* gene driven by its own promoter in the *rbd1* mutant completely rescued growth and wild-type chlorophyll *a* fluorescence patterns (**Figures 1A,B**). Consistently, similar levels of RBD1 protein were detected in WT and complemented plants (**Figure 1D**). These results demonstrate that loss of the RBD1 protein is responsible for the severe mutant phenotype of *rbd1*.

The *rbd1* Mutant Accumulates Low Amount of PSII but Relatively High Levels of PSII Assembly Intermediates

To examine the effects of RBD1 on the abundance of thylakoid complexes, thylakoids freshly isolated from wild type and *rbd1* mutant were solubilized with 1% *n*-dodecyl β -D-maltoside (β -DM), and protein complexes were separated by blue native polyacrylamide gel electrophoresis (BN-PAGE) (**Figure 2A**). The results revealed a drastic reduction of PSII complexes including PSII supercomplexes, PSII dimer, PSII monomer, and CP43-less PSII, whereas accumulation of NDH-PSI supercomplex was identical in wild type and *rbd1* mutant (**Figure 2A**). To quantitate the abundance of PSII subunits in *rbd1*, immunoblotting was performed using WT and *rbd1* thylakoids. Accumulation of the PSII core subunits D1, D2, CP43, CP47, PsbE, and PsbI is significantly reduced to less than 1/8 of WT in *rbd1* (**Figure 2B**). The level of PSII oxygen-evolving complex subunit PsbO and PSI subunits (PsaA and PsaD) in the *rbd1* mutant is reduced to about 1/2 compared with WT. However, the amounts of LHCII complex (Lhcb1), cytochrome *b₆f* complex (Cyt *b₆*), and ATP synthase (CF₁ ϵ) are slightly increased in *rbd1* relative to WT (**Figure 2B**). Similar levels of these thylakoid membrane proteins were observed in the *Chlamydomonas* RBD1-deficient mutant *2apc*. The decrease of PSI in *rbd1* is likely a secondary effect of the drastic reduction of PSII (Calderon et al., 2013). These data indicate that, similar to its *Chlamydomonas* ortholog, Arabidopsis RBD1 is required for the accumulation of PSII complexes (García-Cerdán et al., 2019).

To further investigate the accumulation of the PSII assembly intermediates in *rbd1*, thylakoid protein complexes separated in the first dimension by (1D) BN-PAGE were then resolved into their subunits in the second dimension by (2D) electrophoresis on 15% SDS-urea-PAGE (**Figure 2C**). Immunoblot analysis showed that the PSII core subunits D1, D2, CP43, and CP47 are present as expected in the PSII supercomplexes (PSII-SC), PSII dimer, PSII monomer, and CP43-less PSII in WT and complemented plants (**Figure 2C**). However, in the *rbd1* mutant, D1 and D2 are mainly present in the PSII monomer and CP43 and CP47 are mainly present in the PSII monomer and their assembly intermediates (pre-CP43 and pre-CP47) (**Figure 2C**). Moreover, only trace amounts of D1 and D2 were detected in the PSII reaction center (RC) in WT and complemented plants but a relatively higher level of RC assembly intermediate was

¹<https://www.ncbi.nlm.nih.gov/sra/PRJNA785666>

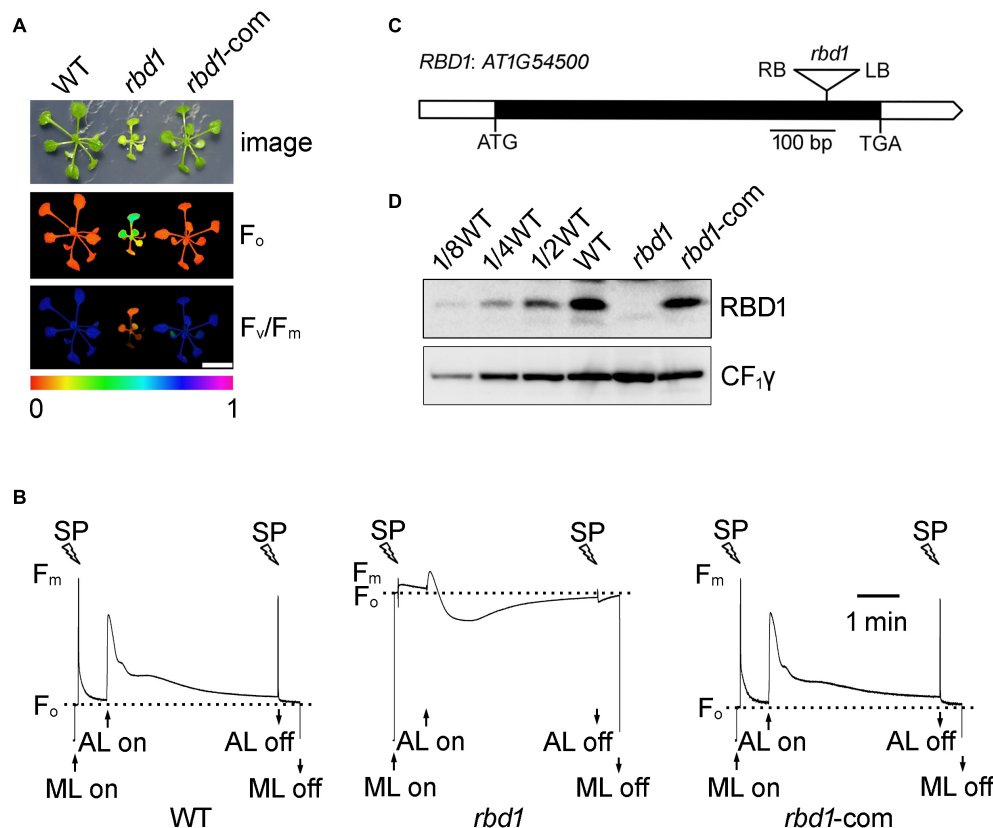


FIGURE 1 | Characterization of the *rbd1* mutant. **(A)** Phenotypes and complementation of the *rbd1* mutant. Growth (upper panel) and chlorophyll a fluorescence (F_o , middle panel; F_v/F_m , lower panel) phenotype of wild type (WT), *rbd1*, and *rbd1-com* plants. Values for F_o and F_v/F_m are indicated using a false color scale at the bottom. *rbd1-com*, *rbd1* mutant complemented using the RBD1 genomic DNA from WT. **(B)** Chlorophyll a fluorescence transients of the *rbd1* mutant. After 20-min dark adaption, minimal fluorescence (F_o) was measured with measuring light (ML) and a saturation pulse (SP) was applied to record maximal fluorescence (F_m). Subsequently, leaves were exposed to actinic light (AL, $64 \mu\text{mol photons m}^{-2} \text{s}^{-1}$) for 4 min. **(C)** Structure of the *RBD1* gene. White and black boxes represent the untranslated and coding regions, respectively. The T-DNA insertion is represented by a triangle. **(D)** Immunoblot analysis of RBD1 protein. Thylakoid proteins extracted from WT, *rbd1*, and *rbd1-com* plants were separated by SDS-urea-PAGE and detected with an antibody against RBD1. CF₁γ is shown as a loading control.

found in the *rbd1* mutant (Figure 2C). These results show that *rbd1* accumulates a high amount of PSII assembly intermediates including PSII RC, pre-CP43, and pre-CP47.

Assembly of PSII Is Impaired in the *rbd1* Mutant

To study the assembly kinetics of PSII in the *rbd1* mutant, chloroplast-encoded proteins were labeled with [³⁵S]-Met for 20 min using primary leaves of 12-day-old plants in the presence of cycloheximide which specifically inhibits cytosolic protein synthesis. After labeling, thylakoids were extracted and solubilized in the SDS sample buffer. Equal amounts of protein were separated by 15% SDS-PAGE and the labeled proteins were visualized by autoradiography. As shown in Figure 3A, the most striking difference is that the rate of synthesis of mature D1 protein is drastically reduced in *rbd1* compared with WT (Figure 3A). In contrast, proteins corresponding to pD1 and D2 were heavily labeled in *rbd1* (Figure 3A). As mature D1 is produced from pD1 by removing the C-terminal 9-AA with the

CtpA enzyme, it is possible that processing of pD1 protein is retarded in *rbd1*, resulting in a higher accumulation of pD1. Since this band also contains D2 protein, it is possible that the rate of synthesis of D2 is increased in *rbd1* compared with WT.

To distinguish between these two possibilities, we performed pulse-chase labeling experiment. After labeling for 20 min (indicated as 0 in Figure 3B), the labeled proteins were chased with unlabeled Met for 30 min (indicated as 30 in Figure 3B). To investigate the dynamic fates of newly synthesized thylakoid proteins, thylakoid protein complexes were separated by 2D BN/SDS-PAGE and individual subunits were visualized by autoradiography. As shown in Figure 3B, in the WT, mature D1, D2, and CP43 proteins were readily detected in the PSII supercomplexes (PSII SC), PSII dimer, PSII monomer, CP43-less PSII, and PSII reaction center (PSII RC) after labeling for 20 min (indicated as 0 in Figure 3B), indicating efficient PSII assembly. At the PSII RC position, the signal of the protein spot corresponding to pD1/D2 is comparable with mature D1 (Figure 3B). 2D BN/SDS-PAGE of labeled proteins in WT showed that the level of labeled D2 protein is significantly lower

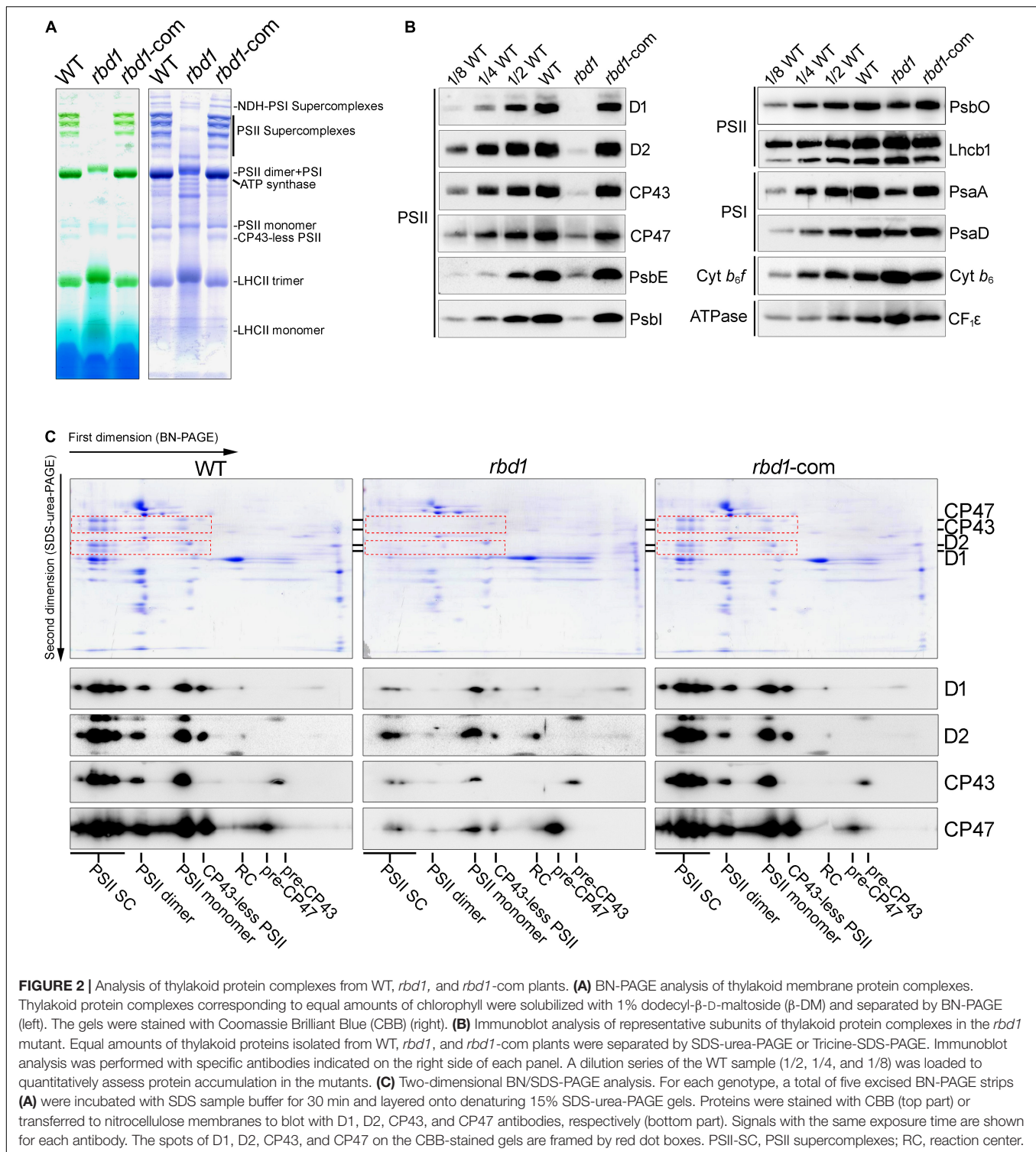


FIGURE 2 | Analysis of thylakoid protein complexes from WT, *rbd1*, and *rbd1-com* plants. **(A)** BN-PAGE analysis of thylakoid membrane protein complexes. Thylakoid protein complexes corresponding to equal amounts of chlorophyll were solubilized with 1% dodecyl-β-D-maltoside (β-DM) and separated by BN-PAGE (left). The gels were stained with Coomassie Brilliant Blue (CBB) (right). **(B)** Immunoblot analysis of representative subunits of thylakoid protein complexes in the *rbd1* mutant. Equal amounts of thylakoid proteins isolated from WT, *rbd1*, and *rbd1-com* plants were separated by SDS-urea-PAGE or Tricine-SDS-PAGE. Immunoblot analysis was performed with specific antibodies indicated on the right side of each panel. A dilution series of the WT sample (1/2, 1/4, and 1/8) was loaded to quantitatively assess protein accumulation in the mutants. **(C)** Two-dimensional BN/SDS-PAGE analysis. For each genotype, a total of five excised BN-PAGE strips **(A)** were incubated with SDS sample buffer for 30 min and layered onto denaturing 15% SDS-urea-PAGE gels. Proteins were stained with CBB (top part) or transferred to nitrocellulose membranes to blot with D1, D2, CP43, and CP47 antibodies, respectively (bottom part). Signals with the same exposure time are shown for each antibody. The spots of D1, D2, CP43, and CP47 on the CBB-stained gels are framed by red dot boxes. PSII-SC, PSII supercomplexes; RC, reaction center.

than that of D1 in the different PSII complexes. Thus, it is reasonable to speculate that the protein spot corresponding to pD1/D2 in the PSII RC complex represents mainly pD1. As expected, during the 30 min chase, pD1 was rapidly processed to mature D1 protein in the PSII RC complex which was further assembled into various PSII complexes in WT (**Figure 3B**).

However, after labeling for 20 min, the majority of mature D1 and pD1/D2 was present in the PSII RC and trace amounts of these proteins were in the free form in *rbd1* (**Figure 3B**). The level of pD1/D2 was significantly higher than mature D1 protein in the PSII RC complex. Even after chasing for 30 min, the majority of D1/pD1 was still present in the PSII RC complex

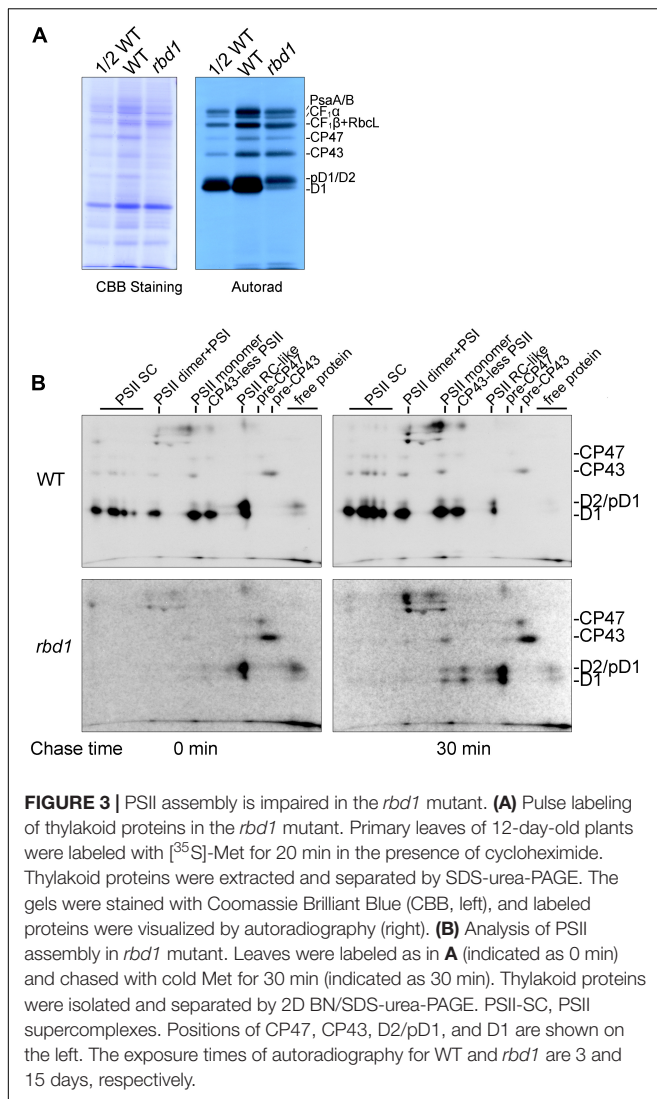


FIGURE 3 | PSII assembly is impaired in the *rbd1* mutant. **(A)** Pulse labeling of thylakoid proteins in the *rbd1* mutant. Primary leaves of 12-day-old plants were labeled with [³⁵S]-Met for 20 min in the presence of cycloheximide. Thylakoid proteins were extracted and separated by SDS-urea-PAGE. The gels were stained with Coomassie Brilliant Blue (CBB, left), and labeled proteins were visualized by autoradiography (right). **(B)** Analysis of PSII assembly in *rbd1* mutant. Leaves were labeled as in **A** (indicated as 0 min) and chased with cold Met for 30 min (indicated as 30 min). Thylakoid proteins were isolated and separated by 2D BN/SDS-urea-PAGE. PSII-SC, PSII supercomplexes. Positions of CP47, CP43, D2/pD1, and D1 are shown on the left. The exposure times of autoradiography for WT and *rbd1* are 3 and 15 days, respectively.

and the level of pD1/D2 was higher than mature D1 in PSII RC (Figure 3B). In addition, CP43 and CP47 were mainly present in the pre-CP43 and pre-CP47 complex, respectively (Figure 3B). These results indicate that PSII assembly of PSII RC complex to CP43-less PSII and other intact PSII complexes is severely impaired in *rbd1*. Since PSII RC contains a high level of mature D1 after chasing for 30 min, it is unlikely that processing of pD1 into D1 represents the main limitation for assembly of PSII in *rbd1*.

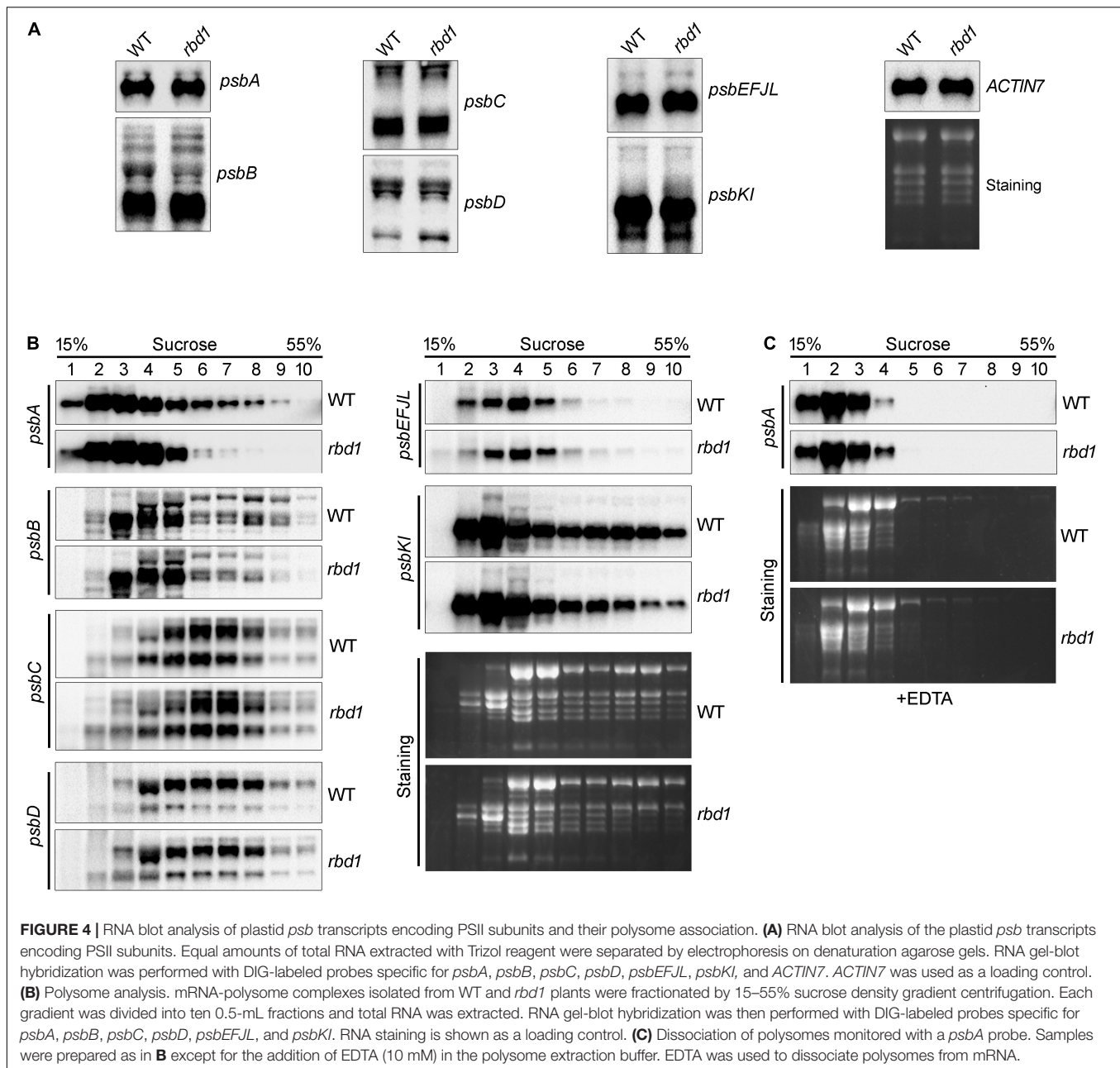
Our protein labeling experiments also showed that the rate of synthesis of the PSI core subunits PsaA/B, ATP synthase subunits CF₁α, as well as the PSII core subunits CP43 and CP47, are slightly reduced in *rbd1* compared with WT (Figure 3A). A similar reduction was also reported for other PSII mutants such as *hcf136*, *hcf244*, *hcf173*, *ohp1*, and *ohp2* (Meurer et al., 1998; Schult et al., 2007; Link et al., 2012; Li et al., 2018) and it is most likely a secondary effect of PSII deficiency.

Polysome Association With *psbA* Is Reduced in the *rbd1* Mutant

To investigate why the rate of synthesis of D1 is reduced in *rbd1*, RNA gel blot and polysome association analysis were performed. As shown in Figure 4A, there was no obvious defect in the accumulation and expression pattern of *psbA*, *psbB*, *psbC*, *psbD*, *psbEFJL*, and *psbKI* in *rbd1* compared with WT indicating that RBD1 is not involved in transcription and post-transcriptional processes of the chloroplast *psb* genes. Polysome association analysis which reflects translation initiation of transcripts showed that the distribution of *psbB*, *psbC*, *psbD*, *psbEFJL*, and *psbKI* transcripts was almost identical between *rbd1* and WT (Figure 4B). In contrast, the distribution of *psbA* transcripts was significantly shifted toward the lower molecular weight polysomal fractions in the *rbd1* mutant compared with WT (Figure 4B) indicating that translation initiation of *psbA* transcript is impaired in *rbd1*, resulting in a reduced synthesis rate of D1 *in vivo*. To confirm that the reduction of *psbA* mRNA in the higher molecular weight fractions in *rbd1* was caused by the dissociation with polysomes we performed a control experiment by treating the extract with EDTA before ultracentrifugation. It is known to cause ribosome dissociation from mRNA. As shown in Figure 4C, EDTA treatment induced shifts of *psbA* transcripts towards lower molecular weight fractions in both the *rbd1* mutant and WT, indicating that the amount of polysomes associated with *psbA* transcripts was reduced.

Ribosome Recruitment to *psbA* mRNA Is Specifically Reduced in *rbd1*

To investigate whether RBD1 is involved in the translation of other transcripts encoding PSII subunits and other thylakoid complexes, ribosome profiling was performed using WT and *rbd1* plants. In this experiment, ribosome-protected mRNA fragments were deep-sequenced and the reads of each transcript can be calculated by normalizing to total chloroplast reads (cpRPKM). We obtained 63,216,962 and 57,604,852 high-quality clean reads in two replicates for WT and *rbd1*, respectively, after the removal of rRNA, tRNAs, snoRNA, snRNA, miRNA, and low-quality reads (Supplementary Table 2). The proportion of total reads that mapped to the reference genome ranged from 70.43% to 89.39%, and 22,719 genes were identified. As shown in Figure 5A, *psbA* mRNA abundance of ribosome occupancy was drastically reduced to about 14% of WT in *rbd1*, consistent with the lower abundance of polysome association of *psbA* mRNA in the mutant (Figure 4B and Supplementary Table 2). The abundance of ribosome footprints for *psbN*, and *psaA* and *psaB* mRNAs encoding PSI subunits were comparable in *rbd1* and WT. The ribosome footprint abundance of other chloroplast transcripts varied between 1.5- and 4-fold increase compared to WT (Figure 5A). Similar results were also reported for the PSII mutants of *hcf244*, *ohp1*, and *ohp2* (Chotewutmontri et al., 2020). They can be explained by the fact that *psbA* ribosome footprints represent a high fraction of the total footprints in WT and the drastic decrease in *psbA* reads in the mutant therefore increases the cpRPKM values for other genes. If one



takes into account this compensation effect, the relatively low *rbd1*/WT cprPKM ratios for *psbN*, *psaA*, and *psaB* suggest that translation of these proteins may be slightly affected. PsbN is not a PSII subunit but it is involved in the PSII RC formation (Torabi et al., 2014). These facts imply that RBD1 and PsbN share some biochemical or genetic interaction during PSII RC biogenesis.

To further investigate the role of RBD1 in *psbA* mRNA translation, we analyzed the distribution of ribosome footprints along the *psbA* mRNA. Several major peaks were detected both in the mutant and wild type that represent the positions of ribosomes paused temporarily along the mRNA during

translation. As expected, the signals of *rbd1* detected in the distribution of *psbA* mRNA were much lower compared to WT because of the lower abundance of ribosome association in *rbd1* (Figure 5B). To facilitate comparison of the ribosome distribution along the *psbA* mRNA in WT and *rbd1*, the Y-axis was adjusted as previously reported (Chotewutmontri et al., 2020). As shown in Figure 5C, the pattern of the ribosome distribution along the *psbA* mRNA in *rbd1* was similar to wild type (Figure 5C). However, a peak was specifically detected in *rbd1* in the region of *psbA* mRNA encoding the latter part of the third transmembrane domain (TMD) (Figure 5C). These results suggest that ribosomes pause during *psbA* translation in *rbd1*

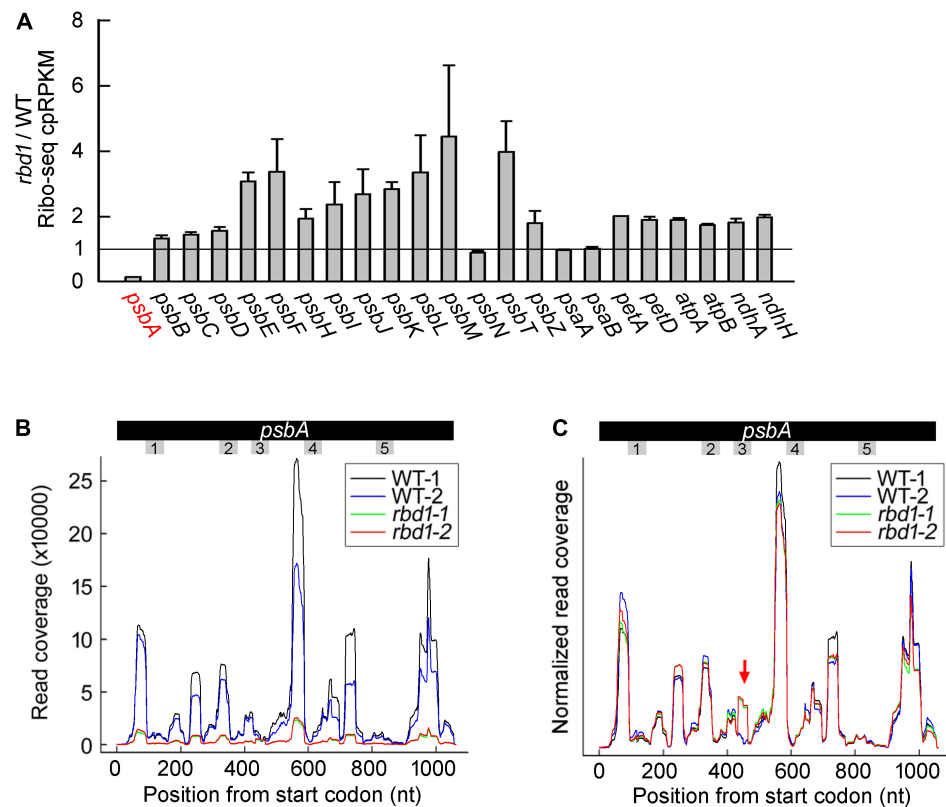


FIGURE 5 | Ribo-seq analysis of the expression of chloroplast gene in the *rbd1* mutant. **(A)** Ribosome footprint abundance for chloroplast genes in *rbd1* relative to wild type. Average of two replicates (mean \pm SD) is shown. cpRPKM, reads per kilobase in the ORF per million reads mapped to chloroplast ORFs. **(B)** Distribution of ribosome footprints along the *psbA* ORF in the two replicates of the *rbd1* mutant (*rbd1-1* and *rbd1-2*) and WT (WT-1 and WT-2). The regions of *psbA* mRNA encoding the transmembrane domains (TMD) are labelled from 1 to 5. **(C)** Normalized reads of **(B)**. The Y-axis was normalized to the sum of the read coverage. The red arrow points to a new pausing site in *rbd1*.

when the third TMD of D1 emerges from the ribosomal tunnel. It is thus likely that integration of the first two, probably also the third, TMDs of D1 is retarded during PSII biogenesis in *rbd1*. RBD1 may, directly or indirectly, facilitate the insertion of D1 into thylakoids to form the functional PSII RC complex during assembly and repair of PSII.

DISCUSSION

Our results show that the levels of the PSII core subunits D1, D2, CP43, and CP47 are reduced to less than 1/8 of WT resulting in a drastic decrease of the various intact PSII complexes as well as PSII activity (Figures 1, 2). Similar phenotypes were also found for the *Chlamydomonas rbd1* and *Synechocystis rubA* deletion mutant (García-Cerdán et al., 2019; Kiss et al., 2019). However, in the *Arabidopsis rbd1* mutant, the steady-state levels of PSII assembly intermediates including PSII RC, pre-CP43, and pre-CP47 complexes are relatively higher compared to WT and the complemented plants (Figure 2C). Consistent with these results, pulse labeling and pulse-chase experiments showed that newly synthesized PSII core subunits are mainly

present in the PSII RC, pre-CP43, and pre-CP47 intermediates after labeling for 20 min and an additional 30-min chase (Figure 3B). These results confirm that RBD1 is required for PSII assembly *in vivo* (García-Cerdán et al., 2019; Kiss et al., 2019).

Although the rate of synthesis of pD1 and D1 is reduced in *rbd1*, newly synthesized pD1/D1/D2 proteins are able to assemble into the PSII RC complex in this mutant (Figure 3). However, formation of the larger PSII complexes is severely decreased (Figure 3B). In higher plants, after the formation of the PSII RC complex, CP47 and several low molecular mass subunits (LMM) attach to RC forming CP43-less PSII. Subsequently, CP43 and other LMM PSII subunits are assembled to form the PSII monomer (Rokka et al., 2005). In *rbd1*, newly synthesized CP47 and CP43 are mainly present in the pre-CP47 and pre-CP43 assembly intermediates, respectively (Figure 3B). Pulse labeling showed that the rate of synthesis of CP47 and CP43 is slightly reduced in *rbd1* comparable with WT (Figure 3A). Also, ribosome occupancy of *psbB* and *psbC* mRNA is not reduced in *rbd1* (Figure 5A). These results suggest that newly synthesized CP47 and CP43 are functional and available for further association with the PSII RC complex. However, they

are unable to sequentially associate with PSII RC during the labeling and chase period of 50 min (**Figure 3B**). Hence, it is reasonable to propose that the newly formed PSII RC complex is largely non-functional and therefore cannot bind antennas CP47 and CP43 to form functional PSII. However, we could not exclude the possibility that PSII RC is functional, but the CP47 and CP43 antennas do not have access to PSII RC in the *rbd1* mutant.

In the *Synechocystis rubA* deletion mutant, however, the rates of synthesis of D1 as well as those of the other core subunits D2, CP43, and CP47 are as in WT (Kiss et al., 2019). Moreover, the majority of newly synthesized D1 and D2 remained in an unassembled state in thylakoids and could not assemble into PSII RC complexes as in the Arabidopsis *rbd1* mutant (**Figure 3B**; Kiss et al., 2019). Since RBD1 in chloroplasts and its cyanobacterial ortholog RubA have conserved rubredoxin and transmembrane domains, it is reasonable to assume that they exert a similar physiological function during PSII assembly. How can one explain the differences between these two species? One explanation could be that the PSII assembly process in cyanobacteria is slightly different. The Arabidopsis *pam68-2* mutant accumulates ~1/10 level of PSII complex compared with WT but in the *Synechocystis* *sllo933*, in which the PAM68 cyanobacterial ortholog Sll0933 is disrupted, the PSII complex accumulates almost normally (Armbruster et al., 2010). Further analysis showed that a high level of PSII RC complex is present in *pam68-2* but almost undetectable in the *sllo933* mutant (Armbruster et al., 2010). Similar phenotypes with different levels of PSII assembly intermediates were also found between the *hcf136* Arabidopsis and *ycf48* cyanobacterial mutant (Meurer et al., 1998; Komenda et al., 2008). Moreover, several specific chloroplast PSII assembly factors are absent in cyanobacteria (Nickelsen and Rengstl, 2013). Reciprocally, cyanobacteria also possess specific PSII assembly factors that are missing in chloroplasts (Nickelsen and Rengstl, 2013). These differences in the PSII assembly process and assembly factors may be the result of different environmental living pressures during evolution. As discussed by Nixon et al. (2010), it is also possible that a more effective protein quality system in chloroplasts may lead to differences in accumulation of PSII assembly intermediates in the mutants mentioned above.

How does RBD1 facilitate formation of the functional PSII RC complex? Our protein labeling experiments show that PSII RC containing mature D1 is produced implying that newly synthesized pD1 protein can be properly inserted into thylakoids in the correct topology for processing by the CtpA enzyme in the lumen. RBD1 contains a redox-active rubredoxin domain with a redox midpoint potential of +114 mV that is capable to transfer electrons to cytochrome *c in vitro* (Calderon et al., 2013). Thus, formation of inactive PSII RC in *rbd1* is most likely due to deficient redox control. It is known that D1 integrates co-translationally into the PSII complex during its assembly (Zhang et al., 1999). Addition of DTT at a low concentration partially activated translation elongation of D1 protein pointing to the existence of a redox-sensitive regulatory component (Zhang et al., 2000). It has also been

reported that two Cys residues of the cyanobacterial ortholog RubA are reversibly oxidized upon a light-to-dark transition (Guo et al., 2014). It is interesting that one of the two Cys residues (Cys-125) in D1 is positioned at the end of the second transmembrane domain (another one is in the middle of the first loop of D1). Therefore, RBD1 might be the redox regulatory component during the biogenesis of pD1, especially at early stages, when ribosomes pause after the first two transmembrane domains have emerged from the ribosomal tunnel in *rbd1* (**Figure 5C**).

An alternative possibility for the function of RBD1 is delivery co-factors into PSII RC, as discussed previously (Kiss et al., 2019). The D1/D2 heterodimer binds several redox components including six chlorophyll *a*, two pheophytin (Pheno) *a*, one non-heme iron, as well as quinones *Q_A* and *Q_B* (Umena et al., 2011). Non-pigmented forms of most chlorophyll-binding proteins are rapidly degraded, suggesting that these co-factors are incorporated into PSII RC during the biogenesis of D1/D2 (Funk et al., 1995). Thus, RBD1 might also facilitate the binding of redox components to D1, such as pheophytin which binds to the residue Glu-130 of D1 at the end of the second transmembrane segment (Giorgi et al., 1996; Sharma et al., 1997). Moreover, it has been shown that iron can be released from the active site of rubredoxin protein under certain conditions (Zheng et al., 2013). Hence, another possibility could be that RBD1 directly delivers the non-heme Fe to the D1/D2 heterodimer.

Our polysome association and ribosome profiling analysis revealed that ribosome occupancy on *psbA* mRNA is drastically reduced in the absence of RBD1 (**Figure 5A**). A similar decrease was also found in the *hcf244*, *ohp1*, and *ohp2* mutants (Chotewutmontri et al., 2020). These results imply that RBD1 and HCF244/OHP1/OHP2 are involved in the translation initiation of D1. However, a peak downstream of the region encoding the latter part of the third transmembrane domain of D1 is relatively enhanced in *rbd1* compared to WT (**Figures 5B,C**), indicating that ribosomes pause in *rbd1* after the second transmembrane domain of D1 is released from the ribosomal tunnel. It is possible that, in the absence of RBD1, the first two transmembrane domains cannot properly insert in the D2-Cyt *b₅₅₉* precomplex because of unavailability for the redox-active cofactors, resulting in ribosome pausing on *psbA* mRNA, and subsequently in the degradation of this ribosome-nascent chain complex, ultimately leading to a decrease of *psbA* mRNA translation (**Figures 3, 5**). A similar scenario may be also valid for the HCF244/OHP1/OHP2 proteins, which were proposed to deliver chlorophyll to PSII RC (Hey and Grimm, 2018; Li et al., 2018; Myouga et al., 2018; Chotewutmontri et al., 2020). In this case, reduction of polysome occupancy on the *psbA* mRNA is likely a secondary effect of membrane integration deficiency of D1.

In summary, we provide evidence that RBD1 is required for the formation of the functional PSII core complex and probably also required for the translation of D1 during the assembly of PSII at early stages in Arabidopsis. Together with the reports on RBD1 from Chlamydomonas and its ortholog from cyanobacteria RubA

(García-Cerdán et al., 2019; Kiss et al., 2019), it is likely that RBD1 orthologs exert a similar role for forming a functional PSII among various photosynthetic organisms.

ONE-SENTENCE SUMMARY

Thylakoid intrinsic protein RBD1 is required for assembly of PSII core complex at early stages.

The author responsible for the distribution of materials integral to the findings presented in this article in accordance with the policy described in the Instructions for Author is: LZ (zhanglin2017@shnu.edu.cn).

DATA AVAILABILITY STATEMENT

The original contributions presented in the study are publicly available. These data can be found here: National Center for Biotechnology Information (NCBI) BioProject database under accession number PRJNA785666.

REFERENCES

- Adman, E., Watenpaugh, K. D., and Jensen, L. H. (1975). NH-S hydrogen bonds in *Peptococcus aerogenes* ferredoxin, *Clostridium pasteurianum* rubredoxin, and *Chromatium* high potential iron protein. *Proc. Natl. Acad. Sci. U.S.A.* 72, 4854–4858. doi: 10.1073/pnas.72.12.4854
- Armbruster, U., Zühlke, J., Rengstl, B., Kreller, R., Makarenko, E., Ruhle, T., et al. (2010). The Arabidopsis thylakoid protein PAM68 is required for efficient D1 biogenesis and photosystem II assembly. *Plant Cell* 22, 3439–3460. doi: 10.1105/tpc.110.077453
- Baena-González, E., and Aro, E.-M. (2002). Biogenesis, assembly and turnover of photosystem II units. *Philos. Trans. R. Soc. Lond. B Biol. Sci.* 357, 1451–1460. doi: 10.1098/rstb.2002.1141
- Beck, J., Lohscheider, J. N., Albert, S., Andersson, U., Mendgen, K. W., Rojas-Stütz, M. C., et al. (2017). Small one-helix proteins are essential for photosynthesis in *Arabidopsis*. *Front. Plant Sci.* 8:7. doi: 10.3389/fpls.2017.00007
- Calderon, R. H., García-Cerdán, J. G., Alizée, M., Cook, R., and Niyogi, K. K. (2013). A conserved rubredoxin is necessary for photosystem II accumulation in diverse oxygenic photoautotrophs. *J. Biol. Chem.* 288, 26688–26696. doi: 10.1074/jbc.M113.487629
- Che, Y., Fu, A., Hou, X., McDonald, K., Buchanan, B. B., Huang, W., et al. (2013). C-terminal processing of reaction center protein D1 is essential for the function and assembly of Photosystem II in *Arabidopsis*. *Proc. Natl. Acad. Sci. U.S.A.* 110, 16247–16252. doi: 10.1073/pnas.1313894110
- Chotewutmontri, P., and Barkan, A. (2018). Multilevel effects of light on ribosome dynamics in chloroplasts program genome-wide and psbA-specific changes in translation. *PLoS Genet.* 14:e1007555. doi: 10.1371/journal.pgen.1007555
- Chotewutmontri, P., Williams-Carrier, R., and Barkan, A. (2020). Exploring the link between photosystem II assembly and translation of the Chloroplast psbA mRNA. *Plants* 9:152. doi: 10.3390/plants9020152
- Clough, S. J., and Bent, A. F. (1998). Floral dip: a simplified method for *Agrobacterium*-mediated transformation of *Arabidopsis thaliana*. *Plant J.* 16, 735–743. doi: 10.1046/j.1365-3113.1998.00343.x
- Funk, C., Adamska, I., Green, B. R., Andersson, B., and Renger, G. (1995). The nuclear-encoded chlorophyll-binding Photosystem II-S protein is stable in the absence of pigments. *J. Biol. Chem.* 270, 30141–30147. doi: 10.1074/jbc.270.50.30141
- García-Cerdán, J. G., Furst, A. L., McDonald, K. L., Schünemann, D., and Niyogi, K. K. (2019). A thylakoid membrane-bound and redox-active rubredoxin (RBD1) functions in de novo assembly and repair of photosystem II. *Proc. Natl. Acad. Sci. U.S.A.* 33, 116–126. doi: 10.1073/pnas.1903314116

AUTHOR CONTRIBUTIONS

LC, HM, and LZ conceived the study and designed the experiments. LC, HM, and JR performed the experiments. HM and LZ produced the figures. LC, HM, LP, and LZ wrote the manuscript. LZ supervised the whole study. All authors analyzed the data.

FUNDING

This work was supported by the Fund of Shanghai Engineering Research Center of Plant Germplasm Resources (Grant No. 17DZ2252700).

SUPPLEMENTARY MATERIAL

The Supplementary Material for this article can be found online at: <https://www.frontiersin.org/articles/10.3389/fpls.2022.824358/full#supplementary-material>

- Giorgi, L. B., Nixon, P. J., Merry, S. A. P., Joseph, D. M., Durrant, J. R., Rivas, J. D., et al. (1996). Comparison of primary charge separation in the photosystem II reaction center complex isolated from wild-type and D1-130 mutants of the cyanobacterium *Synechocystis* PCC 6803. *J. Biol. Chem.* 271, 2093–2101. doi: 10.1074/jbc.271.4.2093
- Guo, J., Nguyen, A. Y., Dai, Z., Su, D., Gaffrey, M. J., Moore, R. J., et al. (2014). Proteome-wide light/dark modulation of thiol oxidation in cyanobacteria revealed by quantitative site-specific redox proteomics. *Mol. Cell Proteomics* 13, 3270–3285. doi: 10.1074/mcp.M114.041160
- Hey, D., and Grimm, B. (2018). ONE-HELIX PROTEIN2 (OHP2) is required for the stability of OHP1 and assembly factor HCF244 and is functionally linked to PSII biogenesis. *Plant Physiol.* 177, 1453–1472. doi: 10.1104/pp.18.00540
- Ingolia, N. T., Brar, G. A., Rouskin, S., McGeachy, A. M., and Weissman, J. S. (2012). The ribosome profiling strategy for monitoring translation in vivo by deep sequencing of ribosome-protected mRNA fragments. *Nat. Protoc.* 7, 1534–1550. doi: 10.1038/nprot.2012.086
- Kiss, E., Knoppova, J., Aznar, G. P., Pilny, J., and Komenda, J. (2019). A photosynthesis-specific rubredoxin-like protein is required for efficient association of the D1 and D2 proteins during the initial steps of photosystem II assembly. *Plant Cell* 31, 2241–2258. doi: 10.1105/tpc.19.00155
- Komenda, J., Nickelsen, J., Tichý, M., Prásl, O., Eichacker, L. A., and Nixon, P. J. (2008). The cyanobacterial homologue of HCF136/YCF48 is a component of an early photosystem II assembly complex and is important for both the efficient assembly and repair of photosystem II in *Synechocystis* sp. PCC 6803. *J. Biol. Chem.* 283, 22390–22399. doi: 10.1074/jbc.M801917200
- Komenda, J., Sobotka, R., and Nixon, P. J. (2012). Assembling and maintaining the Photosystem II complex in chloroplasts and cyanobacteria. *Curr. Opin. Plant Biol.* 15, 245–251. doi: 10.1016/j.pbi.2012.01.017
- Li, Y., Liu, B., Zhang, J., Kong, F., Zhang, L., Meng, H., et al. (2018). OHP1, OHP2, and HCF244 form a transient functional complex with the photosystem II reaction center. *Plant Physiol.* 179, 195–208. doi: 10.1104/pp.18.01231
- Link, S., Engelmann, K., Meierhoff, K., and Westhoff, P. (2012). The atypical shortchain dehydrogenases HCF173 and HCF244 are jointly involved in translational initiation of the psbA mRNA of *Arabidopsis*. *Plant Physiol.* 160, 2202–2218. doi: 10.1104/pp.112.205104
- Lovenberg, W., and Sobel, B. E. (1965). Rubredoxin: a new electron transfer protein from *Clostridium pasteurianum*. *Proc. Natl. Acad. Sci. U.S.A.* 54, 193–199. doi: 10.1073/pnas.54.1.193
- Lyska, D., Meierhoff, K., and Westhoff, P. (2013). How to build functional thylakoid membranes: from plastid transcription to protein complex assembly. *Planta* 237, 413–428. doi: 10.1007/s00425-012-1752-5

- Meurer, J., Plücker, H., Kowallik, K. V., and Westhoff, P. (1998). A nuclear-encoded protein of prokaryotic origin is essential for the stability of photosystem II in *Arabidopsis thaliana*. *EMBO J.* 17, 5286–5297. doi: 10.1093/emboj/17.18.5286
- Morlan, J. D., Qu, K., and Sinicropi, D. V. (2012). Selective depletion of rRNA enables whole transcriptome profiling of archival fixed tissue. *PLoS One* 7:e42882. doi: 10.1371/journal.pone.0042882
- Mulo, P., Sirpiö, S., Suorsa, M., and Aro, E.-M. (2008). Auxiliary proteins involved in the assembly and sustenance of photosystem II. *Photosynth. Res.* 98, 489–501. doi: 10.1007/s11120-008-9320-3
- Myouga, F., Takahashi, K., Tanaka, R., Nagata, N., Kiss, A. Z., Funk, C., et al. (2018). Stable accumulation of photosystem II requires ONE-HELIX PROTEIN1 (OHP1) of the light harvesting-like family. *Plant Physiol.* 176, 2277–2291. doi: 10.1104/pp.17.01782
- Nelson, N., and Junge, W. (2015). Structure and energy transfer in photosystems of oxygenic photosynthesis. *Annu. Rev. Biochem.* 84, 659–683. doi: 10.1146/annurev-biochem-092914-041942
- Nelson, N., and Yocum, C. F. (2006). Structure and function of photosystems I and II. *Annu. Rev. Plant Biol.* 57, 521–565. doi: 10.1146/annurev-arplant.57.032905.105350
- Nickelsen, J., and Rengstl, R. (2013). Photosystem II assembly: from cyanobacteria to plants. *Annu. Rev. Plant Biol.* 64, 605–639. doi: 10.1146/annurev-arplant-050312-120124
- Nixon, P. J., Michoux, F., Yu, J., Boehm, M., and Komenda, J. (2010). Recent advances in understanding the assembly and repair of photosystem II. *Ann. Bot.* 106, 1–16. doi: 10.1093/aob/mcq059
- Plücker, H., Müller, B., Grohmann, D., Westhoff, P., and Eichacker, L. A. (2002). The HCF136 protein is essential for assembly of the photosystem II reaction center in *Arabidopsis thaliana*. *FEBS Lett.* 532, 85–90. doi: 10.1016/s0014-5793(02)03634-7
- Rokka, A., Suora, M., Saleem, A., Battchikova, N., and Aro, E. M. (2005). Synthesis and assembly of thylakoid protein complexes: multiple assembly steps of photosystem II. *Biochem. J.* 388, 159–168. doi: 10.1042/BJ20042098
- Schult, K., Meierhoff, K., Paradies, S., Töller, T., Wolff, P., and Westhoff, P. (2007). The nuclear-encoded factor HCF173 is involved in the initiation of translation of the psbA mRNA in *Arabidopsis thaliana*. *Plant Cell* 19, 1329–1346. doi: 10.1105/tpc.106.042895
- Sharma, J., Panico, M., Shipton, C. A., Nilsson, F., Morris, H. R., and Barber, J. (1997). Primary structure characterization of the photosystem II D1 and D2 subunits. *J. Biol. Chem.* 272, 33158–33166. doi: 10.1074/jbc.272.52.33158
- Shen, J. R. (2015). The structure of photosystem II and the mechanism of water oxidation in photosynthesis. *Annu. Rev. Plant Biol.* 66, 23–48. doi: 10.1146/annurev-arplant-050312-120129
- Torabi, S., Umate, P., Manavski, N., Plöckinger, M., Kleinknecht, L., Bogireddi, H., et al. (2014). PsbN is required for assembly of the photosystem II reaction center in *Nicotiana tabacum*. *Plant Cell* 26, 1183–1199. doi: 10.1105/tpc.113.120444
- Umena, Y., Kawakami, K., Shen, J. R., and Kamiya, N. (2011). Crystal structure of oxygen-evolving photosystem II at a resolution of 1.9 Å. *Nature* 473:55. doi: 10.1038/nature09913
- Yu, J., Knoppová, J., Michoux, F., Bialek, W., Cota, E., Shukla, M. K., et al. (2018). Ycf48 involved in the biogenesis of the oxygen-evolving photosystem II complex is a seven-bladed beta-propeller protein. *Proc. Natl. Acad. Sci. U.S.A.* 115, E7824–E7833. doi: 10.1073/pnas.1800609115
- Zhang, L., Duan, Z., Zhang, J., and Peng, L. (2016). Biogenesis factor required for ATP synthase 3 facilitates assembly of the chloroplast ATP synthase complex. *Plant Physiol.* 171, 1291–1306. doi: 10.1104/pp.16.00248
- Zhang, L., Paakkari, V., van Wijk, K. J., and Aro, E.-M. (1999). Co-translational assembly of the D1 protein into photosystem II. *J. Biol. Chem.* 274, 16062–16067. doi: 10.1074/jbc.274.23.16062
- Zhang, L., Paakkari, V., van Wijk, K. J., and Aro, E.-M. (2000). Biogenesis of the chloroplast-encoded D1 protein: regulation of translation elongation, insertion, and assembly into photosystem II. *Plant Cell* 12, 1769–1781. doi: 10.1105/tpc.12.9.1769
- Zhang, L., Pu, H., Duan, Z., Li, Y., Liu, B., Zhang, Q., et al. (2018). Nucleus-encoded protein BFA1 promotes efficient assembly of the chloroplast ATP synthase coupling factor 1. *Plant Cell* 30, 1770–1788. doi: 10.1105/tpc.18.00075
- Zheng, P., Chou, C. C., Guo, Y., Wang, Y., and Li, H. (2013). Single molecule force spectroscopy reveals the molecular mechanical anisotropy of the FeS4 metal center in rubredoxin. *J. Am. Chem. Soc.* 135, 17783–17792. doi: 10.1021/ja406695g

Conflict of Interest: The authors declare that the research was conducted in the absence of any commercial or financial relationships that could be construed as a potential conflict of interest.

Publisher's Note: All claims expressed in this article are solely those of the authors and do not necessarily represent those of their affiliated organizations, or those of the publisher, the editors and the reviewers. Any product that may be evaluated in this article, or claim that may be made by its manufacturer, is not guaranteed or endorsed by the publisher.

Copyright © 2022 Che, Meng, Ruan, Peng and Zhang. This is an open-access article distributed under the terms of the Creative Commons Attribution License (CC BY). The use, distribution or reproduction in other forums is permitted, provided the original author(s) and the copyright owner(s) are credited and that the original publication in this journal is cited, in accordance with accepted academic practice. No use, distribution or reproduction is permitted which does not comply with these terms.



AtRsmD Is Required for Chloroplast Development and Chloroplast Function in *Arabidopsis thaliana*

Zi-Yuan Wang[†], Wan-Tong Qu[†], Tong Mei, Nan Zhang, Nai-Ying Yang, Xiao-Feng Xu, Hai-Bo Xiong, Zhong-Nan Yang* and Qing-Bo Yu*

Shanghai Key Laboratory of Plant Molecular Sciences, College of Life Sciences, Shanghai Normal University, Shanghai, China

OPEN ACCESS

Edited by:

Hongbo Gao,
Beijing Forestry University, China

Reviewed by:

Aigen Fu,
Northwest University, China
Nadir Zaman,
University of Malakand, Pakistan

*Correspondence:

Zhong-Nan Yang
znyang@shnu.edu.cn
Qing-Bo Yu
yuqing9860@shnu.edu.cn

[†]These authors have contributed
equally to this work and share first
authorship

Specialty section:

This article was submitted to
Plant Physiology,
a section of the journal
Frontiers in Plant Science

Received: 24 January 2022

Accepted: 16 March 2022

Published: 25 April 2022

Citation:

Wang Z-Y, Qu W-T, Mei T,
Zhang N, Yang N-Y, Xu X-F,
Xiong H-B, Yang Z-N and Yu Q-B
(2022) AtRsmD Is Required for
Chloroplast Development
and Chloroplast Function
in *Arabidopsis thaliana*.
Front. Plant Sci. 13:860945.
doi: 10.3389/fpls.2022.860945

AtRsmD was recently demonstrated to be a chloroplast 16S *rRNA* methyltransferase (MTase) for the m²G915 modification in *Arabidopsis*. Here, its function of AtRsmD for chloroplast development and photosynthesis was further analyzed. The *AtRsmD* gene is highly expressed in green photosynthetic tissues. AtRsmD is associated with the thylakoid in chloroplasts. The *atrsmd-2* mutant exhibited impaired photosynthetic efficiency in emerging leaves under normal growth conditions. A few thylakoid lamellas could be observed in the chloroplast from the *atrsmd-2* mutant, and these thylakoids were loosely organized. Knockout of the *AtRsmD* gene had minor effects on chloroplast ribosome biogenesis and RNA loading on chloroplast ribosomes, but it reduced the amounts of chloroplast-encoded photosynthesis-related proteins in the emerging leaves, for example, D1, D2, CP43, and CP47, which reduced the accumulation of the photosynthetic complex. Nevertheless, knockout of the *AtRsmD* gene did not cause a general reduction in chloroplast-encoded proteins in *Arabidopsis* grown under normal growth conditions. Additionally, the *atrsmd-2* mutant exhibited more sensitivity to lincomycin, which specifically inhibits the elongation of nascent polypeptide chains. Cold stress exacerbated the effect on chloroplast ribosome biogenesis in the *atrsmd-2* mutant. All these data suggest that the AtRsmD protein plays distinct regulatory roles in chloroplast translation, which is required for chloroplast development and chloroplast function.

Keywords: AtRsmD, chloroplast, *rRNA* methylation, ribosome, photosynthesis

INTRODUCTION

In all living organisms, ribosomal RNAs (*rRNAs*) constitute the functional center of the ribosome. These RNAs are extensively modified, and the modified nucleotides are usually located in the regions crucial to the function of the ribosome (Urlaub et al., 1997). In *Escherichia coli*, the majority of modified nucleotides in *rRNAs* belong to various types of base and ribose methylated residues (Sergiev et al., 2011), and there are 11 modified nucleotides in 16S *rRNA* (Andersen and Douthwaite, 2006). The three-dimensional locations of these modifications on ribosome crystal structures indicate that these nucleotides are distributed within several discrete regions related to essential ribosomal functions (Brimacombe et al., 1993; Ban et al., 2000; Wimberly et al., 2000; Harms et al., 2001; Yusupov et al., 2001; Schuwirth et al., 2005). *rRNA* modifications play important

roles in efficient protein synthesis (Krzyzosiak et al., 1987; Green and Noller, 1999; Khaitovich et al., 1999). The corresponding enzymes for these sites have been determined and characterized in *E. coli* (Andersen and Douthwaite, 2006). For example, the *yebU* gene encodes a putative m⁵C RNA MTase for the methylation of nucleotide 1407 in 16S rRNA, and the *yebU* knockout strain displays slower growth and reduced fitness in competition with wild-type cells. The *RsmH* gene encodes a conserved MTase that is a specific AdoMet-dependent MTase responsible for the N(4)-methylation of C1402 in 16S rRNA in almost all species of bacteria (Wei et al., 2012). Two *Escherichia coli* guanine-N₂ (m²G) MTases, *rsmC* and *rsmD*, modify nucleotides G1207 and G966 in 16S rRNA, respectively, and they possess a common MTase domain related to the YbiN family of hypothetical MTases in their C-terminus and a variable region in their N-terminus. Knockout of either *rsmC* or *rsmD* results in a mild reduction in cellular growth in *E. coli* (Bujnicki and Rychlewski, 2002; Kimura and Suzuki, 2010). Characterization of these MTase for 16S rRNA methylation has provided a comprehensive understanding of ribosome biogenesis in prokaryotes.

Chloroplasts in plant cells are derived from an endosymbiotic event in which a photosynthetic cyanobacterium was engulfed by an early eukaryotic cell (Keeling, 2013). During host-endosymbiont coevolution, the chloroplast retained a small-scale genome, while many genes were transferred to the nuclear genome (Abdallah et al., 2000). The chloroplast has both the transcriptional and translational machinery for the expression of chloroplast genes. The translational machinery is a bacterial-type 70S ribosome that is composed of a large 50S subunit and a small 30S subunit. The small 30S subunit comprises 25 ribosomal proteins and chloroplast 16S rRNA, while the 50S large subunit consists of 33 ribosomal proteins and three other types of chloroplast rRNAs (23S rRNA, 4.5S rRNA, and 5S rRNA) (Graf et al., 2017; Zoschke and Bock, 2018). Not only do chloroplast ribosomal proteins exhibit high similarities to their counterparts in *E. coli*, but rRNA constituents are also conserved between chloroplasts and *E. coli* (Zoschke and Bock, 2018). Analogous to methylation in *E. coli* rRNAs, this modification occurs in chloroplast rRNAs, and the modification sites and the corresponding enzymes are highly conserved (Zou et al., 2020; Manduzio and Kang, 2021; Ngoc et al., 2021a,b). In contrast, research on rRNA modification in chloroplasts lags behind that in *E. coli*. Two independent groups recently reported that the chloroplast-localized CMAL protein, an ortholog of the bacterial MraW/RsmH protein, is involved in the m⁴C methylation of C1352 in chloroplast 16S rRNA, which plays essential roles in chloroplast development and hormonal responses in higher plants (Zou et al., 2020; Ngoc et al., 2021a). Ngoc et al. (2021b) reported that chloroplast-localized AtRsmD, an ortholog of the MTase for the N₂-methylguanosine (m²G) modification of 16S rRNA in *E. coli*, is involved in m²G methylation at position 915 in chloroplast 16S rRNA in Arabidopsis. The *atrsmd* mutant exhibited no observable differences in seed germination or seedling growth when grown under normal growth conditions; however, the *atrsmd* mutant was hypersensitive to both cold stress and translation inhibitors (Ngoc et al., 2021b). This finding

indicates that AtRsmD is a chloroplast 16S rRNA MTase for the m²G915 modification and that it plays a role in the adaptation of Arabidopsis to cold stress (Ngoc et al., 2021b). Nevertheless, the role of the AtRsmD protein in chloroplast development remains to be further explored.

In this study, we further characterized the *AtRsmD* gene and the corresponding *AtRsmD* deletion mutant, *atrsmd-2*. Knockout of the *AtRsmD* gene impaired chloroplast development and reduced photosynthetic efficiency in emerging leaves in Arabidopsis under normal growth conditions. It did not cause in a general reduction in chloroplast-encoded proteins in Arabidopsis when grown under normal culture conditions but affected the amounts of photosynthetic proteins, such as D1, D2, CP43, and CP47. This reduction interrupted the accumulation of the photosynthetic complex in the *atrsmd-2* mutant. These data suggested that the AtRsmD protein plays distinct regulatory roles in the rapid synthesis of photosynthesis-related proteins, which are required for chloroplast development and chloroplast function.

MATERIALS AND METHODS

Plant Materials and Growth Conditions

The *Arabidopsis thaliana* Col-0 ecotype was used in this study. The T-DNA insertional line (CS832131) was obtained from the Arabidopsis Biological Resource Centre (ABRC; Ohio State University, United States). Plants were grown in a growth chamber with a 16-h light/8-h dark photoperiod at a constant temperature of 22°C. The light intensity was 120 $\mu\text{mol m}^{-2} \text{s}^{-1}$. For growth on agar plates, the seeds were surface-sterilized with 75% alcohol and sown on Murashige-Skoog (MS) medium and 0.7% (w/v) phytoagar with or without the corresponding antibiotics.

For the genomic complementation experiment, the 2,594 bp wild-type genomic fragment of the *AtRsmD* (AT3G28460) gene was amplified with the gene-specific primers listed **Supplementary Table 1** using high-fidelity KOD plus polymerases (TOYOBO)¹ and then subcloned into the modified pCAMBIA1300 binary vector (CAMBIA)² with a three-tandem FLAG tag. The construct was introduced into the *atrsmd-2* mutant via *Agrobacterium tumefaciens* GV3101 (Clough and Bent, 1998). Transgenic lines were screened on MS medium with 80 mg/L hygromycin B (Roche).³

Chlorophyll Fluorescence and Chlorophyll Content Measurements

Chlorophyll fluorescence was determined using an Imaging PAM fluorometer (Walz, Germany). Measurement of chlorophyll fluorescence was performed according to Li et al.'s (2019) report. For chlorophyll content determination, equal fresh weights of Arabidopsis leaves were extracted with equal volumes of 80% (v/v) acetone, and the absorbance of the supernatant was

¹<http://www.toyo-bo-global.com/>

²<http://www.cambia.org>

³<http://www.roche.com>

measured at 663 and 646 nm. Both chlorophyll a and b contents were calculated using the equation of Porra (2002).

Transmission Electron Microscopy Observation

Young primary leaves grown under normal conditions or cold treatments were fixed and embedded as described in a previous report (Yu et al., 2013). Thin sections were prepared with an ultramicrotome and then stained with uranyl acetate and lead citrate. The ultrastructure was examined using a Tecnai Spirit G2 BioTWIN transmission electron microscope.

Subcellular Localization Analysis

The full-length coding sequence of the *AtRsmD* gene was amplified by high-fidelity KOD plus polymerases (TOYOBO)⁴ with the corresponding gene-specific primers and fused in frame with the enhanced green fluorescence protein (eGFP) of the modified pRIN101:eGFP vector (TOYOBO, see text footnote 4) to produce *AtRsmD*:eGFP. Both the construct and free pRIN101:eGFP vector were transformed into *Arabidopsis* protoplasts prepared as described in a previous report, respectively (Yoo et al., 2007). The fluorescence signals were imaged by a laser-scanning confocal microscope (Zeiss, Oberkochen, Germany) with excitation and emission wavelengths of 488 and 545 nm, respectively.

Chloroplast fractions were isolated as described in a previous report (Xiong et al., 2020). Three-week-old leaves from the *AtRsmD*:eGFP stable transgenic lines were homogenized in precooled buffer I (0.33 M sorbitol; 0.02 M Tricine/KOH, pH 8.4; 5 mM EGTA, pH 8.35; 5 mM EDTA, pH 8.0; 10 mM NaHCO₃). After filtration with a double layer of Miracloth, the homogenate was further filtered through 100- and 40- μ m sieves, in order, and the filtrate was centrifuged at 2,000 g for 5 min at 4°C to obtain intact chloroplasts. Following centrifugation, the intact chloroplasts were then resuspended in buffer II (0.33 M sorbitol; 5 mM MgCl₂; 2.5 M EDTA, pH 8.0; 20 mM HEPES/KOH, pH 7.6) and in buffer III (5 mM MgCl₂-6H₂O, 25 M EDTA pH 8.0, 20 mM HEPES/KOH pH 7.6), successively. After centrifugation at 4°C, the supernatant contained stroma, while the sediment contained the thylakoid fractions. The corresponding antibodies were used to perform immunoblotting analysis.

Sequence Alignment and Phylogenetic Tree Construction

Protein sequences were aligned with ClustalW, and the alignment results were displayed with the BoxShade Server.⁵ The phylogenetic tree was constructed and tested using MEGA 3.1⁶ based on the neighbor-joining method.

Nucleic Acid Isolation, cDNA Synthesis, and qPCR Analysis

For genomic DNA isolation, samples were homogenized in lysis buffer [200 mM Tris-HCl, pH 7.5; 25 mM NaCl; 25 mM

EDTA; and 0.5% (w/v) SDS], and the homogenate was isolated with phenol/chloroform (1:1, v/v). After centrifugation, the supernatant was collected, and genomic DNA was precipitated by adding ice-cold isopropyl alcohol. After washing with 70% (v/v) ethanol, the genomic DNA was air-dried and dissolved in double-distilled water. For total RNA isolation, samples were ground in liquid nitrogen, and total RNA was isolated using an RNA isolation kit (Tiangen)⁷ according to the manufacturer's instructions.

Total RNA (5 μ g) was used to synthesize first-strand cDNA with Trans-Script® Fly First-Strand cDNA Synthesis Super-Mix. Quantitative PCR (qPCR) analysis was performed using the gene-specific primers listed in **Supplementary Table 1** and SYBRGREEN I master mix reagent (Toyobo, see text footnote 1) on a real-time RT-PCR system (ABI7300, United States). Reactions were performed in triplicate for each sample, and expression levels were normalized against *TUBLIN4*.

Polysome Association Analysis

Polysome association assays were performed as described previously (Zhang et al., 2018). Total extracts from the young leaves of 2-week-old plants were fractionated in 15–55% sucrose gradients through centrifugation at 45,000 rpm (246,000 g) at 4°C for 65 min. After centrifugation, 10 fractions (0.5 mL each fraction) were collected successively from the sucrose gradients. Then, the total RNA in each fraction was isolated, and an equal proportion of RNA was separated using RNA gel blot analysis.

RNA Gel-Blot Hybridization

RNA hybridization was performed according to the Roche manual as described previously (Yu et al., 2013). Total RNA (5 μ g) from the wild type and *atrsmd-2* mutant was separated using formamide denaturing agarose gel electrophoresis, transferred onto nylon membranes (MILLIPORE), and subjected to RNA gel blotting with digoxigenin (DIG)-labeled nucleic acid probes (DIG Easy Hyb system; Roche). The probes were prepared using a PCR DIG synthesis kit (Roche, see text footnote 3) with the specific primers listed in **Supplementary Table 1**. Total RNA was detected by ethidium bromide staining, and the signals on the RNA gel blot were visualized with a LuminoGraph WSE-6100 (ATTO).

Chloroplast Blue Native PAGE and Two-Dimensional Analysis

Chloroplast BN-PAGE and 2-D analysis were performed according to a previous report (Zhang et al., 2018). Briefly, 1 g of 2-week-old seedlings was homogenized in precooled HMSN buffer (0.4 M sucrose, 10 mM NaCl, 5 mM MgCl₂-6H₂O, and 10 mM HEPES) and then filtered through a multilayer microcloth. The isolated thylakoid pellets were resuspended in buffer [25 mM Bis-Tris-HCl, pH 7.0, 1% n-dodecyl b-D-maltoside (w/v), and 20% glycerol (w/v)] at 1.0 mg chlorophyll/mL and incubated at 4°C for 5 min followed by centrifugation at 12,000 g for 10 min. After one-tenth volume

⁴<http://www.toyobo.co.jp>

⁵<http://arete.ibb.waw.pl/PL/html/boxshade.html>

⁶<http://www.megasoftware.net>

⁷<https://www.tiangen.com/>

of loading buffer [100 mM Bis-Tris-HCl, pH 7.0, 0.5 M 6-amino-n-caproic acid, 5% Serva blue G (w/v), and 30% glycerol (w/v)] was added to the supernatant, and the samples were separated on 0.75-mm 4–12% acrylamide gradient gels in a Tannon vertical electrophoresis device at 4°C. For two-dimensional analysis, excised BN-PAGE lanes were soaked in SDS sample buffer for 30 min and layered onto 1-mm 10% SDS polyacrylamide gels containing 6 M urea. After electrophoresis, the proteins were stained with Coomassie bright blue.

Total Protein Extraction and Immunoblotting Analysis

Total protein was isolated from the young leaves of 2-week-old Arabidopsis seedlings according to a previous report (Zou et al., 2020). Briefly, samples were ground in extraction buffer [25 mM Tris-HCl (pH 7.9), 50 mM NaCl, 1 mM EDTA, 5% glycerol (v/v), and 2% SDS] and subsequently centrifuged at 12,000 g for 10 min. The total protein in the supernatant was quantified using the DC Protein Assay Kit according to the manufacturer's instructions (Bio-Rad Laboratories). Approximately 10 µg of total protein was separated on 10% SDS polyacrylamide gels and transferred onto PVDF membranes. Immunoblotting analysis was performed with specific primary antibodies, and the signals from the secondary conjugated antibodies were detected with enhanced chemiluminescence and a TANNON imaging system.

RESULTS

Knockout of the *AtRsmD* Gene Impaired Photosynthetic Efficiency in Arabidopsis

The chlorophyll fluorescence parameter *Fv/Fm* reflects the maximum quantum efficiency of photosystem II (PSII) photochemistry and has been widely used for early stress detection in plants. To obtain novel insights into the regulation of photosynthetic efficiency in Arabidopsis, we screened Arabidopsis T-DNA insertion lines on a large scale to detect their *Fv/Fm* values. We found that the *Fv/Fm* value of the homozygous T-DNA insertion line CS832131 was only 0.643 ± 0.02 , which was lower than the 0.788 ± 0.02 value found for the control (Figures 1A,B). The homozygous mutants exhibited no obviously visible phenotype (Figure 1B). Measurement of the total chlorophyll contents indicated that the chlorophyll contents in the homozygous mutant were slightly lower than those in the wild type (Figure 1C). PCR sequencing analysis confirmed that the T-DNA is inserted in the fourth intron of the *AT3G28460* gene. RT-PCR analysis showed that the full-length transcript of the *AT3G28460* gene was not detected in the homozygous mutant but was detected in the wild type (Figure 1D), which demonstrated that the line is another mutant for the locus. Therefore, we named the line as the *atrsmd-2* mutant, while a previously reported line (Ngoc et al., 2021b) was named as the *atrsmd-1* mutant.

To verify that the *AT3G28460* locus is responsible for the impaired photosynthetic efficiency in the *atrsmd-2* mutant, we produced a construct carrying the genomic sequence of the

AT3G28460 gene fused with the coding sequence of a three-tandem FLAG tag before its stop codon that was driven by its native promoter, and we transformed it into the *atrsmd-2* mutant via *Agrobacterium tumefaciens* (Clough and Bent, 1998). Three independent transgenic lines carrying the *AtRsmD* genomic fragment were identified to have the *atrsmd-2/-* genotype. RT-PCR results indicated that *AtRsmD* transcripts could be detected in the complemented line (Figure 1D). Immunoblotting analysis detected a protein with the predicted size of 35 kDa in the complemented line, but this protein was absent in both the wild type and *atrsmd-2* mutant (Figure 1E). The values of *Fv/Fm* in the complemented line were restored to the levels of the wild type (Figure 1B). These data showed that knockout of the *AtRsmD* gene impaired the photosynthesis efficiency of photosystem II under normal conditions. Taken together, our data demonstrated that the *AtRsmD*:FLAG fusion protein is able to complement the *atrsmd-2* mutant, and the fusion protein is functional.

Expressional Pattern of the *AtRsmD* Gene and Subcellular Localization of Its Product in Arabidopsis

To examine the expression pattern of the *AtRsmD* gene in different tissues, we performed reverse-transcription (RT)-PCR analysis of various tissues from wild-type plants. Our results showed that the *AtRsmD* transcripts were present in all tissues (Figures 2A,B). The *AtRsmD* transcripts were much more abundant in seedlings and leaves than in the other tissues. These data indicated that the *AtRsmD* gene was highly expressed in these green tissues.

TargetP software predicted that the *AtRsmD* protein contains a potential chloroplast transpeptide at the N-terminus,⁸ and a very recent study demonstrated that the *AtRsmD* protein is localized to the chloroplast (Ngoc et al., 2021b). We made a construct in which the full-length encoding sequence of the *AtRsmD* protein was fused into the coding sequence of eGFP and introduced it into Arabidopsis protoplasts. *AtRsmD*:eGFP fluorescence colocalized with chlorophyll autofluorescence (Figure 2C), demonstrating that the *AtRsmD* protein is localized to the chloroplast. We also checked whether *AtRsmD* is associated with thylakoids. Chloroplast stroma and thylakoids were isolated from the stable *AtRsmD*:eGFP transgenic lines, and then immunoblotting analysis was carried out with the corresponding antibodies. Our immunoblotting analysis showed that *AtRsmD*:eGFP was detected in both chloroplasts and thylakoid fragments (Figure 2D). All these data showed that the *AtRsmD* protein is associated with thylakoids in chloroplasts.

Absence of the *AtRsmD* Protein Impaired the Accumulation of Chloroplast-Encoded Photosynthetic Proteins

The *atrsmd-2* mutant exhibited impaired photosynthetic efficiency (Figure 1B), which could be due to reduced protein levels of photosynthetic complex elements. We investigated

⁸www.cbs.dtu.dk/services/TargetP-1.1/index.php

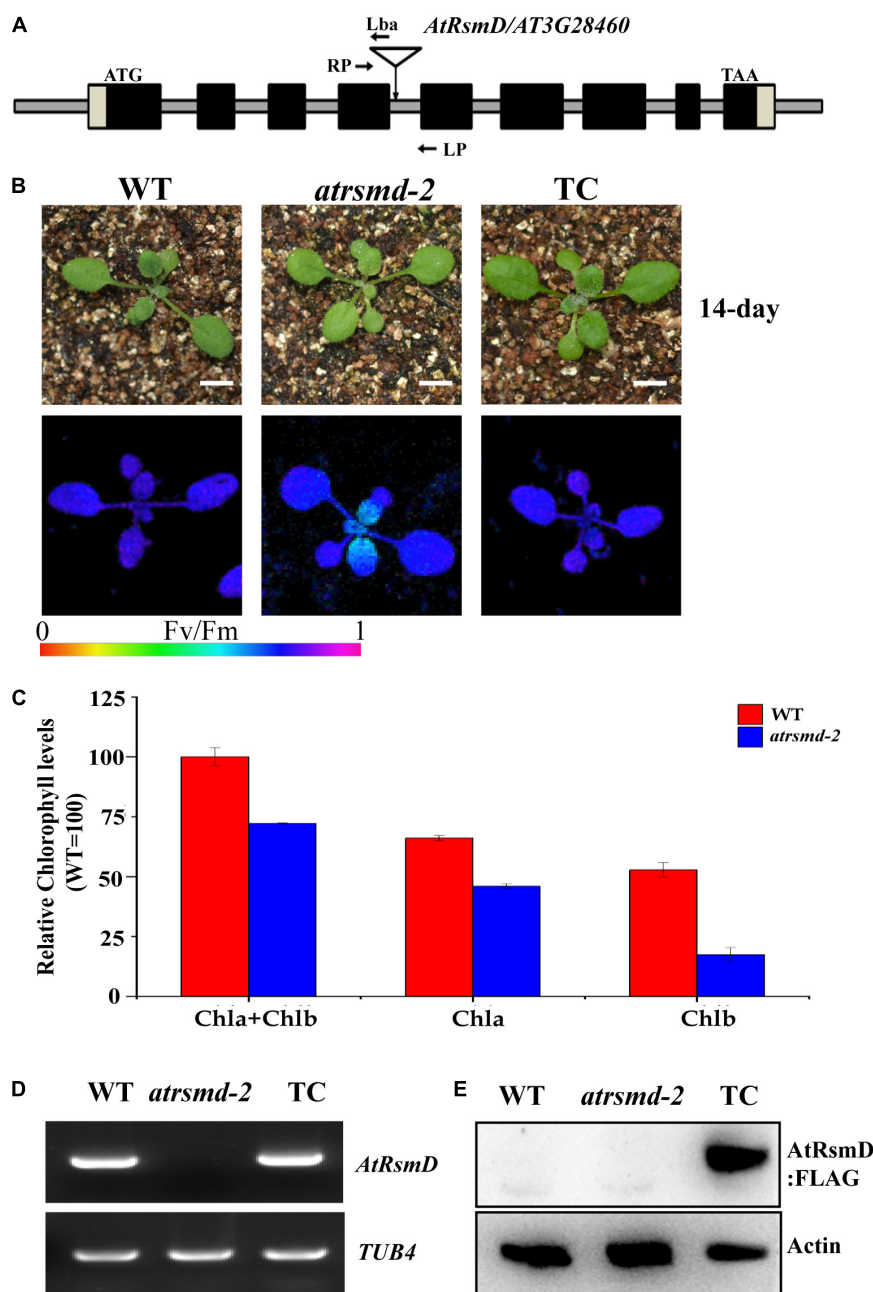


FIGURE 1 | Knockout of the *AtRsmD* gene impaired photosynthetic efficiency in Arabidopsis. **(A)** Schematic illustrating the genomic structures of *AtRsmD* and the location of the T-DNA insertion. Black boxes and striped boxes indicate exons and introns, respectively. The T-DNA insertion site is indicated by an inverted triangle. Lba represents the left border primer of the T-DNA insertion. LP and RP represent the left and right genomic primers around the T-DNA insertion site, respectively. **(B)** Phenotype and F_v/F_m values of 14-day-old seedlings of the wild type (WT), *atrsmd-2* mutant and complemented lines (TC). Bar represents 1 cm. **(C)** Chlorophyll content in the emerging leaves from the 14-day-old wild type and *atrsmd-2* mutant seedlings. **(D)** RT-PCR analysis of the *AtRsmD* gene in the wild type, *atrsmd-2* mutant, and complemented line (TC). *Tubulin 4* was used as a control. **(E)** Immunoblotting analysis of AtRsmD:FLAG in the wild type, *atrsmd-2* mutant, and complemented line (TC) with the anti-FLAG antibody. Actin was used as a control.

whether the absence of *AtRsmD* affects the accumulation of photosynthetic complex elements. Thylakoid membranes were solubilized with 1% dodecyl- β -D-maltopyranoside (DM), and then membrane protein complexes were separated by blue native PAGE (BN-PAGE). Our results showed that the amounts

of supercomplex elements, such as the PSII supercomplex, PSI-PSII dimer, PSII monomer, and LhcII trimers, were clearly reduced in the *atrsmd-2* mutant compared with those of the wild type (Figure 3A). The complexes resolved by BN-PAGE were then separated into their subunits in the second dimension by

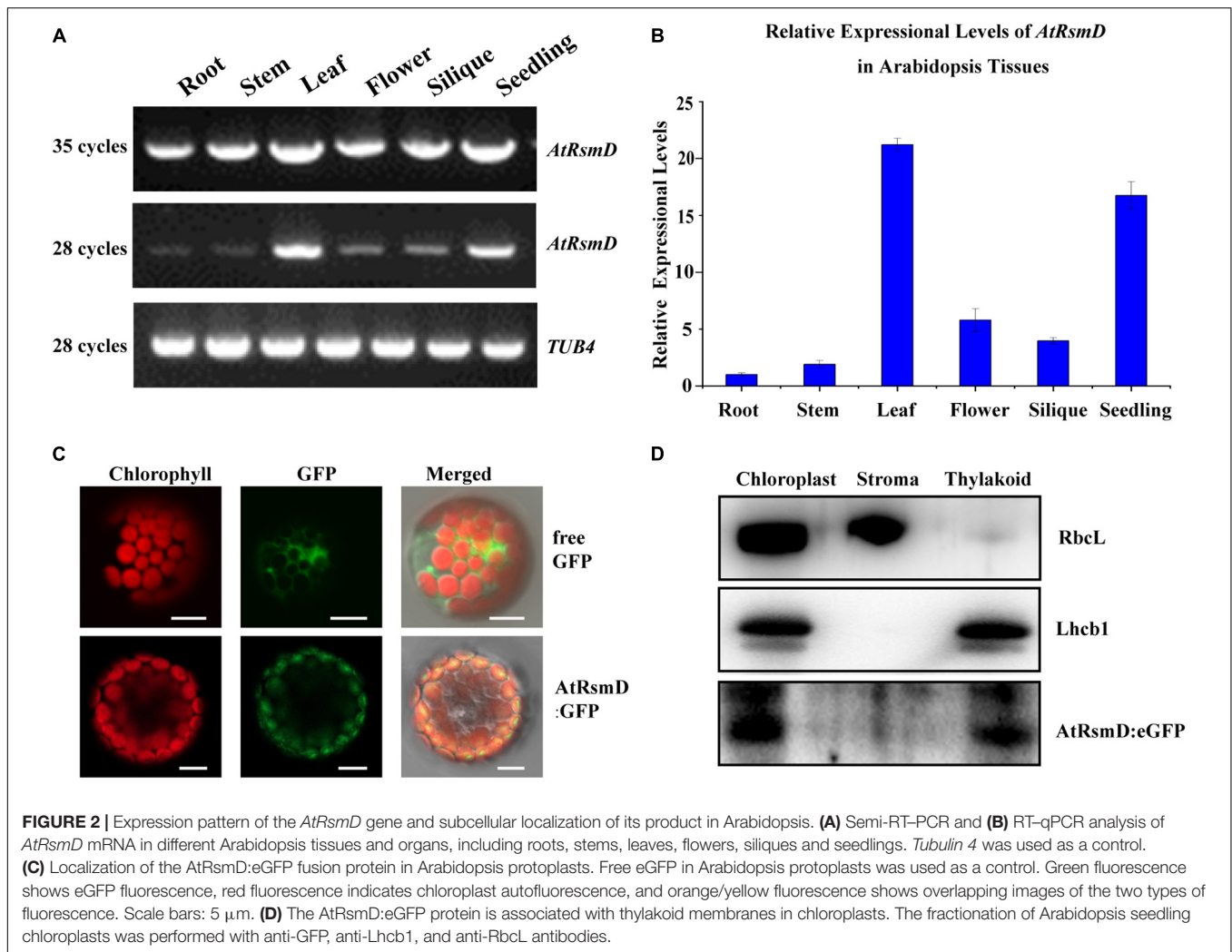


FIGURE 2 | Expression pattern of the *AtRsmD* gene and subcellular localization of its product in Arabidopsis. **(A)** Semi-RT-PCR and **(B)** RT-qPCR analysis of *AtRsmD* mRNA in different Arabidopsis tissues and organs, including roots, stems, leaves, flowers, siliques and seedlings. *Tubulin 4* was used as a control. **(C)** Localization of the *AtRsmD*:eGFP fusion protein in Arabidopsis protoplasts. Free eGFP in Arabidopsis protoplasts was used as a control. Green fluorescence shows eGFP fluorescence, red fluorescence indicates chloroplast autofluorescence, and orange/yellow fluorescence shows overlapping images of the two types of fluorescence. Scale bars: 5 μ m. **(D)** The *AtRsmD*:eGFP protein is associated with thylakoid membranes in chloroplasts. The fractionation of Arabidopsis seedling chloroplasts was performed with anti-GFP, anti-Lhcb1, and anti-RbcL antibodies.

electrophoresis on SDS-PAGE gels and stained with Coomassie brilliant blue R 250. We found that the accumulation of the core subunits of PSII, CP43, CP47, D1, and D2 in the complex was clearly reduced in the *atrsmd-2* mutant (Figure 3B) compared with their counterparts in the wild type. These results showed that assembly of the photosynthetic complex was seriously reduced in the *atrsmd-2* mutant.

To examine the steady-state levels of the thylakoid membrane proteins, immunoblotting analysis was performed with antibodies against specific subunits of the photosynthetic thylakoid membrane complex. Our results showed that the amounts of plastid-encoded photosynthesis-related proteins, including D1, D2, CP43, CP47, and AtpF, were 25–50% those of the wild type (Figure 4). In contrast, other photosynthesis-related proteins, such as AtpA, AtpB, RbcL, PetA, PetD, OEC33, and Lhcb1, accumulated to similar levels as the wild type (Figure 4), while the abundance of the PsaA protein increased in the mutant. These results indicated that knockout of the *AtRsmD* gene interrupted the accumulation of photosynthesis-related proteins, including chloroplast-encoded photosystem II proteins, and affected the assembly of the photosynthetic

complex, which probably impaired photosynthetic efficiency in the *atrsmd-2* mutant.

Absence of *AtRsmD* Affects Chloroplast Transcripts

Since the amounts of several chloroplast-encoded photosynthetic proteins, including D1, D2, CP43, CP47, and AtpF, were clearly reduced in the *atrsmd* mutant, we investigated whether the absence of the *AtRsmD* gene affected the accumulation of their corresponding chloroplast transcripts through RT-qPCR analysis. Our results showed that the chloroplast transcripts *psbA*, *psbB*, *psbC*, *psbD*, and *atpF* were 1–6-fold higher in the *atrsmd-2* mutant than those in the wild type (Figure 5A), although the corresponding photosynthetic proteins were clearly reduced in the mutant. Additionally, we observed that the abundances of the chloroplast transcripts *atpA*, *atpB*, *petA*, *petD*, and *rbcL* were increased. We further investigated the accumulation of the PEP complex in the *atrsmd-2* mutant. The amounts of the core subunit, RpoB, and the essential component, PAP8/pTAC6, were checked in this mutant, and our results showed that

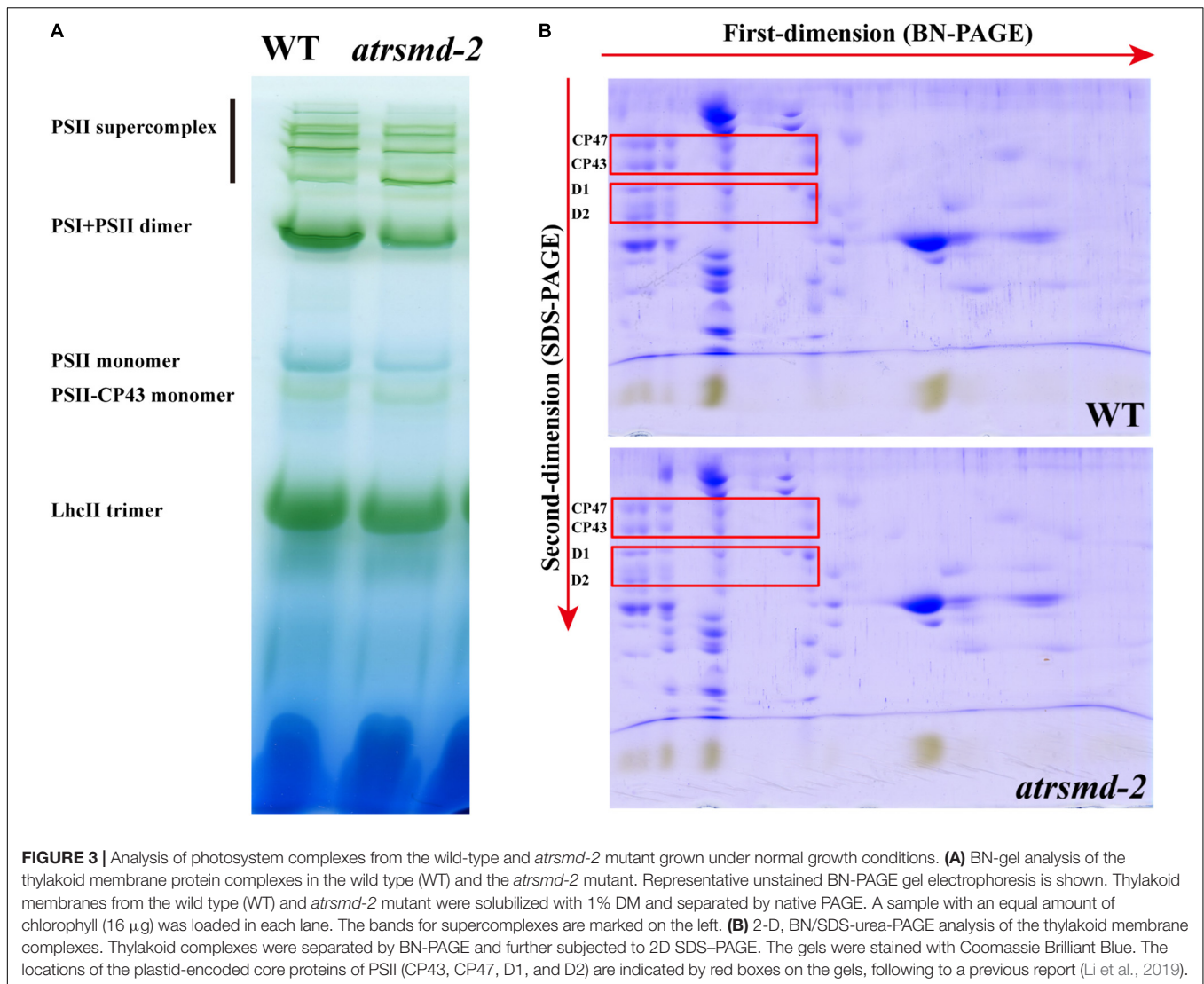


FIGURE 3 | Analysis of photosystem complexes from the wild-type and *atsrsmD-2* mutant grown under normal growth conditions. **(A)** BN-gel analysis of the thylakoid membrane protein complexes in the wild type (WT) and the *atsrsmD-2* mutant. Representative unstained BN-PAGE gel electrophoresis is shown. Thylakoid membranes from the wild type (WT) and *atsrsmD-2* mutant were solubilized with 1% DM and separated by native PAGE. A sample with an equal amount of chlorophyll (16 μ g) was loaded in each lane. The bands for supercomplexes are marked on the left. **(B)** 2-D, BN/SDS-urea-PAGE analysis of the thylakoid membrane complexes. Thylakoid complexes were separated by BN-PAGE and further subjected to 2D SDS-PAGE. The gels were stained with Coomassie Brilliant Blue. The locations of the plastid-encoded core proteins of PSII (CP43, CP47, D1, and D2) are indicated by red boxes on the gels, following to a previous report (Li et al., 2019).

the abundance of these core subunits in the *atsrsmD-2* mutant was slightly increased compared with those in the wild type (Figure 5B). All these results indicated that knockout of the *AtRsmD* gene increased the accumulation of the PEP complex and altered the expression of these chloroplast transcripts in Arabidopsis, which is probably the result of feedback regulation.

Absence of *AtRsmD* Affects the Accumulation of Chloroplast Ribosomes

A previous report indicated that the *AtRsmD* protein is responsible for the methylation of 16S *rRNA* m²G915, and this methylation pattern was missing in the knockout line of the *AtRsmD* gene (Ngoc et al., 2021b). We further investigated the possible impacts of the absence of the *AtRsmD* protein on chloroplast ribosomal biogenesis. The levels of two components of the ribosomal 30S small subunit, PRPS1 (SMALL RIBOSOMAL SUBUNIT 1, bS1c) and PRPS5 (SMALL RIBOSOMAL SUBUNIT 5, uS5c), and two components of the

ribosomal 50S large subunit, PRPL4 (LARGE RIBOSOMAL SUBUNIT 4, uL4c) and PRPL2 (LARGE RIBOSOMAL SUBUNIT 2, uL2c), were slightly reduced in the *atsrsmD-2* mutant grown under normal growth conditions, compared with those in the wild type (Figure 6A). Then, the levels of four chloroplast *rRNA* transcripts (16S *rRNA*, 23S *rRNA*, 5S *rRNA*, and 4.5S *rRNA*) were also investigated in the *atsrsmD-2* mutant using RNA blot analysis (Figures 6B,C). Our results indicated that the amount of the mature form of chloroplast 16S *rRNA* (1.5-knt molecule) in the *atsrsmD-2* mutant was reduced, whereas the amount of the precursor *rRNA* (1.7-kb) molecule was increased (Figure 6C). Levels of the 3.2-, 2.8-, 2.4- and 1.7-knt 23S *rRNA* species were increased in the *atsrsmD-2* mutant. Additionally, the level of one shorter form of the 1.3-knt species was decreased (Figure 6C), while the 1.1-knt form accumulated to a level similar as that in the wild type. In contrast, the levels of 4.5S and 5S *rRNA* transcripts were increased in the *atsrsmD-2* mutant. These data suggest that knockout of the *AtRsmD* gene affected the accumulation of chloroplast *rRNAs* and chloroplast

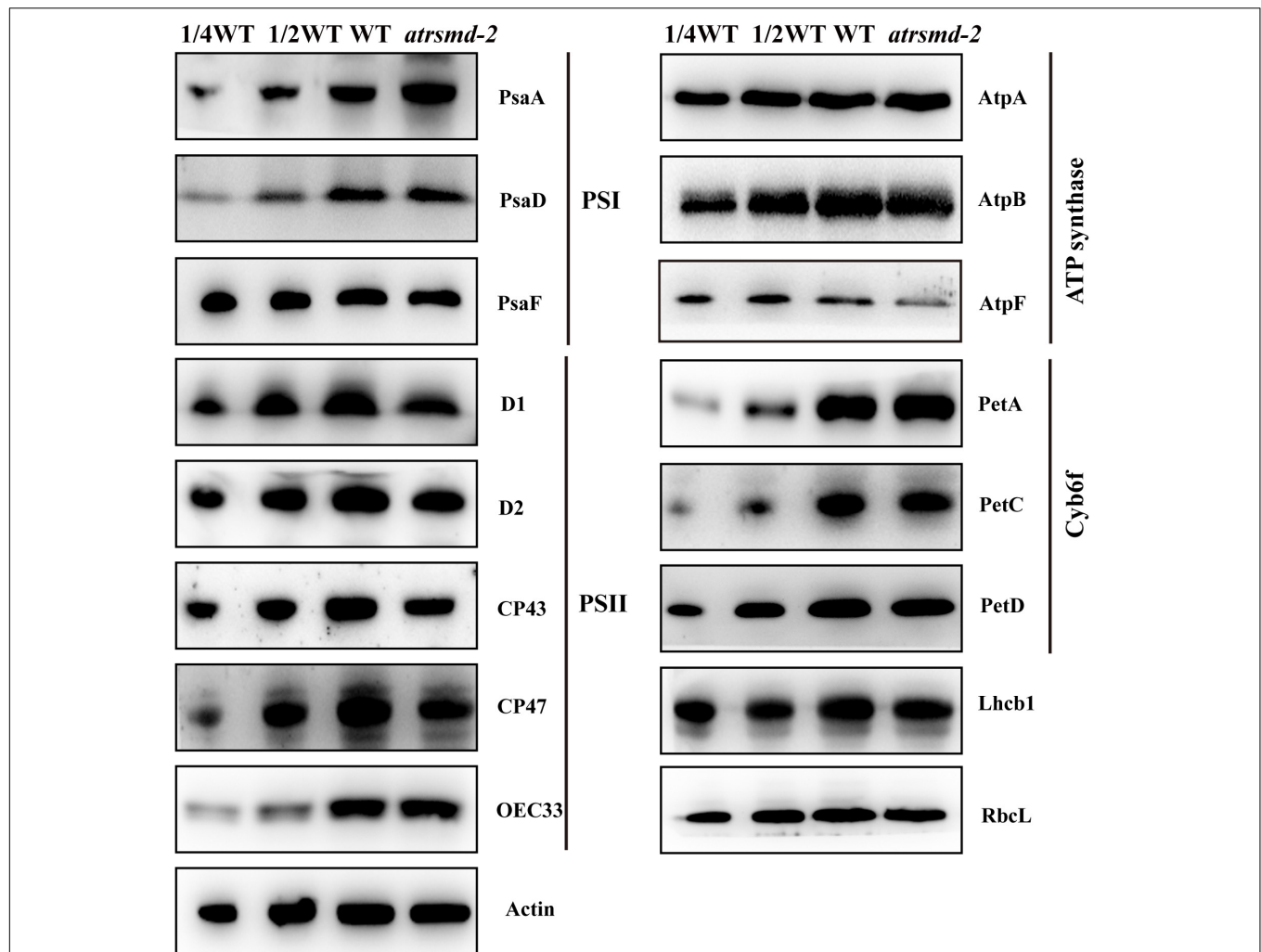


FIGURE 4 | Immunoblot analysis of the photosynthetic proteins from the wild type (WT) and *atrsmD-2* mutant. Total protein samples were prepared from 14-day-old emerging leaves of the wild type and *atrsmD-2* mutant and then separated by SDS-PAGE. Immunoblot analysis of the photosynthetic proteins PsaA, PsaD, PsaF, D1, D2, CP43, CP47, OEC33, AtpA, AtpB, AtpF, PetA, PetC, PetD, Lhcb1, and RbcL using the corresponding antibodies was performed. Total proteins from the WT samples were loaded at three different concentrations (2.5, 5, and 10 μ g), and total proteins from the mutant samples were loaded at 10 μ g.

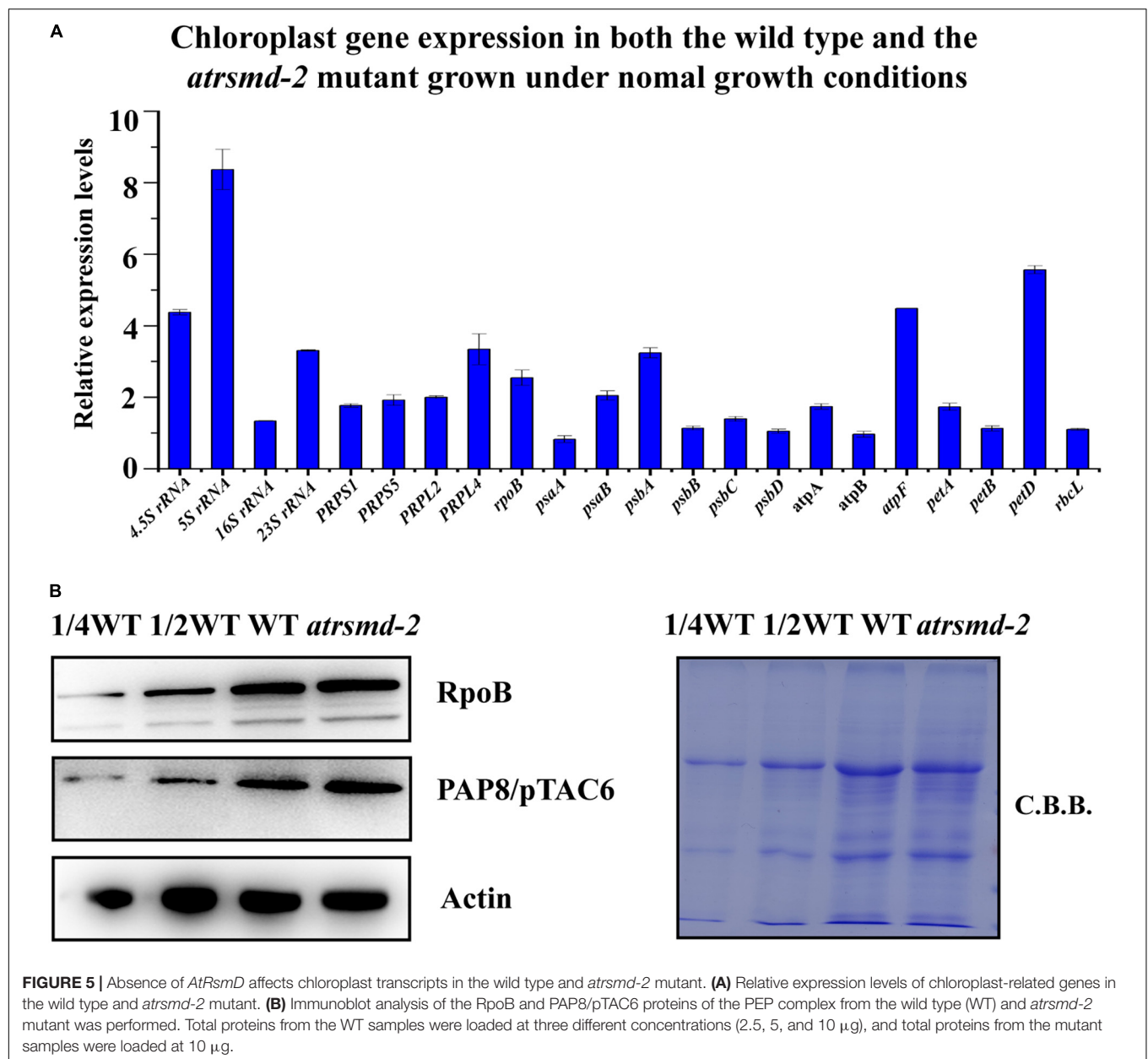
ribosomal proteins. Nevertheless, knockout of the *AtRsmD* gene has a minor effect on chloroplast ribosome biogenesis.

We subsequently investigated the effect of *AtRsmD* gene knockout on chloroplast translation initiation and termination. We examined the association of several plastid-encoded RNAs with chloroplast ribosomes. Polysome-enriched samples were isolated from the emerging young leaves of both the wild-type and *atrsmD-2* mutant under polysome-preserving conditions and further fractionated through sucrose density-gradient centrifugation (Figure 7). Total RNA was isolated from 10 fractions and subjected to denaturing gel electrophoresis and RNA gel blot analyses using selected plastid transcript probes. As shown in Figure 7, we found that the amount of 16S rRNA in the polysomal fragments was slightly greater than that in the monosomal fragments in the *atrsmD-2* mutant compared with that in the wild type. Similar trends were also observed for other transcripts, including 23S rRNA, *psbA*, and *rbcL*. These results

suggested that the knockout of *AtRsmD* had minor effects on the RNA loading of chloroplast ribosomes.

Absence of the *AtRsmD* Protein Enhances the Sensitivity to Cold Stress and Chloroplast Translation Inhibitors

A recent study revealed that loss-of-function mutation of the *AtRsmD* gene enhanced its sensitivity to cold stress and prokaryotic translation inhibitors (Ngoc et al., 2021b). Lincomycin (LIN) and chloramphenicol (CAP) specifically inhibit the elongation of nascent polypeptide chains or block mRNA binding to the ribosome in prokaryotes. Here, we also investigated the effect of these two prokaryotic translation inhibitors on the *atrsmD-2* mutant. The *atrsmD-2* mutant was grown on MS medium plates in the presence of different LIN or CAP concentrations under sterile conditions, while the wild-type



line was used as a control. Five days after germination, the *atrsmd-2* mutant clearly exhibited hypersensitivity to lincomycin, as indicated by the enhanced loss of leaf coloration relative to the wild-type control. In contrast, the *atrsmd-2* mutant is less sensitive to chloramphenicol than it is to lincomycin. Quantification of chlorophyll levels showed that LIN-treated *atrsmd-2* seedlings accumulated significantly less of these pigments than wild-type seedlings (Supplementary Figure 1). These results demonstrated that knockout of *AtRsmD* enhanced the sensitivity to chloroplast translation inhibitors, especially lincomycin, indicating that the *AtRsmD* knockout line has compromised chloroplast ribosome activity.

We also investigated whether the *atrsmd-2* mutant is sensitive to cold stress. Two-week-old *atrsmd-2* mutants grown at 22°C

were transferred to 4°C and grown for another 2 weeks, while the wild-type line was used as a control. For the *atrsmd-2* mutant, yellowing became visible after 1 week of cold treatment and only occurred in the emerging leaves (Supplementary Figure 2A). In contrast, the wild type did not show obvious yellowing of the leaves (Supplementary Figure 2A). Transmission electron microscopy observations showed that a few grana and thylakoids could be observed in the chloroplasts of the *atrsmd-2* mutant, and these membrane systems did not connect well. In contrast, the well-organized stroma and thylakoid systems could be observed in the wild-type chloroplasts (Supplementary Figure 2B). Chloroplasts from pale green leaves have more scattered grana structures in the *atrsmd-2* mutant, and the thylakoid membranes were loosely organized. In contrast, well-organized thylakoids

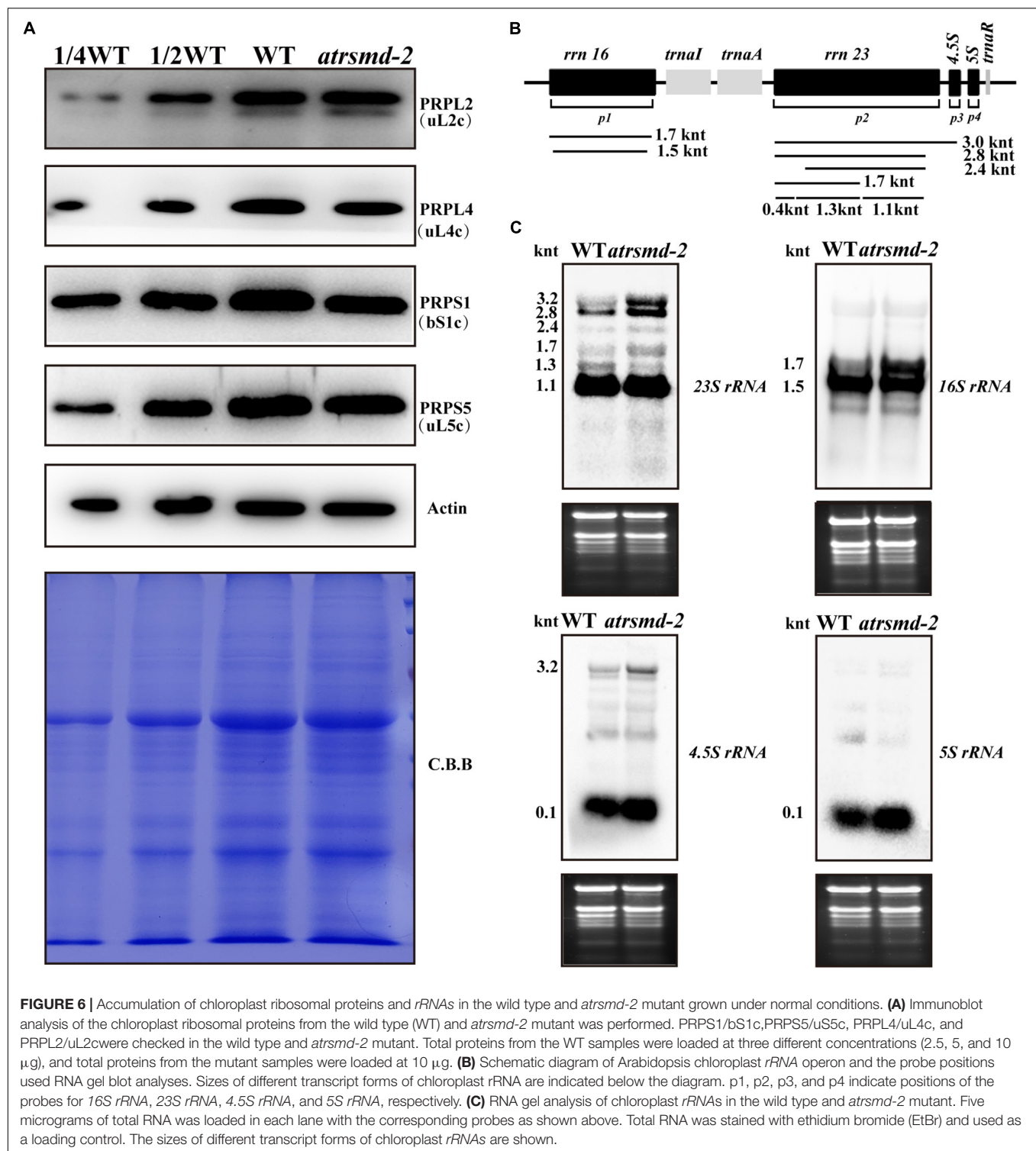
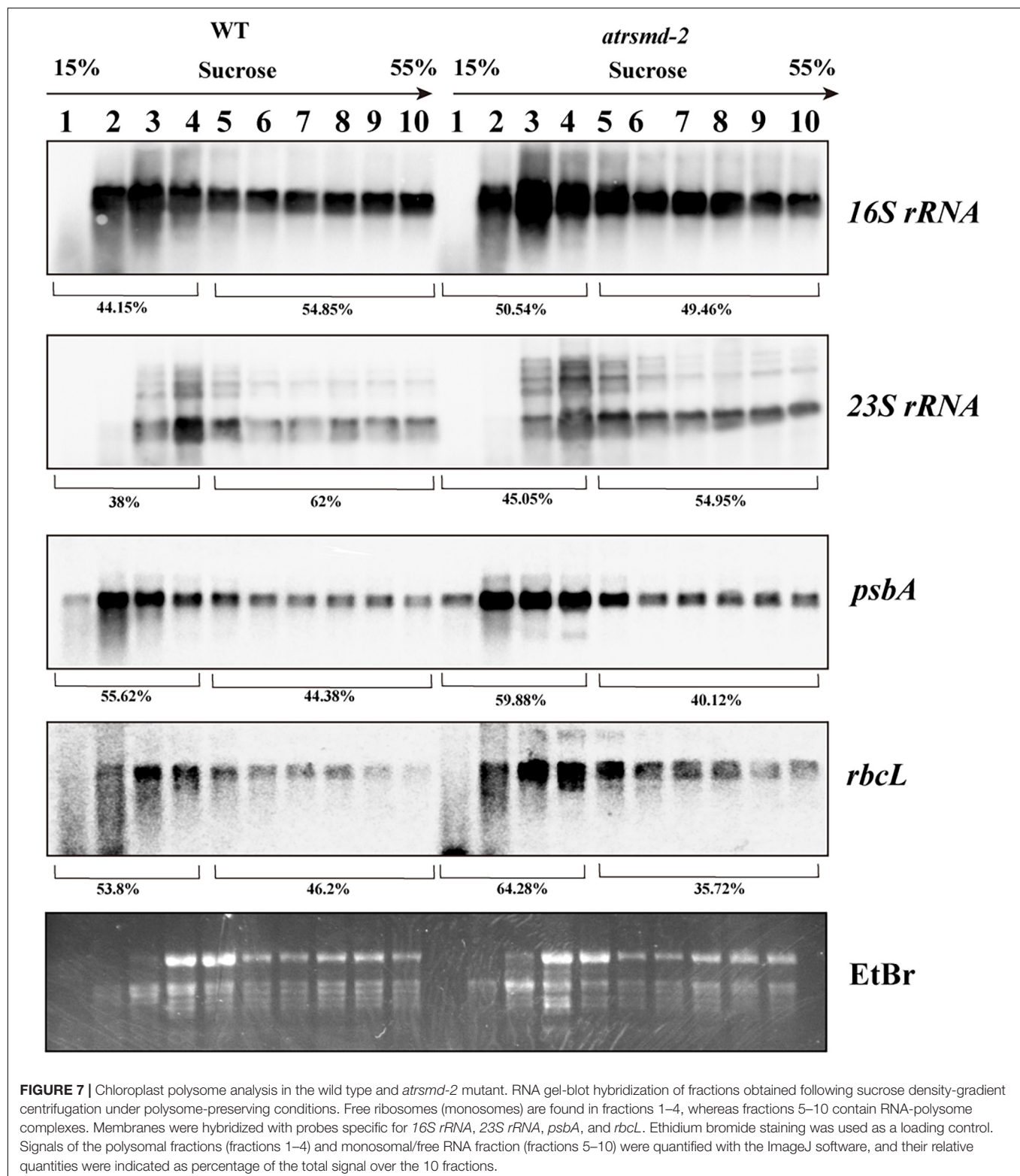


FIGURE 6 | Accumulation of chloroplast ribosomal proteins and *rRNAs* in the wild type and *atrsmD-2* mutant grown under normal conditions. **(A)** Immunoblot analysis of the chloroplast ribosomal proteins from the wild type (WT) and *atrsmD-2* mutant was performed. PRPS1/bS1c, PRPS5/uS5c, PRPL4/uL4c, and PRPL2/uL2c were checked in the wild type and *atrsmD-2* mutant. Total proteins from the WT samples were loaded at three different concentrations (2.5, 5, and 10 μ g), and total proteins from the mutant samples were loaded at 10 μ g. **(B)** Schematic diagram of Arabidopsis chloroplast *rRNA* operon and the probe positions used RNA gel blot analyses. Sizes of different transcript forms of chloroplast *rRNA* are indicated below the diagram. p1, p2, p3, and p4 indicate positions of the probes for 16S *rRNA*, 23S *rRNA*, 4.5S *rRNA*, and 5S *rRNA*, respectively. **(C)** RNA gel analysis of chloroplast *rRNAs* in the wild type and *atrsmD-2* mutant. Five micrograms of total RNA was loaded in each lane with the corresponding probes as shown above. Total RNA was stained with ethidium bromide (EtBr) and used as a loading control. The sizes of different transcript forms of chloroplast *rRNAs* are shown.

could be observed in the wild type (Supplementary Figure 2B). We then checked the abundance of photosynthesis-related proteins, and our results revealed that the amounts of the photosynthesis-related proteins PetD, D1, CP43, OEC33, and AtpF were reduced to 10–50% of those in the wild-type (Supplementary Figure 2C). These results showed that the

accumulation of photosynthesis-related proteins was reduced in the *atrsmD-2* mutant under cold stress conditions. We further examined the amount of chloroplast ribosome proteins, including PRPS1 (bS1c), PRPS5 (uS5c), PRPL2 (uL2c), and PRPL4 (uL4c), in the wild type and *atrsmD-2* mutant. Our immunoblotting data revealed that the amounts of these



chloroplast ribosomal proteins in the *atrsmd-2* mutant were approximately 10–20% of those in the wild type under cold stress (Figure 8A). The levels of chloroplast rRNA transcripts were also investigated using RNA blot analysis in the *atrsmd-2*

mutant. Our results indicated that the amount of the mature form of chloroplast 16S rRNA (1.5-knt molecule) in the *atrsmd-2* mutant was half of that in the wild type, whereas the amount of the precursor rRNA (1.7-knt) molecule was increased

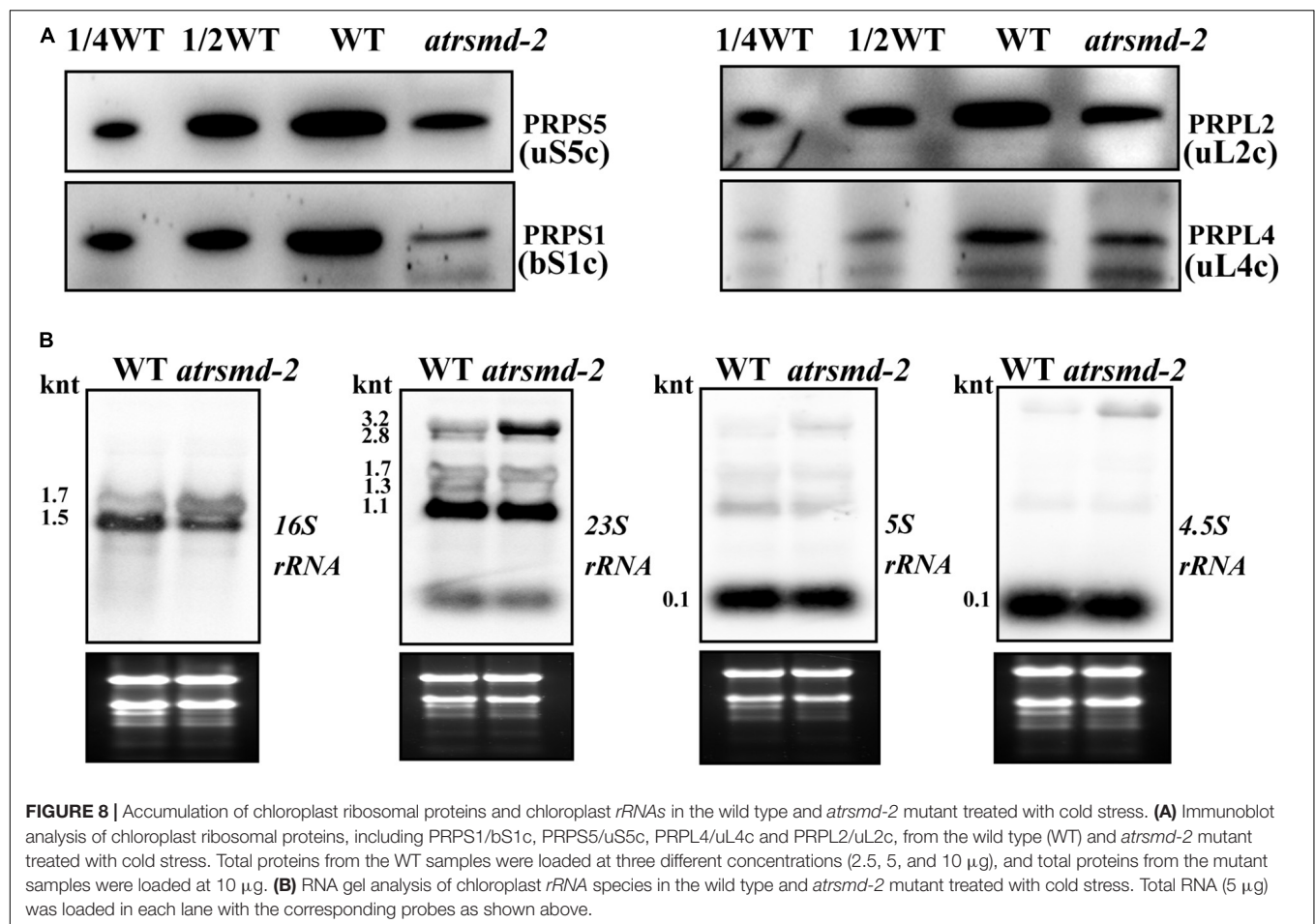


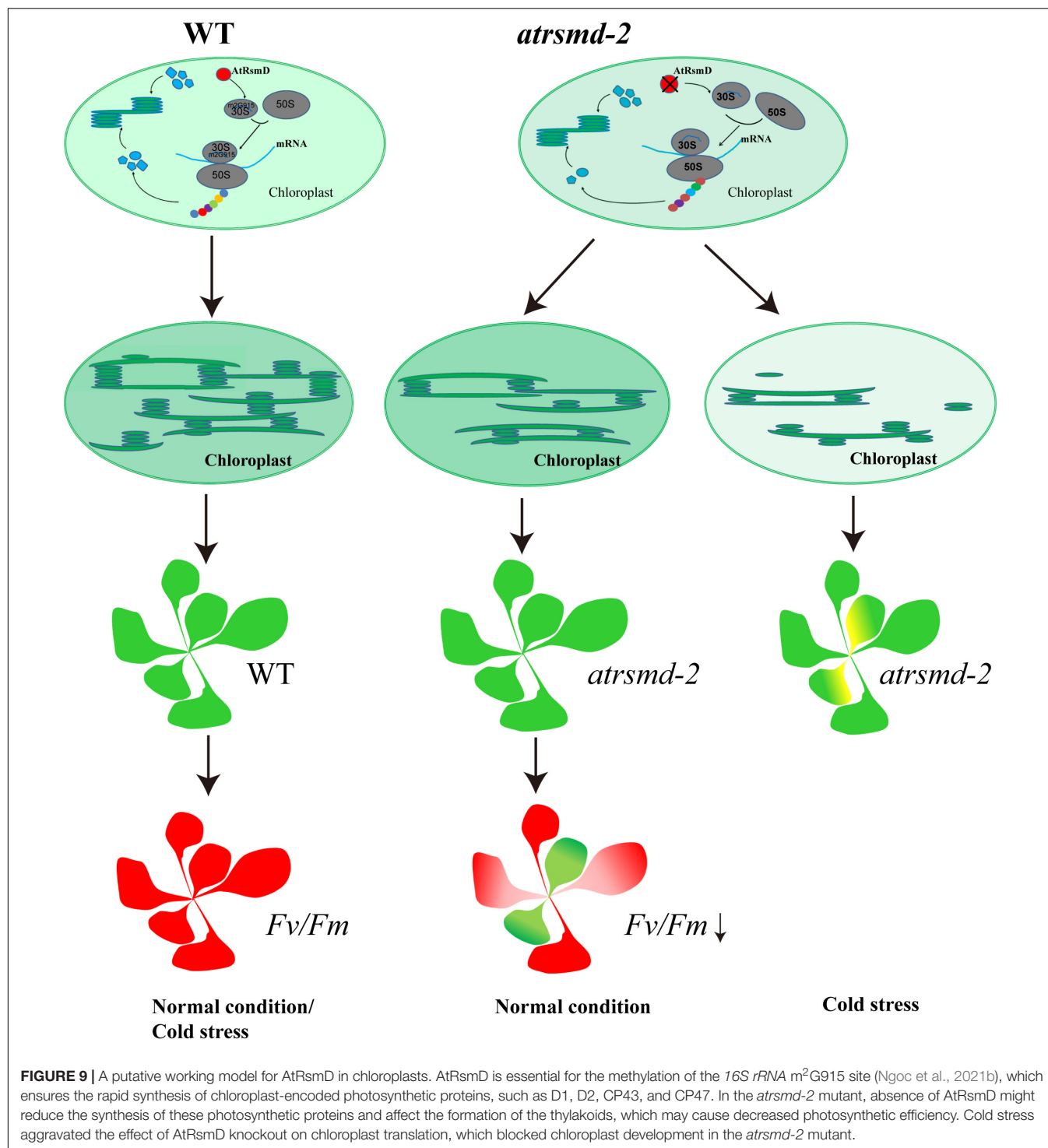
(Figure 8B). The levels of the three 3.2-knt 23S *rRNA* species were increased in *atsrmd-2*, while the level of a shorter form of the 1.3-knt transcript was decreased (Figure 8B). The levels of both the 4.5S and 5S *rRNA* transcripts were clearly reduced in the *atsrmd-2* mutant. These data suggest that the effects of *AtRsmD* gene knockout on chloroplast ribosome assembly and chloroplast protein accumulation were exacerbated, which enhances sensitivity to cold stress.

DISCUSSION

AtRsmD encodes a chloroplast-localized MTase for N₂-methylguanosine (m²G) modification of 16S *rRNA* at position 915 in Arabidopsis chloroplasts, which plays a role in the adaptation of Arabidopsis to cold stress. There were no obvious differences in seedling growth in the knockout mutant when grown under normal growth conditions (Ngoc et al., 2021b). This work extends the previous study and further characterizes the *atsrmd-2* mutant. Our current study sheds light on the important roles of the *AtRsmD* protein in chloroplast development and chloroplast function. Fewer thylakoid membranes were observed in the *atsrmd-2* mutant (Supplementary Figure 2B). Notably, the loss-of-function *atsrmd-2* mutant exhibited

impaired photosynthetic efficiency under normal growth conditions, although no visible phenotype could be observed in the *atsrmd-2* mutant (Figure 1). Impaired photosynthesis is a possible consequence of the reduced levels of chloroplast-encoded photosynthesis-related proteins that hindered the assembly of the photosynthetic super complex (Figures 4, 5). Deletion of the *AtRsmD* gene had minor effects on chloroplast ribosome biogenesis and the RNA loading of chloroplast ribosomes (Figures 6, 7), but the effect on chloroplast ribosome biogenesis and chloroplast development was aggravated when the mutated line was treated with cold stress (Figure 8 and Supplementary Figure 2). Our data and those of a recent report (Ngoc et al., 2021b) together suggested that the *AtRsmD* protein for the m²G915 modification of 16S *rRNA* plays important regulatory roles in chloroplast development and chloroplast function.

16S *rRNA* is a constituent of the 30S small subunit in the prokaryotic-type 70S ribosome that is widely present in prokaryotes and eukaryotic organelles (mitochondria and chloroplasts). The nucleotide residue of 16S *rRNA* tends to be guanosine in bacteria and chloroplasts (Lesnyak et al., 2007), while it is usually uridine in archaea and adenosine in mitochondria (Lesnyak et al., 2007). Accordingly, homologous proteins of *E. coli* RsmD are present in higher plant chloroplasts



(Supplementary Figures 3, 4) but are completely absent in both Archaea and Eukarya. The AtRsmD protein shares highly conserved motifs, such as Dx(F/G/Y)xGxG and (D/N/T)PP(F/Y), with those in *E. coli*; these motifs are required for S-adenosyl-L-methionine (SAM) binding (Supplementary Figure 3; Rana et al., 2013; Ngoc et al., 2021b). Importantly, a recent report demonstrated that AtRsmD is a MTase responsible for

chloroplast 16S rRNA m²G 915 methylation, which is absent in the *atsrmd-1* mutant (Ngoc et al., 2021b). Although we did not investigate modifications to the *atsrmd-2* mutant in this study, genetic analysis demonstrated that the phenotype of *atsrmd-2* is caused by the deletion of AtRsmD. Thus, it is possible that chloroplast 16S rRNA m²G 915 methylation is lacking in the *atsrmd-2* mutant. Chloroplast ribosomes are

attached to the thylakoid membrane (Yamamoto et al., 1981). A chloroplast ribosome proteome study revealed that the homologous protein of RsmD in *Chlamydomonas reinhardtii* comigrated with the 30S ribosome (Westrich et al., 2021). In *E. coli*, the RsmD enzyme methylates the nucleotide of 16S rRNA and is involved in the assembly of the 30S subunit of the ribosome (Lesnyak et al., 2007). AtRsmD also methylates 16S rRNA in chloroplast ribosomes (Ngoc et al., 2021b). An early plastid nucleoid proteomics study has shown that the homologous protein of RsmD in maize is a plastid nucleoid protein (Majeran et al., 2012). Our result also indicates that AtRsmD is associated with the thylakoids (Figure 2D). The thylakoid-associated localization of AtRsmD protein and the high levels of the *AtRsmD* transcript in green tissues are consistent with its putative function.

Methylation of rRNAs has been shown to be a novel cellular regulatory mechanism that is intimately associated with chloroplast translation (Manduzio and Kang, 2021). Multiple nucleotide sites of 16S rRNA are methylated in *E. coli*, and these methylation sites play important regulatory roles in the function of ribosomes (Carrión et al., 1999; Lesnyak et al., 2007). In *E. coli*, C1352 methylation is essential for viability, and the gene *mraW* encoding the corresponding MTase is essential (Carrión et al., 1999). Additionally, the lack of C1352 methylation in 16S rRNA (Zou et al., 2020; Ngoc et al., 2021a) clearly reduced chloroplast translation (Zou et al., 2020), which seriously affected plant growth and development. Thus, methylation of the C1352 nucleotide is essential for maintaining chloroplast function. The G966 nucleotide of *E. coli* 16S rRNA is in direct contact with P-site-bound tRNA and forms a direct contact with the tip of the anticodon loop (Lesnyak et al., 2007). The nucleotide sequence of 16S rRNA is conserved between *E. coli* and chloroplasts (Supplementary Figure 5). Knockout of the *rsmD* gene is viable, and no visible phenotype can be observed in *E. coli* (Jemiolo et al., 1991; Lesnyak et al., 2007; Burakovsky et al., 2012). It seems that no vital function of the ribosome is affected when there is an absence of methylated G966 in *E. coli* (Lesnyak et al., 2007). Similarly, neither germination nor seedling growth of the Arabidopsis *rsmD* mutant were affected under normal growth conditions (Ngoc et al., 2021b). However, our data presented here clearly indicated that the photosynthesis efficiency was reduced in the *atrsmd-2* mutant grown under normal conditions (Figure 1B), although no visible phenotype was observed (Figure 1B). Further observation showed that chloroplast development was impaired in the *atrsmd-2* mutant (Supplementary Figure 2). In accordance with this finding, the chloroplast-encoded photosynthesis-related proteins D1, D2, CP43, CP47, and AtpF were obviously reduced in the *atrsmd-2* mutant, and assembly of the photosynthesis complex was also decreased (Figures 3, 4). Thus, the AtRsmD protein is required for chloroplast development and chloroplast function. In contrast to the effect of the deletion of the CAML protein on chloroplast ribosome biogenesis (Zou et al., 2020), our data indicated that the knockout of the AtRsmD protein had minor effects on chloroplast ribosome biogenesis (Figure 6) and chloroplast RNA loading in Arabidopsis under normal growth conditions (Figure 7). Functional activity of the chloroplast

ribosome is retained in the absence of the 16S rRNA m²G915 modification. Lack of the 16S rRNA m²G915 site did not have a major effect on the translation of photosynthetic proteins because the amounts of the chloroplast-encoded photosynthetic proteins D1 and D2 were reduced in the *atrsmd-2* mutant; however, PsaA and PetA were not reduced (Figure 4). This result is different from the observation of the *cmal* mutant (Zou et al., 2020; Ngoc et al., 2021a), in which the absence of C1352 methylation seriously generally affected chloroplast translation events. Noticeably, the nucleotide modification of the G966 nucleotide influences Watson-Crick positions within the modified base in *E. coli*, since the nucleotide is located in the anticodon region (Moazed and Noller, 1990; Lesnyak et al., 2007). Lack of modification interrupts the hydrophobic interaction with the anticodon of the P-site-bound tRNA, which probably affects the fidelity of chloroplast translation. Nevertheless, it is difficult to check the fidelity of chloroplast translation in the *atrsmd-2* mutant at present. Lack of the m²G915 modification in the 16S rRNA might affect the elongation of polypeptide chains because the *atrsmd-2* mutant exhibited more sensitivity to lincomycin, which specifically inhibits the elongation of nascent polypeptide chains (Supplementary Figure 4). It is likely that the m²G915 modification of the 16S rRNA represents a novel regulatory mechanism for translation in chloroplast-encoded photosynthesis proteins rather than a general regulation of chloroplast translation. Mutants in which chloroplast translation is compromised exhibit sensitivity to cold stress (Tokuhisa et al., 1998; Rogalski et al., 2008; Liu et al., 2010; Fleischmann et al., 2011; Zhang et al., 2016; Pulido et al., 2018). Similar to the *atrsmd-1* mutant described in Ngoc et al. (2021b), the *atrsmd-2* mutant was found to be more sensitive to translational inhibitors (Supplementary Figure 1) and cold stress (Supplementary Figure 2) than the wild-type. Further characterization of the *atrsmd-2* mutant treated with cold stress revealed that defects in chloroplast ribosomal biogenesis were aggravated under cold stress (Figure 8). Our study, together with the report by Ngoc et al. (2021b), showed that knockout of the AtRsmD protein for the methylation of 16S rRNA m²G915 in chloroplasts reduced the accumulation of several important chloroplast-encoded photosynthetic proteins, which could not meet the needs of rapid chloroplast development and thylakoid membrane formation in emerging leaves, and cold stress exacerbated the effect on chloroplast development (Figure 9). Overall, this study combined with a previous report (Ngoc et al., 2021b) showed that the AtRsmD protein involved in the methylation of 16S rRNA m²G915 in chloroplasts is required for chloroplast development and chloroplast function. This work extends our understanding of the significance of the methylation of chloroplast rRNAs in chloroplast development and chloroplast function.

DATA AVAILABILITY STATEMENT

The original contributions presented in the study are included in the article/Supplementary Material, further inquiries can be directed to the corresponding author/s.

AUTHOR CONTRIBUTIONS

Q-BY designed the research and wrote the manuscript. Z-YW, W-TQ, TM, NZ, and N-YY performed the experiments. Z-NY, H-BX, X-FX, and Q-BY analyzed the data. All authors contributed to the article and approved the submitted version.

FUNDING

This work was supported by the National Natural Scientific Foundation of China (grant no. 31570232) and funds from the Shanghai Key Laboratory of Plant Molecular Sciences.

ACKNOWLEDGMENTS

We thank the Arabidopsis Biological Resource Center for providing the T-DNA insertion line (CS832131). We thank Prof. Lianwei Peng for help with BN-PAGE and polysome analysis.

SUPPLEMENTARY MATERIAL

The Supplementary Material for this article can be found online at: <https://www.frontiersin.org/articles/10.3389/fpls.2022.860945/full#supplementary-material>

Supplementary Figure 1 | Absence of AtRsmD enhances the effects of the translation inhibitors LIN and CAP. **(A)** Representative images of 5-day-old wild-type (WT) and *atrsmD-2* mutant plants germinated on Murashige and Skoog (MS) medium containing the indicated concentrations of LIN. The quantification of the total chlorophyll levels (see section “Materials and Methods”) demonstrates the differences between wild-type and mutant plants grown in the presence of LIN. Relative data are shown (wild-type plants grown in the absence of LIN = 100%), and means \pm se values ($n = 3$) are provided. **(B)** Representative images of 5-day-old wild-type (WT) and *atrsmD-2* mutant plants germinated on Murashige and Skoog (MS) medium containing the indicated concentrations of CAP. The quantification of the total chlorophyll levels (see section “Materials and Methods”) demonstrates the differences between wild-type and mutant plants grown in the

presence of CAP. Relative data are shown (wild-type plants grown in the absence of CAP = 100%), and means \pm se values ($n = 3$) are provided.

Supplementary Figure 2 | Chloroplast development in the wild type and *atrsmD-2* mutant treated with cold stress. **(A)** Phenotype of the wild type and *atrsmD-2* mutant treated with cold stress. Bar: 1 cm. **(B)** Chloroplast ultrastructure observation in the wild type and *atrsmD-2* mutant. Bar: 1 μ m. **(C)** Immunoblot analysis of the photosynthetic proteins from the wild type (WT) and *atrsmD-2* mutant that were treated with cold stress. Immunoblot analysis of the photosynthetic proteins PsaA, PsaF, D1, CP43, OEC33, AtpA, AtpC, AtpF, PetC, PetD, and RbcL was performed using the corresponding antibodies. Total proteins from the WT samples were loaded at three different concentrations (2.5, 5, and 10 μ g), and total proteins from the mutant samples were loaded at 10 μ g.

Supplementary Figure 3 | Alignment of *E. coli* RsmD homologous proteins in land plants. Alignment of the amino acid sequence of RsmD homologs in land plants. Sequence identifiers for RsmD homologs are as follows: *Arabidopsis thaliana* (NP_189487.2), *Oryza sativa japonica* group (EEE59885.1), and *Escherichia coli* (EGS2103359.1).

Supplementary Figure 4 | Phylogenetic analysis of the AtRsmD protein and its orthologs from different species. The orthologous proteins are listed as follows: *Camelina sativa* (XP_010514550.1), *Brassica napus* (XP_013711825.1), *Capsella rubella* (XP_023639147.1), *Arabidopsis lyrata* subsp. *lyrata* (XP_002877109.1), *Arabidopsis thaliana* (NP_189487.2), *Ricinus communis* (XP_015573725.1), *Vitis vinifera* (XP_002281501.1), *Oryza sativa japonica* Group (EEE59885.1), *Zea mays* (ACG38583.1), *Physcomitrella patens* (XP_024381071.1), *Selaginella moellendorffii* (EFJ21750.1), *Ostreococcus lucimarinus* CCE9901(XP_001417522.1), *Micromonas pusilla* CCMP1545(XP_003060663.1), *Chloropicon primus* (QDZ19162.1), *Gonium pectoral* (KXZ51239.1), *Chlamydomonas reinhardtii* (XP_042917255.1), *Cyanidioschyzon merolae* strain 10D (XP_005537355.1), *Galdieria sulphuraria* (XP_005703506.1), *Gracilariopsis chorda* (PXF40802.1), *Fischerella thermalis* (WP_102206177.1), *Escherichia coli* (EGS2103359.1), *Oscillatoriales cyanobacterium* MTP1(TAD77760.1), *Synechococcus* sp. PCC 73109 (WP_062431539.1), *Cyanobacteria* (WP_044151411.1), *Synechocystis* sp. PCC 7509 (WP_009631812.1), *Nostoc* sp. 106C (WP_086756145.1), and *Phormidium ambiguum* (WP_073593883.1).

Supplementary Figure 5 | Alignment of 16S rRNAs from different organisms. Sequence identifiers for RsmD homologs are as follows: *Oryza sativa* (MK348618.1), *Brachypodium distachyon* (LR537486.1), *Hordeum vulgare*, (MN171392.1), *Sorghum bicolor* (MK348612.1), *Zea mays* (MK348606.1), *Arabidopsis thaliana* (MK353213.1), *Cyanobacterium* (LN833508.1), *Populus trichocarpa* (AC208048.1), *Glycine max* (DQ317523.1), *Chlamydomonas reinhardtii* (MF083689.2), and *Escherichia coli* (CP056921.1).

REFERENCES

- Abdallah, F., Salamini, F., and Leister, D. (2000). A prediction of the size and evolutionary origin of the proteome of chloroplasts of *Arabidopsis*. *Trends Plant Sci.* 5, 141–142. doi: 10.1016/s1360-1385(00)01574-0
- Andersen, N. M., and Douthwaite, S. (2006). YebU is a m5C methyltransferase specific for 16 S rRNA nucleotide 1407. *J. Mol. Biol.* 359, 777–786. doi: 10.1016/j.jmb.2006.04.007
- Ban, N., Nissen, P., Hansen, J., Moore, P. B., and Steitz, T. A. (2000). The complete atomic structure of the large ribosomal subunit at 2.4 Å resolution. *Science* 289, 905–920. doi: 10.1126/science.289.5481.905
- Brimacombe, R., Mitchell, P., Osswald, M., Stade, K., and Bochkariov, D. (1993). Clustering of modified nucleotides at the functional center of bacterial ribosomal RNA. *FASEB J.* 7, 161–167. doi: 10.1096/fasebj.7.1.8422963
- Bujnicki, J. M., and Rychlewski, L. (2002). RNA:(guanine-N2) methyltransferases RsmC/RsmD and their homologs revisited—bioinformatic analysis and prediction of the active site based on the uncharacterized Mj0882 protein structure. *BMC Bioinformatics* 3:10. doi: 10.1186/1471-2105-3-10
- Burakovsky, D. E., Prokhorova, I. V., Sergiev, P. V., Milón, P., Sergeeva, O. V., Bogdanov, A. A., et al. (2012). Impact of methylations of m2G966/m5C967 in 16S rRNA on bacterial fitness and translation initiation. *Nucleic Acids Res.* 40, 7885–7895. doi: 10.1093/nar/gks508
- Carrión, M., Gómez, M. J., Merchante-Schubert, R., Dongarrá, S. R., and Ayala, J. A. (1999). mraW, an essential gene at the dcw cluster of *Escherichia coli* codes for a cytoplasmic protein with methyltransferase activity. *Biochimie* 81, 879–888. doi: 10.1016/s0300-9084(99)00208-4
- Clough, S. J., and Bent, A. F. (1998). Floral dip: a simplified method for *Agrobacterium*-mediated transformation of *Arabidopsis thaliana*. *Plant J.* 16, 735–743. doi: 10.1046/j.1365-3113.1998.00343.x
- Fleischmann, T. T., Scharff, L. B., Alkatib, S., Hasdorf, S., Schöttler, M. A., and Bock, R. (2011). Nonessential plastid-encoded ribosomal proteins in tobacco: a developmental role for plastid translation and implications for reductive genome evolution. *Plant Cell* 23, 3137–3155. doi: 10.1105/tpc.111.088906
- Graf, M., Arenz, S., Huter, P., Dönhöfer, A., Nováček, J., and Wilson, D. N. (2017). Cryo-EM structure of the spinach chloroplast ribosome reveals the location of plastid-specific ribosomal proteins and extensions. *Nucleic Acids Res.* 45, 2887–2896. doi: 10.1093/nar/gkw1272
- Green, R., and Noller, H. F. (1999). Reconstitution of functional 50S ribosomes from *in vitro* transcripts of *Bacillus stearothermophilus* 23S rRNA. *Biochemistry* 38, 1772–1779. doi: 10.1021/bi982246a
- Harms, J., Schlutzen, F., Zarivach, R., Bashan, A., Gat, S., Agmon, I., et al. (2001). High resolution structure of the large ribosomal subunit from a mesophilic eubacterium. *Cell* 107, 679–688. doi: 10.1016/s0092-8674(01)00546-3
- Jemiolo, D. K., Taurence, J. S., and Giese, S. (1991). Mutations in 16S rRNA in *Escherichia coli* at methyl-modified sites: G966, G967, and G1207. *Nucleic Acids Res.* 19, 4259–4265. doi: 10.1093/nar/19.15.4259

- Keeling, P. J. (2013). The number, speed, and impact of plastid endosymbioses in eukaryotic evolution. *Annu. Rev. Plant Biol.* 64, 583–607. doi: 10.1146/annurev-arplant-050312-120144
- Khaitovich, P., Tenson, T., Kloss, P., and Mankin, A. S. (1999). Reconstitution of functionally active *Thermus aquaticus* large ribosomal subunits with *in vitro* transcribed rRNA. *Biochemistry* 38, 1780–1788. doi: 10.1021/bi9822473
- Kimura, S., and Suzuki, T. (2010). Fine-tuning of the ribosomal decoding center by conserved methyl-modifications in the *Escherichia coli* 16S rRNA. *Nucleic Acids Res.* 38, 1341–1352. doi: 10.1093/nar/gkp1073
- Krzyzosiak, W., Denman, R., Nurse, K., Hellmann, W., Boubik, M., Gehrke, C. W., et al. (1987). *In vitro* synthesis of 16S ribosomal RNA containing single base changes and assembly into functional 30S ribosome. *Biochemistry* 26, 2353–2364. doi: 10.1021/bi00382a042
- Lesnyak, D. V., Osipiuk, J., Skarina, T., Sergiev, P., Bogdanov, A. A., Edwards, A., et al. (2007). Methyltransferase that modifies guanine 966 of the 16S rRNA: functional identification and tertiary structure. *J. Biol. Chem.* 282, 5880–5887. doi: 10.1074/jbc.M608214200
- Li, Y., Liu, B., Zhang, J., Kong, F., Zhang, L., Meng, H., et al. (2019). OHP1, OHP2, and HCF244 form a transient functional complex with the photosystem II reaction center. *Plant Physiol.* 179, 195–208. doi: 10.1104/pp.18.01231
- Liu, X., Rodermeier, S. R., and Yu, F. (2010). A *var2* leaf variegation suppressor locus, *SUPPRESSOR OF VARIEGATION3*, encodes a putative chloroplast translation elongation factor that is important for chloroplast development in the cold. *BMC Plant Biol.* 10:287. doi: 10.1186/1471-2229-10-287
- Majeran, W., Friso, G., Asakura, Y., Qu, X., Huang, M., Ponnala, L., et al. (2012). Nucleoid-enriched proteomes in developing plastids and chloroplasts from maize leaves: a new conceptual framework for nucleoid functions. *Plant Physiol.* 158, 156–189. doi: 10.1104/pp.111.188474
- Manduzio, S., and Kang, H. (2021). RNA methylation in chloroplasts or mitochondria in plants. *RNA Biol.* 18, 2127–2135. doi: 10.1080/15476286.2021.1909321
- Moazed, D., and Noller, H. F. (1990). Binding of tRNA to the ribosomal A and P sites protects two distinct sets of nucleotides in 16S rRNA. *J. Mol. Biol.* 211, 135–145. doi: 10.1016/0022-2836(90)90016-F
- Ngoc, L. N. T., Park, S. J., Huong, T. T., Lee, K. H., and Kang, H. (2021a). N4-methylcytidine rRNA methylation in chloroplasts is crucial for chloroplast function, development, and abscisic acid response in *Arabidopsis*. *J. Integr. Plant Biol.* 63, 570–582. doi: 10.1111/jipb.13009
- Ngoc, L. N. T., Park, S. J., Cai, J., Huong, T. T., Lee, K., and Kang, H. (2021b). RsmD, a Chloroplast rRNA m2G Methyltransferase, Plays a Role in Cold Stress Tolerance by Possibly Affecting Chloroplast Translation in *Arabidopsis*. *Plant Cell Physiol.* 62, 948–958. doi: 10.1093/pcp/pcab060
- Porra, R. J. (2002). The chequered history of the development and use of simultaneous equations for the accurate determination of chlorophylls a and b. *Photosynth. Res.* 73, 149–156. doi: 10.1023/A:1020470224740
- Pulido, P., Zagari, N., Manavski, N., Gawronski, P., Matthes, A., Scharff, L. B., et al. (2018). CHLOROPLAST RIBOSOME ASSOCIATED supports translation under stress and interacts with the ribosomal 30S Subunit. *Plant Physiol.* 177, 1539–1554. doi: 10.1104/pp.18.00602
- Rana, K. A., Chandr, S., Siddiqi, M. I., and Misra-Bhattacharya, S. (2013). Molecular Characterization of an *rsmD*-Like rRNA Methyltransferase from the *Wolbachia* Endosymbiont of *Brugia malayi* and Antifilarial Activity of Specific Inhibitors of the Enzyme. *Antimicrob. Agents Chemother.* 57, 3843–3856. doi: 10.1128/AAC.02264-12
- Rogalski, M., Schöttler, M. A., Thiele, W., Schulze, W. X., and Bock, R. (2008). Rpl33, a nonessential plastid-encoded ribosomal protein in tobacco, is required under cold stress conditions. *Plant Cell* 20, 2221–2237. doi: 10.1105/tpc.108.060392
- Schuwirth, B. S., Borovinskaya, M. A., Hau, C. W., Zhang, W., Vila-Sanjurjo, A., Holton, J. M., et al. (2005). Structures of the bacterial ribosome at 3.5 Å resolution. *Science* 310, 827–834.
- Sergiev, P., Golovina, A., Prokhorova, I., Sergeeva, O., Osterman, I., Nesterchuk, M., et al. (2011). “Modifications of ribosomal RNA: from enzymes to function,” in *Ribosomes: Structure, Function, and Dynamics*, eds M. V. Rodnina, W. Wintermeyer, and R. Green (Wien, NY: Springer), 97–110. doi: 10.1007/978-3-7091-0215-2_9
- Tokuhisa, J. G., Vijayan, P., Feldmann, K. A., and Browse, J. A. (1998). Chloroplast development at low temperatures requires a homolog of DIM1, a yeast gene encoding the 18S rRNA demethylase. *Plant Cell* 10, 699–711. doi: 10.1105/tpc.105.699
- Urlaub, H., Thiede, B., Müller, E. C., Brimacombe, R., and Wittmann-Liebold, B. (1997). Identification and sequence analysis of contact sites between ribosomal proteins and rRNA in *Escherichia coli* 30 S subunits by a new approach using matrix-assisted laser desorption/ionization-mass spectrometry combined with N-terminal microsequencing. *J. Biol. Chem.* 272, 14547–14555. doi: 10.1074/jbc.272.23.14547
- Wei, Y., Zhang, H., Gao, Z. Q., Wang, W. J., Shtykova, E. V., Xu, J. H., et al. (2012). Crystal and solution structures of methyltransferase RsmH provide basis for methylation of C1402 in 16S rRNA. *J. Struct. Biol.* 179, 29–40. doi: 10.1016/j.jsb.2012.04.011
- Westrich, L. D., Gotsmann, V. L., Herkt, C., Ries, F., Kazek, T., Trosch, R., et al. (2021). The versatile interactome of chloroplast ribosomes revealed by affinity purification mass spectrometry. *Nucleic Acids Res.* 49, 400–415. doi: 10.1093/nar/gkaa1192
- Wimberly, B. T., Brodersen, D. E., Clemons, W. M. J., Morgan-Warren, R. J., Carter, A. P., Vonnrhein, C., et al. (2000). Structure of the 30 S ribosomal subunit. *Nature* 407, 327–339.
- Xiong, H. B., Wang, J., Huang, C., Rochaix, J. D., Lin, F. M., Zhang, J. X., et al. (2020). mTERF8, a member of the mitochondrial transcription termination factor family, is involved in the transcription termination of chloroplast Gene psbJ. *Plant Physiol.* 182, 408–423. doi: 10.1104/pp.19.00906
- Yamamoto, T., Burke, J., Autz, G., and Jagendorf, A. T. (1981). Bound Ribosomes of Pea chloroplast thylakoid membranes: location and release *in vitro* by high salt, Puromycin, and RNase. *Plant Physiol.* 67, 940–949. doi: 10.1104/pp.67.5.940
- Yoo, S. D., Cho, Y. H., and Sheen, J. (2007). Arabidopsis mesophyll protoplasts: a versatile cell system for transient gene expression analysis. *Nat. Protoc.* 2, 1565–1572. doi: 10.1038/nprot.2007.199
- Yu, Q. B., Lu, Y., Ma, Q., Zhao, T., Huang, C., Zhao, H. F., et al. (2013). TAC7, an essential component of the plastid transcriptionally active chromosome complex, interacts with FLN1, TAC10, TAC12 and TAC14 to regulate chloroplast gene expression in *Arabidopsis thaliana*. *Physiol. Plant.* 148, 408–421. doi: 10.1111/j.1399-3054.2012.01718.x
- Yusupov, M. M., Yusupova, G. Z., Baucom, A., Lieberman, K., Earnest, T. N., Cate, J. H., et al. (2001). Crystal structure of the ribosome at 5.5 Å resolution. *Science* 292, 883–896.
- Zhang, J., Yuan, H., Yang, Y., Fish, T., Lyi, S. M., Thannhauser, T. W., et al. (2016). Plastid ribosomal protein S5 is involved in photosynthesis, plant development, and cold stress tolerance in *Arabidopsis*. *J. Exp. Bot.* 67, 2731–2744. doi: 10.1093/jxb/erw106
- Zhang, L., Pu, H., Duan, Z., Li, Y., Liu, B., Zhang, Q., et al. (2018). Nucleus-Encoded Protein BFA1 Promotes Efficient Assembly of the Chloroplast ATP Synthase Coupling Factor. *Plant Cell* 30, 1770–1788. doi: 10.1105/tpc.18.00075
- Zoschke, R., and Bock, R. (2018). Chloroplast translation: structural and functional organization, operational control, and regulation. *Plant Cell* 30, 745–770. doi: 10.1105/tpc.18.00016
- Zou, M., Mu, Y., Chai, X., Ouyang, M., Yu, L. J., Zhang, L., et al. (2020). The critical function of the plastid rRNA methyltransferase, CMAL, in ribosome biogenesis and plant development. *Nucleic Acids Res.* 48, 3195–3210. doi: 10.1093/nar/gkaa129

Conflict of Interest: The authors declare that the research was conducted in the absence of any commercial or financial relationships that could be construed as a potential conflict of interest.

Publisher's Note: All claims expressed in this article are solely those of the authors and do not necessarily represent those of their affiliated organizations, or those of the publisher, the editors and the reviewers. Any product that may be evaluated in this article, or claim that may be made by its manufacturer, is not guaranteed or endorsed by the publisher.

Copyright © 2022 Wang, Qu, Mei, Zhang, Yang, Xu, Xiong, Yang and Yu. This is an open-access article distributed under the terms of the Creative Commons Attribution License (CC BY). The use, distribution or reproduction in other forums is permitted, provided the original author(s) and the copyright owner(s) are credited and that the original publication in this journal is cited, in accordance with accepted academic practice. No use, distribution or reproduction is permitted which does not comply with these terms.



A Tissue-Chopping Based Immunofluorescence Staining Method for Chloroplast Proteins

Lulu Wang^{1,2}, Mingdong Tang^{1,2}, Wenwen Huang^{1,2}, Jinjie An^{1,2}, Xiaomin Liu^{1,2*} and Hongbo Gao^{1,2*}

¹ National Engineering Research Center of Tree Breeding and Ecological Restoration, Beijing Forestry University, Beijing, China, ² College of Biological Sciences and Technology, Beijing Forestry University, Beijing, China

OPEN ACCESS

Edited by:

Jirong Huang,
Shanghai Institute for Biological
Sciences (CAS), China

Reviewed by:

Lina Yin,
Northwest A&F University, China
Hiroyoshi Takano,
Kumamoto University, Japan

*Correspondence:

Xiaomin Liu
liuxiaomin@bjfu.edu.cn
Hongbo Gao
gaohongbo@bjfu.edu.cn

Specialty section:

This article was submitted to
Plant Physiology,
a section of the journal
Frontiers in Plant Science

Received: 01 April 2022

Accepted: 19 April 2022

Published: 19 May 2022

Citation:

Wang L, Tang M, Huang W, An J,
Liu X and Gao H (2022) A
Tissue-Chopping Based
Immunofluorescence Staining Method
for Chloroplast Proteins.
Front. Plant Sci. 13:910569.
doi: 10.3389/fpls.2022.910569

Immunofluorescence staining is an important method for detecting the localization of proteins in the cell. It is also frequently used in the localization study of chloroplast-division proteins. Although this method has been improved before by using protoplasts, it still has some limitations. Now we developed a new method to make it much easier. We just broke the plant leaf tissue with a serrated blade, stained the samples directly, and simply lysed the tissue into separable cells. The localization of the target protein can then be observed with a clear view. Since this method directly uses broken leaf pieces, it is very fast. It can also be applied to the plants in which protoplasts are difficult to prepare. We first used this method to observe the localization of a chloroplast division protein FtsZ1 in the wild-type *Arabidopsis*. A ring was clearly seen in the middle of chloroplasts. In addition, we used this method to analyze the localization of FtsZ1 in *arc3* and *pdv2* mutants, as well as in dozens of other species, including some woody plants. This new immunofluorescence staining method is not only easy to use, but also has a wide applicability in various plants.

Keywords: tissue-chopping, immunofluorescence staining, tissue lysis, chloroplast, protein localization

INTRODUCTION

Chloroplasts are photosynthetic organelles encapsulated by double membranes. They propagate by binary division. Chloroplast division maintains the stability of the chloroplast number in plant cells. In the process of chloroplast division, chloroplast division proteins form a ring-like complex in the middle of chloroplasts (Osteryoung and Nunnari, 2003; Chen et al., 2018). Then the ring-like complex constricts, splitting one chloroplast into two daughter chloroplasts (Osteryoung and Pyke, 2014). FtsZ is an essential chloroplast division protein conserved in plants and bacteria (Osteryoung and Nunnari, 2003; Stokes and Osteryoung, 2003). There are two sub-family members in plants, including FtsZ1 and FtsZ2 (Osteryoung and McAndrew, 2001; Stokes and Osteryoung, 2003). The correct localization is essential for chloroplast division proteins to function *in vivo* (Zhang et al., 2013, 2016; Chen et al., 2019).

Immunofluorescence staining is a widely used method to study the localization of proteins in the cell. It is frequently used to study the localization of chloroplast division proteins (Vitha et al., 2001; Li et al., 2016; Wang et al., 2017; Liu et al., 2022). Compared with transforming plants with fluorescent protein tags, immunofluorescence staining does not need to obtain transgenic plants, so it is a good choice to study the localization of proteins in plants that cannot be transformed or are untransformed. Moreover, fluorescent protein tags may change the structure and function of

the fused protein (Hanson and Ziegler, 2004), and interfere their localization in the cell. However, immunofluorescence staining can reflect the natural and real localization of proteins *in vivo*.

Because of the cell wall of plant cells, it is not easy for the antibodies to enter the cell and recognize the target proteins. Immunofluorescence staining method with wax-embedded tissue sections was used to observe the localization of the chloroplast division proteins FtsZ in plants (Vitha et al., 2001). However, this kind of method takes a long time, they need several days, and the operation is cumbersome and laborious (Ovecka et al., 2014).

In comparison with the tissue sectioning method, a new method using isolated protoplasts for the immunofluorescence staining of chloroplast proteins was developed (Li et al., 2016). This method was used in studying the localization of chloroplast division proteins (Wang et al., 2017; Liu et al., 2022). Compared with the immunofluorescence staining method with wax-embedded tissue sections, this method with enzymatic digestion of cell wall is much simpler and less time-consuming. The results can be obtained within only 1 day. However, due to the special composition and structure of plant cell walls, protoplasts of some plants, especially the woody plants, are hard to obtain. Therefore, this method has some limitations.

To overcome the influence of plant cell walls, we developed another immunofluorescence staining method by directly breaking the leaf tissue into irregular small pieces for immunofluorescence staining. There is no need of embedding the tissue in wax and sectioning, and preparation of poly-L-lysine coated slides and protoplasts by enzyme digestion. The entire experiment can be completed in about 8 h. In addition, the difficulty of operation is greatly reduced. The demand for experimental materials is very low, and a leaf area of 1–2 cm² is enough. We can observe the localization of FtsZ1 in many species, including poplar, elm, *Broussonetia papyrifera* and *Ginkgo biloba* with this method. Thus, this new method should have a wide range of applications.

MATERIALS AND METHODS

Plant Materials and Growth Conditions

Arabidopsis thaliana plants used are Columbia-0 (Col) wild type, *pdv2-3* and *arc3-1* (Pyke and Leech, 1994; Chang et al., 2017). *Arabidopsis thaliana*, *Nicotiana benthamiana*, *Brassica oleracea* var. *capitata* L., poplar 84K (*Populus alba* × *P. tremula* var. *glandulosa*) were grown in soil at 22°C with 40–60% relative humidity and 16-h-light/8-h-dark cycles. *Allium tuberosum* Rottler ex Spreng., *Allium sativum* L., *Lactuca sativa* var. *longifolia* Lam., *Apium graveolens* L., *Brassica juncea* (L.) Czern., *Brassica juncea* (L.) Czern., *Brassica rapa* var. *oleifera* DC. and *Spinacia oleracea* L. were bought from a vegetable shop. *Dianthus caryophyllus* L. were bought from a flower shop. All other plants were grown in a greenhouse.

Leaf Breaking and Fixation

All the steps were carried out at room temperature. Leaf tissues were harvested and immediately immersed in fixation solution [0.4 M Mannitol, 20 mM KCl, 20 mM MES (pH 5.7), 4%

paraformaldehyde] in petri dishes and cut into pieces by blades. The sharp blades were surgical blades (K3-23, Shanghai Pudong Jinhuan Medical Products Company Limited). The saw-shaped blades were taken from GLAD ClingWrap (W300N, Clorox China Limited). The broken tissue and the fixation solution were transferred together into a 1.5 mL tube and kept in the dark for 1 h.

Antibody Incubation

Leaf tissues were gently washed with 1 mL 1 × PBS (137 mM NaCl, 2.7 mM KCl, 10 mM Na₂HPO₄•12H₂O, 2 mM KH₂PO₄, pH = 7.4) three times and 5 min each time at least. The sample was covered with 1 mL blocking solution (5% BSA in 1 × PBS with 0.15% Triton X-100) and incubated at room temperature for 30 min. The samples were then incubated with 200 µL anti-FtsZ1 antibodies (Liu et al., 2022) (a dilution of 1:100 with blocking solution) for 2 h in darkness at room temperature. Next, samples were washed with 1 × PBS or 5% BSA in 1 × PBS three times. Then the samples were incubated with 100 µL goat anti-rabbit FITC-conjugated secondary antibodies (JX3004, Jiaxuan Biotech, Beijing) (1:100 dilution in 5% BSA) for 1 h in the dark. The samples were washed with 1 × PBS or 5% BSA in 1 × PBS three times.

Tissue Lysis

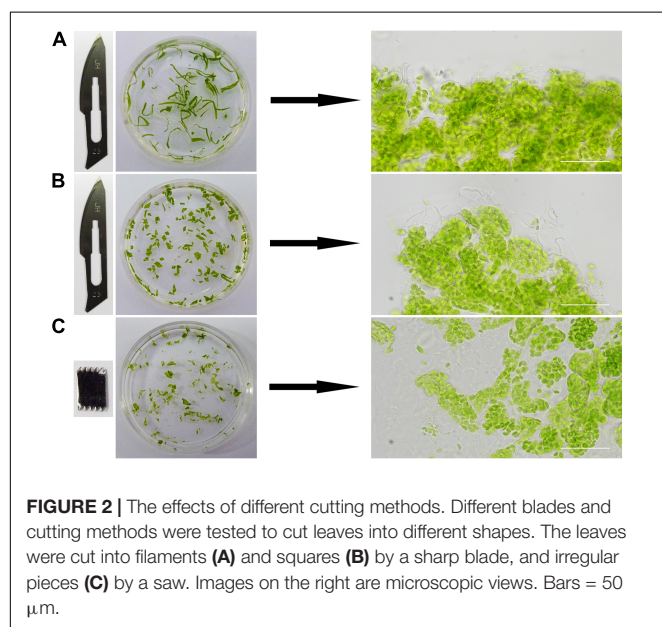
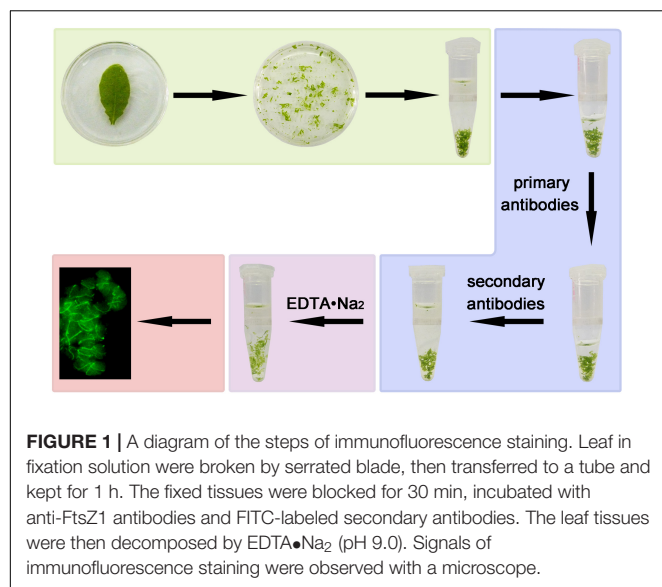
In total, 1 mL EDTA•Na₂ (pH 9.0) was added to samples and incubated at 55°C for 1 h to break the middle lamellar between the cells and lyse the tissue. After removing the EDTA•Na₂ solution, 1 mL fresh home-made anti-fade mounting medium (5 mM Na-Ascorbate, 15 mM Na₂HPO₄ pH 9.0, 50% glycerin) was added to the tube. Samples were stored at 4°C. Images were taken with a microscope (NEXCOPE NE910, Olympus) equipped with a 40× objective and an E3ISPM camera. Image analysis was carried out using ImageJ¹ (version 1.52V) and Photoshop (Adobe Photoshop CC 2015).

RESULTS

The Procedures of Immunofluorescence Staining

We developed an improved method of immunofluorescence staining directly with leaf tissue. This method does not need wax-embedded tissue sections, separation of protoplasts and preparation of poly-L-lysine slides in advance. The leaf tissue is directly chopped with a serrated blade in fixation solution and fixed instantly, and incubated with primary antibodies and FITC-labeled secondary antibodies. Finally, the intercellular pectin between cells is decomposed by EDTA•Na₂ and heated to dissociate the cells for a better view of the signals in the cell (Pyke and Leech, 1991; Tsugama et al., 2011; Gao et al., 2013; Figures 1, 2). The method is very simple and only requires a small amount of material.

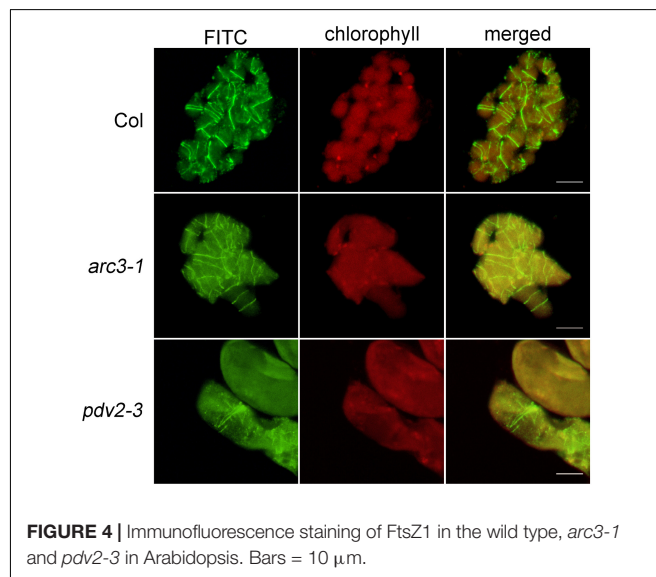
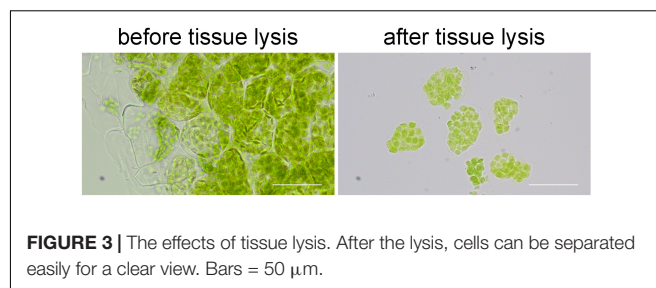
¹<http://rsbweb.nih.gov/ij/>



It Is Better to Cut the Leaf Tissue With a Saw-Shaped Blade

We tried different methods to cut the leaf tissues. At first, a sharp blade was used and the leaf tissues were cut into narrow pieces or small squares (Figures 2A,B). A saw-shaped blade was also used for the cutting and the leaves were cut into irregular small pieces (Figure 2C). The edges of the leaf tissues cut by a sharp blade were regular and sharp (Figures 2A,B). In contrast, those cut by a saw-shaped blade were irregular and coarse (Figure 2C). So, it is apparent that the leaf tissues cut by a saw-shaped blade had much more surface area and cells directly exposed to the solutions and the reagents, which could lead to a better result in the end. This had been confirmed by the final experimental results.

This step required only a few minutes. For tender leaves like *Arabidopsis* leaves, it can be finished in 1 min. For the hard



leaves of woody plants, such as the leaves of poplar, it can be finished in 3–5 mins.

Tissue Lysis Facilitates the Observation of the Signal

When we directly observed the samples after immunofluorescence staining, we found that it was not easy to see the signal of immunofluorescence staining clearly. Because the cells were stuck together in the leaf tissue, the background signals were high and the real signals were blurry. Therefore, we treated the stained tissue with EDTA•Na₂ (pH 9.0) at 55°C for 1 h. This treatment broke the pectin in the middle lamellar, so the cells can be separated easily (Figure 3). To our surprise, the signal of immunofluorescence staining was not affected by this treatment (Figures 4, 5), and it looked much clear since the cells were dispersed.

Immunofluorescence Staining of FtsZ1 in Arabidopsis by the Newly Developed Method

In order to confirm the feasibility of this method, *Arabidopsis* wild type was used at first to observe the localization of the chloroplast division protein FtsZ1. The results indicated that FtsZ1 protein formed a ring and localized to the middle of chloroplasts (Figure 4), as previous reported with other immunofluorescence staining methods (Vitha et al., 2001;

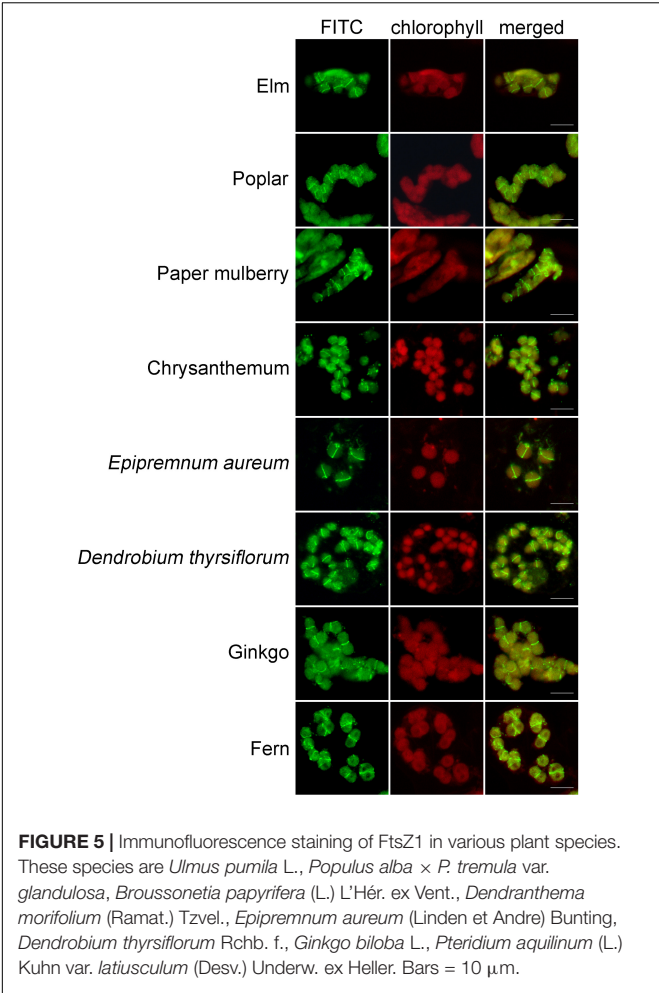


FIGURE 5 | Immunofluorescence staining of FtsZ1 in various plant species. These species are *Ulmus pumila* L., *Populus alba* × *P. tremula* var. *glandulosa*, *Broussonetia papyrifera* (L.) L'Hér. ex Vent., *Dendranthema morifolium* (Ramat.) Tzvel., *Epipremnum aureum* (Linden et Andre) Bunting, *Dendrobium thyrsiflorum* Rchb. f., *Ginkgo biloba* L., *Pteridium aquilinum* (L.) Kuhn var. *latiusculum* (Desv.) Underw. ex Heller. Bars = 10 μm.

Li et al., 2016). Next, we tested this new method with *Arabidopsis* chloroplast division mutants *arc3* and *pdv2* (Pyke and Leech, 1994; Chang et al., 2017). In these mutants, chloroplasts are increased in size and decreased in number, and the FtsZ rings are irregular (Miyagishima et al., 2006; Zhang et al., 2013; Wang et al., 2017). The results showed that FtsZ1 was distributed in large chloroplasts in the *arc3-1* mutant as multiple parallel rings (Figure 4). In the *pdv2-3* mutant, the rings of FtsZ1 were distributed in the middle of the large chloroplasts (Figure 4). The localization results of FtsZ1 in *arc3-1* and *pdv2-3* obtained by this method were also similar to those of previously reported (Miyagishima et al., 2006; Zhang et al., 2013). Therefore, the new immunofluorescence staining method developed in this study is suitable for observing the localization of chloroplast division proteins in *Arabidopsis*.

The New Immunofluorescence Staining Method Can Be Widely Used in Many Other Species

To learn whether this newly-developed method can be applied in other plants, we used the leaves from a wide variety of many other plant species, including some woody plants, for the test.

TABLE 1 | A partial list of the species in which FtsZ1 can be detected with good signals by the newly-developed immunofluorescence staining method.

A partial list of the plant species

<i>Pisum sativum</i> L.
<i>Glycine max</i> (L.) Merr.
<i>Nerium oleander</i> L.
<i>Gossypium hirsutum</i> L.
<i>Dendranthema morifolium</i> (Ramat.) Tzvel.
<i>Lactuca sativa</i> var. <i>longifolia</i> Lam
<i>Ailanthus giraldii</i> Dode
<i>Prunus davidiana</i> (Carrière.) Franch.
<i>Prunus persica</i>
<i>Nicotiana benthamiana</i>
<i>Broussonetia papyrifera</i> (L.) L'Hér. ex Vent.
<i>Apium graveolens</i> L.
<i>Cardamine hirsuta</i> L.
<i>Brassica oleracea</i> var. <i>capitata</i> L.
<i>Brassica juncea</i> (L.) Czern.
<i>Brassica rapa</i> var. <i>oleifera</i> DC.
<i>Dianthus caryophyllus</i> L.
<i>Spinacia oleracea</i> L.
<i>Boehmeria nivea</i> (L.) Gaudich.
<i>Salix matsudana</i> var. <i>pseudomatsudana</i> (Y. L. Chou & Skvortzov) Y. L. Chou
<i>Populus alba</i> × <i>Populus tremula</i> var. <i>glandulosa</i>
<i>Ulmus pumila</i> L.
<i>Murraya exotica</i> L.
<i>Citrus reticulata</i> Blanco
<i>Zanthoxylum bungeanum</i> Maxim.
<i>Cinnamomum camphora</i> (L.) J. Presl
<i>Oxalis corymbosa</i> DC.
<i>Phalaenopsis aphrodite</i> Rchb. f.
<i>Dendrobium thyrsiflorum</i> Rchb. f.
<i>Alstroemeria aurea</i> Graham
<i>Allium tuberosum</i> Rottler ex Spreng.
<i>Allium sativum</i> L.
<i>Allium schoenoprasum</i> L.
<i>Hippeastrum rutilum</i> (Ker-Gawl.) Herb.
<i>Chlorophytum comosum</i> (Thunb.) Baker
<i>Ophiopogon japonicus</i> (L. f.) Ker Gawl.
<i>Cordyline fruticosa</i> (L.) A. Chev.
<i>Philodendron selloum</i> K. Koch
<i>Epipremnum aureum</i> (Linden et Andre) Bunting
<i>Tradescantia fluminensis</i>
<i>Livistona chinensis</i> (Jacq.) R. Br. ex Mart.
<i>Chamaedorea elegans</i> Mart.
<i>Ginkgo biloba</i> L.
<i>Pteridium aquilinum</i> (L.) Kuhn var. <i>latiusculum</i> (Desv.) Underw. ex Heller
<i>Marchantia polymorpha</i> L.

Since FtsZ1 is a well conserved protein in plants, we used the FtsZ1 antibodies as the primary antibodies. In many of the plants, a good signal of FtsZ1 were clearly seen in the cells (Figure 5). FtsZ1 formed a ring in middle of the chloroplasts of those plants, which is consistent with the localization of FtsZ1 in *Arabidopsis*. Figure 5 shows the immunofluorescence staining

of some selected plants. **Table 1** shows a partial list of the tested plants which showed a good signal of FtsZ1. As we can see, those plants include moss, fern, gymnosperm and angiosperms. For some woody plants, such as poplar and ginkgo, a good signal could also be obtained (**Figure 5**). Therefore, this newly-developed method can be applied to many plant species and it has a wide applicability.

DISCUSSION

Immunofluorescence staining is a method widely used to study the localization of proteins in the cells. In this study, we developed a new method for the immunofluorescence staining of chloroplast proteins in plant cells. We found that use a serrated blade, instead of a sharp blade, to cut the leaves into small irregular pieces make the tissues more accessible to the reagents. After the fixation and immunofluorescence staining with the primary and secondary antibodies, those small leaf tissues were lysed by a simple way, which made them easily separated into single cells. This greatly reduced the background noise signal and presented a clear view of the true signal in the cell. Although these treatments seemed to be not new, but they were not used in immunofluorescence staining previously. The combination of these steps made this immunofluorescence staining method superior to the previous ones.

We first tried this method in *Arabidopsis* to detect the localization of a chloroplast division protein, FtsZ1, in the wild type and two chloroplast division mutants. The localization results are very similar to those obtained by other methods (McAndrew et al., 2001; Vitha et al., 2001; Zhang et al., 2013; Li et al., 2016; Chen et al., 2019). The leaves of *Arabidopsis* are tender and easy to operate. We then further test the applicability of this method in various many other plants. Good signals were observed in many of those plants, including some woody plants, such as ginkgo and poplar.

Our new method has some advantages to the previous methods. Firstly, it is very easy and simple. Although the

protoplast-based immunofluorescence staining method is easy too, our method doesn't require preparation of protoplasts and poly-lysine coated glass slides. It is much easier than the wax-embedding and sectioning method too. Secondly, it is very fast. The whole process can be finished in several hours. Thirdly, it only needs a small piece of leaf tissue. An area of 1–2 cm² will be enough for the experiment. Fourthly, it doesn't need enzymes to lyse the leaf tissues. The tissues are directly broken by a saw-shaped blade into small pieces and then simply lysed by EDTA•Na₂ and heating. So, it is very cost-effective. Fifthly, due to the existence of the cell wall, protoplasts are difficult to prepare in many plants, such as woody plants and liverworts. Our tissue-breaking and tissue lysis method can overcome this problem to a large extent and it can be used in a wide variety of plants. Theoretically, this method can also be used for the localization study of many other proteins in the cell. It provides an additional and good choice of the methods for the study of protein localization.

DATA AVAILABILITY STATEMENT

The raw data supporting the conclusions of this article will be made available by the authors, without undue reservation.

AUTHOR CONTRIBUTIONS

HG designed the experiments. LW, MT, WH, and JA carried out the experiments. LW, XL, and HG prepared the manuscript. All authors contributed to the article and approved the submitted version.

FUNDING

This work was supported by grants from the National Natural Science Foundation of China (Nos. 32070696 and 31570182).

REFERENCES

- Chang, N., Sun, Q., Li, Y., Mu, Y., Hu, J., Feng, Y., et al. (2017). PDV2 has a dosage effect on chloroplast division in *Arabidopsis*. *Plant Cell Rep.* 36, 471–480. doi: 10.1007/s00299-016-2096-6
- Chen, C., Cao, L., Yang, Y., Porter, K. J., and Osteryoung, K. W. (2019). ARC3 activation by PARC6 promotes ftsz-ring remodeling at the chloroplast division site. *Plant Cell* 31, 862–885. doi: 10.1105/tpc.18.00948
- Chen, C., Maccready, J. S., Ducat, D. C., and Osteryoung, K. W. (2018). The molecular machinery of chloroplast division. *Plant Physiol.* 176, 138–151. doi: 10.1104/pp.17.01272
- Gao, Y., Liu, H., An, C., Shi, Y., Liu, X., Yuan, W., et al. (2013). *Arabidopsis* FR54/CPD25 and FHY3/CPD45 work cooperatively to promote the expression of the chloroplast division gene ARC5 and chloroplast division. *Plant J.* 75, 795–807. doi: 10.1111/tpj.12240
- Hanson, D. A., and Ziegler, S. F. (2004). Fusion of green fluorescent protein to the C-terminus of granulin alters its intracellular localization in comparison to the native molecule. *J. Negat. Res. Bio.* 3:2. doi: 10.1186/1477-5751-3-2
- Li, Y., Sun, Q., Feng, Y., Liu, X., and Gao, H. (2016). An improved immunofluorescence staining method for chloroplast proteins. *Plant Cell Rep.* 35, 2285–2293. doi: 10.1007/s00299-016-2034-7
- Liu, X., An, J., Wang, L., Sun, Q., An, C., Wu, B., et al. (2022). A novel amphiphilic motif at the C-terminus of FtsZ1 facilitates chloroplast division. *Plant Cell* 34, 419–432. doi: 10.1093/plcell/koab272
- McAndrew, R. S., Froehlich, J. E., Vitha, S., Stokes, K. D., and Osteryoung, K. W. (2001). Colocalization of plastid division proteins in the chloroplast stromal compartment establishes a new functional relationship between FtsZ1 and FtsZ2 in higher plants. *Plant Physiol.* 127, 1656–1666. doi: 10.1104/pp.010542
- Miyagishima, S. Y., Froehlich, J. E., and Osteryoung, K. W. (2006). PDV1 and PDV2 mediate recruitment of the dynamin-related protein ARC5 to the plastid division site. *Plant Cell* 18, 2517–2530. doi: 10.1105/tpc.106.045484
- Osteryoung, K. W., and McAndrew, R. S. (2001). The plastid division machine. *Ann. Rev. Plant Physiol. Plant Mol. Biol.* 52, 315–333. doi: 10.1146/annurev.arplant.52.1.315
- Osteryoung, K. W., and Nunnari, J. (2003). The division of endosymbiotic organelles. *Science* 302, 1698–1704. doi: 10.1126/science.1082192
- Osteryoung, K. W., and Pyke, K. A. (2014). Division and dynamic morphology of plastids. *Ann. Rev. Plant Biol.* 65, 443–472. doi: 10.1146/annurev-arplant-050213-035748
- Ovecka, M., Samajova, O., Baluska, F., and Samaj, J. (2014). Immunofluorescent localization of MAPKs in Steedman's wax sections. *Methods Mol. Biol.* 1171, 117–130. doi: 10.1007/978-1-4939-0922-3_10

- Pyke, K. A., and Leech, R. M. (1991). Rapid image analysis screening procedure for identifying chloroplast number mutants in mesophyll Cells of *Arabidopsis thaliana* (L.) heynh. *Plant Physiol.* 96, 1193–1195. doi: 10.1104/pp.96.4.1193
- Pyke, K. A., and Leech, R. M. (1994). A genetic analysis of chloroplast division and expansion in *Arabidopsis thaliana*. *Plant Physiol.* 104, 201–207. doi: 10.1104/pp.104.1.201
- Stokes, K. D., and Osteryoung, K. W. (2003). Early divergence of the FtsZ1 and FtsZ2 plastid division gene families in photosynthetic eukaryotes. *Gene* 320, 97–108. doi: 10.1016/s0378-1119(03)00814-x
- Tsugama, D., Liu, S., and Takano, T. (2011). A rapid chemical method for lysing *Arabidopsis* cells for protein analysis. *Plant Methods* 7:22. doi: 10.1186/1746-4811-7-22
- Vitha, S., McAndrew, R. S., and Osteryoung, K. W. (2001). FtsZ ring formation at the chloroplast division site in plants. *J. Cell Biol.* 153, 111–120. doi: 10.1083/jcb.153.1.111
- Wang, W., Li, J., Sun, Q., Yu, X., Zhang, W., Jia, N., et al. (2017). Structural insights into the coordination of plastid division by the ARC6-PDV2 complex. *Nat. Plants* 3:17011. doi: 10.1038/nplants.2017.11
- Zhang, M., Chen, C., Froehlich, J. E., Terbush, A. D., and Osteryoung, K. W. (2016). Roles of *Arabidopsis* PARC6 in coordination of the chloroplast division complex and negative regulation of FtsZ assembly. *Plant Physiol.* 170, 250–262. doi: 10.1104/pp.15.01460
- Zhang, M., Schmitz, A. J., Kadirjan-Kalbach, D. K., Terbush, A. D., and Osteryoung, K. W. (2013). Chloroplast division protein ARC3 regulates chloroplast FtsZ-ring assembly and positioning in *Arabidopsis* through interaction with FtsZ2. *Plant Cell* 25, 1787–1802. doi: 10.1105/tpc.113.11.1047

Conflict of Interest: The authors declare that the research was conducted in the absence of any commercial or financial relationships that could be construed as a potential conflict of interest.

Publisher's Note: All claims expressed in this article are solely those of the authors and do not necessarily represent those of their affiliated organizations, or those of the publisher, the editors and the reviewers. Any product that may be evaluated in this article, or claim that may be made by its manufacturer, is not guaranteed or endorsed by the publisher.

Copyright © 2022 Wang, Tang, Huang, An, Liu and Gao. This is an open-access article distributed under the terms of the Creative Commons Attribution License (CC BY). The use, distribution or reproduction in other forums is permitted, provided the original author(s) and the copyright owner(s) are credited and that the original publication in this journal is cited, in accordance with accepted academic practice. No use, distribution or reproduction is permitted which does not comply with these terms.



OPEN ACCESS

EDITED BY

Alistair McCormick,
University of Edinburgh,
United Kingdom

REVIEWED BY

Mirko Zaffagnini,
University of Bologna, Italy
Sally Buck,
Australian National University, Australia

*CORRESPONDENCE

Lin Zhang
zhanglin2017@shnu.edu.cn
Xiaoqin Wang
wangxq@bua.edu.cn

SPECIALTY SECTION

This article was submitted to
Plant Physiology,
a section of the journal
Frontiers in Plant Science

RECEIVED 11 November 2021

ACCEPTED 14 September 2022

PUBLISHED 14 October 2022

CITATION

Li Y, Peng L, Wang X and Zhang L
(2022) Reduction in chloroplastic
ribulose-5-phosphate-3-epimerase
decreases photosynthetic capacity
in Arabidopsis.
Front. Plant Sci. 13:813241.
doi: 10.3389/fpls.2022.813241

COPYRIGHT

© 2022 Li, Peng, Wang and Zhang. This
is an open-access article distributed
under the terms of the [Creative
Commons Attribution License \(CC BY\)](#).
The use, distribution or reproduction
in other forums is permitted, provided
the original author(s) and the
copyright owner(s) are credited and
that the original publication in this
journal is cited, in accordance with
accepted academic practice. No use,
distribution or reproduction is
permitted which does not comply with
these terms.

Reduction in chloroplastic ribulose-5-phosphate-3- epimerase decreases photosynthetic capacity in Arabidopsis

Yonghong Li^{1,2}, Lianwei Peng³, Xiaoqin Wang^{1*}
and Lin Zhang^{3*}

¹Beijing Advanced Innovation Center for Tree Breeding by Molecular Design, Beijing University of Agriculture, Beijing, China, ²School of Biology and Brewing Engineering, TaiShan University, Taian, China, ³Shanghai Key Laboratory of Plant Molecular Sciences, College of Life Sciences, Shanghai Normal University, Shanghai, China

Chloroplast ribulose-5-phosphate-3-epimerase (RPE) is a critical enzyme involved in the Calvin-Benson cycle and oxidative pentose phosphate pathways in higher plants. Three Arabidopsis *rpe* mutants with reduced level of RPE were identified through their high NPQ (nonphotochemical quenching) phenotype upon illumination, and no significant difference of plant size was found between these *rpe* mutants and WT (wild type) plants under growth chamber conditions. A decrease in RPE expression to a certain extent leads to a decrease in CO₂ fixation, V_{cmax} and J_{max} . Photosynthetic linear electron transport was partially inhibited and activity of ATP synthase was also decreased in the *rpe* mutants, but the levels of thylakoid protein complexes and other Calvin-Benson cycle enzymes in *rpe* mutants were not affected. These results demonstrate that some degree of reduction in RPE expression decreases carbon fixation in chloroplasts, which in turn feedback inhibits photosynthetic electron transport and ATP synthase activity due to the photosynthetic control. Taken together, this work provides evidence that RPE plays an important role in the Calvin-Benson cycle and influences the photosynthetic capacity of chloroplasts.

KEYWORDS

photosynthesis, Calvin-Benson cycle, carbon fixation, RPE, photosystem, ATP synthase

Introduction

Photosynthesis is one of the most influential processes for the earth biosphere. It generates O₂ and converts CO₂ into carbohydrates. Photosynthesis is basically composed of the light-dependent reactions and the carbon-fixing reactions (Johnson, 2016). In the light reactions, light excitation energy is absorbed and used to produce ATP and NAD(P)

H for carbon fixation in the carbon-fixing reactions. The Calvin-Benson cycle (CBC) is the primary pathway of carbon fixation in the chloroplast stroma of higher plants, producing sugars and their derivatives for a series of pathways that are necessary for plant growth and development. During photosynthesis, the light and carbon-fixing reactions are tightly linked. When the activity of the carbon-fixing reactions is low, excess of ATP and NAD(P)H can inhibit photosynthetic electron transport and ATP synthase *via* the photosynthetic control mechanism (Foyer et al., 1990).

The Calvin-Benson cycle consists of 13 steps of chemical reactions catalyzed by 11 enzymes. Some intermediates and enzymes of CBC are shared with the respiratory carbon metabolic pathways, such as the oxidative pentose phosphate pathway (OPPP) and the glycolytic pathway (Kaiser, 1979; De Porcellinis et al., 2018). CBC is divided into three phases: (1) Carbon dioxide fixation: ribulose 1, 5-bisphosphate carboxylase/oxygenase (Rubisco) produces 3-phosphoglycerate (3-PGA) by carboxylation of ribulose 1, 5-bisphosphate (RuBP). This is the key step of the CBC (Bracher et al., 2017; Wilson and Hayer-Hartl, 2018). Rubisco is a multi-subunit complex with a molecular mass of ~550 kDa and contains eight large (RbcL) and eight small subunits (RbcS) (Bracher et al., 2017; Wilson and Hayer-Hartl, 2018). (2) Triose reduction: 3-PGA is reduced to glyceraldehyde 3-phosphate (G3P) by 3-phosphoglycerate kinase (PGK) and glyceraldehyde 3-phosphate dehydrogenase (GAPDH). (3) Pentose regeneration: triose phosphate isomerase (TPI), fructose 1,6-bisphosphate aldolase (FBA), fructose 1,6-bisphosphatase (FBPase), transketolase (TKL), ribulose-5-phosphate-3-epimerase (RPE), sedoheptulose-1,7-bisphosphatase (SBPase), ribose 5-phosphate isomerase (RPI), and phosphoribulokinase (PRK) are involved in the resynthesis of RuBP (Reyes-Prieto and Bhattacharya, 2007; Michelet et al., 2013; Sharkey, 2019). In addition to the CBC pathway, these enzymes usually have multiple homologs that have different locations in chloroplasts and cytoplasm, and they participate in other glucose metabolic pathways. For example, there are cytosolic and chloroplast PGK isozymes. The latter have been hypothesized to originate from a cyanobacterial ancestor (Massange-Sanchez et al., 2020). There are also four different GAPDH isoforms localized in the cytosol or in chloroplasts of which only GAPA/B is involved in the CBC (Gani et al., 2016). FBPases are homotetrameric enzymes with different isoforms cFBP (in chloroplasts) and cyFBP (in cytosol) in plants (Serrato et al., 2018).

To enhance CO₂ fixation and photosynthesis, some CBC enzymes were found to be overexpressed in various oxygenic phototrophs. However, their effects on photosynthetic productivity and growth are dependent on the particular enzyme, species, and other factors (De Porcellinis et al., 2018). Other enzymes are thought to have a greater control over carbon flow during photosynthesis than Rubisco, such as SBPase, FBA, and TKL (Raines, 2003; Mu et al., 2021). Overexpression of

SBPase and FBPase has demonstrated the potential of increase carbon fixation, photosynthesis to increase growth, biomass and even seed yield in transgenic plants (Lefebvre et al., 2005; Tamoi et al., 2006; Rosenthal et al., 2011; Simkin et al., 2017; López-Calcano et al., 2020). Overexpression of TKL gene promotes chilling tolerance by increasing the activities of photosynthetic enzymes in cucumber plants (Bi et al., 2019). However, overexpression of plastid transketolase in tobacco results in a thiamine auxotrophic phenotype, which may contribute to the complex regulatory mechanisms maintaining thiamine homeostasis in plants (Khozaei et al., 2015). The importance of the activities of individual enzymes in the CBC cycle for carbon fixation and photosynthesis is complex and not well understood.

RPE catalyzes the interconversion of ribulose-5-phosphate and xylulose-5-phosphate in the CBC and OPPP (Favery et al., 1998). In the Arabidopsis genome, only *At5g61410* was designated as RPE and located in plastids. The Arabidopsis chloroplast *RPE* deletion mutant *rpe* can be germinated only when exogenous carbohydrates are added and are dwarf-like with light-green leaves (Favery et al., 1998; Xiong et al., 2009). It was found that the *RPE* gene affects the early stage of giant cell formation induced by the root-knot nematode (Favery et al., 1998). The lethality of the homozygous *rpe* mutant may be mainly due to the adverse effect on the production of Ru5P in the OPPP pathway, resulting in reduced purine synthesis required for embryonic development (Andriotis and Smith, 2019). In addition to RPE, two other proteins encoded by *At1g63290* and *At3g01850* were proposed to be cytosolic RPE (cyRPE) (Kruger and von Schaewen, 2003; Baune et al., 2020). Cytosolic RPEs have also been shown to be involved in the OPPP which is critical for production of NADPH (Kopriva et al., 2000).

In this study, we have isolated three *rpe* mutants which accumulate low levels of chloroplast RPE protein in Arabidopsis. Reduced CO₂ fixation and photosynthetic electron transport was found in these *rpe* mutants under high light conditions suggesting that RPE plays an important role in the Calvin cycle and influences the photosynthetic capacity of chloroplasts.

Materials and methods

Plant materials and growth conditions

The mutant *rpe-1* was isolated from the pSKI015 T-DNA insertion Arabidopsis mutant pool according to the high level of NPQ upon illumination. T-DNA insertion mutants *rpe-2* (SAIL_1271_E12) and *rpe-3* (SALK_023919C) were obtained from NASC (Nottingham Arabidopsis Stock Centre). Wild-type *Arabidopsis thaliana* (Col ecotype) and mutants were grown on soil under greenhouse conditions (16 h/8 h: light/dark photoperiod, 50 μmol photons m⁻² s⁻¹, 23°C).

Chlorophyll fluorescence measurements

Imaging of chlorophyll fluorescence was performed according to Zhang et al. (2016) with an IMAGING-PAM fluorometer (Walz, Effeltrich, Germany). NPQ induction curves were measured with default programs also using IMAGING-PAM fluorometer and leaves were selected to derive NPQ data.

Light-intensity dependence parameters of ETR II, NPQ, and 1-qL were measured after illumination for two minutes using a Dual-PAM-100 (Walz) with a series of light intensities (9, 38, 77, 117, 221, 397, 665, 1031 $\mu\text{mol photons m}^{-2} \text{s}^{-1}$) as previously reported (Zhang et al., 2016). Light intensity-dependent ETR I and oxidation of the donor side of PSI was measured with a Dual-PAM-100 under a series of light intensities (22, 68, 143, 271, 476, 756, 1194, 1865 $\mu\text{mol photons m}^{-2} \text{s}^{-1}$) after turning on light for 20 s and calculated automatically using Dual-PAM-100 software (Zhang et al., 2016).

Protein extraction and protein gel blot analyses

Thylakoid membrane and stromal proteins isolation, immunoblotting, BN-PAGE and 2D-PAGE analysis were performed as previously described (Zhang et al., 2018). Thylakoid membrane protein was determined by the acetone method for chlorophyll content, chloroplast stromal proteins were determined by dye-binding method according to Bradford.

Antibodies against D1 (ATCG00020, PHY0057), D2 (ATCG00270, PHY0060), LHCI (AT1G76570, PHY0471S), PsaA (ATCG00350, PHY0342), CF1 α/β (ATCG00480, PHY0312), PetC (AT4G03280, PHY2293S), NDHH (ATCG01110, PHY2018A), PGRL1 (AT4G22890, PHY0234A), RbcL (ATCG00490, PHY0346), RPE (AT5G61410, PHY0616), FBA2 (AT4G38970, PHY0406S), PGK1 (AT3G12780, PHY0405S), PRK (AT1G32060, PHY0100A), RCA (AT2G39730, PHY0400S), RPI (AT3G04790, PHY0402S), TPI (AT2G21170, PHY0409S), TKL1 (AT3G60750, PHY0407S), GAP1 (AT3G26650, PHY0408S), SBPase (AT3G55800, PHY0410S) were obtained from PhytoAB (USA).

Subcellular localization of GFP fusion proteins

Subcellular localization was performed as described by Zhang et al. (2016) and full-length of RPE cDNA was cloned into pBI221 vector to express the RPE-GFP fusion protein.

ATP synthase activity measurement

The activity of ATP synthase was measured as described previously (Zhang et al., 2018) using a Dual-PAM-100 (Walz)

with a P515/535 emitter-detector module except that leaves were illuminated for 10 min with 167, 325, and 606 $\mu\text{mol photons m}^{-2} \text{s}^{-1}$ red light after overnight dark-adaption.

Gas exchange measurements

Photosynthetic gas exchange was measured using a GFS-3000 gas exchange measuring system (Walz). Air temperature in the leaf chamber and the relative humidity were maintained at 23°C and 50%, respectively. Air concentrations were controlled at 400 ppm CO₂ and 21% O₂. The CO₂ assimilation rate was determined at 103, 197, and 756 $\mu\text{mol photons m}^{-2} \text{s}^{-1}$ red light with the leaf of mutant and wild-type plants grown for 4 weeks. The steady-state of gas exchange was recorded after 10 min illumination.

A/Ci photosynthetic gas exchange measurements

The A/Ci curve was measured using the GFS-3000 gas exchange system (Walz, Effeltrich, Germany) with leaves of 6-week-old plant. For each line, the measurement was performed on at least five individual plants at 25°C, relative humidity of 60% and 400 ppm of CO₂. Leaves were illuminated using a red light source of Dual-PAM-100 (Walz, Effeltrich, Germany) attached to the gas-exchange system at 1000 $\mu\text{mol photons m}^{-2} \text{s}^{-1}$. Net photosynthesis (A) was measured with three replications under a series of CO₂ concentrations as following: 400, 50, 100, 150, 200, 300, 400, 500, 700, 1000, 1500, and 2000 ppm. A/Ci curves were analyzed using the equations of Farquhar et al. (1980). The maximum Rubisco carboxylation rate (V_{cmax}) and RuBP regeneration rate (J_{max}) were estimated according to the A/Ci curves using the method described previously (Dubois et al., 2007).

Results

Isolation of the *rpe-1* mutant

The mutant *rpe-1* was isolated from a pSKI015 T-DNA insertion mutant pool of Arabidopsis through the high level of NPQ (non-photochemical quenching) after illumination (Figures 1B, C; Supplementary Figure 1). The *rpe-1* mutant did not exhibit a visible growth phenotype under growth chamber conditions, such as leaf size and chlorophyll content (Supplementary Figure 2). The maximum photochemical efficiency (Fv/Fm) was comparable to WT (Figure 1B; Supplementary Figure 1), indicating that the function of Photosystem II (PSII) is not affected in the mutant. In WT plants, NPQ is induced to approximately 0.9 within 60 s of

illumination with AL (Actinic light). Then NPQ was relaxed within two min due to the activation of ATP synthase and the CBC reactions in the chloroplast stroma (Figure 1C, Zhang et al., 2016). In contrast, the NPQ level in *rpe-1* increased continuously to approximately 1.2 after 80 s of illumination and did barely relax during the following period of illumination (Figure 1C).

Identification of the *rpe* mutations

Thermal asymmetric interlaced polymerase chain reaction (TAIL-PCR) revealed that the T-DNA was inserted in the 5'-UTR of the chloroplast *RPE* gene (*At5g61410*) in the *rpe-1* mutant (Figure 1A). We obtained two other mutants *rpe-2* and *rpe-3* in which the T-DNA was also inserted in the 5'-UTR of *RPE* (Figure 1A). All three alleles had similar high NPQ phenotypes upon illumination, although the degree of elevation was different (Figures 1B, C). These results indicate that the T-DNA insertion in the 5'-UTR of *RPE* is responsible for the high-NPQ phenotype in the *rpe* mutants.

RPE is involved in the CBC and OPPP. Transient expression of *RPE*-GFP fusion protein in Arabidopsis protoplasts confirmed that *RPE* is specifically localized in chloroplasts (Figure 2A). Immunoblot analyses of chloroplast membrane and stromal proteins showed that *RPE* is present in the chloroplast stroma (Figure 2B) consistent with the localization of the CBC reactions. As expected, *RPE* protein is reduced to less than 50% of WT level in the three *rpe* mutants (Figures 1D, 2B). Although the T-DNA were all inserted into the 5'-UTR in *rpes*, their germplasm sources were not consistent, resulting in inconsistent protein expression levels. The accumulation of *RPE* in *rpe-1* is less than in *rpe-2* and *rpe-3*, and reduced to

~20% of wild-type levels (Figures 1D, 2B) which is consistent with the NPQ induction curves of these three mutants (Figures 1B, C).

The abundance of the major thylakoid protein complexes did not change in the *rpe* mutants

By using NPQ screening system, we have successfully isolated three mutants accumulating low amounts of chloroplast ATP synthase (*bfa1*, *bfa2*, and *bfa3*, Zhang et al., 2016; Zhang et al., 2018; Zhang et al., 2019). To investigate whether the *rpe* mutants have similar phenotypes of those three mutants, thylakoid protein complexes were analyzed by blue-native PAGE and immunoblot analyses. As shown in Figure 3, thylakoid protein complexes of PSI-NDH supercomplex, PSI monomer, PSII supercomplexes, PSII dimer, PSII monomer, CP43-less PSII, trimeric LHCII, and chloroplast ATP synthase were readily detected in the WT and the *rpe* mutants by BN-PAGE (Figure 3A). The BN-gel was further subjected to 2D SDS-urea-PAGE to resolve into individual subunits. No obvious difference was found in the levels of these subunits between WT and the *rpe* mutants (Figure 3B; Supplementary Figure 3). The $CF_1\alpha/\beta/\gamma$ subunits were detected at the position of the intact ATP synthase and the CF_1 subcomplex at similar levels in WT and the *rpe* mutants indicating that the amount of ATP synthase is not reduced in the mutant. This conclusion is further supported by the immunoblot analysis using a series of antibodies against some of the major subunits of the photosynthetic complexes such as photosystem II (D1, D2 and LHCII), PSI (PsaA), cytochrome *b6f* complex (PetC) and ATP

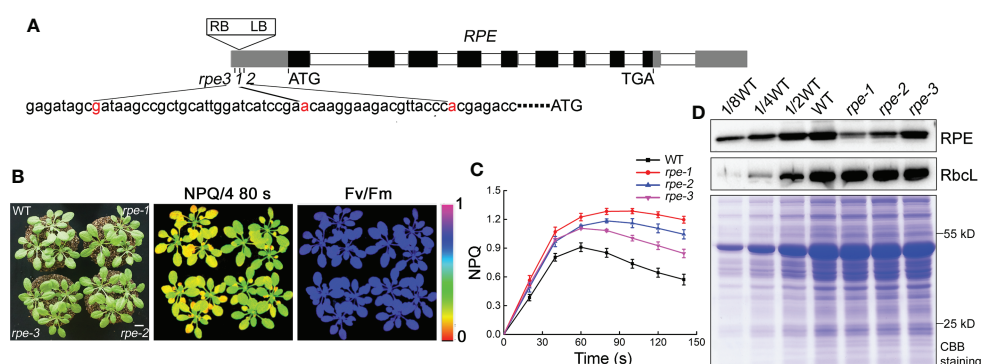


FIGURE 1

Characterization of the *rpe* mutants. (A) Schematic representation of *RPE*. The positions of the T-DNA insertions in the three *rpe* mutants are shown with red nucleotides. (B) Growth, NPQ, and Fv/Fm phenotypes of WT and *rpe* mutants. Four-week-old plants grown on soil at 50 $\mu\text{mol photons m}^{-2} \text{s}^{-1}$ (left panels). Signal intensities for NPQ and Fv/Fm are indicated according to the color scale (0 to 1.0) on the right. The bar represents one centimeter. (C) NPQ induction curves of the *rpe* mutants and WT. NPQ was calculated as $(F_m - F_m')/F_m'$. Data are presented as the means \pm SD ($n=4$). (D) Immunoblot analysis of *RPE* protein in the *rpe* mutants. Chloroplast stroma was isolated and immunoblot analyses were performed. RbcL was used as loading control. Equal amounts of chloroplast stromal proteins were loaded on the gels. The gels were stained with CBB for visualization of the proteins.

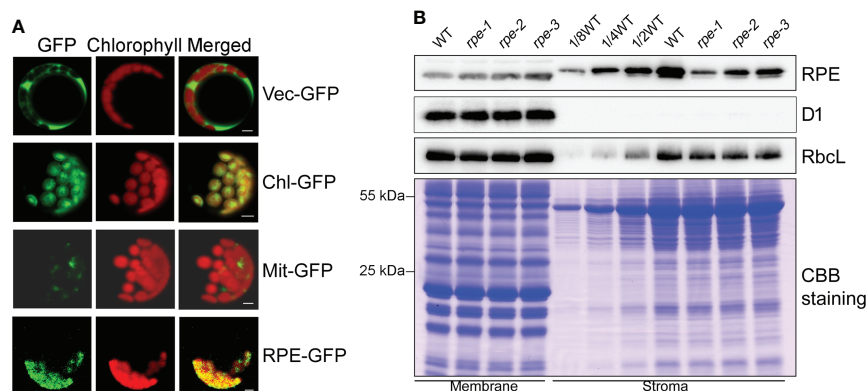


FIGURE 2

Subcellular localization of RPE. (A) Subcellular localization of RPE by GFP assay. RPE-GFP, RPE-GFP fusion; Vec-GFP, empty plasmid control; Chl-GFP, chloroplast control; Mit-GFP, mitochondrial control. Bars=5 μm . (B) Immunolocalization analysis of RPE. Intact chloroplasts isolated from WT and the *rpe* mutants were fractionated into membrane and stromal fractions, and immunoblot analyses were performed. D1 and RbcL were used as loading and fractionation controls. Thylakoids membrane protein containing equal amounts of chlorophyll and equal amounts of chloroplast stromal proteins were loaded on the gels. The gels were also stained with CBB for visualization of the proteins.

synthase ($\text{CF}_1\alpha/\beta$). The levels of these subunits were identical between the *rpe* mutants and the WT (Figure 3C). The level of NADH dehydrogenase-like complex (NDHH) and PGR5/PGRL1 complex (PGRL1) is also not affected in the *rpe* mutants. These results indicate that the RPE deficiency does not affect the accumulation of the major thylakoid complexes involved in photosynthetic electron transport.

CO₂ fixation is decreased in the *rpe* mutants

To determine whether the amounts of other CBC enzymes change when the level of the RPE protein is reduced, we determined their accumulation by immunoblotting. We found that the level of 10 plastid-localized CBC enzymes was almost identical between WT and the *rpe* mutants (Figure 4A) suggesting that the reduction of RPE does not impact the level of other CBC enzymes. Expression of CBC enzymes may not be tightly co-regulated. To explore the impact of RPE deficiency, the CO₂ assimilation rate was measured under different light intensities and atmospheric CO₂ levels. Before the analysis, seedlings were incubated in the dark for 2 h to completely inactivate the CBC enzymes. Under low light conditions at 103 $\mu\text{mol photons m}^{-2} \text{ s}^{-1}$, the CO₂ assimilation rate of the *rpe* mutants was comparable to WT (Figure 4B). This result is consistent with the similar plant size of WT and the *rpe* mutants grown in chamber conditions. Under 197 $\mu\text{mol photons m}^{-2} \text{ s}^{-1}$, the CO₂ assimilation rate of *rpe-1* and *rpe-2* was slightly reduced compared to WT (Figure 4B). Under 756 $\mu\text{mol photons m}^{-2} \text{ s}^{-1}$, even the CO₂ assimilation rate of *rpe-3* was slightly reduced compared to WT. Although this reduction

was more pronounced under 756 $\mu\text{mol photons m}^{-2} \text{ s}^{-1}$, the CO₂ assimilation rate was reduced by only 25% in *rpe-1* (Figure 4B). This indicates that, in the *rpe* mutants, about 20% of RPE protein is capable to assimilate 75% of CO₂ compared to WT, at least under our experimental conditions (Figures 4B, 1D).

Further analysis of the photosynthetic rates of the *rpe* mutants and WT was carried out by determining the response of CO₂ assimilation (*A*) to changes in intercellular CO₂ concentration (*C_i*). The *A/C_i* curve represents the carbon assimilation in mesophyll cells for a given carbon supply through stomata. The dependence of *A/C_i* is determined by the degree of Rubisco saturation, involving carboxylation, regeneration, or the export of TPU (triose phosphate utilization), referred to as “Rubisco limited” or “RuBP limited”, and “TPU limited”. Maximum carboxylation rate (*V_{cmax}*) and RuBP regeneration rate (*J_{max}*) are valuable metrics of photosynthetic performance, which was estimated by FvCB model (Farquhar et al., 1980; Dubois et al., 2007). The *rpe-1* and *rpe-2* had a significantly different response of *A* to that of WT at high *C_i* (Figure 5A). The maximum Rubisco carboxylation rate (*V_{cmax}*) and RuBP regeneration rate (*J_{max}*) in two mutants also showed a decrease relative to the wild-type (Figures 5B, C). The *V_{cmax}* of the *rpe-3* mutant with the least decrease in RPE protein was not different from those of WT, but *J_{max}* showed a slight decrease (Figures 5B, C).

Photosynthetic electron transport and ATP synthase activity are partially inhibited in the *rpe* mutants

In order to determine possible effects on photosynthetic electron transport in the *rpe* mutants, we analyzed the

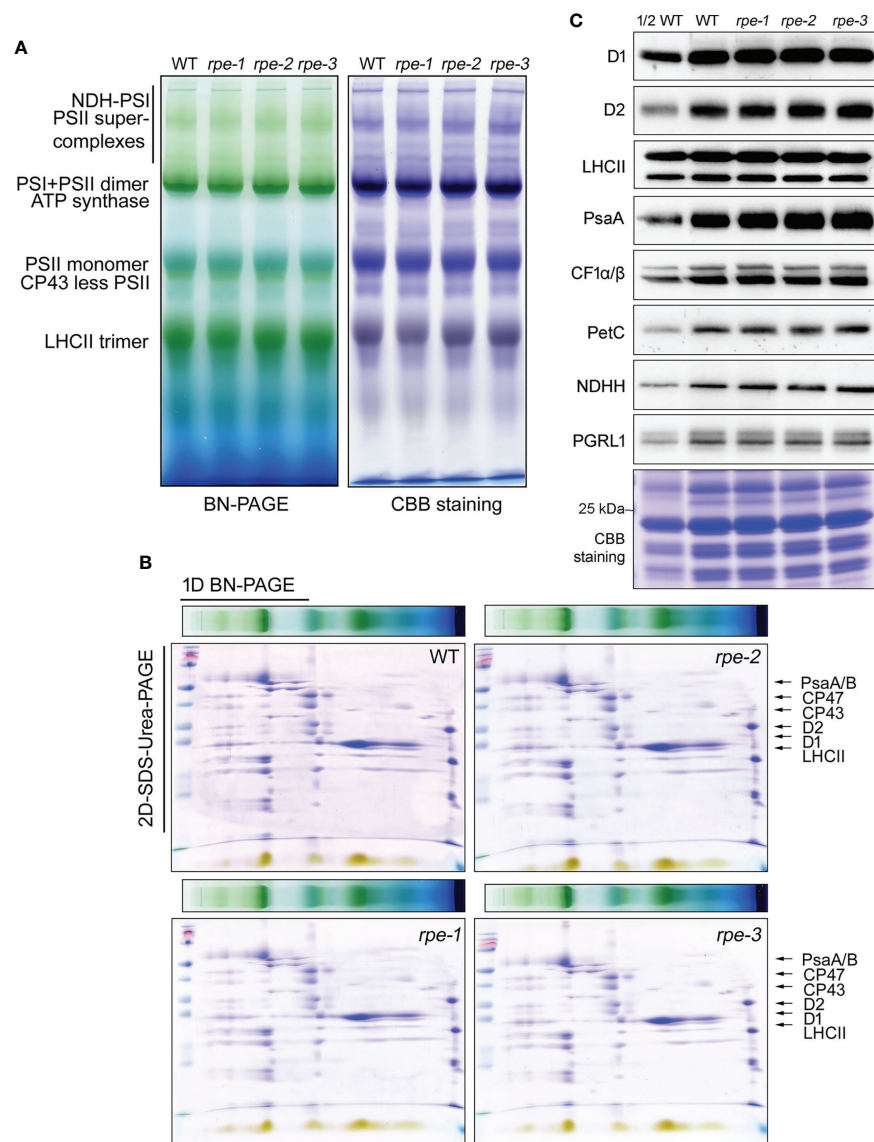


FIGURE 3

Analysis of the photosystem complexes and their core proteins in WT and the *rpe* mutants. (A, B) BN-PAGE (B) and 2D SDS-Urea-PAGE (C) analysis of the thylakoid protein complexes. Thermo Scientific PageRuler Prestained Protein Ladder is used for the protein molecular weight marker (Thermo, 26616). (C) Immunoblot analysis of representative thylakoid proteins. Thylakoid membranes isolated from the WT and the *rpe* mutants were separated by 15% SDS-Urea-PAGE and then probed with antibodies against individual subunits of PSII (D1, D2 and LHCII), PSI (PsaA), chloroplast ATP synthase (CF₁α/β), Cyt *b₆f* (PetC), NADH dehydrogenase-like complex (NDHH), and PGR5/PGRL1 complexes (PGRL1). Thylakoid proteins containing equal amounts of chlorophyll were loaded.

chlorophyll fluorescence parameters under different light intensities. Electron transport rates through PSII (ETR II) and through PSI (ETR I) are indicators of the relative of electron flow through PSII and PSI. Compared with WT, lower ETR II and ETR I values were observed in the *rpe* mutants, especially the *rpe-1* mutant with the lower RPE expression decreased more obviously at light intensities greater than 100 $\mu\text{mol photons m}^{-2} \text{s}^{-1}$ (Figures 6A, D). The steady-state NPQ in the *rpe* mutants was

higher compared with WT at light intensities greater than 100 $\mu\text{mol photons m}^{-2} \text{s}^{-1}$ (Figure 6B) suggesting that more protons accumulated in the thylakoid lumen in the *rpe* mutants compared with WT. The increase of steady-state NPQ in the *rpe* mutants was also consistent with the decrease of RPE expression. We also analyzed the photosynthetic parameter 1-qL, which shows the degree of the reduction state of the plastoquinone pool, in which it is assumed that the redox level

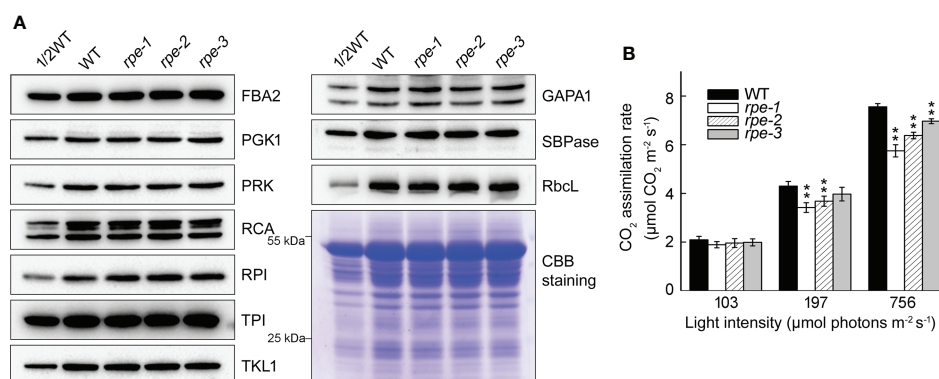


FIGURE 4
Characterization of Calvin-Benson cycle from WT and the *rpe* mutants. (A) Immunoblot analysis of Calvin-Benson cycle enzymes in WT and the *rpe* mutants. Chloroplast stroma was isolated and immunoblot analyses were performed using the indicated antibodies. Equal amounts of chloroplast stromal proteins were loaded. The gels were stained with CBB for visualization of the proteins. (B) CO₂ assimilation rate of WT and the *rpe* mutants under different light intensities. Values are means \pm SD ($n=3$). Significant differences were performed using the Student's *t*-test (** $P < 0.01$).

of the primary quinone acceptor (Q_A) in PSII is in rapid equilibrium with the redox level of the plastoquinone pool (Ohnishi et al., 2021). Higher 1-qL were observed in the *rpe* mutants (Figure 6C) suggesting that the redox state of plastoquinone on the PSII acceptor side is reduced in the *rpe* mutants than in WT. Furthermore, the PSI donor side was more oxidized than WT levels (Figure 6E). All these results indicate that photosynthetic electron transport is affected in the *rpe* mutants and limitation occurs between PSII and PSI.

To detect the changes of ATP synthase activity, we analyzed the light-intensity dependence of gH^+ which reveals the conductivity of the thylakoids to protons in *rpe-1* (Figure 6F). gH^+ was reduced to 67%–85% of wild-type levels in *rpe-1* at the light intensities investigated certifying that ATP synthase activity is reduced in *rpe-1* (Figure 6F).

Discussion

Some of the enzymes involved in the plastid OPPP and CBC pathways are critical for embryo development in *Arabidopsis*. Their absence usually leads to seed abortion, non-viable seeds, or non-viable seedlings (Bryant et al., 2011). Mutations in enzymes (such as PGL3, PGD, and RPI/EMB3119) involved in the oxidation part of OPPP lead to seed abortion beyond the globular stage, possibly due to the inability to synthesize Ru5P, and as a consequence, to the lack of substrates for purine nucleotide synthesis (Andriotis and Smith, 2019). The knock-out *rpe* mutant can develop beyond the globular stage. It is arrested at the cotyledon stage or is seedling-lethal (Favery et al., 1998; Andriotis and Smith, 2019). In our study, we obtained three knock-down *rpe* mutants. Although the accumulation of

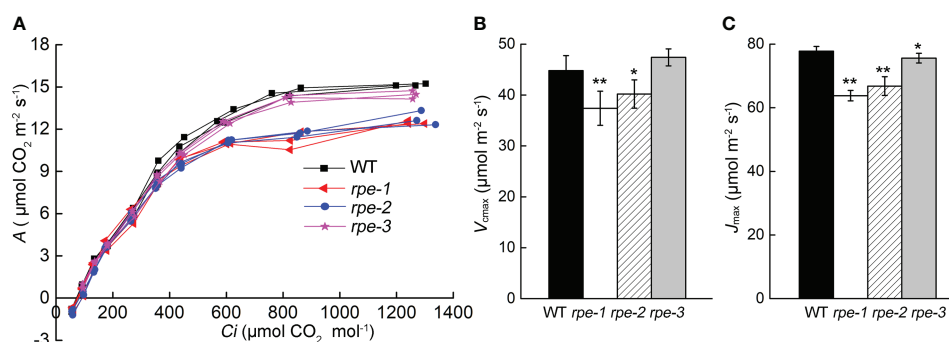


FIGURE 5
CO₂ assimilation rate (A) to changes in intercellular CO₂ (C_i). (A) The curve of A to C_i (the A/C_i curve). Individual measurements on three plants were presented. (B, C) V_{max} (B) and J_{max} (C) of the response of A to C_i . Values are means \pm SD ($n=5$) (* $P < 0.05$; ** $P < 0.01$).

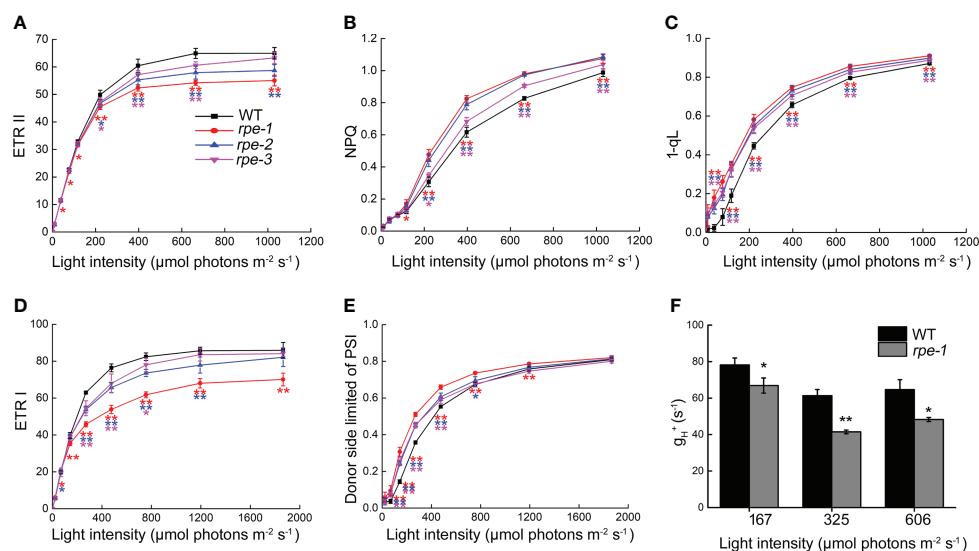


FIGURE 6
Analysis of light intensity dependence of photosynthetic parameters of WT and the *rpe* mutants. **(A)** Electron transport rate around PSII (ETR II). **(B)** Nonphotochemical quenching (NPQ). **(C)** 1-qL of PSII. qL means the fraction of open PSII centers, and 1-qL reflects the PQ redox state of PSII. **(D)** Electron transport rate around PSI (ETR I). **(E)** Donor-side limited PSI (with donor-side oxidized). **(F)** Analysis of ATP synthase activity in WT and *rpe-1*. Values are means \pm SD ($n=3-6$). Significant differences between WT and the *rpe* mutants are indicated by asterisk according to the Student's *t* test (* $P < 0.05$; ** $P < 0.01$). The red, blue, and pink asterisk represents significant differences between WT and *rpe-1*, *rpe-2*, *rpe-3*, respectively.

RPE is reduced to 20–50% in the *rpe* mutants (Figures 1D, 2B), their growth was similar to that of wild type (Figure 1B, Supplementary Figure 2), indicating that as low as 20% of RPE can maintain normal plant growth under growth chamber conditions (Figure 1B). More importantly, even under high light ($756 \mu\text{mol photons m}^{-2} \text{s}^{-1}$), about 75% of WT CO_2 assimilation rate was observed in the *rpe-1* mutant with only about 20% of WT level of RPE (Figure 4B). The Calvin Benson cycle is co-limited by the maximum carboxylation efficiency of Rubisco (V_{cmax}) and the regeneration of the substrate *RuBP* driven by photosynthetic electron transport (J_{max}). The V_{cmax} of the *rpe-3* mutant with approximately 50% reduction in RPE (Figure 1D) was not different from those of WT, and J_{max} showed a slight decrease (Figures 5B, C). The V_{cmax} and J_{max} in *rpe-1* and *rpe-2* mutants with approximately 12.5–25% reduction in RPE were reduced relative to the wild-type (Figure 5B, C). These data demonstrate that a 50% reduction in RPE protein can reduce the synthesis of *Ru5P*, and to a greater extent affect the activity of Rubisco, ultimately limiting photosynthetic carbon assimilation. This is similar to the reduced sedoheptulose-1,7-bisphosphatase levels in transgenic tobacco, reductions in SBPase activity to 38% and 57% of wild-type plants decreased J_{max} , but not V_{cmax} photosynthesis, and in plants with more severe reductions in SBPase activity, both J_{max} and V_{cmax} were reduced (Harrison et al., 1997; Harrison et al., 2001). These findings are also consistent with previous studies and show that some enzymes of the Calvin cycle are present at

levels well above those needed to maintain a sustained rate of CO_2 fixation (Woodrow and Mott, 1993; Miyagawa et al., 2001).

The decrease of Rubisco activity was associated with a decrease of photosynthesis only under high light conditions. Plants grown under moderate light and temperature were barely affected in photosynthesis even when Rubisco activity was reduced by more than 50% (Quick et al., 1991; De Porcellinis et al., 2018). In transgenic tobacco transformed with “antisense” *RbcS*, photosynthesis was inhibited by only 6% when Rubisco was decreased to about 60% of wild-type levels. The reduced amount of Rubisco was compensated by incubating these plants at high pH, Mg^{2+} and CO_2 to increase Rubisco activation (rising from 60 to 100%), with minor effects by an increase of its substrates and a decrease of its product (Quick et al., 1991). The *RbcS*-antisense tobacco with a severe decline in Rubisco content showed slight photoinhibition (Quick et al., 1991). Similar phenotypes were also observed in Arabidopsis *rbcS* mutants (Izumi et al., 2012).

Why are plants with a drastic reduction in RPE and *RbcS* still able to maintain a high activity of CO_2 fixation? Despite decades of research, the function and interaction of different small subunits in Rubisco is still enigmatic. Khumsupan et al. (2020) generated a set of single gene and multi gene knockout mutants for the four *rbcS* members in Arabidopsis, which provides a powerful tool for expanding our understanding of Rubisco structure function relationship in leaves (Khumsupan et al., 2020; Cavanagh, 2020). E.coli expression system

successfully expressing active plant Rubisco and was used to analyze the plant large and small subunits of Rubisco that affect its kinetic properties, overcame a major obstacle in functional studies of plant Rubisco (Aigner et al., 2017; Lin et al., 2020). Martin-Avila et al. (2020) recently provided an effective bioengineering chassis by modifying plant photosynthesis and growth through homogenous plant Rubisco by *rbcL-rbcS* operon chloroplast transformation in an RNAi-RbcS tobacco (Martin-Avila et al., 2020). The excess enzymes of the Calvin cycle may be in response to metabolic and environmental changes. Post-translational modifications (PTMs) of proteins enable rapid function regulation of protein in response to the metabolic and environmental changes (Lehtimäki et al., 2015; Grabsztunowicz et al., 2017). Rubisco subunits have multiple conserved PTMs in higher plants, the conserved N-terminal acetylation of RbcL and other PTMs may be absent in the Arabidopsis Rubisco expressed in *E. coli* (Aigner et al., 2017; Lin et al., 2020). Thioredoxin-mediated redox regulation of enzymes in Calvin cycle has been shown to determine the carbon assimilation efficiency (Lehtimäki et al., 2015). Some proteomics-based approaches suggest that all enzymes of CBC may be subject to redox regulation (Zaffagnini et al., 2012; Morisse et al., 2014). Other types of PTMs, Lys methylation, N-terminal and Lys acetylation, Tyr nitration and S-nitrosylation, sumoylation, glutathionylation and glycosylation of chloroplast proteins have also been described (Lehtimäki et al., 2015). CBC enzymes, including RPE, are subjected to carbonylation, nitration and particularly nitrosylation in leaves, confirming a link between these modifications and photosynthetic mechanisms (Grün et al., 2006; Jasid et al., 2006; Tanou et al., 2012).

Analysis of photosynthetic parameters showed that under a light irradiance of less than about 100 $\mu\text{mol photons m}^{-2} \text{ s}^{-1}$, the steady state rate of electron transport through PSII (ETR II) and PSI (ETR I) are almost similar in the *rpe* mutants and WT, except for a slight change in *rpe-1* (Figures 6A, D). These results are consistent with the normal plant growth and normal accumulation of thylakoid protein complexes under our growth chamber conditions (Figure 1B). However, under irradiance of 197 and 756 $\mu\text{mol photons m}^{-2} \text{ s}^{-1}$, the CO_2 assimilation rate was reduced in the *rpe* mutants (Figure 4B). The decrease in CO_2 assimilation may be caused by the decrease in RuBP regeneration capacity and Rubisco activity caused by the decrease in RPE level (Figure 5). This suggests that an insufficient amount of chloroplast RPE protein is available in the *rpe* mutants under higher light conditions. Also, the cis-element analysis shows that *cRPE* (*RPE* gene localized in chloroplasts) genes are light-responsive (Supplementary Figure 4) suggesting that expression of these genes is regulated by light. Further analyses showed that, under an irradiance of more than 100 $\mu\text{mol photons m}^{-2} \text{ s}^{-1}$, the electron transport rates through PSII (ETR II) and PSI (ETR I) are reduced in the *rpe*

mutants (Figures 6A, D). A higher value of 1-qL, which indicates a more reduced plastoquinone pool, was found in the *rpe* mutants compared with WT (Figure 6C). Chloroplast ATP synthase activity was also decreased in *rpe-1* in comparison to WT (Figure 6F), resulting in an increased accumulation of protons in the thylakoid lumen, and as a consequence, inducing a higher NPQ (Figure 6B). These photosynthetic properties of the *rpe* mutants can be well explained by the mechanism termed photosynthetic control (Foyer et al., 1990). During photosynthesis, reduced CO_2 assimilation in the chloroplast stroma of the *rpe* mutants leads to an over-accumulation of NAD(P)H and ATP, which restricts photosynthetic electron flow and ATP synthase activity by feedback control. Furthermore, increased acidification of the thylakoid lumen in the *rpe* mutants limits photosynthetic electron transport at the position of Cyt *b₆f* complex, resulting in reduced photosynthetic electron transport and an excessive reduction state of the plastoquinone pool (Figures 6C, E; Zhang et al., 2016).

To enhance CO_2 fixation, some of the CBC enzymes have been overexpressed in various oxygenic phototrophs. Our study reveals that chloroplast RPE is important for photosynthesis. Thus RPE may be a potential target for genetic engineering to enhance photosynthesis. It will be interesting to test whether overexpression of RPE can enhance carbon fixation, increase biomass, and improve environmental adaptability under stressful conditions.

Data availability statement

The original contributions presented in the study are included in the article/Supplementary Material. Further inquiries can be directed to the corresponding authors.

Author contributions

YL and LZ conceived the study and designed the experiments. YL performed the experiments. YL and LZ produced the figures. All authors analyzed the data. YL, XW, LP and LZ wrote the manuscript. XW and LZ supervised the whole study. All authors contributed to the article and approved the submitted version.

Funding

This work was supported by the National Natural Science Foundation of China (31871235), the Natural Science Foundation of Shanghai (22ZR1446000) and the Fund of

Shanghai Engineering Research Center of Plant Germplasm Resources (Grant No. 17DZ2252700).

Acknowledgments

We thank the NASC for providing the mutant seeds.

Conflict of interest

The authors declare that the research was conducted in the absence of any commercial or financial relationships that could be construed as a potential conflict of interest.

References

- Aigner, H., Wilson, R. H., Bracher, A., Calisse, L., Bhat, J. Y., Hartl, F. U., et al. (2017). Plant RuBisCo assembly in *E. coli* with five chloroplast chaperones including BSD2. *Science* 358, 1272–1278.
- Andriotis, V. M. E., and Smith, A. M. (2019) The plastidial pentose phosphate pathway is essential for postglobular embryo development in arabidopsis. *Proc. Natl. Acad. Sci. U. S. A.* 116, 15297–15306. doi: 10.1073/pnas.1908556116
- Baune, M. C., Lansing, H., Fischer, K., Meyer, T., Charton, L., Linka, N., et al. (2020). The arabidopsis plastidial glucose-6-phosphate transporter GPT1 is dually targeted to peroxisomes via the endoplasmic reticulum. *Plant Cell* 32, 1703–1726. doi: 10.1105/tpc.19.00959
- Bi, H., Li, F., Wang, H., and Ai, X. (2019). Overexpression of transketolase gene promotes chilling tolerance by increasing the activities of photosynthetic enzymes, alleviating oxidative damage and stabilizing cell structure in *cucumis sativus* L. *Physiol. Plant* 167, 502–515. doi: 10.1111/pp.12903
- Bracher, A., Whitney, S. M., Hartl, F. U., and Hayer-Hartl, M. (2017). Biogenesis and metabolic maintenance of rubisco. *Annu. Rev. Plant Biol.* 68, 29–60. doi: 10.1146/annurev-arplant-043015-111633
- Bryant, N., Lloyd, J., Sweeney, C., Myouga, F., and Meinke, D. (2011). Identification of nuclear genes encoding chloroplast-localized proteins required for embryo development in arabidopsis. *Plant Physiol.* 155, 1678–1689. doi: 10.1104/pp.110.168120
- Cavanagh, A. P. (2020). Big progress for small subunits: new rubisco mutants in arabidopsis. *J. Exp. Bot.* 71, 5721–5724. doi: 10.1093/jxb/eraa360
- De Porcellinis, A. J., Norgaard, H., Brey, L. M. F., Erstad, S. M., Jones, P. R., Heazlewood, J. L., et al. (2018). Overexpression of bifunctional fructose-1,6-bisphosphatase/sedoheptulose-1,7-bisphosphatase leads to enhanced photosynthesis and global reprogramming of carbon metabolism in *synechococcus* sp. *PCC 7002*. *Meta. Eng.* 47, 170–183. doi: 10.1016/j.ymben.2018.03.001
- Dubois, J. B., Fiscus, E. L., Booker, F. L., Flowers, M. D., and Reid, C. D. (2007). Optimizing the statistical estimation of the parameters of the farquhar-von caemmerer-berry model of photosynthesis. *New Phytol.* 176, 402–414. doi: 10.1111/j.1469-8137.2007.02182.x
- Farquhar, G. D., Caemmerer, S. V., and Berry, J. A. (1980). A biochemical model of photosynthetic CO₂ assimilation in leaves of *c-3* species. *Planta* 149, 78–90. doi: 10.1007/BF00386231
- Favery, B., Lecomte, P., Gil, N., Bechtold, N., Bouchez, D., Dalmasso, A., et al. (1998). RPE, a plant gene involved in early developmental steps of nematode feeding cells. *EMBO J.* 17, 6799–6811. doi: 10.1093/emboj/17.23.6799
- Foyer, C., Furbank, R., Harbinson, J., and Horton, P. (1990). The mechanisms contributing to photosynthetic control of electron transport by carbon assimilation in leaves. *Photosynth. Res.* 25, 83–100. doi: 10.1007/BF00035457
- Gani, Z., Boradia, V. M., Raghu Ram, J., Suryavanshi, P. M., Patil, P., Kumar, S., et al. (2016). Purification and characterization of glyceraldehyde-3-phosphate-dehydrogenase (GAPDH) from pea seeds. *Protein Expr. Purif.* 127, 22–27. doi: 10.1016/j.pep.2016.06.014
- Grabsztunowicz, M., Koskela, M. M., and Mulo, P. (2017). Post-translational modifications in regulation of chloroplast function: Recent advances. *Front. Plant Sci.* 8, 240. doi: 10.3389/fpls.2017.00240
- Grün, S., Lindermayr, C., Sell, S., and Durner, J. (2006). Nitric oxide and gene regulation in plants. *J. Exp. Bot.* 57, 507–516. doi: 10.1093/jxb/erj053
- Harrison, E. P., Olcer, H., Lloyd, J. C., Long, S. P., and Raines, C. A. (2001). Small decreases in SBPase cause a linear decline in the apparent RuBP regeneration rate, but do not affect rubisco carboxylation capacity. *J. Exp. Bot.* 52, 1779–1784. doi: 10.1093/jxb/52.362.1779
- Harrison, E. P., Willingham, N. M., Lloyd, J. C., and Raines, C. A. (1997). Reduced sedoheptulose-1,7-bisphosphatase levels in transgenic tobacco lead to decreased photosynthetic capacity and altered carbohydrate accumulation. *Planta* 204, 27–36. doi: 10.1007/s004250050226
- Izumi, M., Tsunoda, H., Suzuki, Y., Makino, A., and Ishida, H. (2012). RBCS1A and RBCS3B, two major members within the arabidopsis RBCS multigene family, function to yield sufficient rubisco content for leaf photosynthetic capacity. *J. Exp. Bot.* 63, 2159–2170. doi: 10.1093/jxb/err434
- Jasid, S., Simontacchi, M., Bartoli, C. G., and Puntarulo, S. (2006). Chloroplasts as a nitric oxide cellular source. effect of reactive nitrogen species on chloroplastic lipids and proteins. *Plant Physiol.* 142, 1246–1255. doi: 10.1104/pp.106.086918
- Johnson, M. P. (2016). Photosynthesis. *Essays Biochem.* 60, 255–273. doi: 10.1042/EBC20160016
- Kaiser, W. M. (1979). Reversible inhibition of the calvin cycle and activation of oxidative pentose phosphate cycle in isolated intact chloroplasts by hydrogen peroxide. *Planta* 145, 377–382. doi: 10.1007/BF00388364
- Khozaei, M., Fisk, S., Lawson, T., Gibon, Y., Sulpice, R., Stitt, M., et al. (2015). Overexpression of plastid transketolase in tobacco results in a thiamine auxotrophic phenotype. *Plant Cell* 27, 432–447. doi: 10.1105/tpc.114.131011
- Khumsupan, P., Kozłowska, M. A., Orr, D. J., Andreou, A. I., Nakayama, N., Patron, N., et al. (2020). Generating and characterizing single- and multigene mutants of the rubisco small subunit family in arabidopsis. *J. Exp. Bot.* 71, 5963–5975. doi: 10.1093/jxb/eraa316
- Kopriva, S., Koprivova, A., and Suss, K. H. (2000). Identification, cloning, and properties of cytosolic d-ribulose-5-phosphate 3-epimerase from higher plants. *J. Biol. Chem.* 275, 1294–1299. doi: 10.1074/jbc.275.2.1294
- Kruger, N. J., and von Schaewen, A. (2003). The oxidative pentose phosphate pathway: structure and organisation. *Curr. Opin. Plant Biol.* 6, 236–246. doi: 10.1016/S1369-5266(03)00039-6
- Lefebvre, S., Lawson, T., Zakhleniuk, O. V., Lloyd, J. C., Raines, C. A., and Fryer, M. (2005). Increased sedoheptulose-1,7-bisphosphatase activity in transgenic tobacco plants stimulates photosynthesis and growth from an early stage in development. *Plant Physiol.* 138, 451–460. doi: 10.1104/pp.104.055046

Publisher's note

All claims expressed in this article are solely those of the authors and do not necessarily represent those of their affiliated organizations, or those of the publisher, the editors and the reviewers. Any product that may be evaluated in this article, or claim that may be made by its manufacturer, is not guaranteed or endorsed by the publisher.

Supplementary material

The Supplementary Material for this article can be found online at: <https://www.frontiersin.org/articles/10.3389/fpls.2022.813241/full#supplementary-material>

- Lehtimäki, N., Koskela, M. M., and Mulo, P. (2015). Posttranslational modifications of chloroplast proteins: An emerging field. *Plant Physiol.* 168, 768–775. doi: 10.1104/pp.15.00117
- Lin, M. T., Stone, W. D., Chaudhari, V., and Hanson, M. R. (2020). Small subunits can determine enzyme kinetics of tobacco Rubisco expressed in *Escherichia coli*. *Nat. Plants* 6, 1289–1299.
- López-Calcano, P. E., Brown, K. L., Simkin, A. J., Fisk, S. J., Viallet-Chabrand, S., Lawson, T., et al. (2020). Stimulating photosynthetic processes increases productivity and water-use efficiency in the field. *Nat. Plants* 6, 1054–1063. doi: 10.1038/s41477-020-0740-1
- Martin-Avila, E., Lim, Y. L., Birch, R., Dirk, L. M. A., Buck, S., Rhodes, T., et al. (2020). Modifying plant photosynthesis and growth via simultaneous chloroplast transformation of Rubisco large and small subunits. *Plant Cell* 32, 2898–2916.
- Massange-Sanchez, J. A., Casados-Vazquez, L. E., Juarez-Colunga, S., Sowers, R. J. H., and Tiessen, A. (2020). The phosphoglycerate kinase (PGK) gene family of maize (*Zea mays* var. B73). *Plants* 9, 1639. doi: 10.3390/plants9121639
- Michelet, L., Zaffagnini, M., Morisse, S., Sparla, F., Pérez-Pérez, M. E., Francia, F., et al. (2013). Redox regulation of the Calvin-Benson cycle: something old, something new. *Front. Plant Sci.* 4, 470. doi: 10.3389/fpls.2013.00470
- Miyagawa, Y., Tamoi, M., and Shigeoka, S. (2001). Overexpression of a cyanobacterial fructose-1,6-/sedoheptulose-1,7-bisphosphatase in tobacco enhances photosynthesis and growth. *Nat. Biotechnol.* 19, 965–969. doi: 10.1038/nbt1001-965
- Morisse, S., Michelet, L., Bedhomme, M., Marchand, C. H., Calvaresi, M., Trost, P., et al. (2014). Thioredoxin-dependent redox regulation of chloroplastic phosphoglycerate kinase from *Chlamydomonas reinhardtii*. *J. Biol. Chem.* 289, 30012–30024. doi: 10.1074/jbc.M114.597997
- Mu, J., Fu, Y., Liu, B., Zhang, Y., Wang, A., Li, Y., et al. (2021). SiFBA5, a cold-responsive factor from *Saussurea involucreata* promotes cold resilience and biomass increase in transgenic tomato plants under cold stress. *BMC Plant Biol.* 21, 75. doi: 10.1186/s12870-021-02851-8
- Ohnishi, M., Furutani, R., Sohtome, T., Suzuki, T., Wada, S., Tanaka, S., et al. (2021). Photosynthetic parameters show specific responses to essential mineral deficiencies. *Antioxidants* 10, 996. doi: 10.3390/antiox10070996
- Quick, W. P., Schurr, U., Scheibe, R., Schulze, E. D., Rodermel, S. R., Bogorad, L., et al. (1991). Decreased ribulose-1,5-bisphosphate carboxylase-oxygenase in transgenic tobacco transformed with “antisense” *rbcS*: I. impact on photosynthesis in ambient growth conditions. *Planta* 183, 542–554. doi: 10.1007/BF00194276
- Raines, C. A. (2003). The Calvin cycle revisited. *Photosynth. Res.* 75, 1–10. doi: 10.1023/A:1022421515027
- Reyes-Prieto, A., and Bhattacharya, D. (2007). Phylogeny of Calvin cycle enzymes supports plantae monophyly. *Mol. Phylogenet. Evol.* 45, 384–391. doi: 10.1016/j.ympev.2007.02.026
- Rosenthal, D. M., Locke, A. M., Khozaei, M., Raines, C. A., Long, S. P., and Ort, D. R. (2011). Over-expressing the C₃ photosynthesis cycle enzyme sedoheptulose-1-7 bisphosphatase improves photosynthetic carbon gain and yield under fully open air CO₂ fumigation (FACE). *BMC. Plant Biol.* 11, 123. doi: 10.1186/1471-2229-11-123
- Serrato, A. J., Romero-Puertas, M. C., Lazaro-Payo, A., and Sahrawy, M. (2018). Regulation by s-nitrosylation of the Calvin-Benson cycle fructose-1,6-bisphosphatase in *Pisum sativum*. *Redox Biol.* 14, 409–416. doi: 10.1016/j.redox.2017.10.008
- Sharkey, T. D. (2019). Discovery of the canonical Calvin-Benson cycle. *Photosynth. Res.* 140, 235–252. doi: 10.1007/s11120-018-0600-2
- Simkin, A. J., Lopez-Calcano, P. E., Davey, P. A., Headland, L. R., Lawson, T., Timm, S., et al. (2017). Simultaneous stimulation of sedoheptulose 1,7-bisphosphatase, fructose 1,6-bisphosphate aldolase and the photorespiratory glycine decarboxylase-h protein increases CO₂ assimilation, vegetative biomass and seed yield in arabidopsis. *Plant Biotechnol. J.* 15, 805–816. doi: 10.1111/pbi.12676
- Tamoi, M., Nagaoka, M., Miyagawa, Y., and Shigeoka, S. (2006). Contribution of fructose-1,6-bisphosphatase and sedoheptulose-1,7-bisphosphatase to the photosynthetic rate and carbon flow in the Calvin cycle in transgenic plants. *Plant Cell Physiol.* 47, 380–390. doi: 10.1093/pcp/pcj004
- Tanou, G., Filippou, P., Belghazi, M., Job, D., Diamantidis, G., Fotopoulos, V., et al. (2012). Oxidative and nitrosative-based signaling and associated post-translational modifications orchestrate the acclimation of citrus plants to salinity stress. *Plant J.* 72, 585–599. doi: 10.1111/j.1365-313X.2012.05100.x
- Wilson, R. H., and Hayer-Hartl, M. (2018). Complex chaperone dependence of rubisco biogenesis. *Biochem.* 57, 3210–3216. doi: 10.1021/acs.biochem.8b00132
- Woodrow, E., and Mott, A. (1993). Modelling C₃ photosynthesis: A sensitivity analysis of the photosynthetic carbon-reduction cycle. *Planta* 191, 421–432. doi: 10.1007/BF00195743
- Xiong, Y., DeFraia, C., Williams, D., Zhang, X., and Mou, Z. (2009). Deficiency in a cytosolic ribose-5-phosphate isomerase causes chloroplast dysfunction, late flowering and premature cell death in arabidopsis. *Physiol. Plant* 137, 249–263. doi: 10.1111/j.1399-3054.2009.01276.x
- Zaffagnini, M., Bedhomme, M., Groni, H., Marchand, C. H., Puppo, C., Gontero, B., et al. (2012). Glutathionylation in the photosynthetic model organism *Chlamydomonas reinhardtii*: A proteomic survey. *Mol. Cell. Proteomics* 11, M111. 014142. doi: 10.1074/mcp.M111.014142
- Zhang, L., Duan, Z., Zhang, J., and Peng, L. (2016). Biogenesis factor required for ATP synthase 3 facilitates assembly of the chloroplast ATP synthase complex. *Plant Physiol.* 171, 1291–1306. doi: 10.1104/pp.16.00248
- Zhang, L., Pu, H., Duan, Z., Li, Y., Liu, B., Zhang, Q., et al. (2018). Nucleus-encoded protein BFA1 promotes efficient assembly of the chloroplast ATP synthase coupling factor 1. *Plant Cell* 30, 1770–1788. doi: 10.1105/tpc.18.00075
- Zhang, L., Zhou, W., Che, L., Rochaix, J. D., Lu, C., Li, W., et al. (2019). PPR protein BFA2 is essential for the accumulation of the atpH/F transcript in chloroplasts. *Front. Plant Sci.* 10, 446. doi: 10.3389/fpls.2019.00446

Frontiers in Plant Science

Cultivates the science of plant biology and its applications

The most cited plant science journal, which advances our understanding of plant biology for sustainable food security, functional ecosystems and human health.

Discover the latest Research Topics

[See more →](#)

Frontiers

Avenue du Tribunal-Fédéral 34
1005 Lausanne, Switzerland
frontiersin.org

Contact us

+41 (0)21 510 17 00
frontiersin.org/about/contact

